

COMPACT OBJECTS IN RELATIVISTIC THEORIES OF GRAVITY

A Dissertation
presented in partial fulfillment of requirements
for the degree of Doctor of Philosophy
in the Department of Physics and Astronomy
The University of Mississippi

by

Hector Okada da Silva

May 2017

Copyright Hector Okada da Silva 2017
ALL RIGHTS RESERVED

ABSTRACT

In this dissertation we discuss several aspects of compact objects, i.e. neutron stars and black holes, in relativistic theories of gravity. We start by studying the role of nuclear physics (encoded in the so-called equation of state) in determining the properties of neutron stars in general relativity. We show that low-mass neutron stars are potentially useful astrophysical laboratories that can be used to constrain the properties of the equation of state. More specifically, we show that various bulk properties of these objects, such as their quadrupole moment and tidal deformability, are tightly correlated.

Next, we develop a formalism that aims to capture how generic modifications from general relativity affect the structure of neutron stars, as predicted by a broad class of gravity theories, in the spirit of the parametrized post-Newtonian formalism (PPN). Our “post-Tolman-Oppenheimer-Volkoff” formalism provides a toolbox to study both stellar structure and the interior/exterior geometries of static, spherically symmetric relativistic stars. We also apply the formalism to parametrize deviations from general relativity in various astrophysical observables related with neutron stars, including surface redshift, apparent radius, Eddington luminosity.

We then turn our attention to what is arguably the most well-motivated and well-investigated generalization of general relativity: scalar-tensor theory. We start by considering theories where gravity is mediated by a single extra scalar degree of freedom (in addition to the metric tensor). An interesting class of scalar-tensor theories passes all experimental tests in the weak-field regime of gravity, yet considerably deviates from general relativity in the strong-field regime in the presence of matter. A common assumption in modeling neutron stars is that the pressure within these object is spatially isotropic. We relax this

assumption and examine how pressure anisotropy affects the mass, radius and moment of inertia of slowly rotating neutron stars, both in general relativity and in scalar-tensor gravity. We show that a sufficient amount of pressure anisotropy results in neutron star models whose properties in scalar-tensor theory deviate significantly from their general relativistic counterparts. Moreover, the presence of anisotropy allows these deviations to be considerable even for values of the theory's coupling parameter for which neutron stars in scalar-tensor theory would be otherwise indistinguishable from those in general relativity.

Within scalar-tensor theory we also investigate the effects of the scalar field on the crustal torsional oscillations of neutron stars, which have been associated to quasi-periodic oscillations in the X-ray spectra in the aftermath of giant flares. We show that the presence of the scalar field has an influence on the thickness of the stellar crust, and investigate how it affects the oscillation frequencies. Deviations from the predictions of general relativity can be large for certain values of the theory's coupling parameter. However, the influence of the scalar field is degenerate with uncertainties in the equation of state of the star's crust and microphysics effects (electron screening) for values of the coupling allowed by binary pulsar observations.

We also derive the stellar structure equations for slowly-rotating neutron stars in a broader class of scalar-tensor theories in which matter and scalar field are coupled through the so-called disformal coupling. We study in great detail how the disformal coupling affects the structure of neutron stars, and we investigate the existence of universal (equation of state-independent) relations connecting the stellar compactness and moment of inertia. In particular, we find that these universal relations can deviate considerably from the predictions of general relativity.

We then study neutron stars in tensor-multi-scalar theories, focusing on a particular model with two scalar degrees of freedom. We start with a detailed exposition of the formulation of this theory and, in particular, we show that it can be transformed into a scalar-tensor theory for a single complex-valued field with non-trivial kinetic term in the action. This

theory possesses a larger parameter space in comparison with the single-field scalar-tensor gravity, and certain combinations of these parameters are currently unconstrained by observations. After a discussion of the formal aspects of the theory, we derive the stellar structure equations for slowly-rotating relativistic stars. Our numerical results reveal that the theory possesses a very rich phenomenology. Additionally, we present the $3 + 1$ decomposition of the field equations, a fundamental requirement to perform numerical relativity evolutions.

Finally, we consider the most general scalar-tensor theory that yields second-order field equations: Horndeski gravity. We first study black hole solutions, and we generalize existing no-hair theorems to the case of slowly rotating black holes. Only a subclass of Horndeski gravity (namely Einstein-dilaton-Gauss-Bonnet gravity) supports asymptotically flat black holes with nontrivial scalar field configurations in first perturbative order in rotation. We also explore the existence of neutron stars in Horndeski gravity. We show that certain subclasses of the theory do not admit neutron star solutions. For the subclasses of the theory where these solutions exist, we study the properties of slowly rotating neutron stars, and obtain novel equation of state-independent relations connecting their compactness and moment of inertia.

ACKNOWLEDGEMENTS

I would like to thank Emanuele Berti for the unique opportunity to work with you, for introducing me to a whole new field of physics and for all the help and encouragement during these years. I feel very honored to be your student.

I was extremely fortunate to have collaborated with a fantastic group of people during the past years. I would like to thank Andrea Maselli, Caio F. B. Macedo, Davide Gerosa, George Pappas, Hajime Sotani, Jeremy Sakstein, Justin Alsing, Kostas Glampedakis, Leonardo Gualtieri, Luís C. B. Crispino, Masato Minamitsuji, Michael Horbatsch, Paolo Pani and Ulrich Sperhake. I learned much from you all. I also acknowledge the many (too many to name individually!) people with whom I have discussed various aspects of the work presented here.

I am pleased to thank Luca Bombelli, Katherine Dooley and Micah B. Milinovich for accepting being part of the dissertation committee.

I am grateful to the Department of Physics and Astronomy, faculty, staff and fellow students, for giving me the opportunity to pursue a degree here and providing all the necessary “boundary conditions” to carry my studies and research. In particular, I would like to thank Alakabha Datta, Josh Gladden, Kevin Beach, Luca Bombelli and Richard Raspet for the excellent courses taught. I also wish to thank Ginger Dykes and Amy Barnes for the always prompt hand to help me with bureaucratic matters. I am also thankful to Thomas Jamerson for being a great mentor during my period as a teaching assistant.

I am very happy to thank the Gravitation at Técnico group, at the Instituto Superior Técnico, for hosting and providing an amazing atmosphere for work during my long-term visits. I would like to thank Vitor Cardoso and Rita Almeida for the opportunity and help.

I also want to thank Andrea Nerozzi, Caio F. B. Macedo, Vincenzo Vitagliano and Ryuichi Fujita for great time sharing offices.

I would like to thank the “Casimir group” at the Universidade Federal do Pará, in particular os grandes cumpadis Danilo T. Alves and Carlos Farina. This work is the continuation of a journey that started long ago with you as guides.

I am extremely thankful to Anastasia for her love, affection and support during all these years.

None of this would have been possible without the unconditional support of my parents José Maria and Keiko, and my brother Vinícius, over the years. *Muito obrigado por tudo.*

PREFACE

The material included in this dissertation is part of my research work carried at the Department of Physics and Astronomy at The University of Mississippi during the period between August 2012 and April 2017, under the supervision of Prof. Emanuele Berti.

The chapters are based on different publications which I co-authored during this period, namely:

- Chapter 2 is based on:

Low-mass neutron stars: universal relations, the nuclear symmetry energy and gravitational radiation

H. O. Silva, H. Sotani and E. Berti

Mon. Not. Roy. Astron. Soc. **459** 4378 (2016)

- Chapter 3 is based on:

Post-Tolman-Oppenheimer-Volkoff formalism for relativistic stars

K. Glampedakis, G. Pappas, H. O. Silva and E. Berti

Phys. Rev. D **92** 024056 (2015)

- Chapter 4 is based on:

Astrophysical applications of the post-Tolman-Oppenheimer-Volkoff formalism

K. Glampedakis, G. Pappas, H. O. Silva and E. Berti

Phys. Rev. D **94** 044030 (2016)

- Chapter 5 is based on:

Slowly rotating anisotropic neutron stars in general relativity and scalar-tensor theory

H. O. Silva, C. F. B. Macedo, E. Berti and L. C. B. Crispino
Class. Quantum Grav. **32** 145008 (2015)

- Chapter 6 is based on:

Torsional oscillations of neutron stars in scalar-tensor theory of gravity

H. O. Silva, H. Sotani, E. Berti and M. Horbatsch
Phys. Rev. D **90** 124044 (2014)

- Chapter 7 is based on:

Relativistic stars in scalar-tensor theories with disformal coupling

M. Minamitsuji and H. O. Silva
Phys. Rev. D **93** 124041 (2016)

- Chapter 8 is based on:

Tensor-multi-scalar theories: relativistic stars and 3 + 1 decomposition

M. Horbatsch, H. O. Silva, D. Gerosa, P. Pani, E. Berti, L. Gualtieri and U. Sperhake
Class. Quantum Grav. **32** 204001 (2015)

- Chapter 9 is based on:

Slowly rotating black hole solutions in Horndeski gravity

A. Maselli, H. O. Silva, M. Minamitsuji and E. Berti
Phys. Rev. D **92** 104049 (2015)

Compact objects in Horndeski gravity

H. O. Silva, A. Maselli, M. Minamitsuji and E. Berti
Int. J. Mod. Phys. D **25** 1641006 (2016)

- Chapter 10 is based on:

Neutron stars in Horndeski gravity

A. Maselli, H. O. Silva, M. Minamitsuji and E. Berti
Phys. Rev. D **93** 124056 (2016)

Another investigation carried out during this period, but not included here is:

- *New signatures of the dynamical Casimir effect in a superconducting circuit*

A. L. C. Rego, H. O. Silva, D. T. Alves and C. Farina

Phys. Rev. D **90** 025003 (2014)

because its falls outside the main theme of this dissertation.

TABLE OF CONTENTS

ABSTRACT	ii
ACKNOWLEDGEMENTS	v
PREFACE	vii
LIST OF FIGURES	xiii
INTRODUCTION	1
LOW-MASS NEUTRON STARS: UNIVERSAL RELATIONS, THE NUCLEAR SYMMETRY ENERGY AND GRAVITATIONAL RADIATION	9
A POST-TOLMAN-OPPENHEIMER-VOLKOFF FORMALISM FOR RELATIVISTIC STARS	31
SOME ASTROPHYSICAL APPLICATIONS OF POST-TOLMAN-OPPENHEIMER-VOLKOFF FORMALISM FOR RELATIVISTIC STARS	74
SLOWLY ROTATING ANISOTROPIC NEUTRON STARS IN GENERAL RELATIVITY AND SCALAR-TENSOR THEORY	100
TORSIONAL OSCILLATIONS OF NEUTRONS STARS IN SCALAR-TENSOR THEORY OF GRAVITY	124
RELATIVISTIC STARS IN SCALAR-TENSOR THEORIES WITH DISFORMAL COUPLING	148

TENSOR-MULTI-SCALAR THEORIES: RELATIVISTIC STARS AND 3+1 DECOM- POSITION	192
SLOWLY-ROTATING BLACK HOLE SOLUTIONS IN HORNDESKI GRAVITY . .	227
NEUTRON STARS IN HORNDESKI GRAVITY	247
BIBLIOGRAPHY	276
APPENDICES	315
DIMENSIONAL ANALYSIS OF POST-NEWTONIAN TERMS	316
THE NEWTONIAN AND RELATIVISTIC LANE-EMDEN EQUATIONS	323
THE PPN POTENTIALS	328
INTEGRAL REPRESENTATION OF THE MOMENT OF INERTIA OF A SLOWLY ROTATING ANISOTROPIC STAR IN SCALAR-TENSOR THEORY	333
A SIMPLE APPROXIMATE FORMULA FOR THE CRUST THICKNESS-TO-RADIUS RATIO OF NEUTRON STARS IN SCALAR TENSOR THEORY	335
EQUIVALENCE OF THE PERTURBATION EQUATIONS IN EINSTEIN AND JOR- DAN FRAMES	337
DISFORMAL INVARIANCE	339
SPHERICAL AND HYPERBOLOIDAL TARGET SPACES	344
SOLAR SYSTEM CONSTRAINTS ON TENSOR-MULTI-SCALAR THEORY . . .	350
LINEARIZED FIELD EQUATIONS AND SCALARIZATION IN TENSOR-MULTI- SCALAR THEORY	353

THE FIELD EQUATIONS OF HORNDESKI GRAVITY	356
VITA	363

LIST OF FIGURES

- 2.1 *Mass-radius curves of NSs for a variety of unified EOSs.* Mass-radius relations for the EOSs adopted in this chapter, and discussed in Sec. 2.2. The curves span NS models starting from $u_c = \rho_c/\rho_0 = 0.9$ up to the value of u_c resulting in the maximum mass allowed by each EOS. The solid horizontal band corresponds to the lowest high-precision NS mass measurement of $M/M_\odot = 1.174 \pm 0.004$ [303]. The dotted horizontal line indicates a conservative lower bound on the mass of $M/M_\odot = 0.89$, see e.g. [459]. Symbols on each line correspond to $u_c = 1.5$ and $u_c = 2.0$, respectively. 15
- 2.2 *Some properties of static NSs.* Left: Dependence of the NS mass M for a nonrotating star on the parameter η introduced in Eq. (2.1) at three given values of the central density: $u_c \equiv \rho_c/\rho_0 = 1.0, 1.5, 2.0$. Right: same, but for the surface gravitational redshift z defined in Eq. (2.4). In both cases, the solid lines represent the fit given in Eq. (2.5) using the fitting parameters listed in Table 2.2. The lower panels show the relative error of the fit with respect to the numerical data, $|y_{\text{data}} - y_{\text{fit}}|/y_{\text{data}}$, as a function of η . The shaded area corresponds to the most plausible range of values for η , namely $67 < \eta < 120$ (see Sec. 2.2.2). This plot reproduces and extends Fig. 2 of [437]. Horizontal dashed lines correspond to a NS with $M/M_\odot = 0.89$ (the value of z was computed using the Shen EOS). 20
- 2.3 *The EOS-independent I-Love-Q relations [514, 515] in the low-mass regime.* The different panels show the I - Q (left), I -Love (center) and Love- Q (right) relations within the range of central energy densities considered here. For reference, the vertical dashed line corresponds to the values of \bar{Q} and $\bar{\lambda}^{(\text{tid})}$ of a NS model using the Shen EOS with $M/M_\odot = 0.89$. The lower panels show that the fractional deviations in the I -Love- Q relations increase for very low mass (i.e., larger values of \bar{Q} and $\bar{\lambda}^{(\text{tid})}$). Nevertheless, near and above the minimum mass value $0.89 M_\odot$ the relations hold within an accuracy $< 2\%$. The explicit functional form of the I -Love- Q relations can be found in Eq. (54) and Table 1 of [515]. Observe that even for very low-mass NSs the universality remains, although it is not captured by the I -Love- Q relations. 23
- 2.4 *The EOS independent Love-Love relations in the low-mass regime.* The Love-Love relation between $\bar{\lambda}^{(\text{tid})}$ and $\bar{\lambda}^{(\text{rot})}$ becomes an equality in the Newtonian – i.e., small- M – limit [325], and deviates from unity (solid line) for more relativistic stars. To make our fits of $\bar{\lambda}^{(\text{tid})}$ and $\bar{\lambda}^{(\text{rot})}$ with respect to η useful in combination with the Love-Love relation, we derived the improved fit of Eq. (2.8), corresponding to the dash-dotted line. This fit is accurate within $< 1\%$ for $M/M_\odot \geq 0.89$ (lower panel). The vertical dashed line corresponds to NS model with mass $M/M_\odot = 0.89$ using the Shen EOS. 24

2.5	<i>Fitting coefficients.</i> Illustration of the behavior of c_0 (circles) and c_1 (squares), appearing in the fitting expressions (2.5) and (2.9), as functions of u_c . The c_i 's are shown for three representative bulk properties of NSs: the mass M (top) fitted using Eqs. (2.5) and (2.6); the dimensionless moment of inertia \bar{I} (center) fitted using Eqs. (2.9) and (2.6); and the dimensionless quadrupole moment \bar{Q} (bottom) fitted using Eqs. (2.9) and (2.6).	25
2.6	<i>Some properties of slowly-rotating NSs - Part I.</i> Left: fit of $\bar{I} \equiv I/M^3$. Right: Fit of the reduced quadrupole moment $\bar{Q} \equiv Q^{(\text{rot})^*}/(M^3\chi^2)$. The horizontal dashed line in the left (right) panel marks the value of \bar{I} (\bar{Q}) for a NS with $M/M_\odot = 0.89$ and the Shen EOS.	26
2.7	<i>Rotational and tidal Love numbers.</i> Left: Fit of the rotational Love number $\bar{\lambda}^{(\text{rot})}$. Right: Fit of the tidal Love number $\bar{\lambda}_{\text{tid}}$. The horizontal dashed line in the left (right) panel marks the value of $\bar{\lambda}^{(\text{rot})}$ ($\bar{\lambda}^{(\text{tid})}$) for a NS with $M/M_\odot = 0.89$ and the Shen EOS.	26
2.8	<i>Some properties of slowly-rotating NSs - Part II.</i> Left: Fit of the quadrupole ellipticity e_Q^* . Right: fit of the $\ell = 2$ rotational apsidal constant $k_2^{(\text{rot})}$. Both quantities behave similarly, becoming nearly independent of η for $\rho_c = 2.0\rho_0$. For large value of η , we see that $k_2^{\text{rot}} \approx 0.7$ irrespective of the central density. The horizontal dashed line in the left (right) panel marks the value of e_Q^* ($k_2^{(\text{rot})}$) for a NS with $M/M_\odot = 0.89$ and the Shen EOS.	27
3.1	<i>The gravity-theory degeneracy problem.</i> The mass-radius relations in different modified theories of gravity for EOS APR [10]. Masses are measured in solar masses, and radii in kilometers. The theory parameters used for this plot are: $\alpha = 20M_\odot^2$ and $\beta^2 = 1$ (EdGB [355]); $c_{14} = 0.3$ (Einstein-Aether [508]); $\beta = -4.5$ (ST theory [353]) and $\kappa = \pm 0.005$ (Eddington-inspired-Born-Infeld gravity [431]). Even if the high-density EOS were known, it would be hard to distinguish the effects of competing theories of gravity on the bulk properties of NSs.	32
3.2	<i>2PN-order post-TOV corrections on the mass-radius curves.</i> We show the modification induced by different families of post-TOV terms on the general relativistic mass-radius curve, assuming the APR EOS. Left to right and top to bottom, the different panels show the effect of the pressure terms, proportional to π_i ($i = 1, \dots, 4$), and of the mass terms, proportional to μ_i ($i = 1, \dots, 5$).	34

- 3.3 *The radial profile of the Λ_2 -function.* We exhibit the behavior of $\bar{\rho}\Lambda_2$, where $\bar{\rho} = \rho/\rho_c$ and Λ_2 is given in Eq. (3.47), for a stellar model using the APR EOS, with $\epsilon_c/c^2 = 0.86 \times 10^{15}$ g/cm³, $M = 1.51M_\odot$ and $R = 12.3$ km. The curves are labelled according to the respective values of (α, β, θ) . From the top row to the bottom row the index θ takes on the values $(0, 1, 2, 3)$, respectively. Despite the multitude of possible dimensionally correct 2PN terms, their self-similarity – which is clear when we compare terms along the bottom-left to top-right diagonals in this “grid” of plots – allows us to group them into a relatively small number of families (see text for details). The contributions plotted in three panels at the bottom right of the grid (marked as “Excluded”) would lead to divergences in the hydrostatic equilibrium equations, and therefore they can be discarded as unphysical. 52
- 3.4 *The family-representative 2PN terms.* Here we show the selected representative terms from each of the families depicted in Fig. 3.3, as listed in Eq. (3.53), for three different EOSs: FPS (left panel), APR (middle panel) and an $n = 0.6$ polytrope (right panel). Each term illustrates the qualitative behavior of each family of possible 2PN contributions to the structure equations. The high degree of invariance of the Λ_2 -profiles with respect to the EOS is evident in this figure. The GR background stellar models utilized in the figure have the following bulk properties: $\epsilon_c = 0.861 \times 10^{15}$ g/cm³ ($\lambda \equiv p_c/\epsilon_c = 0.165$), $M = 1.51 M_\odot$ and $R = 12.3$ km (left panel); $\epsilon_c = 1.450 \times 10^{15}$ g/cm³ ($\lambda = 0.198$), $M = 1.50 M_\odot$ and $R = 10.7$ km (center panel); $\lambda = 0.165$, $M = 1.50 M_\odot$ and $R = 11.75$ km (right panel). 54
- 3.5 *The family-representative terms in the structure equations.* This figure illustrates the behavior of each of the family-representative 2PN terms [see Eq. (3.53)] multiplied by the Newtonian prefactors in the post-TOV equations. The stellar parameters are identical to the ones used in Fig. 3.4. *Left panel:* the combination $(\rho m/r^2) \Lambda_2(\alpha, \beta, \theta)$ appearing in the pressure equation. *Right panel:* the combination $\rho r^2 \Lambda_2(\alpha, \beta, \theta)$ appearing in the mass equation. The top panels correspond to EOS APR; the bottom panels correspond to a relativistic polytrope with polytropic index $n = 0.6$. The divergence at the origin of the F5 term justifies its exclusion from the pressure equation. . . . 55
- 3.6 *Self-similarity in mass-radius curves - I.* Numerical integrations show that 2PN terms belonging to the same family result in self-similar deviations from GR in the mass-radius relation. This figure illustrates this remarkable property for pressure terms (top row) and mass terms (bottom row) belonging to families F2, F3 and F4 (from left to right). In each panel, the solid line corresponds to GR; the long-dashed line to a positive-sign correction due to the chosen term in each family; the short-dashed line to a negative-sign correction due to the chosen term in each family. The various symbols show that nearly identical corrections can be produced using different terms belonging to the same family, as long as we appropriately rescale their post-TOV coefficients. 63
- 3.7 *Self-similarity in mass-radius curves - II.* Same as in Fig. 3.6, but for the F5 family, which only admits post-TOV corrections with $\mu_5 < 0$ (see text). . . . 64

3.8	<i>Fractional deviations induced by the post-TOV parameters on the stellar mass and radius.</i> Here we illustrate the fractional changes caused by the post-TOV parameters in NS masses and radii. For a fixed central energy density and EOS APR, we plot the relative deviations from GR in mass and radius that result from varying the post-TOV parameters within the range indicated in the legends. <i>Top row:</i> $\epsilon_c/c^2 = 8.61 \times 10^{14}$ g/cm ³ , $M_{\text{GR}} = 1.51M_\odot$ and $R_{\text{GR}} = 12.3$ km. <i>Bottom row:</i> $\epsilon_c/c^2 = 1.20 \times 10^{15}$ g/cm ³ , $M_{\text{GR}} = 2.04M_\odot$ and $R_{\text{GR}} = 11.9$ km. <i>Left panels:</i> Effect of the post-TOV terms that enter in the pressure equation. <i>Right panels:</i> Effect of the post-TOV terms that enter in the mass equation. The circles represent contours of fixed relative deviation from GR.	68
3.9	<i>Directions of the post-TOV induced deviations.</i> This schematic diagram shows which sign of individual post-TOV parameters produces smaller or larger masses/radii with respect to GR, cf. Fig. 3.8.	69
3.10	<i>Deviations induced by the post-TOV parameters on the stellar compactness.</i> Here we consider the influence of the post-TOV parameters on the compactness $\mathcal{C} = M/R$ of NSs. Deviations from GR are calculated assuming the same APR EOS models as in the top and bottom rows of Fig. 3.8. <i>Left panels:</i> Effect of the post-TOV terms appearing in the pressure equation. <i>Right panels:</i> Effect of the post-TOV terms appearing in the mass equation.	70
4.1	<i>Errors in M_∞.</i> We show the percent error [% error $\equiv 100 \times (x_{\text{value}} - x_{\text{ref}})/x_{\text{ref}}$] in calculating M_∞ using Eqs. (4.17) and (4.18) with respect to (4.15) for various values of μ_1 using EOS SLy4. The range of μ_1 is chosen such that using any of Eqs. (4.15), (4.17) or (4.18) one can obtain a real root corresponding to M_∞ . The post-TOV models are constructed using a fixed central value of the energy density, which results in either a canonical ($1.4 M_\odot$) or a maximum-mass ($2.05 M_\odot$) NS in GR. <i>Top panel:</i> errors for a maximum-mass GR star. <i>Bottom panel:</i> errors for a canonical-mass GR star. <i>Right panel:</i> the absolute value of the post-TOV correction $\mathcal{F} = 4\pi\mu_1(M_\infty/R)^2$ as a function of μ_1 . The condition $\mathcal{F} \ll 1$ bounds the range of acceptable values of μ_1 for which the expansions leading to Eqs. (4.17) and (4.18) are valid. Errors are below 5 % when $\mu_1 \in [-1.0, 0.1]$	82
4.2	<i>Surface redshift and stellar compactness.</i> Relative percent changes with respect to GR for both z_s and C for different values of χ	85
4.3	<i>Bursting NS constraints.</i> The surfaces are contours of constant $[1 + (2/3)\chi z_s^2] z_s(2 + z_s)/(1 + z_s)^4$ in the (z_s, χ) plane. This quantity is a combination of observables – cf. the right-hand side of Eq. (4.48) – and therefore it is potentially measurable; a measurement will single out a specific contour in this plot. A further measurement of (say) the redshift z_s corresponds to the intersection between one such contour and a line with $z_s = \text{const}$, so it can lead to a determination of χ	88

4.4	<i>ISCO quantities.</i> ISCO quantities as functions of χ . The solid curve corresponds to the relative difference (in percent) of r_{isco} with respect to GR, while the dashed curve corresponds to the relative difference of the orbital frequency at the ISCO, $(\Omega_\varphi)_{\text{isco}}$	93
4.5	<i>Orbital frequencies.</i> Plots of Ω_r against Ω_φ for different values of $\chi = \pm 0.1, \pm 0.5$ and ± 1 . The black solid curve corresponds to the GR case. The dashed curves correspond to positive values of χ (and $r_{\text{isco}} > 6M_\infty$) while the dash-dotted curves correspond to negative values of χ (and $r_{\text{isco}} < 6M_\infty$).	94
5.1	<i>Mass-radius curves for anisotropic stars.</i> Mass-radius relation (top panels) and dimensionless compactness G_*M/Rc^2 as a function of the central density (bottom panels) for anisotropic stars in GR using EOS APR. In the left panels we use the quasi-local model of [228]; in the right panels, the Bowers-Liang model [63]. Different curves correspond to increasing λ_H (or λ_{BL}) in increments of 0.5 between -2 (top) and 2 (bottom). The shaded blue bar corresponds to the mass $M = 2.01 \pm 0.04M_\odot$ of PSR J0348+0432 [19].	112
5.2	<i>Moment of inertia of anisotropic stars.</i> The moment of inertia I as function of the mass M for anisotropic stars in GR using EOS APR, increasing λ_H (or λ_{BL}) in increments of 0.5 between -2 (top curves) and 2 (bottom curves). As in Figure 5.1, the vertical shaded region marks the largest measured NS mass [19].	113
5.3	<i>Scalarized anisotropic stars - I.</i> Spontaneous scalarization in the quasi-local model of Horvat et al. [228]. See the main text for details.	115
5.4	<i>Scalarized anisotropic stars - II.</i> Same as Figure 5.3, but for the Bowers-Liang anisotropy model [63].	116
5.5	<i>Scalarized anisotropic stars - III.</i> Same as Figure 5.2, but in ST theories with different values of β	117
5.6	<i>Scalarization threshold.</i> Critical β for scalarization as a function of the central density (left panel) and of the stellar compactness (right panel) for nonrotating NS models constructed using different nuclear-physics based EOSs, in the absence of anisotropy.	120
5.7	<i>Influence of anisotropy on the scalarization threshold.</i> Left panels: β versus critical central densities for different values of $\lambda_{H,BL}$. Right panels: β versus compactness $G_*M/\tilde{R}c^2$ of the critical solutions for different values of $\lambda_{H,BL}$	121
6.1	<i>The crustal equations of state.</i> Pressure \tilde{p} versus energy density $\tilde{\epsilon}$ for the crust EOSs considered in this work: EOS DH (solid line) and EOS KP (dashed line).	130

6.2	<i>Properties of our stellar models in ST theory.</i> From left to right we show: the mass-radius relation, the scalar field at the center of the star φ_c as a function of the central density $\tilde{\epsilon}_c$, the dimensionless ratio $-\alpha = Q/M$ as a function of the compactness $\tilde{\mathcal{C}}$ and the fractional crust thickness $\tilde{\mathcal{R}}$ as a function of $\tilde{\mathcal{C}}$. The choice of crustal EOS does not sensibly affect the crust thickness and the onset of scalarization. In all panels, curves with various linestyles correspond to stellar models using EOS DH for the NS crust: solid lines correspond to $\beta = 0.0$, dashed lines to $\beta = -4.5$, and dotted lines to $\beta = -6.0$. Different symbols correspond to stellar models using EOS KP for the crust: circles for $\beta = 0.0$, squares for $\beta = -4.5$ and triangles for $\beta = -6.0$	131
6.3	<i>Fractional crust thickness of scalarized stars.</i> Comparison between Eq. (6.23) and the numerical results for $\beta = -6.0$, using $\sigma = 0.02326$. The GR expression (6.22) is also shown. Since the integration of Eqs. (6.12)-(6.15), gives us φ in the Einstein-frame radial coordinate r , the compactness and fractional crust thickness are evaluated in this frame. Notice, however, that even for $\beta = -4.5$ (a value marginally excluded by binary pulsars observations [169]) the percent difference between the compactnesses and fractional crust thicknesses in the two frames is less than 1.0%, and therefore Eq. (6.23) is accurate for all physically sensible values of β	135
6.4	<i>Shear velocity in scalarized stars.</i> Shear velocity profile $\tilde{v}_s(r)$ in the NS crust in the following cases: (i) GR without electron screening (solid line); (ii) GR with electron screening (dashed line); (iii) ST theory ($\beta = -6.0$) without electron screening (dashed-dotted line); (iv) ST theory ($\beta = -6.0$) with electron screening (dotted line). The top panel refers to EOS DH, the bottom panel to EOS KP. The sharp peaks occur near the neutron drip density $\tilde{\epsilon} \approx 3 \times 10^{11}$ g/cm ³ [412].	141
6.5	<i>The oscillation frequency spectra - I.</i> We show the frequencies of the torsional modes in ST theory as a function of M/M_\odot . <i>Top panels:</i> the fundamental torsional mode ${}_0t_2$ without (<i>left</i>) and with (<i>right</i>) electron screening. <i>Lower panels:</i> the first overtone ${}_1t_\ell$ without (<i>left</i>) and with (<i>right</i>) electron screening.	143
6.6	<i>The oscillation frequency spectra - II.</i> Frequencies of the torsional modes in ST theory as a function of β for stellar models with mass $M = 1.8 M_\odot$. Circles and dotted lines correspond to APR+DH; squares and dashed lines correspond to APR+KP. In the right panel we plot the mode frequencies ${}_0t_\ell$ for $\ell = 2, 3, 4$ and 5. In the left panel we show the frequencies of the first overtone ${}_1t_\ell$	144
6.7	<i>Equation of state degeneracy.</i> This plot compares modifications in torsional oscillation frequencies due to the underlying gravitational theory with crustal EOS uncertainties for models constructed using EOS APR in the core. Regions bounded by dashed lines correspond to oscillation frequencies in GR with different crustal EOSs; regions bounded by solid lines correspond to oscillation frequencies in ST theory with different crustal EOSs. The degeneracy between modified gravity and crustal EOS is broken when the two regions do not overlap. Left panels refer to a ST theory with $\beta = -4.5$, right panels to a theory with $\beta = -6.0$ (a value already excluded by binary pulsar experiments [169]).	145

6.8	<i>Comparison between electron screening and scalarization effect on the oscillation spectra.</i> The ratio η defined in Eq. (6.48) for all stellar models considered in this work. Values of $\eta > 1$ mean that the effect of scalarization is larger than that of electron screening. This would only be possible for values of β that are already ruled out by binary pulsar experiments.	146
7.1	<i>The role of Λ in spontaneous scalarization.</i> In both panels we consider stellar models using EOS SLy4 with $\beta_1 = -6.0$, $\beta_2 = 0$ and for $\Lambda = (-500, -3000, 50)$ km^2 . For reference the solid line corresponds to GR. Left panel: The mass-radius relation. Right panel: The dimensionless scalar charge $q \equiv -Q/M$ [118] as a function of the compactness \mathcal{C} . We see that $\Lambda > 0$ slightly increases scalarization with respect to the purely conformal theory (cf. Fig. 7.2). On the other hand, $\Lambda < 0$ can dramatically suppress scalarization. Note also that unlike β_2 , Λ can change the compactness threshold above which scalarization can happen, as predicted by the analysis of Sec. 7.5. These results are qualitatively independent of the choice of EOS.	179
7.2	<i>The role of β_2 in spontaneous scalarization.</i> As in Fig. 7.1, in both panels we consider stellar models using SLy4 EOS but with $\beta_1 = -6.0$ and $\Lambda = -1000$ km^2 for $\beta_2 = (-20, 0, 20)$. For reference the solid line corresponds to GR. Left panel: The mass-radius relation. Right panel: The dimensionless scalar charge $q = -Q/M$ as a function of the compactness \mathcal{C} . We see that β_2 affects highly scalarized stellar models making scalarization stronger (in the sense of increasing the value of q) when $\beta_2 < 0$, or weaker for $\beta_2 > 0$. Observe that β_2 has a negligible effect on weakly scalarized models ($ q \lesssim 0.35$). This is in agreement with its absence from the perturbative analysis of Sec. 7.5. Note that the range of \mathcal{C} for which scalarization occurs is the same, irrespective of the choice of β_2 . Again, these results are qualitatively independent of the choice of EOS.	180
7.3	<i>Radial profiles of some quantities of interest.</i> We show the normalized pressure profile p/p_c (top left), dimensionless mass function μ/M_\odot (top right), scalar field φ (bottom left) and the disformal factor χ (bottom right) in the stellar interior. The radial coordinate was normalized by the Einstein frame radius R . The radial profiles above correspond to three stellar configurations using SLy4 EOS, with fixed baryonic mass $M_b/M_\odot = 1.5$ and theory parameters $(\beta_1, \beta_2, \Lambda) = (-6, 0, 60)$, $(-6, -40, -500)$ and $(-6, 0, 0)$, the latter corresponding to a stellar model in the Damour-Esposito-Farèse theory [118, 120]. While the fluid variables are not dramatically affected, models with $\Lambda > 0$ ($\Lambda < 0$) become more (less) scalarized due to the disformal coupling. The bulk properties of these models are summarized in Table 7.1.	181

7.4	<i>NSs in ST theories with disformal coupling – Part I.</i>	We show NS models for three choices of realistic EOSs, namely APR, SLy4 and FPS, in decreasing order of stiffness. We illustrate the effect of varying the values of β_1 and Λ , while keeping β_2 fixed ($\beta_2 = 0$) for simplicity. The curves corresponding to $\Lambda = 0$, represent stellar models in purely conformal theory [118, 119]. Top panels: Mass-radius relations. Bottom panels: Moment of inertia versus mass. As seen in Fig. 7.1 already, while $\Lambda < 0$ weakens scalarization, $\Lambda > 0$ strengthens the effect. For $\beta_2 = 0$, this latter effect is very mild, being more evident by $\beta_2 < 0$ (cf. Fig. 7.5).	183
7.5	<i>NSs in ST theories with disformal coupling – Part II.</i>	In comparison to Fig. 7.4, here we show the influence of β_2 in spontaneous scalarization while keeping $\Lambda = -1000 \text{ km}^2$. As we have seen in Fig. 7.1 (and by the analytic treatment of Sec. 7.5), negative values of Λ suppress scalarization. This effect is such that for $\beta_1 = -4.5$, scalarization is suppressed altogether (top left panel). For smaller values of β_1 , this value of Λ weakens scalarization and we clearly see that β_2 affects the most scalarized stellar models in the conformal coupling theory. Note that the range covered by the axis here and in Fig. 7.4 is the same, making it clear that scalarization is less strong for the values of β_2 adopted.	184
7.6	<i>Binding energy.</i>	We show the fractional binding energy \mathcal{E}_b as a function of the baryonic mass for stellar models using EOS SLy4 and for theory with $(\beta_1, \beta_2, \Lambda) = (-6, 0, 50)$. Solutions in this theory branch around $M_b/M_\odot \approx 1.1$ with scalarized solutions (solid line) being energetically favorable over the general-relativistic ones (dashed line). The turning point at the solid curve corresponds to the maximum in the M - R relation, cf. Fig. 7.1.	185
7.7	<i>The I-\mathcal{C} relation in ST gravity.</i>	Top panel: The fit (7.94) obtained in the context of GR (thick solid line) is confronted against stellar models obtained in GR (solid line); and ST theories with parameters $(\beta_2, \Lambda) = (-20, -500)$, but with $\beta_1 = -6$ (dashed lines) and $\beta_2 = -7$ (dash-dotted lines), using EOSs APR, SLy4 and FPS. Middle panel: Relative error between the fit for GR against ST theory with $\beta_1 = -6$. Bottom panel: Similarly, but for $\beta_1 = -7$. In all panels the shaded regions correspond to approximately the domain of compactness for which spontaneous scalarization occurs in each theory. While for GR, the errors are typically below 6%, scalarized models can deviate from GR by 20% (for $\beta_1 = -6$) and up to 40% (for $\beta_1 = -7$).	188
8.1	<i>Spontaneous scalarization in a TMS theory with $O(2)$ symmetry.</i>	The value ψ_0 of the scalar field at the center of the star for scalarized solutions in the $O(2)$ -symmetric theory with $\beta_0 = -5.0$ and central baryon density $n_B = 10.4 n_{\text{nuc}}$, where the nuclear density is $n_{\text{nuc}} = 10^{44} \text{ m}^{-3}$. <i>Left panel:</i> spherical target space with $\mathfrak{r}^2 > 0$. <i>Right panel:</i> hyperbolic target space with $\mathfrak{r}^2 < 0$. In both panels the origin corresponds to the neutron star solution in GR.	209

- 8.2 *Stellar properties in the $O(2)$ -symmetric theory.* *Left panel:* The mass-radius relation for different values of τ and $\beta_0 = -5.0$. *Right panel:* Central value of the magnitude of the scalar field $|\psi_0|$ as a function of the stellar compactness $G_*M/(\tilde{R}c^2)$. Here \tilde{R} is the areal Jordan-frame radius of the star. The onset of scalarization does not depend on the value of τ 209
- 8.3 *Radial profiles.* Different panels show the profiles of the mass function m , metric potential ν , total energy density ρ and complex scalar field ψ , in units of $c = G = M_\odot = 1$. The profiles correspond to a scalarized star in the $O(2)$ -symmetric theory with $\beta_0 = -5.0$, $\beta_1 = \alpha = 0$, and fixed baryon mass $M_B = 1.70M_\odot$. The target space curvature is either $\tau = 0.5$ (spherical) or $\tau = 0.5i$ (hyperboloidal). In the spherical case, the scalarized solution has a gravitational mass $M = 1.54 M_\odot$, Jordan-frame areal radius $\tilde{R} = 13.0$ km, total scalar charge $Q = 0.553 M_\odot$ and central scalar magnitude $|\psi_0| = 0.154$. In the hyperbolic case, these quantities are $M = 1.54 M_\odot$, $\tilde{R} = 13.0$ km, $Q = 0.393M_\odot$ and $|\psi_0| = 0.110$. For comparison, the GR solution with the same baryonic mass has $M = 1.54M_\odot$ and $R = \tilde{R} = 13.2$ km. 210
- 8.4 *Symmetry breaking of the space of solutions.* When $\beta_1 \neq 0$, the $O(2)$ -symmetric solution-space analyzed in the previous section (cf. Fig. 8.1) collapses down to a $(Z_2 \times Z_2)$ -symmetric solution-space. This property of the theory is here illustrated for stellar models with the same equation of state and central energy density as in Fig. 8.1, $\beta_0 = -5.0$ and $\tau = 5.0$ 212
- 8.5 *Minimal baryonic mass of scalarized models.* The baryon mass of scalarized solutions at the onset of scalarization as a function of (i) $\beta_0 + \beta_1$ for models where $\text{Re}[\psi]$ is non-zero (left panel) and (ii) $\beta_0 - \beta_1$ for models where $\text{Im}[\psi]$ is non-zero (right panel). Each panel contains 6 curves, corresponding to the three values of β_1 at fixed $\tau = \infty$ (dashed curves) and the same three values of β_1 at $\tau = 1/2$ (dotted curves). The three dashed curves and the three dotted curves, respectively, are indistinguishable in the plot and the two families of dashed and dotted curves are only distinguishable in the inset, where we zoom into a smaller region. In both panels, the vertical long-dashed curve denotes the value $\beta_0 \pm \beta_1 = -4.35$ above which we no longer identify scalarized models, in agreement with Eq. (J.5). From Eq. (8.25) it is clear that the natural parameters are $\beta_0 + \beta_1$ and $\beta_0 - \beta_1$ when the theory is written in terms of the real and imaginary part of ψ , respectively. 213
- 8.6 *Mass-radius relations in the full TMS theory.* Analogous to the left panel of Fig. 8.2 for three values of the curvature radius of the target metric ($\tau = \infty$, $\tau = 1$ and $\tau = 0.5$), $\beta_0 + \beta_1 = -5$ (left panel) and $\beta_0 + \beta_1 = -10$ (right panel). Here we only consider models where $\text{Re}[\psi] \neq 0$. The gravitational mass M is shown as a function of the Jordan-frame radius \tilde{R} . For comparison, we include in both panels the GR curve. Note the different axis ranges in the two panels. When $\tau \rightarrow \infty$, the theory reduces to a ST theory with one scalar and effective coupling $\beta = \beta_0 + \beta_1$, and the observational constraint $\beta_0 + \beta_1 \gtrsim -4.5$ is in place [169]. However, such lower bound might be less stringent when τ is finite. 215

8.7	<i>Scalar field amplitudes in the full TMS theory - I.</i> Scalar field amplitude at the stellar center ψ_0 for stellar models with $\beta_0 = -5$, $ \alpha = 0.001$ and fixed baryon mass $M_B = 1.8 M_\odot$. The different panels show the solutions found for different values of β_1 as indicated in each panel. In each case, we vary the phase of α from 0 to 2π in steps of $\pi/6$. In contrast to the $\alpha = 0$ case in Fig. 8.4, the breaking of the $O(2)$ symmetry occurs gradually as β_1 is increased away from 0.	217
8.8	<i>Scalar field amplitudes in the full TMS theory - II.</i> The data of the upper left panel of Fig. 8.7 are shown on different scales to resolve the fine structure of the solutions in the ψ_0 plane. In each panel the vertical extent is equal to the horizontal.	217
9.1	<i>Hair (and its absence) in Horndeski gravity.</i> A schematic representation of the Hui-Nicolis no-hair theorem for shift-symmetric Horndeski gravity, and two possible ways of violating it (adapted from Ref. [418]).	241
10.1	<i>Mass-radius curves for different EOS models, selected values of q_∞, and $\eta = \pm 1$.</i> The various panels correspond to EOS APR (top left), SLy4 (top right), GNH3 (bottom left) and a polytropic (bottom right). Configurations with radii smaller than that identified by the orange cross do not satisfy the condition (10.34). The horizontal colored band corresponds to $M = 2.01 \pm 0.04 M_\odot$, the most massive NS mass known to date [138]. Note that the various panels have different x -axis ranges.	261
10.2	<i>Moment of inertia I as a function of the mass M.</i> The various panels correspond to EOS APR (top-left), SLy4 (top-right), GNH3 (bottom left) and a polytropic (bottom right). Configurations with masses larger than that identified by the orange cross do not satisfy the condition (10.34).	262
10.3	<i>The $I - q_\infty$ relations.</i> Top panel: The moment of inertia I versus charge q_∞ for a canonical NS with $M = 1.4 M_\odot$ and $\eta = -1$, and the realistic EOSs APR, GNH3, and SLy4. Bottom panel: Relative percentage errors between the numerical data and the relation (10.64).	272
10.4	<i>The $\bar{I} - \mathcal{C}$ relations.</i> Top panel: $\bar{I} - \mathcal{C}$ relation for different values of the scalar charge q_∞ and the realistic EOS APR (blue), GNH3 (red), SLy4 (green). The solid curve represents the fit given by Eq. (10.39), obtained in [71]. Bottom panel: Relative errors between the numerical data and the analytic relation. For illustrative purposes, we show the cases $q_\infty = 0$ and $q_\infty = 0.064$. For the latter, deviations from GR are more dramatic.	272
10.5	<i>Relative errors between the improved fits and the numerical data.</i> Top panel: $q_\infty = 0$. Middle panel: $q_\infty = 0.064$ and $\eta = 1$. Lower panel: $q_\infty = 0.064$ and $\eta = -1$	273
C.1	<i>Integral PN potentials and 1PN terms.</i> The radial profiles of the integral potentials U , E/m_N and Ω/m_N are well fitted by linear functions of the non-integral potentials p/ρ and $r^3 p/m_N$. In all plots, the radial coordinate is normalized to the stellar radius R	330

CHAPTER 1

INTRODUCTION

1.1 General relativity and beyond

General Relativity (GR) is the theory of spacetime and gravity, formulated in final form by Albert Einstein in 1915. The theory superseded the gravitational theory of Isaac Newton, formulated in the mid-17th century, which had so accurately explained gravitational phenomena on a vast scale, from the falling of objects on Earth to the motion of celestial bodies.

In the years following 1905, when Einstein presented his theory of special relativity, he embarked on an effort to formulate a relativistic theory of gravity. As early as 1907, he had already introduced the core idea behind what would later become GR. In a 1907 paper, in addition to assuming the weak equivalence principle (WEP), Einstein argues that given two systems, one in a static uniform gravitational field and one in uniform accelerated motion with respect to the first, one *cannot* use the laws of physics to distinguish them. He writes that “*we shall therefore assume complete physical equivalence between the gravitational field and the corresponding acceleration of the reference system.*” From this assumption it follows that time flows faster in a gravitational potential. This effect is known as gravitational redshift. Moreover, light would be deflected by the gravitational field of a massive body. During this period Einstein’s attention was much more focused on the fast development of quantum mechanics. It would not be until 1911 that he would turn his efforts back to the development of a relativistic theory of gravity. This culminated with a series of four papers in November 1915 [310]. The last of these paper contains the final formulation of GR.

For a long time it was generally accepted that GR would have little or negligible

effects in astrophysics. This scenario started to change in the 1960s in a quick succession of events (narrated in [502, 503]). Important for us are: (i) the discovery of the first *quasar*, a small region of spacetime sourcing the emission of a very large amount of energy through electromagnetic radiation, and (ii) the development of a competing theory to GR (Brans-Dicke theory [64]). The first discovery led astrophysicists to consider GR to explain quasars. At present, the outpouring of energy from quasars is understood as sourced by the accretion of matter by supermassive BHs. As for Brans-Dicke theory, it showed that it was possible to formulate consistent alternative theories to GR that were compatible (at the time) with available experimental tests of relativistic gravity. Shortly after the discovery of the first quasar, in 1967 Bell and Hewish discovered the first pulsar, a magnetized rotating NS¹. This class of stars were first proposed by Baade and Zwicky in 1934. Estimates of their masses and radii revealed that these objects are very dense and possess strong gravitational fields which prompts the use of GR in their description [343].

It quickly became clear that relativistic gravity *does* play an important role in the description of certain systems in the Universe, and the field of *relativistic astrophysics* was born. In this context it is natural to ask whether GR is the correct description of relativistic gravity. The following decades witnessed a flourishing of precision tests of relativistic gravity, made possible by technological advances and theoretical progress in the understanding of metric theories of gravity, epitomized by the parametrized post-Newtonian (PPN) formalism [502, 335]. Over the years we have seen GR passing with flying colors all the stringent experimental tests it was subjected to [499]. However, all of these tests probe gravity in the weak-field regime [51], with the possible exception of compact binary systems [496]. GR, and all metric theories of gravity for that matter, predict the emission of gravitational radiation from binary systems consisting of a pair of objects (stars and/or BHs) orbiting each other. While the motion of the binary constituents is not highly relativistic, they are strongly self-

¹The combined effect of magnetic field and rotation causes these NSs to emit radiation from their magnetic poles. This signal is detectable by telescopes only when the radiation is pointed towards Earth. Since the star rotates, the signal appears and fades periodically, much like as if we were facing a light-house, hence the name pulsar.

gravitating objects. The energy lost in the process causes a shrinking of the system’s orbit, which can be measured with great precision. The study of binary systems provides us with an indirect verification of the existence of gravitational waves. The agreement between the general relativistic predictions and the observational data from PSR B1913+16 (a double NS system) resulted in the Nobel Prize won by Hulse and Taylor in 1993. More recently, the (two) spectacular direct detections of gravitational-waves produced by the late inspiral and merger of two black holes (BHs) by the LIGO/Virgo Scientific Collaboration [3, 2] has offered us the first glimpse of the highly dynamical, fully nonlinear, strong-field regime of gravity, and GR is consistent with the observational data [4, 527]. We can anticipate that the new field of gravitational wave astronomy opens to us a new window to explore the nature of gravity in its most extremal manifestations.

At present there are compelling reasons to believe that GR must be modified in both its low- and large-energy limits [51]. In the infrared (low-energy) limit, cosmology tells us that a large fraction of the energy content of the Universe is due to dark matter (accounting for e.g, the “missing mass” in galactic systems) and dark energy (responsible for the small cosmological constant that makes the Universe expand at an accelerating rate). Attempts have been made to explain these entities in terms of modifications of GR. In the ultraviolet (high-energy) limit, GR is non-renormalizable; this problem can be cured by high-energy corrections to the theory. Corrections to GR appear, for instance, in the low-energy limit of string theory.

1.2 Compact objects as strong-gravity probes

As we have discussed there are classes of objects in our Universe whose description requires relativistic gravity. We elaborate more on NSs and BHs next.

1.2.1 Neutron stars

NSs [193] are the remnants of supernovae, the most energetic events in the Universe since the Big Bang. They are extremely compact and dense stars, with a typical mass of

$M = 1.4M_{\odot}$ ($M_{\odot} \approx 2 \times 10^{30}$ kg denotes the Sun’s mass) packed in a small sphere of merely 10 km. Moreover, NSs known as magnetars can harbor ultra-strong magnetic fields [478], about 10^{13} times stronger than the Earth’s. Other NSs, known as pulsars, can spin incredibly fast, with periods of revolution of the order of a dozen milliseconds [292]. In their interior, gravity is so strong and matter has such high densities (supranuclear) that these conditions are not reproducible by any terrestrial experiment. In fact, one of the greatest uncertainties in the description of these objects is in the equation of state of matter: we do not know with certainty the correct description of matter at the supranuclear densities in the interior of NSs. This translates into uncertainties in the bulk properties of NSs, such as the mass and radius. On the gravitational side, NSs are relativistic objects requiring the use of general relativity in their description. It is therefore natural to ask if NSs can carry observable imprints of gravitational theories beyond GR.

In summary, these celestial bodies provide us with a unique astrophysical laboratory for testing our understanding of fundamental aspects of physics. Future Earth and space-based experiments such as the SKA [493], NICER [25], AXTAR [386] and eXTP [529] will open a new era of precision measurements of NS properties and thereby allow us to test fundamental physics.

1.2.2 Black holes

One of the most surprising consequences of GR is the prediction of the existence of objects whose gravity is so strong that even light can not escape from their attraction. They are characterized by the presence of an event horizon, a no-return boundary in spacetime. These objects, called BHs by Wheeler, are poetically described by Chandrasekhar [93] as “*the most perfect macroscopic objects there are in the Universe*”, for “*the only elements in their construction are our concepts of space and time*”. BHs are not only perfect, in the sense described by Chandrasekhar, but they are also the simplest objects, since the uniqueness theorems developed during the 1970s – the so-called “Golden Age” of relativity – state

that the most general BH solution in vacuum in GR is completely described by only two parameters: their mass M and angular momentum J . This solution, obtained by Kerr [244], is expected to describe astrophysical BHs such as Sagittarius A* at the center of our own galaxy. The uniqueness theorem led to what became known as the *no-hair* conjecture, which states that the final outcome of gravitational collapse must be a Kerr BH.

BHs are also predicted in many gravitational theories which contain extra scalar degrees of freedom (such as Brans-Dicke theory [205]). Under certain assumptions, the no-hair conjecture holds and BH solutions in these theories are the same as in GR. BH solutions with some type of hair can be constructed either by relaxing some the theorem's assumptions, or by considering different types of fields [213].

BHs as predicted in some modified theories of gravity will differ from the Kerr solution, and therefore could lead to potentially observable effects in different astrophysical scenarios. It is expected that within the few next years we will be able to study with unprecedented levels of accuracy (e.g. with the Event Horizon Telescope [166, 165]) our galaxy's very own BH. Therefore, it is important to investigate these objects in modified theories of gravity [488] and to confront the predictions of these theories against observations [378, 73, 236, 380, 31].

In summary, the next generation of astrophysical observatories combined with the emergence of gravitational wave astronomy, will allows us to probe the strong-field limit of relativistic gravity for the first time. In some sense, the situation is similar to that of the 1960s and 1970s, when technology allowed us for the first time to do precision measurements of relativistic effects within of our Solar System.

1.3 Outline of this work

The present work on compact objects is organized in nine chapters, eight of which concern NSs and one focusing on BHs.

We start our investigation with Chapter 2, examining the interplay between nuclear physics and NSs in GR. As already mentioned, one of the outstanding problems in astro-

physics is the determination of the equation of state at the supranuclear densities found inside NSs. As a small contribution to help solving this problem, we show that various properties of low-mass NSs (e.g. their tidal deformability and quadrupole moment) are tightly correlated with certain parameters that describe the equation of state. This opens the possibility to use future NS observations to extract information about nuclear matter within these objects.

Chapter 3 addresses one of the most important difficulties in testing GR with NSs: the gravity theory-equation of state degeneracy, i.e., how can we disentangle our ignorance about the equation of state inside NSs from deviations (if any) induced by beyond-GR theories of gravity? To tackle this problem, we lay the foundations of a program to study NSs in a theory-agnostic manner, drawing inspiration from the PPN formalism. Our formalism, that we call “post-Tolman-Oppenheimer-Volkoff” (post-TOV), is applicable to static, spherically symmetric NSs, and allows us to study changes in the masses and radii due to a large class of possible extensions of GR through a finite set of post-TOV parameters.

In Chapter 4 we carry a step further in the program initiated in the previous chapter and examine how the post-TOV formalism can be applied in a number of interesting astrophysical scenarios. We use the formalism to parametrize deviations from GR in various astrophysical observables, including surface redshift, apparent radius, Eddington luminosity and orbital frequencies, the latter being important in attempts to explain the origin of quasi-periodic frequencies observed in the X-ray spectra of accreting NSs. Future observations of these observables can in principle be used to constrain the post-TOV parameters.

A basic assumption in the study of NSs is that the pressure of the matter within these objects is isotropic. In Chapter 5 we relax this assumption and investigate in detail the impact of anisotropy on the structure of NSs, both in GR and in scalar-tensor (ST) theory. This will be our first direct encounter with ST theories, which we study further in the next chapters. In addition to the mass and radius, we compute the NS moment of inertia within a slow-rotation approximation. We show how the presence of anisotropy affects

these quantities and (in the case of ST theory) how it influences the phenomenon known as spontaneous scalarization. We show that in certain circumstances anisotropy can not only facilitate scalarization, but also enhance its effect, leading to NS models that deviate largely from those predicted by GR.

In Chapter 6 we turn our attention to asteroseismology. In particular, we study the so-called crustal torsional oscillations, presumably connected to quasi-periodic oscillations in the aftermath of giant flares in NSs. Our goal here is to see, in the context of ST gravity, whether the presence of a scalar field in the star can leave some observable imprint in the oscillation spectrum. We conclude that while this could indeed be possible, current constraints on ST gravity imply that the effect of the scalar field is degenerate with uncertainties in the description of the microphysics in the star's crust.

Chapters 5 and 6 examined the implications of the simplest version of ST gravity. In the next two chapters we extend this simple version of the theory in two directions. In Chapter 7, we consider a much broader class of ST theories in which matter is coupled to the scalar field through the so-called disformal coupling. We obtain the stellar structure equations in this theory, examine in great detail how it impacts the bulk properties of slowly rotating NSs, and examine the existence of universal (equation of state-independent) relations connecting the star's moment of inertia and compactness.

All of the previous chapters considered ST theories with a single scalar field. In Chapter 8 we study the simplest multi-ST theory with two scalar fields. We elaborate on the formal aspects of the theory, explore NS solutions, and develop the 3 + 1-decomposition of the field equations, necessary for future numerical relativity simulations of the theory. Our preliminary analysis of NS models reveal a very rich phenomenology, whose full details remains to be explored.

In Chapter 9 we consider BHs in the most general single-scalar ST gravity, known as Horndeski gravity. We generalize known no-hair theorems to slowly rotating solutions, showing that at first order in rotation only a single subclass of the theory (Einstein-dilaton-

Gauss-Bonnet gravity) admits asymptotically flat solution with scalar hair.

We close our dissertation with Chapter 10, where we study slowly rotating NSs in Horndeski gravity, focusing on subclasses of the theory which have received considerable interest in the context of cosmology and generalizing previous results in the literature. We show that some subclasses of Horndeski gravity do not admit the existence of NSs casting doubts on their viability. For subclasses of the theory in which NSs exist, we again investigate the existence of equation of state-independent relations connecting the moment of inertia and compactness of these stars.

CHAPTER 2

LOW-MASS NEUTRON STARS: UNIVERSAL RELATIONS, THE NUCLEAR SYMMETRY ENERGY AND GRAVITATIONAL RADIATION

2.1 Introduction

The equilibrium of spherically symmetric, nonrotating neutron stars (NSs) in general relativity is governed by the Tolman-Oppenheimer-Volkoff (TOV) equations, that follow from Einstein's equations with a perfect-fluid stress energy tensor [457, 412, 171]. When supplemented with an equation of state (EOS) relating the density and pressure of the perfect fluid, the TOV equations form a closed system of ordinary differential equations, whose solutions are obtained (in general) by numerical integration. The solutions form a single-parameter family, where the parameter can be chosen to be the central total energy density ρ_c . Despite recent progress, the EOS is still largely unknown at the energy densities $\rho > \rho_0$ (where $\rho_0/c^2 \equiv 2.68 \times 10^{14}$ g/cm³ is the nuclear saturation density) characterizing the NS core. Uncertainties in the EOS translate into uncertainties in the NS mass-radius relation: for a typical NS mass $M \sim 1.4M_\odot$, EOSs compatible with our current knowledge of nuclear physics predict radii R ranging between 6 and 16 km [453].

Unlike black holes, which are vacuum solutions of Einstein's equations, NS structure depends on the coupling of gravity with matter. Therefore NSs can probe (and possibly rule out) theories of gravity that are close to general relativity in vacuum, but differ in the description of the coupling between matter and gravity in the strong-field regime [51]. In fact, given the strength of their gravitational field, the high density of matter at their cores and the existence of pulsars with fast spin and large magnetic fields, NSs are ideal laboratories to study all fundamental interactions [278, 275, 274, 376]. However, tests of strong gravity

with NSs are made more difficult by two fundamental degeneracies: (i) uncertainties in the EOS can mimic the modifications to the bulk properties of NSs that may be induced by hypothetical strong-field modifications of general relativity; (ii) different theories of gravity can give rise to similar modifications in the bulk properties of NSs [184].

These issues are partially alleviated by exploiting the recently discovered “universal” (EOS-independent) relations showing that rotating NSs are, in fact, relatively simple objects. Let M be the mass of a nonrotating star, J the angular momentum, $\chi = J/M^2$ the dimensionless spin, I the moment of inertia, Q the quadrupole moment and $\lambda^{(\text{tid})}$ the tidal Love number, a measure of stellar deformability (here and throughout this Chapter we use geometrical units $G = c = 1$). Working in the slow-rotation approximation, Yagi and Yunes [515, 514] discovered that universal (EOS-independent) “ I -Love- Q ” relations connect the three normalized quantities $\bar{I} = I/M^3$, $\bar{\lambda}^{(\text{tid})} = \lambda^{(\text{tid})}/M^5$ and $\bar{Q} = -Q^{(\text{rot})}/(M^3\chi^2)$. Subsequent work relaxed the slow-rotation approximation, showing that the universality still holds [152, 364, 86, 510].

Most investigations of relativistic stellar structure focus on NSs with the “canonical” $1.4M_\odot$ mass or higher. From a nuclear physics standpoint, recent measurements of masses $M \gtrsim 2M_\odot$ have ruled out EOS models that are unable to support such high masses [138, 19]¹. Large-mass NSs are more compact, and therefore more interesting for tests of strong gravity. From an astrophysical point of view, the large-mass regime is also interesting to improve our understanding of core-collapse physics. Observations of NS binaries (particularly via radio pulsars) and black hole X-ray binaries indicate that there may be a mass gap between the two populations: the highest measured NS masses just exceed $2M_\odot$ [273], while black hole masses may only start at $\sim 4\text{--}5.5M_\odot$ [346, 159], depending on the assumed shape of the distribution (but see who point out that selection biases could yield lower black hole masses [264]). Gravitational-wave observations of merging compact binaries will offer a

¹Here we will consider some EOS models that do not respect this constraint. This is because we are primarily interested in densities $\rho \sim \rho_0$, and (conservatively) we assume no correlation between the EOS near the saturation density and the EOS at higher densities [451].

unique opportunity to probe the existence of this “mass gap” [145, 298, 288, 458, 41, 98].

Our focus here is instead on low-mass NSs. There are observational and theoretical reasons why this regime is interesting. The lowest well-constrained NS masses currently measured are in the range $1.0\text{--}1.1M_{\odot}$ [273]. Recently [303] claimed a precise measurement of $M/M_{\odot} = 1.174 \pm 0.004$ in a double NS system with large mass asymmetry. While the minimum mass of a star constructed from a cold dense matter EOS is quite small ($< 0.1M_{\odot}$), the minimum mass of a hot protoneutron star is considerably larger, in the range $0.89\text{--}1.13M_{\odot}$ for the models considered by [459]. This minimum mass provides a practical lower bound on NS masses formed from supernovae, unless lower-mass stars form by fragmentation see e.g. the speculative scenario of Ref. [372]. Estimates based on the baryonic mass of the iron core of the supernova progenitor give a minimum mass of $\sim 1.15\text{--}1.2M_{\odot}$, as discussed in Sec. 3.3 of [273]. Tauris et al. [471] estimate that the minimum mass of a NS formed in an ultra-stripped supernova is $1.1M_{\odot}$. Note that uncertainties in supernova physics affect all of these bounds, and (if confirmed) the recent observations of Ref. [303] are only marginally compatible with the iron core bound. To summarize: it is commonly believed that the minimum mass of NSs in the universe should be around the minimum observed mass ($\sim 1M_{\odot}$) and that NS masses $\lesssim 1.2M_{\odot}$ would challenge the paradigm of NS formation by gravitational collapse, but these conclusions are uncertain due to our limited understanding of supernova physics. Therefore the discovery of low-mass NSs may give us important clues on their formation mechanism: for example, observations of NSs with mass $M \lesssim 1M_{\odot}$ could validate the astrophysical viability of the proto-NS fragmentation scenario proposed by [372].

Another key motivation for this work is that the low-mass regime is sensitive to – and carries information on – the isospin dependence of nuclear forces, and in particular on the nuclear symmetry energy [454, 474, 281, 277, 282, 331]. Sotani et al. [437] recently computed the structure of low-mass nonrotating NSs for a wide range of EOSs. They found that their mass M and surface redshift z can be fitted by simple functions of the central energy density

ρ_c and of the dimensionful parameter

$$\eta \equiv (K_0 L^2)^{1/3}, \quad (2.1)$$

where K_0 is the incompressibility of symmetric nuclear matter and L is the slope of the symmetry energy at saturation density (note that K_0 , L and η all have units of energy). Therefore, at least in principle, measurements of M and z could be used to constrain η ; in fact, the NS radius is highly correlated with the NS matter pressure at densities close to nuclear saturation density. A practical complication is that the determination of z and of the stellar radius, e.g. via photospheric radius expansion bursts and thermal emissions from quiescent low-mass X-ray binaries, is model-dependent and affected by systematic errors. Therefore, at present, no individual observation can determine NS radii to better than $\sim 20\%$ accuracy. This translates into nearly a 100% error in the determination of L , since $L \sim R^4$ [277].

A possible way to circumvent this problem is to rely on the fact that all NSs in nature are spinning. Considering rotating NSs is of interest because near-future experiments in the electromagnetic spectrum – such as NICER [176], LOFT [162], Astro-H [467] and SKA [493] – or in the gravitational-wave spectrum – such as Advanced LIGO [1], Advanced Virgo [6], KAGRA [421] and the Einstein Telescope [404] – could measure or constrain the additional multipoles that determine the structure of rotating NSs or other properties (such as the “Love numbers”) that are related to their deformability. Spin-orbit coupling in binary pulsars may allow us to measure the moment of inertia [116, 276, 35, 263] and gravitational-wave observations may be used to infer the tidal Love numbers, as well as additional information on the EOS [325, 53, 167, 388, 220, 487, 123, 135, 387, 160, 516, 266, 99, 519, 143]. Quite remarkably, measurements of the moment of inertia within an accuracy $\sim 10\%$ *alone* can yield tight constraints on the pressure over a range of densities [451]. The correlation between the moment of inertia and the tidal deformability (the “ I -Love” relation) is very tight for

massive NSs [515, 514], but not so much in the low-mass regime: see e.g. Fig. 2.3 below.

One of the main results of this chapter is that all of the properties of rotating and tidally deformed stars can be expressed as simple functions of ρ_c and η . Therefore measurements of any two bulk properties of a low-mass NS – for example, the mass M and the moment of inertia I – can be used to determine a region in the ρ_c - η plane, permitting to estimate η .

This chapter is organized as follows. In Section 2.2 we discuss the EOS models used in this chapter and the properties of nuclear matter that are relevant in the low-mass regime. In Section 2.3 we present our numerical results for the bulk properties of nonrotating and slowly rotating NSs, and we fit the properties of slowly rotating NSs by nearly universal functions of the central density ρ_c and of the parameter η . In the concluding Section 2.4 we discuss possible observational applications and future extensions of our work.

2.2 Low-mass neutron star properties and the nuclear symmetry energy

In this section we introduce some notation for the properties of uniform nuclear matter near saturation density, and we describe the EOS models used in our numerical work.

2.2.1 Properties of uniform nuclear matter

The energy of uniform nuclear matter at zero temperature can be expanded around the saturation point of symmetric nuclear matter (i.e., matter composed of an equal number of neutrons and protons). If n_b is the nucleon number density and $\alpha \equiv (n_n - n_p)/n_b$, where n_n (n_p) is the neutron (proton) number density, the bulk energy per nucleon w of uniform nuclear matter can be written as

$$w = w_0 + \frac{K_0}{18n_0^2}(n_b - n_0)^2 + \left[S_0 + \frac{L}{3n_0}(n_b - n_0) \right] \alpha^2, \quad (2.2)$$

where w_0 , n_0 and K_0 are the saturation energy, the saturation density and the incompressibility of symmetric nuclear matter, while S_0 and L are associated with the symmetry energy

coefficient $S(n_b)$:

$$S_0 = S(n_0), \quad L = 3n_0 \left(\frac{dS}{dn_b} \right) \Big|_{n_b=n_0}. \quad (2.3)$$

The parameters w_0 , n_0 and S_0 can be relatively easily determined from empirical data for the masses and radii of stable nuclei. The parameters K_0 and L , which determine the stiffness of neutron-rich nuclear matter, are more difficult to fix, and they affect the structure of low-mass NSs.

Different EOS models are based on different theoretical and computational approaches in nuclear physics. In order to derive empirical formulas expressing the properties of low-mass NSs that do not rely on specific EOSs, following [437] we adopt several tabulated EOS models that can be separated into three categories:

- (1) The phenomenological EOS model constructed by Oyamatsu and Iida [344]. The bulk energy $w(n_b, \alpha)$ is constructed to reproduce Eq. (2.2) in the limit where $n_b \rightarrow n_0$ and $\alpha \rightarrow 0$, and the optimal values of w_0 , n_0 , and S_0 are determined by requiring that the density profile of stable nuclei (determined within the extended Thomas-Fermi theory for given values of L and K_0) reproduce experimental nuclear data. The EOSs in this category will be labeled as OI K/Y , where $K = K_0$ and $Y = -K_0 S_0 / (3n_0 L)$. At variance with [437] we will omit the OI 180/350 EOS, because the associated values of K_0 and L are ruled out by current nuclear physics constraints (cf. Sec. 2.2.2).
- (2) Two EOS models based on the relativistic framework. One of these models (Shen) is constructed within relativistic mean field theory together with the TM1 nuclear interaction [414]; the second (Miyatsu) is based on the relativistic Hartree-Fock theory with the chiral quark-meson coupling model [324]. The spherical nuclei in the crust region are determined using the Thomas-Fermi theory.
- (3) Five EOS models based on the Skyrme-type effective interactions: FPS, SLy4, BSk19, BSk20, and BSk21 [290, 155, 189, 368, 367, 375].

All of these models are *unified* EOSs, i.e., both the crust and core regions can be described with the same EOS with specific values of K_0 and L . From the EOS tables we can compute K_0 , L and the auxiliary dimensionful parameter η introduced in Eq. (2.1) above, with the results listed in Table 2.1. The mass-radius relations predicted by these EOS models for nonrotating low-mass NSs are shown in Fig. 2.1.

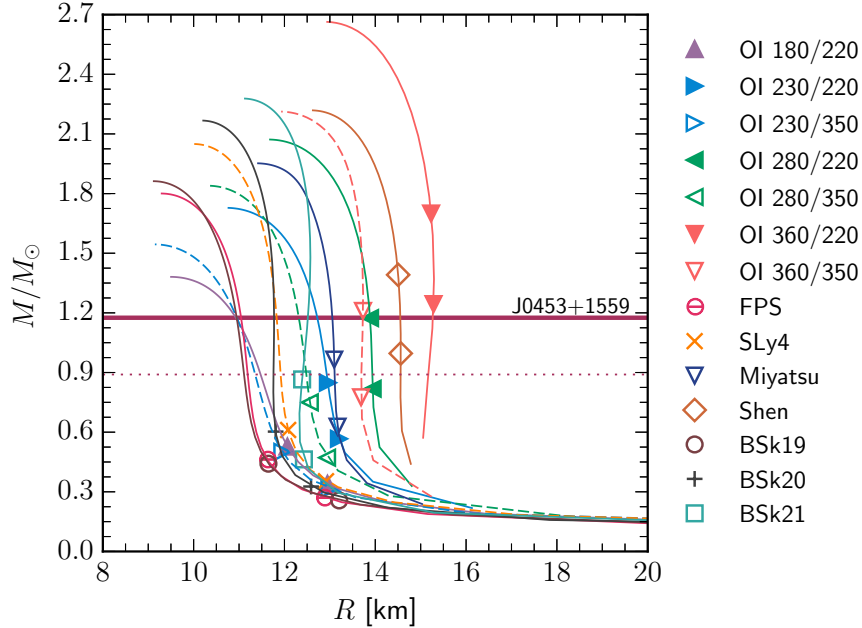


Figure 2.1: *Mass-radius curves of NSs for a variety of unified EOSs.* Mass-radius relations for the EOSs adopted in this chapter, and discussed in Sec. 2.2. The curves span NS models starting from $u_c = \rho_c/\rho_0 = 0.9$ up to the value of u_c resulting in the maximum mass allowed by each EOS. The solid horizontal band corresponds to the lowest high-precision NS mass measurement of $M/M_\odot = 1.174 \pm 0.004$ [303]. The dotted horizontal line indicates a conservative lower bound on the mass of $M/M_\odot = 0.89$, see e.g. [459]. Symbols on each line correspond to $u_c = 1.5$ and $u_c = 2.0$, respectively.

2.2.2 Experimental constraints

An extensive discussion of theoretical and experimental constraints on the properties of uniform nuclear matter can be found Refs. [281], [277] and [331]. Generally accepted values of K_0 are in the range $K_0 = 230 \pm 40$ MeV [245]. The current consensus in the

EOS	K_0 (MeV)	L (MeV)	η (MeV)
OI 180/220	180	52.2	78.9
OI 230/350	230	42.6	74.7
OI 230/220	230	73.4	107
OI 280/350	280	54.9	94.5
OI 280/220*	280	97.5	139
OI 360/350*	360	76.4	128
OI 360/220*	360	146	197
Shen*	281	114	154
Miyatsu	274	77.1	118
FPS	261	34.9	68.2
SLy4*	230	45.9	78.5
BSk19	237	31.9	62.3
BSk20*	241	37.9	69.6
BSk21*	246	46.6	81.1

Table 2.1: Parameters of the EOSs used in this work. EOSs which result in NSs with a maximum mass larger than $2M_\odot$ are indicated by an asterisk.

nuclear physics community is that values of L in the range $L = 60 \pm 20$ MeV are plausible² but higher values are not excluded [331].

There are proposals to constrain nuclear saturation parameters, and in particular the value of L , via astronomical observations. This approach is completely different from constraints based on nuclear physics experiments. Under the assumption that the observed frequencies of quasiperiodic oscillations (QPOs) in NSs are related to crustal torsional oscillations, Sotani et al. [441] found the constraint $101 < L < 131$ MeV when all the observed frequencies are interpreted as torsional oscillations, or $58 < L < 85$ MeV when the second lowest frequency is assumed to have a different origin. The inclusion of electron screening effects can modify the former constraint on L to the range $97 < L < 127$ MeV [436]. Furthermore, in some cases having information on the mass and radius of low-mass NSs may allow us to constrain EOS parameters. For example, the observation of the X-ray burster

²Lattimer and Steiner [277] suggest a tighter plausible range of $44 \text{ MeV} < L < 66 \text{ MeV}$ (see the discussion of their Figure 1), but we will follow Newton et al. [331] in an attempt to be more conservative.

4U 1724-307 [464] allows to set the constraint $\eta \gtrsim 130$ MeV [435]. These astrophysical constraints seem incompatible with constraints on L obtained from the terrestrial nuclear experiments quoted above [281, 277, 331]. One possible reason for this discrepancy may be that the constraints from nuclear experiments were obtained from almost stable nuclei, whose neutron excess α in Eq. (2.2) is very small, while NS matter deviates significantly from symmetric nuclear matter. Indeed, some nuclear experiments with unstable nuclei suggest the possibility that L may have larger values [475, 521].

If we adopt as fiducial values $40 \text{ MeV} < L < 80 \text{ MeV}$ – recalling that higher values cannot be excluded [331] – and $K_0 = 230 \pm 40 \text{ MeV}$ [245], respectively, we can conclude that a plausible range for η is $67 < \eta < 120$, and that higher values of η may be possible. This should be kept in mind in Section 2.3 below, where we discuss how the bulk properties of NSs depend on η .

2.3 Neutron star structure

2.3.1 Nonrotating neutron stars

For nonrotating NSs, the effect of the nuclear symmetry parameters introduced above on the mass-radius relation $M(R)$ was investigated by [437]. The main finding of their work was that the NS mass M and the surface gravitational redshift z , defined as

$$z \equiv \left(1 - \frac{2M}{R}\right)^{-1/2} - 1, \quad (2.4)$$

can be expressed as smooth functions of η of the form

$$y = c_0 + c_1 \left(\frac{\eta}{100 \text{ MeV}}\right), \quad (2.5)$$

where y collectively denotes either M or z . We also note that these relations can be combined to write the radius R as a function of η .

Using Eqs. (2.5) and (2.6) – Quantities at order $\mathcal{O}(\epsilon^0)$ in rotation							
Quantity	$c_{0,0}$	$c_{0,1}$	$c_{0,2}$	$c_{1,0}$	$c_{1,1}$	$c_{1,2}$	σ
M	0.34626	-0.82183	0.29265	-0.60780	1.2996	-0.25890	0.086 / 0.076
$z = (1 - 2M/R)^{-1/2} - 1$	0.0040470	-0.059527	0.026591	-0.042719	0.10673	-0.014208	0.100 / 0.089
Using Eqs. (2.9) and (2.6) – Quantities at order $\mathcal{O}(\epsilon^1)$ and $\mathcal{O}(\epsilon^2)$ in rotation							
Quantity	$c_{0,0}$	$c_{0,1}$	$c_{0,2}$	$c_{1,0}$	$c_{1,1}$	$c_{1,2}$	σ
$\bar{I} = I/M^3$	4.1429	-2.2458	0.46120	-0.23654	-0.26292	0.083322	0.122 / 0.083
$\bar{Q} = -Q^{(\text{rot})^*}/(M^3\chi^2)$	2.9160	-1.3835	0.24677	-0.25594	-0.093784	0.015956	0.120 / 0.114
$\bar{\lambda}^{(\text{rot})} = \lambda^{(\text{rot})}/M^5$	11.203	-5.8769	1.1697	-0.24302	-0.21457	0.055320	0.424 / 0.237
$k_2^{(\text{rot})} = (3/2)\lambda^{(\text{rot})}/R^5$	-3.9878	3.3914	-0.91026	-3.4378	2.6267	-0.53179	0.273 / 0.272
$e_Q^* = -Q^{(\text{rot})^*}/I$	-2.1203	1.8784	-0.52335	-4.0307	3.0883	-0.55984	0.129 / 0.126
Using Eqs. (2.9) and (2.6) – Tidally deformed star							
Quantity	$c_{0,0}$	$c_{0,1}$	$c_{0,2}$	$c_{1,0}$	$c_{1,1}$	$c_{1,2}$	σ
$\bar{\lambda}^{(\text{tid})} = \lambda^{(\text{tid})}/M^5$	11.238	-5.9413	1.1450	-0.21434	-0.25432	0.052281	0.462 / 0.263

Table 2.2: Numerical values of the constant in the fitting expressions and of the rms percentage error σ (last column), computed with / without EOS BSk21.

The coefficients c_i depend on the ratio $u_c \equiv \rho_c/\rho_0$ which specifies the central density of the stellar model. Following [437], we will fit these coefficient using a quadratic polynomial in u_c :

$$c_i = c_{i,0} + c_{i,1} u_c + c_{i,2} u_c^2. \quad (2.6)$$

Therefore each of our empirical formulas will depend on six constant parameters $c_{i,j}$.

In Fig. 2.2 we confirm the main results of [437]. The left (right) panel shows that, quite independently of the chosen EOS, the mass M (the redshift z , respectively) is indeed well fitted by a linear function of η for any fixed value of the central density u_c : the plots show this explicitly in the three cases $u_c = 1$, $u_c = 1.5$ and $u_c = 2$. The bottom insets show that the fractional differences $\delta y \equiv |y_{\text{data}} - y_{\text{fit}}|/y_{\text{data}}$ for M and z are typically below $\sim 10\%$ (with the exception of EOS BSk21) whenever $\eta \gtrsim 67$ MeV.

The values of the fitting constants are listed in the top two rows of Table 2.2. To quantify the accuracy of these fits, Table 2.2 also lists the rms relative error

$$\sigma \equiv \sqrt{\frac{1}{N} \sum_{i=1}^N \left(1 - \frac{y_i^{\text{fit}}}{y_i^{\text{data}}}\right)^2}, \quad (2.7)$$

where the sum runs over all stellar models $i = 1, \dots, N$. Two EOS models, namely BSk20 and BSk21 (and particularly the latter), deviate more from our best-fit function as ρ_c increases. As pointed out by [437], these deviations are of the order of the uncertainties on the mass M due to three-neutron interactions obtained from the quantum Monte Carlo evaluations [175]. Therefore in Table 2.2 we list the values of σ obtained either including or omitting EOS BSk21, the EOS for which the errors are larger.

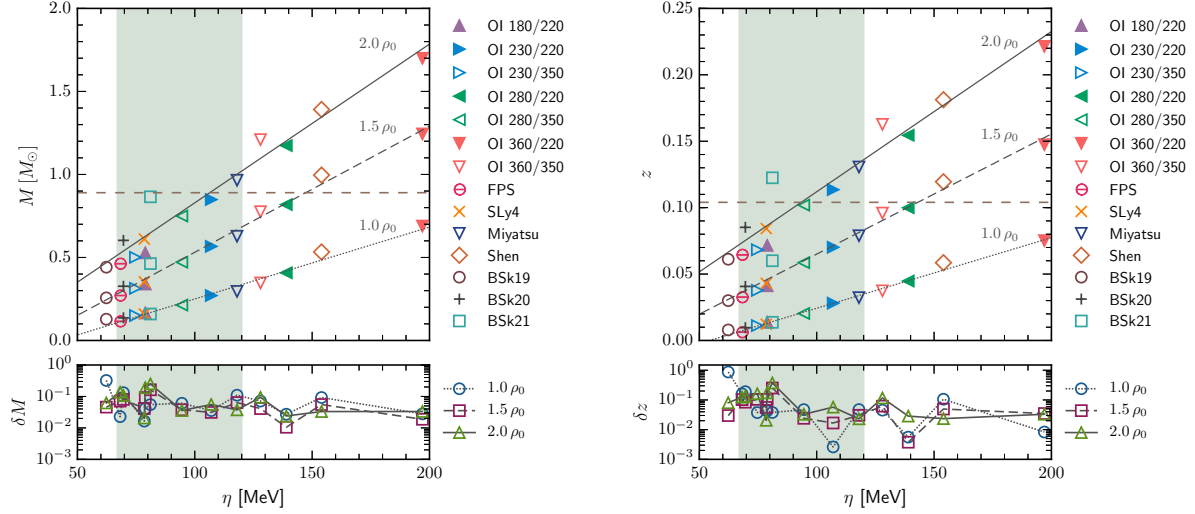


Figure 2.2: *Some properties of static NSs.* Left: Dependence of the NS mass M for a nonrotating star on the parameter η introduced in Eq. (2.1) at three given values of the central density: $u_c \equiv \rho_c/\rho_0 = 1.0, 1.5, 2.0$. Right: same, but for the surface gravitational redshift z defined in Eq. (2.4). In both cases, the solid lines represent the fit given in Eq. (2.5) using the fitting parameters listed in Table 2.2. The lower panels show the relative error of the fit with respect to the numerical data, $|y_{\text{data}} - y_{\text{fit}}|/y_{\text{data}}$, as a function of η . The shaded area corresponds to the most plausible range of values for η , namely $67 < \eta < 120$ (see Sec. 2.2.2). This plot reproduces and extends Fig. 2 of [437]. Horizontal dashed lines correspond to a NS with $M/M_\odot = 0.89$ (the value of z was computed using the Shen EOS).

2.3.2 Slowly rotating and tidally deformed neutron stars

In general, rotating stellar models in general relativity must be constructed numerically by solving a complicated system of partial differential equations. These numerical calculations (reviewed in Refs. [457, 171]) suggest that uniformly rotating NSs with physically motivated EOSs have dimensionless angular momentum $\chi \lesssim 0.7$ [111, 54, 289], but the spin magnitudes of NSs in binary systems observable by Advanced LIGO are likely to be much smaller than this theoretical upper bound [299, 74]. The spin period of isolated NSs at birth should be in the range 10-140 ms (or $\chi \lesssim 0.04$ [291]). Accretion from a binary companion can spin up NSs, but it is unlikely to produce periods less than 1 ms i.e. $\chi \lesssim 0.4$ [87]. The fastest spinning observed pulsar, PSR J1748-2446ad, has a period of 1.4 ms $\chi \sim 0.3$ [215]; the fastest known pulsar in a NS-NS system, J0737-3039A, has a period of 22.70 ms with a

corresponding dimensionless angular momentum of $\chi \sim 0.02$ [75].

The perturbative formalism to construct slowly rotating NS models was developed in the seminal works by Hartle and Thorne in the 60s [203, 202]. The formalism basically consists of an expansion in terms of the small parameter $\epsilon \equiv \Omega/\Omega^* \ll 1$, where Ω is the stellar angular velocity and $\Omega^* \equiv \sqrt{M/R^3}$ is a characteristic rotation frequency, comparable in order of magnitude to the mass-shedding frequency of the star. Subsequent work extended the formalism up to fourth order in ϵ , showing that the equilibrium properties of slowly rotating solutions compare favorably with numerical codes for arbitrary rotation rates [55, 42, 510] even for the fastest known millisecond pulsar PSR J1748-2446ad [215]. This pulsar spins well below the estimated $\epsilon \approx 0.5$ for which the Hartle-Thorne approximative scheme agrees very well with full numerical calculations. Therefore the slow-rotation approximation is more than adequate to extend the work on low-mass NSs by [437].

We use the stellar structure equations as presented by [465], correcting the misprints listed by [55]. Our numerical results were validated by comparison against the tables by [55]. For the dimensionless bulk properties we follow the definitions of [515]. The explicit form of the structure equations, their derivation and details of the integration procedure can be found in these references.

At order $\mathcal{O}(\epsilon^0)$ in the perturbative expansion, a static nonrotating star is characterized by its gravitational mass M and radius R . Sometimes it is useful to replace the radius by the surface redshift z defined in Eq. (2.4).

At first order in rotation, i.e. $\mathcal{O}(\epsilon^1)$, the star is also characterized by its moment of inertia I . Given I , we can define a dimensionless moment of inertia $\bar{I} \equiv I/M^3$ as well as a spin parameter $\chi \equiv I\Omega/M^2$ [515].

At second order in rotation, i.e. $\mathcal{O}(\epsilon^2)$, the star deviates from its spherical shape and acquires a rotational quadrupole moment $Q^{(\text{rot})^*}$. For convenience, we define the dimensionless rotation-induced quadrupole moment $\bar{Q} \equiv -Q^{(\text{rot})^*}/(M^3\chi^2)$. The $\ell = 2$ rotational Love number $\lambda^{(\text{rot})}$ can be defined in terms of $Q^{(\text{rot})^*}$ as $\lambda^{(\text{rot})} \equiv -Q^{(\text{rot})^*}/\Omega^2$, and it can be made

dimensionless by defining $\bar{\lambda}^{(\text{rot})} \equiv \bar{I}^2 \bar{Q}$. A quantity closely related with $\lambda^{(\text{rot})}$ is the $\ell = 2$ apsidal constant, defined as $k_2^{(\text{rot})} \equiv (3/2)\lambda^{(\text{rot})}/R^5$ (note that [53] used a different definition). Following [108], we can also define the quadrupolar rotational ellipticity³ $e_Q^* \equiv -Q^{(\text{rot})^*}/I$. Note that all of the barred quantities defined above (as well as $k_2^{(\text{rot})}$) are independent of the actual value of the rotation parameter ϵ .

2.3.3 Tidally deformed neutron stars

We will also be interested in the tidal deformation of a NS due the presence of an orbiting companion, e.g. in a binary system. The response to tidal deformations is encoded in the so-called $\ell = 2$ tidal Love number $\lambda^{(\text{tid})}$ [218, 219, 122, 60, 487], which is potentially measurable by advanced gravitational-wave interferometers. This quantity is in general spin-dependent [269, 360, 359, 268], but for simplicity we will assume that the tidally deformed NS is nonrotating. The tidal Love number can be put in a dimensionless form by defining $\bar{\lambda}^{(\text{tid})} \equiv \lambda^{(\text{tid})}/M^5$. We calculated the tidal Love number using the structure equations as presented by [373], and validated our results by comparison against [515].

2.3.4 Empirical relations for slowly rotating and tidally deformed neutron stars

We constructed NS models for all of the 14 EOS models listed in Table 2.1. We integrated the structure equations for central total energy densities within the range $u_c \equiv \rho_c/\rho_0 \in [1.0, 2.0]$ in increments $\Delta u_c = 0.1$, for a total of 154 stellar models. We verified that the normalized binding energy $M_b/M - 1$ (where M_b is the baryonic mass) is positive, so that all of these stellar configurations are bound.

Our results for the I -Love- Q relations are shown in Fig. 2.3, which confirms the main findings of [515]: the universality holds within a few percent, except for very low-mass stars. This breakdown of the I -Love- Q relations was already visible e.g. in Fig. 9 of [515], but it is much more noticeable in the low-mass range explored in this work. Yagi et al. [511]

³This quantity is different from the surface ellipticity $e_s \equiv r_e/r_p - 1$, where r_e and r_p are the equatorial and polar radii of the oblate rotating star, respectively. The surface ellipticity is related to the so-called “eccentricity” $e \equiv [(r_e/r_p)^2 - 1]^{1/2}$ (see e.g. [55]) by $e^2 = e_s^2 + 2e_s$, and it describes the geometry of the star.

suggested that the I -Love- Q relations hold because of an approximate self-similarity in the star’s isodensity contours. This approximate symmetry only holds for compact stars, but it is broken in low-mass NSs, white dwarfs and ordinary stars. Indeed, the I -Love- Q relations presented in [511] were obtained by fitting data in the range $\bar{Q} < 20$ and $\bar{\lambda}^{(\text{tid})} < 2 \times 10^4$ [507].

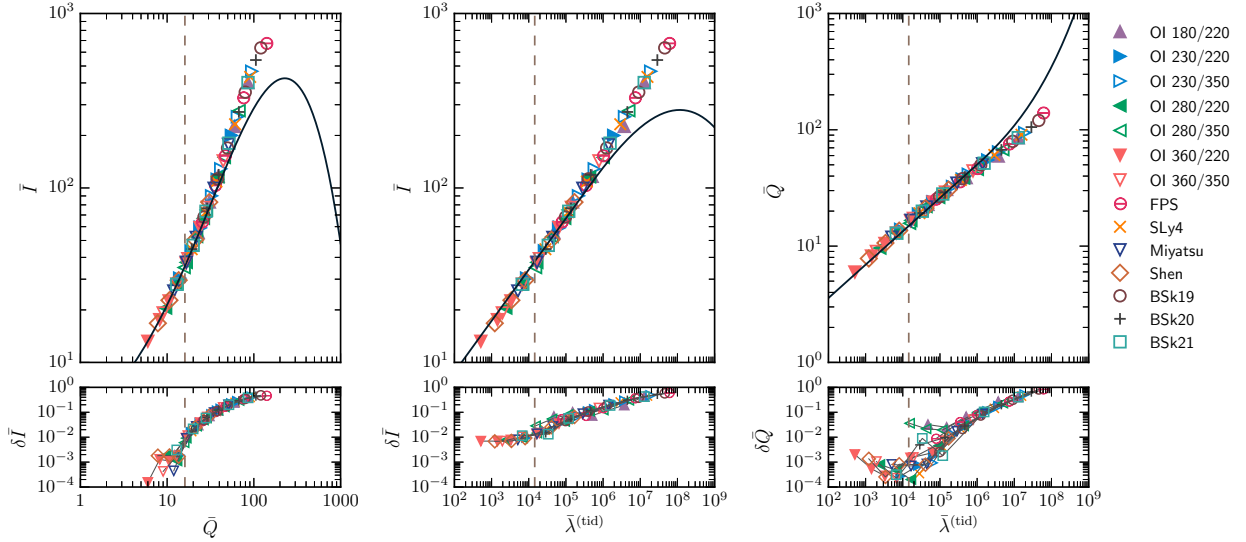


Figure 2.3: The EOS-independent I -Love- Q relations [514, 515] in the low-mass regime. The different panels show the I - Q (left), I -Love (center) and Love- Q (right) relations within the range of central energy densities considered here. For reference, the vertical dashed line corresponds to the values of \bar{Q} and $\bar{\lambda}^{(\text{tid})}$ of a NS model using the Shen EOS with $M/M_{\odot} = 0.89$. The lower panels show that the fractional deviations in the I -Love- Q relations increase for very low mass (i.e., larger values of \bar{Q} and $\bar{\lambda}^{(\text{tid})}$). Nevertheless, near and above the minimum mass value $0.89 M_{\odot}$ the relations hold within an accuracy $< 2\%$. The explicit functional form of the I -Love- Q relations can be found in Eq. (54) and Table 1 of [515]. Observe that even for very low-mass NSs the universality remains, although it is not captured by the I -Love- Q relations.

In Fig. 2.4 we show that a universal “Love-Love” relation also holds between the tidal and rotational Love numbers. A well-known result in Newtonian gravity is that tidal and rotational Love numbers are the same [325]. This equality no longer holds true for relativistic

stars [53, 515]. Therefore we propose a different fit, namely:

$$\ln \bar{\lambda}^{(\text{rot})} = \sum_{j=0}^4 k_j (\ln \bar{\lambda}^{(\text{tid})})^j, \quad (2.8)$$

where $k_0 = 2.1089$, $k_1 = 6.5084 \times 10^{-1}$, $k_2 = 2.4688 \times 10^{-2}$, $k_3 = -8.9891 \times 10^{-4}$ and $k_4 = 1.3985 \times 10^{-5}$. This fit uses data in the central density range $u_c \in [0.9, 2.0]$, and it works accurately in the range of masses of our interest.

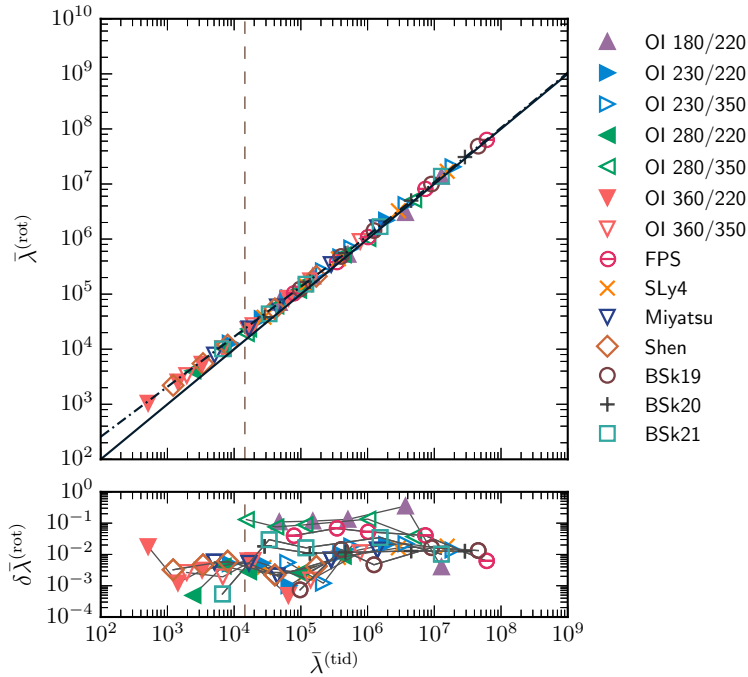


Figure 2.4: *The EOS independent Love-Love relations in the low-mass regime.* The Love-Love relation between $\bar{\lambda}^{(\text{tid})}$ and $\bar{\lambda}^{(\text{rot})}$ becomes an equality in the Newtonian – i.e., small- M – limit [325], and deviates from unity (solid line) for more relativistic stars. To make our fits of $\bar{\lambda}^{(\text{tid})}$ and $\bar{\lambda}^{(\text{rot})}$ with respect to η useful in combination with the Love-Love relation, we derived the improved fit of Eq. (2.8), corresponding to the dash-dotted line. This fit is accurate within $< 1\%$ for $M/M_\odot \geq 0.89$ (lower panel). The vertical dashed line corresponds to NS model with mass $M/M_\odot = 0.89$ using the Shen EOS.

Using these numerical calculations we then fitted the various bulk properties of NSs as functions of η and of the central density. The quantities characterizing rotating stars – namely \bar{I} , \bar{Q} , the $\ell = 2$ rotational Love number $\bar{\lambda}^{(\text{rot})} \equiv \bar{I}^2 \bar{Q}$, the $\ell = 2$ apsidal constant $k_2^{(\text{rot})}$

and the quadrupolar ellipticity e_Q^* – are well fitted by functions of the form

$$\log_{10} y = c_0 \left(\frac{\eta}{100 \text{ MeV}} \right)^{c_1}. \quad (2.9)$$

Just as for the nonrotating bulk properties of NSs, the coefficients c_i depend on the ratio $u_c \equiv \rho_c/\rho_0$, which specifies the central density of the stellar model. Following [437], we fitted the c_i 's by quadratic polynomials of the form (2.6), so that each of our empirical formulas depends on six constant parameters $c_{i,j}$.

The quality of the fits is shown in the three panels of Fig. 2.5 for three representative bulk NS properties, namely the mass M , the dimensionless moment of inertia \bar{I} and the dimensionless quadrupole moment \bar{Q} . In summary: the nonrotating bulk properties of NSs can be expressed as functions of η of the form (2.5) combined with Eq. (2.6); the bulk properties of rotating and tidally deformed NSs can be fitted by functions of the form (2.9) combined with Eq. (2.6). The fitting coefficients are listed in Table 2.2, that collects the main results of our investigation.

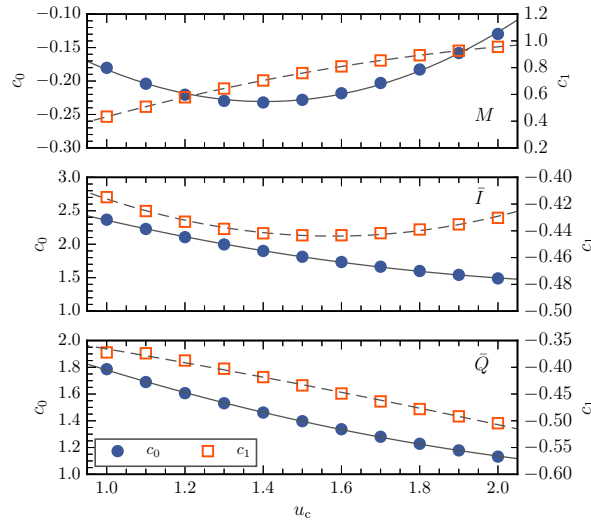


Figure 2.5: *Fitting coefficients.* Illustration of the behavior of c_0 (circles) and c_1 (squares), appearing in the fitting expressions (2.5) and (2.9), as functions of u_c . The c_i 's are shown for three representative bulk properties of NSs: the mass M (top) fitted using Eqs. (2.5) and (2.6); the dimensionless moment of inertia \bar{I} (center) fitted using Eqs. (2.9) and (2.6); and the dimensionless quadrupole moment \bar{Q} (bottom) fitted using Eqs. (2.9) and (2.6).

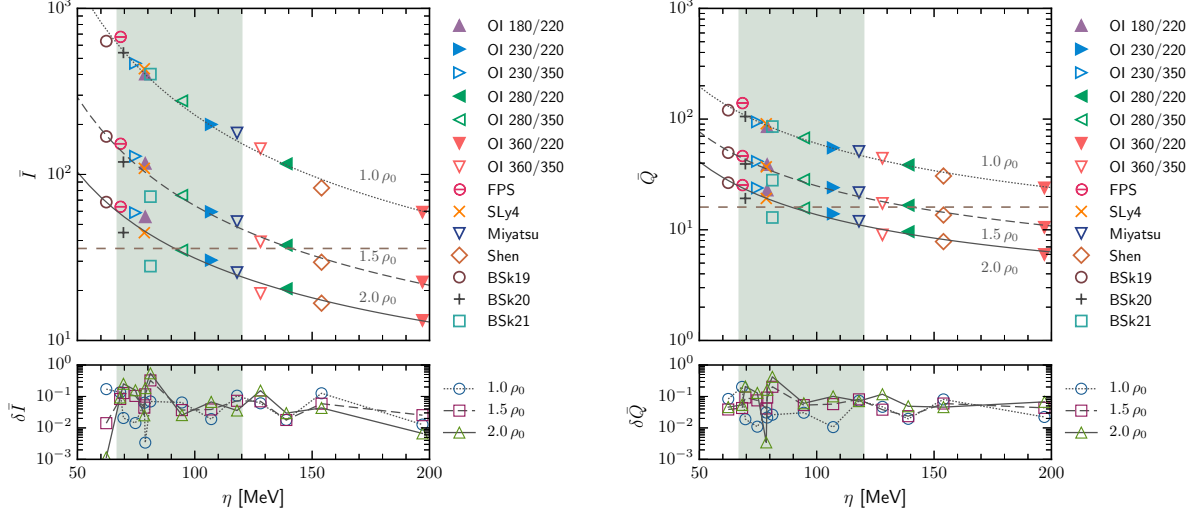


Figure 2.6: *Some properties of slowly-rotating NSs - Part I.* Left: fit of $\bar{I} \equiv I/M^3$. Right: Fit of the reduced quadrupole moment $\bar{Q} \equiv Q^{(\text{rot})}/(M^3\chi^2)$. The horizontal dashed line in the left (right) panel marks the value of \bar{I} (\bar{Q}) for a NS with $M/M_\odot = 0.89$ and the Shen EOS.

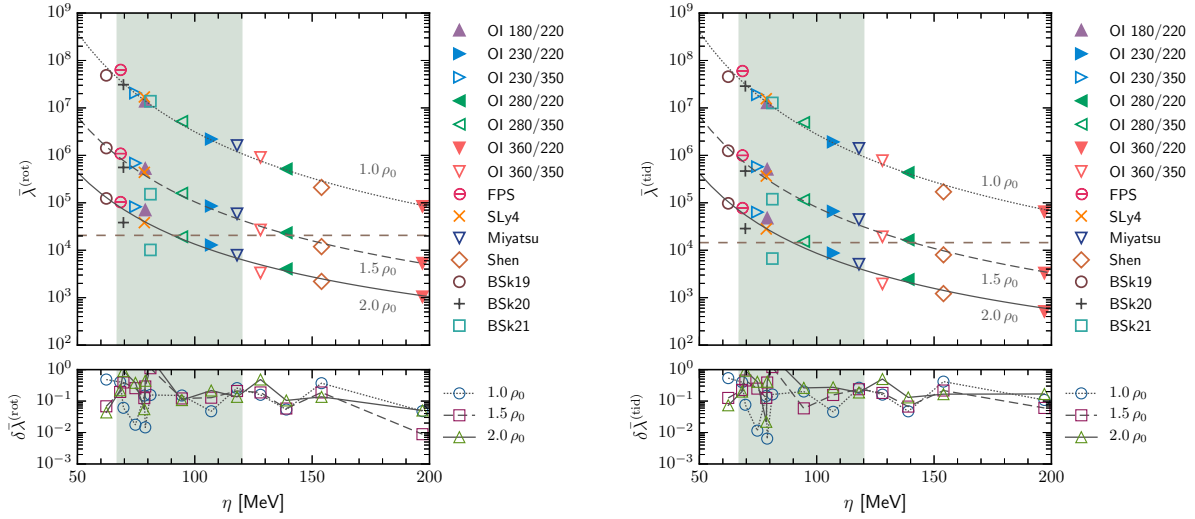


Figure 2.7: *Rotational and tidal Love numbers.* Left: Fit of the rotational Love number $\bar{\lambda}^{(\text{rot})}$. Right: Fit of the tidal Love number $\bar{\lambda}^{(\text{tid})}$. The horizontal dashed line in the left (right) panel marks the value of $\bar{\lambda}^{(\text{rot})}$ ($\bar{\lambda}^{(\text{tid})}$) for a NS with $M/M_\odot = 0.89$ and the Shen EOS.

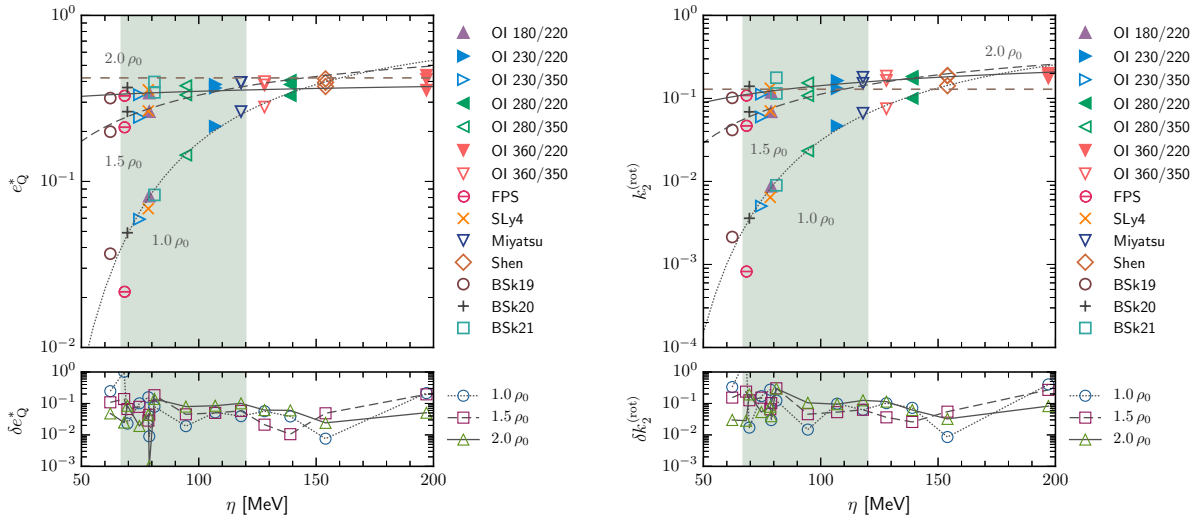


Figure 2.8: *Some properties of slowly-rotating NSs - Part II.* Left: Fit of the quadrupole ellipticity e_Q^* . Right: fit of the $\ell = 2$ rotational apsidal constant $k_2^{(\text{rot})}$. Both quantities behave similarly, becoming nearly independent of η for $\rho_c = 2.0\rho_0$. For large value of η , we see that $k_2^{\text{rot}} \approx 0.7$ irrespective of the central density. The horizontal dashed line in the left (right) panel marks the value of e_Q^* ($k_2^{(\text{rot})}$) for a NS with $M/M_\odot = 0.89$ and the Shen EOS.

The fits and their accuracy are also presented graphically in Figures 2.6–2.8. In the lower panel of each figure we plot the fractional differences δy . As in Fig. 2.2, the shaded area corresponds to the most plausible range of values for η as discussed in Sec. 2.2.2. These figures show that in general the fits work quite well in our fiducial range, i.e. for $\eta > 67$ MeV, with larger errors for small η .

2.4 Conclusions and outlook

In this chapter we have integrated the Hartle-Thorne equations for an extensive set of EOS models. We have computed the bulk properties of nonrotating (mass M and radius R , or equivalently mass M and surface redshift z), rotating (moment of inertia I , quadrupole moment Q , quadrupole ellipticity e_Q , rotational Love number $\lambda^{(\text{rot})}$, $\ell = 2$ apsidal constant $k_2^{(\text{rot})}$) and tidally deformed ($\ell = 2$ tidal Love number $\lambda^{(\text{tid})}$) low-mass NSs. All of these bulk NS properties can be fitted by relatively simple functions of the central density (more precisely, of $u_c \equiv \rho_c/\rho_0$) and of the parameter $\eta \equiv (K_0 L^2)^{1/3}$, where K_0 is the incompress-

ibility of symmetric nuclear matter and L is the slope of the symmetry energy at saturation density. The coefficients of these fitting relations are summarized in Table 2.2.

The main conclusion of our study is that the measurement of *any two* of these bulk properties in low-mass NSs can be used – at least in principle – to infer the values of ρ_c and η , providing important information on the EOS. However there are some important practical caveats.

First and foremost – as shown in the lower panels of Figures 2.6–2.8 – the fitting relations are approximate, with relative errors that typically get larger for the lowest plausible values of η . Furthermore, as discussed in the literature, constraints on the bulk properties of NSs and on the EOS require Monte Carlo simulations or dedicated Bayesian studies which are beyond the scope of this chapter [452, 453, 451, 277].

Even assuming accurate measurements of two of the bulk properties of a given NS – to be concrete, say M and I – a conceptual limitation is that not all EOSs predict the existence of NSs with “realistic” masses (say, $M > 0.89M_\odot$) in the range $1 \leq u_c \leq 2$ where our fitting relations have been derived (cf. Fig. 2.1). This problem can in principle be circumvented, because the measurement of M and I can be used to infer *both* u_c and η , and thus to verify whether the NS really has central densities in the range of interest. However it is possible that systematic errors could spoil these consistency tests. For example one could imagine a situation where the “true” central density corresponds to (for example) $u_c = 3$, but since we are applying the fitting relations outside of their region of validity, we recover values of $u_c \in [1, 2]$ and get a wrong estimate for η [507]. These data analysis issues deserve further study.

The recent discovery of universal I -Love- Q relations is also helpful. For example we can imagine measuring (say) M , R and \bar{I} and getting information on the remaining bulk properties by exploiting the I -Love- Q relations. A measurement of multiple parameters for the same astrophysical NS can be combined with our fitting formulas either to check the consistency of the inferred values of u_c and η , or to reduce statistical and/or systematic

errors.

We conclude by speculating on some observational possibilities to implement this program. Perhaps the most promising avenue in the near future is the measurement of mass and moment of inertia through relativistic spin-orbit coupling in systems such as the “double pulsar” PSR J0737-3039 [75], especially considering that a 10% measurement of the moment of inertia *alone* can yield tight constraints on the pressure over a range of densities to within 50 – 60% [451]. This possibility was discussed by various authors [116, 276, 35]. The experimental challenges associated with these measurements in the case of the double pulsar are reviewed in for instance in Section 6 of Kramer et al. [263].

In the near future it may also be possible to constrain η by gravitational-wave observations. Low-mass isolated NSs are relatively promising gravitational-wave sources because they are more deformable and their crusts can support larger ellipticities, generating stronger gravitational-wave signals [226, 238, 237] (cf. also our Figs. 2.6 and 2.7). However the characteristic gravitational-wave amplitude depends on a (generally unknown) geometrical factor involving the orientation of the NS and the antenna pattern of the detectors see e.g. [62, 142]. It has recently been proposed that gravitational-wave measurements of a *stochastic* gravitational-wave background from rotating NSs could be used to constrain the average NS ellipticity, and (if constraints on the masses can be obtained) these measurements could also constrain η . This possibility seems most promising for third-generation detectors such as the Einstein Telescope [468].

Ono et al. [342] proposed to estimate the mass of an isolated rapidly rotating NS by exploiting the mass-dependent logarithmic phase shift caused by the Shapiro time delay. According to their Monte Carlo simulations, the mass of a NS with spin frequency $f = 500$ Hz and ellipticity 10^{-6} at 1 kpc is typically measurable with an accuracy of 20% using the Einstein Telescope. Higher-order terms in the Shapiro time delay will depend on the higher multipole moments I and Q , and they may allow us to measure these moments and constrain η . It may also be possible to combine the empirical relations of the present work

with similar fitting relations that have been developed in the context of gravitational-wave asteroseismology, see e.g. [146].

Last but not least, as mentioned in the Sec. 2.1, Advanced LIGO observations of binary systems involving NSs could yield measurements of masses and tidal Love numbers [325, 53, 167, 388, 220, 487, 123, 135, 387, 266, 519, 143, 9]. Recent studies pointed out that systematic errors on these measurements are large and that better waveform models are necessary [160, 516, 489, 99], but effective-one-body methods and numerical simulations are making remarkable progress in this direction [48, 46, 47, 45].

CHAPTER 3

A POST-TOLMAN-OPPENHEIMER-VOLKOFF FORMALISM FOR RELATIVISTIC STARS

3.1 Introduction

NSs play a special role among astrophysical objects, because they are excellent laboratories for matter under extreme conditions (unlike BHs) and *also* excellent laboratories to probe strong gravity (unlike ordinary stars or white dwarfs) [51]. For these reasons NSs are among the main targets of future observatories such as the SKA [493], NICER [25], LOFT [161] and AXTAR [386]. These experiments have the potential to measure NS masses and radii to unprecedented levels [379, 317, 318]. If GR is assumed to be the correct theory of gravity, the observed mass-radius relation will constrain the EOS of matter at supranuclear densities, which is inaccessible to laboratory experiments [278, 275, 345, 452, 208, 316]. A procedure to reconstruct the EOS from observations of the mass-radius relation (working within GR) was developed in a series of papers by Lindblom and collaborators [284, 286, 287]; see [285] for a review.

Besides their interest for nuclear physics, NSs are also unique probes of strong-field gravitational physics. For any given EOS, theories that modify the strong-field dynamics of GR generally predict bulk observable properties (NS mass, radius, moment of inertia and higher multipole moments) that are different from those in Einstein's theory. However, a survey of the literature on NSs in modified theories of gravity (see e.g. Table 3 of [51]) reveals a high degree of degeneracy in the salient properties of relativistic stars. As we show in Fig. 3.1, if we assume a nuclear-physics motivated EOS (specifically, EOS APR [10] in the figure), modifications in the gravity sector are usually equivalent to systematic shifts of the

GR mass-radius curves towards either higher masses and larger radii (as in the case of ST theories [353, 153]), lower masses and smaller radii (as in the case of Einstein-dilaton-Gauss-Bonnet (EdGB) gravity [355, 247, 248] and Lorentz-violating theories [509, 508]) or both, as in Eddington-inspired-Born-Infeld gravity with different signs of the coupling parameter [358, 431].

Systematic shifts in the mass-radius relation could be attributed either to the poorly known physics controlling the high-density EOS, or to modifications in the theory of gravity itself. This EOS/gravity degeneracy is intrinsic in all attempts to constrain strong gravity through astrophysical observations of NSs: chapter 4 of [51] reviews various proposals to solve this problem, e.g. through the recently discovered universal relations between the bulk properties of NSs [514, 515, 364, 510].

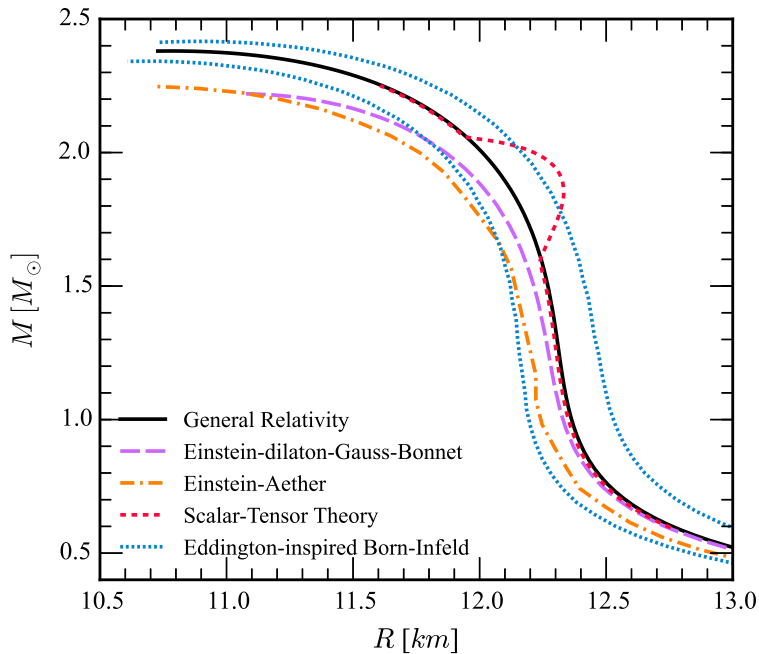


Figure 3.1: *The gravity-theory degeneracy problem.* The mass-radius relations in different modified theories of gravity for EOS APR [10]. Masses are measured in solar masses, and radii in kilometers. The theory parameters used for this plot are: $\alpha = 20M_{\odot}^2$ and $\beta^2 = 1$ (EdGB [355]); $c_{14} = 0.3$ (Einstein-Aether [508]); $\beta = -4.5$ (ST theory [353]) and $\kappa = \pm 0.005$ (Eddington-inspired-Born-Infeld gravity [431]). Even if the high-density EOS were known, it would be hard to distinguish the effects of competing theories of gravity on the bulk properties of NSs.

In any case, different gravitational theories span (at least qualitatively) the same parameter space in terms of their predictions for relativistic stellar models. Gravity-induced modifications usually look like smooth deformations of the general relativistic predictions. A notable exception are cases where nonperturbative effects induce phase transitions, as in the “spontaneous scalarization” scenario first proposed in [118], where modifications only occur in a specific range for the central density.

With the possible exception of nonperturbative phase transitions, these considerations suggest that the broad features of a large class of modified gravity theories can be reproduced, at least for small deviations from GR, by a perturbative expansion around a background solution given by the standard TOV equations, which determine the structure of relativistic stellar models in GR [323, 369].

Instead of committing to one particular pet theory, in this we formulate a parametrized “post-TOV” framework for relativistic stars based on the well-known PPN theory developed by Nordtvedt and Will [501, 335]; see e.g. [369] for introductions to the formalism. The foundations of PN theory for fluid configurations in GR were laid in classic work by Chandrasekhar and collaborators [89, 92]. Various authors studied stellar structure using the PN approximation, both in GR [26, 469, 416, 191] and in modified theories of gravity, such as ST theory [339, 506]. To our knowledge, after some early work that will be discussed below [490, 106, 413], the investigation of compact stars within the PPN approximation has remained dormant for more than thirty years. In the intervening time the PPN parameters have been extremely well constrained by Solar System and binary pulsar observations at 1PN order (see [499] for a review of current bounds).

In this chapter we build a phenomenological post-TOV framework by considering 1PN and 2PN order corrections to the TOV equations. Our strategy is, at heart, quite simple: from a suitable set of PPN hydrostatic equilibrium equations we isolate the purely non-GR pieces. These PPN terms are subsequently added “by hand” to the *full* general relativistic TOV equations, hence producing a set of parametrized post-TOV equations (cf. [525] for

a similar “post-Einsteinian” parametrization in the context of gravitational radiation from binary systems). The formalism introduces a new set of 2PN parameters that are presently unconstrained by weak-field experiments, and that encompass the dominant corrections to the bulk properties of NSs in GR in a wide class of modified gravity theories.

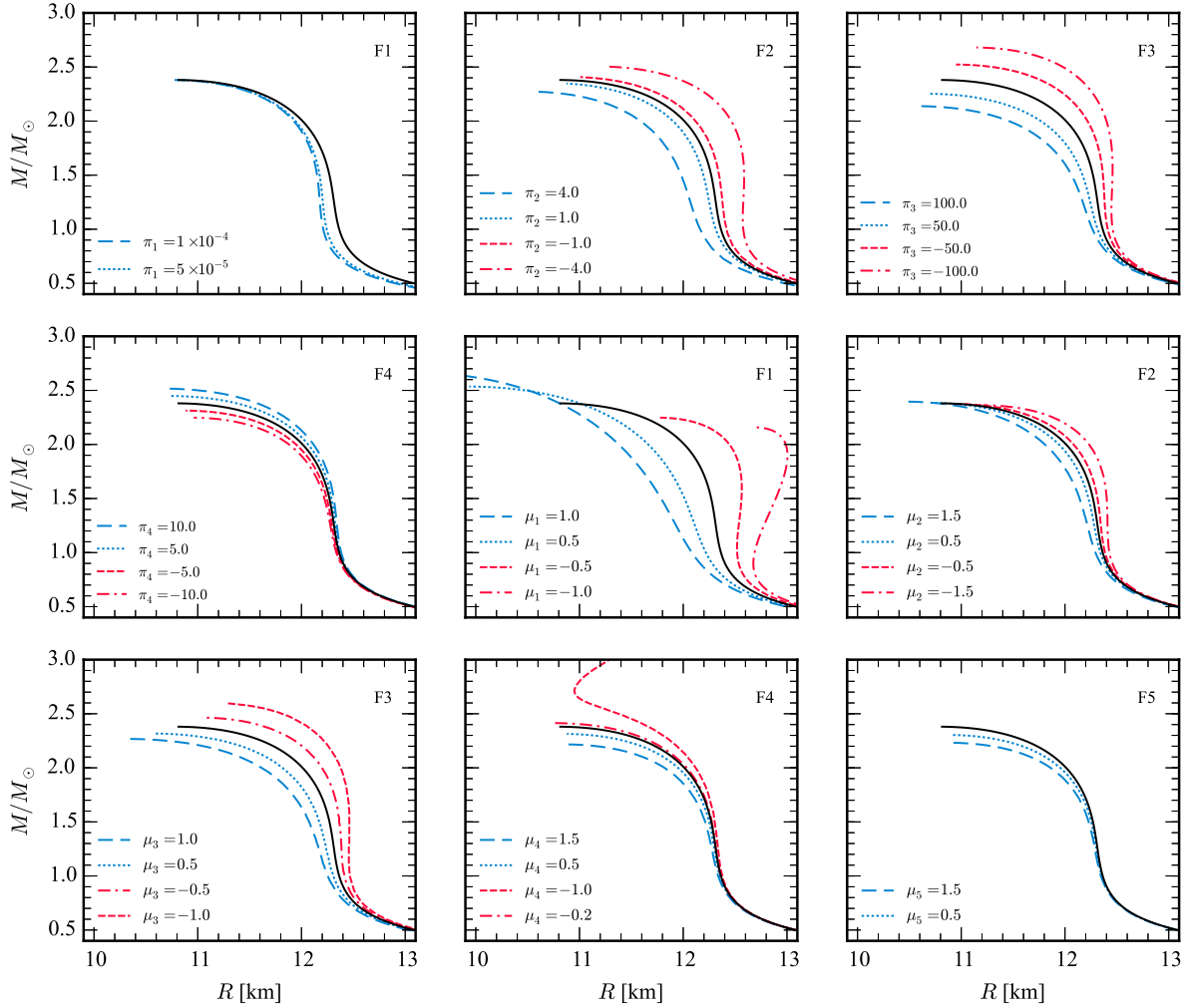


Figure 3.2: *2PN-order post-TOV corrections on the mass-radius curves.* We show the modification induced by different families of post-TOV terms on the general relativistic mass-radius curve, assuming the APR EOS. Left to right and top to bottom, the different panels show the effect of the pressure terms, proportional to π_i ($i = 1, \dots, 4$), and of the mass terms, proportional to μ_i ($i = 1, \dots, 5$).

3.1.1 Executive summary of this chapter

Since this chapter is rather technical (and quite long), we summarize our main conclusions here. The core of our proposal is to use the following set of “post-TOV” equations of structure for spherically symmetric stars (from now on we use geometrical units $G = c = 1$):

$$\frac{dp}{dr} = \left(\frac{dp}{dr} \right)_{\text{GR}} - \frac{\rho m}{r^2} (\mathcal{P}_1 + \mathcal{P}_2), \quad (3.1a)$$

$$\frac{dm}{dr} = \left(\frac{dm}{dr} \right)_{\text{GR}} + 4\pi r^2 \rho (\mathcal{M}_1 + \mathcal{M}_2), \quad (3.1b)$$

where

$$\mathcal{P}_1 \equiv \delta_1 \frac{m}{r} + 4\pi \delta_2 \frac{r^3 p}{m}, \quad (3.2a)$$

$$\mathcal{M}_1 \equiv \delta_3 \frac{m}{r} + \delta_4 \Pi, \quad (3.2b)$$

$$\mathcal{P}_2 \equiv \pi_1 \frac{m^3}{r^5 \rho} + \pi_2 \frac{m^2}{r^2} + \pi_3 r^2 p + \pi_4 \frac{\Pi p}{\rho}, \quad (3.2c)$$

$$\mathcal{M}_2 \equiv \mu_1 \frac{m^3}{r^5 \rho} + \mu_2 \frac{m^2}{r^2} + \mu_3 r^2 p + \mu_4 \frac{\Pi p}{\rho} + \mu_5 \Pi^3 \frac{r}{m}. \quad (3.2d)$$

Here r is the circumferential radius, m is the mass function, p is the fluid pressure, ρ is the baryonic rest mass density, ϵ is the total energy density, and $\Pi \equiv (\epsilon - \rho)/\rho$ is the internal energy per unit baryonic mass. A “GR” subscript denotes the standard TOV equations in GR [cf. Eq. (3.7) below, where we appended a subscript “T” to the mass function for reasons that will become apparent later]; δ_i, π_i ($i = 1, \dots, 4$) and μ_i ($i = 1, \dots, 5$) are phenomenological post-TOV parameters. The GR limit of the formalism corresponds to setting all of these parameters to zero, i.e. $\delta_i, \pi_i, \mu_i \rightarrow 0$.

The dimensionless combinations $\mathcal{P}_1, \mathcal{M}_1$ and $\mathcal{P}_2, \mathcal{M}_2$ represent a parametrized departure from the GR stellar structure and are linear combinations of 1PN- and 2PN-order terms, respectively. In particular, the coefficients δ_i attached to the 1PN terms are simple algebraic

combinations of the traditional PPN parameters: see Eqs. (3.35) and (3.36) below. As such, they are constrained to be very close to zero by existing Solar System and binary pulsar observations¹: $|\delta_i| \ll 1$. This result translates to negligibly small 1PN terms in Eq. (3.1): $\mathcal{P}_1, \mathcal{M}_1 \ll 1$. On the other hand, π_i and μ_i are presently unconstrained, and consequently $\mathcal{P}_2, \mathcal{M}_2$ should be viewed as describing the dominant (significant) departure from GR.

Each of the two combinations \mathcal{P}_2 and \mathcal{M}_2 involves no more than five dimensionless 2PN terms, but as we show in Section 3.3.2 these terms are representative of five distinct “families” consisting of a large number of 2PN terms. Each family is defined by the property that all of its members lead to approximately self-similar changes in the stellar mass-radius curves when included in $\mathcal{P}_2, \mathcal{M}_2$. In other words, as we verified by numerical calculations, we can account for several terms belonging to the same family by taking just one term from that family (either the dominant one or, when convenient, a much simpler subdominant one) and varying the corresponding post-TOV coefficient π_i or μ_i .

The qualitative effect of each of the 2PN-order post-TOV terms on the mass-radius relation is illustrated in Fig. 3.2. The values of the π_i and μ_i coefficients in each panel of this figure were chosen with purely illustrative purposes, i.e., we chose these coefficients to be large enough that they can produce visible deviations on the scale of the plot. A first noteworthy feature is that pressure terms *typically* induce corrections that are about an order of magnitude smaller than mass terms². This can be seen by the larger range of π_i ’s needed to produce visible changes in the mass-radius curve ($|\pi_2| \leq 4$, $|\pi_3| \leq 100$ and $|\pi_4| \leq 10$) when compared to the corresponding corrections in the mass-function equation ($|\mu_2| \leq 1$, $|\mu_3| \leq 1$ and $|\mu_4| \leq 1.5$, respectively). Some terms (such as those proportional to π_2 , π_3 , π_4 , μ_3 and μ_5) induce smooth rigid shifts of the mass-radius curve, similar to those that would be produced by a softening or stiffening of the nuclear EOS. Other terms (like those proportional to μ_1 , μ_2 and μ_4) produce more peculiar features that are more or less localized in a finite range

¹Using the latest constraints on the PPN parameters [499] we obtain the following upper limits: $|\delta_1| \lesssim 6 \times 10^{-4}$, $|\delta_2| \lesssim 7 \times 10^{-3}$, $|\delta_3| \lesssim 7 \times 10^{-3}$, $|\delta_4| \lesssim 10^{-8}$.

²A notable exception to this rule is the π_1 term, for reasons that will be explained in Section 3.4 below.

of central densities. This is interesting, because (for example) it is plausible to conjecture that some combination of the μ_1 and μ_2 corrections may reproduce the qualitative features of a highly non-perturbative phenomenon such as spontaneous scalarization, despite the intrinsically perturbative nature of our formalism.

The punchline here is that each post-TOV correction is qualitatively different, so we can use the post-TOV formalism as a toolbox to reproduce the mass-radius curves shown in Fig. 3.1 for various modified theories of gravity. More ambitiously, it would be interesting to address the inverse problem, i.e. to find out how the post-TOV parameters are related to the dominant corrections induced by each different theory. These issues are beyond the scope of the content in this chapter, but they are obviously crucial to relate our formalism to experiments, and we plan to address them in future work.

The second main result of this chapter has to do with the “completeness” of our post-TOV formalism, in the sense that the stellar structure Eqs. (3.1) – if we neglect the small terms $\mathcal{P}_1, \mathcal{M}_1$ – can be formally derived by a covariantly conserved perfect fluid stress energy tensor. That is:

$$\nabla_\nu T^{\mu\nu} = 0, \quad T^{\mu\nu} = (\epsilon_{\text{eff}} + p)u^\mu u^\nu + pg^{\mu\nu}, \quad (3.3)$$

where the effective, gravity-modified energy density is

$$\epsilon_{\text{eff}} = \epsilon + \rho\mathcal{M}_2, \quad (3.4)$$

and the covariant derivative is compatible with the effective post-TOV metric

$$g_{\mu\nu} = \text{diag}[e^{\nu(r)}, (1 - 2m(r)/r)^{-1}, r^2, r^2 \sin^2 \theta], \quad (3.5)$$

with

$$\frac{d\nu}{dr} = \frac{2}{r^2} \left[(1 - \mathcal{M}_2) \frac{m + 4\pi r^3 p}{1 - 2m/r} + m\mathcal{P}_2 \right]. \quad (3.6)$$

Our phenomenological post-TOV formalism is expected to encompass a large number of alternative theories of gravity, but it is not completely general, and future extensions may be possible or even desirable. As we stated earlier, theories which produce non-perturbative phase transitions in their stellar structure equations may not be accurately modelled. The formalism is also limited by the choice of acceptable 2PN terms out of all dimensionally possible combinations, based on criteria that have bearing on the structure of the gravitational field equations (see Section 3.3.2 below).

3.1.2 Organization of this chapter

This chapter is organized as follows. In Section 3.2 we introduce the PPN formalism and review previous applications to relativistic stars (in particular work by Wagoner and Malone [490] as well as Ciufolini and Ruffini [106]). In Section 3.3 we develop the post-TOV formalism to 1PN order (where all parameters are already constrained to be very close to their GR values by Solar System and binary pulsar experiments), and then to 2PN order. We also show the equivalence between the 2PN post-TOV equations and GR with a gravity-modified EOS under a minimal set of reasonable assumptions. In Section 3.4 we present some numerical results illustrating the relative importance of the different post-TOV corrections. Some technical material is collected in three appendices. Appendix A gives details of the dimensional analysis arguments used to select the relevant set of 2PN post-TOV coefficients. In Appendix B we present a brief summary of the relativistic Lane-Emden theory, which plays an auxiliary role in the construction of our formalism. Finally, Appendix C shows that certain integral potentials appearing at 1PN order in the stellar structure equations (namely, the gravitational potential U , the internal energy E and the gravitational potential energy Ω) can be approximated by linear combinations of non-integral potentials, so these integral potentials are “redundant” and can be discarded when building our post-TOV expansion.

3.2 Setting the stage: stellar structure within PPN theory

3.2.1 The TOV equations

A convenient starting point for our analysis are the standard general relativistic TOV equations, describing hydrostatic equilibrium in spherical symmetry [369]. These are given by the familiar formulae:

$$\left(\frac{dp}{dr}\right)_{\text{GR}} = -\frac{(\epsilon + p)(m_{\text{T}} + 4\pi r^3 p)}{r^2(1 - 2m_{\text{T}}/r)}, \quad (3.7a)$$

$$\left(\frac{dm_{\text{T}}}{dr}\right)_{\text{GR}} = 4\pi r^2 \epsilon, \quad (3.7b)$$

where p and ϵ are the fluid’s pressure and energy density, respectively, and m_{T} is the mass function (the subscript is used to distinguish this mass function from similar quantities appearing in PPN theory, see below).

For later convenience we also write down the 1PN-order expansion of these equations (for simplicity the subscript “GR” is omitted):

$$\frac{dp}{dr} = -\frac{m_{\text{T}}\rho}{r^2} \left(1 + \Pi + \frac{p}{\rho} + \frac{2m_{\text{T}}}{r} + 4\pi \frac{r^3 p}{m_{\text{T}}}\right) + \mathcal{O}(2\text{PN}), \quad (3.8a)$$

$$\frac{dm_{\text{T}}}{dr} = 4\pi r^2 \rho(1 + \Pi). \quad (3.8b)$$

where we have introduced the baryonic rest-mass density ρ and the dimensionless internal energy per unit mass, $\Pi \equiv (\epsilon - \rho)/\rho$. It can be noticed that the mass function equation only contains 1PN corrections to the Newtonian equations of hydrostatic equilibrium, while higher-order corrections appear in the pressure equation.

3.2.2 The PPN stellar structure equations

The PPN formalism [501, 335] was first employed for building static, spherically symmetric models of compact stars by Wagoner & Malone [490], and subsequently by Ciufolini & Ruffini [106]. This early work is briefly reviewed here since it will provide the stepping

stone towards formulating our post-TOV equations.

A convenient starting point is the set of stellar structure equations derived by Ciufolini and Ruffini [106] from the original Will-Nordtvedt PPN theory [501, 335]. These are (cf. Eqs. (14) of [106]):

$$\frac{dp}{dr} = -\frac{\epsilon\bar{m}}{r^2} \left[1 + (5 + 3\gamma - 6\beta + \zeta_2)\frac{\bar{m}}{r} + \frac{p}{\epsilon} + \zeta_3\frac{E}{\bar{m}} + (\gamma + \zeta_4)\frac{4\pi r^3 p}{\bar{m}} + \frac{1}{2}(11 + \gamma - 12\beta + \zeta_2 - 2\zeta_4)\frac{\Omega}{\bar{m}} \right], \quad (3.9a)$$

$$\frac{d\bar{m}}{dr} = 4\pi r^2 \epsilon, \quad (3.9b)$$

where $\{\beta, \gamma, \zeta_1, \zeta_2, \zeta_3, \zeta_4, \alpha_1, \alpha_2, \alpha_3\}$ are the standard set of nine PPN parameters. In the GR limit $\beta = \gamma = 1$ and $\zeta_i = \alpha_i = 0$ ($i = 1, \dots, 4$) [499].

It should be pointed out that the basic parameters p, \bar{m} (as well as the radial coordinate r) entering Eqs. (3.9) may not be the same as the corresponding ones in the TOV equations. This is a reflection of the “gauge” freedom in defining these parameters in a number of equivalent ways. Indeed, below we are going to exploit this freedom and obtain an “improved” set of PPN equations by a suitable redefinition of the mass function. On the other hand, following [106], we will stick to the same p and r throughout this analysis, implicitly assuming that they are the *same* variables as the ones in the TOV equations (3.7).

The potentials Ω and E appearing in Eq. (3.9a) obey

$$\frac{d\Omega}{dr} = -4\pi r \rho \bar{m}, \quad \frac{dE}{dr} = 4\pi r^2 \rho \Pi. \quad (3.10)$$

The more familiar Newtonian gravitational potential U , solution of $\nabla^2 U = -4\pi\rho$, is not featured in Eqs. (3.9) as a result of a change of radial coordinate and a redefinition of the mass function \bar{m} with respect to the original PPN theory parameters (see [106] for details).

The stellar structure equations can be manipulated further by switching to a new

mass function:

$$m(r) = \bar{m} + AE + B\Omega + C\frac{\bar{m}^2}{r} + D(4\pi r^3 p), \quad (3.11)$$

where A , B , C , and D are free constants. As evident, \bar{m} and m differ at 1PN level. The constants A and B can be chosen so that the terms proportional to E and Ω in Eq. (3.9a) are eliminated. This is achieved for

$$A = \zeta_3, \quad B = \frac{1}{2}(11 + \gamma - 12\beta + \zeta_2 - 2\zeta_4). \quad (3.12)$$

The resulting “new” set of PPN stellar structure equations is

$$\frac{dp}{dr} = -\frac{\rho m}{r^2} \left[1 + \Pi + \frac{p}{\rho} + (5 + 3\gamma - 6\beta + \zeta_2 - C) \frac{m}{r} + (\gamma + \zeta_4 - D) 4\pi \frac{r^3 p}{m} \right], \quad (3.13a)$$

$$\frac{dm}{dr} = 4\pi r^2 \rho \left[1 + (1 + \zeta_3)\Pi + 3D\frac{p}{\rho} - \frac{C}{4\pi} \frac{m^2}{\rho r^4} - \frac{1}{2}(11 + \gamma - 12\beta + \zeta_2 - 2\zeta_4 - 4C + 2D) \frac{m}{r} \right]. \quad (3.13b)$$

These expressions still contain the gauge freedom associated with the definition of the mass function m in the form of the yet unspecified constants C and D . In particular, the Wagoner-Malone hydrostatic equilibrium equations [490] represent a special case of these expressions, and it is straightforward to see that they can be recovered for

$$D = \gamma + \zeta_4, \quad C = \frac{1}{2}(7 + 3\gamma - 8\beta + \zeta_2). \quad (3.14)$$

Making this choice for the constants on the right-hand side of Eq. (3.11) leads to a new mass function, say \tilde{m} , and to the following structure equations, which match Eqs. (6) and (7) of

[490]:

$$\frac{dp}{dr} = -\frac{\rho\tilde{m}}{r^2} \left(1 + \Pi + \frac{p}{\rho} + a\frac{\tilde{m}}{r} \right), \quad (3.15a)$$

$$\frac{d\tilde{m}}{dr} = 4\pi r^2 \rho \left[1 + (1 + \zeta_3)\Pi + a\frac{\tilde{m}}{r} + 3(\gamma + \zeta_4)\frac{p}{\rho} - \frac{b}{4\pi} \frac{\tilde{m}^2}{\rho r^4} \right], \quad (3.15b)$$

where $a \equiv (3 + 3\gamma - 4\beta + \zeta_2)/2$ and the constant b in the notation of [490] is our C , i.e. $b = (7 + 3\gamma - 8\beta + \zeta_2)/2$.

A comparison between the two sets of PPN equations (3.9) and (3.15) discussed in this section reveals that the Wagoner-Malone equations are simpler, in the sense that they do not depend on the auxiliary potentials Ω and E . This advantage, however, is partially offset by the more complicated expression for the mass function equation. If we compare the GR limit of Wagoner-Malone equations (3.15) against the 1PN expansion of the TOV equations, Eqs (3.8), we find that the two sets coincide provided we identify $\bar{m} = m_{\text{T}}$, i.e.

$$\tilde{m} = m_{\text{T}} + \frac{m_{\text{T}}^2}{r} + 4\pi r^3 p, \quad (3.16)$$

where the last equation follows by taking the GR limit of Eq. (3.11) in combination with Eqs. (3.12) and (3.14). Clearly, the fact that $\tilde{m} \neq m_{\text{T}}$ in the GR limit is an unsatisfactory property of the Wagoner-Malone equations.

It would be desirable to have a set of structure equations that – unlike the set (3.9) – does not involve integral potentials, and such that – unlike the set (3.15) – the mass function is compatible with the GR limit. Fortunately, it is not too difficult to find a new set of PPN equations for which $m = m_{\text{T}}$. In the following section we will propose an improved set of PPN stellar structure equations that satisfies these requirements.

3.2.3 An improved set of PPN equations

We can exploit the degree of freedom associated with the constants C, D in Eqs. (3.13) and produce a new set of PPN equations that exactly match the 1PN TOV equations in the

GR limit with $m = m_{\Gamma}$. It is easy to see that this can be achieved by making the trivial choice

$$C = D = 0. \quad (3.17)$$

Note that the constants A and B are still given by Eqs. (3.12). The resulting PPN equations are

$$\frac{dp}{dr} = -\frac{\rho m}{r^2} \left[1 + \Pi + \frac{p}{\rho} + (5 + 3\gamma - 6\beta + \zeta_2) \frac{m}{r} + (\gamma + \zeta_4) 4\pi \frac{r^3 p}{m} \right], \quad (3.18a)$$

$$\frac{dm}{dr} = 4\pi r^2 \rho \left[1 + (1 + \zeta_3)\Pi - \frac{1}{2} (11 + \gamma - 12\beta + \zeta_2 - 2\zeta_4) \frac{m}{r} \right]. \quad (3.18b)$$

As advertised, in the GR limit these equations reduce to Eqs. (3.8) with $m = m_{\Gamma}$. The same equations will be used in Section 3.3 below in the construction of the desired post-TOV equations.

3.2.4 The physical interpretation of the mass function

Within the framework of PPN theory, inertial mass and active/passive gravitational mass³ are, in general, distinct notions. In the context of compact stars, expressions for all three kinds of mass are given in [106]:

$$M_{\text{in}} = \bar{m}(\bar{R}) + \left(\frac{17}{2} + \frac{3}{2}\gamma - 10\beta + \frac{5}{2}\zeta_2 \right) \Omega(\bar{R}), \quad (3.19)$$

$$\begin{aligned} M_{\text{a}} &= M_{\text{in}} + \left(4\beta - \gamma - 3 - \frac{1}{2}\alpha_3 - \frac{1}{3}\zeta_1 - 2\zeta_2 \right) \Omega(\bar{R}) \\ &\quad + \zeta_3 E(\bar{R}) - \left(\frac{3}{2}\alpha_3 - 3\zeta_4 + \zeta_1 \right) P, \end{aligned} \quad (3.20)$$

$$M_{\text{p}} = M_{\text{in}} + \left(4\beta - \gamma - 3 - \alpha_1 + \frac{2}{3}\alpha_2 - \frac{2}{3}\zeta_1 - \frac{1}{3}\zeta_2 \right) \Omega(\bar{R}), \quad (3.21)$$

³The inertial mass quantifies the resultant acceleration of a body when a force (of any nature) is applied to it. The active gravitational mass is the source (in Newtonian gravity) of the gravitational field, whose strength is proportional to this mass. When placed in a gravitational field, a test body will experience an acceleration proportional to its passive gravitational mass.

where \bar{R} is the stellar radius associated with the mass function $\bar{m}(r)$ – i.e. with the set of equations (3.9) – and

$$P = 4\pi \int_0^{\bar{R}} dr r^2 p. \quad (3.22)$$

is the volume-integrated pressure.

In GR the three masses are of course identical, $M_{\text{in}} = M_{\text{a}} = M_{\text{p}}$. As argued in [106], any theory conserving the four-momentum of an isolated system should incorporate the equality of the two gravitational masses, i.e. $M_{\text{a}} = M_{\text{p}}$. If adopted, this equality leads to following three algebraic relations for the PPN parameters:

$$\zeta_3 = 0, \quad (3.23)$$

$$\zeta_1 - 3\zeta_4 + \frac{3}{2}\alpha_3 = 0, \quad (3.24)$$

$$\zeta_1 + 3\alpha_1 - 2\alpha_2 - 5\zeta_2 - \frac{3}{2}\alpha_3 = 0. \quad (3.25)$$

We can subsequently write for the common gravitational mass:

$$M_{\text{g}} = M_{\text{a}} = M_{\text{p}} = \bar{m}(\bar{R}) + F\Omega(\bar{R}), \quad (3.26)$$

with

$$F = \frac{1}{2} \left(11 + \gamma - 12\beta - \alpha_3 + \zeta_2 - \frac{2}{3}\zeta_1 \right). \quad (3.27)$$

For our new PPN equations with $C = D = 0$ the mass equality $M_{\text{a}} = M_{\text{p}}$ implies

$$m(r) = \bar{m}(r) + \frac{1}{2} (11 + \gamma - 12\beta + \zeta_2 - 2\zeta_4) \Omega(r). \quad (3.28)$$

Then with the help of Eq. (3.24) it is easy to see that

$$M_{\text{g}} = m(\bar{R}) + \left(\zeta_4 - \frac{1}{2}\alpha_3 - \frac{1}{3}\zeta_1 \right) \Omega(\bar{R}) = m(\bar{R}). \quad (3.29)$$

If R is the stellar radius associated with our PPN equations (3.18), the difference $\delta R = R - \bar{R}$ is a 1PN-order quantity. We can then approximately write

$$m(\bar{R}) \approx m(R) - \frac{dm}{dr}(R) \delta R. \quad (3.30)$$

However, Eq. (3.18b) implies that $dm/dr(R) = 0$ if $\rho(R) = 0$ at the stellar surface. This is indeed the case for a realistic EOS. Therefore, we have shown that at 1PN precision the mass of the system is given by

$$M_g = m(R). \quad (3.31)$$

This elegant result is one more attractive property of the new PPN equations.

3.3 The Post-TOV formalism

The logic underpinning the formalism we are seeking is that of parametrizing the deviation of the stellar structure equations from their GR counterparts, thus producing a set of post-TOV equations. As already pointed out in the introduction, the post-TOV formalism is merely a useful parametrized framework rather than the product of a specific, self-consistent modified gravity theory (in the spirit of PPN theory). In this sense our formalism is akin to the existing “quasi-Kerr” or “bumpy” Kerr metrics, designed to study deviations from the Kerr spacetime in GR (see e.g. [110, 182, 82]).

By design the post-TOV formalism should be a more powerful tool for building relativistic stars than the PPN framework; after all, the latter is based on a PN approximation of strong gravity. However, and as it will become clear from the analysis of this section, our formalism has its own limitations, the most important one being the fact that the deviations from GR are introduced in the form of PN corrections. This could mean that the structure of compact stars with a high degree of departure from GR may not be accurately captured by the formalism.

3.3.1 Post-TOV equations: 1PN order

The recipe for formulating leading-order post-TOV equations is rather simple: from a suitable set of PPN hydrostatic equilibrium equations we isolate the purely non-GR pieces. These 1PN terms are subsequently added “by hand” to the full general relativistic TOV equations, hence producing a set of parametrized post-Einsteinian equations. It should be pointed out that this procedure can only be applied at the level of 1PN corrections. Higher-order corrections should be sought by other means, such as dimensional analysis (see Section 3.3.2).

In principle, either set of equations, (3.9) [106] or (3.15) [490], could have been used. However, our improved PPN equations (3.18) seem to be best suited for this task.

Considering Eqs. (3.18), we first isolate the terms that represent a genuine deviation from GR. These are the second terms appearing in the following equations:

$$\begin{aligned} \frac{dp}{dr} = & -\frac{\rho m}{r^2} \left(1 + \Pi + \frac{p}{\rho} + \frac{2m}{r} + 4\pi \frac{r^3 p}{m} \right) \\ & - \frac{\rho m}{r^2} \left[(3 + 3\gamma - 6\beta + \zeta_2) \frac{m}{r} + (\gamma - 1 + \zeta_4) 4\pi \frac{r^3 p}{m} \right], \end{aligned} \quad (3.32a)$$

$$\frac{dm}{dr} = 4\pi r^2 \rho (1 + \Pi) d + 4\pi r^2 \rho \left[\zeta_3 \Pi - \frac{1}{2} (11 + \gamma - 12\beta + \zeta_2 - 2\zeta_4) \frac{m}{r} \right]. \quad (3.32b)$$

The second step consists of adding the non-GR terms to the TOV equations (3.7). We obtain (recall that $m = m_{\Gamma}$)

$$\frac{dp}{dr} = -\frac{(\epsilon + p)}{r^2} \left(\frac{m + 4\pi r^3 p}{1 - 2m/r} \right) - \frac{\rho m}{r^2} \left(\delta_1 \frac{m}{r} + \delta_2 4\pi \frac{r^3 p}{m} \right), \quad (3.33)$$

$$\frac{dm}{dr} = 4\pi r^2 \left[\epsilon + \rho \left(\delta_3 \frac{m}{r} + \delta_4 \Pi \right) \right], \quad (3.34)$$

where we have introduced the constant post-TOV parameters:

$$\delta_1 \equiv 3(1 + \gamma) - 6\beta + \zeta_2, \quad \delta_2 \equiv \gamma - 1 + \zeta_4, \quad (3.35)$$

$$\delta_3 \equiv -\frac{1}{2}(11 + \gamma - 12\beta + \zeta_2 - 2\zeta_4), \quad \delta_4 \equiv \zeta_3. \quad (3.36)$$

As expected, $\delta_i = 0$ in the limit of GR.

The above equations can be written in a more compact form:

$$\frac{dp}{dr} = \left(\frac{dp}{dr}\right)_{\text{GR}} - \frac{\rho m}{r^2} \left(\delta_1 \frac{m}{r} + \delta_2 4\pi \frac{r^3 p}{m}\right), \quad (3.37a)$$

$$\frac{dm}{dr} = \left(\frac{dm}{dr}\right)_{\text{GR}} + 4\pi r^2 \rho \left(\delta_3 \frac{m}{r} + \delta_4 \Pi\right). \quad (3.37b)$$

These expressions represent our main result for the *leading-order* post-TOV stellar structure equations. They describe the 1PN-level corrections produced by an arbitrary deviation from GR that is compatible with PPN theory. In other words, Eqs. (3.37) encapsulate the stellar structure physics (at this order) for any member of the PPN family of gravity theories.

We could in principle introduce other 1PN order terms, in the spirit of the general parametrized framework of deviating from GR that we have described in the beginning of this section. But the introduction of such terms would correspond to either redefinitions of coordinates and/or the mass function at 1PN level, as we have already seen, or deviations from special relativity, which we would prefer not to include.

Unfortunately, it turns out that Eqs. (3.37) are of limited practical value. As discussed in the executive summary, the modern limits on the PPN parameters suggest that these corrections are very close to their GR values, because $\beta, \gamma \approx 1$ and $\alpha_i, \zeta_i \ll 1$, making all the δ_i parameters very small. We should not therefore expect any notable deviation from GR at the level of the leading-order post-TOV equations. We verified this claim by explicit calculations of NS stellar models with different EOSs.

Any significant deviations from compact stars in GR have to be sought at 2PN order and beyond, where the existing observational limits leave much room for the practitioner of alternative theories of gravity. This calls for the formulation of a higher-order set of post-TOV equations, a task to which we now turn.

3.3.2 Post-TOV equations: 2PN order

In this section we shall formulate post-TOV equations with 2PN-accurate correction terms. Unlike the calculation of the preceding section, we now have to build these equations “from scratch”, given that the general PPN theory has not yet been extended to 2PN order. Inevitably, the procedure for building the various 2PN terms will turn out to be somewhat more complicated than the one of the preceding section, heavily relying on dimensional analysis for constructing these terms out of the available fluid parameters. Moreover, at 2PN order we also need to consider terms that involve the integral potentials U , E and Ω (recall that these were eliminated at 1PN order by a suitable redefinition of the mass function). However, as shown numerically and via analytical arguments in Appendix C, the integral potentials can be approximated to a high precision, and for a variety of EOSs, by simple linear combinations of the non-integral PN terms. As a result, they do not have to be considered separately in the post-TOV expansion.

To begin with, we can get an idea of the form of some of the 2PN terms we are looking for by expanding the TOV equations (3.7) to that order. Let us first consider the pressure equation (3.7a):

$$\frac{dp}{dr} = -\frac{\rho m}{r^2} \left[\left(1 + \Pi + \frac{p}{\rho} \right) \left(1 + \frac{2m}{r} + 4\pi \frac{r^3 p}{m} \right) + \frac{4m^2}{r^2} + 8\pi r^2 p \right] + \mathcal{O}(3\text{PN}). \quad (3.38)$$

As anticipated, all 1PN terms appearing here are also present in our PPN equation (3.18a). The produced 2PN corrections are proportional to the following combinations:

$$\frac{m^2}{r^2}, \quad \Pi \frac{m}{r}, \quad r^2 p, \quad \frac{mp}{r\rho}, \quad \Pi \frac{r^3 p}{m}, \quad \frac{r^3 p^2}{\rho m}. \quad (3.39)$$

Additional 2PN terms that do not appear in the TOV equations can be constructed by forming products of the available 1PN terms. The largest set of 1PN terms can be found in the general PPN equations (3.13):

$$\text{1PN : } \quad \Pi, \frac{p}{\rho}, \frac{m}{r}, \frac{r^3 p}{m}, \frac{m^2}{\rho r^4}. \quad (3.40)$$

We can observe that all terms, except the last one, also appear in our final PPN equations (3.18). From these we can reproduce the set (3.39) as well as the additional 2PN terms:

$$\frac{r^6 p^2}{m^2}, \quad \Pi \frac{m^2}{\rho r^4}, \quad \frac{m^3}{\rho r^5}, \quad \Pi^2, \quad \Pi \frac{p}{\rho}, \quad \underbrace{\frac{p^2}{\rho^2}, \frac{m^4}{\rho^2 r^8}, \frac{m^2 p}{\rho^2 r^4}}. \quad (3.41)$$

We have set apart the last three (underbraced) terms of this set because, as a result of their $\sim 1/\rho^2$ scaling, these terms will be discarded. In fact, the same fate will be shared by any term $\sim \rho^\beta$ with $\beta \leq -2$.

There are various reasons why we believe that this selection rule should be imposed. In our opinion these reasons are quite convincing, but they fall short from constituting a watertight argument: in all fairness, if we had a single truly compelling reason, we would not need more than one.

The first line of reasoning to exclude the presence of negative powers of ρ (and of the other fluid parameters) in the PN terms is based on the regularity of these terms at the stellar surface, where $p, \rho, \Pi \rightarrow 0$ for any realistic EOS. A PN term like the second one in the underbraced group of the set (3.41) will lead to a term diverging as $\sim 1/\rho$ at the stellar surface in the stellar structure equations, and therefore it is not an acceptable PN correction. Although this surface regularity argument is powerful, it obviously works only for terms that do not scale with positive powers of p or Π .

The second (heuristic) argument applies to gravity theories with the following (sym-

bolic) structure:

$$\{\text{geometry}\} = 8\pi T^{\mu\nu}, \quad (3.42)$$

$$\nabla_\nu T^{\mu\nu} = 0 \rightarrow \frac{dp}{dr} = (\epsilon + p)\{\text{geometry}\}, \quad (3.43)$$

where “geometry” stands for combinations of the metric and its derivatives, and the last equation assumes a perfect fluid stress-energy tensor. The stress-energy tensor and the right-hand side of Eq. (3.43) feature $\epsilon + p = \rho(1 + \Pi + p/\rho)$ and p *linearly*. It can then be argued that the solution of the field equations for the metric and its derivatives will display a

$$\{\text{geometry}\} \sim (\epsilon + \tau p)^n \sim \rho^n \left(1 + \Pi + \tau \frac{p}{\rho}\right)^n \quad (3.44)$$

dependence with respect to the fluid variables (where τ and n are $\mathcal{O}(1)$ numbers). Such a solution should lead to pressure-dependent PN terms of the form:

$$\text{PN term} \sim (r^2 \rho)^{n-1} \left(\frac{p}{\rho}\right)^k, \quad k = n, n-1, \dots \quad (3.45)$$

where one ρ factor has been removed and absorbed in the Newtonian prefactor of the structure equations, while at the same time the r^2 factor has been added in order to produce a dimensionless quantity. A key observation is that the form (3.45) assumes a theory that does *not* depend on *dimensional* coupling constants. Now, according to (3.45) the highest negative power of ρ corresponds to $k = n$, which means that the scaling with respect to the density should be:

$$\text{PN term} \sim \rho^\beta, \quad \beta \geq -1 \quad (3.46)$$

Based on these arguments, we deem acceptable those PN terms which scale with ρ as in (3.46). This choice is also consistent with the previous PPN formulae, see Eqs. (3.13). A similar argument can be used to exclude terms with negative powers of p and Π ⁴.

⁴A related argument for excluding high powers of $1/\rho$ is the following. By virtue of the field equations,

Equation (3.39) and the top row of Eq. (3.41) represent a large set of 2PN terms emerging from the expansion of the TOV equation and from products of the various known 1PN terms. This set is large but not necessarily complete. Inevitably, a systematic approach to the problem of “guessing” 2PN terms should involve dimensional analysis. To improve readability we relegate our dimensional analysis considerations to Appendix A, and here we only quote the main result. The *most general* form for 2PN order terms is given by the dimensionless combination:

$$\Lambda_2 \sim \Pi^\theta (r^2 p)^\alpha (r^2 \rho)^\beta \left(\frac{m}{r}\right)^{2-2\alpha-\beta-\theta}, \quad (3.47)$$

where α, β, θ are integers with $\beta \geq -1$, while different bounds on θ and α apply to the two hydrostatic equilibrium equations:

$$\frac{dp}{dr} : \quad 0 \leq \theta \leq 2, \quad 0 \leq \alpha \leq 2 - \theta, \quad (3.48)$$

$$\frac{dm}{dr} : \quad 0 \leq \theta \leq 3, \quad 0 \leq \alpha \leq 3 - \theta. \quad (3.49)$$

The lower bounds on the three parameters α, β, θ are dictated by the same considerations discussed below Eq. (3.41), namely, regularity at the surface and consistency with the fact that gravitational field equations of the general form (3.43) are unlikely to generate negative powers higher than $1/\rho$. The upper bounds on α and θ are imposed by the regularity at $r = 0$ of the stellar structure terms arising from Λ_2 (see Appendix A).

the Ricci scalar is usually proportional to the energy density of matter (at least in the Newtonian limit, if the modified theory reproduces GR in the weak field regime): $R \sim \rho$. If inverse powers of ρ are produced by gravity modifications, they should therefore originate from terms $\sim 1/R^n$ in the action of the theory. These terms are usually associated with ghosts or instabilities [124], and therefore their presence is problematic.

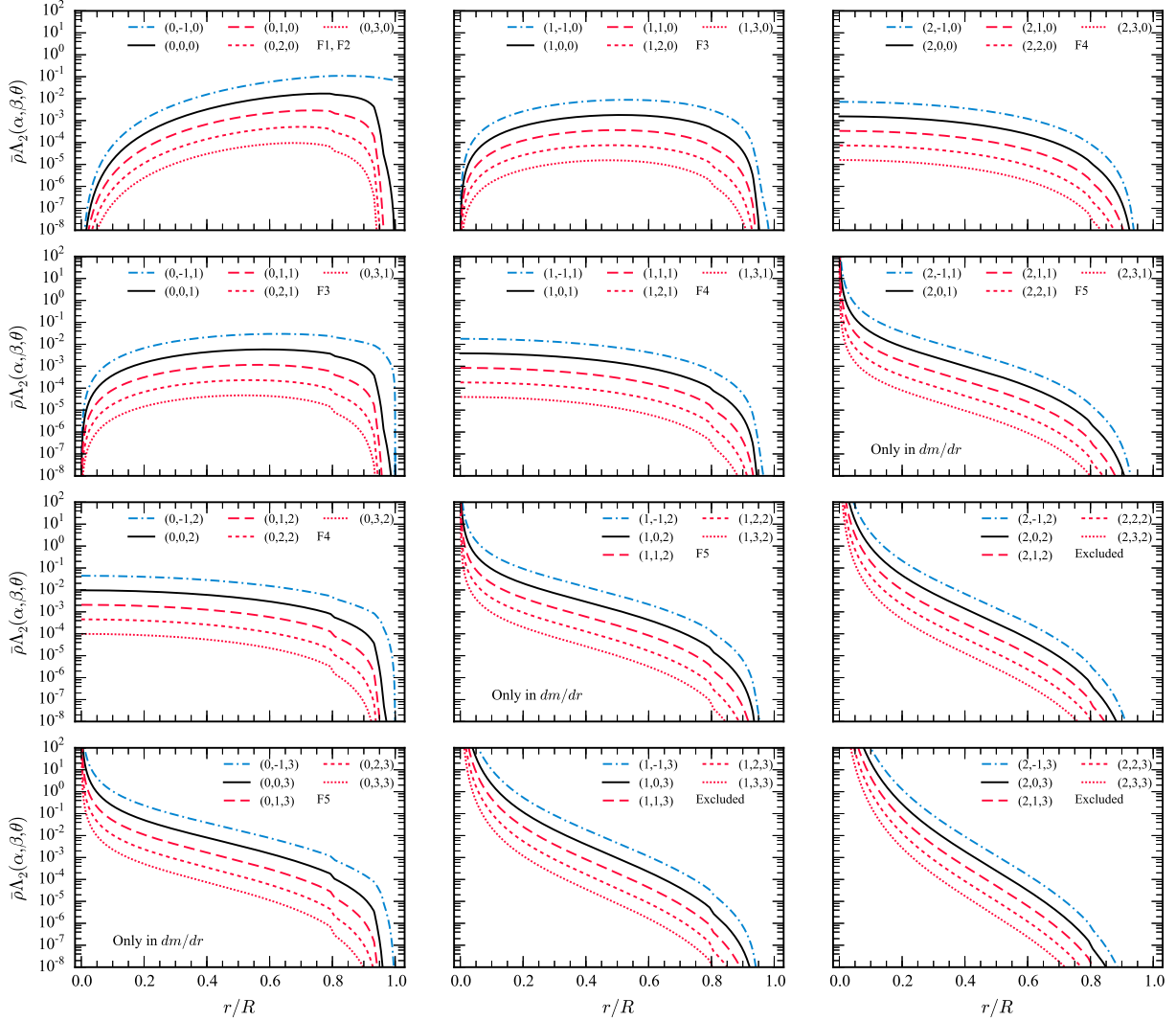


Figure 3.3: *The radial profile of the Λ_2 -function.* We exhibit the behavior of $\bar{\rho}\Lambda_2$, where $\bar{\rho} = \rho/\rho_c$ and Λ_2 is given in Eq. (3.47), for a stellar model using the APR EOS, with $\epsilon_c/c^2 = 0.86 \times 10^{15}$ g/cm³, $M = 1.51M_\odot$ and $R = 12.3$ km. The curves are labelled according to the respective values of (α, β, θ) . From the top row to the bottom row the index θ takes on the values $(0, 1, 2, 3)$, respectively. Despite the multitude of possible dimensionally correct 2PN terms, their self-similarity – which is clear when we compare terms along the bottom-left to top-right diagonals in this “grid” of plots – allows us to group them into a relatively small number of families (see text for details). The contributions plotted in three panels at the bottom right of the grid (marked as “Excluded”) would lead to divergences in the hydrostatic equilibrium equations, and therefore they can be discarded as unphysical.

From the general expression (3.47) we can reproduce all previous 1PN and 2PN terms and generate an infinite number of new ones. This possibility could have been a fatal blow

to our post-TOV programme. Fortunately, the day is saved by the fact that the magnitude of Λ_2 decays rapidly throughout the star as β increases. This trend is clearly visible in the numerical results shown in Fig. 3.3 (see discussion below).

For all practical purposes these results imply that the first few members of the $\beta = -1, 0, 1, \dots$ sequence are sufficient to construct accurate post-TOV expansions. A sample set of such dominant 2PN terms is:

$$\begin{aligned}
2\text{PN} : \quad & \frac{m^3}{r^5\rho}, \frac{m^2}{r^2}, r\rho m, \frac{mp}{r\rho}, r^2p, \frac{r^3p^2}{\rho m}, \frac{r^6p^2}{m^2}, \\
& \frac{r^7p^3}{\rho m^3}, \frac{r^{10}p^3}{m^4}, \Pi \frac{m^2}{r^4\rho}, \Pi \frac{m}{r}, \Pi r^2\rho, \Pi \frac{p}{\rho}, \\
& \Pi \frac{r^3p}{m}, \Pi \frac{r^4p^2}{\rho m^2}, \Pi \frac{r^7p^2}{m^3}, \Pi^2 \frac{m}{\rho r^3}, \Pi^2, \Pi^2 \frac{rp}{m\rho}, \\
& \Pi^2 \frac{r^4p}{m^2}, \frac{\Pi^3}{r^2\rho}, \Pi^3 \frac{r}{m}.
\end{aligned} \tag{3.50}$$

This set is markedly larger than the previous sets (3.39) and (3.41) (whose acceptable terms form a subset of the new set), but a complete post-TOV formalism would have to include all (or almost all) of these terms, with twice the number of free coefficient in the dp/dr and dm/dr equations. Fortunately, as it turns out, the same job can be done with a much smaller subset of 2PN terms. This is possible because the various 2PN terms can be divided into *five “families”*, each family comprising terms with similar profiles. When incorporated in the post-TOV equations, terms belonging to a given family lead to *self-similar* modifications in the mass-radius curves for a given EOS.

Insight into the behavior of the $\Lambda_2(\alpha, \beta, \theta)$ terms can be gained by direct numerical calculations of their radial profiles in relativistic stars. We carried out such calculations for a variety of realistic EOSs as well as relativistic polytropes, and for different choices of central density, verifying that all cases lead to very similar results, as discussed below. More specifically, we considered EOS A [350], FPS [170], SLy4 [192, 155] and N [410] in increasing order of stiffness, as well as relativistic polytropes with indices $n = 0.4, 0.6,$ and 1.0 : see

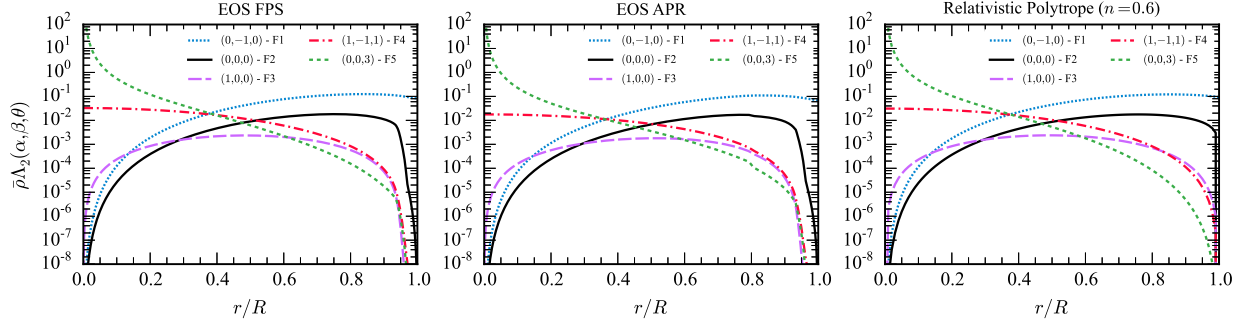


Figure 3.4: *The family-representative 2PN terms.* Here we show the selected representative terms from each of the families depicted in Fig. 3.3, as listed in Eq. (3.53), for three different EOSs: FPS (left panel), APR (middle panel) and an $n = 0.6$ polytrope (right panel). Each term illustrates the qualitative behavior of each family of possible 2PN contributions to the structure equations. The high degree of invariance of the Λ_2 -profiles with respect to the EOS is evident in this figure. The GR background stellar models utilized in the figure have the following bulk properties: $\epsilon_c = 0.861 \times 10^{15}$ g/cm³ ($\lambda \equiv p_c/\epsilon_c = 0.165$), $M = 1.51 M_\odot$ and $R = 12.3$ km (left panel); $\epsilon_c = 1.450 \times 10^{15}$ g/cm³ ($\lambda = 0.198$), $M = 1.50 M_\odot$ and $R = 10.7$ km (center panel); $\lambda = 0.165$, $M = 1.50 M_\odot$ and $R = 11.75$ km (right panel).

Appendix B, and in particular Eq. (B.7). Note that the polytropic models are parametrized by $\lambda = p_c/\epsilon_c$ instead of ϵ_c alone (the subscript “c” indicates a quantity evaluated at the center), but this is equivalent to the central density parametrization. The polytropic models are also invariant with respect to the scale factor $K^{n/2}$; this can be adjusted to generate polytropic models of (say) the same mass (for a given λ) as that of a specific tabulated-EOS model.

Rather than computing Λ_2 itself, from a phenomenological point of view it makes more sense to consider the combination $\rho\Lambda_2$. The reason is that this combination appears in both the pressure and mass equations, and furthermore it has the desirable feature of being regular at the surface for $\beta = -1$. More specifically, in Fig. 3.3 we plot the dimensionless combination $\bar{\rho}\Lambda_2(\alpha, \beta, \theta)$, where $\bar{\rho} = \rho/\rho_c$. Our sample NS model was built using the EOS APR with central density $\epsilon_c/c^2 = 0.86 \times 10^{15}$ g/cm³, corresponding to mass $M = 1.51M_\odot$ and radius $R = 12.3$ km, but we have verified that our qualitative conclusions remain the same for different models and different EOSs.

Figure 3.3 reveals two key trends: (i) the clear β -ordering of the $\rho\Lambda_2$ profiles, with

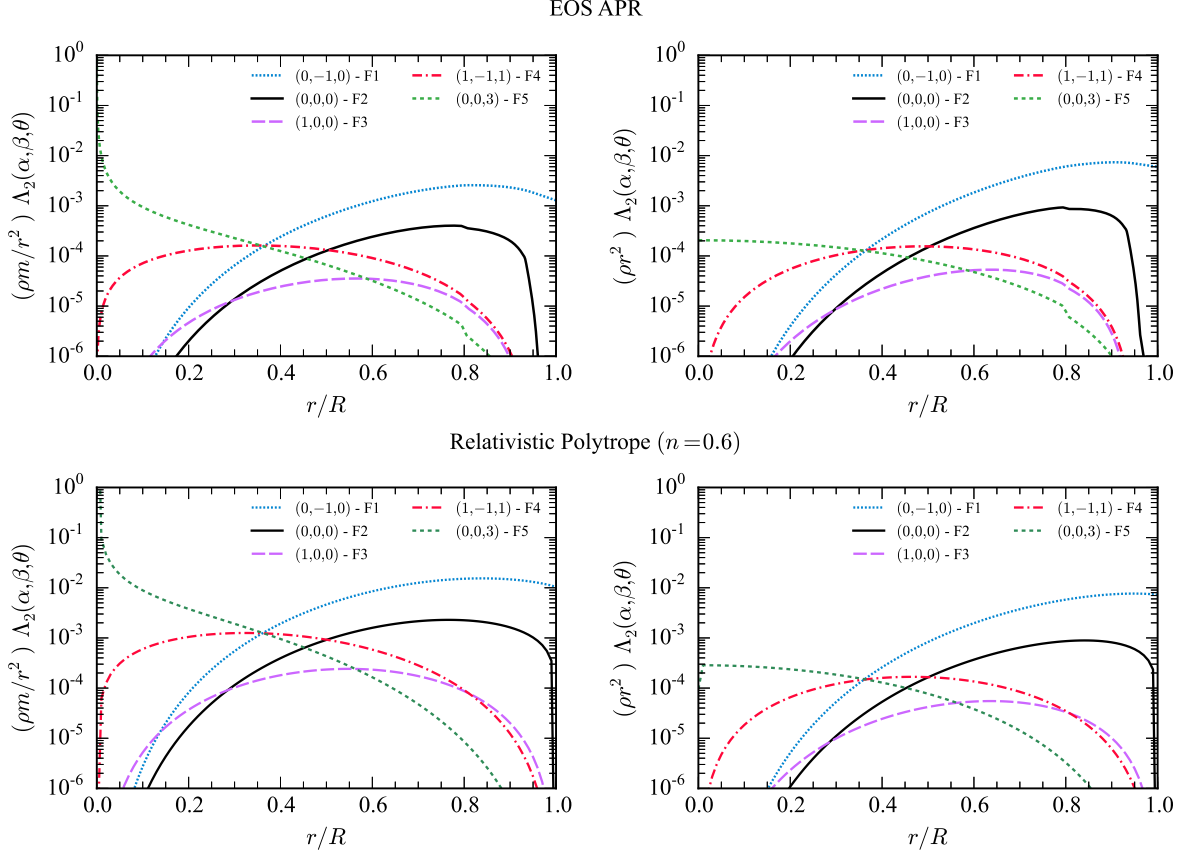


Figure 3.5: *The family-representative terms in the structure equations.* This figure illustrates the behavior of each of the family-representative 2PN terms [see Eq. (3.53)] multiplied by the Newtonian prefactors in the post-TOV equations. The stellar parameters are identical to the ones used in Fig. 3.4. *Left panel:* the combination $(\rho m/r^2) \Lambda_2(\alpha, \beta, \theta)$ appearing in the pressure equation. *Right panel:* the combination $\rho r^2 \Lambda_2(\alpha, \beta, \theta)$ appearing in the mass equation. The top panels correspond to EOS APR; the bottom panels correspond to a relativistic polytrope with polytropic index $n = 0.6$. The divergence at the origin of the F5 term justifies its exclusion from the pressure equation.

$\beta = -1$ always associated with the dominant term for fixed α and θ , and (ii) the remarkable similarity in the shape of the profiles of terms with dissimilar (α, β, θ) triads along the bottom-left to top-right diagonals in the “grid” of Fig. 3.3. This property defines distinct families of 2PN terms and implies that the terms of each family cause self-similar changes in the mass-radius curves of the various post-TOV stellar models.

We have identified five 2PN families (labeled “F1”, ..., “F5” in the various panels of Fig. 3.3, and described in more detail in Table 3.1):

(i) F1: This is a single-member family comprising only the $\rho\Lambda_2(0, -1, 0)$ term in the top-left panel, which is zero at $r = 0$ but finite at $r = R$.

(ii) F2: The members of this family vanish at $r = 0$ and $r = R$, and have a peak near the surface. These are the $\rho\Lambda_2(0, \beta, 0)$ terms with $\beta \geq 0$ in the top-left panel.

(iii) F3: These terms also vanish at both $r = 0$ and $r = R$, but display an approximately flat profile inside the star. They correspond to $\rho\Lambda_2(1, \beta, 0)$ (top-middle panel) and $\rho\Lambda_2(0, \beta, 1)$ (top-right panel) for $\beta \geq -1$.

(iv) F4: This family comprises terms that are finite at $r = 0$ but zero at $r = R$. These are the $\rho\Lambda_2(2, \beta, 0)$ (bottom-left panel) and $\rho\Lambda_2(1, \beta, 1)$ (bottom-middle panel) terms with $\beta \geq -1$.

(v) F5: These terms by themselves diverge at $r = 0$ and vanish at $r = R$, but they become well-behaved when inserted in the stellar mass-function equation, where they are multiplied by the factor r^2 : cf. Eq. (A.24). These terms correspond to $\rho\Lambda_2(2, \beta, 1)$, and from the constraints (3.48) and (3.49) we conclude that *the members of this family can only appear in the mass equation*.

There is an intuitive way to explain the existence of the above families. As an example we consider F3, where the seemingly unrelated terms $\Lambda_2(1, \beta, 0)$ and $\Lambda_2(0, \beta, 1)$ yield similar profiles. Consider

$$\Lambda_2(0, \beta, 1) \sim r^{-1+3\beta} \frac{\Pi\rho^\beta}{m^{\beta-1}}. \quad (3.51)$$

By means of the approximations $m \sim \rho r^3$, $\Pi \sim p/\rho$ (the latter approximation is motivated by the exact thermodynamical relation $\Pi = np/\rho$ for relativistic polytropes with index n , see Appendix B) we find

$$\Lambda_2(0, \beta, 1) \sim r^{2+3\beta} p \left(\frac{\rho}{m}\right)^\beta \sim \Lambda_2(1, \beta, 0). \quad (3.52)$$

Similarly we can show that $\Lambda_2(2, \beta, 0) \sim \Lambda_2(1, \beta, 1)$ for the F4 family. The argument can be generalized to show that terms along the diagonals of Fig. 3.3 are equivalent.

Table 3.1 summarizes the taxonomy of the most important terms of each family according to the above criteria. The impact of each of these terms as a post-TOV correction has been tested for a variety of EOSs. The results reveal that the members of a given family lead to self-similar modifications to the stellar mass-radius curves. A sample of these numerical results is shown in Fig. 3.2, which is further discussed in Section 3.4 below.

Family	2PN term	(α, β, θ)	Dominant / Chosen?
F1	$m^3/(r^5\rho)$	$(0, -1, 0)$	D/C
F2	$(m/r)^2$	$(0, 0, 0)$	D/C
F2	$rm\rho$	$(0, 1, 0)$	–
F3	$mp/(r\rho)$	$(1, -1, 0)$	–
F3	r^2p	$(1, 0, 0)$	C
F3	$\Pi m^2/(r^4\rho)$	$(0, -1, 1)$	D
F3	$\Pi m/r$	$(0, 0, 1)$	–
F3	$r^2\Pi\rho$	$(0, 1, 1)$	–
F4	$r^3p^2/(\rho m)$	$(2, -1, 0)$	–
F4	$r^6p^2/(m^2)$	$(2, 0, 0)$	–
F4	$\Pi p/\rho$	$(1, -1, 1)$	C
F4	$\Pi r^3p/m$	$(1, 0, 1)$	–
F4	$\Pi^2 m/(r^3\rho)$	$(0, -1, 2)$	D
F4	Π^2	$(0, 0, 2)$	–
F5	$\Pi r^4p^2/(\rho m^2)$	$(2, -1, 1)$	–
F5	$\Pi r^7p^2/m^3$	$(2, 0, 1)$	–
F5	$\Pi^2 rp/m\rho$	$(1, -1, 2)$	–
F5	$\Pi^2 r^4p/m^2$	$(1, 0, 2)$	–
F5	$\Pi^3/(r^2\rho)$	$(0, -1, 3)$	D
F5	$\Pi^3 r/m$	$(0, 0, 3)$	C

Table 3.1: Taxonomy of the dominant 2PN terms. The self-similarity between the radial profiles of the various 2PN terms listed in Eq. (3.50) (and illustrated in Fig. 3.3) allows us to group them into five distinct families. This table spells out the explicit form of the various terms, and indicates which term in each family is dominant (D) according to our numerical calculations, and which one was chosen (C) as representative of each family.

This remarkable self-similarity property means that we can simply select one term from each family and emulate the effect of *all* significant 2PN terms of the same family by simply varying the post-TOV coefficient associated with the selected term.

In doing so, it is reasonable to choose the simplest terms as family representatives. The five terms we select based on this reasoning are:

$$\text{F-representatives : } \frac{m^3}{r^5\rho}, \frac{m^2}{r^2}, r^2p, \Pi\frac{p}{\rho}, \Pi^3\frac{r}{m}. \quad (3.53)$$

The phenomenologically relevant radial profiles of $\bar{\rho}\Lambda_2(\alpha, \beta, \theta)$ produced by these terms are shown in Fig. 3.4 for three choices of EOS: FPS, APR and an $n = 0.6$ polytrope. The most striking feature of this figure is the close resemblance of the Λ_2 profiles of identical (α, β, θ) triads for different EOSs, which lends support to the EOS-independence of our selection of post-TOV terms.

The family-representative terms (3.53) are again shown in Fig. 3.5, where we plot the combinations that appear in the dp/dr and dm/dr equations, i.e. $m\rho\Lambda_2/r^2$ and $r^2\rho\Lambda_2$, respectively (in the latter term we have omitted a trivial prefactor of 4π). We consider two different EOSs: APR and an $n = 0.6$ polytrope. All terms displayed are regular at both $r = 0$ and $r = R$ with the exception of the F5 term in the dp/dr equation, which is divergent at $r = 0$ and must be excluded. Once again, the variations in the radial profiles due to considering different EOSs are extremely mild.

We have thus obtained a *minimum* set of representative 2PN terms, listed in Eq. (3.53), which in reality encompasses a much larger set, like the one obtained from the combination of Eqs. (3.41) and (3.50), as well as terms that involve the integral potentials.

After this admittedly tedious procedure we can finally assemble our 2PN-order post-TOV equations for the pressure and the mass. These are (omitting the negligibly small 1PN corrections):

$$\frac{dp}{dr} = \left(\frac{dp}{dr}\right)_{\text{GR}} - \frac{\rho m}{r^2} \left(\pi_1 \frac{m^3}{r^5\rho} + \pi_2 \frac{m^2}{r^2} + \pi_3 r^2 p + \pi_4 \Pi \frac{p}{\rho} \right), \quad (3.54a)$$

$$\frac{dm}{dr} = \left(\frac{dm}{dr}\right)_{\text{GR}} + 4\pi r^2 \rho \left(\mu_1 \frac{m^3}{r^5\rho} + \mu_2 \frac{m^2}{r^2} + \mu_3 r^2 p + \mu_4 \Pi \frac{p}{\rho} + \mu_5 \Pi^3 \frac{r}{m} \right). \quad (3.54b)$$

where, as anticipated in the executive summary, π_i ($i = 1, \dots, 4$) and μ_i ($i = 1, \dots, 5$) are free parameters controlling the size of the corresponding departure from GR.

3.3.3 Completing the formalism: the post-TOV metric and stress-energy tensor

So far, our post-TOV formalism comprises no more than a pair of stellar structure equations, Eqs. (3.54a) and (3.54b), which can be used for the description of static and spherically symmetric compact stars. In this section we show that there is more to the formalism than meets the eye: to a high precision it is a “complete” toolkit, in the sense that (i) it can be reformulated in terms of a spherically symmetric metric $g_{\mu\nu}$ and a perfect fluid stress-energy tensor $T^{\mu\nu}$, and (ii) these two structures are related through the covariant conservation law $\nabla_\nu T^{\mu\nu} = 0$ (where ∇_ν is the metric-compatible covariant derivative), hence respecting the equivalence principle. Remarkably, it also turns out that the metric and matter degrees of freedom can be related as in GR, which implies that the post-TOV formalism is *equivalent* to stellar structure in GR with a *gravity-modified* EOS for matter and an *effective* spacetime geometry.

In order to establish the above statements we begin with the following general result. Assume the static spherically symmetric metric

$$ds^2 = g_{\mu\nu} dx^\mu dx^\nu = -e^{\nu(r)} dt^2 + \left(1 - \frac{2\mathcal{M}(r)}{r}\right)^{-1} dr^2 + r^2 d\Omega^2 \quad (3.55)$$

and a perfect-fluid stress-energy tensor (with energy density \mathcal{E} and pressure \mathcal{P})

$$T^{\mu\nu} = (\mathcal{E} + \mathcal{P})u^\mu u^\nu + \mathcal{P}g^{\mu\nu}. \quad (3.56)$$

For a static spherical fluid ball, the energy-momentum conservation equation

$$\nabla_\nu T^{\mu\nu} = 0 \quad (3.57)$$

leads to

$$\frac{d\mathcal{P}}{dr} = -(\mathcal{E} + \mathcal{P})\Gamma_{rt}^t = -\frac{1}{2}(\mathcal{E} + \mathcal{P})\frac{d\nu}{dr}, \quad (3.58)$$

where Γ_{rt}^t is a Christoffel symbol. As long as we consider theories respecting (3.57) with a metric-compatible covariant derivative, this result is independent of the gravitational field equations.

For the mass function $\mathcal{M}(r)$ we can always write a relation of the form

$$\frac{d\mathcal{M}}{dr} = 4\pi r^2 \mathcal{E} [1 + Z(r)], \quad (3.59)$$

where $Z(r)$ is a theory-dependent function. Einstein's theory is recovered by setting $Z = 0$, as required by the field equations of GR.

To establish the properties described at the beginning of this section we will show that we can successfully map our post-TOV equations onto Eqs. (3.58) and (3.59) (with $Z = 0$).

The full post-TOV equations, Eqs. (3.54), can be written in the form:

$$\frac{dp}{dr} = -\frac{(\epsilon + p)}{r^2}\Gamma(r) - \frac{\rho m}{r^2} \left[\left(1 + \Pi + \frac{p}{\rho} \right) \mathcal{P}_1 + \tilde{\mathcal{P}}_2 \right], \quad (3.60)$$

$$\frac{dm}{dr} = 4\pi r^2 \epsilon + 4\pi r^2 \rho [\mathcal{M}_1 + \mathcal{M}_2], \quad (3.61)$$

where $\mathcal{P}_1, \mathcal{P}_2$ have been defined in Eqs. (3.2),

$$\tilde{\mathcal{P}}_2 \equiv \mathcal{P}_2 - \left(\Pi + \frac{p}{\rho} \right) \mathcal{P}_1 \quad (3.62)$$

is a 2PN-order term, and $\Gamma(r) \equiv (m + 4\pi r^3 p)/(1 - 2m/r)$.

Based on these expressions, we can define the effective energy density

$$\epsilon_{\text{eff}} \equiv \epsilon + \rho(\mathcal{M}_1 + \mathcal{M}_2), \quad (3.63)$$

which implies

$$\frac{dm}{dr} = 4\pi r^2 \epsilon_{\text{eff}}. \quad (3.64)$$

Using (3.63) in the pressure equation we have

$$\frac{dp}{dr} = -[\epsilon_{\text{eff}} + p - \rho(\mathcal{M}_1 + \mathcal{M}_2)] \frac{\Gamma}{r^2} - \frac{m}{r^2} [(\epsilon + p)\mathcal{P}_1 + (\epsilon_{\text{eff}} + p)\tilde{\mathcal{P}}_2], \quad (3.65)$$

where we have used the fact that in any 2PN term we can replace the factor ρ by $\epsilon_{\text{eff}} + p$, at the cost of introducing 3PN terms. Using (3.63) once more in the last term, and after some rearrangement, we obtain,

$$\frac{dp}{dr} = -\frac{(\epsilon_{\text{eff}} + p)}{r^2} \left[(1 - \mathcal{M}_2)\Gamma + m(\mathcal{P}_1 + \tilde{\mathcal{P}}_2 - \mathcal{M}_1\mathcal{P}_1) \right] + \frac{\rho}{r^2} \mathcal{M}_1 \Gamma. \quad (3.66)$$

Given that $\mathcal{M}_1 \ll 1$, the last term can be safely omitted and we are left with

$$\begin{aligned} \frac{dp}{dr} &\approx -\frac{(\epsilon_{\text{eff}} + p)}{r^2} \left[(1 - \mathcal{M}_2)\Gamma + m(\mathcal{P}_1 + \tilde{\mathcal{P}}_2 - \mathcal{M}_1\mathcal{P}_1) \right] \\ &\approx -\frac{(\epsilon_{\text{eff}} + p)}{r^2} [(1 - \mathcal{M}_2)\Gamma + m\mathcal{P}_2], \end{aligned} \quad (3.67)$$

which is of the form (3.58). Note that in this and the following expressions the small $\mathcal{M}_1, \mathcal{P}_1$ terms can be omitted.

The resulting mapping is:

$$\mathcal{P} = p, \quad \mathcal{M} = m, \quad \mathcal{E} = \epsilon_{\text{eff}}. \quad (3.68)$$

It follows that the effective post-TOV metric is

$$g_{\mu\nu} = \text{diag}[e^{\nu(r)}, (1 - 2m(r)/r)^{-1}, r^2, r^2 \sin^2 \theta], \quad (3.69)$$

with

$$\frac{d\nu}{dr} \approx \frac{2}{r^2} \left[(1 - \mathcal{M}_2)\Gamma + m(\mathcal{P}_1 + \tilde{\mathcal{P}}_2 - \mathcal{M}_1\mathcal{P}_1) \right] \quad (3.70)$$

$$\approx \frac{2}{r^2} [(1 - \mathcal{M}_2)\Gamma + m\mathcal{P}_2] . \quad (3.71)$$

From this result we can see that r represents the circumferential radius of the $r = \text{constant}$ spheres and therefore the post-TOV radius R (where $p(R) = 0$) coincides with the circumferential radius of the star.

Finally, the effective post-TOV stress-energy tensor is

$$T^{\mu\nu} = (\epsilon_{\text{eff}} + p)u^\mu u^\nu + pg^{\mu\nu} , \quad (3.72)$$

and it is covariantly conserved with respect to the metric (3.69).

These expressions clearly demonstrate that our post-TOV formalism is completely equivalent to GR with an effective EOS:

$$p(\epsilon) \rightarrow p(\epsilon_{\text{eff}}) , \quad (3.73)$$

$$\epsilon_{\text{eff}} \approx \epsilon + \rho\mathcal{M}_2 . \quad (3.74)$$

As is evident from this last expression, ϵ_{eff} represents a gravity-shifted parameter with respect to the physical energy density ϵ . This result highlights a key characteristic of compact relativistic stars when studied in the context of alternative theories of gravity, namely, the intrinsic degeneracy between the physics of the matter and gravity sectors.

Whether the above effective description (and in particular its effective geometry part) can give observables that have a correspondence to observables of an underlying theory or not depends on the nature of that theory. As long as the underlying theory admits a PN expansion, the physical description that arises from the effective formalism should match that of the physical theory.

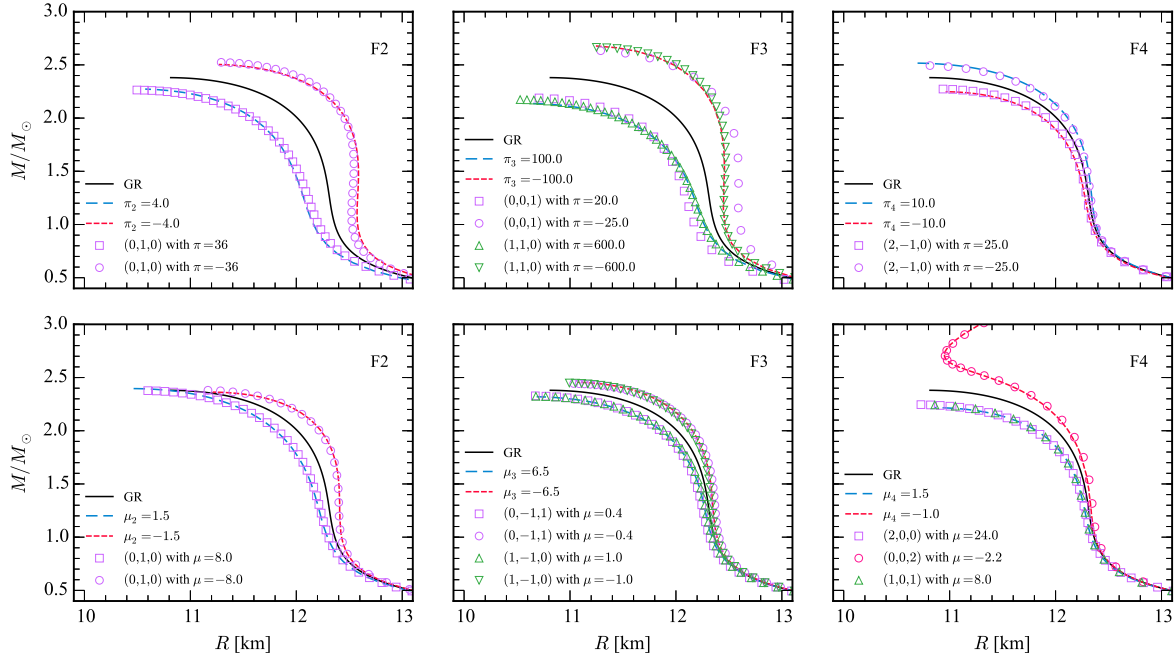


Figure 3.6: *Self-similarity in mass-radius curves - I.* Numerical integrations show that 2PN terms belonging to the same family result in self-similar deviations from GR in the mass-radius relation. This figure illustrates this remarkable property for pressure terms (top row) and mass terms (bottom row) belonging to families F2, F3 and F4 (from left to right). In each panel, the solid line corresponds to GR; the long-dashed line to a positive-sign correction due to the chosen term in each family; the short-dashed line to a negative-sign correction due to the chosen term in each family. The various symbols show that nearly identical corrections can be produced using different terms belonging to the same family, as long as we appropriately rescale their post-TOV coefficients.

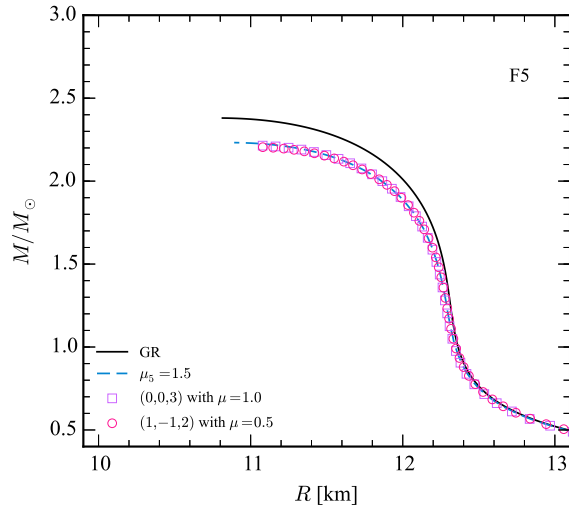


Figure 3.7: *Self-similarity in mass-radius curves - II.* Same as in Fig. 3.6, but for the F5 family, which only admits post-TOV corrections with $\mu_5 < 0$ (see text).

3.4 Numerical results

In this section we provide a more detailed discussion of our numerical techniques and results, focusing on the mass-radius curves produced by the integration of the post-TOV equations (3.54) [or equivalently Eqs. (3.1)].

First, let us briefly summarize the integration procedure we have followed in this chapter. We have carried out two kinds of computations: (i) “background” models – these involve the integration of the general relativistic TOV equations – with the purpose of studying the radial profiles of the post-TOV correction terms, (ii) the integration of the full post-TOV equations, typically including the representative term of a single 2PN family.

The post-TOV structure equations (3.1a) and (3.1b) are integrated simultaneously starting at the origin $r = 0$, for fixed values of the coefficients π_i , μ_i , and for a range of central energy density values. The chosen central energy density ϵ_c fixes the central pressure $p_c = p(\epsilon_c)$, the central mass density $\rho_c = m_b n_b(\epsilon_c)$ and the central internal energy $\Pi_c = (\epsilon_c - \rho_c)/\rho_c$, where $m_b = 1.66 \times 10^{-24}$ g is the baryonic mass and n_b is the baryon number density. In general, $p(\epsilon)$ and $n_b(\epsilon)$ are computed using tabulated EOS data. Once the initial conditions have been specified, Eqs. (3.1a) and (3.1b) are integrated outward up

to the stellar radius R , where $p(R) = 0$. The gravitational mass is obtained as $M = m(R)$.

The integration procedure for realistic EOS background models is virtually the same as the one just described. We have also employed a number of polytropic background models; for these the integration procedure is slightly different (see Appendix B for details), and it is based on the simpler Lane-Emden formulation, where the pressure is replaced by the density ρ in the structure equations and the stellar model is parameterized by the ratio $\lambda = p_c/\epsilon_c$ rather than ϵ_c alone (this formulation is of course equivalent to the one using tabulated EOSs). The added advantage of this approach is its scale invariance with respect to the polytropic constant K . This means that K can be freely adjusted to generate a model with (say) a specific mass M . This scaling procedure also fixes the radius R .

The main installment of our mass-radius results has already been presented in Fig. 3.2 of the executive summary (Section 3.1.1). As discussed there, the various post-TOV correction terms, representing the five 2PN families of Section 3.3.2, cause qualitatively different modifications to the mass-radius curves.

As a rule of thumb, the corrections to the pressure equation lead to markedly weaker mass-radius modifications than the corrections to the mass equation, for the same magnitude of π_i and μ_i . The effective-metric formulation of the post-TOV formalism suggests a simple qualitative explanation of this observation. The mass corrections \mathcal{M}_2 change both the effective EOS and the strength of gravity, as measured by $\nu(r)$, while the pressure corrections \mathcal{P}_2 are only associated with a change in the strength of gravity [cf. Eqs. (3.71) and (3.74)], and it is well known that changes in the EOS outweigh gravity modifications in terms of their effect on the mass-radius relation.

A notable exception is the single-member family F1 [given by $m^3/(r^5\rho)$], for which the pressure correction term dominates over its mass counterpart. In fact, the F1 pressure term leads to the largest mass-radius changes, as evidenced by the π_1 values used in Fig. 3.2. It is not too difficult to explain why this happens: near the stellar surface, where all three fluid parameters p, ρ, Π are close to zero, the F1 correction terms remain finite and dominate

over all other terms in the post-TOV equations (this can be clearly seen in Fig. 3.5), thus taking control of the pressure and mass derivatives.

Another noteworthy point is that, when considering individual post-TOV terms, it is not always possible to integrate the equations for both positive and negative values of the corresponding coefficient. This is the case for family F5 in Fig. 3.2, where the integration fails for $\mu_5 < 0$. We have found that this is caused by an unphysical negative slope dm/dr near the origin.

The remarkable self-similarity in the radial profiles of 2PN terms belonging to the same family has been illustrated in Fig. 3.3 (see Section 3.3.2). With hindsight, this property should not come as a total surprise, given the approximate correlations among the fluid variables: $m \sim \rho r^3$, $\Pi \sim p/\rho$.

The emergence of the same self-similarity in the mass-radius curves is something far less anticipated and even more striking. This property, which has allowed us to formulate a practical and versatile set of post-TOV equations, is illustrated in Figs. 3.6 and 3.7, where we show mass-radius results for each 2PN family, considering both the pressure and the mass equation and for the same APR EOS stellar model as in Fig. 3.2. Each panel is devoted to a particular family, and it shows the mass-radius curves resulting from the integration of the post-TOV equations when various terms from Table 3.1 are included as corrections (notice that F1 is missing from these plots for the obvious reason that it consists of only one post-TOV correction).

In all cases considered, the terms of the same family are found to cause *nearly identical mass-radius changes* by a suitable rescaling of the relevant coefficient π_i or μ_i . This behavior is most striking for family F4, where different post-TOV corrections in the mass equations lead to the same characteristic back-bending behavior in the mass-radius curve. The only notable exception to this remarkable scaling property is the (0, 0, 1) member of the F3 family, proportional to $\Pi m/r$, which can be rescaled to agree with other members of the family at high densities but partially fails to capture the behavior of the mass-radius curve at low

densities. This partial symmetry breaking can be understood by looking at the leftmost panel on the second row of Fig. 3.3: the behavior of this term near the surface is not as smooth as for other members of this family. In our opinion this does not warrant extensions of the formalism to include another family, but this is definitely a possibility that could be considered in the future, given the approximate nature of the self-similarity argument.

Another important aspect of the post-TOV results is their “directionality” in the mass-radius plane, in the sense that a given correction term could affect more the mass than the radius, or vice versa. This kind of information cannot be easily extracted from a traditional mass-radius plot such as Fig. 3.2, but becomes very visible if we display the same results in terms of the fractional changes $\delta M/M_{\text{GR}} \equiv (M - M_{\text{GR}})/M_{\text{GR}}$ and $\delta R/R_{\text{GR}} \equiv (R - R_{\text{GR}})/R_{\text{GR}}$ from the corresponding GR values.

“Dart-board” plots of these fractional changes are shown in Fig. 3.8. The aforementioned directionality of the various post-TOV corrections is clearly visible in this figure. Individual correction terms are seen to drive nearly *linear* departures (at least up to a $\sim 10\%$ level) from the center of the “board.” Moreover, certain terms are mutually (nearly) orthogonal, although not aligned with the mass or radius axis. In some cases this happens between the pressure and mass terms of the same family, e.g. family F2. In general, the departures from the GR model are more isotropically scattered when caused by the corrections \mathcal{M}_2 in the dm/dr equation, whereas the pressure corrections \mathcal{P}_2 are clearly more concentrated near the direction of the mass axis. This behavior fits nicely with the effective-EOS interpretation of how \mathcal{M}_2 and \mathcal{P}_2 corrections change the mass-radius diagram. As expected, \mathcal{M}_2 corrections affect the stiffness of the effective EOS with significant effects on the radius, while \mathcal{P}_2 corrections change the strength of gravity, and this mostly affects how much mass a particular model can support.

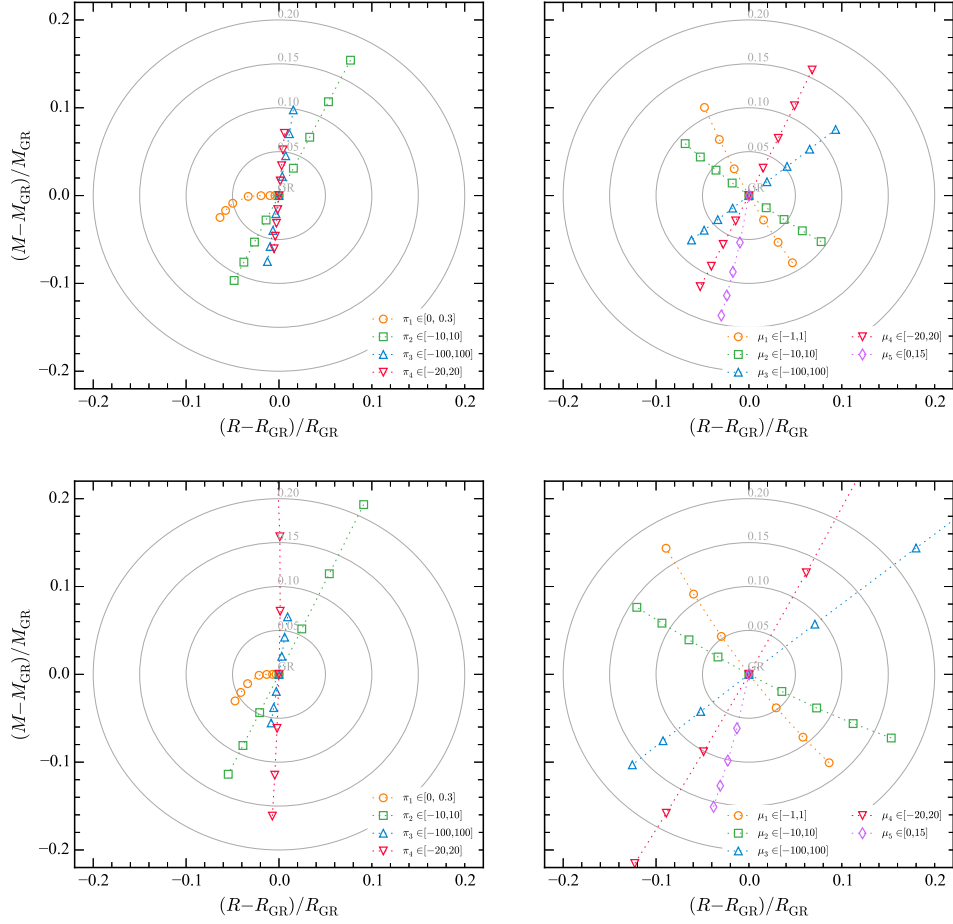


Figure 3.8: *Fractional deviations induced by the post-TOV parameters on the stellar mass and radius.* Here we illustrate the fractional changes caused by the post-TOV parameters in NS masses and radii. For a fixed central energy density and EOS APR, we plot the relative deviations from GR in mass and radius that result from varying the post-TOV parameters within the range indicated in the legends. *Top row:* $\epsilon_c/c^2 = 8.61 \times 10^{14}$ g/cm³, $M_{\text{GR}} = 1.51M_{\odot}$ and $R_{\text{GR}} = 12.3$ km. *Bottom row:* $\epsilon_c/c^2 = 1.20 \times 10^{15}$ g/cm³, $M_{\text{GR}} = 2.04M_{\odot}$ and $R_{\text{GR}} = 11.9$ km. *Left panels:* Effect of the post-TOV terms that enter in the pressure equation. *Right panels:* Effect of the post-TOV terms that enter in the mass equation. The circles represent contours of fixed relative deviation from GR.

These trends remain unchanged as the central energy density (and the stellar mass) increases (see bottom panels of Fig. 3.8). The pressure correction term associated with π_1 (family F1) provides the exception to the rule: a sequence of $\pi_1 > 0$ values leads to a non-linear trajectory, with initially just the radius decreasing and then followed by a comparable fractional decrease in the mass. Negative values of π_1 are not shown because they lead to

unphysical models where in the outer low-density layers of the star dp/dr becomes nearly zero but never negative, thus preventing us from finding the exact location of the surface (as we have pointed out earlier in this section, this behavior is related to the non-zero value of the F1 term at the surface).

Fig. 3.9 provides a schematic chart of the correlation between the sign of the π_i , μ_i coefficients and the sign of the associated variations δM , δR . Interestingly, the π_i terms are limited to just two of the four possible quadrants (note the anti-correlation between the signs of π_1 and the other π_i). This translates to variations that simultaneously make the star bigger (smaller) and heavier (lighter), i.e. $\delta R > 0$, $\delta M > 0$ (or $\delta R < 0$, $\delta M < 0$). In contrast, the μ_i terms occupy all four quadrants, with the F3, F4, F5 families leading to $\delta R \delta M > 0$ variations, and F1, F2 giving rise to the opposite arrangement, $\delta R \delta M < 0$.

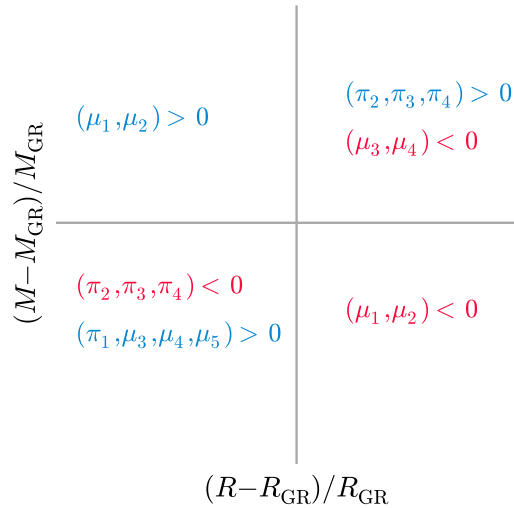


Figure 3.9: *Directions of the post-TOV induced deviations.* This schematic diagram shows which sign of individual post-TOV parameters produces smaller or larger masses/radii with respect to GR, cf. Fig. 3.8.

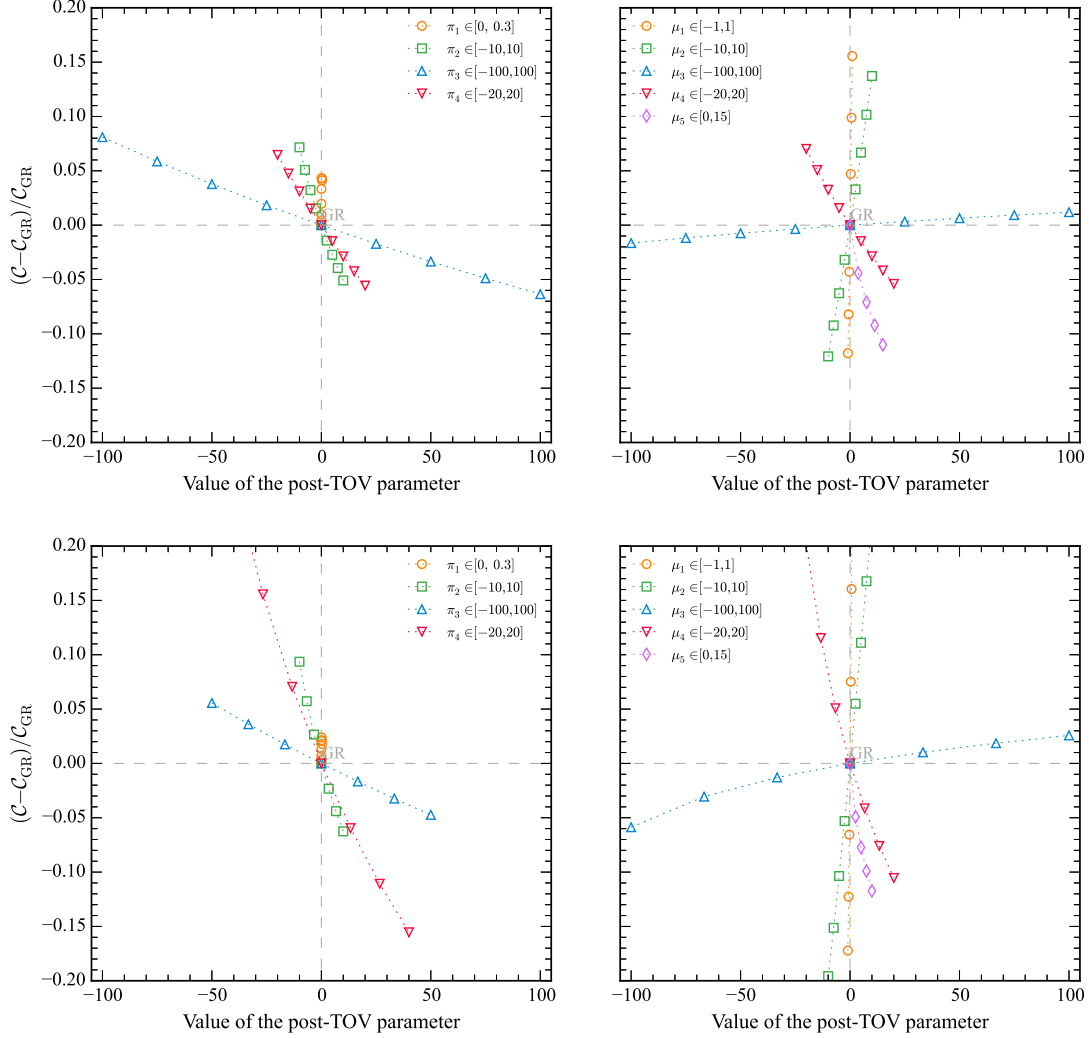


Figure 3.10: *Deviations induced by the post-TOV parameters on the stellar compactness.* Here we consider the influence of the post-TOV parameters on the compactness $\mathcal{C} = M/R$ of NSs. Deviations from GR are calculated assuming the same APR EOS models as in the top and bottom rows of Fig. 3.8. *Left panels:* Effect of the post-TOV terms appearing in the pressure equation. *Right panels:* Effect of the post-TOV terms appearing in the mass equation.

The linear patterns of Fig. 3.8 suggest that the mass and radius variations, for a given $\sigma_i = \{\pi_i \neq \pi_1, \mu_i\}$, obey the empirical relations,

$$\frac{\delta M}{M_{\text{GR}}} \approx \sigma_i K_M, \quad \frac{\delta R}{R_{\text{GR}}} \approx \sigma_i K_R, \quad (3.75)$$

where the structure parameters K_M, K_R are functions of the EOS and of ϵ_c , but independent of σ_i . Given the nonlinear character of the post-TOV equations, this conclusion is clearly nontrivial. We can recast this result in terms of the variation of the stellar compactness $\mathcal{C} \equiv M/R$,

$$\frac{\delta\mathcal{C}}{\mathcal{C}_{\text{GR}}} \approx \sigma_i (K_M - K_R). \quad (3.76)$$

This almost linear $\delta\mathcal{C}(\sigma_i)$ dependence⁵ can indeed be seen in the numerical results shown in Fig. 3.10, where we consider the same stellar models as in Fig. 3.8.

The results presented in this section provide a wealth of information on the character of the post-TOV corrections on stellar structure. It is likely that a more systematic study of the self-similar F-families will reveal additional layers of information and provide clues as to why the 2PN terms change the bulk properties of the star the way they do, as a function of the central density. Such a study provides an attractive subject for future work.

3.5 Conclusions and outlook

In this chapter we presented a first step towards establishing a parametrized perturbative framework that should, at least in principle, encompass all modifications to the bulk properties of NSs induced by modified theories of gravity. As in the original formulation of the PPN formalism, along the way we were forced to make some reasonable simplifying assumptions in order to reduce the complexity (and increase the practicality) of our parametrization. These reasonable assumptions may well fail to match the well-known creativity of theorists, and it will be interesting to see how the formalism can be extended and improved.

In future work we could use our basic post-TOV equations to recover stellar structure

⁵It is interesting to note that the qualitative effect of the post-TOV terms in the pressure equation can be understood by analogy with the case of anisotropic stars in GR (which we will explore with great detail in Chapter 5). The post-TOV pressure equation takes the form $dp/dr = (dp/dr)_{\text{GR}} - \rho m \pi_i f_i(r)/r^2$, with $f_i(r) > 0$, whereas anisotropic stars obey $dp_r/dr = (dp_r/dr)_{\text{GR}} - 2\sigma/r$, with $\sigma = p_r - p_q$ being the difference between the radial and tangential pressure. These two expressions can be matched if $2r\sigma = \rho m \pi_i f_i(r)$. The compactness of anisotropic stars is known to decrease (increase) when σ increases (decreases) [417]. This conclusion is in good qualitative agreement with the results shown in the left panel of Fig. 3.10.

calculations in some popular theories of gravity, such as those shown in Fig. 3.1. It is particularly interesting to compare the formalism against theories that violate some of our basic assumptions, such as ST gravity with spontaneous scalarization (which introduces intrinsically nonperturbative effects [118]) or Eddington-inspired-Born-Infeld gravity, with its lack of a Newtonian limit and its unorthodox dependence on the stress-energy tensor [358, 137].

We have already obtained some interesting results in this context: for example, our conclusion that the 2PN post-TOV equations are equivalent to an effective modified perfect-fluid EOS (see Section 3.3.3) has an interesting parallel with the results by Delsate et al. [137], who reached a similar conclusion for Eddington-inspired-Born-Infeld gravity.

There are several interesting extensions of our work that should be addressed in the future. The most obvious one is to assess whether post-TOV parameters can indeed reproduce the mass-radius curve in various classes of alternative theories, and whether the post-TOV parameters encode specific information on the physical parameters underlying specific theories. This study will hopefully lead to a better understanding of the generality of the EOS/gravity-theory degeneracy.

From a data analysis point of view, it is important to understand whether physical measurements of masses and radii (or perhaps more realistically, measurements of masses and surface redshifts/stellar compactnesses) can lead to constraints on the post-TOV parameters under specific assumptions on the high-density EOS. The answer to this question obviously depends on the relative magnitude of modified gravity effects and EOS uncertainties. It will be interesting to quantify what uncertainties in the EOS are acceptable if we want to experimentally constrain post-TOV parameters at meaningful levels.

Other obvious extensions are (i) the generalization of the post-TOV framework to slowly and possibly fast rotating relativistic stars, and (ii) stability investigations within the post-TOV framework. We hope that our work will stimulate further activity in this field. Stability studies in a post-TOV context may reveal that certain generic features of modified

gravity lead to instabilities even for nonrotating stars, possibly excluding whole classes of modified gravity theories.

Last but not least, we would like to point out that our post-TOV toolkit is not (nor was it designed to be) a self-consistent PN expansion, but rather a phenomenological parametrization of the leading-order (unconstrained) deviations from GR. A systematic and self-consistent PPN expansion extending the PN stellar structure works cited in the introduction [26, 469, 416, 191] is an interesting but quite distinct area of investigation that should also be pursued in the future.

In the next chapter we will develop an exterior post-Schwarzschild metric that will allow us to extend the applicability of the post-TOV, having astrophysical application in mind [185]. This extension of our formalism is applicable to situations involving bursting NSs (along the lines of [377]), geodesic motion around NSs and quasi-periodic oscillations [130], and NSs cooling curves [374, 77]. It is possible that the combination of multiple observables may lift the EOS/gravity degeneracy.

CHAPTER 4

SOME ASTROPHYSICAL APPLICATIONS OF
POST-TOLMAN-OPPENHEIMER-VOLKOFF FORMALISM FOR RELATIVISTIC
STARS

4.1 Introduction

Compact stars are ideal astrophysical environments to probe the coupling between matter and gravity in a high-density, strong gravity regime not accessible in the laboratory. Cosmological observations and high-energy physics considerations have spurred extensive research on the properties of NSs, whether isolated or in binary systems, in modified theories of gravity (see e.g. [51, 526] for reviews). Different extensions of GR affect the bulk properties of the star (such as the mass M and radius R) in similar ways for given assumptions on the EOS of high-density matter. Therefore it is interesting to understand whether these deviations from the predictions of GR can be understood within a simple parametrized formalism. The development of such a generic framework to understand how NS properties are affected in modified gravity is even more pressing now that gravitational-wave observations are finally a reality [3], since the observation of NS mergers could allow us to probe the dynamical behavior of these objects in extreme environments.

In Chapter 3 we developed a post-Tolman-Oppenheimer-Volkoff (henceforth, post-TOV) formalism valid for spherical stars [184]. The basic idea is quite simple. The structure of nonrotating, relativistic stars can be determined by integrating two ordinary differential equations: one of these equations gives the “mass function” and the other equation – a generalization of the hydrostatic equilibrium condition in Newtonian gravity – determines the pressure profile and the stellar radius, defined as the point where the pressure vanishes.

The post-TOV formalism, introduced in Chapter 4 and reviewed in Section 4.2 below, adds a relatively small number of parametrized corrections with parameters μ_i ($i = 1, \dots, 5$) and π_i ($i = 1 \dots, 4$) to the mass and pressure equations. These corrections have two properties: (i) they are of second post-Newtonian (PN) order, because first-order deviations are already tightly constrained by observations; and (ii) they are general enough to capture in a phenomenological way all possible deviations from the mass-radius relation in GR. Other parametrizations were explored in [408, 486] by modifying *ad hoc* the TOV equations.

In this chapter we turn to the investigation of astrophysical applications of the formalism. Part of our analysis is inspired by previous work by Psaltis [377], who showed that, under the assumption of spherical symmetry, many properties of NSs in metric theories of gravity can be calculated using only conservation laws, Killing symmetries, and the Einstein equivalence principle, without requiring the validity of the GR field equations. Psaltis computed the gravitational redshift of a surface atomic line z_s , the Eddington luminosity at infinity L_E^∞ (thought to be equal to the touchdown luminosity of a radius-expansion burst), and the apparent surface area of a NS (which is potentially measurable during the cooling tails of bursts).

We first extend our previous work to study the exterior of neutron stars. Then we compute the surface redshift z_s , the apparent radius R_{app} and the Eddington luminosity at infinity L_E^∞ . In addition, we study geodesic motion in the NS spacetime within the post-TOV formalism. We focus on the orbital and epicyclic frequencies, that according to some models – such as the relativistic precession model [455, 456] and the epicyclic resonance model [5] – may be related with the quasiperiodic oscillations (QPOs) observed in the x-ray spectra of accreting NSs.

Our main result is that, at leading order, all of these quantities depend on just *two* post-TOV parameters: μ_1 and the combination

$$\chi \equiv \pi_2 - \mu_2 - 2\pi\mu_1. \quad (4.1)$$

We also express the leading multipoles in a multipolar expansion of the NS spacetime in terms of μ_1 and χ , and we discuss the possibility to measure (or set upper bounds on) these parameters with astrophysical observations.

The plan of the chapter is as follows. In Sec. 4.2 we present a short review of the post-TOV formalism developed in [184] and introduced in the Chapter 3. In Sec. 4.3 we extend the formalism to deal with the stellar exterior, computing a “post-Schwarzschild” exterior metric. In Sec. 4.4 we compute the surface redshift z_s and relate it to the stellar compactness M/R . In Sec. 4.5, following [377], we study the properties of bursting NSs in the post-TOV framework. In Sec. 4.6 we calculate the orbital frequencies. In Sec. 4.7 we look at the leading-order multipoles of post-TOV stars. Then we present some conclusions and possible directions for future work.

4.2 Overview of the post-TOV formalism

Let us begin with a review of the post-TOV formalism introduced in Chapter 3. The core of this formalism consists of the following set of “post-TOV” structure equations for static spherically symmetric stars (we use geometrical units $G = c = 1$):

$$\frac{dp}{dr} = \left(\frac{dp}{dr} \right)_{\text{GR}} - \frac{\rho m}{r^2} (\mathcal{P}_1 + \mathcal{P}_2), \quad (4.2a)$$

$$\frac{dm}{dr} = \left(\frac{dm}{dr} \right)_{\text{GR}} + 4\pi r^2 \rho (\mathcal{M}_1 + \mathcal{M}_2), \quad (4.2b)$$

where

$$\mathcal{P}_1 \equiv \delta_1 \frac{m}{r} + 4\pi \delta_2 \frac{r^3 p}{m}, \quad \mathcal{M}_1 \equiv \delta_3 \frac{m}{r} + \delta_4 \Pi, \quad (4.3a)$$

$$\mathcal{P}_2 \equiv \pi_1 \frac{m^3}{r^5 \rho} + \pi_2 \frac{m^2}{r^2} + \pi_3 r^2 p + \pi_4 \frac{\Pi p}{\rho}, \quad (4.3b)$$

$$\mathcal{M}_2 \equiv \mu_1 \frac{m^3}{r^5 \rho} + \mu_2 \frac{m^2}{r^2} + \mu_3 r^2 p + \mu_4 \frac{\Pi p}{\rho} + \mu_5 \Pi^3 \frac{r}{m}. \quad (4.3c)$$

Here r is the circumferential radius, m is the mass function, p is the fluid pressure, ρ is the baryonic rest mass density, ϵ is the total energy density and $\Pi \equiv (\epsilon - \rho)/\rho$ is the internal energy per unit baryonic mass. A “GR” subscript denotes the standard TOV equations in GR, i.e.

$$\left(\frac{dp}{dr}\right)_{\text{GR}} = -\frac{(\epsilon + p)(m_{\text{T}} + 4\pi r^3 p)}{r^2(1 - 2m_{\text{T}}/r)}, \quad (4.4a)$$

$$\left(\frac{dm}{dr}\right)_{\text{GR}} = \frac{dm_{\text{T}}}{dr} = 4\pi r^2 \epsilon, \quad (4.4b)$$

where m_{T} is the GR mass function.

The dimensionless combinations $\mathcal{P}_1, \mathcal{M}_1$ and $\mathcal{P}_2, \mathcal{M}_2$ represent a parametrized departure from the GR stellar structure and are linear combinations of 1PN- and 2PN-order terms, respectively. These terms feature the phenomenological post-TOV parameters δ_i ($i = 1, \dots, 4$), π_i ($i = 1, \dots, 4$) and μ_i ($i = 1, \dots, 5$). In particular, the coefficients δ_i attached to the 1PN terms are simple algebraic combinations of the traditional PPN parameters $\delta_1 \equiv 3(1 + \gamma) - 6\beta + \zeta_2$, $\delta_2 \equiv \gamma - 1 + \zeta_4$, $\delta_3 \equiv -\frac{1}{2}(11 + \gamma - 12\beta + \zeta_2 - 2\zeta_4)$, $\delta_4 \equiv \zeta_3$. As such, they are constrained to be very close to zero by existing Solar System and binary pulsar observations¹: $|\delta_i| \ll 1$. This result translates to negligibly small 1PN terms in Eq. (4.2): $\mathcal{P}_1 \ll 1$, $\mathcal{M}_1 \ll 1$. On the other hand, π_i and μ_i are presently unconstrained, and consequently $\mathcal{P}_2, \mathcal{M}_2$ should be viewed as describing the dominant (significant) departure from GR. The GR limit of the formalism corresponds to setting all of these parameters to zero, i.e. $\delta_i, \pi_i, \mu_i \rightarrow 0$.

Alternatively, the stellar structure equations (4.2) can be formally derived – if we neglect the small terms $\mathcal{P}_1, \mathcal{M}_1$ – from a covariantly conserved perfect fluid stress energy tensor [184]:

$$\nabla_{\nu} T^{\mu\nu} = 0, \quad T^{\mu\nu} = (\epsilon_{\text{eff}} + p)u^{\mu}u^{\nu} + pg^{\mu\nu}, \quad (4.5)$$

¹We may recall from Chapter 3 that using the latest constraints on the PPN parameters [500] we obtain the following upper limits: $|\delta_1| \lesssim 6 \times 10^{-4}$, $|\delta_2| \lesssim 7 \times 10^{-3}$, $|\delta_3| \lesssim 7 \times 10^{-3}$, $|\delta_4| \lesssim 10^{-8}$.

where the effective, gravity-modified energy density is

$$\epsilon_{\text{eff}} = \epsilon + \rho\mathcal{M}_2, \quad (4.6)$$

and the covariant derivative is compatible with the effective post-TOV metric

$$g_{\mu\nu} = \text{diag}[-e^{\nu(r)}, (1 - 2m(r)/r)^{-1}, r^2, r^2 \sin^2 \theta], \quad (4.7)$$

with

$$\frac{d\nu}{dr} = \frac{2}{r^2} \left[(1 - \mathcal{M}_2) \frac{m + 4\pi r^3 p}{1 - 2m/r} + m\mathcal{P}_2 \right]. \quad (4.8)$$

This post-TOV metric is valid in the *interior* of the star. In the following section we discuss how an *exterior* post-TOV metric can be constructed within our framework.

4.3 The exterior “post-Schwarzschild” metric

For the applications of the post-TOV formalism considered in this work, we must specify how the g_{tt} and g_{rr} metric elements are calculated in the interior and exterior regions of the fluid distribution. In this section we will construct an exterior spacetime in a post-Schwarzschild form.

From the effective post-TOV metric, we have that *inside* the fluid body $g_{tt} = -\exp[\nu(r)]$, where $\nu(r)$ is determined in terms of the fluid variables and post-TOV parameters from Eq. (4.8). We will assume that *outside* the fluid distribution the *same* effective metric expression holds.² Then we get the equations

$$\frac{d\nu}{dr} = \left(\frac{d\nu}{dr} \right)_{\text{GR}} + \frac{2}{r^2} \left[-\mu_2 \frac{m^2}{r^2} \frac{m}{1 - 2m/r} + \pi_2 \frac{m^3}{r^2} \right], \quad (4.9)$$

$$\frac{dm}{dr} = 4\pi\mu_1 \frac{m^3}{r^3}, \quad (4.10)$$

²This assumption is based on simplicity. While we keep an agnostic view on the validity of Birkhoff’s theorem within our formalism (and in modified gravity theories in general), the interior post-TOV metric is arguably the best guide towards the construction of the exterior metric.

where

$$\left(\frac{d\nu}{dr}\right)_{\text{GR}} \equiv \frac{2}{r^2} \frac{m}{1 - 2m/r}. \quad (4.11)$$

These equations originate from the general expressions (4.8) and (4.2b) after setting all fluid parameters to zero, i.e. $p = \epsilon = \rho = \Pi = 0$, and keeping the surviving terms in \mathcal{M}_2 and \mathcal{P}_2 . It is not difficult to see that, in the nomenclature of [184], the only 2PN post-TOV terms that can appear in the exterior equations are those of “family F1” and “family F2.” The F1 term (coefficient π_1) should not appear in the \mathcal{P}_2 correction of the *interior* $d\nu/dr$ equation because it is divergent at the surface. This implies that the F1 term should not appear in the dp/dr equation either.

As it stands, Eq. (4.9) contains higher than 2PN order terms. It should therefore be PN-expanded with respect to the post-TOV terms:

$$\frac{d\nu}{dr} = \left(\frac{d\nu}{dr}\right)_{\text{GR}} + 2(\pi_2 - \mu_2) \frac{m^3}{r^4}. \quad (4.12)$$

Thus (4.12) and (4.10) are our “final” post-TOV equations for the stellar exterior.

The mass equation is decoupled and can be directly integrated. The result is

$$m(r) = \frac{r}{\sqrt{4\pi\mu_1 + Kr^2}}, \quad (4.13)$$

where K is an integration constant. The fact that $dm/dr \neq 0$ outside the star implies the presence of an “atmosphere” due to the non-GR degree of freedom. This is reminiscent of the exterior structure of NSs in scalar-tensor theories [118]. The constant K is fixed by setting $m(r \rightarrow \infty)$ equal to the system’s ADM mass M_∞ . Then,

$$m(r) = M_\infty \left(1 + 4\pi\mu_1 \frac{M_\infty^2}{r^2}\right)^{-1/2}. \quad (4.14)$$

Thus the ADM mass is related to the Schwarzschild mass $M \equiv m(R)$ by

$$M = M_\infty \left(1 + 4\pi\mu_1 \frac{M_\infty^2}{R^2} \right)^{-1/2}. \quad (4.15)$$

As expected, in the GR limit the two masses coincide

$$m(r > R) = M_\infty = M. \quad (4.16)$$

Assuming a post-TOV correction $\mathcal{F} \equiv 4\pi|\mu_1|(M_\infty/R)^2 \ll 1$ we can reexpand our result (4.15),

$$M = M_\infty \left(1 - 2\pi\mu_1 \frac{M_\infty^2}{R^2} \right). \quad (4.17)$$

The inverse relation $M_\infty = M_\infty(M)$ reads³

$$M_\infty = M \left(1 + 2\pi\mu_1 \frac{M^2}{R^2} \right). \quad (4.18)$$

The three mass relations (4.15), (4.17) and (4.18) are equivalent in the $\mathcal{F} \ll 1$ limit. Equations (4.15) and (4.14) are “exact” post-TOV results and do not require \mathcal{F} or μ_1 to be much smaller than unity, although Eq. (4.15) does place a lower limit on μ_1 because the argument of the square root must be nonnegative. Unfortunately, the use of (4.14) in the calculation of the metric components leads to very cumbersome expressions.

To make progress (while also keeping up with the post-TOV spirit), we hereafter use the $\mathcal{F} \ll 1$ approximations (4.17) and (4.18). This step, however, introduces a certain degree of error. This is quantified in Fig. 4.1 (left panel), where we show the relative percent error in calculating M_∞ using the post-TOV expanded Eqs. (4.17) and (4.18) rather than Eq. (4.15). Using EOS Sly4 [155], we considered values of μ_1 for which Eqs. (4.15) and (4.17) admit

³At first glance, obtaining $M_\infty(M)$ entails solving a cubic equation. However, the procedure is greatly simplified if we recall that the post-TOV formalism must reduce to GR for $\{\mu_i, \pi_i\} \rightarrow 0$. Having that in mind we can treat μ_1 as a small parameter and solve (4.17) perturbatively. The only regular solution in the $\mu_1 \rightarrow 0$ limit is Eq. (4.18).

a positive solution for M_∞ . As test beds, we consider NSs with central energy densities which result in a canonical $1.4M_\odot$ and the maximum allowed mass in GR, i.e. $2.05M_\odot$. As evident from Fig. 4.1, the error can become significant as we increase the value of $|\mu_1|$. By demanding that the errors remain within 5% we can narrow down the admissible values of μ_1 to $[-1.0, 0.1]$. We observe that while M_∞ can deviate greatly from the GR value (e.g. M_∞ reduces by $\approx 21\%$ when $\mu_1 = -1.0$ with respect to a $1.4M_\odot$ NS), \mathcal{F} remains below unity (see right panel of Fig. 4.1). This is because large negative values of the parameter μ_1 make the star less compact (i.e. Newtonian), as evidenced in Fig. 1 of [184].

We emphasize that the larger errors for some values of μ_1 are not an issue with the post-TOV formalism itself, but serve to constrain the values of μ_1 for which the perturbative expansion is valid. From a practical point of view, excluding large values of $|\mu_1|$ is a sensible strategy, since the resulting stellar parameters are so different with respect to their GR values that these cannot be considered as meaningful post-TOV corrections. Hereafter, whenever we refer to M_∞ we mean the mass calculated using Eq. (4.18) with $\mu_1 \in [-1.0, 0.1]$.

Within this approximation we are free to use the Taylor-expanded form of (4.14), i.e.

$$m(r) = M_\infty \left(1 - 2\pi\mu_1 M_\infty^2 / r^2\right). \quad (4.19)$$

This expression leads to the exterior g_{rr} metric

$$g_{rr}(r) = \left(1 - \frac{2M_\infty}{r}\right)^{-1} - 4\pi\mu_1 \frac{M_\infty^3}{r^3} + \mathcal{O}\left(\frac{\mu_1 M_\infty^4}{r^4}\right). \quad (4.20)$$

This expression allows us to identify M_∞ as the spacetime's gravitating mass (see also the result for g_{tt} below).

The next step is to use our result for $m(r)$ in (4.12) and integrate to obtain $\nu(r)$. After expanding to 2PN post-TOV order we obtain:

$$\frac{d\nu}{dr} = \frac{2M_\infty}{r^2} \left(1 - \frac{2M_\infty}{r}\right)^{-1} + 2\chi \frac{M_\infty^3}{r^4}. \quad (4.21)$$

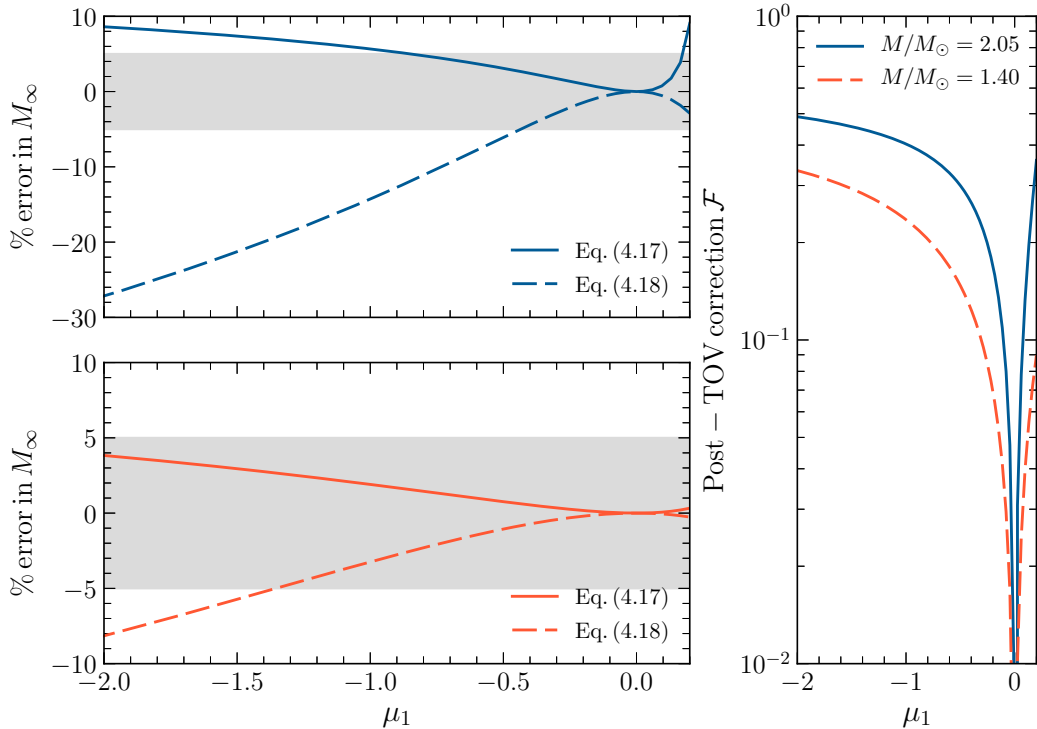


Figure 4.1: *Errors in M_∞ .* We show the percent error [$\% \text{ error} \equiv 100 \times (x_{\text{value}} - x_{\text{ref}})/x_{\text{ref}}$] in calculating M_∞ using Eqs. (4.17) and (4.18) with respect to (4.15) for various values of μ_1 using EOS SLy4. The range of μ_1 is chosen such that using any of Eqs. (4.15), (4.17) or (4.18) one can obtain a real root corresponding to M_∞ . The post-TOV models are constructed using a fixed central value of the energy density, which results in either a canonical ($1.4 M_\odot$) or a maximum-mass ($2.05 M_\odot$) NS in GR. *Top panel:* errors for a maximum-mass GR star. *Bottom panel:* errors for a canonical-mass GR star. *Right panel:* the absolute value of the post-TOV correction $\mathcal{F} = 4\pi\mu_1(M_\infty/R)^2$ as a function of μ_1 . The condition $\mathcal{F} \ll 1$ bounds the range of acceptable values of μ_1 for which the expansions leading to Eqs. (4.17) and (4.18) are valid. Errors are below 5 % when $\mu_1 \in [-1.0, 0.1]$.

where the parameter χ , defined in Eq. (4.1), quantifies the departure from the Schwarzschild metric. Integrating,

$$\nu(r) = \log\left(1 - \frac{2M_\infty}{r}\right) - \frac{2\chi}{3} \frac{M_\infty^3}{r^3}, \quad (4.22)$$

where the integration constant has been eliminated by requiring asymptotic flatness. The resulting exterior g_{tt} metric component is

$$g_{tt}(r) = -\left(1 - \frac{2M_\infty}{r}\right) + \frac{2\chi}{3} \frac{M_\infty^3}{r^3} + \mathcal{O}\left(\frac{\chi M_\infty^4}{r^4}\right). \quad (4.23)$$

Equations (4.23) and (4.20) represent our final results for the 2PN-accurate exterior post-Schwarzschild metric. From this construction it follows that post-TOV stars for which $\mu_1 = \mu_2 = \pi_2 = 0$ have the Schwarzschild metric as the exterior spacetime. The following sections describe how the exterior metric can be used to compute observables of relevance for NS astrophysics.

4.4 Surface redshift and stellar compactness

The surface redshift is among the most basic NS observables that could be affected by a change in the gravity theory. The surface redshift is defined in the usual way as

$$z_s \equiv \frac{\lambda_\infty - \lambda_s}{\lambda_s} = \frac{f_s}{f_\infty} - 1, \quad (4.24)$$

where λ and f are the wavelength and frequency of a photon, respectively. Here and below, the subscripts s and ∞ will denote the value of various quantities at the stellar surface $r = R$ and at spatial infinity. The familiar redshift formula

$$\frac{f_\infty}{f_s} = \left[\frac{g_{tt}(R)}{g_{tt}(\infty)} \right]^{1/2} \quad (4.25)$$

is valid for any static spacetime, regardless of the form of the field equations. Using the metric (4.23), we easily obtain (at first post-TOV order)

$$\frac{f_s}{f_\infty} = \left(1 - \frac{2M_\infty}{R} \right)^{-1/2} + \frac{\chi}{3} \frac{M_\infty^3}{R^3}. \quad (4.26)$$

Given that the frequency shift depends only on the ratio M_∞/R , it is more convenient to work in terms of the stellar compactness

$$C = M_\infty/R. \quad (4.27)$$

Then from the definition of the surface redshift we obtain

$$z_s = z_{\text{GR}} + \frac{\chi}{3}C^3, \quad (4.28)$$

where

$$z_{\text{GR}} \equiv (1 - 2C)^{-1/2} - 1 \quad (4.29)$$

is the standard redshift formula in GR, while the second term represents the post-TOV correction. Observe that z_s can be smaller or larger than z_{GR} depending on the sign of the parameter χ . This is shown in Fig. 4.2 (left panel), where we plot the percent difference $\delta z_s/z_s \equiv 100 \times (z_s - z_{\text{GR}})/z_{\text{GR}}$ as a function of C for two representative cases ($\chi = \pm 0.1$).

A characteristic property of the redshift is that it is a function of C , and as such it cannot be used to disentangle mass and radius individually. A given *observed* surface redshift z_{obs} can be experimentally interpreted either as $z_{\text{obs}} = z_{\text{GR}}(C)$ or $z_{\text{obs}} = z_s(C, \chi)$, and therefore lead to different estimates for C (for a given χ). Figure 4.2 (right panel), where we plot the percent difference $\delta C/C \equiv 100 \times (C - C_{\text{GR}})/C_{\text{GR}}$ as a function of z_s , shows how much the inferred compactness would differ in the two cases where $\chi = \pm 0.1$. A positive (negative) χ leads to a lower (higher) inferred compactness with respect to GR. The figure suggests that the “error” in C becomes significant for redshifts $z_s \gtrsim 1$.

It is a straightforward exercise to invert the redshift formula and obtain a post-TOV expression $C = C(z_s)$. We first write

$$1 + z_s = \frac{1}{\sqrt{-g_{tt}(R)}} \Rightarrow g_{tt}(R) = -\frac{1}{(1 + z_s)^2}. \quad (4.30)$$

Upon inserting the post-Schwarzschild metric (4.23) we get a cubic equation for the compactness,

$$-1 + \frac{1}{(1 + z_s)^2} + 2C + \frac{2}{3}\chi C^3 = 0. \quad (4.31)$$

In solving this equation we take into account that the small parameters are C and $z_s \sim \mathcal{O}(C)$

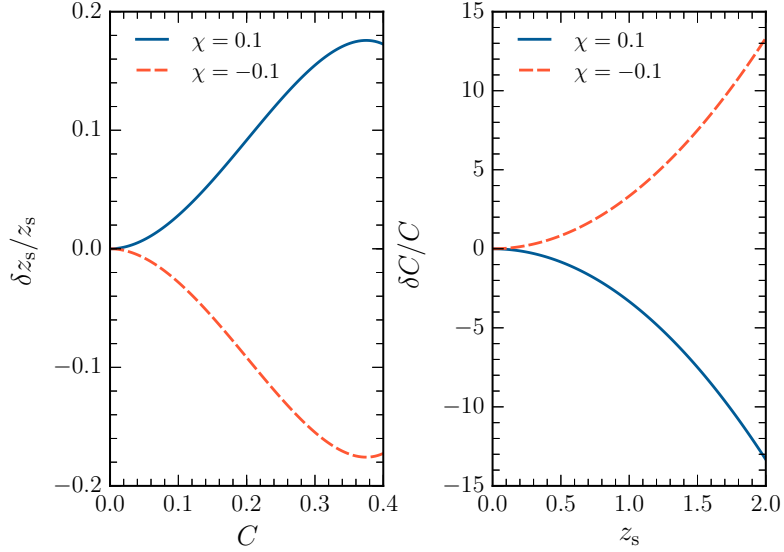


Figure 4.2: *Surface redshift and stellar compactness.* Relative percent changes with respect to GR for both z_s and C for different values of χ .

and that the $\chi \rightarrow 0$ limit should be smooth. We find

$$C = C_{\text{GR}} \left(1 - \frac{1}{3} \chi z_s^2 \right), \quad (4.32)$$

where

$$C_{\text{GR}} = \frac{1}{2} [1 - (1 + z_s)^{-2}], \quad (4.33)$$

is the corresponding solution in GR.

As was the case for the post-TOV redshift formula, the compactness of a post-TOV star can be pushed above (below) the GR value by choosing a negative (positive) parameter χ .

The two main results of this section, Eqs. (4.28) and (4.32), are also interesting from a different perspective, namely, their dependence on the single post-TOV parameter χ . This dependence entails a degeneracy with respect to the coefficient triad $\{\mu_1, \mu_2, \pi_2\}$ when (for example) a NS redshift observation is used as a gravity theory discriminator. The redshift/compactness χ -degeneracy is another reminder of the intrinsic difficulty in

distinguishing non-GR theories of gravity from NS physics (see e.g. discussion around Fig. 1 in [184]).

4.5 Bursting neutron stars

A potential test bed for measuring deviations from GR with a parametrized scheme like our post-TOV formalism is provided by accreting NSs exhibiting the so-called type I bursts. These are x-ray flashes powered by the nuclear detonation of accreted matter on the stellar surface layers [280]. The luminosity associated with these events can reach the Eddington limit and may cause a photospheric radius expansion (see e.g. [265, 452]), thus offering a number of observational “handles” to the system (see below for more details).

A paper by Psaltis [377] proposed type I bursting NSs as a means to constrain possible deviations from GR. Psaltis’ analysis, based on a static and spherically symmetric model for describing the spacetime outside a nonrotating NS, is general enough to allow a direct adaptation to the post-TOV scheme. For that reason we can omit most of the technical details discussed in [377] and instead focus on the key results derived in that paper.

There is a number of observable quantities associated with type I bursting NSs that can be used to set up a test of GR. The first one is the surface redshift z_s ; in Sec. 4.4 we have derived post-TOV formulas for z_s and the stellar compactness C , which are used below in the derivation of a constraint equation between the post-Schwarzschild metric and the various observables.

The luminosity (as measured at infinity) of a source located at a (luminosity) distance D is

$$L_\infty = 4\pi D^2 F_\infty, \quad (4.34)$$

where F_∞ is the (observable) flux. This luminosity can be written in a blackbody form with the help of an apparent surface area S_{app} and a color temperature (as measured at infinity) \bar{T}_∞ :

$$4\pi D^2 F_\infty = \sigma_{\text{SB}} S_{\text{app}} \bar{T}_\infty^4, \quad (4.35)$$

where σ_{SB} is the Stefan-Boltzmann constant. We then define the second observable parameter used in this analysis, i.e. the apparent radius

$$R_{\text{app}} \equiv \left(\frac{S_{\text{app}}}{4\pi} \right)^{1/2} = D \left(\frac{F_{\infty}}{\sigma_{\text{SB}} \bar{T}_{\infty}^4} \right)^{1/2}. \quad (4.36)$$

As evident from its form, R_{app} is independent of the underpinning gravitational theory, at least to the extent that the theory does not appreciably modify the (luminosity) distance to the source.

The surface color temperature is related to the intrinsic effective temperature T_{eff} via the standard color correction factor f_c [296, 463],

$$\bar{T}_s = f_c T_{\text{eff}}. \quad (4.37)$$

The observed temperature at infinity picks up a redshift factor with respect to its local surface value, that is,

$$\bar{T}_{\infty} = f_c \sqrt{-g_{tt}(R)} T_{\text{eff}}. \quad (4.38)$$

The effective temperature is the one related to the source's intrinsic luminosity,

$$L_s = 4\pi R^2 \sigma_{\text{SB}} T_{\text{eff}}^4. \quad (4.39)$$

As shown in [377],

$$L_{\infty} = -g_{tt}(R) L_s = 4\pi R^2 \sigma_{\text{SB}} \left(\frac{\bar{T}_{\infty}}{f_c} \right)^4 [-g_{tt}(R)]^{-1}. \quad (4.40)$$

Combining this with the preceding formulas leads to

$$\frac{R_{\text{app}}}{R} = \frac{1 + z_s}{f_c^2}. \quad (4.41)$$

The third relevant observable is the Eddington luminosity/flux at infinity. This is given by [377]

$$L_E^\infty = 4\pi D^2 F_E^\infty = \frac{4\pi}{\kappa} \frac{R^2}{(1+z_s)^2} g_{\text{eff}}, \quad (4.42)$$

where κ is the opacity of the matter interacting with the radiation field⁴ and g_{eff} is an effective surface gravitational acceleration, defined as

$$g_{\text{eff}} = \frac{1}{2\sqrt{g_{rr}(R)}} \frac{g'_{tt}(R)}{g_{tt}(R)}. \quad (4.43)$$

This parameter is key to the present analysis as it encodes the departure from the general relativistic Schwarzschild metric.

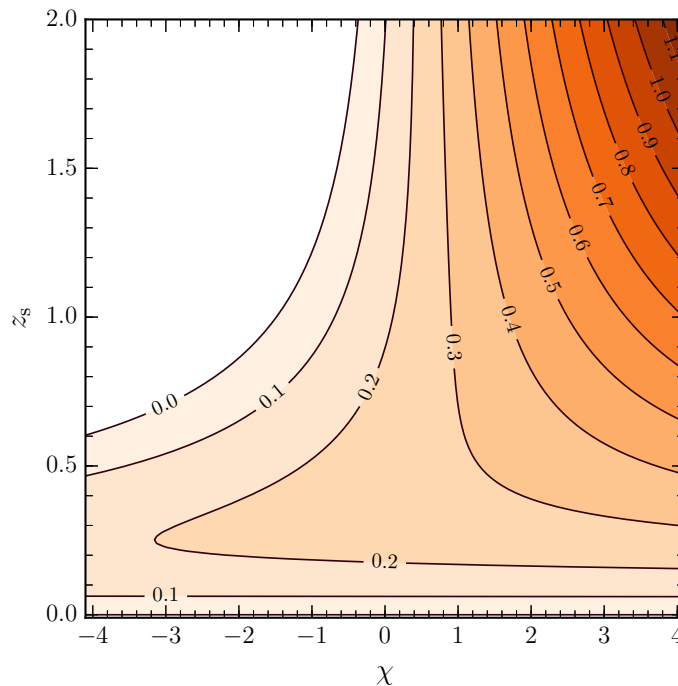


Figure 4.3: *Bursting NS constraints.* The surfaces are contours of constant $[1 + (2/3)\chi z_s^2] z_s (2 + z_s) / (1 + z_s)^4$ in the (z_s, χ) plane. This quantity is a combination of observables – cf. the right-hand side of Eq. (4.48) – and therefore it is potentially measurable; a measurement will single out a specific contour in this plot. A further measurement of (say) the redshift z_s corresponds to the intersection between one such contour and a line with $z_s = \text{const}$, so it can lead to a determination of χ .

⁴Typically, this interaction manifests itself as Thomson scattering in a hydrogen-helium plasma, in which case the opacity is $\kappa \approx 0.2(1 + X) \text{ cm}^2/\text{gr}$ where X is the hydrogen mass fraction [452].

Having at our disposal the above three observable combinations, the strategy is to combine them and derive a constraint equation between the observables and the spacetime metric. To this end, we first need to eliminate the not directly observable stellar radius R between (4.41) and (4.42) and subsequently solve with respect to g_{eff} . We obtain

$$g_{\text{eff}} = \kappa \sigma_{\text{SB}} \frac{F_{\text{E}}^{\infty}}{F_{\infty}} \left(\frac{\bar{T}_{\infty}}{f_{\text{c}}} \right)^4 (1 + z_{\text{s}})^4. \quad (4.44)$$

The remaining task is to express g_{eff} in terms of z_{s} . Using the post-Schwarzschild metric, Eqs. (4.20) and (4.23), in (4.44) we obtain the post-TOV result

$$g_{\text{eff}} = \frac{C}{R} (1 + z_{\text{s}}) (1 + \chi C^2). \quad (4.45)$$

Making use of Eq. (4.32) for the compactness leads to the desired result [cf. Eq. (39) in [377]]:

$$g_{\text{eff}} = \frac{z_{\text{s}} (2 + z_{\text{s}})}{2R (1 + z_{\text{s}})} \left(1 + \frac{2}{3} \chi z_{\text{s}}^2 \right), \quad (4.46)$$

where, as evident, the prefactor represents the GR result. Finally, after eliminating R with the help of (4.41) and (4.36), we obtain the ‘‘observable’’ effective gravity:

$$g_{\text{eff}} = \frac{z_{\text{s}} (2 + z_{\text{s}})}{2D f_{\text{c}}^2} \left(1 + \frac{2}{3} \chi z_{\text{s}}^2 \right) \left(\frac{\sigma_{\text{SB}} \bar{T}_{\infty}^4}{F_{\infty}} \right)^{1/2}. \quad (4.47)$$

This can then be combined with (4.44) to give

$$\frac{z_{\text{s}} (2 + z_{\text{s}})}{(1 + z_{\text{s}})^4} \left(1 + \frac{2}{3} \chi z_{\text{s}}^2 \right) = 2D \kappa \frac{F_{\text{E}}^{\infty}}{f_{\text{c}}^2} \left(\frac{\sigma_{\text{SB}} \bar{T}_{\infty}^4}{F_{\infty}} \right)^{1/2}, \quad (4.48)$$

and consequently

$$\chi = \frac{3}{2z_{\text{s}}^2} \left[2D \kappa \frac{(1 + z_{\text{s}})^4}{z_{\text{s}} (2 + z_{\text{s}})} \frac{F_{\text{E}}^{\infty}}{f_{\text{c}}^2} \left(\frac{\sigma_{\text{SB}} \bar{T}_{\infty}^4}{F_{\infty}} \right)^{1/2} - 1 \right]. \quad (4.49)$$

This equation is the main result of this section and provides, at least as a proof of principle, a quantitative connection between the post-Schwarzschild correction to the exterior metric [in the form of the χ coefficient defined in Eq. (4.1)] and observable quantities in a type I bursting NS. Reference [377] arrives at a similar result [their Eq. (49)] which has the same physical meaning, but is not identical to Eq. (4.48) due to the different assumed form of the exterior metric.

Our results are illustrated in Fig. 4.3, where we show the left-hand side of Eq. (4.48) as a contour plot in the (z_s, χ) plane. Each contour represents a specific measurement of this observable quantity. An additional surface redshift measurement can lead, at least in principle, to the determination of the post-TOV parameter χ , as given by Eq. (4.49).

4.6 Quasiperiodic oscillations

The post-Schwarzschild metric allows us to compute the geodesic motion of particles in the exterior spacetime of post-TOV NSs. Geodesics in NS spacetimes play a key role in the theoretical modeling of the QPOs observed in the x-ray spectra of accreting NSs. The detailed physical mechanism(s) responsible for the QPO-like time variability in the flux of these systems is still a matter of debate, but some of the most popular models are based on the notion of a radiating hot “blob” of matter moving in nearly circular geodesic orbits. The QPO frequencies are identified either with the orbital frequencies, or with simple combinations of the orbital frequencies. The most popular models are variants of the relativistic precession [455, 456] and epicyclic resonance [5] models.

In this section we discuss the relevant orbital frequencies within the post-TOV formalism and derive formulas that could easily be used in the aforementioned QPO models. In principle, matching the orbital frequencies to the QPO data would allow one to extract post-TOV parameters such as χ and μ_1 (see [391, 361, 362] for a similar exercise in the context of GR and scalar-tensor theory).

For nearly circular orbits in a spherically symmetric spacetime, the only perturbations

of interest are the radial ones (i.e., there is periastron precession but no Lense-Thirring nodal precession) and therefore we can associate two frequencies to every circular orbit: the orbital azimuthal frequency of the circular orbit Ω_φ and the radial epicyclic frequency Ω_r .

Geodesics in a static, spherically symmetric spacetime are characterized by the two usual conserved quantities, the energy $E = -g_{tt}\dot{t}$ and the angular momentum $L = g_{\phi\phi}\dot{\phi}$. Here both constants are defined per unit particle mass, and the dots stand for differentiation with respect to proper time. The four-velocity normalization condition $u^a u_a = -1$ yields an effective potential equation for the particle's radial motion,

$$g_{rr}\dot{r}^2 = -\frac{E^2}{g_{tt}} - \frac{L^2}{g_{\phi\phi}} - 1 \equiv V_{\text{eff}}(r). \quad (4.50)$$

The conditions for circular orbits are $V_{\text{eff}}(r) = V'_{\text{eff}}(r) = 0$, where the prime denotes differentiation with respect to the radial coordinate. Hereafter r will denote the circular orbit radius. From these conditions we can determine the orbital frequency $\Omega_\varphi \equiv \dot{\phi}/\dot{t}$ measured by an observer at infinity.⁵ The square of the orbital frequency is then given as

$$\Omega_\varphi^2 = -\frac{g'_{tt}}{g'_{\phi\phi}} = \frac{M_\infty}{r^3} \left(1 + \chi \frac{M_\infty^2}{r^2} \right). \quad (4.51)$$

The Schwarzschild frequency is recovered for $\chi = 0$.

The radial epicyclic frequency can be calculated from the equation for radially perturbed circular orbits, which follows from Eq. (4.50):

$$\Omega_r^2 = -\frac{g^{rr}}{2\dot{t}^2} V''_{\text{eff}}(r) \approx \frac{M_\infty}{r^3} \left[1 - \frac{6M_\infty}{r} - \frac{\chi M_\infty^2}{r^2} + \mathcal{O}(r^{-3}) \right] \quad (4.52a)$$

$$= \Omega_\varphi^2 \left[1 - \frac{6M_\infty}{r} - \frac{2\chi M_\infty^2}{r^2} + \mathcal{O}(r^{-3}) \right], \quad (4.52b)$$

⁵Apart from its implications for the QPOs, the post-TOV corrected orbital frequency would imply a shift in the corotation radius r_{co} in an accreting system. This radius is defined as $\Omega_* = \Omega_\varphi(r_{\text{co}})$, where Ω_* is the stellar angular frequency, and plays a key role in determining the torque-spin equilibrium in magnetic field-disk coupling models. Using the above definition we find the following result for the post-TOV corotation radius: $r_{\text{co}} = M_\infty (M_\infty \Omega_*)^{-2/3} [1 + (\chi/3)(M_\infty \Omega_*)^{4/3}]$.

where again the frequency is calculated with respect to observers at infinity. From the post-TOV expanded result we can see that the first two terms correspond to the Schwarzschild epicyclic frequency. The additional post-TOV terms in these formulas produce a shift in the frequency and radius of the innermost stable circular orbit (ISCO) with respect to their GR values – the latter quantity is determined by the condition $\Omega_r^2 = 0$, which in GR leads to the well-known result $r_{\text{isco}} = 6M_\infty$. The corresponding post-TOV ISCO is obtained from (4.52a), up to linear order in χ , as:

$$r_{\text{isco}} \approx 6M_\infty \left(1 + \frac{19}{324}\chi \right). \quad (4.53)$$

The post-TOV ISCO parameters r_{isco} and $(\Omega_\varphi)_{\text{isco}}$ are plotted in Fig. 4.4 as functions of the parameter χ . As evident from Eq. (4.53), a positive (negative) χ implies $r_{\text{isco}} > 6M_\infty$ ($r_{\text{isco}} < 6M_\infty$). If one takes Eq. (4.52a) at face value for the given post-Schwarzschild metric, for negative enough values of χ there is no ISCO solution, but this occurs well beyond the point where it is safe to use our perturbative formalism. The orbital frequency profile remains rather simple, with $(\Omega_\varphi)_{\text{isco}}$ exceeding the GR value when $r_{\text{isco}} < 6M_\infty$ (and vice versa).

Besides the frequency pair $\{\Omega_\varphi, \Omega_r\}$, a third prominent quantity in the QPO models is the frequency

$$\Omega_{\text{per}} = \Omega_\varphi - \Omega_r, \quad (4.54)$$

associated with the orbital periastron precession (for example, in the relativistic precession model [455, 456] this frequency is typically associated with the low-frequency QPO) .

Given our earlier results, it is straightforward to derive a series expansion in powers of $1/r$ for Ω_{per} . However, it is usually more desirable to produce a series expansion with respect to an observable quantity, such as the circular orbital velocity $U_\infty = (M_\infty \Omega_\varphi)^{1/3}$. This can be done by first expanding U_∞ with respect to $1/r$ and then inverting the expansion, thus

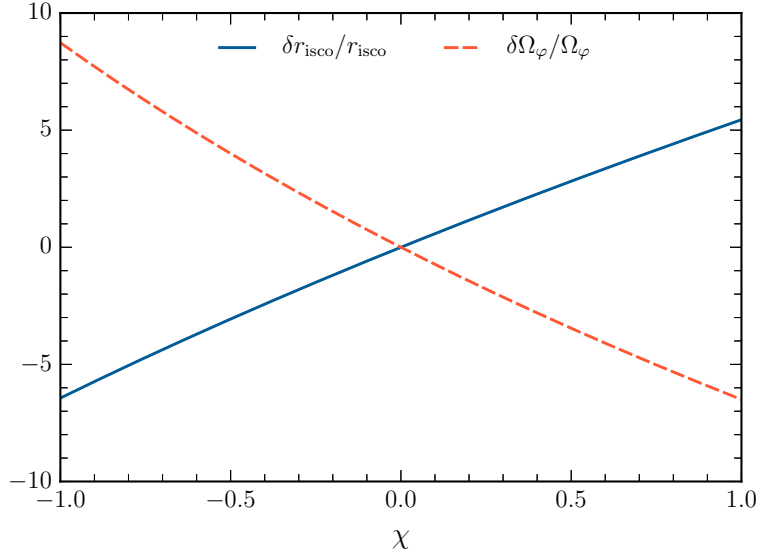


Figure 4.4: *ISCO quantities.* ISCO quantities as functions of χ . The solid curve corresponds to the relative difference (in percent) of r_{isco} with respect to GR, while the dashed curve corresponds to the relative difference of the orbital frequency at the ISCO, $(\Omega_\varphi)_{\text{isco}}$.

producing a series in U_∞ . The outcome of this recipe is

$$\frac{\Omega_{\text{per}}}{\Omega_\varphi} = 1 - \frac{\Omega_r}{\Omega_\varphi} = 3U_\infty^2 + \left(\frac{9}{2} + \chi\right)U_\infty^4 + \mathcal{O}(U_\infty^6). \quad (4.55)$$

A similar “Keplerian” version of this expression can be produced if we opt for using the velocity U_K and mass M_K that an observer would infer from the motion of (say) a binary system under the assumption of exactly Keplerian orbits. These are $U_K = (M_K \Omega_\varphi)^{1/3}$ and $M_K = r^3 \Omega_\varphi^2$, so that $M_K = M_\infty (1 + \chi M_\infty^2 / r^2)$. The resulting series is identical to Eq. (4.55) when truncated to U_K^4 order. Higher-order terms, however, are different (see the following section).

The above results for the frequencies $\{\Omega_\varphi, \Omega_r, \Omega_{\text{per}}\}$ suggest that a QPO-based test of GR within the post-TOV formalism could in principle allow the extraction of the post-TOV parameter χ . In this sense these frequencies probe the same kind of deviation from GR (and suffer from the same degree of degeneracy) as the observations of bursting NSs discussed in Section 4.5.

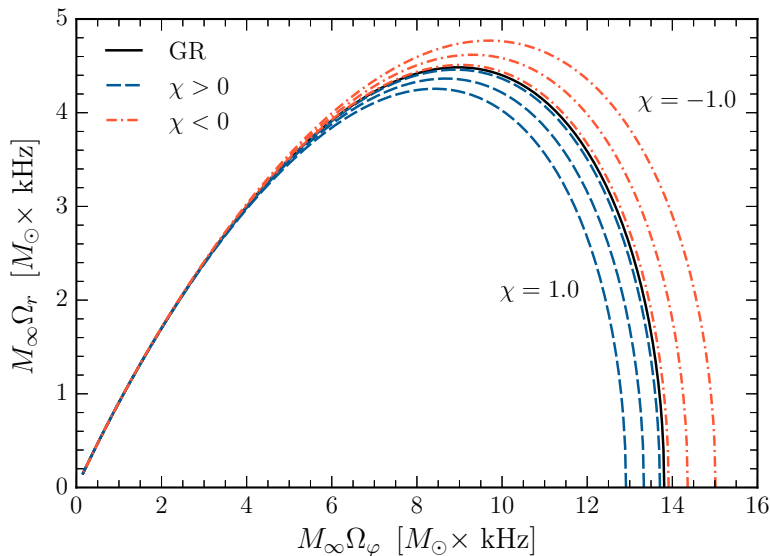


Figure 4.5: *Orbital frequencies.* Plots of Ω_r against Ω_ϕ for different values of $\chi = \pm 0.1, \pm 0.5$ and ± 1 . The black solid curve corresponds to the GR case. The dashed curves correspond to positive values of χ (and $r_{\text{ischo}} > 6M_\infty$) while the dash-dotted curves correspond to negative values of χ (and $r_{\text{ischo}} < 6M_\infty$).

We conclude this section by sketching how this procedure works in practice in the context of the relativistic precession model. The twin kHz QPO frequencies $\{\nu_1, \nu_2\}$ seen in the flux of bright low-mass x-ray binaries are identified with the azimuthal and periastron precession orbital frequencies. More specifically, the high-frequency member of the pair is identified with the azimuthal frequency ($\nu_2 = \nu_\phi = \Omega_\phi/2\pi$), while the low-frequency member is identified with the periastron precession ($\nu_1 = \nu_{\text{per}} = \Omega_{\text{per}}/2\pi$). With this interpretation, the QPO separation is equal to the radial epicyclic frequency: $\Delta\nu = \nu_2 - \nu_1 = \Omega_r/2\pi$.

We use our previous results [Eqs. (4.51), (4.52b), (4.55)] to plot these orbital frequencies (clearly, $\nu_1/\nu_2 = \Omega_{\text{per}}/\Omega_\phi$ and $\Delta\nu/\nu_2 = \Omega_r/\Omega_\phi$) as functions of each other and for varying χ . As it turns out, deviations from GR are best illustrated by plotting $\Omega_r(\Omega_\phi)$ (or equivalently $\Delta\nu(\nu_2)$). In Fig. 4.5 we plot the dimensionless combinations $M_\infty\Omega_r$, $M_\infty\Omega_\phi$ (in units of kHz for the frequencies and solar masses for M_∞). As we can see, the post-TOV models considered here ($-1 < \chi < 1$) are qualitatively similar to the GR result (black solid curve), all cases showing the characteristic hump in Ω_r as Ω_ϕ increases (so that the orbital

radius decreases). This feature is evidently associated with the existence of an ISCO (where $\Omega_r \rightarrow 0$) and is consistent with a similar trend seen in observations [456].

4.7 Multipolar structure of the spacetime

Expansions like Eq. (4.55) contain information about the multipolar structure of the background spacetime. That expansion can be directly compared against a similar expansion derived by Ryan [391] for an axisymmetric, stationary spacetime in GR with an arbitrary set of mass ($M_0 = M_\infty, M_2, M_4, \dots$) and current (S_1, S_3, S_5, \dots) Geroch-Hansen multipole moments [179, 180, 197]:⁶

$$\begin{aligned} \frac{\Omega_{\text{per}}}{\Omega_\varphi} &= 3U^2 - 4 \frac{S_1}{M_\infty^2} U^3 + \left(\frac{9}{2} - \frac{3}{2} \frac{M_2}{M_\infty^3} \right) U^4 - 10 \frac{S_1}{M_\infty^2} U^5 \\ &+ \left(\frac{27}{2} - 2 \frac{S_1^2}{M_\infty^4} - \frac{21}{2} \frac{M_2}{M_\infty^3} \right) U^6 + \mathcal{O}(U^7). \end{aligned} \quad (4.56)$$

where $U = (M_\infty \Omega_\varphi)^{1/3}$ denotes the orbital velocity.

To understand the PN accuracy of the post-TOV expansion in this context, it is useful to consider the effect of higher PN order terms in the metric. Imagine that the g_{tt} and g_{rr} metric components [see Eqs. (4.20) and (4.23)] included 3PN corrections of the schematic form,

$$g_{tt}(r) = g_{tt}^{2\text{PN}} + \alpha_{tt} \frac{M_\infty^3}{r^3}, \quad (4.57)$$

$$g_{rr}(r) = g_{rr}^{2\text{PN}} + \alpha_{rr} \frac{M_\infty^3}{r^3}. \quad (4.58)$$

We can use the coefficients α_{tt} and α_{rr} as bookkeeping parameters in order to understand how these omitted higher-order contributions affect the results of the previous section. The recalculation of the various expressions reveals that the orbital frequency remains un-

⁶A multipolar expansion in scalar-tensor theory can be found in [363]. Specific calculations were also carried out in other theories: for example, the quadrupole moment was computed in Einstein-dilaton-Gauss-Bonnet gravity [247].

changed to 2PN order; the 3PN term of Eq. (4.57) contributes at the next order, as expected. The same applies to the epicyclic frequency, as we can see for example from the modified Eq. (4.52b), where the next-order correction is a mixture of $g_{rr}^{2\text{PN}}$ and the 3PN term in g_{tt} :

$$\Omega_r^2 = \Omega_\varphi^2 \left[1 - \frac{6M_\infty}{r} - \frac{2\chi M_\infty^2}{r^2} + \frac{(4\pi\mu_1 - 6\alpha_{tt})M_\infty^3}{r^3} + \mathcal{O}(r^{-4}) \right]. \quad (4.59)$$

Proceeding in a similar way we find the next-order correction to the Ryan-like expansion (4.55):

$$\frac{\Omega_{\text{per}}}{\Omega_\varphi} = 3U_\infty^2 + \left(\frac{9}{2} + \chi \right) U_\infty^4 + \left[\frac{27}{2} + 2(\chi - \pi\mu_1) + 3\alpha_{tt} \right] U_\infty^6 + \mathcal{O}(U_\infty^8). \quad (4.60)$$

We can see that the 3PN term ‘‘contaminates’’ the PN correction that was omitted in Eq. (4.55). Repeating the same exercise for the Keplerian version of the multipole expansion (i.e. where the orbital velocity U_∞ is replaced by U_K) we find

$$\frac{\Omega_{\text{per}}}{\Omega_\varphi} = 3U_K^2 + \left(\frac{9}{2} + \chi \right) U_K^4 + \left(\frac{27}{2} - 2\pi\mu_1 + 3\alpha_{tt} \right) U_K^6 + \mathcal{O}(U_K^8). \quad (4.61)$$

At the PN order considered in the previous section the two expressions were identical but, as we can see, they differ at the next order.

We now have Ryan-type multipole expansions of the post-Schwarzschild spacetime up to 3PN in the circular orbital velocity, which we can compare against Eq. (4.56) to draw (with some caution) analogies and differences between GR and modified theories of gravity.

For instance, odd powers of U_∞ are missing in Eq. (4.60) because the nonrotating post-Schwarzschild spacetime has vanishing current multipole moments. Furthermore, we can see that the quadrupole moment M_2 , first appearing in the coefficient of U_∞^4 in Eq. (4.56), can be associated with χ . The parameter χ is an *effective* quadrupole moment in the sense that

$$M_2^{\text{eff}} = -\frac{2}{3}\chi M_\infty^3. \quad (4.62)$$

Indeed, this relation implies that a positive (negative) χ could be associated with an oblate (prolate) source of the gravitational field.

The identification (4.62) holds at $\mathcal{O}(U_\infty^4)$. The next-order term U_∞^6 would, in general, lead to a different effective M_2 . Hence, the comparison between the U_∞^4 and U_∞^6 terms could provide a null test for the GR-predicted quadrupole. However, there is a special case where these two terms could be consistent with the same effective quadrupole (4.62): this occurs when the post-TOV parameters satisfy the condition $5\chi = -2\pi\mu_1 + 3\alpha_{tt}$, in which case the expansion (4.60) behaves as a ‘‘GR mimicker’’.

A different kind of ‘‘multipole’’ expansion in powers of $1/r$ can be applied to the metric functions $\nu(r), m(r)$ [see Eqs. (4.9)–(4.11)], leading to an alternative calculation of the ADM mass M_∞ of a post-TOV star. We consider the expansions

$$\nu(r) = \sum_{n=0}^{\infty} \frac{\nu_n}{r^n}, \quad m(r) = \sum_{n=0}^{\infty} \frac{m_n}{r^n}, \quad (4.63)$$

where ν_n and m_n are constant coefficients. In addition, we impose that $\nu_0 = 0$ and $m_0 = M_\infty$. We subsequently substitute these expansions into Eqs. (4.9) and (4.10), expand for $r/R \gg 1$, and then solve for the coefficients. The outcome of this exercise in the vacuum exterior spacetime is

$$m(r) = M_\infty - 2\pi\mu_1 \frac{M_\infty^3}{r^2} + \mathcal{O}(r^{-4}), \quad (4.64)$$

$$\nu(r) = -\frac{2M_\infty}{r} - \frac{2M_\infty^2}{r^2} - \frac{2}{3} \frac{M_\infty^3}{r^3} (4 + \chi) + \mathcal{O}(r^{-4}). \quad (4.65)$$

As expected, the top equation is consistent with our earlier result, Eq. (4.19). To get an agreement between Eqs. (4.22) and (4.65) we must expand the logarithm appearing in the former equation in powers of M_∞/r , thus recovering Eq. (4.65).

4.8 Conclusions

In this chapter we have demonstrated the applicability of the post-TOV formalism to a number of facets of NS astrophysics. Let us summarize our main results. The exterior post-Schwarzschild metric [Eqs. (4.20) and (4.23)] depends only on the ADM mass M_∞ [given by Eq. (4.18)] and on just two post-TOV parameters μ_1 and χ . These are subsequently used to produce a post-TOV formula for the surface redshift, Eq. (4.28), which is a function of the stellar compactness and χ . Next, we have shown how a basic post-TOV model for type I bursting NSs can be constructed. The key equation here is (4.49), which gives χ (the only post-TOV parameter appearing in the model) in terms of observable quantities. We also computed geodesic motion in the post-Schwarzschild exterior of post-TOV NS models, finding expressions for the orbital, epicyclic and periastron precession frequencies of nearly circular orbits [Eqs. (4.51), (4.52b), (4.55)] and for the ISCO radius [Eq. (4.53)]. These results can be fed into models for QPOs from accreting NSs, such as the relativistic precession model. Finally, on a more theoretical level, we have sketched how the post-TOV parameters enter in the spacetime’s multipolar structure [Eq. (4.61)].

The meticulous reader may have noticed that, in spite of the exterior metric being a function $g_{tt}(\chi)$ and $g_{rr}(\mu_1)$, all other post-TOV results feature only χ , while μ_1 is either not present or enters at higher order. This is not a coincidence: these quantities either depend solely on g_{tt} (e.g. the redshift) or receive their leading-order contributions from g_{tt} (e.g. the orbital frequencies).

The post-TOV formalism developed in [184] and in this paper can be viewed as a basic “stage-one” version of a more general framework. There are several directions one can follow for taking the formalism to a more sophisticated level, and here we discuss just a couple of possibilities.

An obvious improvement is the addition of stellar rotation. This is necessary because all astrophysical compact stars rotate, some of them quite rapidly, and the influence of rotation is ubiquitous, affecting to some extent all of the effects discussed in this chapter. As

a first stab at the problem, it would make sense to work in the Hartle-Thorne slow rotation approximation [203, 204], which should be accurate enough for all but the fastest spinning neutron stars [55].

There are equally important possibilities for improvement on the modified gravity sector of the formalism. The present post-TOV theory is oblivious to the existence of dimensionful coupling constants, such as the ones appearing in many modified theories of gravity [e.g. $f(R)$ theories or theories quadratic in the curvature]. These coupling parameters should be added to the existing set of fluid parameters, and participate in the algorithmic generation of “families” of post-TOV terms (see [184] for details). The extended set of parameters will most likely lead to a proliferation of post-TOV terms, and result in more complicated stellar structure equations than the ones used so far [i.e. Eqs. (4.2)]. Among other things, this enhancement may allow one to study in more generality to what extent other theories of gravity are mapped onto the post-TOV formalism. Another limitation of the formalism is that it is intrinsically perturbative with respect to GR solutions. It is important to generalize to theories of gravity that present screening mechanisms; the viability of perturbative expansions in these theories is a topic of active research (see e.g. [85, 27, 530, 309]).

CHAPTER 5

SLOWLY ROTATING ANISOTROPIC NEUTRON STARS IN GENERAL RELATIVITY AND SCALAR-TENSOR THEORY

5.1 Introduction

Most investigations of the structure of NSs assume isotropic matter with a perfect-fluid EOS relating the pressure and density in the stellar interior. However, various physical effects can lead to local anisotropies (see [214] for a review). Anisotropy can occur for stars with a solid core [246] or strong magnetic fields [522, 168, 242]. Spaghetti- and lasagna-like structures would induce anisotropic elastic properties that could be important for NS quakes [210]. Nuclear matter may be anisotropic at very high densities [390, 78], where the nuclear interactions must be treated relativistically and phase transitions (e.g. to pion condensates [405] or to a superfluid state [83]) may occur. For example, Nelmes and Piette [329] recently considered NS structure within the Skyrme model, a low energy, effective field theory for Quantum Chromodynamics (QCD), finding significant anisotropic strains for stars with mass $M \gtrsim 1.5M_{\odot}$ (see also [7, 8]). From a mathematical point of view, two-fluid systems can be shown to be equivalent to a single anisotropic fluid [279]. Anisotropy affects the bulk observable properties of NSs, such as the mass-radius relation and the surface redshift [63, 209, 139, 141]: it can increase the maximum NS mass for a given EOS [63, 228] and stabilize otherwise unstable stellar configurations [140]. Incidentally, exotic compact objects such as gravastars [84] and boson stars [407, 294] are also equivalent to anisotropic fluids (i.e., they have anisotropic pressure).

It is known that rotation can induce anisotropy in the pressure due to anisotropic velocity distributions in low-density systems [214], but to the best of our knowledge – with

the exception of some work by Bayin [34] – slowly rotating anisotropic stars have never been investigated in GR. The goal of this chapter is to fill this gap using two different phenomenological models for anisotropy [63, 228], and to extend the analysis of slowly rotating anisotropic stars to ST theories of gravity.

ST theories are among the simplest and best studied extensions of GR [172]. In addition to the metric, in these theories gravity is also mediated by a scalar field. ST theories arise naturally from the dimensional reduction of higher-dimensional proposals to unify gravity with the Standard Model, and they encompass $f(R)$ theories of gravity as special cases [444, 124]. The simplest variant of ST theory, Brans-Dicke theory, is tightly constrained experimentally [499], but certain versions of the theory could in principle differ from GR by experimentally measurable amounts in the strong-field regime, as shown by Damour and Esposito-Farèse [117, 118].

From an astrophysical standpoint, compact objects such as BHs and NSs are the most plausible candidates to test strong-field gravity [51]. Compared to BHs, NSs are a more promising strong-field laboratory to distinguish ST gravity from GR, because a large class of ST theories admits the *same* black-hole solutions as GR (see [445] and references therein), and the dynamics of BHs can differ from GR only if the BHs are surrounded by exotic forms of matter [450, 150, 80, 79] or if the asymptotic behavior of the scalar field is nontrivial [224, 49].

The study of NS structure in GR is textbook material [201, 323, 412, 171], and there is an extensive literature on stellar configurations in ST theories as well (see e.g. [223, 355] and references therein). One of the most intriguing phenomena in this context is “spontaneous scalarization” [118], a phase transition analogous to the familiar spontaneous magnetization in solid state physics [119]: in a certain range of central densities, asymptotically flat solutions with a nonzero scalar field are possible and energetically favored with respect to the corresponding GR solutions.

In the absence of anisotropy, the degree of scalarization depends on a certain (real)

theory parameter β , defined in Eq. (5.2) below. Theory predicts that scalarization cannot occur (in the absence of anisotropy) when $\beta \gtrsim -4.35$ [199]. Present binary pulsar observations yield a rather tight experimental constraint: $\beta \gtrsim -4.5$ [169, 496]. One of our main findings is that the effects of scalarization, as well as the critical $|\beta|$ for spontaneous scalarization to occur, increase (decrease) for configurations in which the tangential pressure is bigger (smaller) than the radial pressure. Therefore binary pulsars can be used to constrain the degree of anisotropy at fixed β , or to constrain β for a given degree of anisotropy. This may open the door to experimental constraints on the Skyrme model via binary pulsar observations. Other notable findings of this study are (i) an investigation of the dependence of the stellar moment of inertia on the degree of anisotropy λ (more precisely, λ_{H} and λ_{BL} , because we consider two different anisotropy models [63, 228]); and (ii) an investigation of the threshold for scalarization for different values of β and λ in terms of a simple linear stability criterion, along the lines of recent work for BHs surrounded by matter [80, 79].

5.1.1 Organization of this chapter

In Section 5.2 we introduce the equations of motion in ST theory and the stress-energy tensor describing anisotropic fluids that will be used in the rest of the chapter. In Section 5.3 we present the equations of structure for relativistic stars at first order in the slow-rotation expansion. The macroscopic properties of NSs obtained by integrating these equations for two different models of anisotropic stars are presented in Section 5.4. Section 5.4.3 shows that a linear approximation is sufficient to identify the threshold for spontaneous scalarization for different values of β and λ . Section 5.5 summarizes our main conclusions and points out possible avenues for future work. Finally, in Appendix D we give a detailed derivation of an integral formula to compute the moment of inertia. Throughout this chapter, quantities associated with the Einstein (Jordan) frame will be labeled with an asterisk (tilde). We use geometrical units ($c = G_* = 1$) unless stated otherwise and signature $(-, +, +, +)$.

5.2 Anisotropic fluids in scalar-tensor theory of gravity

5.2.1 Overview of the theory

We consider a massless ST theory described by an Einstein-frame action [118, 119]

$$S = \frac{c^4}{16\pi G_*} \int d^4x \frac{\sqrt{-g_*}}{c} (R_* - 2g_*^{\mu\nu} \partial_\mu \varphi \partial_\nu \varphi) + S_M [\psi_M; A^2(\varphi)g_{*\mu\nu}] , \quad (5.1)$$

where G_* is the bare gravitational constant, $g_* \equiv \det [g_{*\mu\nu}]$ is the determinant of the Einstein-frame metric $g_{*\mu\nu}$, R_* is the Ricci curvature scalar of the metric $g_{*\mu\nu}$, and φ is a massless scalar field. S_M is the action of the matter fields, collectively represented by ψ_M . Free particles follow geodesics of the Jordan-frame metric $\tilde{g}_{\mu\nu} \equiv A^2(\varphi)g_{*\mu\nu}$, where $A(\varphi)$ is a conformal factor. In this work we assume that $A(\varphi)$ has the form

$$A(\varphi) \equiv e^{\frac{1}{2}\beta\varphi^2} , \quad (5.2)$$

where β is the theory's free parameter and, as we recalled in the introduction, current binary pulsar observations constrain it to the range $\beta \gtrsim -4.5$ [169, 496].

The field equations of this theory, obtained by varying the action S with respect to $g_*^{\mu\nu}$ and φ , are given by

$$R_{*\mu\nu} = 2\partial_\mu \varphi \partial_\nu \varphi + 8\pi \left(T_{*\mu\nu} - \frac{1}{2} T_* g_{*\mu\nu} \right) , \quad (5.3)$$

$$\square_* \varphi = -4\pi \alpha(\varphi) T_* , \quad (5.4)$$

where $R_{*\mu\nu}$ is the Ricci tensor, $\alpha(\varphi) \equiv d \log A(\varphi) / d\varphi$ (in the language of [118, 119]) is the “scalar-matter coupling function” and \square_* is the d'Alembertian operator associated to the metric $g_{*\mu\nu}$. GR is obtained in the limit where the scalar field decouples from matter, i.e. $\alpha(\varphi) \rightarrow 0$. Under the particular choice of the conformal factor (5.2), this is equivalent to letting $\beta = 0$. In this chapter, all equations will be derived within the context of ST gravity

and the particular limit of GR will be taken when necessary.

Finally, $T_*^{\mu\nu}$ is the energy-momentum tensor of the matter fields, defined as

$$T_*^{\mu\nu} \equiv \frac{2}{\sqrt{-g_*}} \frac{\delta S_M [\psi_M, A^2(\varphi) g_{*\mu\nu}]}{\delta g_{*\mu\nu}}, \quad (5.5)$$

and $T_* \equiv T_*^{\mu\nu} g_{*\mu\nu}$ is its trace. The energy-momentum tensor in the Jordan frame $\tilde{T}^{\mu\nu}$, with trace $\tilde{T} \equiv \tilde{T}^{\mu\nu} \tilde{g}_{\mu\nu}$, is defined in an analogous fashion:

$$\tilde{T}^{\mu\nu} \equiv \frac{2}{\sqrt{-\tilde{g}}} \frac{\delta S_M [\psi_M, \tilde{g}_{\mu\nu}]}{\delta \tilde{g}_{\mu\nu}}. \quad (5.6)$$

The two energy-momentum tensors (and their traces) are related as follows:

$$T_*^{\mu\nu} = A^6(\varphi) \tilde{T}^{\mu\nu}, \quad T_{*\mu\nu} = A^2(\varphi) \tilde{T}_{\mu\nu}, \quad T_* = A^4(\varphi) \tilde{T}. \quad (5.7)$$

The covariant divergence of the energy-momentum tensor satisfies

$$\nabla_{*\mu} T_*^{\mu\nu} = \alpha(\varphi) T_* \nabla_*^\nu \varphi, \quad (5.8)$$

$$\tilde{\nabla}_\mu \tilde{T}^{\mu\nu} = 0, \quad (5.9)$$

in the Einstein and Jordan frames, respectively.

5.2.2 Anisotropic fluids

An anisotropic fluid with radial pressure \tilde{p} , tangential pressure \tilde{q} and total energy density $\tilde{\epsilon}$ can be modeled by the Jordan-frame energy-momentum tensor [63, 147]

$$\tilde{T}_{\mu\nu} = \tilde{\epsilon} \tilde{u}_\mu \tilde{u}_\nu + \tilde{p} \tilde{k}_\mu \tilde{k}_\nu + \tilde{q} \tilde{\Pi}_{\mu\nu}, \quad (5.10)$$

where \tilde{u}_μ is the fluid four-velocity, \tilde{k}_μ is a unit radial vector ($\tilde{k}_\mu \tilde{k}^\mu = 1$) satisfying $\tilde{u}^\mu \tilde{k}_\mu = 0$, and $\tilde{\Pi}_{\mu\nu} \equiv \tilde{g}_{\mu\nu} + \tilde{u}_\mu \tilde{u}_\nu - \tilde{k}_\mu \tilde{k}_\nu$. $\tilde{\Pi}_{\mu\nu}$ is a projection operator onto a two-surface orthogonal

to both \tilde{u}_μ and \tilde{k}_μ : indeed, defining a projected vector $\tilde{A}^\mu \equiv \tilde{\Pi}^{\mu\nu}\tilde{V}_\nu$, one can easily verify that $\tilde{u}_\mu\tilde{A}^\mu = \tilde{k}_\mu\tilde{A}^\mu = 0$. At the center of symmetry of the fluid distribution the tangential pressure \tilde{q} must vanish, since \tilde{k}^μ is not defined there [147]. The trace of the Einstein-frame stress-energy tensor for an anisotropic fluid is

$$T_* = A^4(\varphi) [-(\tilde{\epsilon} - 3\tilde{p}) - 2(\tilde{p} - \tilde{q})] . \quad (5.11)$$

As emphasized by Bowers and Liang [63], \tilde{p} and \tilde{q} contain contributions from fluid pressures and other possible stresses inside the star, therefore they should not be confused with purely hydrostatic pressure. Additional stresses could be caused, for instance, by the presence of a solid core [246], strong magnetic fields [522] or a multi-fluid mixture [279]. The derivation of a microphysical model for anisotropy is a delicate issue, so we will adopt a phenomenological approach. We will assume that \tilde{p} is described by a barotropic EOS, i.e. $\tilde{p} = \tilde{p}(\tilde{\epsilon})$. For brevity in this chapter we focus on the APR EOS [10], but we have verified that our qualitative results do not depend on this choice. The APR EOS supports NS models with a maximum mass M larger than $2.0M_\odot$, and therefore it is compatible with the recent observations of the $M = 1.97 \pm 0.04M_\odot$ pulsar PSR J1614-2230 [138] and of the $M = 2.01 \pm 0.04M_\odot$ pulsar PSR J0348+0432 [19].

The functional form of the anisotropy $\tilde{\sigma} \equiv \tilde{p} - \tilde{q}$ [63, 147, 183] depends on microscopic relationships between \tilde{p} , \tilde{q} and $\tilde{\epsilon}$, that unfortunately are not known. However we can introduce physically motivated functional relations for $\tilde{\sigma}$ that allow for a smooth transition between the isotropic and anisotropic regimes. Many such functional forms have been studied in the literature. As an application of our general formalism we will consider two of these phenomenological relations, described below.

5.2.2.1 Quasi-local equation of state

Horvat et al. [228] proposed the following quasi-local equation for $\tilde{\sigma}$:

$$\tilde{\sigma} \equiv \lambda_{\text{H}} \tilde{p} \tilde{\gamma}, \quad (5.12)$$

where $\tilde{\gamma} \equiv 2\mu(r)/r$. The “mass function” $\mu(r)$, defined in Eq. (5.15) below, is essentially the mass contained within the radius r , so the quantity $\tilde{\gamma}$ is a local measure of compactness, whereas λ_{H} is a free (constant) parameter that controls the degree of anisotropy.

The calculations of [405] show that, if anisotropy occurs due to pion condensation, $0 \leq \tilde{\sigma}/\tilde{p} \leq 1$, therefore λ_{H} could be of order unity [147]. More recently, Nelmes and Piette [329] considered NS structure within a model consisting of a Skyrme crystal, which allows for the presence of anisotropic strains. They found that λ_{H} , as defined in Eq. (5.12), has a nearly constant value $\lambda_{\text{H}} \approx -2$ throughout the NS interior. The nonradial oscillations of anisotropic stars were studied in [147] using the model of Eq. (5.12). Following Doneva and Yazadjiev [147], we will consider values of λ_{H} in the range $-2 \leq \lambda_{\text{H}} \leq 2$.

5.2.2.2 Bowers-Liang model

As a second possibility we will consider the functional form for $\tilde{\sigma}$ proposed by Bowers and Liang [63], who suggested the relation¹

$$\tilde{\sigma} \equiv \frac{1}{3} \lambda_{\text{BL}} (\tilde{\epsilon} + 3\tilde{p}) (\tilde{\epsilon} + \tilde{p}) \left(1 - \frac{2\mu}{r}\right)^{-1} r^2. \quad (5.13)$$

The model is based on the following assumptions: (i) the anisotropy should vanish quadratically at the origin (the necessity for this requirement will become clear in Sec. 5.3), (ii) the anisotropy should depend nonlinearly on \tilde{p} , and (iii) the anisotropy is (in part) gravitationally induced. The parameter λ_{BL} controls the amount of anisotropy in the fluid.

¹The factor of 1/3 in Eq. (5.13) is chosen for convenience. Also, there is a sign difference between our definition of $\tilde{\sigma}$ and the one in [63]. Our parameter λ_{BL} is related with the Bowers-Liang (physically equivalent) parameter C by $\lambda_{\text{BL}} = -3C$.

This ansatz was used in [63] to obtain an exact solution for incompressible stars with $\tilde{\epsilon} = \tilde{\epsilon}_0 = \text{constant}$. In their simple model, the requirement that equilibrium configurations should have finite central pressure \tilde{p}_c implies that $\lambda_{\text{BL}} \geq -2$. The Newtonian limit of the Bowers-Liang ansatz was also considered in a recent study of the correspondence between superradiance and tidal friction [183]. In our calculations we will assume that $-2 \leq \lambda_{\text{BL}} \leq 2$.

5.3 Stellar structure in the slow-rotation approximation

In this section we approximate the metric of a slowly, rigidly rotating, anisotropic star following the seminal work by Hartle and Thorne [203, 204]. The idea is to consider the effects of rotation as perturbations of the spherically symmetric background spacetime of a static star. We generalize the results of [203, 204] (in GR) and [119] (in ST theory) to account for anisotropic fluids up to first order in rotation, so we can study how anisotropy and scalarization affect the moment of inertia of the star and the dragging of inertial frames. Our calculation have been generalized to higher orders in perturbation theory (in GR) by Yagi and Yunes [517, 518, 520].

We remark that the moment of inertia I , the star's uniform angular velocity Ω and the angular momentum $J \equiv I\Omega$ are the same in the Jordan and Einstein frames (cf. [119, 353]). Therefore, to simplify the notation, we will drop asterisks and tildes on these quantities. Working at order $\mathcal{O}(\Omega)$, the line element of a stationary axisymmetric spacetime in the Jordan frame reads

$$d\tilde{s}^2 = A^2(\varphi) \left[-e^{2\Phi(r)} dt^2 + e^{2\Lambda(r)} dr^2 + r^2 d\theta^2 + r^2 \sin^2 \theta d\phi^2 - 2\omega(r, \theta) r^2 \sin^2 \theta dt d\phi \right], \quad (5.14)$$

where

$$e^{-2\Lambda(r)} \equiv 1 - \frac{2\mu(r)}{r}, \quad (5.15)$$

$\mu(r)$ is the mass function and $\omega(r, \theta) \sim \mathcal{O}(\Omega)$ is the angular velocity acquired by a particle falling from infinity as measured by a static asymptotic observer [203].

The four-velocity of the rotating fluid is such that $\tilde{u}_\mu \tilde{u}^\mu = -1$, and it has components [203]

$$\tilde{u}^0 = [-(\tilde{g}_{00} + 2\Omega\tilde{g}_{03} + \Omega^2\tilde{g}_{33})]^{-1/2}, \quad (5.16)$$

$$\tilde{u}^1 = \tilde{u}^2 = 0, \quad (5.17)$$

$$\tilde{u}^3 = \Omega\tilde{u}^0. \quad (5.18)$$

Using (5.14), at first order in the slow-rotation parameter we obtain:

$$\tilde{u}^\mu = A^{-1}(\varphi) (e^{-\Phi}, 0, 0, \Omega e^{-\Phi}). \quad (5.19)$$

Following the standard procedure [323, 203, 449], the field equations (5.3), (5.4) and (5.8) with the metric given by (5.1) yield the following set of ordinary differential equations:

$$\frac{d\mu}{dr} = 4\pi A^4(\varphi) r^2 \tilde{\epsilon} + \frac{1}{2} r (r - 2\mu) \psi^2, \quad (5.20)$$

$$\frac{d\Phi}{dr} = 4\pi A^4(\varphi) \frac{r^2 \tilde{p}}{r - 2\mu} + \frac{1}{2} r \psi^2 + \frac{\mu}{r(r - 2\mu)}, \quad (5.21)$$

$$\begin{aligned} \frac{d\psi}{dr} = & 4\pi A^4(\varphi) \frac{r}{r - 2\mu} [\alpha(\varphi)(\tilde{\epsilon} - 3\tilde{p}) + r(\tilde{\epsilon} - \tilde{p})\psi] - \frac{2(r - \mu)}{r(r - 2\mu)} \psi \\ & + 8\pi A^4(\varphi) \alpha(\varphi) \frac{r\tilde{\sigma}}{r - 2\mu}, \end{aligned} \quad (5.22)$$

$$\frac{d\tilde{p}}{dr} = -(\tilde{\epsilon} + \tilde{p}) \left[\frac{d\Phi}{dr} + \alpha(\varphi)\psi \right] - 2\tilde{\sigma} \left[\frac{1}{r} + \alpha(\varphi)\psi \right], \quad (5.23)$$

$$\frac{d\varpi}{dr} = 4\pi A^4(\varphi) \frac{r^2}{r - 2\mu} (\tilde{\epsilon} + \tilde{p}) \left(\varpi + \frac{4\bar{\omega}}{r} \right) + \left(r\psi^2 - \frac{4}{r} \right) \varpi - 16\pi A^4(\varphi) \frac{r\tilde{\sigma}}{r - 2\mu} \bar{\omega}, \quad (5.24)$$

where we defined $\psi \equiv d\varphi/dr$, $\varpi \equiv d\bar{\omega}/dr$, and $\bar{\omega} \equiv \Omega - \omega$. The equations above reduce to the Tolman-Oppenheimer-Volkoff (TOV) equations for anisotropic stars in GR [63] when $\alpha \rightarrow 0$, to the results of [118] in the isotropic limit $\tilde{\sigma} \rightarrow 0$, and to the usual TOV equations when both quantities are equal to zero [323]. In the GR limit, our frame-dragging equation

(5.24) agrees with Bayin's [34] result².

To obtain the interior solution we integrate the generalized TOV equations (5.20)-(5.24) from a point r_c close to the stellar center $r = 0$ outwards up to a point $r = r_s$ where the pressure vanishes, i.e. $\tilde{p}(r_s) = 0$. This point specifies the Einstein-frame radius $R_* \equiv r_s$ of the star. If $\varphi_s = \varphi(r_s)$, the Jordan-frame radius \tilde{R} is

$$\tilde{R} = A(\varphi_s) R_* . \quad (5.25)$$

In practice, to improve numerical stability, given $\tilde{\epsilon}_c$, Φ_c , φ_c and μ_c (where the subscript c means that all quantities are evaluated at $r = 0$) we use the following series expansions:

$$\mu = \frac{4}{3}\pi A_c^4 \tilde{\epsilon}_c r^3 + \mathcal{O}(r^4), \quad (5.26a)$$

$$\Phi = \Phi_c + \frac{2}{3}\pi A_c^4 (\tilde{\epsilon}_c + 3\tilde{p}_c) r^2 + \mathcal{O}(r^4), \quad (5.26b)$$

$$\begin{aligned} \tilde{p} &= \tilde{p}_c + \frac{2}{3}\pi r^2 A_c^4 (\tilde{\epsilon}_c + \tilde{p}_c) [3\tilde{p}_c (\alpha_c^2 - 1) - \tilde{\epsilon}_c (\alpha_c^2 + 1)] \\ &\quad - \frac{1}{3}r^2(2r\sigma_3 + 3\sigma_2) + \mathcal{O}(r^4), \end{aligned} \quad (5.26c)$$

$$\varphi = \varphi_c + \frac{2\pi}{3}A_c^4 \alpha_c (\tilde{\epsilon}_c - 3\tilde{p}_c) r^2 + \mathcal{O}(r^4), \quad (5.26d)$$

$$\bar{\omega} = \bar{\omega}_c + \frac{8\pi}{5}A_c^4 \bar{\omega}_c (\tilde{\epsilon}_c + \tilde{p}_c) r^2 + \mathcal{O}(r^4), \quad (5.26e)$$

$$\tilde{\sigma} = \sigma_2 r^2 + \sigma_3 r^3 + \mathcal{O}(r^4), \quad (5.26f)$$

where σ_2 and σ_3 depend on the particular anisotropy model.

In the vacuum exterior we have $\tilde{p} = \tilde{\epsilon} = \tilde{\sigma} = 0$. Eqs. (5.20)-(5.22) must be integrated outwards starting from the stellar radius to obtain the stellar mass, angular momentum and

²In principle, as mentioned in the introduction, rotation may induce anisotropy. Therefore the Horvat et al. and Bowers-Liang models for $\tilde{\sigma}$ should contain terms proportional to Ω . However, Eq. (5.24) implies that such terms in $\tilde{\sigma}$ would lead to corrections of second order in the angular velocity Ω . These corrections are beyond the scope of the $\mathcal{O}(\Omega)$ approximation considered in our work.

scalar charge. For large r we can expand the relevant functions as follows:

$$\mu(r) = M - \frac{Q^2}{2r} - \frac{MQ^2}{2r^2} + \mathcal{O}(r^{-3}), \quad (5.27a)$$

$$e^{2\Phi} = 1 - \frac{2M}{r} + \mathcal{O}(r^{-3}), \quad (5.27b)$$

$$\varphi(r) = \varphi_\infty + \frac{Q}{r} + \frac{MQ}{r^2} + \mathcal{O}(r^{-3}), \quad (5.27c)$$

$$\bar{\omega}(r) = \Omega - \frac{2J}{r^3} + \mathcal{O}(r^{-4}), \quad (5.27d)$$

where M is the ADM mass of the NS, Q is the scalar charge, J is the star's angular momentum and φ_∞ is the (constant) cosmological value of the scalar field, here assumed to be zero. Under this assumption the mass M is the same in the Jordan and Einstein frames [353]. By matching the numerical solution integrated from the surface of the star with the asymptotic expansions (5.27a)–(5.27d) we can compute M , Q and J .

We compute the moment of inertia of the star I in two equivalent ways. The first method consists of extracting the angular momentum as described above and using

$$I = \frac{J}{\Omega}. \quad (5.28)$$

In alternative, we can compute I through an integral within the star. Combining Eqs. (5.15), (5.20)–(5.21) and (5.24) we obtain the following integral expression:

$$I = \frac{8\pi}{3} \int_0^{R_*} A^4(\varphi) e^{\Lambda-\Phi} r^4 (\tilde{\epsilon} + \tilde{p}) \left(1 - \frac{\tilde{\sigma}}{\tilde{\epsilon} + \tilde{p}} \right) \left(\frac{\bar{\omega}}{\Omega} \right) dr \quad (5.29)$$

(see Appendix D for details). As $A(\varphi) \rightarrow 1$ and $\tilde{\sigma} \rightarrow 0$ we recover Hartle's result [203], and in the isotropic limit $\tilde{\sigma} \rightarrow 0$ we match the result of [449]. The numerical values of I obtained with (5.28) and (5.29) are in excellent agreement.

For each stellar model we also calculate the *baryonic mass* \tilde{M}_b , defined as [118]

$$\tilde{M}_b \equiv 4\pi\tilde{m}_b \int_0^{R_*} \tilde{n} A^3(\varphi) \frac{r^2}{\sqrt{1 - 2\mu/r}} dr, \quad (5.30)$$

where $\tilde{m}_b = 1.66 \times 10^{-24}$ g is the atomic mass unit and \tilde{n} is the baryonic number density.

5.4 Numerical results

The tools developed so far allow us to investigate the effect of anisotropy on the bulk properties of rotating stars. In Section 5.4.1 we will focus on slowly rotating stars in GR. To the best of our knowledge – and to our surprise – rotating anisotropic stars have not been studied in the GR literature, with the only exception of a rather mathematical paper by Bayin [34]. In Section 5.4.2 we extend our study to ST theories. Our main motivation here is to understand whether anisotropy may increase the critical value $\beta = \beta_{\text{crit}}$ above which spontaneous scalarization cannot happen, and therefore allow for observationally interesting modifications to the structure of NSs that would still be compatible with the stringent bounds from binary pulsars [169, 496].

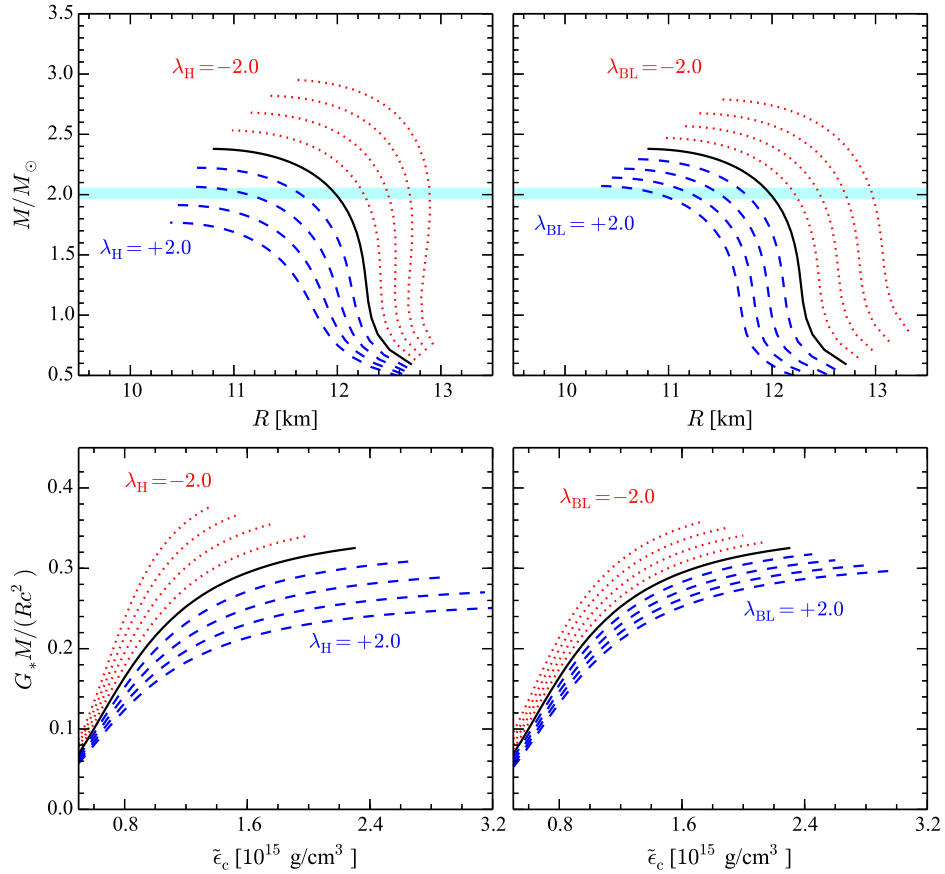


Figure 5.1: *Mass-radius curves for anisotropic stars.* Mass-radius relation (top panels) and dimensionless compactness G_*M/Rc^2 as a function of the central density (bottom panels) for anisotropic stars in GR using EOS APR. In the left panels we use the quasi-local model of [228]; in the right panels, the Bowers-Liang model [63]. Different curves correspond to increasing λ_H (or λ_{BL}) in increments of 0.5 between -2 (top) and 2 (bottom). The shaded blue bar corresponds to the mass $M = 2.01 \pm 0.04M_\odot$ of PSR J0348+0432 [19].

5.4.1 The effect of anisotropy in GR

In the top panels of Figure 5.1 we show the mass-radius relation for anisotropic NS models in GR. All curves are truncated at the central density corresponding to the maximum NS mass, because models with larger central densities are unstable to radial perturbations [201, 323]. Solid lines correspond to $\tilde{\sigma} = 0$, i.e. the isotropic fluid limit. The horizontal shaded band in the upper panels represents the largest measured NS mass $M = 2.01 \pm 0.04M_\odot$ (PSR J0348+0432: cf. [19]).

Recall that $\tilde{\sigma} = \tilde{p} - \tilde{q}$ is proportional to λ_H and λ_{BL} (with a positive proportionality constant) in both models, and that \tilde{p} and \tilde{q} represent the “radial” and “tangential” pressures, respectively. Therefore positive values of λ_H and λ_{BL} mean that the radial pressure is larger than the tangential pressure (dashed lines); the opposite is true when the anisotropy parameters are negative (dotted lines).

The trend in the top panels of Figure 5.1 is clear: for both anisotropy models, positive (negative) anisotropy parameters yield smaller (larger) radii at fixed mass, and smaller masses at fixed radius. The lower panels of Figure 5.1 show that the stellar compactness $G_*M/(Rc^2)$ decreases (for a given EOS and fixed central density) as the anisotropy degree increases. Nuclear matter EOSs are usually ordered in terms of a “stiffness” parameter, with stiffer EOSs corresponding to larger sound speeds (more incompressible matter) in the stellar interior, and larger values of the compactness M/R . The qualitative effect of increasing anisotropy (with our sign conventions) is *opposite* (for a given EOS) to the qualitative effect of increasing stiffness.

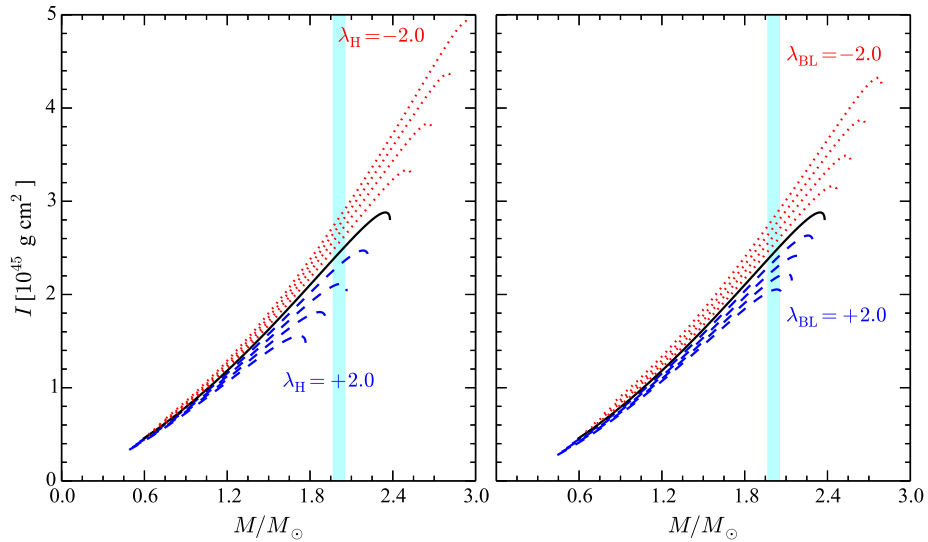


Figure 5.2: *Moment of inertia of anisotropic stars.* The moment of inertia I as function of the mass M for anisotropic stars in GR using EOS APR, increasing λ_H (or λ_{BL}) in increments of 0.5 between -2 (top curves) and 2 (bottom curves). As in Figure 5.1, the vertical shaded region marks the largest measured NS mass [19].

Figure 5.2 is, to our knowledge, the first calculation of the effect of anisotropy on the moment of inertia I . As in Figure 5.1, solid lines corresponds to the isotropic limit. In the right panel we use the quasi-local model of [228]; in the left panel, the Bowers-Liang model [63]. Hypothetical future observations of the moment of inertia of star A, from the double pulsar PSR J0737-3039 [293, 276, 263], or preferably from large-mass NSs, may be used to constrain the degree of anisotropy under the assumptions that GR is valid and that the nuclear EOS is known.

5.4.2 The effect of anisotropy on spontaneous scalarization

In Figures 5.3 and 5.4 we display the properties of nonrotating, spontaneously scalarized stars within the anisotropy models of Horvat et al. [228] and Bowers-Liang [63], respectively. The main panel in each Figure shows the mass-radius relation as the anisotropy parameter increases (in increments of 1, and from top to bottom) in the range $-2 \leq \lambda_H \leq 2$ (Figure 5.3) or $-2 \leq \lambda_{BL} \leq 2$ (Figure 5.4). Solid lines correspond to the GR limit; dotted, dashed and dash-dotted lines correspond to $\beta = -4.3, -4.4$ and -4.5 , as indicated in the legend. The lower panels show the scalar charge Q/M as a function of the baryonic mass. In each of these panels we plot the scalar charge for a fixed value of β and different anisotropy parameters.

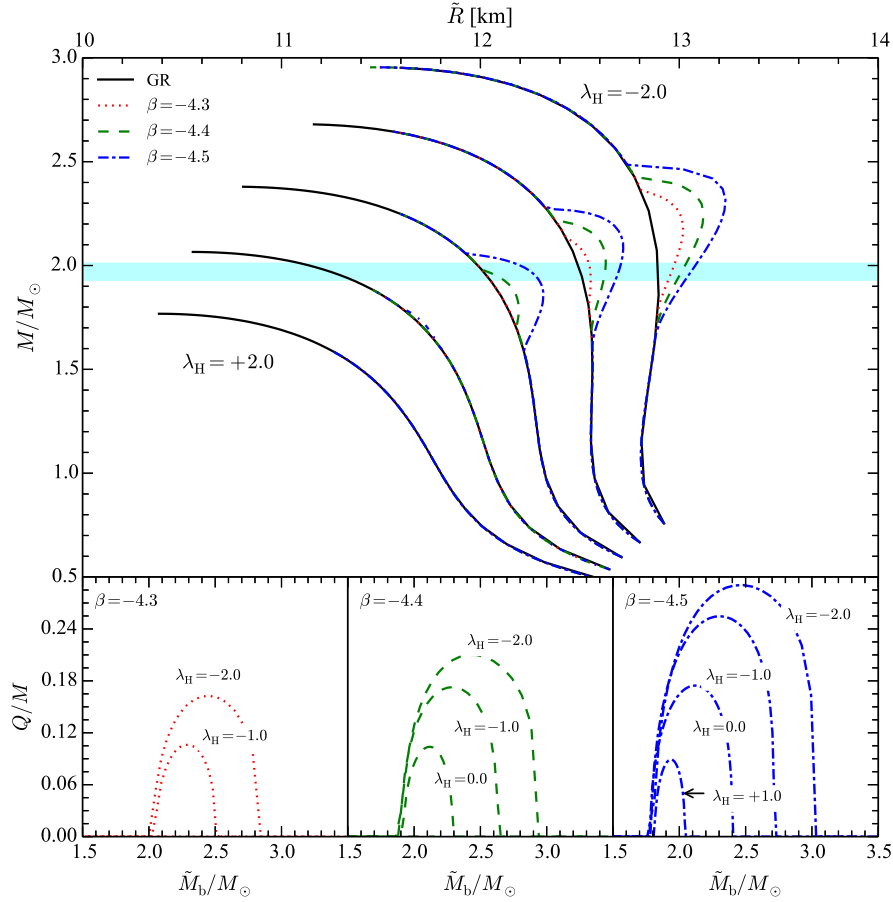


Figure 5.3: *Scalarized anisotropic stars - I.* Spontaneous scalarization in the quasi-local model of Horvat et al. [228]. See the main text for details.

For isotropic EOSs in GR, Harada [199] used catastrophe theory to show that scalarization is only possible when $\beta \lesssim -4.35$. We find that scalarization can occur for larger values of β in the presence of anisotropy. For example, for a value of $\lambda_H \sim -2$ (compatible with the Skyrme model predictions of [329]) scalarization is possible when $\beta \simeq -4.15$, and for $\beta \simeq -4.3$ scalarization produces rather large ($\approx 10\%$) deviations in the mass-radius relation. This qualitative conclusion applies to both anisotropy models considered by us. The lower panels show that: (i) for fixed β (i.e., for a fixed theory) and for a fixed central density, the “strength” of scalarization – as measured by the scalar charge of the star – increases for large negative λ ’s, i.e. when the tangential pressure is significantly larger than

the radial pressure, for both anisotropy models; (ii) scalarization occurs in a much wider range of baryonic masses, all of which are compatible with the range where anisotropy would be expected according to the Skyrme model predictions of [329]. These calculations are of course preliminary and should be refined using microphysical EOS models.

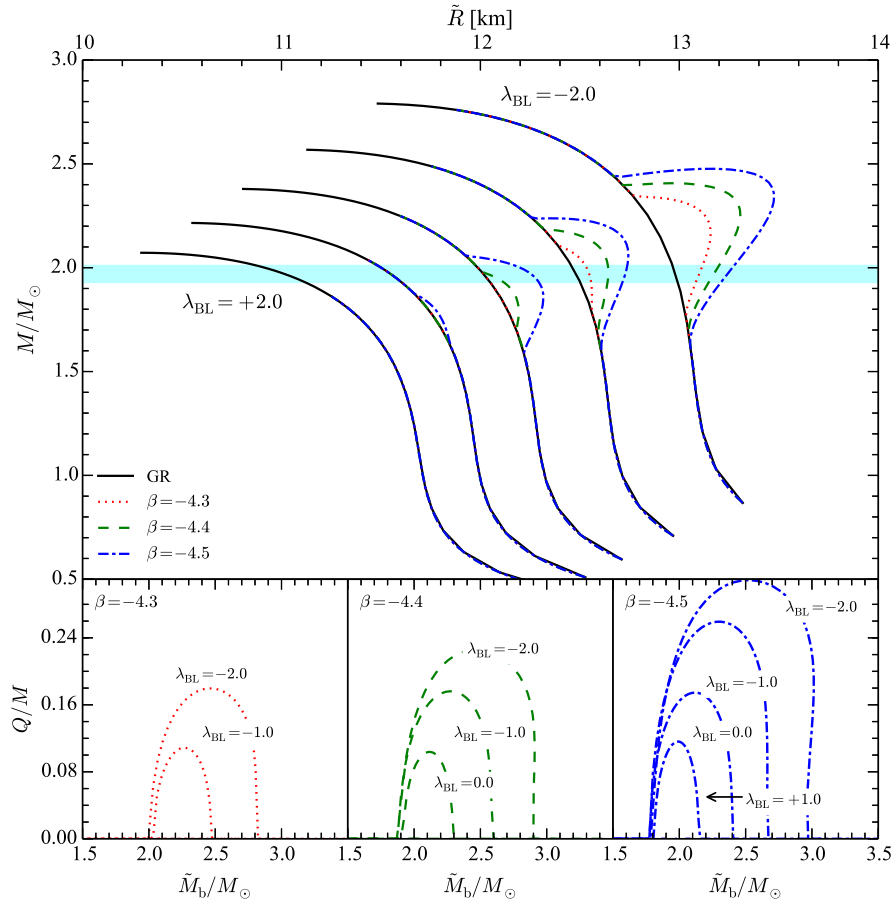


Figure 5.4: *Scalarized anisotropic stars - II.* Same as Figure 5.3, but for the Bowers-Liang anisotropy model [63].

Let us remark once again that the scalarization threshold in the absence of anisotropy is to a very good approximation EOS-independent, and stars only acquire significant scalar charge when $\beta < -4.35$ (as shown in [199] and in Figure 5.6 below).

In the admittedly unlikely event that binary pulsar observations were to hint at

scalarization with $\beta > -4.35$, this would be strong evidence for the presence of anisotropy³ and even lead to experimental constraints on the Skyrme model and QCD.

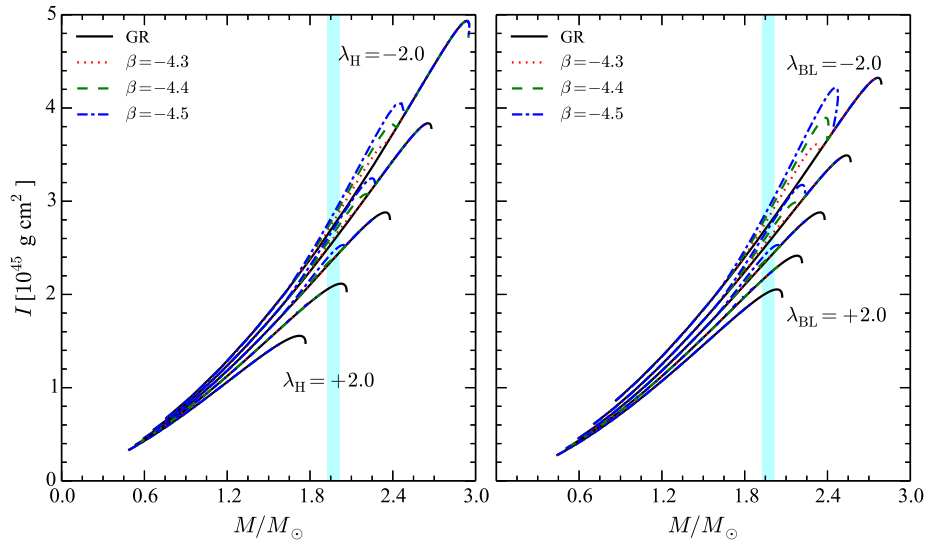


Figure 5.5: *Scalarized anisotropic stars - III.* Same as Figure 5.2, but in ST theories with different values of β .

As in Figure 5.2, in the left panel of Figure 5.5 we show the moment of inertia as a function of the stellar mass for the quasi-local model of [228], while the right panel refers to the Bowers-Liang model [63]. Solid lines corresponds to the GR limit for different anisotropy parameters. Unsurprisingly, the largest modifications to the moment of inertia occur for large negative λ 's, and they follow the same trends highlighted in our discussion of the mass-radius relation.

5.4.3 Critical scalarization point in the linearized approximation

The condition for spontaneous scalarization to occur can be found in a linearized approximation to the scalar-field equation of motion. The idea is that *at the onset* of scalarization the scalar field must be small, so we can neglect its backreaction on the geometry and

³An important caveat here is that *fast* rotation can also strengthen the effects of scalarization: according to [153], scalarization can occur for $\beta < -3.9$ for NSs spinning at the mass-shedding limit. However the NSs found in binary pulsar systems are relatively old, as they are expected to be spinning well below the mass-shedding limit, where the slow-rotation approximation works very well [55].

look for bound states of the scalar field by dropping terms quadratic in the field [118, 119]. Here we study general conditions for the existence of bound states in the linearized regime, and we show that (as expected based on the previous argument) the linearized theory does indeed give results in excellent agreement with the full, nonlinear calculation.

Redefining the scalar field as $\varphi(t, r) = r^{-1}\Psi(r)e^{-i\nu t}$ and neglecting terms $\mathcal{O}(\varphi^2)$, Eq. (5.4) can be written as a Schrödinger-like equation:

$$\frac{d^2\Psi}{dx^2} + [\nu^2 - V_{\text{eff}}(x)] \Psi = 0, \quad (5.31)$$

where the tortoise radial coordinate x is defined by $dx \equiv dr e^{-\Phi}/\sqrt{1 - 2\mu/r}$. The effective potential is

$$V_{\text{eff}}(r) \equiv e^{2\Phi} \left[\mu_{\text{eff}}^2(r) + \frac{2\mu}{r^3} + 4\pi(\tilde{p} - \tilde{\epsilon}) \right], \quad (5.32)$$

where we have introduced an effective (position-dependent) mass

$$\mu_{\text{eff}}^2(r) \equiv -4\pi\beta T_*. \quad (5.33)$$

Eq. (5.31) with the potential (5.32) is a wave equation for a scalar field with effective mass μ_{eff} . From Eq. (5.11) we see that anisotropy affects the effective mass (and therefore the scalarization threshold) because T_* contains a term proportional to $\tilde{\sigma}$, that in turn is proportional to either λ_{H} or λ_{BL} : cf. Eqs. (5.12) and (5.13). The case of spontaneous scalarization around BHs (studied in [80, 79]) can be recovered by setting $\tilde{\epsilon} = \tilde{p} = 0$.

The scalarization threshold can be analyzed by looking for the zero-energy ($\nu \sim 0$) bound state solutions of Eq. (5.31). In this case, the scalar field satisfies the following boundary conditions:

$$\Psi \sim \begin{cases} \varphi_c r & \text{as } r \rightarrow 0, \\ \varphi_\infty & \text{as } r \rightarrow \infty, \end{cases} \quad (5.34)$$

and we impose $\Psi'(r \rightarrow \infty) = 0$, where the prime denotes derivative with respect to r . To

obtain the scalarization threshold we integrate Eq. (5.31) outwards, starting from $r = 0$, with the above boundary conditions. Since the equation is linear, φ_c is arbitrary. At infinity we impose that the first derivative of Ψ with respect to r must be zero. This is a two-point boundary value problem that can be solved with a standard shooting method to find the critical value of the central density $\tilde{\epsilon}_c$ for which the above conditions are satisfied, given fixed values of β and λ_H (or λ_{BL}). The solution is some

$$\tilde{\epsilon}_i = \tilde{\epsilon}_i(\beta), \quad (5.35)$$

where $\tilde{\epsilon}_i$ is the smallest critical density at which scalarization can occur for the given β . The largest critical density producing scalarization can be similarly obtained by looking for zero-energy bound state solutions to find some

$$\tilde{\epsilon}_f = \tilde{\epsilon}_f(\beta). \quad (5.36)$$

It can be shown that in these two regimes (i.e., at the starting and ending points of the scalarization regime) the derivative of $\Psi'(r \rightarrow \infty)$ with respect to $\tilde{\epsilon}_c$ has opposite signs:

$$\frac{\partial}{\partial \tilde{\epsilon}_c} \Psi'(r \rightarrow \infty) \begin{cases} < 0 & \text{for } \tilde{\epsilon}_c = \tilde{\epsilon}_i, \\ > 0 & \text{for } \tilde{\epsilon}_c = \tilde{\epsilon}_f. \end{cases} \quad (5.37)$$

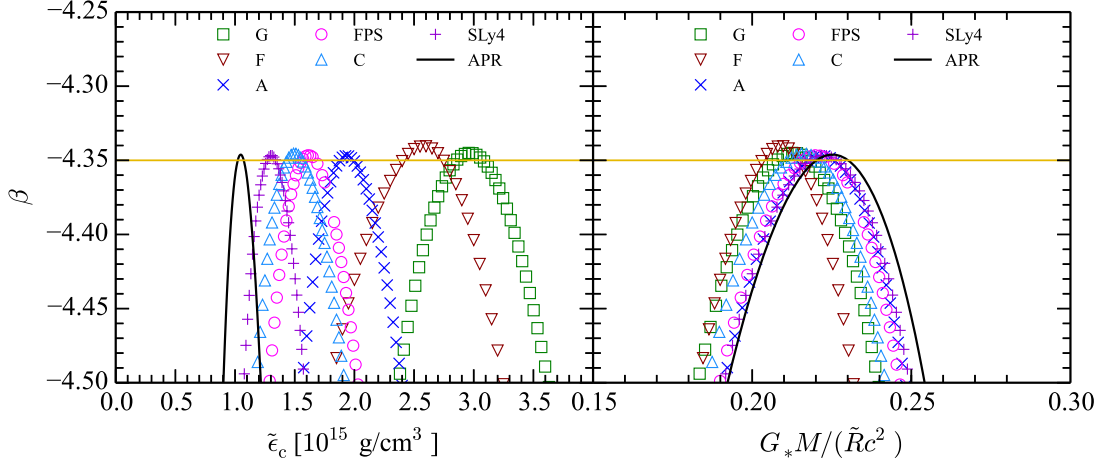


Figure 5.6: *Scalarization threshold.* Critical β for scalarization as a function of the central density (left panel) and of the stellar compactness (right panel) for nonrotating NS models constructed using different nuclear-physics based EOSs, in the absence of anisotropy.

As a warm-up, in Figure 5.6 we compute the scalarization threshold for nonrotating isotropic stars with several nuclear-physics based EOSs. The original references for the subset of EOSs used here can be found in [260] (the one exception is SLy4: cf. [155]). The EOSs are sorted by stiffness, with APR EOS being the stiffest and G EOS the softest in our catalog. As a trend, for stiffer EOSs scalarization occurs at lower values of the central densities and at higher values of the compactness. The most remarkable fact is that the value $\beta = \beta_{\max}$ above which scalarization cannot occur is very narrow: it ranges from $\beta_{\max} = -4.3462$ for APR EOS to $\beta_{\max} = -4.3405$ for F EOS [24]. This is consistent with Harada’s study based on catastrophe theory, that predicts a threshold value $\beta_{\max} \simeq -4.35$ (horizontal line in the figure) in the absence of anisotropy [199] (see also [336]).

In Table 5.1 we compare the values for $\tilde{\epsilon}_i$ and $\tilde{\epsilon}_f$ computed using (i) the linearized method described in this Section, and (ii) the full nonlinear set of equations for anisotropic models constructed using the APR EOS. The results agree remarkably well, showing that the onset of scalarization can be analyzed to an excellent degree of accuracy by neglecting the backreaction effects of the scalar field on the geometry. The last column of Table 5.1 lists β_{\max} , the value of β above which scalarization cannot happen. We do not present results for

λ_H	Linearized		Full nonlinear		
	$\tilde{\epsilon}_i(\text{g cm}^{-3})$	$\tilde{\epsilon}_f(\text{g cm}^{-3})$	$\tilde{\epsilon}_i(\text{g cm}^{-3})$	$\tilde{\epsilon}_f(\text{g cm}^{-3})$	β_{max}
-2	6.983×10^{14}	9.141×10^{14}	6.980×10^{14}	9.140×10^{14}	-4.150
-1	7.819×10^{14}	1.053×10^{15}	7.817×10^{14}	1.053×10^{15}	-4.239
0	9.021×10^{14}	1.216×10^{15}	9.021×10^{14}	1.216×10^{15}	-4.346
1	1.127×10^{15}	1.340×10^{15}	1.126×10^{15}	1.341×10^{15}	-4.471

Table 5.1: Critical density values obtained through the linearized theory and the full nonlinear equations for APR EOS, different values of the Horvat et al. anisotropy parameter λ_H and $\beta = -4.5$: for these choices of parameters, the solution is scalarized if $\tilde{\epsilon}_i < \tilde{\epsilon}_c < \tilde{\epsilon}_f$. The last column lists the critical value $\beta = \beta_{\text{max}}$ above which scalarization is not possible.

$\lambda_H = 2$ because the resulting β_{max} is already ruled out by binary pulsar observations [169].

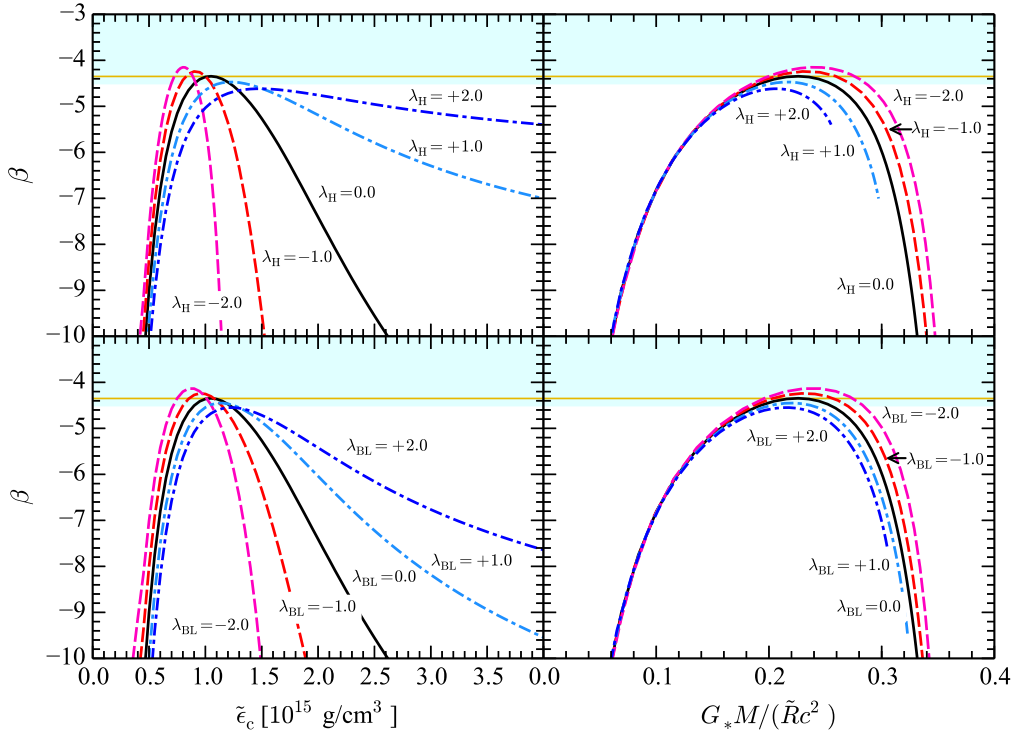


Figure 5.7: Influence of anisotropy on the scalarization threshold. Left panels: β versus critical central densities for different values of $\lambda_{H,BL}$. Right panels: β versus compactness $G_*M/\tilde{R}c^2$ of the critical solutions for different values of $\lambda_{H,BL}$.

In the left panels of Figure 5.7 we analyze the dependence of the critical β on the central density, focusing on EOS APR and selecting different values of the anisotropy parameters λ_{BL} (top) and λ_H (bottom). The shaded region at the top ($\beta \gtrsim -4.5$) is allowed

by current binary pulsar observations [169, 496]. The horizontal line is the roughly EOS-independent threshold $\beta_{\max} \simeq -4.35$ for isotropic stars. For a given theory, the starting and ending points of the scalarization regime are those for which a $\beta = \text{constant}$ (horizontal) line crosses the curves. Anisotropic models have two distinctive features: (1) when the tangential pressure is larger than the radial pressure (dashed lines in Figure 5.7) scalarization can occur even for $\beta \geq -4.35$ (for example, for the Horvat et al. model with $\lambda_{\text{H}} = -2$ we have $\beta_{\text{crit}} = -4.1513$, and for the Bowers-Liang model with $\lambda_{\text{BL}} = -2$ we have $\beta_{\text{crit}} = -4.1354$; cf. Table 5.1, Figure 5.4 and Figure 5.3); (2) when the tangential pressure is smaller than the radial pressure (dash-dotted lines in Figure 5.7) scalarized solutions may exist for a much wider range of $\tilde{\epsilon}_{\text{c}}$.

In the right panels of Figure 5.7 we plot the critical β as a function of the stellar compactness $G_*M/\tilde{R}c^2$. For low compactness ($M/\tilde{R} \lesssim 0.15$) all curves have the same behaviour regardless of λ_{H} or λ_{BL} . This universality has two reasons: (1) all modern nuclear-physics based EOS have the same Newtonian limit (cf. [357] for an analytic treatment of this regime for constant density stars); (2) for any given EOS, the effects of anisotropy are suppressed in the Newtonian regime, where pressures and densities are low and the local compactness parameter is small: cf. Eqs. (5.12) and (5.13).

5.5 Conclusions

Binary pulsar observations require $\beta \gtrsim -4.5$ [169, 496], and even more stringent constraints are expected in the near future. As shown in Figure 5.6, most “ordinary” nuclear-physics based EOSs for nuclear matter predict that scalarization can only occur for $\beta < \beta_{\max} = -4.35$. As binary pulsar observations get closer and closer to the limit $\beta \gtrsim -4.35$, the spontaneous scalarization mechanism originally proposed by Damour and Esposito-Farèse [118, 119] looks more and more unlikely to be realized in Nature if neutron stars are isotropic.

The admittedly unlikely event of a binary-pulsar observation of scalarization with $\beta > -4.35$ would be strong evidence for the presence of anisotropy, and it may even lead to

experimental constraints on the Skyrme model and QCD. An important caveat here is that *fast* rotation can also strengthen the effects of scalarization: according to [153], scalarization can occur for $\beta < -3.9$ when NSs spin at the mass-shedding limit. However the NSs found in binary pulsar systems are relatively old, are they are expected to spin well below the mass-shedding limit, where the slow-rotation approximation works very well [55].

Our work can be extended in several directions. An obvious extension is to consider the effects of anisotropy at second or higher order in the Hartle-Thorne expansion. This would allow us to assess whether the recently discovered “I-Love-Q” and “three-hair” universal relations between the multipole moments of the spacetime hold in the presence of anisotropy *and* scalarization [514, 515, 364, 510, 353]. In the context of GR, work towards this directions has recently been done by [518, 517, 512, 520]. A second obvious extension could consider fast rotating, anisotropic stars (cf. [153, 151]), the orbital and epicyclic frequencies around these objects [130, 154] and surface redshift [129, 376].

Anisotropy can lower the threshold for scalarization to occur, and this could be of interest to test ST theories through gravitational-wave asteroseismology [438, 439, 420] (we will discuss this in Chapter 6). We also remark that our study used simplified, phenomenological models for anisotropy, when of course it would be desirable to study realistic microphysical models. Last but not least, our study should be extended to evaluate the stellar sensitivities [497, 528], possible following [300], and to identify exclusion regions in the (β, λ) parameter space using binary pulsar observations (cf. e.g. [14]).

CHAPTER 6

TORSIONAL OSCILLATIONS OF NEUTRONS STARS IN SCALAR–TENSOR THEORY OF GRAVITY

6.1 Introduction

Observations of QPOs following giant flares in soft gamma-ray repeaters [234, 461, 462] suggest a close coupling between the seismic motion of the crust after a major quake and the modes of oscillations in a magnetar. The analysis of X-ray data in SGR 1900+14 [461] and SGR 1806-20 [462] has unveiled a number of periodicities, with frequencies that agree reasonably well with the expected torsional (or toroidal shear) oscillation modes of the NS crust: see e.g. [494] for a review, and [230] for recent progress in explaining apparent discrepancies between theoretical models and observations. These observations are very exciting because they allow us, for the very first time, to test NS oscillation models.

The foundations of crustal torsional oscillation theory in GR were laid in a classic paper by Schumaker and Thorne [406]. Recent work motivated by QPO observations explored how torsional oscillation frequencies are affected by various physical effects, including crustal elasticity [402], magnetic fields [422, 109, 173], superfluidity [440], the nuclear symmetry energy [134, 231, 441] and electron screening [430].

The main motivation of this chapter is to answer the following question: could torsional oscillation frequencies carry observable imprints of strong-field dynamics, and possibly hint at dynamics beyond GR? Vice versa, can we ignore effects due to hypothetical strong-field modifications of GR when we explore the dependence of torsional oscillation frequencies on the various physical mechanisms listed above?

We address these questions within the simplest class of modifications of GR, namely

ST theory. Damour and Esposito-Farèse [118] showed that a wide class of ST theories can pass Solar System tests and exhibit nonperturbative strong-field deviations away from GR (“spontaneous scalarization”) that can potentially be measured by observations of the bulk properties of NSs, and of binary systems containing NSs. The magnitude of these deviations is very sensitive to the value of a certain theory parameter β , defined in Eq. (6.16) below¹.

Static NSs in theories with spontaneous scalarization were first studied in [118]. Their stability was investigated using catastrophe theory by Harada [198, 199]. The formation of scalarized NSs in gravitational collapse was studied in [336, 338], and a possible mechanism to “seed” macroscopic scalar fields from quantum vacuum instabilities was recently suggested [283, 357, 314]. Slowly rotating NSs were studied at first [119, 429] and second [353] order in rotation by extending the Hartle-Thorne formalism [203, 204]. Recent work [153, 154, 151] addressed the properties of rapidly rotating NS models.

Widely-separated binary systems of compact objects in ST theory have been studied in [117, 119, 121], and the results have been combined with binary pulsar timing data in order to obtain bounds on scalar-matter coupling parameters, in particular β . Recent pulsar timing data continue to improve these bounds [169, 19]. Recently there has been interest in close binaries and mergers, and it was found that *dynamical scalarization* may take place: a close NS binary may scalarize even if the NSs would not scalarize in isolation [32, 415, 348]. The possibility of exploiting this mechanism in order to obtain bounds on scalar-matter coupling parameters from future gravitational wave observations has been explored in [400, 470].

A second motivation for this study comes from the surprising finding that there are universal “I-Love-Q” relations between a NS’s moment of inertia, tidal Love number and quadrupole moment in GR [514, 515]. These relations are “universal” in the sense that they are independent of the poorly known equation of state (EOS) of matter at high densities. Yagi and Yunes [514, 515] pointed out that if these relations were different in alternative theories of gravity, measurements of these bulk NS properties could be used to constrain alternative

¹There exists a threshold $\beta_c \sim -4.5$, whose exact value depends on the NS equation of state. Scalarization is possible when $\beta < \beta_c$.

theories or even hint at possible strong-field modifications of GR. However, stellar structure calculations in ST theories show that the I-Love-Q relations are remarkably insensitive to scalarization for values of the theory parameters allowed by binary pulsar tests [353, 151]. If the static properties of NSs (multipole moments and tidal deformation coefficients) cannot be used for this purpose, it seems natural to explore QPOs and torsional oscillation frequencies as promising observational avenues to look for smoking guns of new physics.

Several papers have investigated the signature of alternative theories of gravity on the NS oscillation spectrum. Blazquez-Salcedo et al. studied axial perturbations in Einstein-dilaton-Gauss-Bonnet theory [61]. Sotani et al. studied nonradial oscillations in ST gravity [438, 439, 432], tensor-scalar-vector [423, 424, 426, 428] and Eddington-inspired Born-Infeld gravity [433]. In particular, Refs. [438, 439] showed that the nonradial oscillation frequencies of NSs can change when the effects of scalarization are large enough to modify the bulk properties of the star by an appreciable amount. These studies were motivated by gravitational-wave asteroseismology, i.e. by the prospect of constraining the stellar properties and the EOS from direct observations of gravitational radiation from oscillating NSs. This is one of the major science goals of third-generation gravitational-wave detectors such as the Einstein Telescope, but it seems highly unlikely that we will measure NS oscillation accurately enough to constrain alternative theories of gravity with upcoming second-generation experiments, such as Advanced LIGO and Virgo (cf. [16, 17] for reviews). The connection between torsional oscillations and QPOs means that our results have more immediate experimental relevance.

Another noteworthy aspect of our study is that, whereas models of NSs in alternative theories of gravity usually adopt simple EOS models, none of these investigations have studied the effect of scalarization on the structure of the NS crust. Here we show quantitatively the connection between the crustal depth, the threshold for scalarization and the scalar field profile in a scalarized star.

6.1.1 Organization of this chapter

The plan of the chapter is as follows. In Sec. 6.2 we give the equations of hydrostatic equilibrium and we present numerical results for the equilibrium structure using different models for the EOS prevailing in the crust. In Sec. 6.3 we derive the perturbation equation describing torsional oscillations in ST theory in the Cowling approximation, and we describe the numerical method we used to solve the corresponding eigenvalue problem. Sec. 6.4 shows our numerical results for the oscillation spectra. In the conclusions, Sec. 6.5 we discuss the implications and possible extensions of our work. Appendix E provides the derivation of an approximate analytical expression for the ratio between the crust thickness and the stellar radius in ST theory, that generalizes a similar result by Samuelsson and Andersson [402] in GR. We carry out most of the work in the Einstein frame, but in Appendix F we show that the Einstein- or Jordan-frame formulations are equivalent, in the sense that the energy-momentum conservation law in either frame leads to the same perturbation equations.

6.2 Stellar models in scalar-tensor theory

6.2.1 Action and field equations

We consider the Einstein-frame action [118]

$$S = \frac{c^4}{16\pi G_*} \int d^4x \frac{\sqrt{-g_*}}{c} (R_* - 2g_*^{\mu\nu} \partial_\mu \varphi \partial_\nu \varphi) + S_M[\psi_M; A^2(\varphi)g_{*\mu\nu}] , \quad (6.1)$$

where G_* is the bare gravitational constant, $g_* \equiv \det[g_{*\mu\nu}]$ is the determinant of the Einstein-frame metric $g_{*\mu\nu}$, R_* is the Ricci curvature scalar of the metric $g_{*\mu\nu}$ and φ is a massless scalar field. S_M is the action of the matter fields ψ_M , coupled to the Einstein-frame metric $g_{*\mu\nu}$ and scalar field φ via the Jordan-frame metric $\tilde{g}_{\mu\nu} \equiv A^2(\varphi)g_{*\mu\nu}$, where $A(\varphi)$ is a conformal factor. Throughout this chapter we use geometrical units ($c = 1 = G_*$) and a mostly plus metric signature $(-, +, +, +)$. Quantities associated with the Einstein (Jordan) frame will be labeled with an asterisk (tilde).

The field equations of this theory, obtained by varying the action S with respect to $g_*^{\mu\nu}$ and φ , respectively, are given by

$$R_{*\mu\nu} = 2\partial_\mu\varphi\partial_\nu\varphi + 8\pi \left(T_{*\mu\nu} - \frac{1}{2}T_*g_{*\mu\nu} \right), \quad (6.2)$$

$$\square_*\varphi = -4\pi\alpha(\varphi)T_*, \quad (6.3)$$

where $R_{*\mu\nu}$ is the Ricci tensor, $\alpha(\varphi) \equiv d\log A(\varphi)/d\varphi$ is usually called the ‘‘scalar-matter coupling function’’, $T_*^{\mu\nu}$ is the matter field energy-momentum tensor defined as

$$T_*^{\mu\nu} \equiv \frac{2}{\sqrt{-g_*}} \frac{\delta S_M[\psi_M, A^2(\varphi)g_{*\mu\nu}]}{\delta g_{*\mu\nu}}, \quad (6.4)$$

and $T_* \equiv T_*^{\mu\nu}g_{*\mu\nu}$ is its trace. The energy-momentum tensor in the Jordan frame $\tilde{T}^{\mu\nu}$, with trace $\tilde{T} \equiv \tilde{T}^{\mu\nu}\tilde{g}_{\mu\nu}$, is defined as

$$\tilde{T}^{\mu\nu} \equiv \frac{2}{\sqrt{-\tilde{g}}} \frac{\delta S_M[\psi_M, \tilde{g}_{\mu\nu}]}{\delta \tilde{g}_{\mu\nu}}. \quad (6.5)$$

The energy-momentum tensors (and their traces) in these two conformally related representations of the theory are related as follows:

$$T_*^{\mu\nu} = A^6(\varphi)\tilde{T}^{\mu\nu}, \quad T_{*\mu\nu} = A^2(\varphi)\tilde{T}_{\mu\nu}, \quad T_* = A^4(\varphi)\tilde{T}. \quad (6.6)$$

Moreover, the covariant divergence of the energy-momentum tensor in the Einstein and Jordan frames can be shown to be

$$\nabla_{*\mu}T_*^{\mu\nu} = \alpha(\varphi)T_*\nabla_*^\nu\varphi, \quad (6.7)$$

$$\tilde{\nabla}_\mu\tilde{T}^{\mu\nu} = 0. \quad (6.8)$$

In the limit $\alpha(\varphi) \rightarrow 0$ the scalar field decouples from matter, and the theory reduces to GR.

6.2.2 The equations of hydrostatic equilibrium

The line element describing the space-time of a static, spherically symmetric star in Schwarzschild coordinates is given by

$$ds_*^2 = -e^{2\Phi} dt^2 + e^{2\Lambda} dr^2 + r^2 d\theta^2 + r^2 \sin^2 \theta d\phi^2 \quad (6.9)$$

in the Einstein frame, and by

$$d\tilde{s}^2 = A^2(\varphi) \left(-e^{2\Phi} dt^2 + e^{2\Lambda} dr^2 + r^2 d\theta^2 + r^2 \sin^2 \theta d\phi^2 \right) \quad (6.10)$$

in the Jordan frame, where Φ and Λ are functions of the radial coordinate r . By symmetry, the scalar field φ also depends only on r . We assume the energy-momentum tensor $\tilde{T}_{\mu\nu}$ to be that of a perfect fluid:

$$\tilde{T}_{\mu\nu} = (\tilde{\epsilon} + \tilde{p}) \tilde{u}_\mu \tilde{u}_\nu + \tilde{p} \tilde{g}_{\mu\nu}, \quad (6.11)$$

where $\tilde{\epsilon}$ is the energy density, \tilde{p} the pressure and \tilde{u}_μ the fluid's four-velocity. Using Eqs. (6.9) and (6.11), the field equations (6.2) and (6.3) yield the following equations that describe a static spherically symmetric star in hydrostatic equilibrium in ST theory [118, 119]:

$$\frac{dm}{dr} = 4\pi A^4(\varphi) r^2 \tilde{\epsilon} + \frac{1}{2} r(r-2m) \psi^2, \quad (6.12)$$

$$\frac{d\Phi}{dr} = 4\pi A^4(\varphi) \frac{r^2 \tilde{p}}{r-2m} + \frac{1}{2} r \psi^2 + \frac{m}{r(r-2m)}, \quad (6.13)$$

$$\frac{d\psi}{dr} = 4\pi A^4(\varphi) \frac{r}{r-2m} [\alpha(\varphi)(\tilde{\epsilon} - 3\tilde{p}) + r(\tilde{\epsilon} - \tilde{p})\psi] - \frac{2(r-m)}{r(r-2m)} \psi, \quad (6.14)$$

$$\frac{d\tilde{p}}{dr} = -(\tilde{\epsilon} + \tilde{p}) \left[\frac{d\Phi}{dr} + \alpha(\varphi)\psi \right]. \quad (6.15)$$

Here $m = m(r)$ is the mass function, defined in terms of $\Lambda(r)$ as $m \equiv (r/2)(1 - e^{-2\Lambda})$, and we introduced $\psi \equiv d\varphi/dr$.

Hereafter, following Damour and Esposito-Farèse [118, 119], we will focus on the ST

theory specified by the choice

$$A(\varphi) = e^{\frac{1}{2}\beta\varphi^2}. \quad (6.16)$$

For sufficiently large and negative values of β , as discussed in the introduction, NSs in this theory can undergo a phase transition called *spontaneous scalarization* and acquire a nonvanishing scalar charge associated with a nontrivial scalar field configuration. These scalarized solutions of the field equations are more energetically favorable than non-scalarized solutions.

To close this system of equations we must complement it with an EOS $\tilde{p} = \tilde{p}(\tilde{\epsilon})$. In this chapter, we construct our stellar models adopting two EOSs for the NS core, namely EOS APR [10] and EOS MS0 [328], while for the NS crust we use the EOSs derived by Kobyakov and Pethick (henceforth KP, [255]) and by Douchin and Haensel (henceforth DH, [155]). These crust EOSs have densities $\tilde{\epsilon}_b$ at the crust basis equal to $\tilde{\epsilon}_b = 1.504 \times 10^{14}$ g/cm³ for EOS KP, and $\tilde{\epsilon}_b = 1.285 \times 10^{14}$ g/cm³ for EOS DH. For a comparison between the physical assumptions involved in the construction of these two EOSs, see e.g. [430]. In Fig. 6.1 we display the relation between pressure and energy density for EOSs DH and KP.

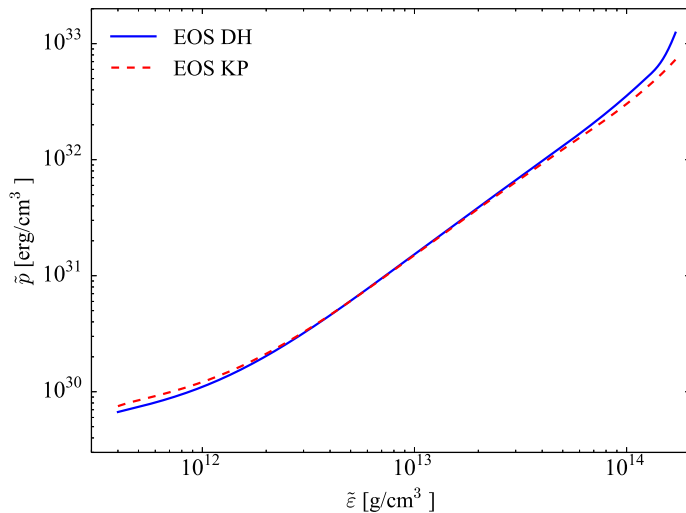


Figure 6.1: *The crustal equations of state.* Pressure \tilde{p} versus energy density $\tilde{\epsilon}$ for the crust EOSs considered in this work: EOS DH (solid line) and EOS KP (dashed line).

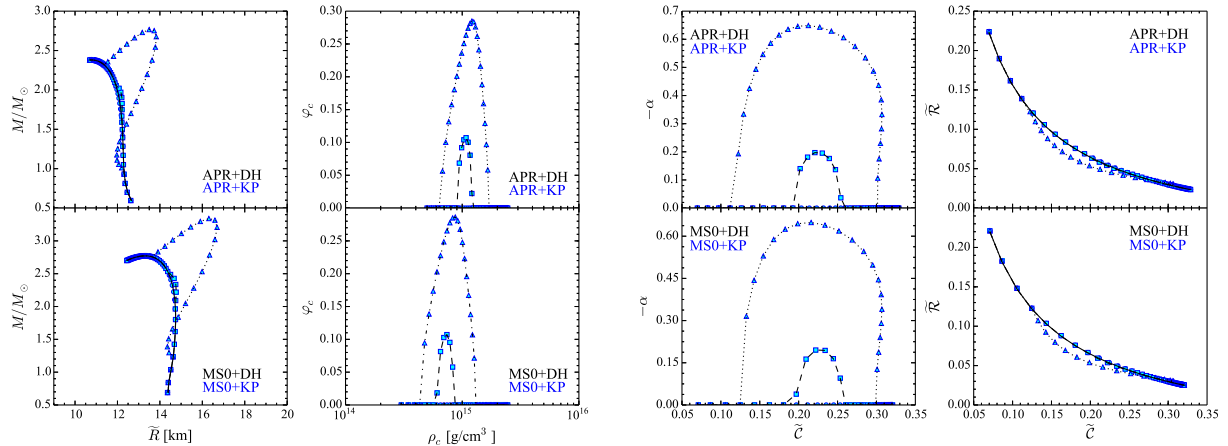


Figure 6.2: *Properties of our stellar models in ST theory.* From left to right we show: the mass-radius relation, the scalar field at the center of the star φ_c as a function of the central density $\tilde{\epsilon}_c$, the dimensionless ratio $-\alpha = Q/M$ as a function of the compactness \tilde{C} and the fractional crust thickness \tilde{R} as a function of \tilde{C} . The choice of crustal EOS does not sensibly affect the crust thickness and the onset of scalarization. In all panels, curves with various linestyles correspond to stellar models using EOS DH for the NS crust: solid lines correspond to $\beta = 0.0$, dashed lines to $\beta = -4.5$, and dotted lines to $\beta = -6.0$. Different symbols correspond to stellar models using EOS KP for the crust: circles for $\beta = 0.0$, squares for $\beta = -4.5$ and triangles for $\beta = -6.0$.

6.2.3 Numerical results for unperturbed stars

To obtain the equilibrium stellar models we integrate numerically Eqs. (6.12)-(6.15) outwards starting from $r = 0$ with initial conditions $m(0) = 0$, $\Phi(0) = \Phi_c$, $\varphi(0) = \varphi_c$, $\psi(0) = 0$ and $\tilde{\epsilon}(0) = \tilde{\epsilon}_c$, using one of the two EOSs (APR or MS0) for the core region. The point $r = r_b$ such that $\tilde{\epsilon}(r_b) = \tilde{\epsilon}_b$ determines the location of the crust basis. The integration then proceeds until we reach a point $r = r_s$ for which $\tilde{p}(r_s) = 0$, which defines the Einstein-frame radius of the star. The radii r_b and r_s can be converted to the physical (Jordan) frame using the relations $\tilde{R}_b = A(\varphi_b) r_b$ and $\tilde{R} = A(\varphi_s) r_s$, where $\varphi_b = \varphi(r_b)$ and $\varphi_s = \varphi(r_s)$. We can then define the crust thickness as $\Delta\tilde{R} \equiv \tilde{R} - \tilde{R}_b$. For convenience, we also introduce the dimensionless fractional crust thickness $\tilde{\mathcal{R}} \equiv \Delta\tilde{R}/\tilde{R}$. We remark that the theory is invariant under reflection symmetry ($\varphi \rightarrow -\varphi$), and therefore, for simplicity, we shall only consider positive values of the scalar field.

At spatial infinity ($r \rightarrow \infty$) the metric $g_{*\mu\nu}$ and the scalar field φ behave asymptoti-

cally as

$$g_{*tt} = -1 + \frac{2M}{r} + \mathcal{O}\left(\frac{1}{r^2}\right), \quad (6.17a)$$

$$g_{*rr} = 1 + \frac{2M}{r} + \mathcal{O}\left(\frac{1}{r^2}\right), \quad (6.17b)$$

$$\varphi = \varphi_\infty + \frac{Q}{r} + \mathcal{O}\left(\frac{1}{r^2}\right), \quad (6.17c)$$

where M is the ADM mass and Q is the scalar charge. The values of the various variables at the stellar surfaces (labeled with the subscript s) can be used to calculate M , Q and the asymptotic value of the scalar field $\varphi_\infty \equiv \varphi(r \rightarrow \infty)$ via the following expressions [118]:

$$M = r_s^2 \Phi'_s \left(1 - \frac{2m_s}{r_s}\right)^{1/2} \exp \left\{ -\frac{\Phi'_s}{(\Phi_s'^2 + \psi_s^2)^{1/2}} \operatorname{arctanh} \left[\frac{(\Phi_s'^2 + \psi_s^2)^{1/2}}{\Phi'_s + 1/r_s} \right] \right\}, \quad (6.18)$$

$$Q = -\frac{\psi_s}{\Phi'_s} M, \quad (6.19)$$

$$\varphi_\infty = \varphi_s + \frac{\psi_s}{(\Phi_s'^2 + \psi_s^2)^{1/2}} \operatorname{arctanh} \left[\frac{(\Phi_s'^2 + \psi_s^2)^{1/2}}{\Phi'_s + 1/r_s} \right], \quad (6.20)$$

where Φ'_s can be calculated with the aid of Eq. (6.13) as

$$\Phi'_s = \frac{1}{2} r_s \psi_s^2 + \frac{m_s}{r_s (r_s - 2m_s)}, \quad (6.21)$$

and primes indicate partial derivatives with respect to the radial coordinate r . From now on, we will assume that $\varphi_\infty = 0$.

To obtain solutions of Eqs. (6.12)-(6.15) satisfying this assumption, we apply the shooting method in order to find the central values of the scalar field φ_c such that the required value of φ_∞ is obtained. As a check of our code we compared our results against the ones presented in Refs. [154] (in ST theory) and [260, 55] (in GR), finding excellent agreement.

In Fig. 6.2 we present general properties of stellar models constructed by solving

Eqs. (6.12)-(6.15) combining EOS APR and EOS MS0 (for the NS core) with EOS KP and EOS DH (for the NS crust). The top row refers to the APR EOS, and the bottom row refers to the MS0 EOS; results for different crust models are shown using different linestyles in each inset.

The leftmost column shows the mass-radius relation. Deviations from GR due to spontaneous scalarization are clearly visible; we also see that the choice of crustal EOS has negligible influence on the mass-radius relation, for both “ordinary” and scalarized stars. The second column shows the central value of the scalar field φ_c as a function of the central density $\tilde{\epsilon}_c$. The scalar field at the center acquires a nonzero value (i.e., the NS becomes scalarized) around $\tilde{\epsilon}_c \approx 4 \times 10^{14} - 6 \times 10^{14} \text{ g/cm}^3$, and it has a maximum around $\tilde{\epsilon}_c \approx 7 \times 10^{14} - 9 \times 10^{14} \text{ g/cm}^3$. In the third column we plot the dimensionless scalar charge $\alpha \equiv -Q/M$ as a function of the compactness $\tilde{\mathcal{C}} \equiv M/\tilde{R}$ (both expressed in geometrical units). Finally, the rightmost column shows $\tilde{\mathcal{R}}$ as a function of the compactness $\tilde{\mathcal{C}}$. In comparison with their GR counterparts, for scalarized stars the crust represents a smaller fraction of the NS interior. Note also that deviations in the crust thickness due to scalarization and nonzero scalar charges develop in the same range of compactness $\tilde{\mathcal{C}}$, as expected.

These plots show that the choice of crustal EOS has negligible effects on the bulk properties of the star. This is not surprising, considering that EOSs DH and KP have very similar crust basis densities $\tilde{\epsilon}_b$ and $\tilde{p}(\tilde{\epsilon})$ (cf. Fig. 6.1). However, as we will see in Sec. 6.3.2, different crustal EOSs result in rather different elastic properties for the crust, and they do have an effect on torsional oscillation frequencies.

6.2.4 An approximate formula for \mathcal{R}

Samuelsson and Andersson [402] obtained a simple approximate analytical expression for the ratio between the crust thickness and stellar radius \mathcal{R} , within GR, in terms of the star’s compactness \mathcal{C} :

$$\mathcal{R} = \left(\frac{\mathcal{C}}{\sigma} e^{2\Lambda} + 1 \right)^{-1}, \quad (6.22)$$

where $e^{-2\Lambda} = 1 - 2\mathcal{C}$ and $\sigma \approx 0.02326$ is a constant found by curve fitting, which in general depends on the crustal EOS [401].

In Appendix E we show that this result can be generalized to ST theory as follows:

$$\mathcal{R} = \frac{\sigma}{2\beta\zeta} \left(\mathcal{F} - \sqrt{\mathcal{F}^2 - \frac{4\beta\zeta}{\sigma}} \right), \quad (6.23)$$

where we introduced

$$\mathcal{F} \equiv 1 + \frac{1}{\sigma} (\mathcal{C}e^{2\Lambda} + \beta\zeta) \quad (6.24)$$

and $\zeta = \zeta(\mathcal{C}) \equiv \varphi_s \psi_s r_s$, which is obtained by interpolation, given a family of stellar models, as a function of \mathcal{C} . We make the same approximations used in [402], and in addition we assume the scalar field to be constant throughout the NS crust. From Eq. (6.23) we can also calculate the first correction to Eq. (6.22) in powers of $\beta\zeta$, due the presence of the scalar field in a scalarized NS:

$$\mathcal{R} \approx \left(\frac{\mathcal{C}}{\sigma} e^{2\Lambda} + 1 \right)^{-1} - 2\mathcal{C}e^{2\Lambda} \frac{(\beta\zeta)^2}{\sigma^3} \left(\frac{\mathcal{C}}{\sigma} e^{2\Lambda} + 1 \right)^{-3}, \quad (6.25)$$

where the minus sign indicates that \mathcal{R} is smaller for such stars in comparison to nonscalarized ones, as observed in Figs. 6.2 and 6.3.

To illustrate how accurately Eq. (6.23) describes the behavior of \mathcal{R} observed in Fig. 6.2, in Fig. 6.3 we plot \mathcal{R} , choosing EOS APR to describe the NS core, as a function of \mathcal{C} for $\beta = -6.0$ (the case in which deviations from GR are greatest). We find good agreement between the approximate expression and data obtained by numerically solving Eqs. (6.12)-(6.15). As can be seen, the same value of σ obtained in [402] for the EOS used in [401] is accurate enough for both EOS DH and EOS KP.

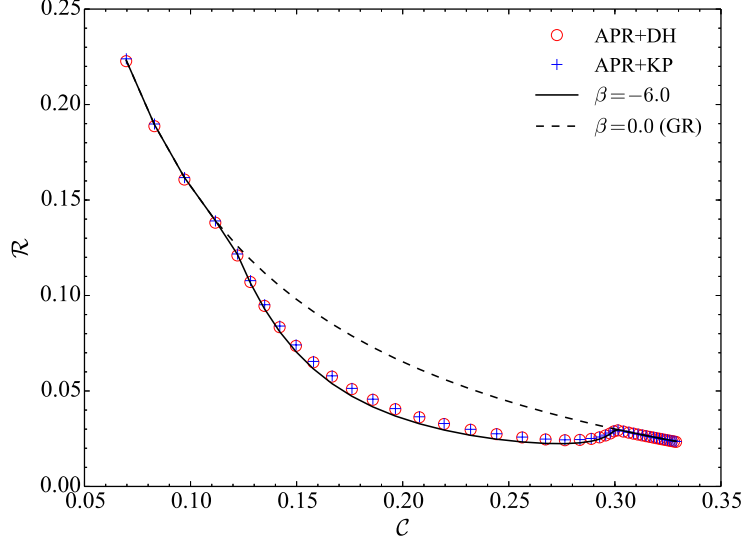


Figure 6.3: *Fractional crust thickness of scalarized stars.* Comparison between Eq. (6.23) and the numerical results for $\beta = -6.0$, using $\sigma = 0.02326$. The GR expression (6.22) is also shown. Since the integration of Eqs. (6.12)-(6.15), gives us φ in the Einstein-frame radial coordinate r , the compactness and fractional crust thickness are evaluated in this frame. Notice, however, that even for $\beta = -4.5$ (a value marginally excluded by binary pulsars observations [169]) the percent difference between the compactnesses and fractional crust thicknesses in the two frames is less than 1.0%, and therefore Eq. (6.23) is accurate for all physically sensible values of β .

6.3 Torsional perturbations in the Cowling approximation

6.3.1 Derivation of the perturbation equations

Let us now derive the equation describing torsional oscillations in ST theory. We begin by introducing a small fluid perturbation described by a Lagrangian displacement vector

$$\tilde{\xi}^i = \left(0, 0, \tilde{\mathcal{Y}}(t, r) \frac{1}{\sin \theta} \partial_\theta P_\ell(\cos \theta) \right), \quad (6.26)$$

where $P_\ell(\cos \theta)$ is the Legendre polynomial of order ℓ . For notational convenience, in Eq. (6.26) we omit the sum over ℓ . The perturbation of the fluid four-velocity $\delta \tilde{u}^3 = \tilde{u}^0 (\partial \tilde{\xi}^3 / \partial t)$ is

$$\delta \tilde{u}^3 = A^{-1}(\varphi) e^{-\Phi} \dot{\tilde{\mathcal{Y}}}(t, r) \frac{1}{\sin \theta} \partial_\theta P_\ell(\cos \theta), \quad (6.27)$$

where the dot represents a partial derivative with respect to the time coordinate t .

In this work we use the Cowling approximation [308, 164], i.e. we assume that matter perturbations do not result in perturbations on the metric $\tilde{g}_{\alpha\beta}$: $\delta\tilde{g}_{\mu\nu} = 0$. In spherically symmetric, perfect fluid NSs, the pressure \tilde{p} , the energy density $\tilde{\epsilon}$ and the scalar field φ are unaffected by odd (axial) perturbations (see e.g. [91] for a discussion within GR). Metric perturbations are effectively variations of the gravitational potential induced by fluid perturbations (in GR) and scalar field perturbations (in ST theory). Therefore the Cowling approximation is adequate to study torsional oscillations, that are odd (axial) in character. Within this approximation, the perturbed perfect fluid energy-momentum tensor (6.11), including the shear tensor contribution $\delta\tilde{S}_{\mu\nu}$, is

$$\delta\tilde{T}_{\mu\nu} = (\tilde{p} + \tilde{\epsilon}) (\delta\tilde{u}_\mu\tilde{u}_\nu + \tilde{u}_\mu\delta\tilde{u}_\nu) - 2\tilde{\mu}\delta\tilde{S}_{\mu\nu}. \quad (6.28)$$

where we have introduced the shear modulus $\tilde{\mu} = \tilde{\mu}(r)$. While the first term in Eq. (6.28) is simple to calculate, to obtain $\delta\tilde{S}_{\mu\nu}$ we must first use the fact that $\delta\tilde{\sigma}_{\mu\nu} \equiv \mathcal{L}_{\tilde{u}}\delta\tilde{S}_{\mu\nu} = A^{-1}(\varphi)\exp(-\Phi)\partial_0\delta\tilde{S}_{\mu\nu}$, where the perturbed rate of shear $\delta\tilde{\sigma}_{\mu\nu} = \delta\tilde{\sigma}_{\nu\mu}$ is given by

$$\begin{aligned} \delta\tilde{\sigma}_{\mu\nu} = & \frac{1}{2} \left(\delta\tilde{P}^\alpha{}_\nu \tilde{\nabla}_\alpha \tilde{u}_\mu + \delta\tilde{P}^\alpha{}_\mu \tilde{\nabla}_\alpha \tilde{u}_\nu + \tilde{P}^\alpha{}_\nu \tilde{\nabla}_\alpha \delta\tilde{u}_\mu + \tilde{P}^\alpha{}_\mu \tilde{\nabla}_\alpha \delta\tilde{u}_\nu \right) \\ & - \frac{1}{3} \left(\delta\tilde{P}_{\mu\nu} \tilde{\nabla}_\alpha \tilde{u}^\alpha + \tilde{P}_{\mu\nu} \tilde{\nabla}_\alpha \delta\tilde{u}^\alpha \right), \end{aligned} \quad (6.29)$$

$\delta\tilde{P}_{\mu\nu}$ denotes the perturbed projection operator

$$\delta\tilde{P}_{\mu\nu} = \delta\tilde{u}_\mu\tilde{u}_\nu + \tilde{u}_\mu\delta\tilde{u}_\nu, \quad (6.30)$$

and $\mathcal{L}_{\tilde{u}}$ is the Lie derivative along the worldline of a fluid element [406]. The nonzero

components of the perturbed rate of shear $\delta\tilde{\sigma}_{\mu\nu}$ can then be shown to be

$$\delta\tilde{\sigma}_{13} = \frac{1}{2}A(\varphi)e^{-\Phi}\dot{\mathcal{Y}}'(t, r)r^2\sin\theta\partial_\theta P_\ell(\cos\theta), \quad (6.31)$$

$$\delta\tilde{\sigma}_{23} = \frac{1}{2}A(\varphi)e^{-\Phi}\dot{\mathcal{Y}}(t, r)r^2\sin^2\theta\partial_\theta\left[\frac{1}{\sin\theta}\partial_\theta P_\ell(\cos\theta)\right]. \quad (6.32)$$

Using Eqs. (6.31) and (6.32), the perturbed shear tensor has components

$$\delta\tilde{S}_{13} = \frac{1}{2}A^2(\varphi)\tilde{\mathcal{Y}}'(t, r)r^2\sin\theta\partial_\theta P_\ell(\cos\theta), \quad (6.33)$$

$$\delta\tilde{S}_{23} = \frac{1}{2}A^2(\varphi)\tilde{\mathcal{Y}}(t, r)r^2\sin^2\theta\partial_\theta\left[\frac{1}{\sin\theta}\partial_\theta P_\ell(\cos\theta)\right]. \quad (6.34)$$

Combining these results, we find that the nonzero components of the perturbed energy-momentum tensor are

$$\delta\tilde{T}_{03} = -(\tilde{p} + \tilde{\epsilon})A^2(\varphi)\dot{\mathcal{Y}}r^2\sin\theta\partial_\theta P_\ell(\cos\theta), \quad (6.35)$$

$$\delta\tilde{T}_{13} = -\tilde{\mu}A^2(\varphi)\tilde{\mathcal{Y}}'(t, r)r^2\sin\theta\partial_\theta P_\ell(\cos\theta), \quad (6.36)$$

$$\delta\tilde{T}_{23} = -\tilde{\mu}A^2(\varphi)\tilde{\mathcal{Y}}(t, r)r^2\sin^2\theta\partial_\theta\left[\frac{1}{\sin\theta}\partial_\theta P_\ell(\cos\theta)\right]. \quad (6.37)$$

In the GR limit – obtained by taking $A(\varphi) = 1$, and consequently $\alpha(\varphi) = 0$ – the above results are in agreement with [406] when we neglect metric perturbations in their equations.

In the Cowling approximation, the variation of the energy-momentum conservation law in the Jordan frame [438] can be obtained from Eq. (6.8)

$$\begin{aligned} \tilde{\nabla}_\nu\delta\tilde{T}^\nu{}_\mu &= \partial_\nu\delta\tilde{T}^\nu{}_\mu + \Gamma_{*\alpha\nu}^\nu\delta\tilde{T}^\alpha{}_\mu - \Gamma_{*\mu\nu}^\alpha\delta\tilde{T}^\nu{}_\alpha + 4\alpha(\varphi)\partial_\alpha\varphi\delta\tilde{T}^\alpha{}_\mu - \alpha(\varphi)\partial_\mu\varphi\delta\tilde{T}^\alpha{}_\alpha \\ &= 0, \end{aligned} \quad (6.38)$$

where $\Gamma_{*\mu\nu}^\alpha$ denotes the Christoffel symbols of the Einstein-frame metric, related to they

Jordan frame counterparts by

$$\tilde{\Gamma}_{\mu\nu}^{\sigma} = \Gamma_{*\mu\nu}^{\sigma} + \alpha(\varphi) \left(\delta_{\nu}^{\sigma} \partial_{\mu} \varphi + \delta_{\mu}^{\sigma} \partial_{\nu} \varphi - g_{*}^{\sigma\rho} g_{*\mu\nu} \partial_{\rho} \varphi \right). \quad (6.39)$$

In Appendix F we show that Eq. (6.38) can also be obtained starting from the energy-momentum conservation law (6.7) in the Einstein frame, and therefore the perturbation equations in the two frames are equivalent.

By setting $\mu = 3$ and making use of Eqs. (6.35)-(6.37) we obtain the following differential equation for $\tilde{\mathcal{Y}}(t, r)$:

$$\tilde{\mathcal{Y}}''(r) + \left[\frac{4}{r} + \Phi' - \Lambda' + \frac{\tilde{\mu}'}{\tilde{\mu}} + 4\alpha(\varphi)\psi \right] \tilde{\mathcal{Y}}'(r) + \left[\left(\frac{\omega}{\tilde{v}_s} \right)^2 e^{-2\Phi} - \frac{(\ell+2)(\ell-1)}{r^2} \right] e^{2\Lambda} \tilde{\mathcal{Y}}(r) = 0,$$

where we have assumed a harmonic time dependence $\tilde{\mathcal{Y}}(t, r) = \tilde{\mathcal{Y}}(r)e^{i\omega t}$ for the perturbation variable, and we have introduced the shear wave velocity $\tilde{v}_s^2 \equiv \tilde{\mu}/(\tilde{p} + \tilde{\epsilon})$.

We can recast Eq. (6.40) in a form identical to the GR case (cf. [406, 430]) if we introduce an effective shear modulus $\tilde{\mu}_{\text{eff}} \equiv A^4(\varphi)\tilde{\mu}$, an effective wave velocity $\tilde{v}_{\text{eff}}^2 \equiv A^4(\varphi)\tilde{v}_s^2$ and a rescaled frequency $\tilde{\omega} = A^2(\varphi)\omega$:

$$\tilde{\mathcal{Y}}''(r) + \left[\frac{4}{r} + \Phi' - \Lambda' + \frac{\tilde{\mu}'_{\text{eff}}}{\tilde{\mu}_{\text{eff}}} \right] \tilde{\mathcal{Y}}'(r) + \left[\left(\frac{\tilde{\omega}}{\tilde{v}_{\text{eff}}} \right)^2 e^{-2\Phi} - \frac{(\ell+2)(\ell-1)}{r^2} \right] e^{2\Lambda} \tilde{\mathcal{Y}}(r) = 0. \quad (6.40)$$

Given the definition of the conformal factor (6.16), the factor $A^4(\varphi)$ is always less than unity when $\beta < 0$, and therefore $\tilde{\mu}_{\text{eff}}/\tilde{\mu} \leq 1$.

To obtain the oscillation frequencies we must integrate Eq. (6.40) numerically with appropriate boundary conditions. We assume that torsional oscillations are confined to the NS crust, so our boundary conditions are a zero-torque condition at $r = r_s$ and a zero-traction condition at r_b . These boundary conditions follow from the fact that the shear modulus is zero in the NS core and outside the star, and they imply that $\tilde{\mathcal{Y}}(r)$ must satisfy Neumann boundary conditions, i.e. $\tilde{\mathcal{Y}}'(r) = 0$ at both $r = r_b$ and $r = r_s$ [406, 430, 422].

Our integrations of Eq. (6.40) are performed in the Einstein frame, but since $\varphi_\infty = 0$, the torsional oscillation frequencies measured at infinity are the same in the Einstein and Jordan frames.

Following common practice in the literature, we will present numerical results for the torsional oscillation frequencies ${}_n t_\ell \equiv \omega/(2\pi)$. Here n is the number of radial nodes of the function $\tilde{\mathcal{Y}}(r)$ in the crust region, and ℓ is the usual angular index associated with the Legendre polynomials $P_\ell(\cos\theta)$.

6.3.2 The shear modulus

Torsional oscillations depend on the elastic properties of the solid NS crust [88], characterized by the shear stress tensor². A crucial element in describing the elastic properties of the NS crust is the shear modulus $\tilde{\mu}$. Assuming the NS crust to be a body-centered cubic (bcc) lattice, Ogata and Ichimaru [340] (see also [460]) showed that the shear modulus in the limit of zero temperature can be approximated as

$$\tilde{\mu} = 0.1194 n \frac{(Ze)^2}{\tilde{a}}, \quad (6.41)$$

where n is the ion number density, Ze the charge of the nuclei and $\tilde{a}^3 = 3/(4\pi n)$ is the radius of the Wigner-Seitz cell containing one nucleus. Although it is often assumed that the electrons are uniformly distributed in the NS crust, one can also calculate the correction to the shear modulus due a nonuniformity of the electron density distribution, i.e. electron screening effects [255, 227]. Kobayakov and Pethick [255] obtained the following electron screening correction term to Eq. (6.41):

$$\tilde{\mu} = 0.1194 n \left(1 - 0.010 Z^{2/3}\right) \frac{(Ze)^2}{\tilde{a}}. \quad (6.42)$$

²Any deformation of an elastic medium can be decomposed into compressional and shear components. Matter in the NS crust is essentially incompressible, and this is why only a shear stress tensor is studied in the literature [88, 340].

For $Z = 40$, electron screening can reduce the shear modulus by $\approx 11.7\%$. As discussed in [430], this reduces the fundamental mode frequency ${}_0t_2$ by roughly 6% in GR, independently of whether we use EOS DH or KP.

In our calculations we consider both Eqs. (6.41) and (6.42) to see whether one would be able, in principle, to distinguish modifications of the torsional oscillations spectrum due to a modified theory of gravity from microphysics effects (electron screening being one of the simplest examples to investigate).

The impact of electron screening effects can be visualized by plotting the shear velocity $\tilde{v}_s^2 = \tilde{\mu}/(\tilde{\epsilon} + \tilde{p})$ in the crust region. Fig. 6.4 shows \tilde{v}_s^2 for NS models in GR and in a ST theory with $\beta = -6.0$, using both EOS DH and KP, with and without electron screening effects. All NS models shown in the figure have radius $R = 15.21$ km and mass $M = 2.046 M_\odot$. The (density-weighted) shear velocity

$$\langle \tilde{v}_s \rangle = \frac{\int_{r_b}^{r_s} \tilde{\epsilon}(r) \tilde{v}_s(r) r^2 dr}{\int_{r_b}^{r_s} \tilde{v}_s(r) r^2 dr}, \quad (6.43)$$

is always close to $\approx 1 \times 10^8$ cm/s, in remarkable agreement with early estimates by Schumaker and Thorne [406] (see also [196]).

6.3.3 Numerical procedure

To numerically integrate Eq. (6.40) and obtain the frequencies ${}_n t_\ell$, it is convenient to introduce two new variables $\tilde{\mathcal{Y}}_1(r)$ and $\tilde{\mathcal{Y}}_2(r)$, defined as

$$\tilde{\mathcal{Y}}_1(r) \equiv r^{1-\ell} \tilde{\mathcal{Y}}(r), \quad (6.44)$$

$$\tilde{\mathcal{Y}}_2(r) \equiv \tilde{\mu}_{\text{eff}} e^{\Phi-\Lambda} r^{2-\ell} \tilde{\mathcal{Y}}'(r). \quad (6.45)$$

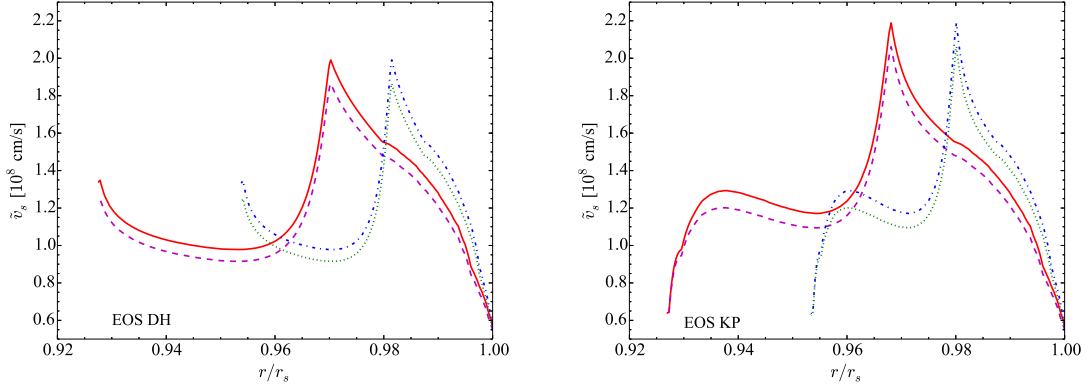


Figure 6.4: *Shear velocity in scalarized stars.* Shear velocity profile $\tilde{v}_s(r)$ in the NS crust in the following cases: (i) GR without electron screening (solid line); (ii) GR with electron screening (dashed line); (iii) ST theory ($\beta = -6.0$) without electron screening (dashed-dotted line); (iv) ST theory ($\beta = -6.0$) with electron screening (dotted line). The top panel refers to EOS DH, the bottom panel to EOS KP. The sharp peaks occur near the neutron drip density $\tilde{\epsilon} \approx 3 \times 10^{11}$ g/cm³ [412].

In terms of these variables, Eq. (6.40) can be decomposed into a system of two first-order coupled differential equations:

$$\tilde{\mathcal{Y}}_1'(r) = -\frac{\ell-1}{r} \tilde{\mathcal{Y}}_1(r) + \frac{e^{\Lambda-\Phi}}{\tilde{\mu}_{\text{eff}} r} \tilde{\mathcal{Y}}_2(r), \quad (6.46)$$

$$\tilde{\mathcal{Y}}_2'(r) = -\frac{\ell+2}{r} \tilde{\mathcal{Y}}_2(r) - e^{\Phi+\Lambda} \left[(\tilde{\epsilon} + \tilde{p}) r \tilde{\omega}^2 e^{-2\Phi} - (\ell+2)(\ell-1) \frac{\tilde{\mu}_{\text{eff}}}{r} \right] \tilde{\mathcal{Y}}_1(r). \quad (6.47)$$

The advantage of this approach is that it eliminates the necessity of computing the derivative of the shear modulus $\tilde{\mu}$, which is known only in tabulated form. In terms of $\tilde{\mathcal{Y}}_2(r)$, the zero-traction and zero-torque conditions translate into the requirements that $\tilde{\mathcal{Y}}_2(r_b) = \tilde{\mathcal{Y}}_2(r_s) = 0$. The same change of variables was used in [422] in the context of magnetized stars (see also [315]).

Using Eqs. (6.46) and (6.47) we can now find the frequencies ${}_n t_\ell$ by applying a shooting method (see e.g. [260]). Choosing $\tilde{\mathcal{Y}}_1(r)$ to be normalized to unity, and setting $\tilde{\mathcal{Y}}_2(r) = 0$ at the stellar surface $r = R$, we integrate Eqs. (6.12)-(6.15), (6.46) and (6.47) inwards for a trial value of ω until we reach the crust basis at $r = r_b$, where we must have $\tilde{\mathcal{Y}}_2(r_b) = 0$.

Depending on whether or not this condition is satisfied, we adjust the trial value of ω until we find $\tilde{\mathcal{Y}}_2(r_b) = 0$ within a certain tolerance. In this way the determination of ω becomes a root finding problem, which can be solved using (for instance) the bisection method.

6.4 The oscillation spectra

With our equilibrium NS models and our numerical framework to deal with crustal perturbations, we are finally in a position to compute and discuss the spectrum of torsional oscillation frequencies in ST theory. The spectrum depends quite sensitively on the bulk properties of the star (mass M , radius \tilde{R} , crust thickness $\Delta\tilde{R}$), on the choice of crustal EOS, and on the scalar field profile in the crust region.

In Fig. 6.5 we show the torsional oscillation frequencies for the fundamental mode ${}_0t_2$ (top panels) and first overtone ${}_1t_2$ (bottom panels) as a function of the mass M for NS models with all possible combinations of core EOS (MS0, APR) and crust EOS (DH, KP). We show results for three different values of β : $\beta = 0$ (GR), $\beta = -4.5$ (marginally excluded by binary pulsar observations) and $\beta = -6$ (observationally excluded, but shown nonetheless to maximize the effects of scalarization). By comparing the left and right panels we can quantify the influence of electron screening effects (everything else being the same): electron screening typically lowers the oscillation spectra, in agreement with the findings of Ref. [430]. For stellar models built using EOS MS0 and for the conservative value $\beta = -4.5$, modifications from GR occur at values of $M \simeq 2.0 M_\odot$, close to the largest observed NS mass [138, 19]. Therefore from now on we will focus on EOS APR.

Notice that the first overtone is more sensitive to scalarization than the fundamental mode. This is confirmed in Fig. 6.6, where we show the frequencies of the ${}_0t_\ell$ and ${}_1t_\ell$ modes for a fixed stellar mass $M = 1.8 M_\odot$ as a function of β . Newtonian estimates [196] (see also [402] for GR with similar conclusion), show that the overtones scale roughly as $\approx n/\Delta\tilde{R}$ and are essentially independent of ℓ , as long as ℓ is not much larger than n . As shown by Eq. (6.23) and in Fig. 6.3, scalarization decreases the crust thickness. The shrinking

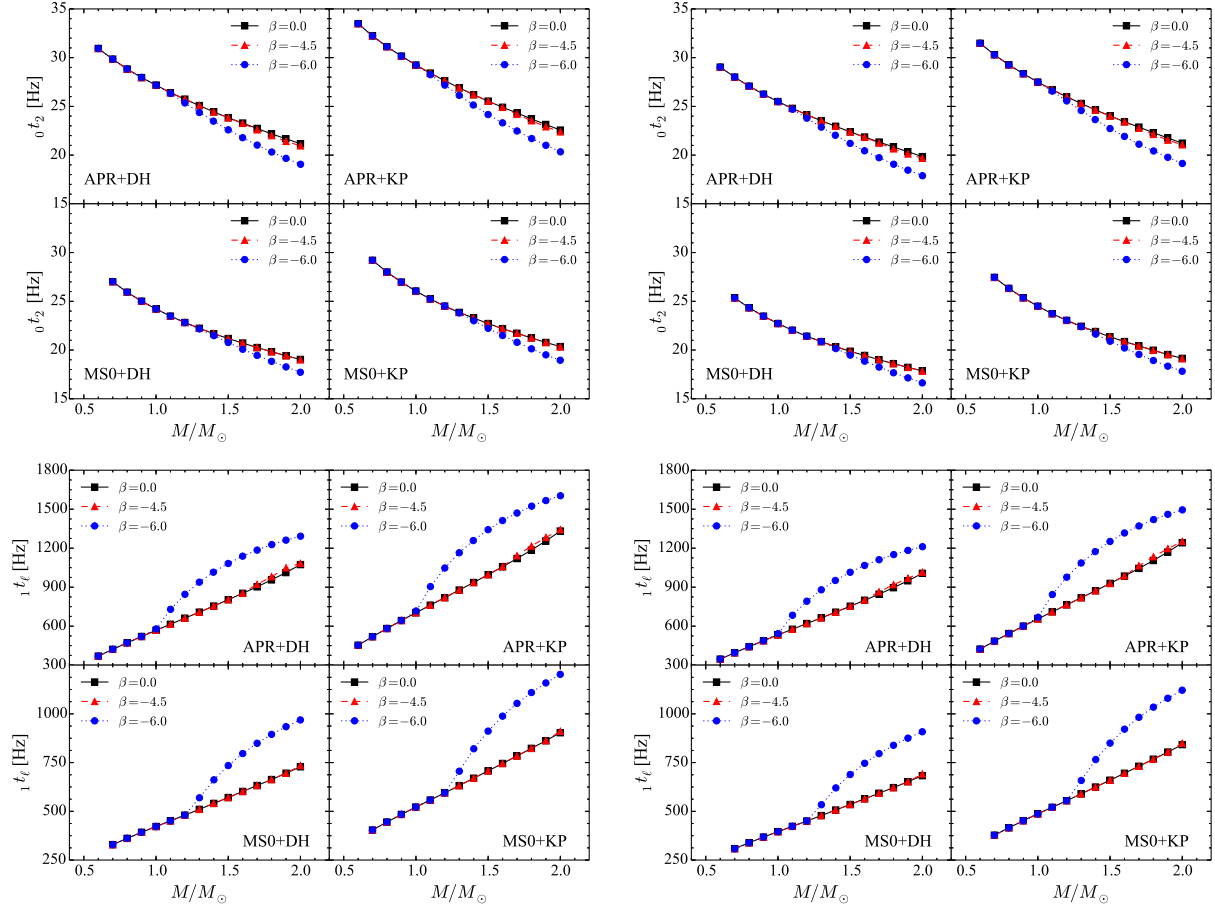


Figure 6.5: *The oscillation frequency spectra - I.* We show the frequencies of the torsional modes in ST theory as a function of M/M_{\odot} . *Top panels:* the fundamental torsional mode ${}_0t_2$ without (*left*) and with (*right*) electron screening. *Lower panels:* the first overtone ${}_1t_1$ without (*left*) and with (*right*) electron screening.

crust thickness compensates for the reduced effective shear modulus, and the net effect is an increase of the oscillation frequencies. Notice also that in ST theory the frequencies of the fundamental torsional oscillation mode decrease as we decrease β (the opposite happens in tensor-vector-scalar theory [428]).

In Fig. 6.7 we address the following question: are uncertainties in the EOS small enough to allow for tests of the underlying gravitational theory based on measurements of torsional oscillation frequencies in QPOs? Unfortunately, the answer is in the negative. Shaded regions in the plot are bounded by the values of the torsional oscillation frequencies computed using EOS DH and KP for the crust. One region (bounded by dashed lines)

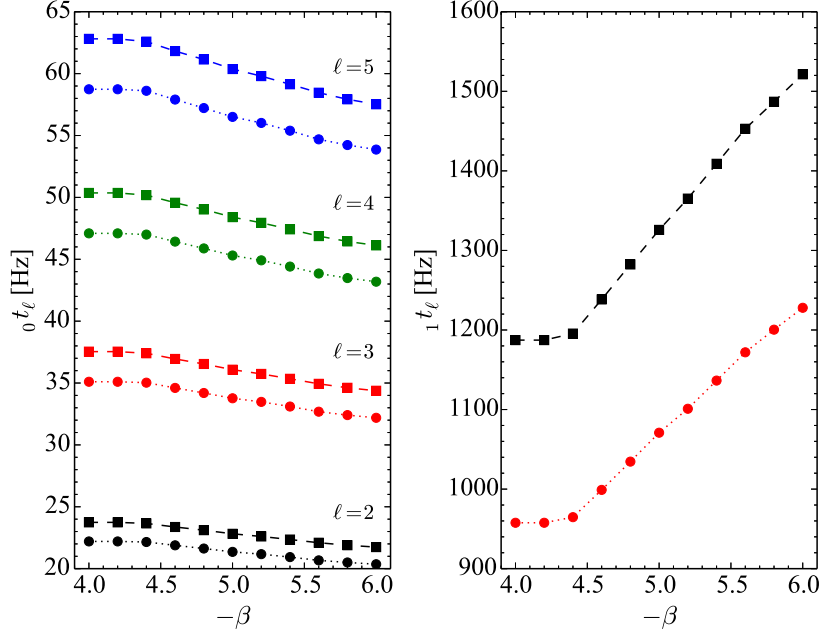


Figure 6.6: *The oscillation frequency spectra - II.* Frequencies of the torsional modes in ST theory as a function of β for stellar models with mass $M = 1.8 M_{\odot}$. Circles and dotted lines correspond to APR+DH; squares and dashed lines correspond to APR+KP. In the right panel we plot the mode frequencies ${}_0t_{\ell}$ for $\ell = 2, 3, 4$ and 5 . In the left panel we show the frequencies of the first overtone ${}_1t_{\ell}$.

corresponds to GR, while the other (solid lines) to ST theory. These regions are meant to roughly quantify the EOS uncertainty *within each theory*. Horizontal lines in the left panels mark the QPO frequency of 28 Hz observed in SGR 1900+14 [461], and identified with the ${}_0t_2$ mode. The plots show that for a theory parameter $\beta = -4.5$ (marginally ruled out by binary pulsar observations [169]) the predictions of GR and ST theory are indistinguishable within uncertainties in the crustal EOS. The bottom-left panel shows that, in principle, a ST theory with $\beta = -6.0$ could be distinguished from GR if we were to observe QPOs with frequencies smaller than 24 Hz in magnetars with $M \gtrsim 1.6 M_{\odot}$. However, such a large value of β is already excluded by binary pulsar experiments. The right panel carries out a similar analysis for the first overtone ${}_1t_{\ell}$. The horizontal line indicates the QPO frequency of 626.46 ± 0.02 Hz detected in SGR 1806-20 [462], and identified with the first overtone ${}_1t_{\ell}$. The conclusions are similar: for $\beta = -4.5$, the predictions of GR and ST theory are

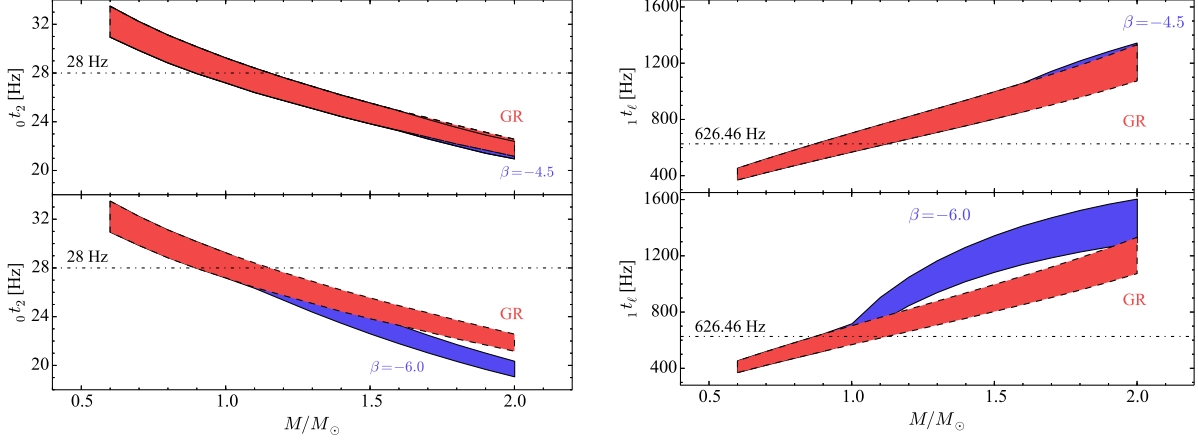


Figure 6.7: *Equation of state degeneracy.* This plot compares modifications in torsional oscillation frequencies due to the underlying gravitational theory with crustal EOS uncertainties for models constructed using EOS APR in the core. Regions bounded by dashed lines correspond to oscillation frequencies in GR with different crustal EOSs; regions bounded by solid lines correspond to oscillation frequencies in ST theory with different crustal EOSs. The degeneracy between modified gravity and crustal EOS is broken when the two regions do not overlap. Left panels refer to a ST theory with $\beta = -4.5$, right panels to a theory with $\beta = -6.0$ (a value already excluded by binary pulsar experiments [169]).

indistinguishable within uncertainties in the crustal EOS.

Let us now focus on the fundamental mode ${}_0t_2$, which has been identified with QPOs in both SGR 1900+14 (28 ± 0.5 Hz) [461] and SGR 1806-20 (30.4 ± 0.3 Hz) [462]. To quantify the relative effect of scalarization and electron screening, assuming the crustal EOS to be known, we introduce the ratio

$$\eta \equiv \frac{|{}_0t_2[\text{ST}] - {}_0t_2[\text{GR}]|}{|{}_0\bar{t}_2[\text{GR}] - {}_0t_2[\text{GR}]|}, \quad (6.48)$$

where ${}_0t_2[\text{GR}]$ (${}_0t_2[\text{ST}]$) is the fundamental mode frequency in GR (ST theory) ignoring electron screening, and ${}_0\bar{t}_2[\text{GR}]$ is the corresponding frequency in GR computed by taking into account electron screening. Electron screening has a larger impact than scalarization whenever $\eta < 1$.

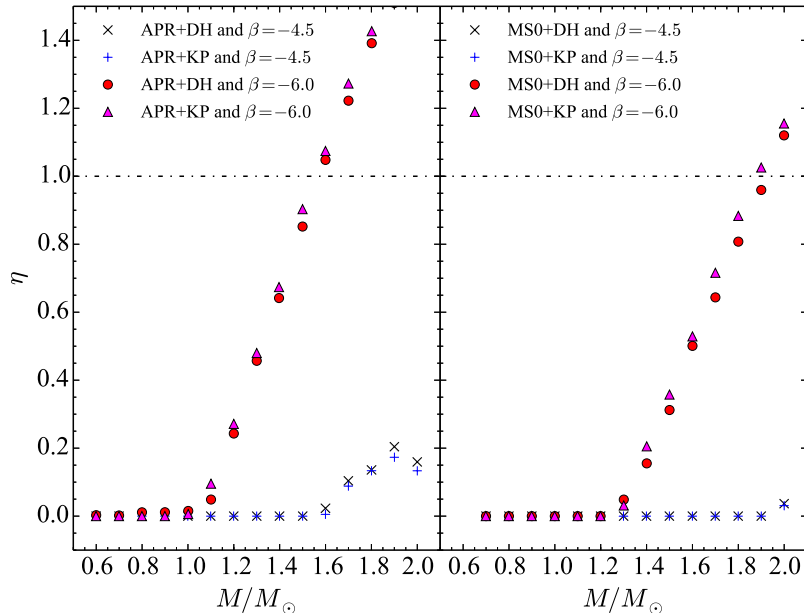


Figure 6.8: Comparison between electron screening and scalarization effect on the oscillation spectra. The ratio η defined in Eq. (6.48) for all stellar models considered in this work. Values of $\eta > 1$ mean that the effect of scalarization is larger than that of electron screening. This would only be possible for values of β that are already ruled out by binary pulsar experiments.

In Fig. 6.8 we show η as a function of the mass M for all combinations of core and crust EOS considered in this chapter. The punchline of this plot is consistent with our previous findings: the effect of electron screening is always dominant over scalarization for values of β that are compatible with current binary pulsar experiments. Unrealistically large values of β (e.g., $\beta = -6$) would be needed to constrain ST theories via torsional oscillation frequencies.

6.5 Conclusions

We studied torsional oscillations in NS crusts in ST theories of gravity allowing for spontaneous scalarization. Working in the Cowling approximation, we showed that the “master equation” governing torsional oscillations – our Eq. (6.40) – has the same form as in GR [406] if we introduce an effective shear modulus $\tilde{\mu}_{\text{eff}}$, an effective wave velocity \tilde{v}_{eff} and a rescaled frequency $\tilde{\omega}$. In general, a smaller effective shear modulus reduces the oscillation

frequencies. However we showed both analytically and numerically that the NS crust becomes thinner under scalarization, and a thinner crust tends to increase the overtone frequencies. Our numerical calculations show that the reduced shear modulus is the dominant effect for the fundamental mode, while the change in crust thickness is dominant for the first overtone.

We found that the dominant torsional oscillation frequencies in ST theory are essentially indistinguishable from those in GR for all values of $\beta \geq -4.5$ that are still allowed by binary pulsar observations. One of the simplest microphysics effects that might affect the torsional oscillation frequencies, namely electron screening [430], has a much more important effect on torsional oscillation frequencies than scalarization. More noticeable deviations from GR would occur for (say) $\beta = -6.0$, but such large values of β are already ruled out by binary-pulsar observations [169]. We expect scalarization to be subdominant when compared to other uncertainties in the microphysics, such as nonuniform nuclear structures (pastas) [427] and superfluidity of dripped neutrons [440].

Given the similarities between torsional oscillation frequencies in GR and ST theory, we can conjecture that the inclusion of slow rotation in our model will result in torsional modes growing due to the Chandrasekhar-Friedmann-Schutz instability [485]. The inclusion of slow rotation adds an extra term proportional to the frame dragging function ϖ (cf. [203]) in the perturbation equation (6.40). Previous studies of slowly rotating NSs in ST theory [429] showed that scalarization affects ϖ , and therefore it will affect torsional modes for rotating stars.

One important omission in our study is the effect of magnetic fields, a crucial ingredient for realistic comparisons with QPO observations in magnetars. Very few works have studied NSs with magnetic fields in alternative theories of gravity (see e.g. [195, 434]). Couplings between the scalar field and magnetic fields may produce larger deviations of the torsional oscillations frequencies with respect to GR. This is an interesting topic for future study.

CHAPTER 7

RELATIVISTIC STARS IN SCALAR-TENSOR THEORIES WITH DISFORMAL COUPLING

7.1 Introduction

Although Einstein's GR has passed all the experimental tests of gravity in the weak-field/slow-motion regimes with flying colors [499], it remains fairly unconstrained in the strong-gravity regime [51] and on the cosmological scales [107]. The recent observation of gravitational waves generated during the merger of two BHs by the LIGO/Virgo Collaboration, in accordance with general-relativistic predictions [3, 4], has offered us a first glimpse of gravity in a fully nonlinear and highly dynamical regime whose theoretical implications are still being explored [527]. Nevertheless, the pressing issues on understanding the nature of dark matter and dark energy, the inflationary evolution of the early Universe and the quest for an ultraviolet completion of GR have served as driving forces in the exploration of modifications to GR [107, 51].

In general modifications of GR introduce new gravitational degree(s) of freedom in addition to the metric tensor and can be described by a ST theory of gravity [172]. On the theoretical side, ST theories should not contain Ostrogradski ghosts [505], i.e. the equations of motion should be written in terms of the second-order differential equations despite the possible existence of the higher-order derivative interactions at the action level. On the experimental/observational side, any extension of GR must pass all the current weak-field tests which GR has successfully passed. Therefore realistic modifications of gravity should contain a mechanism to suppress scalar interactions at small scales [480, 70] or (to be interesting) satisfy weak-field tests, but deviate from GR at some energy scale. Some models satisfying

these requirements belongs to the so-called Horndeski theory [225, 131, 133, 254], the most general ST theory with second-order equations of motion.

In ST theories, the scalar field may directly couple to matter, and hence matter does not follow geodesics associated with the metric $g_{\mu\nu}$ but with another $\tilde{g}_{\mu\nu}$. In the simplest case these two metrics are related as

$$\tilde{g}_{\mu\nu} = A^2(\varphi)g_{\mu\nu}, \quad (7.1)$$

which is known as the conformal coupling [107]. The two frames described by $g_{\mu\nu}$ and $\tilde{g}_{\mu\nu}$ are often referred to as the Einstein and Jordan frames, respectively.

7.1.1 Spontaneous scalarization

For relativistic stars, such as NSs, the conformal coupling to matter can trigger a tachyonic instability (due to a negative effective mass) of the scalar field when the star has a compactness above a certain threshold. This instability *spontaneously scalarizes* the NS, whereupon it harbors a nontrivial scalar field configuration which smoothly decays outside the star. In its simplest realization, scalarization occurs when the conformal factor in Eq. (7.1) is chosen as $A(\varphi) = \exp(\beta_1\varphi^2/2)$, where β_1 is a free parameter of the theory and φ is a massless scalar field. This theory passes all weak-field tests, but the presence of the scalar field can significantly modify the bulk properties of NSs, such as masses and radii, in comparison with GR. This effect was first analyzed for isolated NSs by Damour and Esposito-Farèse [118, 119]. The properties and observational consequences of this phenomenon were studied in a number of situations, including stability [198, 101], asteroseismology [438, 439, 432, 420], slow (and rapidly) rotating NS solutions [119, 429, 153, 151, 353], its influence on geodesic motion of particles around NSs [130, 154], tidal interactions [353] and the multipolar structure of the spacetime [366, 365]. Moreover, the dynamical process of scalarization was studied in Ref. [336] and stellar collapse (including the associated process of scalar radiation emission) was investigated in Refs. [200, 337, 181]. We refer the reader to Ref. [223] for an

extensive literature review.

Additionally, a semiclassical version of this effect [283] (cf. also [270, 314, 271, 312] and [357] for a connection with the Damour-Esposito-Farèse model [118, 119]) has been shown to *awaken the vacuum* state of a quantum field leading to an exponential growth of its vacuum energy density in the background of a relativistic star.

These nontrivial excitations of scalar fields induced by relativistic stars are a consequence of the generic absence of a “no-hair theorem” for these objects (see Refs. [513, 512, 33] for counterexamples), in contrast to the case of BHs, and can potentially be an important source for signatures of the presence of fundamental gravitational scalar degrees of freedom through astronomical observations [376, 51], including the measurements of gravitational and scalar radiation signals [526].

The phenomenological implications of spontaneous scalarization have also been explored in binary NS mergers [32, 348, 470, 409] and in BHs surrounded by matter [79, 80]. In the former situation, a *dynamical* scalarization allows binary members to scalarize under conditions where this would not happen if they were isolated. This effect can dramatically change the dynamics of the system in the final cycles before the merger with potentially observable consequences. In the latter case, the presence of matter can cause the appearance of a nontrivial scalar field configuration, growing “hair” on the BH.

On the experimental side, binary-pulsar observations [169] have set stringent bounds on β_1 , whose value is presently constrained to be $\beta_1 \gtrsim -4.5$. This tightly constrains the effects of spontaneous scalarization in isolated NSs, for it has been shown that independently of the choice of the equation of state (EOS) scalarization can occur only if $\beta_1 \lesssim -4.35$ for NSs modeled by a perfect fluid [199, 336, 417]. These two results confine β_1 to a very limited range, in which, even if it exists in nature, the effects of scalarization on isolated NSs are bound to be small; see Refs. [417, 153] for examples where the threshold value of β_1 can be increased and Refs. [311, 349, 313] for recent work exploring the large positive β_1 region of the theory.

7.1.2 Disformal coupling

It was recently understood that modern ST theories of gravity, under the umbrella of Horndeski gravity [225, 132], offer a more general class of coupling [57, 532] between the scalar field and matter through the so-called *disformal coupling* [37]

$$\tilde{g}_{\mu\nu} = A^2(\varphi) [g_{\mu\nu} + \Lambda B^2(\varphi) \varphi_\mu \varphi_\nu] , \quad (7.2)$$

where $\varphi_\mu = \nabla_\mu \varphi$ is the covariant derivative of the scalar field associated with the gravity frame metric $g_{\mu\nu}$, and Λ is a constant with dimensions of (length)². For $\Lambda = 0$ we recover the purely conformal case of Eq. (7.1). Disformal transformations were originally introduced by Bekenstein and consist of the most general coupling constructed from the metric $g_{\mu\nu}$ and the scalar field φ that respects causality and the weak equivalence principle [37]. Disformal couplings have been investigated so far mainly in the context of cosmology [258, 396, 397]. They also arise in higher-dimensional gravitational theories with moving branes [533, 257], in relativistic extensions of modified Newtonian theories, (the tensor-vector-scalar theories) [38, 39], and in the decoupling limit of the nonlinear massive gravity [127, 126, 43, 72]. Moreover, in Ref. [57] it was shown that the mathematical structure of Horndeski theory is preserved under the transformation (7.2), namely if the ST theory written in terms of $g_{\mu\nu}$ belongs to a class of the Horndeski theory the same theory rewritten in terms of $\tilde{g}_{\mu\nu}$ belongs to another class of the Horndeski theory. Thus disformal transformations provide a natural generalization of conformal transformations.

Disformal coupling was also considered in models of a varying speed of light [295] and inflation [241, 482]. The invariance of cosmological observables in the frames related by the disformal relation (7.2) was verified in Refs. [113, 320, 477, 492, 327, 144]. Although applications to early Universe models are still limited, disformal couplings have been extensively applied to late-time cosmology [393, 481, 397, 258, 533, 531, 259, 125, 58, 194]. A new screening mechanism of the scalar force in the high-density region was proposed in Ref. [259],

where in the presence of disformal coupling the nonrelativistic limit of the scalar field equation seemed to be independent of the local energy density. However, a reanalysis suggested that no new screening mechanism from disformal coupling could work [393, 233]. It was also argued that disformal coupling could not contribute to a chameleon screening mechanism around a nonrelativistic source [334]. Experimental and observational constraints on disformal coupling to particular matter sectors have also been investigated. Disformal couplings to baryons and photons have been severely constrained in terms of the nondetection of new physics in collider experiments [241, 65, 66, 68, 267, 69], the absence of spectral distortion of the cosmic microwave background and the violation of distance reciprocal relations [484, 67, 68, 483], respectively. On the other hand, disformal coupling to the dark sector has been proposed in [330, 481] and is presently less constrained in comparison with coupling to visible matter sectors.

When conformal and disformal couplings are *universal* to all the matter species, they can only be constrained through experimental tests of gravity. A detailed study of ST theory with the pure disformal coupling $A(\varphi) = 1$ and $B(\varphi) = 1$ in the weak-field limit was presented in [393] and the post-Newtonian (PN) corrections due to the presence of pure disformal coupling were computed [233]. In these papers [393, 233], in contrast to the claim of Refs. [533, 259], it was shown that no screening mechanism which could suppress the scalar force in the vicinity of the source exists and the difference of the parametrized post-Newtonian (PPN) parameters from GR are of order $|\Lambda|H_0^2$, where $H_0(\sim 10^{-28} \text{ cm}^{-1})$ is the present-day Hubble scale. The strongest bound on $|\Lambda|$ comes from the constraints on the PPN preferred frame parameter α_2 . The near perfect alignment between the Sun's spin axis and the orbital angular momenta of the planets provides the constraint $\alpha_2 < 4 \times 10^{-5}$ (see Ref. [232] for a discussion), which implies that $|\Lambda| \lesssim 10^{-6}H_0^{-2}(\sim 10^{40} \text{ km}^2)$. With the inclusion of the conformal factor, i.e. $A(\varphi) \neq 1$, the authors of Ref. [233] argued that the Cassini bound $|\gamma - 1| < 2.1 \times 10^{-5}$ [56] imposes a constraint on $\alpha(\varphi_0)$, where φ_0 is the

cosmological background value of the scalar field and

$$\alpha(\varphi) \equiv \frac{d \log A(\varphi)}{d\varphi}, \quad \beta(\varphi) \equiv \frac{d \log B(\varphi)}{d\varphi}. \quad (7.3)$$

On the other hand the disformal part of the coupling $\beta(\varphi_0)$ remains unconstrained, because corrections to the PPN parameters which include $\beta(\varphi)$ are subdominant compared to the conformal part. These weaker constraints on the disformal coupling parameters are due to the fact that in the nonrelativistic regime with negligible pressure and a slowly evolving scalar field the disformal coupling becomes negligible. We also point out that in the weak-field regime such as in the Solar System, typical densities are small therefore preventing the appearance of ghosts in the theory for negative values of Λ .

In the strong-gravity regime such as that found in the interior of NSs, the pressure cannot be neglected and the disformal coupling is expected to be as important as the conformal one. This would affect the spontaneous scalarization mechanism and consequently influence the structure (and stability) of relativistic stars, or have significant impact on gravitational-wave astronomy [51]. The influence of disformal coupling on the stability of matter configurations around BHs was analyzed in Ref. [256]. The authors of Ref. [256] derived the stability conditions of the system by generalizing the case of pure conformal coupling [79, 80]. They also generalized these works to ST theories with noncanonical kinetic terms and disformal coupling, finding that the disformal coupling could make matter configurations more unstable, triggering spontaneous scalarization. In the present work within the same class of ST theory considered in Ref. [256], we will study relativistic stars and investigate the influence of disformal coupling on the scalarization of NSs.

7.1.3 Organization of this chapter

We have organized this chapter as follows. In Sec. 7.2 we review the fundamentals of ST theories with generalized kinetic term and disformal coupling. In Sec. 7.3 we present a general formulation to analyze the structure of slowly rotating stars in theories with disformal

coupling. In Sec. 7.4, as a case study, we consider a canonical scalar field with a generic scalar field potential. We particularize the stellar structure equations to this model and discuss how to solve them numerically. In Sec. 7.5 we explore the consequences of the disformal coupling by studying small scalar perturbations to an incompressible relativistic star in GR. In particular we investigate the conditions for which spontaneous scalarization happens. In Sec. 7.6 we present our numerical studies about the influence of disformal coupling on the spontaneous scalarization by solving the full stellar structure equations. In Sec. 7.7 as an application of our numerical integrations, we examine the EOS independence between the moment of inertia and compactness of NSs in ST theory comparing it against the results obtained in GR. Finally, in Sec. 7.8 we summarize our main findings and point out possible future avenues of research.

7.2 Scalar-tensor theory with the disformal coupling

We consider ST theories in which matter is disformally coupled to the scalar field. The action in the Einstein frame reads

$$S = \frac{1}{2\kappa} \int d^4x \sqrt{-g} [R + 2P(X, \varphi)] + \int d^4x \sqrt{-\tilde{g}(\varphi, \varphi_\mu)} \mathcal{L}_m[\tilde{g}_{\mu\nu}(\varphi, \varphi_\mu), \Psi], \quad (7.4)$$

where x^μ ($\mu = 0, 1, 2, 3$) represents the coordinate system of the spacetime, $g_{\mu\nu}$ and $\tilde{g}_{\mu\nu}$ are respectively the Einstein and Jordan frame metrics disformally related by (7.2), $g \equiv \det(g_{\mu\nu})$ and $\tilde{g} \equiv \det(\tilde{g}_{\mu\nu})$, R is the Ricci scalar curvature associated with $g_{\mu\nu}$, $\kappa \equiv (8\pi G)/c^4$, where G is the gravitational constant defined in the Einstein frame and c is the speed of light in vacuum. $P(X, \varphi)$ is an arbitrary function of the scalar field φ and $X \equiv -\frac{1}{2}g^{\mu\nu}\varphi_\mu\varphi_\nu$, and \mathcal{L}_m represents the Lagrangian density of matter fields Ψ . We note that the canonical scalar field corresponds to the case of $P(X, \varphi) = 2X - V(\varphi)$, but we will not restrict the form of $P(X, \varphi)$ at this stage. In this chapter, exceptionally, we will *not* omit G and c .

Varying the action (7.4) with respect to the Einstein frame metric $g_{\mu\nu}$, we obtain the

Einstein field equations

$$G^{\mu\nu} = \kappa \left(T_{(m)}^{\mu\nu} + T_{(\varphi)}^{\mu\nu} \right), \quad (7.5)$$

where the energy-momentum tensors of the matter fields Ψ and scalar field φ are given by

$$T_{(m)}^{\mu\nu} = \frac{2}{\sqrt{-g}} \frac{\delta \left(\sqrt{-\tilde{g}} \mathcal{L}_m [\tilde{g}(\varphi), \Psi] \right)}{\delta g_{\mu\nu}}, \quad (7.6)$$

and

$$\begin{aligned} T_{(\varphi)}^{\mu\nu} &\equiv \frac{1}{\kappa} \frac{2}{\sqrt{-g}} \frac{\delta \left(\sqrt{-g} P(X, \varphi) \right)}{\delta g_{\mu\nu}}, \\ &= \frac{1}{\kappa} \left(P_X \varphi^\mu \varphi^\nu + P g^{\mu\nu} \right), \end{aligned} \quad (7.7)$$

respectively, where $P_X \equiv \partial_X P$ and $\varphi^\mu \equiv g^{\mu\nu} \varphi_\nu$. From Eq. (7.2), the inverse Jordan frame metric $\tilde{g}^{\mu\nu}$ is related to the inverse Einstein frame metric $g^{\mu\nu}$ by

$$\tilde{g}^{\mu\nu} = A^{-2}(\varphi) \left[g^{\mu\nu} - \frac{\Lambda B^2(\varphi)}{\chi(X, \varphi)} \varphi^\mu \varphi^\nu \right], \quad (7.8)$$

where we have defined

$$\chi(X, \varphi) \equiv 1 - 2\Lambda B^2(\varphi) X. \quad (7.9)$$

The volume element in the Jordan frame $\sqrt{-\tilde{g}}$ is given by $\sqrt{-\tilde{g}} = A^4(\varphi) \sqrt{-g} \sqrt{\chi(X, \varphi)}$.

In order to keep the Lorentzian signature of the Jordan frame metric $\tilde{g}_{\mu\nu}$, χ must be non-negative. We note that in the purely conformal coupling limit $\Lambda = 0$ and $\chi = 1$.

The contravariant energy-momentum tensor in the Jordan frame $\tilde{T}_{(m)}^{\mu\nu}$ is related to that in the Einstein frame by

$$\begin{aligned} \tilde{T}_{(m)}^{\mu\nu} &\equiv \frac{2}{\sqrt{-\tilde{g}}} \frac{\delta \left(\sqrt{-\tilde{g}} \mathcal{L}_m [\tilde{g}, \Psi] \right)}{\delta \tilde{g}_{\mu\nu}}, \\ &= \sqrt{\frac{g}{\tilde{g}}} \frac{\delta g_{\alpha\beta}}{\delta \tilde{g}_{\mu\nu}} T_{(m)}^{\alpha\beta} = \frac{A^{-6}(\varphi)}{\sqrt{\chi(X, \varphi)}} T_{(m)}^{\mu\nu}. \end{aligned} \quad (7.10)$$

The mixed and covariant energy-momentum tensors in the Jordan frame are respectively given by

$$\tilde{T}_{(m)\mu}{}^{\nu} = \frac{A^{-4}(\varphi)}{\sqrt{\chi(X, \varphi)}} (\delta_{\mu}^{\alpha} + \Lambda B^2(\varphi) \varphi_{\mu} \varphi^{\alpha}) T_{(m)\alpha}{}^{\nu}, \quad (7.11a)$$

$$\tilde{T}_{(m)\mu\nu} = \frac{A^{-2}(\varphi)}{\sqrt{\chi(X, \varphi)}} (\delta_{\mu}^{\alpha} + \Lambda B^2(\varphi) \varphi_{\mu} \varphi^{\alpha}) (\delta_{\nu}^{\beta} + \Lambda B^2(\varphi) \varphi_{\nu} \varphi^{\beta}) T_{(m)\alpha\beta}, \quad (7.11b)$$

and

$$T_{(m)}^{\mu\nu} = A^6(\varphi) \sqrt{\chi(X, \varphi)} \tilde{T}_{(m)}^{\mu\nu}, \quad (7.12a)$$

$$T_{(m)\nu}{}^{\mu} = A^4(\varphi) \sqrt{\chi(X, \varphi)} \left(\delta_{\nu}^{\rho} - \frac{\Lambda B^2(\varphi) \varphi^{\rho} \varphi_{\nu}}{\chi(X, \varphi)} \right) \tilde{T}_{(m)\rho}{}^{\mu}, \quad (7.12b)$$

$$T_{(m)\mu\nu} = A^2(\varphi) \sqrt{\chi(X, \varphi)} \left(\delta_{\mu}^{\rho} - \frac{\Lambda B^2(\varphi) \varphi^{\rho} \varphi_{\mu}}{\chi(X, \varphi)} \right) \left(\delta_{\nu}^{\sigma} - \frac{\Lambda B^2(\varphi) \varphi^{\sigma} \varphi_{\nu}}{\chi(X, \varphi)} \right) \tilde{T}_{(m)\rho\sigma}. \quad (7.12c)$$

In terms of the covariant tensors, the Einstein equations in the Einstein frame (7.5) can be recast as

$$\begin{aligned} G_{\mu\nu} &= \kappa A^2(\varphi) \sqrt{\chi(X, \varphi)} \left(\delta_{\mu}^{\rho} - \frac{\Lambda B^2(\varphi) \varphi^{\rho} \varphi_{\mu}}{\chi(X, \varphi)} \right) \left(\delta_{\nu}^{\sigma} - \frac{\Lambda B^2(\varphi) \varphi^{\sigma} \varphi_{\nu}}{\chi(X, \varphi)} \right) \tilde{T}_{(m)\rho\sigma} \\ &\quad + P_X \varphi_{\mu} \varphi_{\nu} + g_{\mu\nu} P. \end{aligned} \quad (7.13)$$

Varying the action (7.4) with respect to the scalar field φ , we obtain the scalar field equation of motion

$$P_X \square \varphi + P_{\varphi} - P_{XX} \varphi^{\rho} \varphi^{\sigma} \varphi_{\rho\sigma} - 2X P_{X\varphi} = \kappa \mathcal{Q}, \quad (7.14)$$

where the function \mathcal{Q} characterizes the strength of the coupling of matter to the scalar field

$$\mathcal{Q} \equiv \Lambda \nabla_{\rho} \left(B^2(\varphi) T_{(m)}^{\rho\sigma} \varphi_{\sigma} \right) - \alpha(\varphi) T_{(m)} - \Lambda B^2(\varphi) [\alpha(\varphi) + \beta(\varphi)] T_{(m)}^{\rho\sigma} \varphi_{\rho} \varphi_{\sigma}, \quad (7.15)$$

where $T_{(m)} \equiv g^{\rho\sigma} T_{(m)\rho\sigma}$ is the trace of $T_{(m)\rho\sigma}$, and $\alpha(\varphi)$ and $\beta(\varphi)$ were defined in Eq. (7.3).

Taking the divergence of Eq. (7.5), employing the contracted Bianchi identity $\nabla_\rho G^{\rho\sigma} = 0$, and using the scalar field equation of motion (7.14), we obtain

$$\nabla_\rho T_{(m)}^{\rho\sigma} = -\nabla_\rho T_{(\varphi)}^{\rho\sigma} = -\mathcal{Q}\varphi^\sigma, \quad (7.16)$$

and the coupling strength \mathcal{Q} can be rewritten

$$\mathcal{Q} = \Lambda B^2(\varphi) \left(\nabla_\rho T_{(m)}^{\rho\sigma} \right) \varphi_\sigma + \mathcal{Y}, \quad (7.17)$$

where we have introduced

$$\mathcal{Y} \equiv \Lambda B^2(\varphi) \left\{ [\beta(\varphi) - \alpha(\varphi)] T_{(m)}^{\rho\sigma} \varphi_\rho \varphi_\sigma + T_{(m)}^{\rho\sigma} \varphi_{\rho\sigma} \right\} - \alpha(\varphi) T_{(m)}. \quad (7.18)$$

Multiplying Eq. (7.16) by φ_σ and solving it with respect to $\left(\nabla_\rho T_{(m)}^{\rho\sigma} \right) \varphi_\sigma$, we obtain

$$\chi \left(\nabla_\rho T_{(m)}^{\rho\sigma} \right) \varphi_\sigma = 2X\mathcal{Y}. \quad (7.19)$$

Then, substituting it in Eq. (7.17), using $\mathcal{Q} = \mathcal{Y}/\chi$, and finally eliminating \mathcal{Q} from Eq. (7.14), we obtain the reduced scalar field equation of motion

$$\begin{aligned} P_X \square \varphi + P_\varphi - P_{XX} \varphi^\rho \varphi^\sigma \varphi_{\rho\sigma} - 2X P_{X\varphi} &= \frac{\kappa}{\chi(X, \varphi)} \\ &\times \left\{ \Lambda B^2(\varphi) \left[(\beta(\varphi) - \alpha(\varphi)) T_{(m)}^{\rho\sigma} \varphi_\rho \varphi_\sigma + T_{(m)}^{\rho\sigma} \varphi_{\rho\sigma} \right] - \alpha(\varphi) T_{(m)} \right\}. \end{aligned} \quad (7.20)$$

7.3 The equations of stellar structure

7.3.1 Equations of motion

In this section, we consider a static and spherically symmetric spacetime with line element

$$ds^2 = g_{\mu\nu} dx^\mu dx^\nu = -e^{\nu(r)} c^2 dt^2 + e^{\lambda(r)} dr^2 + r^2 \gamma_{ij} d\theta^i d\theta^j, \quad (7.21)$$

where $\nu(r)$ and $\lambda(r)$ are functions of the radial coordinate r only, γ_{ij} is the metric of the unit 2-sphere, and the coordinates θ^i ($i = 1, 2$) run over the directions of the unit 2-sphere, such that $\gamma_{ij}d\theta^i d\theta^j = d\theta^2 + \sin^2\theta d\phi^2$. We also assume by symmetry that the scalar field is only a function of r , $\varphi = \varphi(r)$. Hence the coupling functions $A(\varphi)$ and $B(\varphi)$ are also only functions of r through $\varphi(r)$.

We assume that in the Jordan frame only diagonal components of the energy-momentum tensor of matter are nonvanishing

$$\tilde{T}_{(m)}{}^t{}_t = -\tilde{\rho}c^2, \quad \tilde{T}_{(m)}{}^r{}_r = \tilde{p}_r, \quad \tilde{T}_{(m)}{}^i{}_j = \tilde{p}_t\delta^i{}_j, \quad (7.22)$$

where $\tilde{\rho}$, \tilde{p}_r and \tilde{p}_t are respectively the energy density, radial and tangential pressures of an anisotropic fluid in the Jordan frame [63]. Using Eq. (7.12b), they are related to the components of the energy-momentum tensor of matter in the Einstein frame, which are represented by the quantities without a *tilde*, by

$$\rho = A^4(\varphi)\sqrt{\chi}\tilde{\rho}, \quad p_r = \frac{A^4(\varphi)}{\sqrt{\chi}}\tilde{p}_r, \quad p_t = A^4(\varphi)\sqrt{\chi}\tilde{p}_t, \quad (7.23)$$

where in the background given by Eq. (7.21), the quantity χ defined in Eq. (7.9) reduces to

$$\chi = 1 + e^{-\lambda}\Lambda B^2(\varphi)(\varphi')^2. \quad (7.24)$$

We note that even if the fluid in the Jordan frame has an isotropic pressure, $\tilde{p}_r = \tilde{p}_t$, it is transformed into an anisotropic one in the Einstein frame i.e. $p_r \neq p_t$ in the presence of disformal coupling $\chi \neq 1$.

The (t, t) , (r, r) and the trace of (i, j) components of the Einstein equations (7.13)

are given by

$$\frac{1}{r^2} [1 - e^{-\lambda}(1 - r\lambda')] = -P + A^4(\varphi)\sqrt{\chi}\kappa\tilde{\rho}c^2, \quad (7.25)$$

$$\frac{e^\lambda}{r^2} [1 - e^{-\lambda}(1 + r\nu')] = -(\varphi')^2 P_X - e^\lambda \left[P + \frac{A^4(\varphi)}{\sqrt{\chi}}(\kappa\tilde{p}_r) \right], \quad (7.26)$$

$$\frac{1}{2} \left[\nu'' + \left(\frac{\nu'}{2} + \frac{1}{r} \right) (\nu' - \lambda') \right] = e^\lambda [P + A^4(\varphi)\sqrt{\chi}(\kappa\tilde{p}_t)]. \quad (7.27)$$

On the other hand, the scalar field equation of motion (7.20) reduces to

$$\begin{aligned} & \chi \left\{ P_X e^{-\lambda} \left[\varphi'' + \left(\frac{\nu'}{2} - \frac{\lambda'}{2} + \frac{2}{r} \right) \varphi' \right] + P_\varphi - P_{XX} e^{-2\lambda} (\varphi')^2 \left(\varphi'' - \frac{\lambda'}{2} \varphi' \right) + e^{-\lambda} (\varphi')^2 P_{X\varphi} \right\} \\ &= \kappa \frac{A^4(\varphi)}{\varphi'} \left\{ \frac{\tilde{p}_r}{\sqrt{\chi}} \left[-\alpha(\varphi)\varphi' + \Lambda B^2(\varphi) e^{-\lambda} \varphi' \left(\varphi'' + \left(\beta(\varphi)\varphi' - \alpha(\varphi)\varphi' - \frac{\lambda'}{2} \right) \varphi' \right) \right] \right. \\ & \left. - \sqrt{\chi} \left[\alpha(\varphi)\varphi' (-\tilde{\rho}c^2 + 2\tilde{p}_t) + \Lambda B^2(\varphi) e^{-\lambda} \left(\frac{\nu'}{2} \tilde{\rho}c^2 - \frac{2}{r} \tilde{p}_t \right) (\varphi')^2 \right] \right\}. \end{aligned} \quad (7.28)$$

The nontrivial radial component of the energy-momentum conservation law in the Einstein frame (7.16) gives us

$$\frac{d\tilde{p}_r}{dr} = - \left[\frac{\nu'}{2} + \alpha(\varphi)\varphi' \right] (\tilde{\rho}c^2 + \tilde{p}_r) - 2 \left[\frac{1}{r} + \alpha(\varphi)\varphi' \right] \tilde{\sigma}, \quad (7.29)$$

where we have defined $\tilde{\sigma} \equiv \tilde{p}_r - \tilde{p}_t$, which measures the degree of anisotropy of the fluid [63].

The same result can be obtained from the conservation law in the Jordan frame $\tilde{\nabla}_\rho \tilde{T}^{\rho r} = 0$, where $\tilde{\nabla}_\rho$ represents the covariant derivative associated with the Jordan frame metric $\tilde{g}_{\mu\nu}$.

The conservation law (7.29) depends implicitly on $B(\varphi)$ and its derivative through ν' [cf. Eq. (7.26)].

7.3.2 The reduced equations of motion

We then reduce the set of equations (7.25)-(7.27), (7.28) and (7.29) into a form more convenient for a numerical integration. We introduce the mass function $\mu(r)$ through

$$e^{-\lambda(r)} \equiv 1 - \frac{2\mu(r)}{r}, \quad (7.30)$$

and replace all $\lambda(r)$ dependence with $\mu(r)$. We also introduce the first-order derivative of the scalar field $\psi(r)$, i.e.

$$\psi \equiv \frac{d\varphi}{dr}. \quad (7.31)$$

We can write the kinetic energy as

$$X = -\frac{r-2\mu}{2r}\psi^2 \quad (7.32)$$

and χ can then be expressed as

$$\chi = 1 + \frac{r-2\mu}{r}\Lambda B^2(\varphi)\psi^2. \quad (7.33)$$

The (t, t) component of the Einstein equations [cf. Eq (7.25)] determines the gradient of μ

$$\frac{d\mu}{dr} = \frac{r^2}{2} [A^4(\varphi)\sqrt{\chi}\kappa\tilde{\rho}c^2 - P]. \quad (7.34)$$

Similarly, the (r, r) component of the Einstein equations (7.26) reduces to

$$\frac{d\nu}{dr} = \frac{2\mu}{r(r-2\mu)} + r \left\{ \psi^2 P_X + \frac{r}{r-2\mu} \left[P + \frac{A^4(\varphi)}{\sqrt{\chi}}(\kappa\tilde{p}_r) \right] \right\}. \quad (7.35)$$

The conservation law (7.29) combined with Eq. (7.35) leads to

$$\begin{aligned} \frac{d\tilde{p}_r}{dr} = & - \left\{ \alpha(\varphi)\psi + \frac{\mu}{r(r-2\mu)} + \frac{r}{2} \left[\psi^2 P_X + \frac{r}{r-2\mu} \left(P + \frac{A^4(\varphi)}{\sqrt{\chi}} (\kappa\tilde{p}_r) \right) \right] \right\} (\tilde{\rho}c^2 + \tilde{p}_r) \\ & - 2 \left[\frac{1}{r} + \alpha(\varphi)\psi \right] \tilde{\sigma}. \end{aligned} \quad (7.36)$$

Finally, the scalar field equation of motion (7.28) reduces to

$$\begin{aligned} & \left[\chi (P_X - e^{-\lambda}\psi^2 P_{XX}) - \kappa\Lambda A^4(\varphi) B^2(\varphi) \frac{\tilde{p}_r}{\sqrt{\chi}} \right] \psi' \\ & + \left\{ \chi \left[\left(\frac{\nu'}{2} - \frac{\lambda'}{2} + \frac{2}{r} \right) P_X + \frac{\lambda'}{2} e^{-\lambda}\psi^2 P_{XX} + \psi P_{X\varphi} \right] \right. \\ & \left. - \kappa\Lambda A^4(\varphi) B^2(\varphi) \left[\sqrt{\chi} \left(-\frac{\nu'}{2} \tilde{\rho}c^2 + \frac{2}{r} \tilde{p}_t \right) + \frac{\tilde{p}_r}{\sqrt{\chi}} \left(\beta(\varphi)\psi - \alpha(\varphi)\psi - \frac{\lambda'}{2} \right) \right] \right\} \psi \\ & = -e^\lambda \chi P_\varphi + \kappa A^4(\varphi) \alpha(\varphi) e^\lambda \left[-\frac{\tilde{p}_r}{\sqrt{\chi}} + \sqrt{\chi} (\tilde{\rho}c^2 - 2\tilde{p}_t) \right]. \end{aligned} \quad (7.37)$$

Eliminating λ' and ν' from Eq. (7.37), and using Eqs. (7.25)-(7.26), the scalar field equation of motion (7.37) can be rewritten as

$$C_2 \frac{d\psi}{dr} = -C_1 \psi + \frac{r}{r-2\mu} \left\{ -\chi P_\varphi + \kappa A^4(\varphi) \alpha(\varphi) \left[-\frac{\tilde{p}_r}{\sqrt{\chi}} - \sqrt{\chi} (-\tilde{\rho}c^2 + 2\tilde{p}_t) \right] \right\}, \quad (7.38)$$

where we introduced

$$C_2 = \chi \left[P_X - \left(1 - \frac{2\mu}{r} \right) \psi^2 P_{XX} \right] - \kappa\Lambda A^4(\varphi) B^2(\varphi) \frac{\tilde{p}_r}{\sqrt{\chi}}, \quad (7.39)$$

$$\begin{aligned} C_1 = & \chi \left\{ P_X \left[\frac{2(r-\mu)}{r(r-2\mu)} + \frac{r}{2} \psi^2 P_X + \frac{r^2}{r-2\mu} \left(P - \frac{\kappa}{2} A^4(\varphi) \left(\sqrt{\chi} \tilde{\rho}c^2 - \frac{\tilde{p}_r}{\sqrt{\chi}} \right) \right) \right] \right. \\ & \left. + \frac{1}{2} \left[-\frac{2\mu}{r^2} + r(-P + A^4(\varphi)\sqrt{\chi}(\kappa\tilde{\rho}c^2)) \right] \psi^2 P_{XX} + \psi P_{X\varphi} \right\} \\ & - \kappa\Lambda A^4(\varphi) B^2(\varphi) \left\{ -\frac{1}{r-2\mu} \left(\frac{\mu}{r} + \frac{r^2 P}{2} \right) \left(\sqrt{\chi} \tilde{\rho}c^2 - \frac{\tilde{p}_r}{\sqrt{\chi}} \right) - \frac{\tilde{\rho}c^2 \sqrt{\chi}}{2} \psi^2 P_{Xr} \right. \\ & \left. - \frac{\kappa r^2}{r-2\mu} (\tilde{\rho}c^2 \tilde{p}_r) A^4(\varphi) + \frac{2\sqrt{\chi}}{r} \tilde{p}_t + \frac{\psi}{\sqrt{\chi}} [\beta(\varphi) - \alpha(\varphi)] \tilde{p}_r \right\}. \end{aligned} \quad (7.40)$$

The set of Eqs. (7.31), (7.34), (7.35), (7.36) and (7.38) together with a given EOS

$$\tilde{p}_r = \tilde{p}_r(\tilde{\rho}), \quad \tilde{p}_t = \tilde{p}_t(\tilde{\rho}), \quad (7.41)$$

form a closed system of equations to analyze the structure of relativistic stars in the ST theory (7.4).

7.3.3 Slowly rotating stars

In this subsection, we extend our calculation to the case of slowly rotating stars. Once the set of the equations of motion for a static and spherically symmetric star is given, it is simple to take first-order corrections due to rotation into consideration using the Hartle-Thorne scheme [203, 204]. At first order in the Hartle-Thorne perturbative expansion, we derive our results in a manner as general as possible, similarly to the previous section.

In the Einstein frame, the line element including the first-order correction due to rotation is given by

$$ds^2 = -e^{\nu(r)} c^2 dt^2 + e^{\lambda(r)} dr^2 + r^2 (d\theta^2 + \sin^2 \theta d\phi^2) + 2(\omega - \Omega) r^2 \sin^2 \theta dt d\phi, \quad (7.42)$$

where $\omega(r)$ is a function of r , which is of the same order as the star's angular velocity Ω . We can construct the Jordan frame line element using Eqs. (7.2) and (7.8). The construction of the energy-momentum tensor for the anisotropic fluid in the Jordan frame is similar to what was done before, except that now, the normalization of the four-velocity, demands that

$$\tilde{u}^t = \left[- \left(\tilde{g}_{tt} + 2\tilde{\Omega}\tilde{g}_{t\phi} + \tilde{\Omega}^2\tilde{g}_{\phi\phi} \right) \right]^{-1/2}, \quad \tilde{u}^r = \tilde{u}^\theta = 0, \quad \tilde{u}^\phi = \tilde{\Omega}\tilde{u}^t, \quad (7.43)$$

where $\tilde{\Omega}$ is the star's angular velocity in the Jordan frame [measured in the coordinates of

$$x^\mu = (t, r, \theta, \phi),$$

$$\tilde{g}_{tt} = A^2 g_{tt}, \quad \tilde{g}_{rr} = A^2 \left[g_{rr} + \Lambda B^2 (\varphi')^2 \right], \quad (7.44a)$$

$$\tilde{g}_{ij} = A^2 g_{ij}, \quad (i, j = \theta, \phi) \quad (7.44b)$$

$$\tilde{g}_{t\phi} = A^2 g_{t\phi}, \quad (7.44c)$$

and we must expand all expressions, keeping only terms of order $\mathcal{O}(\Omega)$. As shown in the Appendix G the star's angular velocity is disformally invariant, $\tilde{\Omega} = \Omega$. We also note that rotation can induce a dependence of the scalar field on θ , which appears however only at more than second order in rotation, $\mathcal{O}(\Omega^2)$ [353]. Thus in our case, the scalar field configuration remains the same as in the nonrotating situation.

At the first order in rotation, the diagonal components of the Einstein equations and the scalar field equation of motion remain the same as Eqs. (7.31), (7.34), (7.35), (7.36) and (7.38). A new equation comes however from the (t, ϕ) component of the Einstein equation:

$$\frac{d^2\omega}{dr^2} - \left(\frac{4}{r} - \frac{\lambda' + \nu'}{2} \right) \frac{d\omega}{dr} + 2\kappa A^4(\varphi) r \sqrt{\chi} \frac{(\tilde{\rho}c^2 + \tilde{p}_r - \tilde{\sigma})}{(r - 2\mu)} \omega(r) = 0. \quad (7.45)$$

By eliminating ν' and λ' with the use of Eqs. (7.34) and (7.35), we obtain the frame-dragging equation

$$\begin{aligned} \frac{d^2\omega}{dr^2} + \left[\frac{1}{2} r P_X \psi^2 + \frac{\kappa r^2 A^4(\varphi)}{2\sqrt{\chi}(r - 2\mu)} (\tilde{p}_r + \chi \tilde{\rho}c^2) - \frac{4}{r} \right] \frac{d\omega}{dr} \\ + 2\kappa A^4(\varphi) r \sqrt{\chi} \frac{(\tilde{\rho}c^2 + \tilde{p}_r - \tilde{\sigma})}{(r - 2\mu)} \omega(r) = 0. \end{aligned} \quad (7.46)$$

Equation (7.46) can be solved together with Eqs. (7.31), (7.34), (7.35), (7.36) and (7.38). Together these equations fully describe a slowly rotating anisotropic relativistic star in the theory described by the action (7.4).

7.3.4 Particular limits

The equations obtained in the previous section represent the most general set of stellar structure equations for a broad class of ST theories with a single scalar degree of freedom with a disformal coupling between the scalar field and a spherically symmetric slowly rotating anisotropic fluid distribution. Because of its generality, we can recover many particular cases previously studied in the literature:

1. In the limit of the pure conformal coupling, $\Lambda \rightarrow 0$ (thus $\chi \rightarrow 1$), we recover the case studied in Chapter 5 (cf. [417]).
2. If we additionally assume isotropic pressure $\tilde{p}_r = \tilde{p}_t = \tilde{p}$, we recover the standard equations given in Refs. [118, 119] and studied in Chapter 6 (cf. [420]).
3. If we assume a kinetic term of the form $P(X, \varphi) = 2X - V(\varphi)$, where $V(\varphi)$ is a mass term $m^2\varphi^2$, isotropic pressure and purely conformal coupling we recover the massive ST theory studied in Refs. [381, 523, 148] and the asymmetron scenario proposed in Ref. [100] by appropriately choosing $A(\varphi)$.

7.4 Scalar-tensor theory with a canonical scalar field

7.4.1 Stellar structure equations

Now let us apply the general formulation developed in the previous section to the canonical scalar field with the potential $V(\varphi)$, i.e. $P = 2X - V(\varphi)$. The stellar structure

equations (7.31), (7.34), (7.35), (7.36) and (7.38) reduce to

$$\frac{d\mu}{dr} = \frac{r(r-2\mu)}{2}\psi^2 + \frac{r^2}{2}V(\varphi) + A^4(\varphi)\sqrt{\chi} \left(\frac{\kappa}{2}\tilde{\rho}c^2r^2 \right), \quad (7.47a)$$

$$\frac{d\nu}{dr} = \frac{2\mu}{r(r-2\mu)} + r\psi^2 - \frac{r^2}{r-2\mu}V(\varphi) + \frac{r^2}{r-2\mu} \frac{A^4(\varphi)}{\sqrt{\chi}}(\kappa\tilde{p}_r), \quad (7.47b)$$

$$\begin{aligned} \frac{d\tilde{p}_r}{dr} = & - \left[\alpha(\varphi)\psi + \frac{\mu}{r(r-2\mu)} + \frac{r}{2}\psi^2 - \frac{r^2}{2(r-2\mu)}V(\varphi) \right. \\ & \left. + \frac{r^2}{r-2\mu} \frac{A^4(\varphi)}{\sqrt{\chi}} \left(\frac{\kappa}{2}\tilde{p}_r \right) \right] (\tilde{\rho}c^2 + \tilde{p}_r) - 2 \left(\frac{1}{r} + \alpha(\varphi)\psi \right) \tilde{\sigma}, \end{aligned} \quad (7.47c)$$

$$\frac{d\varphi}{dr} = \psi, \quad (7.47d)$$

$$C_2 \frac{d\psi}{dr} = -C_1\psi + \frac{r\chi V_\varphi(\varphi)}{r-2\mu} + \frac{\kappa r}{r-2\mu} A^4(\varphi)\alpha(\varphi) \left[-\frac{\tilde{p}_r}{\sqrt{\chi}} + \sqrt{\chi}(\tilde{\rho}c^2 - 2\tilde{p}_r) + 2\sqrt{\chi}\tilde{\sigma} \right], \quad (7.47e)$$

where

$$\begin{aligned} C_1 = & \frac{2\chi}{r-2\mu} \left[\frac{2(r-\mu)}{r} - r^2V(\varphi) - \frac{\kappa}{2}A^4(\varphi)r^2 \left(\sqrt{\chi}\tilde{\rho}c^2 - \frac{\tilde{p}_r}{\sqrt{\chi}} \right) \right] - \kappa\Lambda A^4(\varphi)B^2(\varphi) \\ & \times \left\{ -\frac{\mu}{r(r-2\mu)} \left(\sqrt{\chi}\tilde{\rho}c^2 - \frac{\tilde{p}_r}{\sqrt{\chi}} \right) - \frac{r\psi^2}{2} \left(\sqrt{\chi}\tilde{\rho}c^2 + \frac{\tilde{p}_r}{\sqrt{\chi}} \right) + \frac{r^2V(\varphi)}{2(r-2\mu)} \right. \\ & \left. \times \left(\sqrt{\chi}\tilde{\rho}c^2 - \frac{\tilde{p}_r}{\sqrt{\chi}} \right) - \kappa A^4(\varphi) \frac{r^2}{r-2\mu} \tilde{p}_r \tilde{\rho}c^2 + \frac{2\sqrt{\chi}}{r} (\tilde{p}_r - \tilde{\sigma}) + \frac{\psi}{\sqrt{\chi}} [\beta(\varphi) - \alpha(\varphi)] \tilde{p}_r \right\}, \end{aligned} \quad (7.48)$$

and

$$C_2 = 2\chi - \kappa\Lambda A(\varphi)^4 B(\varphi)^2 \frac{\tilde{p}_r}{\sqrt{\chi}}. \quad (7.49)$$

In the case of a slowly rotating star, the frame-dragging equation (7.46) becomes

$$\frac{d^2\omega}{dr^2} - \left[r\psi^2 + \frac{\kappa r^2 A^4(\varphi)}{2(r-2\mu)} \left(\frac{\tilde{\rho}c^2}{\sqrt{\chi}} + \sqrt{\chi}\tilde{p}_r \right) - \frac{4}{r} \right] \frac{d\omega}{dr} - 2\kappa A^4(\varphi)r\sqrt{\chi} \frac{(\tilde{\rho}c^2 + \tilde{p}_r - \tilde{\sigma})}{(r-2\mu)} \omega(r) = 0. \quad (7.50)$$

Through the Einstein equation (7.26), we find that if $\Lambda > 0$ the second term of C_2 in Eq. (7.49) is of order $\mathcal{O}(\Lambda B^2/r^2)$, from which we can estimate the radius within which the contributions of disformal coupling to the gradient terms become comparable to the standard ones in the ST theory as $R_D \equiv \sqrt{\Lambda}B(\varphi)$. If $R_D > R$, where $r = R$ is the star's radius, the contributions of disformal coupling to the gradient terms become important throughout the star, while if $R_D < R$ they could be important only in a portion of the star's interior $r < R_D$. When $B \rightarrow 1$, $R_D \approx \sqrt{\Lambda}$ and therefore $\sqrt{\Lambda}$ characterizes the length scale for which the disformal coupling effects become apparent. As the radius of a typical NS is about 10 km, the effects of disformal coupling of the star become apparent when $\Lambda > \mathcal{O}(100 \text{ km}^2)$.

We note that in the presence of the disformal coupling, when integrating the scalar field equation (7.38), the coefficient C_2 in the $d\psi/dr$ equation may vanish at some $r = R_*$, i.e. $C_2(R_*) = 0$. This could happen when both $\Lambda > 0$ and the pressure at the center of the star is large enough such that $C_2 < 0$ in the vicinity of $r = 0$. In such a case, as we integrate the equations outwards, since the radial pressure \tilde{p}_r decreases and vanishes at the surface of the star, there must be a point R_* where C_2 vanishes. This point represents a singularity of our equations and a regular stellar model cannot be constructed. The nonexistence of a regular relativistic star for a large positive Λ is one of the most important consequences due to the disformal coupling. The appearance of the singularity is due to the fact that the gradient term in the scalar field equation of motion (7.47e) picks a wrong sign (i.e., negative speed of sound) and is an illustration of the gradient instability pointed out in Refs. [259, 43, 59].

7.4.2 Interior solutions

From this section onwards, we focus on the case of isotropic pressure $\tilde{p} = \tilde{p}_r = \tilde{p}_t$. We then derive the boundary conditions at the center of the star, $r = 0$, which have to be specified when integrating Eqs. (7.47) and (7.50). We assume that at $r = 0$, $\tilde{\rho}(0) = \tilde{\rho}_c$. The

remaining metric and matter variables can be expanded as

$$\mu(r) = \frac{1}{6} [\kappa \tilde{\rho}_c c^2 A^4(\varphi_c) + V(\varphi_c)] r^3 + \mathcal{O}(r^5), \quad (7.51a)$$

$$\nu(r) = \frac{1}{6} [\kappa (\tilde{\rho}_c c^2 + 3\tilde{p}_c) A^4(\varphi_c) - 2V(\varphi_c)] r^2 + \mathcal{O}(r^4), \quad (7.51b)$$

$$\varphi(r) = \varphi_c + \frac{\kappa A^4(\varphi_c) \alpha(\varphi_c) (\tilde{\rho}_c c^2 - 3\tilde{p}_c) + V_\varphi(\varphi_c)}{12 [2 - \kappa \Lambda \tilde{p}_c A^4(\varphi_c) B^2(\varphi_c)]} r^2 + \mathcal{O}(r^4), \quad (7.51c)$$

$$\begin{aligned} \tilde{p}(r) = \tilde{p}_c - \frac{1}{12} (\tilde{\rho}_c c^2 + \tilde{p}_c) & \left\{ \kappa A^4(\varphi_c) \left[\tilde{\rho}_c c^2 + 3\tilde{p}_c + \alpha(\varphi_c)^2 \frac{\tilde{\rho}_c c^2 - 3\tilde{p}_c}{1 - \frac{\kappa}{2} \Lambda \tilde{p}_c A^4(\varphi_c) B^2(\varphi_c)} \right] \right. \\ & \left. - 2V(\varphi_c) \left[1 - \frac{\alpha(\varphi_c) V_\varphi(\varphi_c)}{2V(\varphi_c)} \frac{1}{1 - \frac{\kappa}{2} \Lambda \tilde{p}_c A^4(\varphi_c) B^2(\varphi_c)} \right] \right\} r^2 + \mathcal{O}(r^4), \end{aligned} \quad (7.51d)$$

where \tilde{p}_c is fixed by $\tilde{\rho}_c$ through the EOS, i.e. $\tilde{p}_c = \tilde{p}(\tilde{\rho}_c)$. The central value of the scalar field φ_c is fixed by demanding that outside the star the scalar field approaches a given cosmological value φ_0 as $r \rightarrow \infty$, which is consistent with observational constraints. We will come back to this in Sec. 7.4.3.

As a well-behaved stellar model requires $\tilde{p}''(0) < 0$, we impose

$$\begin{aligned} & \kappa A^4(\varphi_c) \left[\tilde{\rho}_c c^2 + 3\tilde{p}_c + \alpha(\varphi_c)^2 \frac{\tilde{\rho}_c c^2 - 3\tilde{p}_c}{1 - \frac{\kappa}{2} \Lambda \tilde{p}_c A^4(\varphi_c) B^2(\varphi_c)} \right] \\ & - 2V(\varphi_c) \left[1 - \frac{\alpha(\varphi_c) V_\varphi(\varphi_c)}{2V(\varphi_c)} \frac{1}{1 - \frac{\kappa}{2} \Lambda \tilde{p}_c A^4(\varphi_c) B^2(\varphi_c)} \right] > 0. \end{aligned} \quad (7.52)$$

For a large positive disformal coupling parameter $\Lambda > 0$ and a large pressure at the center \tilde{p}_c such that $|1 - \frac{\kappa \Lambda}{2} \tilde{p}_c A^4(\varphi_c) B^2(\varphi_c)| \ll 1$, the r^2 terms of the scalar field and pressure diverge and the Taylor series solution (7.51) breaks down. Such a property is a direct consequence of the appearance of the singularity inside the star which was mentioned in the previous subsection. Assuming that $A(\varphi_c) \approx 1$ and $B(\varphi_c) \approx 1$, the maximal positive value of Λ_{\max} can be roughly estimated as

$$\Lambda_{\max} \approx \frac{2}{\kappa \tilde{p}_c} = \frac{c^4}{4\pi G \tilde{p}_c} \approx 10^2 \text{ km}^2, \quad (7.53)$$

for $\tilde{p}_c = 10^{36}$ dyne/cm², which agrees with the numerical analysis done in Sec. 7.6. On the other hand, for a large negative value of the disformal coupling $\Lambda < 0$, no singularity appears, from Eq. (7.51c) the r^2 correction to the scalar field amplitude is suppressed, and $\varphi(r) \rightarrow \varphi_c$ everywhere inside the star. This indicates that $A(\varphi_c) \approx \text{constant}$, and for a vanishing potential $V(\varphi) = 0$ the stellar configuration approaches that in GR.

In the case of slowly rotating stars, the boundary condition for ω near the origin reads

$$\omega = \omega_c \left[1 + \frac{\kappa}{5} A^4(\varphi_c) (\tilde{\rho}_c c^2 + \tilde{p}_c) r^2 \right] + \mathcal{O}(r^4). \quad (7.54)$$

7.4.2.1 Stellar models in purely disformal theories

It is interesting to analyze the stellar structure equations in the purely disformal coupling limit, when $A(\varphi) = 1$. In this case we find that the expansions near the origin are

$$\mu(r) = \frac{1}{6} [\kappa \tilde{\rho}_c c^2 + V(\varphi_c)] r^3 + \mathcal{O}(r^5), \quad (7.55a)$$

$$\nu(r) = \frac{1}{6} [\kappa (\tilde{\rho}_c c^2 + 3\tilde{p}_c) - 2V(\varphi_c)] r^2 + \mathcal{O}(r^4), \quad (7.55b)$$

$$\varphi(r) = \varphi_c + \frac{V_\varphi(\varphi_c)}{12 [1 - \frac{\kappa}{2} \Lambda \tilde{p}_c B^2(\varphi_c)]} r^2 + \mathcal{O}(r^4), \quad (7.55c)$$

$$\tilde{p}(r) = \tilde{p}_c - \frac{1}{12} (\tilde{p}_c + \tilde{\rho}_c c^2) [\kappa (\tilde{\rho}_c c^2 + 3\tilde{p}_c) - 2V(\varphi_c)] r^2 + \mathcal{O}(r^4), \quad (7.55d)$$

Thus for $V(\varphi) = 0$, $\varphi = \varphi_c$ everywhere, and the disformal coupling term does not modify the stellar structure with respect to GR. Only with a nontrivial potential $V(\varphi)$, the disformal coupling can modify the profile of the scalar field inside the NS. It was argued in Ref. [393] that for a simple mass term potential $V_\varphi \sim m^2 \varphi$, where m is the mass of the scalar field, disformal contributions can be neglected and the NS solution is the same as in GR.

7.4.2.2 Metric functions in the Jordan frame

Finally, we mention the behaviors of the metric functions in the Jordan frame. In the Appendix we derive the relationship of the physical quantities defined in the two frames.

The boundary conditions (7.51) indicate that in the singular stellar solution of the Einstein frame the metric functions μ and ν remain regular. Using Eqs. (G.3) and (G.9), the metric functions in the Jordan frame behave as

$$\bar{\nu}(r) = \ln A(\varphi_c)^2 + \frac{1}{6} \left[(\tilde{\rho}_c c^2 + 3\tilde{p}_c) - 2V(\varphi_c) + \alpha(\varphi_c) \frac{\kappa A^4(\varphi_c) \alpha(\tilde{\rho}_c c^2 - 3\tilde{p}_c) + V'(\varphi_c)}{1 - \frac{\kappa\Lambda}{2} A^4(\varphi_c) B^2(\varphi_c) \tilde{p}_c} \right] r^2 + \mathcal{O}(r^4), \quad (7.56)$$

$$\bar{\mu}(r) = \frac{A(\varphi_c)}{18} \left[3(A^4(\varphi_c) \tilde{\rho}_c c^2 + V(\varphi_c)) + 3\alpha(\varphi_c) \frac{\kappa A^4(\varphi_c) \alpha(\tilde{\rho}_c c^2 - 3\tilde{p}_c) + V'(\varphi_c)}{1 - \frac{\kappa\Lambda}{2} A^4(\varphi_c) B^2(\varphi_c) \tilde{p}_c} + \Lambda B^2(\varphi_c) \frac{(\kappa A^4(\varphi_c) \alpha(\tilde{\rho}_c c^2 - 3\tilde{p}_c) + V'(\varphi_c))^2}{4(1 - \frac{\kappa\Lambda}{2} A^4(\varphi_c) B^2(\varphi_c) \tilde{p}_c)^2} \right] r^3 + \mathcal{O}(r^5). \quad (7.57)$$

Therefore, for $|1 - \frac{\kappa\Lambda}{2} A^4(\varphi_c) B^2(\varphi_c) \tilde{p}_c| \ll 1$, the Taylor series solutions for $\bar{\mu}(r)$ and $\bar{\nu}(r)$ break down, which indicates that the metric functions in the Jordan frame $\bar{\mu}$ and $\bar{\nu}$ diverge at some finite radius and a curvature singularity appears there.

7.4.3 Exterior solution

In the vacuum region outside the star $r > R$, the fluid variables $\tilde{\rho}$, \tilde{p}_r and \tilde{p}_t vanish. The exterior solution should be the vacuum solution of GR coupled to the massless canonical scalar field. The following exact solution can be obtained [118, 120]

$$ds^2 = -e^{\nu(\rho)} c^2 dt^2 + e^{-\nu(\rho)} \left[d\rho^2 + \left(\rho^2 - \frac{2Gs}{c^2} \rho \right) \gamma_{ij} d\theta^i d\theta^j \right], \quad (7.58)$$

$$\nu(\rho) = \nu_0 + \ln \left(1 - \frac{2Gs}{c^2 \rho} \right)^{\frac{M}{s}}, \quad (7.59)$$

$$\varphi(\rho) = \varphi_0 - \frac{Q}{2M} \ln \left(1 - \frac{2Gs}{c^2 \rho} \right)^{\frac{M}{s}}, \quad (7.60)$$

where ν_0 represents the freedom of the rescaling of the time coordinate, φ_0 is the cosmological value of the scalar field at $r \rightarrow \infty$, M and Q are the integration constants and $s \equiv \sqrt{M^2 + Q^2}$. The metric (7.58) can be rewritten in terms of the Schwarzschild-like

coordinate r by the transformations

$$r(\rho) = \rho \left(1 - \frac{2Gs}{c^2\rho} \right)^{\frac{s-M}{2s}}, \quad (7.61)$$

$$\mu(\rho) = M \left[1 - \frac{G(s-M)^2}{2M\rho c^2 \left(1 - \frac{2Gs}{c^2\rho} \right)} \right] \left(1 - \frac{2Gs}{c^2\rho} \right)^{\frac{s-M}{2s}}. \quad (7.62)$$

As $r \rightarrow \infty$, the solution (7.58) behaves as

$$\mu(r) = \frac{GM}{c^2} - \frac{G^2Q^2}{2c^4r} + \mathcal{O}\left(\frac{1}{r^2}\right), \quad (7.63a)$$

$$\nu(r) = \nu_0 - \frac{2GM}{c^2r} + \mathcal{O}\left(\frac{1}{r^2}\right), \quad (7.63b)$$

$$\varphi(r) = \varphi_0 + \frac{GQ}{c^2r} + \mathcal{O}\left(\frac{1}{r^2}\right). \quad (7.63c)$$

Thus the integration constants M and Q correspond to the Arnowitt-Deser-Misner (ADM) mass and the scalar charge in the Einstein frame, respectively. For later convenience we also define the fractional binding energy

$$\mathcal{E}_b \equiv \frac{M_b}{M} - 1, \quad (7.64)$$

which is positive for bound (but not necessarily stable) configurations. We note that for the vanishing scalar field at asymptotic infinity the ADM mass is disformally invariant, $\bar{M} = M$ [see Eq. (G.10)].

In the slowly rotating case, the integration of Eq. (7.45) in vacuum $\tilde{\rho} = \tilde{p}_t = 0$ gives

$$\omega' = \frac{6G}{c^2r^4} e^{\frac{\lambda+\nu}{2}} J, \quad (7.65)$$

where J is the integration constant. In the vacuum case, we can find the exact exterior

solution at the first order in rotation [119]. Expanding it in the vicinity of $r \rightarrow \infty$ gives

$$\omega = \Omega - \frac{2GJ}{c^2 r^3} + O\left(\frac{1}{r^5}\right). \quad (7.66)$$

Thus J corresponds to the angular momentum in the exterior spacetime.

7.4.4 Matching

At the surface of the star, the interior solution is matched to the exterior solution (7.58). Then the cosmological value of the scalar field φ_0 , the ADM mass M and the scalar charge Q are evaluated as

$$\varphi_0 = \varphi_s + \ln\left(\frac{x_1 + x_2}{x_1 - x_2}\right)^{\frac{\psi_s}{x_2}}, \quad (7.67a)$$

$$M = \frac{c^2 R^2 \nu'_s}{2G} \left(1 - \frac{2\mu_s}{R}\right)^{\frac{1}{2}} \left(\frac{x_1 + x_2}{x_1 - x_2}\right)^{-\frac{\nu'_s}{2x_2}}, \quad (7.67b)$$

$$q \equiv \frac{Q}{M} = -\frac{2\psi_s}{\nu'_s}. \quad (7.67c)$$

where we introduced $x_1 \equiv \nu'_s + 2/R$ and $x_2 \equiv \sqrt{\nu'^2_s + 4\psi_s^2}$. We also defined $\mu_s \equiv \mu(R)$ and $\nu_s \equiv \nu(R)$

In the case of a slowly rotating star, the angular velocity and angular momentum of the star, Ω and J , are evaluated as

$$\Omega = \omega_s - \frac{3c^4 J}{4G^2 M^3 (3 - \alpha(\varphi_s)^2)} \left[\frac{4}{x_1^2 - x_2^2} \left(\frac{x_1 - x_2}{x_1 + x_2}\right)^{\frac{2\nu'_s}{x_2}} \left(\frac{3\nu'_s}{R} + \frac{1}{R^2} + 3\nu'^2_s - \psi_s^2\right) - 1 \right], \quad (7.68)$$

$$J = \frac{c^2 R^4}{6G} \sqrt{1 - \frac{2\mu_s}{R}} e^{-\frac{\nu'_s}{2}} \omega'_s. \quad (7.69)$$

The moment of inertia can be obtained by

$$I \equiv \frac{J}{\Omega}, \quad (7.70)$$

or equivalently by integrating Eq. (7.45), using Eqs. (7.34) and (7.35)

$$I = \frac{8\pi}{3c^2} \int_0^R dr A^4(\varphi) \sqrt{\chi} r^4 e^{-\frac{\nu-\lambda}{2}} (\tilde{\rho}c^2 + \tilde{p}_t) \left(\frac{\omega}{\Omega}\right). \quad (7.71)$$

We observe that this relation for the moment of inertia holds for any choice of $P(X, \varphi)$, $A(\varphi)$ and $B(\varphi)$. In the purely conformal theory we obtain the result of Ref. [417].

For a given EOS the equations of motion (7.47) and (7.50) are numerically integrated from $r = 0$ up to the surface of the star $r = R$, where the pressure vanishes $\tilde{p}(R) = 0$. With the values of various variables at the surface at hand, we can compute φ_0 , M , q and I using the matching conditions.

From the Einstein frame radius R , we can calculate the physical Jordan frame radius \tilde{R} through [cf. Eq. (7.2)]

$$\tilde{R} \equiv \sqrt{A^2(\varphi_s) [R^2 + \Lambda B^2(\varphi_s) \psi_s^2]} \quad (7.72)$$

where we introduced $\varphi_s \equiv \varphi(R)$ and $\psi_s \equiv \psi(R)$. For a vanishing scalar field we have $\tilde{R} = R$.

The total baryonic mass of the star M_b can be obtained by integrating

$$M_b = \int_0^R dr A^3(\varphi) \sqrt{\chi} \frac{4\pi \tilde{m}_b r^2}{\sqrt{1 - \frac{2\mu}{r}}} \tilde{n}(r), \quad (7.73)$$

where $\tilde{m}_b = 1.66 \times 10^{-24}$ g is the atomic mass unit and \tilde{n} is the baryonic number density.

In the Appendix we show that the physical quantities related to the rotation of fluid and spacetime, namely I and J as well as ω and Ω , are invariant under the disformal transformation (7.2).

7.5 A toy model of spontaneous scalarization with an incompressible fluid

Before carrying out the full numerical integrations of the stellar structure equations it is illuminating to study under which conditions scalarization can occur in our model. This can be accomplished by studying a simple toy model where a scalar field lives on the background of an incompressible fluid star. The results obtained in this section will be validated in Sec. 7.6.

Let us start by assuming that the star has a constant density ρ (incompressible) and an isotropic pressure $p = p_r = p_t$. The scalar field φ is massless, and has a canonical kinetic term and small amplitude, such that we can linearize the equations of motion. The conformal and disformal coupling functions can be expanded as

$$\begin{aligned} A(\varphi) &= 1 + \frac{1}{2}\beta_1\varphi^2 + \mathcal{O}(\varphi^3), \\ B(\varphi) &= 1 + \frac{1}{2}\beta_2\varphi^2 + \mathcal{O}(\varphi^3), \end{aligned} \tag{7.74}$$

where we have defined $\beta_1 \equiv A_{\varphi\varphi}(0)$ and $\beta_2 \equiv B_{\varphi\varphi}(0)$. As at the background level the scalar field is trivial $\varphi = 0$, the Jordan and Einstein frames coincide, and $\tilde{\rho} = \rho$ and $\tilde{p} = p$. For an incompressible star, the Einstein field equations admit an exact solution of the form (7.21) given by [201]

$$e^{\lambda(r)} = \left(1 - \frac{2GMr^2}{c^2R^3}\right)^{-1}, \tag{7.75a}$$

$$e^{\nu(r)} = \left[\frac{3}{2}\left(1 - \frac{2GM}{c^2R}\right)^{1/2} - \frac{1}{2}\left(1 - \frac{2GMr^2}{c^2R^3}\right)^{1/2}\right]^2, \tag{7.75b}$$

$$p(r) = \rho c^2 \frac{\left(1 - \frac{2GMr^2}{c^2R^3}\right)^{1/2} - \left(1 - \frac{2GM}{c^2R}\right)^{1/2}}{3\left(1 - \frac{2GM}{c^2R}\right)^{1/2} - \left(1 - \frac{2GMr^2}{c^2R^3}\right)^{1/2}}, \tag{7.75c}$$

where $r = R$ is the surface of the star, at which $p(R) = 0$. Here, M and C are the total mass

and compactness of the star:

$$M = \frac{4\pi R^3}{3}\rho, \quad \mathcal{C} = \frac{GM}{c^2 R}. \quad (7.76)$$

We then consider the perturbations to the background (7.75) induced by the fluctuations of φ . Since the corrections to the Einstein equations appear in $\mathcal{O}(\varphi^2, \varphi_\mu^2)$, at the leading order of φ only the scalar field equation of motion becomes nontrivial. In the linearized approximation, $\chi = 1 + \mathcal{O}(\varphi_\mu^2)$, $\alpha = \beta_1\varphi + \mathcal{O}(\varphi^2)$ and $\beta = \beta_2\varphi + \mathcal{O}(\varphi^2)$, and the scalar field equation of motion (7.20) for the massless and minimally coupled scalar field $P = 2X$ reduces to

$$\left(g^{\rho\sigma} - \frac{\kappa\Lambda}{2}T_{(m)}^{\rho\sigma}\right)\varphi_{\rho\sigma} = -\frac{\kappa\beta_1}{2}T_{(m)}{}^\rho{}_\rho\varphi + \mathcal{O}(\varphi^2, \varphi_\mu^2). \quad (7.77)$$

Thus, as expected, in the Einstein frame the corrections from disformal coupling appear as the modification of the kinetic term via the coupling to the energy-momentum tensor.

Taking the s -wave configuration for a stationary field, $\dot{\varphi} = \ddot{\varphi} = 0$, we get

$$\begin{aligned} \varphi'' + \frac{\frac{\nu' - \lambda'}{2} + \frac{2}{r} - \frac{\kappa\Lambda}{2} \left[-\frac{\nu'}{2}\rho c^2 + \left(-\frac{\lambda'}{2} + \frac{2}{r}\right)p(r) \right]}{1 - \frac{\kappa\Lambda}{2}p(r)}\varphi' - \frac{\kappa\beta_1}{2}e^{\lambda(r)}\frac{\rho c^2 - 3p(r)}{1 - \frac{\kappa\Lambda}{2}p(r)}\varphi \\ + \mathcal{O}(\varphi^2, \varphi'^2) = 0. \end{aligned} \quad (7.78)$$

Inside the star, the scalar field equation of motion in the stationary background (7.78) can be expanded as

$$\varphi'' + \frac{2}{r} \left[1 + \mathcal{O}\left(\mathcal{C}\frac{r^2}{R^2}\right) \right] \varphi' + u \left[1 + \mathcal{O}\left(\mathcal{C}\frac{r^2}{R^2}\right) \right] \varphi = 0, \quad (7.79)$$

where we have defined

$$u \equiv \frac{6(3\sqrt{1-2\mathcal{C}}-2)\mathcal{C}}{(3\sqrt{1-2\mathcal{C}}-1)R^2 + 3\mathcal{C}(\sqrt{1-2\mathcal{C}}-1)\Lambda}|\beta_1|. \quad (7.80)$$

By neglecting the correction terms of order $\mathcal{O}(\mathcal{C}r^2/R^2)$ in Eq. (7.79), the approximated solution inside the star satisfying the regularity boundary condition at the center, $\varphi(0) = \varphi_c$ and $\varphi'(0) = 0$, is given by

$$\varphi(r) \approx \varphi_c \frac{\sin(\sqrt{u}r)}{\sqrt{u}r}. \quad (7.81)$$

We note that at the surface of the star, $r = R$, the corrections to this approximate solution (7.81) would be of $\mathcal{O}(\mathcal{C})$, which is negligible for $\mathcal{C} \ll 1$ and gives at most a 10% error even for $\mathcal{C} \simeq 0.1$. Thus the solution (7.81) provides a good approximation to the precise interior solution of Eq. (7.78), up to corrections of $\mathcal{O}(10\%)$ for typical NSs.

Outside the star ($\tilde{\rho} = \tilde{p} = 0$) the scalar field equation of motion (7.78) reduces to

$$\varphi'' + \left(\frac{1}{r} + \frac{1}{r - \frac{2GM}{c^2}} \right) \varphi' = 0. \quad (7.82)$$

The exterior solution of the scalar field is given by

$$\varphi(r) = \varphi_0 + \frac{Q}{2M} \ln \left(1 - \frac{2GM}{c^2 r} \right), \quad (7.83)$$

which can be expanded as

$$\varphi(r) = \varphi_0 - \frac{GQ}{c^2 r} + \mathcal{O} \left(\frac{1}{r^2} \right), \quad (7.84)$$

where Q denotes scalar charge. Matching at the surface $r = R$ gives

$$\frac{GQ}{c^2 R \varphi_0} = - \frac{2\mathcal{C} (1 - 2\mathcal{C}) (\sqrt{u}R - \tan(\sqrt{u}R))}{\Xi}, \quad (7.85)$$

$$\frac{\varphi_c}{\varphi_0} = - \frac{2\mathcal{C}\sqrt{u}R}{\cos(\sqrt{u}R)} \frac{1}{\Xi}, \quad (7.86)$$

where we introduced

$$\Xi = (1 - 2\mathcal{C}) \sqrt{u}R \ln(1 - 2\mathcal{C}) - [2\mathcal{C} + (1 - 2\mathcal{C}) \ln(1 - 2\mathcal{C})] \tan(R\sqrt{u}) \quad (7.87)$$

The scalar charge Q and the central value of the scalar field φ_c blow up when

$$\frac{\tan(\sqrt{u}R)}{\sqrt{u}R} = \frac{(1 - 2\mathcal{C}) \ln(1 - 2\mathcal{C})}{2\mathcal{C} + (1 - 2\mathcal{C}) \ln(1 - 2\mathcal{C})}. \quad (7.88)$$

Thus, inside the star, the scalar field can be enhanced and the scalarization takes place when

$$\sqrt{u}R \approx \frac{\pi}{2} \left(1 + \frac{4}{\pi^2} \mathcal{C} \right). \quad (7.89)$$

The condition (7.89) can be rewritten as

$$|\beta_1^{\text{crit}}| \approx \frac{\pi^2}{24\mathcal{C}} \frac{3\sqrt{1 - 2\mathcal{C}} - 1 + 3\mathcal{C}(\sqrt{1 - 2\mathcal{C}} - 1) \frac{\Lambda}{R^2}}{3\sqrt{1 - 2\mathcal{C}} - 2} \left(1 + \frac{4}{\pi^2} \mathcal{C} \right)^2, \quad (7.90)$$

where β_1^{crit} is the critical value of β_1 for which scalarization can be triggered.

For small compactness $\mathcal{C} \ll 1$, we find at leading order

$$|\beta_1^{\text{crit}}| \approx \frac{\pi^2}{12\mathcal{C}} \left(1 - \frac{3\mathcal{C}^2}{2R^2} \Lambda \right). \quad (7.91)$$

For a typical NS, the compactness parameter $\mathcal{C} \simeq 0.2$, and if Λ is negligibly small $|\beta_1^{\text{crit}}| = \pi^2/(12\mathcal{C}) \simeq 4.1$, which agrees with the ordinary scalarization threshold [118, 198]. On the other hand, disformal coupling becomes important when $\Lambda \simeq (R/\mathcal{C})^2$, which for $R \sim 10$ km and $\mathcal{C} \simeq 0.2$, corresponds to $\Lambda \simeq 2500$ km².

In the other limit, for sufficiently large negative disformal coupling parameters $|\Lambda| \gg (R/\mathcal{C})^2$, as $uR^2 \simeq 2R^2/(|\Lambda|\mathcal{C}^2) \ll 1$, from Eqs. (7.85) and (7.86) we have

$$\frac{GQ}{c^2 R \varphi_0} \simeq -\frac{1 - 2\mathcal{C}}{3} uR^2 \ll 1 \quad \text{and} \quad \varphi_c \simeq \varphi_0, \quad (7.92)$$

and the scalar field excitation is suppressed inside the star; the stellar configuration is that of GR.

In the next section, we will show explicit examples of the numerical integrations of the stellar structure and scalar field equations [cf. Eqs. (7.47) and (7.50)], and explore how the disformal coupling affects the standard scalarization mechanism in the models proposed in Refs. [118, 119]. We will confirm our main conclusions from the perturbative calculations presented here.

7.6 Numerical results

Having gained analytical insight into the effect of the disformal coupling on spontaneous scalarization, we now will perform full numerical integrations of the stellar structure equations.

For simplicity, we will focus on the simple case of a canonical scalar field without a potential, $V(\varphi) = 0$, and we will assume the special form of the coupling functions that enter Eq. (7.2)

$$A(\varphi) = e^{\frac{1}{2}\beta_1\varphi^2}, \quad B(\varphi) = e^{\frac{1}{2}\beta_2\varphi^2}, \quad (7.93)$$

as a *minimal* model to include the disformal coupling in our problem. In the absence of the disformal coupling function ($\Lambda = 0$), this model reduces to that studied originally by Damour and Esposito-Farèse [118, 119]. Another input from the theory is the cosmological value of the scalar field φ_0 , which for simplicity we take to be zero throughout this section. We also studied the case $\varphi_0 = 10^{-3}$, which does not alter our conclusions.

Under these assumptions our model is invariant under the transformation $\varphi \rightarrow -\varphi$ (reflection symmetry). Therefore for each scalarized NS with scalar field configuration φ , there exists a reflection-symmetric counterpart with $\varphi \rightarrow -\varphi$. For both families of solutions the bulk properties (such as masses, radii and moment of inertia) are the same, while the scalar charges Q have opposite sign, but the same magnitudes. Moreover, $\varphi = 0$ is a trivial solution of the stellar structure equations. These solutions are equivalent to NSs in GR.

In this section we sample the $(\beta_1, \beta_2, \Lambda)$ parameter space of the theory, analyzing each parameter's influence on NS models and on spontaneous scalarization. As mentioned in Sec. 7.1, binary-pulsar observations have set a constraint of $\beta_1 \gtrsim -4.5$ in what corresponds to the purely conformal coupling ($\Lambda = 0$) limit of our model. This lower bound on β_1 is not expected to apply for our more general model and therefore, so far, the set of parameters $(\beta_1, \beta_2, \Lambda)$ are largely unconstrained.

7.6.1 Equation of state

To numerically integrate the stellar structure equations we must complement them with a choice of EOS. Here we consider three realistic EOSs, namely APR [10], SLy4 [155] and FPS [170], in decreasing order of stiffness. The first two support NSs with masses larger than the $M = 2.01 \pm 0.04 M_\odot$ lower bound from the pulsar PSR J0348+0432 in GR [138]. On the other hand, EOS FPS has a maximum mass of $\sim 1.8 M_\odot$ in GR and is in principle ruled out by Ref. [138]. Nevertheless, as we will see this EOS can support NSs with $M \gtrsim 2 M_\odot$, albeit scalarized, for certain values of the theory's parameters.

With this set of EOSs we validated our numerical code by reproducing the results of Refs. [154, 417] in the purely conformal coupling limit. Our results including the presence of the disformal coupling are presented next.

7.6.2 Stellar models in the minimal scalar-tensor theory with disformal coupling

In Sec. 7.5 we found that β_1 always needs to be sufficiently negative for scalarization to be triggered. For this reason, let us first analyze how Λ and β_2 affect scalarized nonrotating NSs assuming a fixed value of β_1 .

In Fig. 7.1, we consider what happens when we change the value of Λ while maintaining β_1 and β_2 fixed. We observe that for sufficiently negative values of Λ the effects of scalarization become suppressed. This can be qualitatively understood from Eq. (7.91): as $\Lambda/R^2 \rightarrow -\infty$ we need $|\beta_1^{\text{crit}}| \rightarrow \infty$ for scalarization to happen. For fixed values of β_1 and \mathcal{C} , there will be a sufficiently negative value of Λ , for which $\beta_1^{\text{crit}} > \beta_1$ and scalarization

ceases to occur. Although in Fig. 7.1 we show $\Lambda = -3000 \text{ km}^2$, we have confirmed this by constructing stellar models for even smaller values of Λ . Also, in agreement with Sec. 7.5, we see that Λ alters the threshold for scalarization. This is most clearly seen in the right panel of Fig. 7.1, where for different values of Λ scalarization starts (evidenced by a nonzero scalar charge q) when different values of compactness \mathcal{C} are reached.¹ In particular, for $\Lambda > 0$, because of the minus sign in the disformal term in Eq. (7.91), NSs can scalarize for smaller values of \mathcal{C} , while the opposite happens when $\Lambda < 0$. We remark that for large positive Λ the structure equations become singular at the origin as discussed in Sec. 7.4. This prevents nonrelativistic stars, for which $\mathcal{C} \rightarrow 0$, from scalarizing.

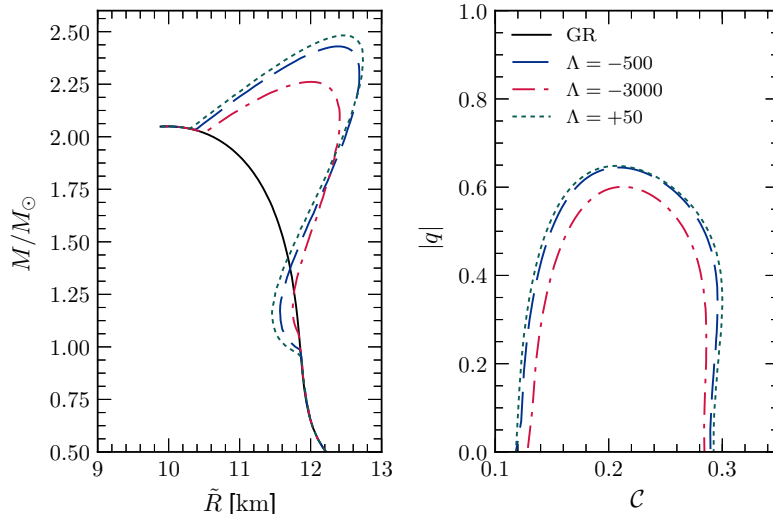


Figure 7.1: *The role of Λ in spontaneous scalarization.* In both panels we consider stellar models using EOS SLy4 with $\beta_1 = -6.0$, $\beta_2 = 0$ and for $\Lambda = (-500, -3000, 50) \text{ km}^2$. For reference the solid line corresponds to GR. Left panel: The mass-radius relation. Right panel: The dimensionless scalar charge $q \equiv -Q/M$ [118] as a function of the compactness \mathcal{C} . We see that $\Lambda > 0$ slightly increases scalarization with respect to the purely conformal theory (cf. Fig. 7.2). On the other hand, $\Lambda < 0$ can dramatically suppress scalarization. Note also that unlike β_2 , Λ can change the compactness threshold above which scalarization can happen, as predicted by the analysis of Sec. 7.5. These results are qualitatively independent of the choice of EOS.

¹In the preceding section, because of the weak (scalar) field approximation the Jordan and Einstein frame radii are approximately the same, i.e. $\tilde{R} = R$. This is not the case in this section and hereafter the compactness uses the Jordan frame radius, i.e. $\mathcal{C} = GM/(c^2\tilde{R})$.

In Fig. 7.2, we consider what happens when we change the value of β_2 while maintaining β_1 and Λ fixed. We see that in agreement with Eq. (7.91), the parameter β_2 does not affect the threshold for scalarization. Moreover, we observe that $\beta_2 < 0$ ($\beta_2 > 0$) makes scalarization more (less) evident with respect to $\beta_2 = 0$. In fact, in Eqs. (7.49) and (7.48), we see that β_1 and β_2 contribute to the scalar field equation through the factors $\Lambda A^4 B^2$ and $\beta - \alpha$, which have competing effects in sourcing the scalar field for $\beta_1 < 0$ and $\beta_2 \neq 0$. Our numerical integrations indicate that the former is dominant and that $\beta_2 \neq 0$ affects only very compact NSs ($\mathcal{C} \gtrsim 0.15$ in the example of Fig. 7.2).

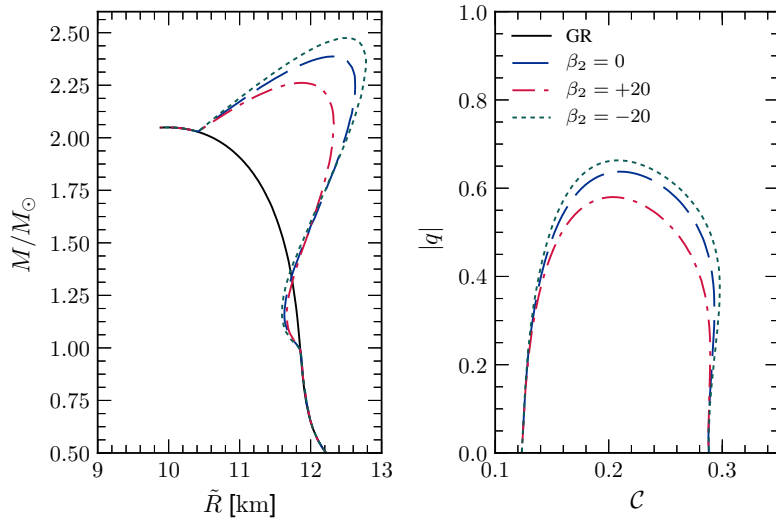


Figure 7.2: *The role of β_2 in spontaneous scalarization.* As in Fig. 7.1, in both panels we consider stellar models using SLy4 EOS but with $\beta_1 = -6.0$ and $\Lambda = -1000 \text{ km}^2$ for $\beta_2 = (-20, 0, 20)$. For reference the solid line corresponds to GR. Left panel: The mass-radius relation. Right panel: The dimensionless scalar charge $q = -Q/M$ as a function of the compactness \mathcal{C} . We see that β_2 affects highly scalarized stellar models making scalarization stronger (in the sense of increasing the value of q) when $\beta_2 < 0$, or weaker for $\beta_2 > 0$. Observe that β_2 has a negligible effect on weakly scalarized models ($|q| \lesssim 0.35$). This is in agreement with its absence from the perturbative analysis of Sec. 7.5. Note that the range of \mathcal{C} for which scalarization occurs is the same, irrespective of the choice of β_2 . Again, these results are qualitatively independent of the choice of EOS.

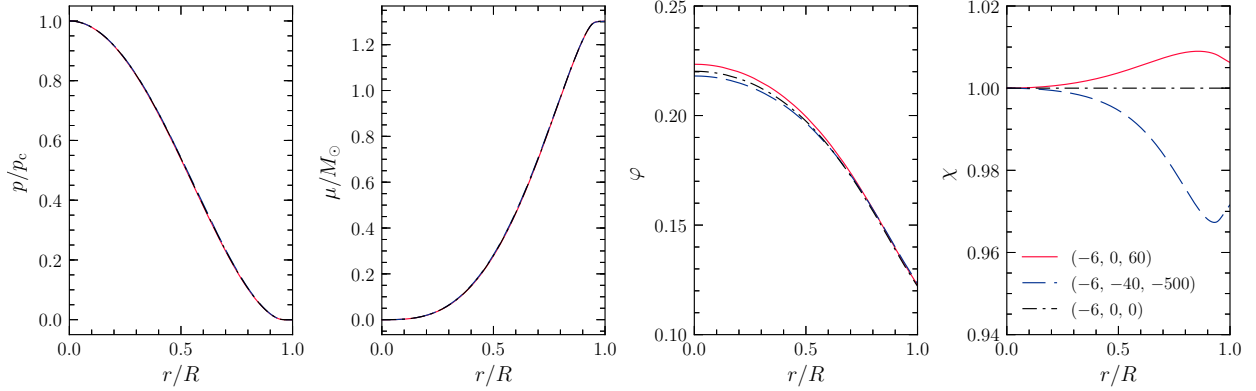


Figure 7.3: *Radial profiles of some quantities of interest.* We show the normalized pressure profile p/p_c (top left), dimensionless mass function μ/M_\odot (top right), scalar field φ (bottom left) and the disformal factor χ (bottom right) in the stellar interior. The radial coordinate was normalized by the Einstein frame radius R . The radial profiles above correspond to three stellar configurations using SLy4 EOS, with fixed baryonic mass $M_b/M_\odot = 1.5$ and theory parameters $(\beta_1, \beta_2, \Lambda) = (-6, 0, 60)$, $(-6, -40, -500)$ and $(-6, 0, 0)$, the latter corresponding to a stellar model in the Damour-Esposito-Farèse theory [118, 120]. While the fluid variables are not dramatically affected, models with $\Lambda > 0$ ($\Lambda < 0$) become more (less) scalarized due to the disformal coupling. The bulk properties of these models are summarized in Table 7.1.

It is also of interest to see how scalarization affects the interior of NSs. In Fig. 7.3, we show the normalized pressure profile p/p_c (top left), the dimensionless mass function μ/M_\odot (top right), the scalar field φ (bottom left) and the disformal factor χ (bottom right) in the stellar interior. The radial coordinate was normalized by the Einstein frame radius R . The quantities correspond to three stellar configurations using SLy4 EOS with fixed baryonic mass $M_b/M_\odot = 1.5$, which in GR yields a canonical NS with mass $M \approx 1.4 M_\odot$, for the sample values of $(\beta_1, \beta_2, \Lambda)$ indicated in Table 7.1. In agreement with our previous discussion we see that NSs with $\Lambda > 0$ ($\Lambda < 0$) support a larger (smaller) value of φ_c , which translates to a larger (smaller) value of q . It is particularly important to observe that χ is non-negative for all NS models, guaranteeing the Lorentzian signature of the spacetime [cf. Eq. (7.9)].

$(\beta_1, \beta_2, \Lambda)$	\tilde{R} [km]	M [M_\odot]	I [10^{45} g cm ²]	φ_c	q
GR	11.72	1.363	1.319	–	–
(−6, 0, 0)	11.60	1.354	1.431	0.220	0.613
(−6, −40, −500)	11.64	1.355	1.440	0.218	0.620
(−6, 0, 60)	11.59	1.354	1.430	0.223	0.614

Table 7.1: The properties of NSs in GR and ST theory using EOS SLy4 and fixed baryonic mass $M_b/M_\odot = 1.5$. The radial profiles of some of the physical variables involved in the integration of the stellar model are shown in Fig. 7.3.

In Fig. 7.4 we show the mass-radius curves (top panels) and moment of inertia-mass (lower panels) for increasing values of β_1 (from left to right), for three realistic EOSs, keeping $\beta_2 = 0$, but using different values of Λ . As we anticipated in Fig. 7.1, negative values of Λ reduce the effects of scalarization, while positive values increase them. The case $\Lambda = 0$ corresponds to the purely conformal theory of Ref. [118]. We observe that scalarized NS models branch from the GR family at different points for different values of Λ (when β_1 is fixed). In agreement with our previous discussion, sufficiently negative values of Λ can completely suppress scalarization. Indeed for $\beta = -4.5$ the solutions with $\Lambda = -1000$ km² are identical to GR, while scalarized solutions exist when $\Lambda = 0$. Additionally, we observe degeneracy between families of solutions in theories with different parameters. For instance, the maximum mass for a NS assuming EOS APR is approximately the same, $M/M_\odot \approx 2.38$, for both $\beta_1 = -5.5$, $\Lambda = 0$ and $\beta_1 = -6.0$, $\Lambda = -1000$ km². We also point out the degeneracy between the choice of EOS and of the parameters of the theory. For instance, the maximum mass predicted by EOS FPS in the theory with $\beta_1 = -5.5$ and $\Lambda = 50$ km² is approximately the same as that predicted by GR, but for EOS SLy4, i.e $M/M_\odot \approx 2.05$. We emphasize that these two types of degeneracies are not exclusive to the theory we are considering, but are generic to *any* modification to GR [184] (and emphasized in Chapter 3).

In Fig. 7.5, we exhibit the mass-radius (top panels) and moment of inertia-mass (lower panels) for increasing values of β_1 (from left to right), but now keeping $\Lambda = -1000$ km² and changing the value of β_2 . Once more, sufficiently negative values of Λ can completely

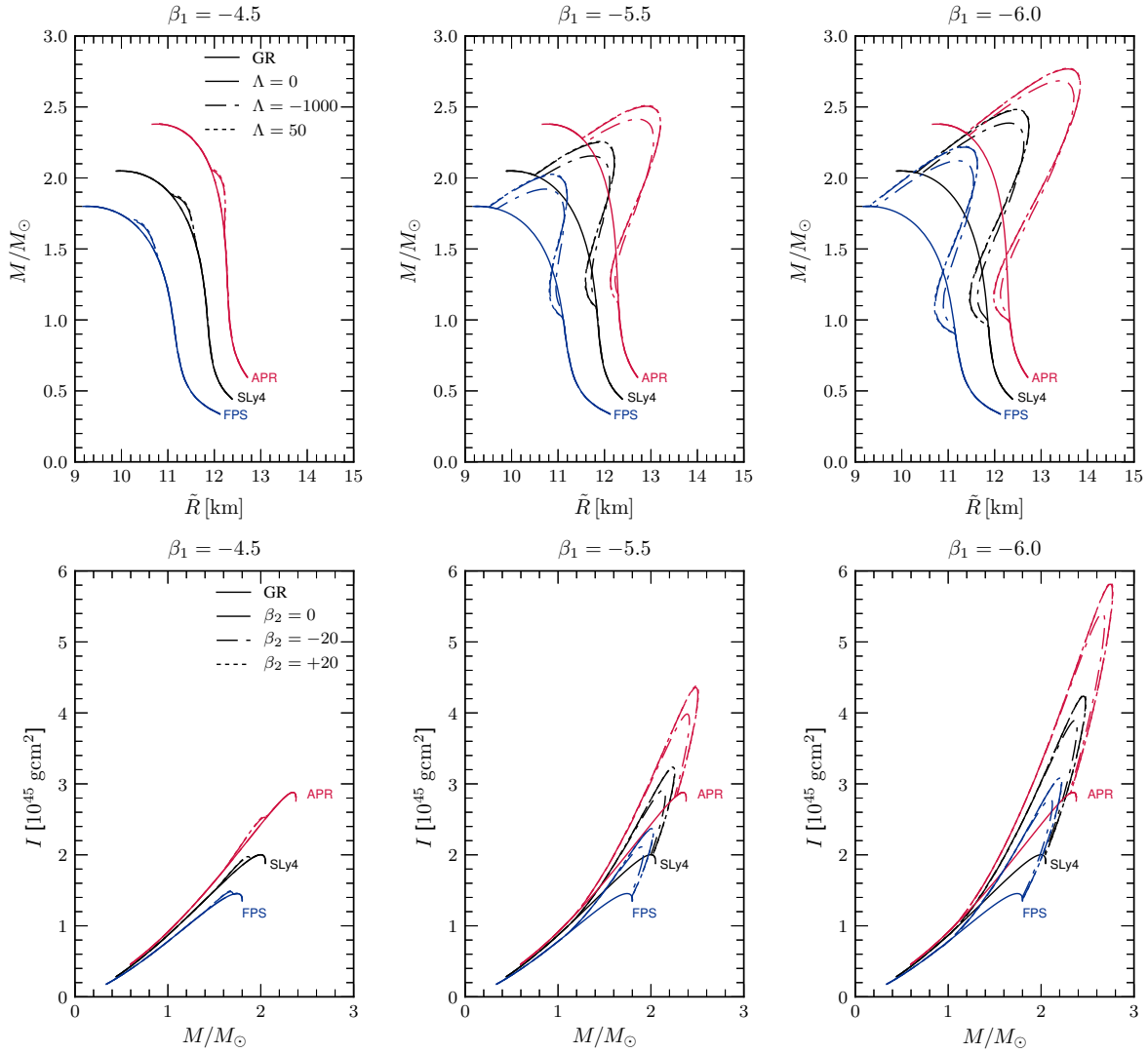


Figure 7.4: *NSs in ST theories with disformal coupling – Part I.* We show NS models for three choices of realistic EOSs, namely APR, SLy4 and FPS, in decreasing order of stiffness. We illustrate the effect of varying the values of β_1 and Λ , while keeping β_2 fixed ($\beta_2 = 0$) for simplicity. The curves corresponding to $\Lambda = 0$, represent stellar models in purely conformal theory [118, 119]. Top panels: Mass-radius relations. Bottom panels: Moment of inertia versus mass. As seen in Fig. 7.1 already, while $\Lambda < 0$ weakens scalarization, $\Lambda > 0$ strengthens the effect. For $\beta_2 = 0$, this latter effect is very mild, being more evident by $\beta_2 < 0$ (cf. Fig. 7.5).

suppress scalarization. This is clearly seen in the panels for $\beta_1 = -4.5$, where $\Lambda = -1000$ km^2 , suppresses scalarization for all values of β_2 considered. We observe that independently of the choice of EOS, $\beta_2 > 0$ ($\beta_2 < 0$) yields smaller (larger) deviations from GR.

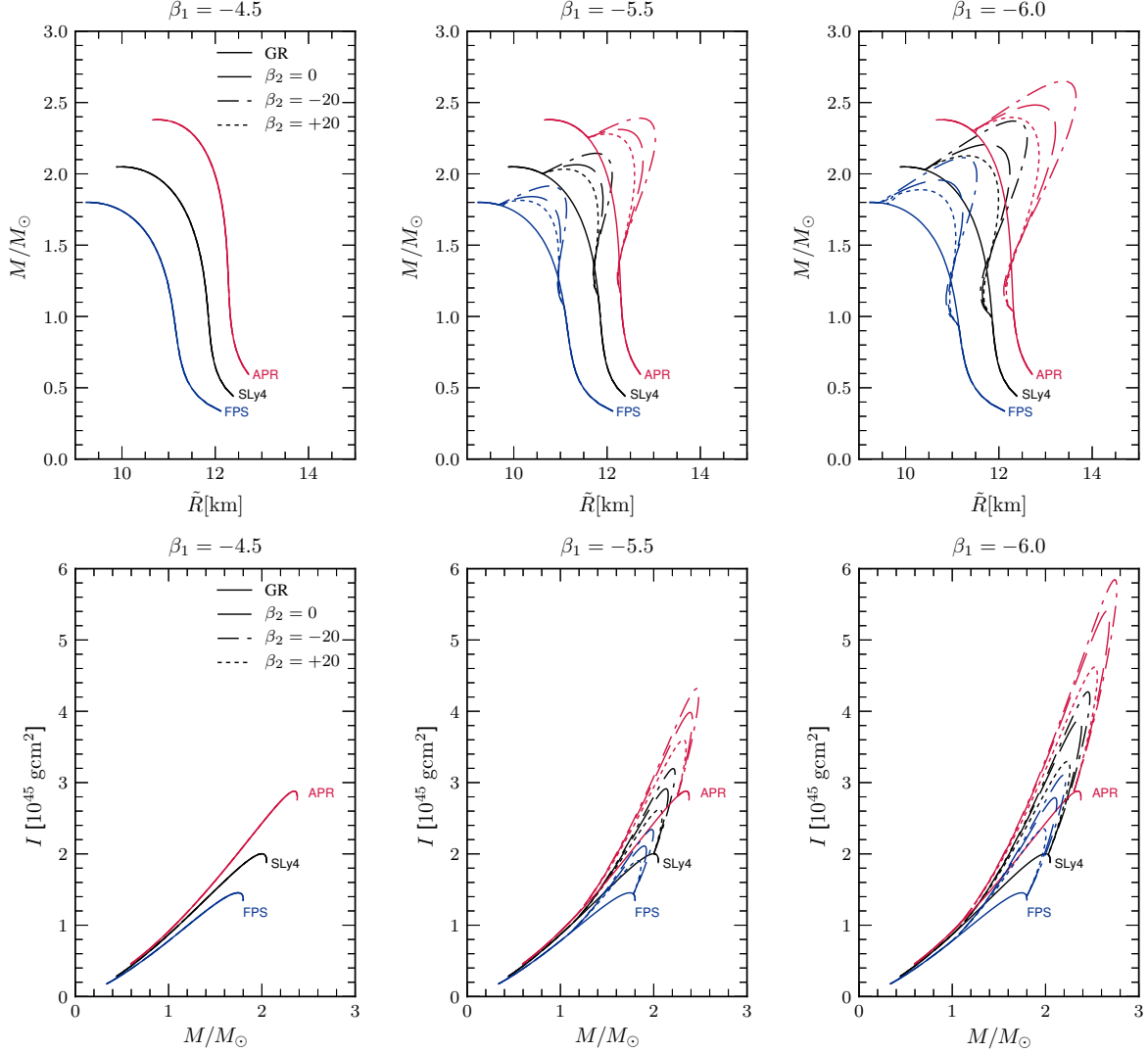


Figure 7.5: *NSs in ST theories with disformal coupling – Part II.* In comparison to Fig. 7.4, here we show the influence of β_2 in spontaneous scalarization while keeping $\Lambda = -1000$ km^2 . As we have seen in Fig. 7.1 (and by the analytic treatment of Sec. 7.5), negative values of Λ suppress scalarization. This effect is such that for $\beta_1 = -4.5$, scalarization is suppressed altogether (top left panel). For smaller values of β_1 , this value of Λ weakens scalarization and we clearly see that β_2 affects the most scalarized stellar models in the conformal coupling theory. Note that the range covered by the axis here and in Fig. 7.4 is the same, making it clear that scalarization is less strong for the values of β_2 adopted.

7.6.3 Stability of the solutions

Let us briefly comment on the stability of the scalarized solutions obtained in this section. In general, for a given set of parameters $(\beta_1, \beta_2, \Lambda)$ and fixed values of M_b and φ_0 , we have more than one stellar configuration with different values of the mass M . Following the arguments of Refs. [118, 198, 223], we take the solution of smallest mass M , i.e., larger fractional binding energy \mathcal{E}_b defined in Eq. (7.64), to be the one which is energetically favorable to be realized in nature. In Fig. 7.6, we show \mathcal{E}_b as a function of M_b for the two families of solutions in a theory with $(\beta_1, \beta_2, \Lambda) = (-6, 0, 50)$ and $\varphi_0 = 0$. The dashed line corresponds to solutions which are indistinguishable from the ones obtained in GR, while the solid line (which branches off from the former around $M_b/M_\odot \approx 1.1$) corresponds to scalarized solutions. We see that scalarized stellar configurations in our model are energetically favorable, as happens in the case of purely conformal coupling theory [118, 198, 223].

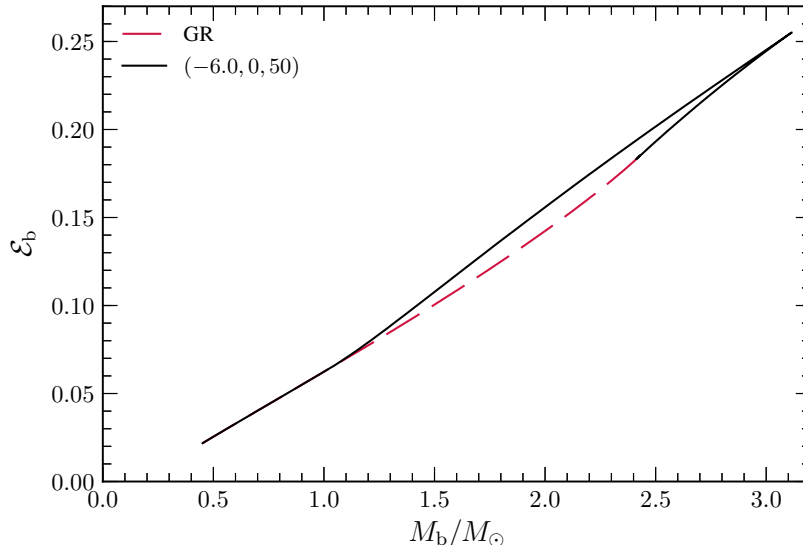


Figure 7.6: *Binding energy.* We show the fractional binding energy \mathcal{E}_b as a function of the baryonic mass for stellar models using EOS SLy4 and for theory with $(\beta_1, \beta_2, \Lambda) = (-6, 0, 50)$. Solutions in this theory branch around $M_b/M_\odot \approx 1.1$ with scalarized solutions (solid line) being energetically favorable over the general-relativistic ones (dashed line). The turning point at the solid curve corresponds to the maximum in the M - R relation, cf. Fig. 7.1.

7.7 An application: EOS-independent $I - \mathcal{C}$ relations

As we have seen in the previous sections the presence of the disformal coupling modifies the structure of NSs making ST theories generically predict different bulk properties with respect to GR. However, as we discussed based on Figs. 7.4 and 7.5, modifications caused by scalarization are usually degenerate with the choice of EOS, severely limiting our ability to constrain the parameters of the theory using current NS observations (see e.g. Ref. [206]). Moreover, different theory parameters can yield similar stellar models for a fixed EOS.

An interesting possibility to circumvent these problems is to search for EOS-independent (or at least weakly EOS-dependent) properties of NSs. Accumulating evidence favoring the existence of such EOS independence between certain properties of NSs, culminated with the discovery of the I -Love- Q relations [514, 515] connecting the moment of inertia, the tidal Love number and the rotational quadrupole moment (all made dimensionless by certain multiplicative factors) of NSs in GR.

If such relations hold in modified theories of gravitation they can potentially be combined with future NS measurements to constrain competing theories of gravity. This attractive idea was explored in the context of dynamical Chern-Simons theory [515], Eddington-inspired Born-Infeld gravity [411], Einstein-dilaton-Gauss-Bonnet (EdGB) gravity [247, 248], $f(R)$ theories [149] and the Damour-Esposito-Farèse model of ST gravity [153, 353].

Within the present framework we cannot compute the I -Love- Q relations, since while on one hand we can compute I , the tidal Love number requires an analysis of tidal interactions, and the rotational quadrupole moment Q requires pushing the Hartle-Thorne perturbative expansion up to order $\mathcal{O}(\Omega^2)$. Nevertheless, we can investigate whether the recently proposed I - \mathcal{C} relations [71] between the moment of inertia I and the compactness \mathcal{C} remain valid in our theory. For a recent study in the Damour-Esposito-Farèse and R^2 theories, see Ref. [448]. This relation was also studied for EdGB and the subclass of Horndeski gravity with nonminimal coupling between the scalar field and the Einstein tensor in Ref. [307].

The relation proposed in Ref. [71] for the moment of inertia $\bar{I} \equiv I/M^3$ and the compactness \mathcal{C} is

$$\bar{I} = a_1 \mathcal{C}^{-1} + a_2 \mathcal{C}^{-2} + a_3 \mathcal{C}^{-3} + a_4 \mathcal{C}^{-4}, \quad (7.94)$$

where the coefficients a_i ($i = 1, \dots, 4$) are given by $a_1 = 8.134 \times 10^{-1}$, $a_2 = 2.101 \times 10^{-1}$, $a_3 = 3.175 \times 10^{-3}$ and $a_4 = -2.717 \times 10^{-4}$. This result is valid for slowly rotating NSs in GR, although it can easily be adapted for rapidly rotating NSs [71]. The coefficients in Eq. (7.94) are obtained by fitting the equation to a large sample of EOSs. For earlier work considering a different normalization for \bar{I} , namely $I/(MR^2)$, see e.g. Refs. [385, 272, 36, 276, 479].

We confront this fit against stellar models in two ST theories with the parameters $(\beta_1, \beta_2, \Lambda)$ having the values $(-6, -20, -500)$ and $(-7, -20, -500)$ that support highly scalarized solutions. As seen in Fig. 7.7, the deviations from GR can be quite large, up to 40% for the theory with $\beta_1 = -7$ in the range of compactness for which spontaneous scalarization happens (cf. Fig. 7.7, bottom panel). Nevertheless, the EOS independence between \bar{I} and \mathcal{C} remains even when scalarization occurs (cf. Fig. 7.7, top panel).

Since our model is largely unconstrained observationally, measurements of the moment of inertia and compactness of NSs could in principle be used to constrain it or, more optimistically, indicate the occurrence of spontaneous scalarization in NSs. This is in contrast with the standard Damour-Esposito-Farèse model, for which the theory's parameters are so tightly constrained by binary pulsar observations [18], that spontaneous scalarization (if it exists) is bound to have a negligible influence on the I - \mathcal{C} relation [448]. We stress however that in general it will be difficult to constrain the parameter space $(\beta_1, \beta_2, \Lambda)$ only through the I - \mathcal{C} relation. The reason is in the degeneracy of stellar models for different values of the parameters; see the discussion in Sec. 7.6.2.

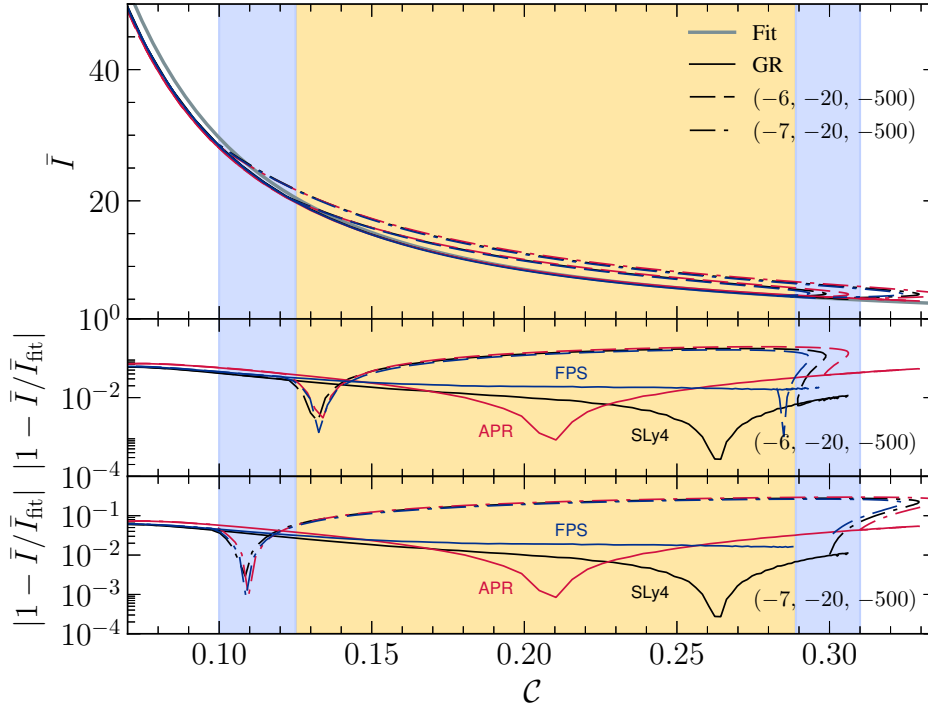


Figure 7.7: *The I - C relation in ST gravity.* Top panel: The fit (7.94) obtained in the context of GR (thick solid line) is confronted against stellar models obtained in GR (solid line); and ST theories with parameters $(\beta_2, \Lambda) = (-20, -500)$, but with $\beta_1 = -6$ (dashed lines) and $\beta_2 = -7$ (dash-dotted lines), using EOSs APR, SLy4 and FPS. Middle panel: Relative error between the fit for GR against ST theory with $\beta_1 = -6$. Bottom panel: Similarly, but for $\beta_1 = -7$. In all panels the shaded regions correspond to approximately the domain of compactness for which spontaneous scalarization occurs in each theory. While for GR, the errors are typically below 6%, scalarized models can deviate from GR by 20% (for $\beta_1 = -6$) and up to 40% (for $\beta_1 = -7$).

7.8 Conclusions and outlook

In this chapter we have presented a general formulation to analyze the structure of relativistic stars in ST theories with disformal coupling, including the leading-order corrections due to slow rotation. The disformal coupling is negligibly small in comparison with conformal coupling in the weak-gravity or slow-motion regimes, where the scalar field is slowly evolving and typical pressures are much smaller than the energy density scales, but it may be comparable to the ordinary conformal coupling in the strong-gravity regime found

inside relativistic stars. Our calculation covers a variety of ST models, especially, conformal and disformal couplings to matter, nonstandard scalar kinetic terms and generic scalar potential terms.

After obtaining the stellar structure equations, we have particularly focused on the case of a canonical scalar field with a generic scalar potential. We showed that in the absence of both conformal coupling and a scalar potential, the disformal coupling does not modify the stellar structure with respect to GR. On the other hand, this result shows us that inside relativistic stars the effects of disformal coupling always appear *only* when there is conformal coupling to matter and/or a nontrivial potential term. The strength of disformal coupling crucially depends on the coupling strength Λ in Eq. (7.2) with dimensions of (length)². For a canonical scalar field, Λ has to be of $\mathcal{O}(10^3)$ km² to significantly influence the structure of NSs.

In our numerical analyses, we have investigated the effects of the disformal coupling on the spontaneous scalarization of NSs in the ST theory with purely conformal coupling. We found that the effects of disformal coupling depend on the sign of Λ . We showed that for negative values of Λ the mass and moment of inertia of NSs decrease, approaching the values in GR for sufficiently large negative values of Λ . We speculate that this is the consequence of a mechanism similar to the disformal screening proposed in Ref. [259] where in a high density or a large disformal coupling limit the response of the scalar field becomes insensitive to the local matter density, exemplified here by studying relativistic stars. On the other hand, for positive values of Λ , we showed that the mass and moment of inertia increase but for too large positive values of Λ the stellar structure equation becomes singular and a regular NS solution cannot be found. This allowed us to derive a mild upper bound of $\Lambda \lesssim 100$ km², that does not depend on the choice of the EOS.

We have also tested the applicability of a recently proposed EOS-independent relation between the dimensionless moment of inertia I/M^3 and the compactness \mathcal{C} for NSs in GR. We found that for a certain domain of the theory's parameter space, the deviations from GR can

be as large as $\sim 40\%$, suggesting that future measurements of NS moment of inertia might be used to test ST theories with disformal coupling. Because of the large dimensionality of the parameter space, modifications with respect to GR are generically degenerate between different choices of β_1 , β_2 and Λ . Thereby, even though deviations from GR can be larger, it seems unlikely that constraints can be put on the theory’s parameters using exclusively the I - \mathcal{C} relation. In this regard, it would be worth extending our work and studying how the I -Love- Q relations are affected by the disformal coupling, generalizing the works of Refs. [353, 151, 153] for ST theories with disformal coupling.

Still in this direction, one could investigate whether the “three-hair” relations – EOS-independent relations connecting higher-order multipole moments of rotating NSs in terms of the first three multipole moments in GR [364, 510, 297] - remain valid in ST theory, including those with disformal coupling. This could be accomplished by combining the formalism developed in [366] with numerical solutions for rotating NSs such as those obtained in Ref. [153].

Although the main subject of our study was to investigate the hydrostatic equilibrium configurations in ST theories with disformal coupling, let us briefly comment on the gravitational (core) collapse resulting in the formation of a NS (see e.g. Ref. [181]). A fully numerical analysis of dynamical collapse in this theory is beyond the scope of our chapter, but an important issue in this dynamical process may be the possible appearance of ghost instabilities for negative values of Λ [241, 259, 43, 59]. During collapse, matter density at a given position increases, and if at some instant it reaches the threshold value where the effective kinetic term in the scalar field equation vanishes, the time evolution afterwards cannot be determined. For a canonical scalar field $P = 2X$, in a linearized approximation where $\chi \simeq 1$ and $B(\varphi) \simeq 1$, the effective kinetic term of the equation of motion (7.20) is roughly given by

$$-\left(1 - \frac{\kappa|\Lambda|}{2}\tilde{\rho}c^2\right)\ddot{\varphi}, \tag{7.95}$$

where a dot represents a time derivative. The sign of the kinetic term may change in the region of a critical density higher than $\tilde{\rho}_{\text{crit}} = 2/(\kappa c^2 |\Lambda|)$. The choice of $\Lambda = -100 \text{ km}^2$ gives $\tilde{\rho}_{\text{crit}} \simeq 10^{15} \text{ g/cm}^3$, which is a typical central density of NSs. Thus for $|\Lambda| \lesssim 100 \text{ km}^2$ a NS is not expected to suffer an instability while for other values it might occur in the interior of the star. Of course, for a more precise estimation, nonlinear interactions between the dynamical scalar field, spacetime and matter must be taken into consideration. A detailed study of time-dependent processes in our theory is definitely important, but is left for future work.

Another interesting prospect for future work would be to study compact binaries within our model. The most stringent test of ST gravity comes from the measurement of the orbital decay of binaries with asymmetric masses, which constrains the emission of dipolar scalar radiation by the system [169]. We expect that the disformal coupling parameters β_2 and Λ should play a role in the orbital evolution of a binary system by influencing the emission of scalar radiation from the system. In fact, both parameters are expected to modify the so-called sensitivities [497, 528] that enter at the lowest PN orders sourcing the emission of dipolar scalar radiation. An investigation of compact binaries within our model could, combined with current observational data, yield tight constraints on disformal coupling. Moreover one could study NS solutions for other classes of ST theories not considered here. This task is facilitated by the generality of our calculations presented in Sec. 7.3.

CHAPTER 8

TENSOR-MULTI-SCALAR THEORIES: RELATIVISTIC STARS AND 3+1 DECOMPOSITION

8.1 Introduction

Modifications of GR often lead to the introduction of additional degrees of freedom [51]. The simplest and best studied extension of GR is ST theory, in which one or more scalar fields are included in the gravitational sector of the action through a non-minimal coupling between the Ricci scalar and a function of the scalar field(s). A further motivation to study ST theories is that they appear in different contexts in high-energy physics: they can be obtained as the low-energy limit of string theories [370], in Kaluza-Klein-like models [156] or in braneworld scenarios [382, 383]. Moreover, ST theories play an important role in cosmology [107].

Almost 60 years ago, in an attempt to implement Mach’s ideas in a relativistic theory of gravity, Jordan, Fierz, Brans and Dicke proposed a specific ST theory (commonly referred to as “Brans-Dicke theory”) as a possible modification of GR [239, 163, 64]. Their theory is still viable, but it has since been constrained to be extremely close to GR by Solar System and binary pulsar observations [499]. Brans-Dicke theory was generalized by Bergmann and Wagoner, who considered the most general ST theory with a single scalar field and an action at most quadratic in derivatives of the fields [44, 491]. In 1992 Damour and Esposito-Farèse introduced and investigated TMS theory, a generalization of the Bergmann-Wagoner theory to an arbitrary number of scalar fields [117]. Multiple scalar degrees of freedom are a generic prediction of string theories and theories involving extra dimensions (see e.g. [240, 11, 114, 115]). In recent years, Bergmann-Wagoner theory has been extensively studied in the case of

a single scalar field (see e.g. [101, 172, 223, 442] and references therein). In comparison, very limited attention has been devoted to the phenomenological implications of TMS theory.

Even in the simplest case of a single scalar, extensively studied by us in Chapter 5 and 6, ST theories give rise to interesting phenomenology. Although their action is linear in the curvature tensor, and scalar-matter couplings are highly constrained by observational bounds from the Solar System [56], ST theories can modify the strong-field regime of GR. Indeed, the equations of structure describing compact stars can admit non-perturbative solutions where the scalar fields can have large amplitudes [118]. This phenomenon, called *spontaneous scalarization*, can significantly affect the masses and radii of NSs. Spontaneous scalarization is strongly constrained by binary pulsar observations [169], but it could still leave a signature in the late inspiral of compact binaries through the so-called “dynamical scalarization” [32, 348, 415], which may be observable by advanced gravitational-wave detectors [400, 470].

In this article we study the phenomenology of TMS theories. The importance of our work for BH physics is to a significant extent of indirect nature. Stellar collapse represents, of course, one of the most important channels for BH formation, and ST theories of gravity are more likely to produce experimental signatures during BH formation than in the dynamics of the remnant “quiescent” BH spacetimes [337, 200].

The reason is that there are strong no-hair theorems¹ implying that stationary, vacuum BH solutions in ST and TMS theories must be identical to GR (cf. [117, 40, 445, 216, 102, 217] and also [443]). In addition, it has been shown that the dynamics of black-hole binaries in ST theory is undistinguishable from that in GR up to 2.5 post-Newtonian order [497, 322] or – in the case of extreme mass-ratio – to all post-Newtonian orders [524]. This result does not apply in the presence of non-trivial boundary conditions [224, 207, 49], but in this case violations of the no-hair theorem would most likely be unobservable. Nev-

¹Hairy BH solutions are possible in presence of a complex scalar field (i.e. two real scalar fields), as long as its phase is time-dependent [212]. No-hair theorems can also be evaded if the potential is non-convex; in this case the solutions are unstable, but their growth time can be extremely large [213].

ertheless, BH binaries have been studied in the framework of single-scalar theories using numerical relativity (cf. [207, 49]), and the extension of such studies to TMS theories may still reveal surprising discoveries.

In order to pave the way for numerical investigations of BHs and NSs in TMS theories, in Section 8.4 we write down the TMS field equations in a 3+1 formalism that is suitable for numerical evolutions of compact binary systems.

A promising avenue to understand the experimental implications of TMS theories (following the reasoning of [118, 119]) is to focus first on the coupling between the various scalars and matter. The scalar fields take values in a coordinate patch of a Riemannian *target-space* manifold. It is natural to ask whether this additional geometric structure can leave a detectable signature in compact stars and/or in the late inspiral of compact binaries, while still allowing for solutions compatible with binary pulsar observations.

This chapter is a preliminary investigation in this direction. We will mainly focus on a simple non-trivial TMS model with two scalar fields and a vanishing potential. This model contains the main novel features that distinguish TMS theories from single-scalar theories, i.e. the presence of a target-space manifold with non-trivial Riemannian structure and non-vanishing curvature, and the presence of a continuous symmetry that is spontaneously broken by scalarized solutions. A more systematic study of scalarization in this prototype TMS theory will be the topic of a future publication, and it should give us useful insight into strong-field effects that characterize more general TMS theories.

8.1.1 Organization of this chapter

The plan of the chapter is as follows. In Section 8.2 we introduce the action and the field equations of TMS theory. We then specialize the field equations to the case of two scalar fields with vanishing potential and a maximally symmetric target-space manifold. In Section 8.3 we derive the equations for slowly rotating relativistic stars, and we perform numerical integrations of these equations in the non-rotating case. In Section 8.4 we derive

the $3+1$ decomposition of the TMS field equations, which can be used to perform fully non-linear numerical evolutions. In Section 8.5 we draw some conclusions and point out possible directions for future work. The Appendices contain some technical material on the structure of target spaces in our model (H), experimental constraints (I) and perturbative arguments to predict the spontaneous scalarization threshold in models with two scalar fields (J).

8.2 Tensor-multi-scalar theories: action, field equations, scalar-matter couplings, and symmetries

8.2.1 Units, notation and conventions

Throughout the chapter we use units with $c = 1$. The gravitational constant measured in a Cavendish experiment is denoted by G , while the “bare” gravitational constant appearing in the action is denoted by G_\star : the relation between the two constants is written down explicitly in Eq. (I.1). Indices on space-time tensors are denoted by Greek letters and take values $0, \dots, 3$, and space-time coordinates are denoted by x^μ . The Lorentzian space-time metric is taken to have signature $(-, +, +, +)$, and its components are denoted by $g_{\mu\nu}(x)$. The conventions for the Riemann curvature tensor and its contractions, as well as the notation for symmetrization and anti-symmetrization of tensors, are those of Misner, Thorne, and Wheeler [323].

The N -tuple of scalar fields $\varphi^A(x) = (\varphi^1(x), \dots, \varphi^N(x))$ takes values in a coordinate patch of an N -dimensional Riemannian target-space manifold. Indices on target-space tensors are denoted by early capital Roman letters A, B, C, \dots , and take integer values $1, \dots, N$. Components of the Riemannian target-space metric are denoted by $\gamma_{AB}(\varphi)$, and the associated Christoffel symbols are denoted by $\gamma^C_{AB}(\varphi)$. The target-space Riemann curvature tensor is denoted by $\mathcal{R}^A_{BCD}(\varphi)$, with obvious notation for derived quantities such as the Ricci tensor and the Ricci scalar. If the target space has a Hermitian structure², then indices on complexified tensors are denoted by lower-case Roman letters, and take values

²For an introduction to Hermitian structures and complex differential geometry, see e.g. [326].

$1, 2, \dots, N/2$. Holomorphic coordinates are denoted by $(\varphi^a, \bar{\varphi}^a)$, and the components of the Hermitian metric in these coordinates are denoted by $\gamma_{\bar{a}b}(\varphi, \bar{\varphi})$. For reference, in Tables 8.1 and 8.2 we provide an overview of the meaning of the various symbols and conventions used in this chapter.

8.2.2 Action and field equations for N real scalars

We consider a gravitational theory with metric tensor $g_{\mu\nu}$, and scalar fields $\varphi^1, \dots, \varphi^N$ which take values in a coordinate patch of an N -dimensional target-space manifold. We assume that all non-gravitational fields, denoted collectively by Ψ , couple only to the Jordan-frame metric $\tilde{g}_{\mu\nu} = A^2(\varphi)g_{\mu\nu}$, so that the matter action has the functional form $S_m[\Psi; \tilde{g}_{\mu\nu}]$. This assumption guarantees that the WEP, which has been experimentally verified with great accuracy [499], will hold. The quantity $A(\varphi)$ is a conformal factor relating the metrics $\tilde{g}_{\mu\nu}$ and $g_{\mu\nu}$.

The most general action which is invariant under space-time and target-space diffeomorphisms (up to boundary terms and field redefinitions), and has at most two space-time derivatives, can be written in the form [117]

$$S = \frac{1}{4\pi G_\star} \int d^4x \sqrt{-g} \left[\frac{R}{4} - \frac{1}{2} g^{\mu\nu} \gamma_{AB}(\varphi) \partial_\mu \varphi^A \partial_\nu \varphi^B - V(\varphi) \right] + S_m[A^2(\varphi)g_{\mu\nu}; \Psi], \quad (8.1)$$

where G_\star is a bare gravitational constant, and g and R are the determinant and Ricci scalar of $g_{\mu\nu}$, respectively. The positive-definiteness of the target-space Riemannian metric $\gamma_{AB}(\varphi)$ guarantees the absence of negative-energy excitations. The scalars φ^A are dimensionless and the potential $V(\varphi)$ has length dimensions minus two. The conformal factor $A(\varphi)$ is dimensionless. In the case of a single scalar ($N = 1$), the target-space metric $\gamma_{AB}(\varphi)$ reduces to a scalar function $\gamma(\varphi)$, and the choice $\gamma(\varphi) = 1$ can be made without loss of generality.

The field equations of the theory, obtained by varying the action (8.1) with respect

G	Gravitational constant from a Cavendish experiment
G_\star	Bare gravitational constants appearing in the action
μ, ν, ρ	Spacetime indices
x^μ	Spacetime coordinates
$g_{\mu\nu}$	Spacetime metric in the Einstein frame
∇_μ	Covariant derivative associated with $g_{\mu\nu}$
$R^\mu{}_{\nu\rho\sigma}$	Spacetime Riemann tensor
A, B, C	Scalar-field indices in real notation
N	Number of scalar fields
φ^A	Gravitational scalar fields in real notation
γ_{AB}	Target-space metric in real notation
γ_{BC}^A	Christoffel symbols on the target space in real notation
$\mathcal{R}^A{}_{BCD}$	Target-space Riemann tensor
Ψ	Non-gravitational fields
$\tilde{g}_{\mu\nu}$	Spacetime metric in the Jordan frame
$A(\varphi)$	Einstein-Jordan frame conformal factor
$V(\varphi)$	Scalar-field potential
a, b, c	Scalar-field indices in complex notation
$\varphi^a, \bar{\varphi}^a$	Gravitational scalar fields in complex notation
$\gamma_{\bar{a}b}$	Target-space metric in complex notation
$\gamma_{\bar{b}c}^a, \gamma_{bc}^a$	Christoffel symbols on the target space in complex notation
\mathbf{r}	Target-space curvature radius ($N = 2$)
$\kappa(\varphi, \bar{\varphi})$	Scalar-matter coupling function ($N = 2$), see Eq. (8.19)
$\alpha^*, \bar{\alpha}^*$	Linear-term coefficients in the expansion of $\log A(\psi, \bar{\psi})$
$\beta_0, \beta_1^*, \bar{\beta}_1^*$	Quadratic-term coefficients in the expansion of $\log A(\psi, \bar{\psi})$
θ	Generic rotation angle in the target-space complex plane
α, β_1	Redefinition of α^*, β_1^* , after rotation
$\psi, \bar{\psi}$	Redefinition of the fields $\varphi, \bar{\varphi}$ after rotation
Z	$\text{Re}[\psi]$
W	$\text{Im}[\psi]$

Table 8.1: Variables and conventions used in this chapter – Part I. Quantities defining the theory

t, r, θ, ϕ	Spacetime coordinates for stellar models
$\nu(r)$	Lapse function
$m(r) = r\mu(r)$	Mass function
$\omega(r)$	Fluid differential angular velocity
Ω	Angular velocity of the star
ρ	Fluid mass-energy density
P	Fluid pressure
n_B	Baryon density
u^μ, \tilde{u}^μ	Fluid 4-velocity in the Einstein/Jordan frame
Subscript “0”	Previous quantities evaluated at the star’s center, $r = 0$
R, \tilde{R}	Stellar radius in the Einstein/Jordan frame
ψ_∞	Asymptotic value of the scalar field
M	Gravitational mass of the star
Q	Scalar charge of the star
M_B	Baryonic mass of the star
K, n_0, m_b, γ	Equation of state parameters, see Eq. (8.36)

Table 8.2: Variables and conventions used in this chapter – Part II. Quantities characterizing the stellar configurations.

to $g^{\mu\nu}$ and φ , take the form

$$R_{\mu\nu} = 2\gamma_{AB}(\varphi)\nabla_\mu\varphi^A\nabla_\nu\varphi^B + 2V(\varphi)g_{\mu\nu} + 8\pi G_\star \left(T_{\mu\nu} - \frac{1}{2}Tg_{\mu\nu} \right), \quad (8.2)$$

$$\square\varphi^A = -\gamma^A_{BC}(\varphi)g^{\mu\nu}\nabla_\mu\varphi^B\nabla_\nu\varphi^C + \gamma^{AB}(\varphi)\frac{\partial V(\varphi)}{\partial\varphi^B} - 4\pi G_\star\gamma^{AB}(\varphi)\frac{\partial\log A(\varphi)}{\partial\varphi^B}T. \quad (8.3)$$

Here ∇_μ is the covariant derivative associated with $g_{\mu\nu}$, and $\square \equiv \nabla^\mu\nabla_\mu$ is the corresponding d’Alembertian operator. The Ricci tensor built out of the metric $g_{\mu\nu}$ is denoted as $R_{\mu\nu}$. The energy-momentum tensor $T_{\mu\nu}$ of the non-gravitational fields is defined by

$$T_{\mu\nu} \equiv -\frac{2}{\sqrt{-g}}\frac{\delta S_m[A^2(\varphi)g_{\rho\sigma}; \Psi]}{\delta g^{\mu\nu}}, \quad (8.4)$$

and its trace is given by $T \equiv g^{\mu\nu}T_{\mu\nu}$.

The energy conservation equation reads

$$\nabla^\mu [T_{\mu\nu} + T_{\mu\nu}^{(\varphi)}] = 0, \quad (8.5)$$

or, more explicitly,

$$\nabla^\mu T_{\mu\nu} = \frac{\partial \log A(\varphi)}{\partial \varphi^A} T \nabla_\nu \varphi^A. \quad (8.6)$$

Here

$$\begin{aligned} T_{\mu\nu}^{(\varphi)} &\equiv -\frac{2}{\sqrt{-g}} \frac{\delta S_\varphi[g_{\rho\sigma}; \varphi]}{\delta g^{\mu\nu}}, \\ &= \frac{1}{4\pi G_\star} \left[\gamma_{AB}(\varphi) \left(\nabla_\mu \varphi^A \nabla_\nu \varphi^B - \frac{1}{2} g_{\mu\nu} g^{\rho\sigma} \nabla_\rho \varphi^A \nabla_\sigma \varphi^B \right) - V(\varphi) g_{\mu\nu} \right] \end{aligned} \quad (8.7)$$

is an effective energy-momentum tensor for the scalar fields, where S_φ denotes the scalar kinetic and potential contributions to the action (8.1). One may build an energy-momentum tensor which is conserved with respect to the Levi-Civita connection of the Jordan-frame metric, and whose components are directly related to physically observable quantities as

$$\tilde{T}_{\mu\nu} \equiv -\frac{2}{\sqrt{-\tilde{g}}} \frac{\delta S_m[\tilde{g}_{\rho\sigma}; \Psi]}{\delta \tilde{g}^{\mu\nu}} = A^{-2}(\varphi) T_{\mu\nu}. \quad (8.8)$$

8.2.3 Complexification

If the target space has a Hermitian structure, then it is useful to write the action in terms of holomorphic coordinates and complexified tensors:

$$S = \frac{1}{4\pi G_\star} \int d^4x \sqrt{-g} \left[\frac{R}{4} - g^{\mu\nu} \gamma_{\bar{a}b}(\varphi, \bar{\varphi}) \nabla_\mu \bar{\varphi}^a \nabla_\nu \varphi^b - V(\varphi, \bar{\varphi}) \right] + S_m[A^2(\varphi, \bar{\varphi}) g_{\mu\nu}; \Psi]. \quad (8.9)$$

The complexified field equations are:

$$R_{\mu\nu} = 4\gamma_{\bar{a}b}(\varphi, \bar{\varphi}) \nabla_{(\mu} \bar{\varphi}^a \nabla_{\nu)} \varphi^b + 2V(\varphi, \bar{\varphi}) g_{\mu\nu} + 8\pi G_\star \left(T_{\mu\nu} - \frac{1}{2} T g_{\mu\nu} \right), \quad (8.10)$$

$$\begin{aligned} \square \varphi^a &= -\gamma^a_{\bar{b}c}(\varphi, \bar{\varphi}) g^{\mu\nu} \nabla_\mu \varphi^b \nabla_\nu \varphi^c - 2\gamma^a_{\bar{b}c}(\varphi, \bar{\varphi}) g^{\mu\nu} \nabla_\mu \bar{\varphi}^b \nabla_\nu \varphi^c \\ &+ \gamma^{a\bar{b}}(\varphi, \bar{\varphi}) \frac{\partial V(\varphi, \bar{\varphi})}{\partial \bar{\varphi}^b} - 4\pi G_\star \gamma^{a\bar{b}}(\varphi, \bar{\varphi}) \frac{\partial \log A(\varphi, \bar{\varphi})}{\partial \bar{\varphi}^b} T. \end{aligned} \quad (8.11)$$

Note that for Kähler manifolds (and in particular one-complex-dimensional manifolds)

$$\gamma^a_{\bar{b}c}(\varphi, \bar{\varphi}) = 0, \quad \gamma^a_{bc}(\varphi, \bar{\varphi}) = \gamma^{a\bar{d}}(\varphi, \bar{\varphi}) \frac{\partial \gamma_{c\bar{d}}(\varphi, \bar{\varphi})}{\partial \varphi^b}, \quad (8.12)$$

so in this particular case the scalar field equations would simplify considerably.

8.2.4 A two-real-scalar model with maximally symmetric target space

The simplest extension of a ST theory with a single real scalar field is the case of two real scalar fields. We will mostly focus on this model to illustrate the basic features of the new phenomenology arising in TMS theories relative to the case of a single real scalar. If the target space is assumed to be maximally symmetric, then there are three possibilities for its geometry: flat, spherical, or hyperbolic. In the flat case, the target space may be trivially identified with the complex plane \mathbb{C} . In the spherical case, the target space may be conformally mapped to the one-point-compactification $\hat{\mathbb{C}}$ of the complex plane \mathbb{C} by means of stereographic projection. In the case of a hyperboloid of two sheets, the target space may be conformally mapped to $\hat{\mathbb{C}} \setminus S^1$, also by means of stereographic projection (we shall neglect the case of a hyperboloid of one sheet); see Appendix H for details. Using the complex formulation discussed in Section 8.2.3, we work with a single complex scalar rather than two real scalars, for which the action (8.9) reduces to

$$S = \frac{1}{4\pi G_\star} \int d^4x \sqrt{-g} \left[\frac{R}{4} - g^{\mu\nu} \gamma(\varphi, \bar{\varphi}) \nabla_\mu \bar{\varphi} \nabla_\nu \varphi - V(\varphi, \bar{\varphi}) \right] + S_m[A^2(\varphi, \bar{\varphi}) g_{\mu\nu}; \Psi], \quad (8.13)$$

and the field equations are

$$R_{\mu\nu} = 4\gamma(\varphi, \bar{\varphi}) \nabla_{(\mu} \bar{\varphi} \nabla_{\nu)} \varphi + 2V(\varphi, \bar{\varphi}) g_{\mu\nu} + 8\pi G_\star \left(T_{\mu\nu} - \frac{1}{2} T g_{\mu\nu} \right), \quad (8.14)$$

$$\begin{aligned} \square \varphi = & -\frac{\partial \log \gamma(\varphi, \bar{\varphi})}{\partial \varphi} g^{\mu\nu} \nabla_\mu \varphi \nabla_\nu \varphi + \gamma^{-1}(\varphi, \bar{\varphi}) \frac{\partial V(\varphi, \bar{\varphi})}{\partial \bar{\varphi}} \\ & - 4\pi G_\star \gamma^{-1}(\varphi, \bar{\varphi}) \frac{\partial \log A(\varphi, \bar{\varphi})}{\partial \bar{\varphi}} T. \end{aligned} \quad (8.15)$$

Hereafter we assume that the potential vanishes, i.e. $V(\varphi, \bar{\varphi}) = 0$, and that the target space is maximally symmetric. Therefore, upon stereographic projection and field redefinition (see Appendix H), the target-space metric can be written as

$$\gamma(\varphi, \bar{\varphi}) = \frac{1}{2} \left(1 + \frac{\bar{\varphi}\varphi}{4\mathbf{r}^2} \right)^{-2}, \quad (8.16)$$

where \mathbf{r} is the radius of curvature of the target-space geometry: for a spherical geometry we have $\mathbf{r}^2 > 0$, for a hyperbolic geometry $\mathbf{r}^2 < 0$, and in the limit $\mathbf{r} \rightarrow \infty$ the geometry is flat.

With the above choices, the field equations become

$$R_{\mu\nu} = 2 \left(1 + \frac{\bar{\varphi}\varphi}{4\mathbf{r}^2} \right)^{-2} \partial_{(\mu} \bar{\varphi} \partial_{\nu)} \varphi + 8\pi G_{\star} \left(T_{\mu\nu} - \frac{1}{2} T g_{\mu\nu} \right), \quad (8.17)$$

$$\square\varphi = \left(\frac{2\bar{\varphi}}{\bar{\varphi}\varphi + 4\mathbf{r}^2} \right) g^{\mu\nu} \partial_{\mu}\varphi \partial_{\nu}\varphi - 4\pi G_{\star} \left(1 + \frac{\bar{\varphi}\varphi}{4\mathbf{r}^2} \right) \bar{\kappa}(\varphi, \bar{\varphi}) T, \quad (8.18)$$

where we introduced

$$\kappa(\varphi, \bar{\varphi}) \equiv 2 \left(1 + \frac{\bar{\varphi}\varphi}{4\mathbf{r}^2} \right) \frac{\partial \log A(\varphi, \bar{\varphi})}{\partial \varphi}, \quad (8.19)$$

the so-called scalar-matter coupling function.

The function $A(\varphi, \bar{\varphi})$, whose derivative enters into the field equations, determines the scalar-matter coupling through Eq. (8.19). Without loss of generality we assume that far away from the source the field vanishes, i.e. that the asymptotic value of the scalar field is $\varphi_{\infty} = 0$. We then expand the function $\log A$ in a series about $\varphi = 0$:

$$\log A(\varphi, \bar{\varphi}) = \alpha^* \varphi + \bar{\alpha}^* \bar{\varphi} + \frac{1}{2} \beta_0 \varphi \bar{\varphi} + \frac{1}{4} \beta_1^* \varphi^2 + \frac{1}{4} \bar{\beta}_1^* \bar{\varphi}^2 + \dots, \quad (8.20)$$

where β_0 is real, while α^* and β_1^* are in general complex numbers³. Although the five real

³At the onset of spontaneous scalarization $|\varphi| \ll 1$, and we can always expand the conformal factor as in Eq. (8.20). For scalarized solutions the field amplitude may be large, the higher-order terms in the expansion may not be negligible, and the expansion (8.20) should be considered as an ansatz for the conformal factor. For a general functional form of the conformal factor, the series expansion used here (and in Ref. [118]) can only provide a qualitative description of the scalarized solution.

parameters $\text{Re}[\alpha^*]$, $\text{Im}[\alpha^*]$, β_0 , $\text{Re}[\beta_1^*]$, $\text{Im}[\beta_1^*]$ are defined in terms of a specific target-space coordinate system, the four real quantities ($|\alpha^*|$, β_0 , $|\beta_1^*|$, $\arg \alpha^* - \frac{1}{2} \arg \beta_1^*$) may be expressed solely in terms of target-space scalar quantities, and thus have an invariant geometric meaning⁴. The remaining real parameter is an unmeasurable overall complex phase.

To make this explicit, redefine $\beta_1^* \equiv \beta_1 e^{i\theta}$, where θ is chosen such that β_1 is real. Then, after defining $\alpha^* \equiv \alpha e^{i\theta/2}$ and a new field $\psi \equiv \varphi e^{i\theta/2}$, the field equations become

$$R_{\mu\nu} = 2 \left(1 + \frac{\bar{\psi}\psi}{4\mathbf{r}^2} \right)^{-2} \partial_{(\mu} \bar{\psi} \partial_{\nu)} \psi + 8\pi G_\star \left(T_{\mu\nu} - \frac{1}{2} T g_{\mu\nu} \right), \quad (8.21)$$

$$\square \psi = \left(\frac{2\bar{\psi}}{\bar{\psi}\psi + 4\mathbf{r}^2} \right) g^{\mu\nu} \partial_\mu \psi \partial_\nu \psi - 4\pi G_\star \left(1 + \frac{\bar{\psi}\psi}{4\mathbf{r}^2} \right) \bar{\kappa}(\psi, \bar{\psi}) T, \quad (8.22)$$

where the function κ is defined in Eq. (8.19) and

$$\log A(\psi, \bar{\psi}) = \alpha\psi + \bar{\alpha}\bar{\psi} + \frac{1}{2}\beta_0\psi\bar{\psi} + \frac{1}{4}\beta_1\psi^2 + \frac{1}{4}\beta_1\bar{\psi}^2 + \dots \quad (8.23)$$

Therefore, any solution of the original theory (formulated with respect to φ and complex coupling coefficients α^* and β_1^*) can be obtained from a theory where we consider the field ψ , a real-valued β_1 and a generically complex α . The solution for the theory corresponding to the conformal factor (8.20) is then given by a simple rotation, $\varphi = \psi \exp(-i\theta/2)$.

The model just described represents the simplest, yet quite comprehensive, generalization of the model of single ST theory investigated originally in Ref. [118].

Note that the quantity $|\alpha|^2 \equiv \alpha\bar{\alpha} \equiv \text{Re}[\alpha]^2 + \text{Im}[\alpha]^2$ is strongly constrained by observations (cf. Appendix I), similarly to the single-scalar case. When $\alpha = 0$, the conformal coupling reduces to

$$\log A(\psi, \bar{\psi}) = \frac{1}{2}\beta_0\psi\bar{\psi} + \frac{1}{4}\beta_1\psi^2 + \frac{1}{4}\beta_1\bar{\psi}^2, \quad (8.24)$$

where we neglected higher-order terms in the scalar field. However, in TMS theories α is

⁴The eigenvalues of the quadratic form in (8.20), given by $\beta_0 \pm |\beta_1^*|$, are target-space scalars. The phase difference $\arg \alpha^* - \frac{1}{2} \arg \beta_1^*$ arises when this quadratic form is contracted with α^* , see Eq. (I.6).

a complex quantity and its argument, $\arg \alpha$, is completely unconstrained in the weak-field regime. In Section 8.3.2.2 we will show that compact stars in theories with $\alpha = 0$ and $\alpha \neq 0$ are rather different.

The field equations can be also written in terms of two real scalars. For this purpose, let us split the field ψ into real and imaginary parts: $\psi \equiv \text{Re}[\psi] + i \text{Im}[\psi]$. Then the conformal factor (8.24), again in the $\alpha = \bar{\alpha} = 0$ case, reads:

$$\log A(\psi, \bar{\psi}) = \frac{1}{2} [(\beta_0 + \beta_1)\text{Re}[\psi]^2 + (\beta_0 - \beta_1)\text{Im}[\psi]^2]. \quad (8.25)$$

The structure of this TMS theory is ultimately determined by three real parameters: $\beta_0 + \beta_1$, $\beta_0 - \beta_1$ and the target-space curvature defined by \mathbf{r}^2 . When $\alpha \neq 0$, two further parameters ($|\alpha|$ and $\arg \alpha$) are necessary to define the theory.

8.3 Stellar structure in tensor-multi-scalar theories

In this section we consider the structure of relativistic stars in the context of the TMS theory introduced in Section 8.2.4. We first derive the equations of structure for a slowly rotating star in the Hartle-Thorne formalism [203, 204] (Section 8.3.1), then we integrate these equations and discuss some properties of scalarized solutions in increasingly complex scenarios (Section 8.3.2).

8.3.1 Equations of hydrostatic equilibrium

We describe a stationary, axisymmetric star, composed by a perfect fluid, slowly rotating with angular velocity Ω , using coordinates $x^\mu = (t, r, \theta, \phi)$ and the line element

$$g_{\mu\nu} dx^\mu dx^\nu = -e^{\nu(r)} dt^2 + \frac{dr^2}{1 - 2\mu(r)} + r^2(d\theta^2 + \sin^2 \theta d\phi^2) + 2[\omega(r) - \Omega] r^2 \sin^2 \theta dt d\phi. \quad (8.26)$$

where we neglect terms of order $\sim \Omega^2$ and higher in the metric and in the hydrodynamical quantities. The variable $\mu(r)$ is related to the more familiar mass function $m(r)$ by $\mu = m/r$.

The energy-momentum tensor of the perfect fluid takes the usual form

$$T^{\mu\nu} = A^4(\psi, \bar{\psi}) [(\rho + P)u^\mu u^\nu + P g^{\mu\nu}] , \quad (8.27)$$

where ρ , P , and $\tilde{u}^\mu = A^{-1}(\psi, \bar{\psi})u^\mu$ are the mass-energy density, pressure, and four-velocity of the fluid, respectively, and

$$u^\mu = e^{-\nu/2}(1, 0, 0, \Omega) . \quad (8.28)$$

With these choices, the field equations (8.2)–(8.3) reduce to a system of coupled ordinary differential equations, namely

$$(r\mu)' = \frac{1}{2}(1 - 2\mu)r^2 \left(1 + \frac{\bar{\psi}\psi}{4r^2}\right)^{-2} \bar{\psi}'\psi' + 4\pi G_\star A^4(\psi, \bar{\psi})r^2\rho , \quad (8.29)$$

$$P' = -(\rho c^2 + P) \left\{ \frac{\nu'}{2} + \frac{1}{2} \left(1 + \frac{\bar{\psi}\psi}{4r^2}\right)^{-1} [\kappa(\psi, \bar{\psi})\psi' + \bar{\kappa}(\psi, \bar{\psi})\bar{\psi}'] \right\} , \quad (8.30)$$

$$\nu' = \frac{2\mu}{r(1 - 2\mu)} + r \left(1 + \frac{\bar{\psi}\psi}{4r^2}\right)^{-2} \bar{\psi}'\psi' + \frac{8\pi G_\star A^4(\psi, \bar{\psi})rP}{1 - 2\mu} , \quad (8.31)$$

$$\begin{aligned} \psi'' &= \frac{2\bar{\psi}\psi'^2}{\bar{\psi}\psi + 4r^2} - \frac{2(1 - \mu)}{r(1 - 2\mu)}\psi' \\ &+ \frac{4\pi G_\star A^4(\psi, \bar{\psi})}{1 - 2\mu} \left[(\rho - 3P) \left(1 + \frac{\bar{\psi}\psi}{4r^2}\right) \bar{\kappa}(\psi, \bar{\psi}) + r\psi'(\rho - P) \right] , \end{aligned} \quad (8.32)$$

$$\omega'' = \left[r \left(1 + \frac{\bar{\psi}\psi}{4r^2}\right)^{-2} \bar{\psi}'\psi' - \frac{4}{r} \right] \omega' + \frac{4\pi G_\star A^4(\psi, \bar{\psi})r(\rho c^2 + P)}{1 - 2\mu} \left(\omega' + \frac{4}{r}\omega \right) , \quad (8.33)$$

where primes denote derivatives with respect to the radial coordinate $x^1 = r$. As usual, the system is closed by specifying a barotropic equation of state $P = P(\rho)$.

For the purpose of numerical integration, it is useful to work out series expansions of

the functions $\mu(r)$, $\nu(r)$, $P(r)$, $\psi(r)$, and $\omega(r)$ about $r = 0$:

$$\mu(r) = \frac{4\pi G_\star}{3} A_0^4 \rho_0 r^2 + \mathcal{O}(r^4), \quad (8.34a)$$

$$\nu(r) = \nu_0 + \frac{4\pi G_\star}{3} A_0^4 (\rho_0 + 3P_0) r^2 + \mathcal{O}(r^4), \quad (8.34b)$$

$$P(r) = P_0 - \frac{2\pi G_\star}{3} A_0^4 (\rho_0 + P_0) [\rho_0 + 3P_0 + \bar{\kappa}_0 \kappa_0 (\rho_0 - 3P_0)] r^2 + \mathcal{O}(r^4), \quad (8.34c)$$

$$\psi(r) = \psi_0 + \frac{2\pi G_\star}{3} A_0^4 \bar{\kappa}_0 (\rho_0 - 3P_0) \left(1 + \frac{\bar{\psi}_0 \psi_0}{4\mathbf{r}^2} \right) r^2 + \mathcal{O}(r^4), \quad (8.34d)$$

$$\omega(r) = \omega_0 + \frac{8\pi G_\star}{5} \omega_0 A_0^4 (\rho_0 + P_0) r^2 + \mathcal{O}(r^4). \quad (8.34e)$$

Here the subscript 0 denotes evaluation at the stellar center $r = 0$.

When ψ and $\bar{\psi}$ are constant and $A(\psi, \bar{\psi}) = 1$ the field equations reduce to the standard Tolman-Oppenheimer-Volkoff equations in GR. Indeed, GR solutions are part of the solution spectrum of TMS theories with $\alpha = 0$ in Eq. (8.23), as in the usual single-scalar case [117, 118]. On the other hand, when $\alpha \neq 0$ the scalar field is forced to have a non-trivial profile in the presence of matter ($T \neq 0$).

Furthermore, even when $\alpha = 0$, other solutions characterized by a non-trivial profile for the scalar fields can co-exist with the GR solutions; in Appendix J we give a simple interpretation of these ‘‘spontaneously scalarized’’ solutions in terms of a tachyonic instability of relativistic GR solutions. Besides their gravitational mass M and radius R , scalarized NSs are characterized by their scalar charge Q , which is generally a complex number for the complex scalar field ψ discussed here⁵.

The gravitational mass M and the scalar charge Q of stellar models in TMS theories can be computed by integration in the vacuum exterior region, where $P = \rho = 0$. We integrate the structure equations outwards from $r = 0$ up to a point $r = R$ such that $P(R) = 0$, which determines the stellar surface in the Einstein frame. The areal radius \tilde{R}

⁵Note that Q is defined in terms of a specific target-space coordinate system. Observable quantities must be invariant under changes of coordinates, and can thus only depend on target-space scalars such as $|Q|^2$, or $|Q_A - Q_B|^2$ (for a binary system with bodies A and B), or more complicated contractions.

in the Jordan frame can be obtained rescaling R by the conformal factor $A(\psi, \bar{\psi})$, which depends on the value of the scalar field ψ and its complex conjugate $\bar{\psi}$ at $r = R$. The values of the mass function m , of the scalar field ψ and of its derivative ψ' at $r = R$ are used as initial conditions to integrate the structure equations in the exterior region. In practice, the integration is terminated at some finite but large grid point where $r = R_\infty$. From the values of m , ψ and ψ' at R_∞ we can determine M and Q by solving the system of equations

$$m(r) = M - \frac{|Q|^2}{2r} - \frac{M|Q|^2}{2r^2} + \mathcal{O}\left(\frac{1}{r^3}\right), \quad (8.35a)$$

$$\psi(r) = \psi_\infty + \frac{Q}{r} + \frac{QM}{r^2} + \mathcal{O}\left(\frac{1}{r^3}\right), \quad (8.35b)$$

$$\psi'(r) = -\frac{Q}{r^2} + \mathcal{O}\left(\frac{1}{r^3}\right). \quad (8.35c)$$

where ψ_∞ is the constant background value of the scalar field. Therefore we have three equations to solve for three unknowns: M , Q and ψ_∞ . The physical solution of interest is the one corresponding to the particular central value of the scalar field ψ_0 (which can be found e.g. by a shooting method) such that the background field vanishes, i.e. $\psi_\infty = 0$.

As an alternative integration technique, we have also implemented a compactified coordinate grid in the vacuum exterior introducing a variable $y \equiv 1/r$, which results in a regular set of differential equations that is readily integrated to spatial infinity at $y = 0$. The gravitational mass M , scalar charge Q and asymptotic scalar field magnitude are then directly obtained from $m(y = 0)$, $\psi(y = 0)$ and $\partial_y \psi(y = 0)$, and numerical shooting provides a fast-converging algorithm to enforce the boundary condition $\lim_{y \rightarrow 0} \psi = 0$. The two independent integrators yield bulk stellar properties that agree within $\sim 1\%$ or better.

8.3.2 Numerical integration and results

In this section we discuss the result of the numerical integration of the hydrostatic equilibrium equations in the TMS theory of Section 8.2.4. Our main interest is to understand scalarization in this model, and for simplicity in this chapter we will focus on static stars.

We will use the polytropic equation of state labeled “EOS1” in Ref. [337], for which the pressure P and the energy density ρ are given as functions of the baryonic density n_B by

$$P = Kn_0 m_B \left(\frac{n_B}{n_0} \right)^\gamma, \quad \rho = n_B m_B + K \frac{n_0 m_B}{\gamma - 1} \left(\frac{n_B}{n_0} \right)^\gamma, \quad (8.36)$$

where $n_0 = 0.1 \text{ fm}^{-3}$, $m_B = 1.66 \times 10^{-27} \text{ kg}$, $K = 0.0195$ and $\gamma = 2.34$. Therefore, the function $\rho = \rho(P)$ can be constructed parametrically by varying n_B .

8.3.2.1 The $O(2)$ symmetric theory

In the absence of a scalar potential, the gravitational part of the action (8.1) is invariant under the target-space isometry group G . For our simple two-real-scalar model with maximally symmetric target space, G is the orthogonal group $O(3)$ in the case of spherical geometry, the indefinite orthogonal group $O(2,1)$ in the case of hyperbolic geometry, and the inhomogeneous orthogonal group $IO(2) = \mathbb{R}^2 \times O(2)$ in the case of flat geometry.

When scalar-matter couplings are introduced, the action is no longer invariant under all of G , but only under some subgroup $H < G$. As a first example, let us consider the particular case in which $\beta_1 = \alpha = 0$. In this case the conformal factor $A(\psi, \bar{\psi})$ given in Eq. (8.24) reduces to

$$A(\psi, \bar{\psi}) = \exp \left(\frac{1}{2} \beta_0 \psi \bar{\psi} \right), \quad (8.37)$$

where again we have neglected higher-order terms in the scalar field. This equation is obviously invariant under rotations in the complex plane ($\psi \rightarrow \psi e^{i\theta}$) and complex conjugation ($\psi \rightarrow \bar{\psi}$). Therefore, $H = O(2)$. Note that the boundary condition $\psi_\infty = 0$ is H -invariant. We refer to this special case as the $O(2)$ -symmetric TMS theory. In this theory, a GR stellar configuration with $\psi \equiv 0$ is always a solution that is $O(2)$ -invariant.

We now construct scalarized solutions, which spontaneously break the $O(2)$ symmetry. They depend on the two real parameters (β_0 and \mathbf{r}^2) of this theory, as well as the central baryon density n_B . The $O(2)$ -symmetric character of the scalarized solution space

is exhibited in Fig. 8.1, where we show that, for given values of \mathfrak{r} and n_B , there exists an infinite number of scalarized solutions characterized by a different value of the complex field ψ_0 at the center of the star. The different values of the scalar field are related by a phase rotation, and the masses and radii of neutron star models along each of the circles shown in Fig. 8.1 are identical. The target-space curvature \mathfrak{r} has the effect of suppressing ($\mathfrak{r}^2 < 0$) or increasing ($\mathfrak{r}^2 > 0$) the value of $|\psi_0|$, and consequently of the scalar charge Q . Therefore a spherical target space ($\mathfrak{r}^2 > 0$) produces stronger scalarization effects in the mass-radius relations with respect to the case of a flat target-space metric, as illustrated in Fig. 8.2. On the other hand, a hyperbolic target space ($\mathfrak{r}^2 < 0$) tends to reduce the effects of spontaneous scalarization. This can be intuitively, if not rigorously, understood by a glance at Eqs. (8.18) and (8.19): the curvature term plays the role of an “effective (field-dependent) gravitational constant” which is either larger or smaller than the “bare” gravitational constant depending on whether $\mathfrak{r}^2 > 0$ or $\mathfrak{r}^2 < 0$. In both cases, as $\mathfrak{r} \rightarrow \infty$ the solution reduces (modulo a trivial phase rotation) to that of a ST theory with a single real scalar field ψ and scalar-matter coupling $A(\psi) = \exp(\frac{1}{2}\beta_0\psi^2)$. We remark that due to the $O(2)$ symmetry, all solutions of this theory are equivalent to solutions with $\text{Im}[\psi] = 0$; as discussed in Section 8.3.2.2 below, these are effectively – modulo a field redefinition – solutions of a single-scalar theory.

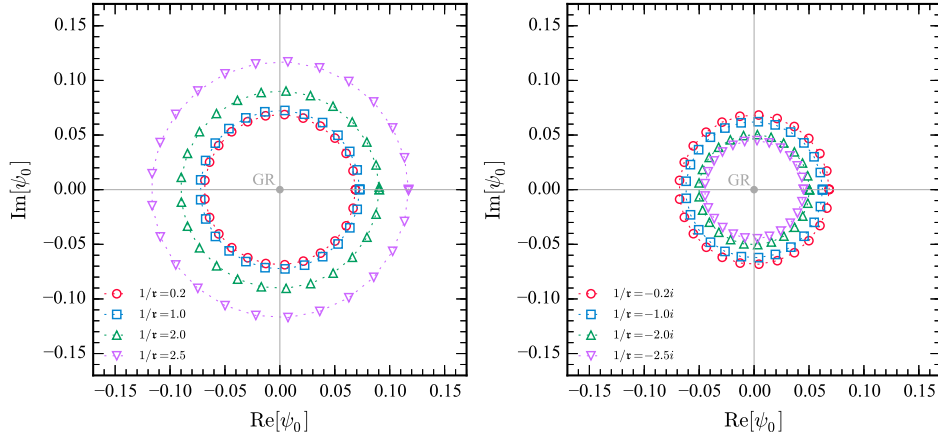


Figure 8.1: *Spontaneous scalarization in a TMS theory with $O(2)$ symmetry.* The value ψ_0 of the scalar field at the center of the star for scalarized solutions in the $O(2)$ -symmetric theory with $\beta_0 = -5.0$ and central baryon density $n_B = 10.4 n_{\text{nuc}}$, where the nuclear density is $n_{\text{nuc}} = 10^{44} \text{ m}^{-3}$. *Left panel:* spherical target space with $\mathfrak{r}^2 > 0$. *Right panel:* hyperbolic target space with $\mathfrak{r}^2 < 0$. In both panels the origin corresponds to the neutron star solution in GR.

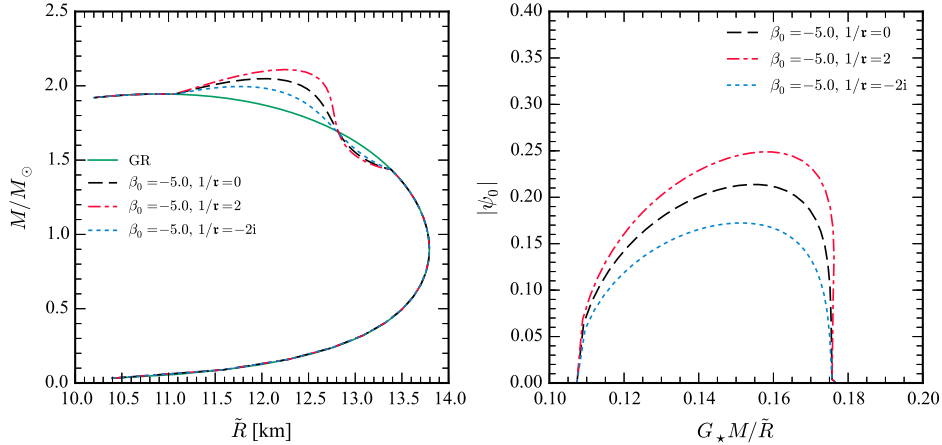


Figure 8.2: *Stellar properties in the $O(2)$ -symmetric theory.* *Left panel:* The mass-radius relation for different values of \mathfrak{r} and $\beta_0 = -5.0$. *Right panel:* Central value of the magnitude of the scalar field $|\psi_0|$ as a function of the stellar compactness $G_\star M / (\tilde{R}c^2)$. Here \tilde{R} is the areal Jordan-frame radius of the star. The onset of scalarization does not depend on the value of \mathfrak{r} .

Finally, in Fig. 8.3 we illustrate the radial profiles of the mass function m , metric potential ν , mass-energy density ρ and scalar field ψ for scalarized stellar models with fixed baryonic mass $M_B = 1.70 M_\odot$ in theories with $\beta_0 = -5.0$ and $\mathfrak{r}^2 = \pm 1/4$.

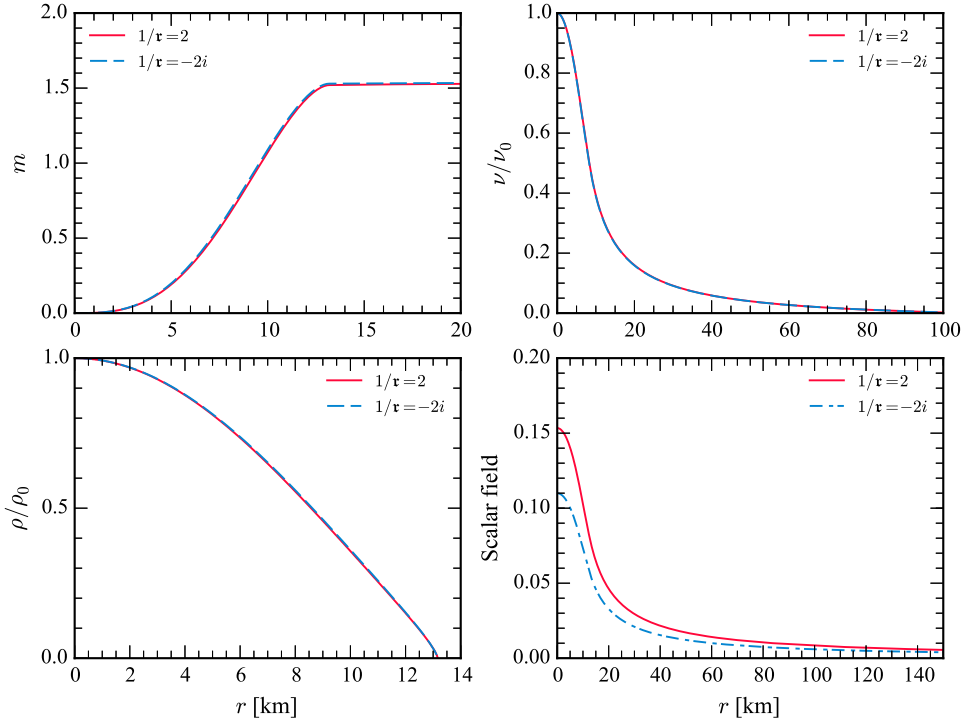


Figure 8.3: *Radial profiles.* Different panels show the profiles of the mass function m , metric potential ν , total energy density ρ and complex scalar field ψ , in units of $c = G = M_\odot = 1$. The profiles correspond to a scalarized star in the $O(2)$ -symmetric theory with $\beta_0 = -5.0$, $\beta_1 = \alpha = 0$, and fixed baryon mass $M_B = 1.70M_\odot$. The target space curvature is either $\tau = 0.5$ (spherical) or $\tau = 0.5i$ (hyperboloidal). In the spherical case, the scalarized solution has a gravitational mass $M = 1.54 M_\odot$, Jordan-frame areal radius $\tilde{R} = 13.0$ km, total scalar charge $Q = 0.553 M_\odot$ and central scalar magnitude $|\psi_0| = 0.154$. In the hyperbolic case, these quantities are $M = 1.54 M_\odot$, $\tilde{R} = 13.0$ km, $Q = 0.393M_\odot$ and $|\psi_0| = 0.110$. For comparison, the GR solution with the same baryonic mass has $M = 1.54M_\odot$ and $R = \tilde{R} = 13.2$ km.

8.3.2.2 The full TMS theory

We now turn our attention to the existence of scalarized stellar models in the theory defined by Eq. (8.23), which depends on three real parameters (β_0 , β_1 and \mathbf{r}^2) and the complex constant α . When $\alpha = 0$ and $\beta_1 \neq 0$, this theory is invariant under the symmetry group $Z_2 \times Z_2$ generated by conjugation ($\psi \rightarrow \bar{\psi}$) and inversion ($\psi \rightarrow -\psi$). Introduction of $\alpha \in \mathbb{R}$ partially breaks this symmetry down to Z_2 , consisting of conjugation only, whereas introduction of $\alpha \in \mathbb{C} \setminus \mathbb{R}$ fully breaks this symmetry.

An interesting question is whether there exists a region of the parameter space of this theory in which *both* fields scalarize⁶. We first searched for such “biscalarized” solutions in the $Z_2 \times Z_2$ theory with $\alpha = 0$, considering a wide range of the $(\beta_0, \beta_1, \mathbf{r})$ space, but we could not find any. However, the situation is dramatically different when $\alpha \neq 0$. Crucially, $|\alpha|$ has to be small enough to satisfy the observational bounds summarized in Appendix I, and in particular Eq. (I.3), but $\arg \alpha$ is completely unconstrained by weak-field observations. Our numerical findings are in agreement with an approximate analytical model which will be presented elsewhere [222]. In the following we discuss the cases $\alpha = 0$ and $\alpha \neq 0$ separately.

Case $\alpha = 0$: breaking the $O(2)$ symmetry down to $Z_2 \times Z_2$ When $\alpha = 0$ but $\beta_1 \neq 0$, we found solutions where only *either the real or the imaginary part* of the scalar field has a non-trivial profile. Therefore, in this case the circle shown in Fig. 8.1 for the $O(2)$ -symmetric theory collapses down to four discrete points on the real and imaginary axes (cf. Fig. 8.4).

⁶This question is not invariant under field redefinitions. More precisely, we ask whether there exists a doubly scalarized solution which can not be described by an effective single-real-scalar theory.

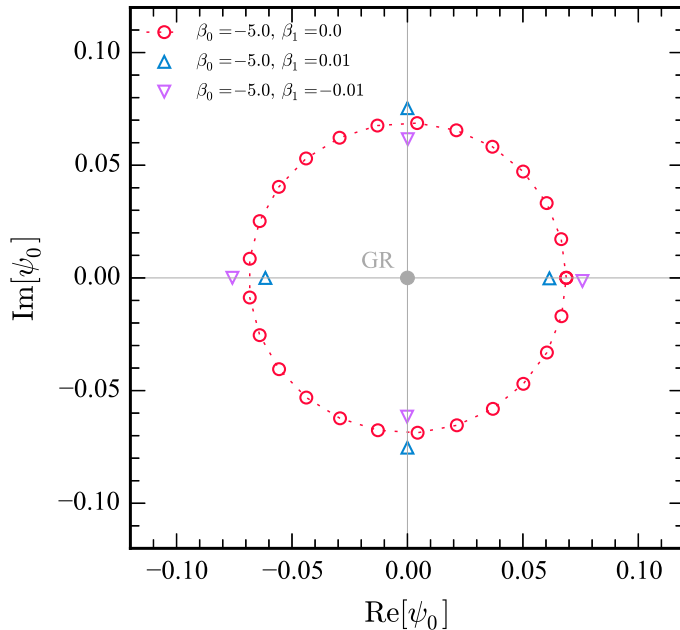


Figure 8.4: *Symmetry breaking of the space of solutions.* When $\beta_1 \neq 0$, the $O(2)$ -symmetric solution-space analyzed in the previous section (cf. Fig. 8.1) collapses down to a $(Z_2 \times Z_2)$ -symmetric solution-space. This property of the theory is here illustrated for stellar models with the same equation of state and central energy density as in Fig. 8.1, $\beta_0 = -5.0$ and $\tau = 5.0$.

In Appendix J we perform a linear analysis of the field equations, deriving the conditions for scalarization to occur. From Eqs. (J.2), (J.3) and (J.5) we expect that scalarized models exist if $\beta_0 + \beta_1 \lesssim -4.35$ when $\text{Re}[\psi] \neq 0$, or $\beta_0 - \beta_1 \lesssim -4.35$ when instead $\text{Im}[\psi] \neq 0$. We have checked this expectation by calculating models for the parameter sets (i) $1/\tau = 0$, $\beta_1 = 0$ and (ii) $1/\tau = 2$, $\beta_1 = 0$. For each of these cases, we have varied the central density from 10^{-5} km^{-2} to 0.0015 km^{-2} in steps of 10^{-5} km^{-2} . We applied our shooting algorithm for a scalar field amplitude $|\psi(r=0)| \in [0, 1]$ in steps of 0.1, choosing discrete values of the complex phase $\theta = 0, \pi/2, \pi, 3\pi/2$, and varying $\beta_0 \in [-20, 3]$ in steps of 0.01. For all values of the central density and β_0 , the shooting method identifies one GR solution model with vanishing scalar charge. For sufficiently negative β_0 , we additionally identify scalarized models. Among these models we then identify for a given value of β_0 the scalarized model with the lowest baryon mass, and thus generate a scalarization plot analogous to Fig. 2

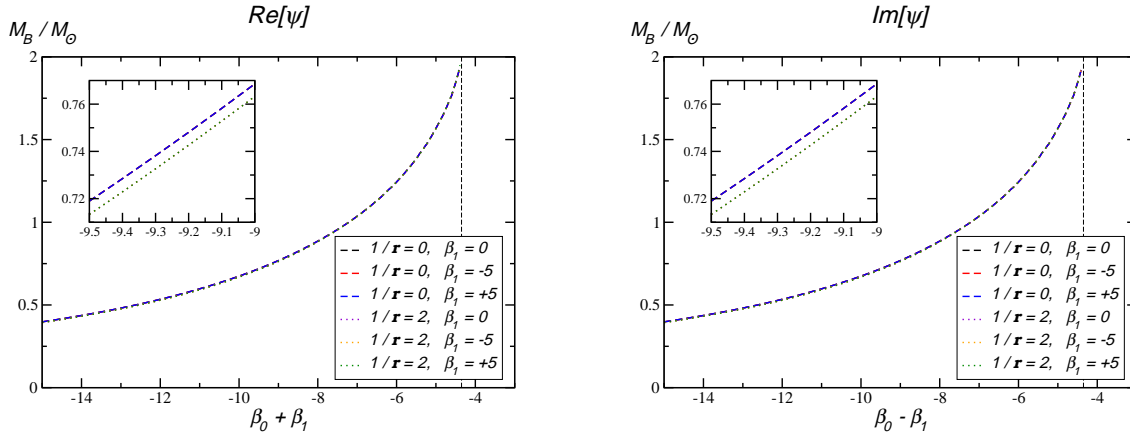


Figure 8.5: *Minimal baryonic mass of scalarized models.* The baryon mass of scalarized solutions at the onset of scalarization as a function of (i) $\beta_0 + \beta_1$ for models where $\text{Re}[\psi]$ is non-zero (left panel) and (ii) $\beta_0 - \beta_1$ for models where $\text{Im}[\psi]$ is non-zero (right panel). Each panel contains 6 curves, corresponding to the three values of β_1 at fixed $\tau = \infty$ (dashed curves) and the same three values of β_1 at $\tau = 1/2$ (dotted curves). The three dashed curves and the three dotted curves, respectively, are indistinguishable in the plot and the two families of dashed and dotted curves are only distinguishable in the inset, where we zoom into a smaller region. In both panels, the vertical long-dashed curve denotes the value $\beta_0 \pm \beta_1 = -4.35$ above which we no longer identify scalarized models, in agreement with Eq. (J.5). From Eq. (8.25) it is clear that the natural parameters are $\beta_0 + \beta_1$ and $\beta_0 - \beta_1$ when the theory is written in terms of the real and imaginary part of ψ , respectively.

in [119] for ST theory with a single scalar field. The result is shown in Fig. 8.5. The small difference between the curves for different curvature radius τ likely arises from the small but finite amplitude of the scalar field appearing in the lowest-mass scalarized binaries, which is a byproduct of finite discretization in the mass parameter space. In the continuum limit of infinitesimal amplitudes of the scalar field in scalarized models, we expect this difference to disappear completely and the dotted and dashed curves to overlap. This is indeed supported by an analytic calculation.⁷ These results confirm the prediction of Eq. (J.5) and agree (qualitatively and quantitatively) with the single-scalar case shown in Fig. 2 of [119].

Indeed, in this case the analogy with the single-scalar case can be made more formal.

Let us consider without loss of generality the subspace of the solution space in which the

⁷This calculation uses Riemann-normal coordinates at φ_∞ in target space, and finds that target-space-curvature terms appear in the field equations at third order in the scalar-amplitude expansion. Details will be published elsewhere [222].

scalar field is real, i.e. $Z = \text{Re}[\psi] \neq 0$, $W = \text{Im}[\psi] = 0$. The kinetic term can be put in the canonical form by a scalar field redefinition, i.e.

$$K = -\frac{1}{2} \left(1 + \frac{Z^2}{4\mathbf{r}^2} \right)^{-2} \partial_\mu Z \partial^\mu Z = -\frac{1}{2} \partial_\mu \tilde{Z} \partial^\mu \tilde{Z}, \quad (8.38)$$

where the two fields are related by $Z = 2\mathbf{r} \tan\left(\frac{\tilde{Z}}{2\mathbf{r}}\right)$, and $-\pi\mathbf{r} < \tilde{Z} < \pi\mathbf{r}$. For $|Z| \ll \mathbf{r}$ we have

$$\tilde{Z} = Z - \frac{Z^3}{12\mathbf{r}^2} + O(Z^5), \quad Z = \tilde{Z} + \frac{\tilde{Z}^3}{12\mathbf{r}^2} + O(\tilde{Z}^5). \quad (8.39)$$

Replacing this Taylor expansion in the conformal factor (8.24) we see that the parameters β_0, β_1 remain the same. In particular, we obtain $A(\tilde{Z}) = \exp\left[(\beta_0 + \beta_1)\tilde{Z}^2/2\right]$ (plus higher-order terms), i.e., the coupling function coincides with that of a single-scalar theory with coupling constant $\beta = \beta_0 + \beta_1$. Thus, as long as $|Z| \ll \mathbf{r}$, the theory with $\alpha = 0$ is equivalent to a ST theory with one scalar and coupling $\beta = \beta_0 + \beta_1$ (or $\beta = \beta_0 - \beta_1$, in which case only $W = \text{Im}[\psi]$ scalarizes). Clearly, this proof also includes the limit $\mathbf{r} \rightarrow \infty$, where the solutions reduce exactly to those of a single-scalar theory with the identification $\beta \equiv \beta_0 + \beta_1$.

When the condition $|Z| \ll \mathbf{r}$ is not fulfilled, the theory is still equivalent to a ST theory with one scalar field, but the form of the conformal factor A changes. These theories only differ by higher-order terms in the series expansion (8.20), (8.22), which are negligible at the onset of the scalarization.

In Fig. 8.6 we show the mass-radius relation of scalarized neutron star solutions in the non- $O(2)$ symmetric theory for different values of \mathbf{r} and $\beta_0 + \beta_1$. When the coupling is large, we observe that the solutions can differ dramatically from their GR counterpart.

Case $\alpha \neq 0$: multi-scalarization When $\alpha \neq 0$, GR configurations are not solutions of the field equations. In particular, a constant (or vanishing) scalar field does not satisfy Eq. (8.18) when $T \neq 0$. Therefore it is not surprising that when $\alpha \neq 0$ we can find solutions

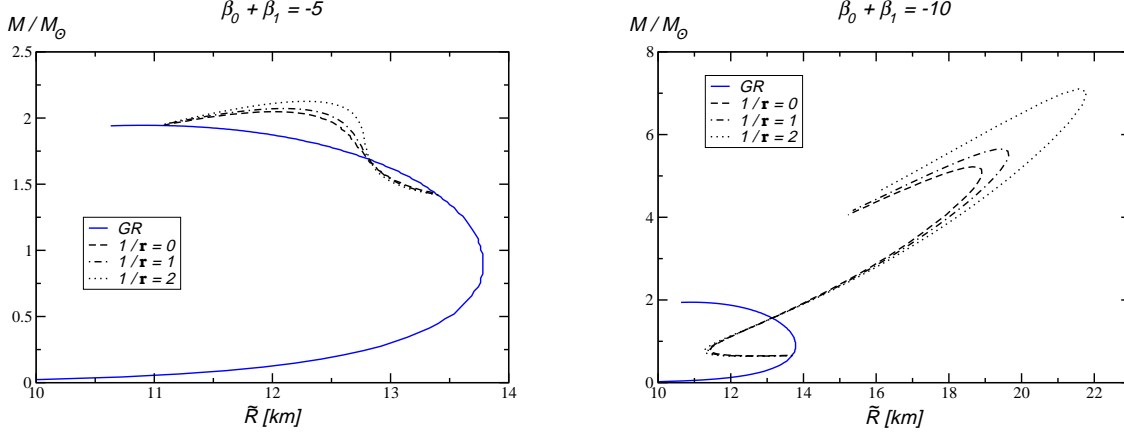


Figure 8.6: *Mass-radius relations in the full TMS theory.* Analogous to the left panel of Fig. 8.2 for three values of the curvature radius of the target metric ($\mathfrak{r} = \infty$, $\mathfrak{r} = 1$ and $\mathfrak{r} = 0.5$), $\beta_0 + \beta_1 = -5$ (left panel) and $\beta_0 + \beta_1 = -10$ (right panel). Here we only consider models where $\text{Re}[\psi] \neq 0$. The gravitational mass M is shown as a function of the Jordan-frame radius \tilde{R} . For comparison, we include in both panels the GR curve. Note the different axis ranges in the two panels. When $\mathfrak{r} \rightarrow \infty$, the theory reduces to a ST theory with one scalar and effective coupling $\beta = \beta_0 + \beta_1$, and the observational constraint $\beta_0 + \beta_1 \gtrsim -4.5$ is in place [169]. However, such lower bound might be less stringent when \mathfrak{r} is finite.

with two non-trivial scalar profiles even when $\beta_0 = \beta_1 = 0$. A more interesting question is whether there are stellar configurations in which both scalar fields have a large amplitude. As we have seen, these “biscalarized” solutions are absent in the $\alpha = 0$ case. Here we present preliminary results that demonstrate the existence of interesting biscalarized solutions as long as $\alpha \neq 0$.

For concreteness we set $|\alpha| = 10^{-3}$: such a small value of $|\alpha|$ satisfies the experimental bounds discussed in Appendix I (but we have also studied the case where $|\alpha| = 10^{-4}$, with qualitatively similar results).

In this preliminary study we vary $\arg \alpha$ in the range $[0, 2\pi]$ in steps of $\pi/6$ and we set $1/\mathfrak{r} = 0$ (i.e., we consider a flat target space). A finite target-space curvature \mathfrak{r} does not change the picture qualitatively; a more detailed analysis will be presented elsewhere [222]. Our search yields several models with non-zero scalar field, as shown in Figs. 8.7 and 8.8, where dots denote the real and imaginary parts of the central value of the scalar field ψ_0 for

which solutions were found.

For the time being, we wish to remark two very interesting (and perhaps unexpected) features of these biscalarized solutions:

- 1) Figure 8.7 shows that the solutions are at least approximately $O(2)$ symmetric when $\beta_1 \sim |\alpha|$, and the $O(2)$ symmetry is broken (the solution “circles” turn into “crosses”) when $\beta_1 \gg |\alpha|$. The cross-like shape of the scalarized solutions in the $\text{Re}[\psi_0]$, $\text{Im}[\psi_0]$ plane collapses towards a set of solutions on the vertical line $\text{Re}[\psi_0] = 0$ for the larger values of β_1 (bottom panels in Fig. 8.7). This behavior can be interpreted as an approximation to the spontaneous scalarization for the case $\alpha = 0$ displayed in Fig. 8.5, and discussed in the text around Eqs. (8.38) and (8.39). There we observed that spontaneous scalarization of $\text{Re}[\psi]$ occurs (in analogy with the single-field case) if $\beta_0 + \beta_1 \lesssim -4.35$, and scalarized models with a large imaginary part $\text{Im}[\psi]$ exist if $\beta_0 - \beta_1 \lesssim -4.35$. The biscalarized models in Fig. 8.5 have been calculated for fixed $\beta_0 = -5$. For $\beta_1 \gtrsim 0.65$ we therefore enter the regime where $\beta_0 + \beta_1 \gtrsim -4.35$, and we no longer expect to find models with strongly scalarized $\text{Re}[\psi]$. The condition $\beta_0 - \beta_1 \lesssim -4.35$ for scalarization of $\text{Im}[\psi]$, however, remains satisfied, so that scalarized models should cluster close to the $\text{Re}[\psi_0]$ -axis. This is indeed observed in the bottom panels of Fig. 8.7. Note that in this case the condition $\beta_1 \gtrsim 0.65 \gg |\alpha| = 10^{-3}$ is satisfied, in close correspondence to the case $\alpha = 0$ of Fig. 8.5.
- 2) Figure 8.8 (which is a “zoom-in” on the top-left panel of Figure 8.7) indicates additional fine structure in the space of solutions, with at least three different families of scalarized solutions having remarkably different values of the scalar field (and therefore of the scalar charge).

When $\mathbf{r} \rightarrow \infty$, binary pulsar observations in the single-scalar case would impose a constraint equivalent to $\beta_0 + \beta_1 \gtrsim -4.5$ [169]. More work is required to clarify whether a similar constraint is in place also for multiple scalars. Preliminary calculations indicate that

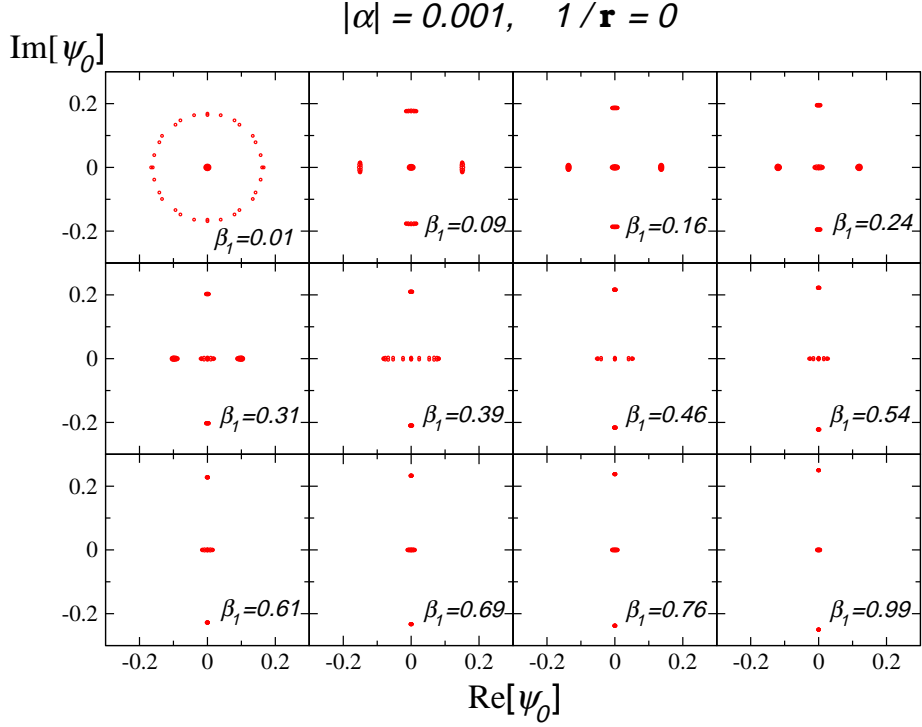


Figure 8.7: *Scalar field amplitudes in the full TMS theory - I.* Scalar field amplitude at the stellar center ψ_0 for stellar models with $\beta_0 = -5$, $|\alpha| = 0.001$ and fixed baryon mass $M_B = 1.8 M_\odot$. The different panels show the solutions found for different values of β_1 as indicated in each panel. In each case, we vary the phase of α from 0 to 2π in steps of $\pi/6$. In contrast to the $\alpha = 0$ case in Fig. 8.4, the breaking of the $O(2)$ symmetry occurs gradually as β_1 is increased away from 0.

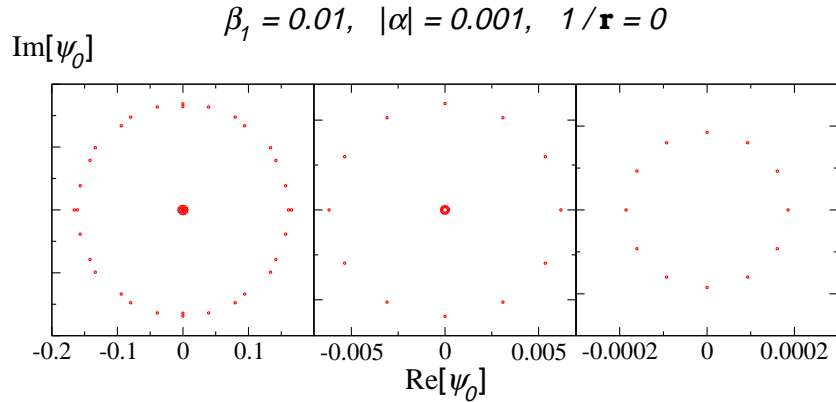


Figure 8.8: *Scalar field amplitudes in the full TMS theory - II.* The data of the upper left panel of Fig. 8.7 are shown on different scales to resolve the fine structure of the solutions in the ψ_0 plane. In each panel the vertical extent is equal to the horizontal.

the target-space curvature should affect the energy flux from compact binaries at high post-Newtonian order. However, it is unclear whether the formalism of [117] for describing orbital binary dynamics is applicable to the theory studied in this chapter, due to the discontinuity at $\alpha = 0$. Furthermore, for multiple scalars, it is possible that some combination of β_0 and β_1 other than their sum may be constrained by binary pulsar observations. A detailed answer to this question requires two theoretical developments that are currently missing: (1) the investigation of stellar structure in generic TMS theories to understand the effect of the theory parameters on stellar properties, and (2) an implementation of these stellar structure calculations in flux formulas similar to those derived in [117] (or generalizations thereof). These are important tasks that should be addressed in future work. In Fig. 8.6 we adopt an agnostic point of view and use large values of $\beta_0 + \beta_1$ in order to illustrate the effect of scalarization in TMS theory in some extreme cases. The phenomenological implications and the stability of biscalarized stellar models will be discussed elsewhere [222].

8.4 3+1 formulation of the field equations for numerical relativity

Studies of the strong-field dynamics of compact stars and BHs, whether isolated or in binary systems, require the fully non-linear theory without any symmetry assumptions. Such studies can now be carried out using numerical relativity techniques, and they have already led to new insights into the behavior of ST theories. For example, numerical simulations of neutron star binaries in single-scalar theories have identified a new phenomenon (“dynamical scalarization”) occurring in the late stages of the inspiral, just before merger [32, 415, 371]. Similarly, studies of equilibrium sequences of neutron star binaries have shown that dynamical scalarization can lead to a reduction of the number of gravitational-wave cycles with respect to GR [470]. Scalar radiation has also been identified in the inspiral of black hole binaries when the binary is embedded in a non-trivial scalar background gradient [207, 49]. All numerical studies rely on a formulation of the theory suitable for numerical implementation, which is most commonly achieved in terms of a space-time (or 3+1) decomposition of

the field equations. Here we present the 3+1 formulation of the field equations for general multi-scalar theories. The work presented in this section is a prerequisite for future numerical studies of multi-scalar theories, and we hope that it will motivate other researchers to investigate this interesting, unexplored topic.

8.4.1 Action, stress-energy tensor and field equations

We consider a multi-scalar theory described by the action (8.1):

$$S = \frac{1}{4\pi G_\star} \int d^4x \sqrt{-g} \left[\frac{R}{4} - \frac{1}{2} g^{\mu\nu} \gamma_{AB}(\varphi) \partial_\mu \varphi^A \partial_\nu \varphi^B - V(\varphi) \right] + S_m[A^2(\varphi)g_{\mu\nu}; \Psi]. \quad (8.40)$$

For computational purposes it is useful to consider the scalar fields themselves as ordinary matter, described by the stress-energy tensor $T_{\mu\nu}^{(\varphi)}$ defined in Eq. (8.7):

$$8\pi G_\star T_{\mu\nu}^{(\varphi)} = 2\gamma_{AB} \left(\partial_\mu \varphi^A \partial_\nu \varphi^B - \frac{1}{2} g_{\mu\nu} g^{\alpha\beta} \partial_\alpha \varphi^A \partial_\beta \varphi^B \right) - 2g_{\mu\nu} V, \quad (8.41)$$

while $T_{\mu\nu}$, defined in Eq. (8.4), is associated to the fields Ψ (for instance, the fluid composing a neutron star). The total stress-energy tensor, then, is $T_{\mu\nu} + T_{\mu\nu}^{(\varphi)}$. This allows us to use the 3 + 1 decomposition of Einstein's equations given in [12], with the replacement $T_{\mu\nu} \rightarrow T_{\mu\nu} + T_{\mu\nu}^{(\varphi)}$. Since

$$\frac{16\pi G_\star}{\sqrt{-g}} \frac{\delta S}{\delta g^{\mu\nu}} = R_{\mu\nu} - 2\gamma_{AB} \partial_\mu \varphi^A \partial_\nu \varphi^B - \frac{1}{2} g_{\mu\nu} (R - 2\gamma_{AB} g^{\alpha\beta} \partial_\alpha \varphi^A \partial_\beta \varphi^B - 4V) - 8\pi G_\star T_{\mu\nu} = 0, \quad (8.42)$$

Einstein's equations have the form $R_{\mu\nu} - (1/2)g_{\mu\nu}R = 8\pi G_\star(T_{\mu\nu} + T_{\mu\nu}^{(\varphi)})$. The trace of Eq. (8.42) yields

$$-R + 2\gamma_{AB} g^{\alpha\beta} \partial_\alpha \varphi^A \partial_\beta \varphi^B + 8V - 8\pi G_\star T = 0, \quad (8.43)$$

where $T = g^{\mu\nu} T_{\mu\nu}$, and therefore we have

$$R_{\mu\nu} - 2\gamma_{AB} \partial_\mu \varphi^A \partial_\nu \varphi^B - 2g_{\mu\nu} V - 8\pi G_\star \left(T_{\mu\nu} - \frac{1}{2} g_{\mu\nu} T \right) = 0. \quad (8.44)$$

By varying the action (8.40) with respect to φ^A one gets the scalar field equation

$$4\pi G_\star \frac{\gamma^{AB}}{\sqrt{-g}} \frac{\delta S}{\delta \varphi^B} = \square \varphi^A + \gamma_{CD}^A g^{\mu\nu} \partial_\mu \varphi^C \partial_\nu \varphi^D - \gamma^{AB} \frac{\partial V}{\partial \varphi^B} + 4\pi G_\star \gamma^{AB} \frac{\partial \log A}{\partial \varphi^B} T = 0, \quad (8.45)$$

where γ_{CD}^A are the Christoffel symbols on the target space.

8.4.2 The 3 + 1 decomposition

As discussed in Ref. [49] (see also [12]), we consider a slicing of the spacetime in a set of surfaces Σ . We introduce the normal n_μ to those surfaces and the projector

$$h_{\mu\nu} = g_{\mu\nu} + n_\mu n_\nu, \quad (8.46)$$

and write the metric in the form ($\mu, \nu = 0, \dots, 3$; $i, j = 1, 2, 3$)

$$ds^2 = g_{\mu\nu} dx^\mu dx^\nu = -\alpha^2 dt^2 + h_{ij} (dx^i + \beta^i dt)(dx^j + \beta^j dt), \quad (8.47)$$

where α , β^i and h_{ij} are the lapse, the shift, and the metric on Σ , respectively. We remark that in these coordinates $n_i = 0$, therefore the 3-dimensional metric coincides with the projector (8.46) restricted to the spatial indices. It is also worth noting that $h^{0\mu} = 0$, and $g^{\mu\nu} h_{\mu\nu} = 3$.

We define the covariant derivative on Σ as $D_i \equiv h_i^\alpha \nabla_\alpha$. Since $\partial_t = \alpha n + \beta$, the Lie derivative with respect to n is $\mathcal{L}_n = (\partial_t - \mathcal{L}_\beta)/\alpha$. The extrinsic curvature is defined as

$$K_{\mu\nu} \equiv -h_\mu^\sigma \nabla_\sigma n_\nu. \quad (8.48)$$

Its contravariant form is purely spatial, i.e., $K^{0\mu} = 0$. The extrinsic curvature satisfies the relation $K_{ij} = \mathcal{L}_n h_{ij}/2$, so the evolution equation for the metric reads

$$\mathcal{L}_n h_{ij} = -2K_{ij}. \quad (8.49)$$

Other useful relations are [398, 12]

$$\nabla^\mu n_\mu = -K, \quad n^\mu \nabla_\mu n^\nu = D^\nu(\ln \alpha), \quad (8.50)$$

where we defined $K \equiv g_{\mu\nu} K^{\mu\nu}$.

In the same way, we can define the curvature of each of the scalar fields as $K_\varphi^A \equiv -\mathcal{L}_n \varphi^A / 2$. Consequently, the evolution equation for the scalar fields reads

$$\mathcal{L}_n \varphi^A = -2K_\varphi^A, \quad (8.51)$$

where we note that $\mathcal{L}_n \varphi^A = n^\mu \varphi_{,\mu}^A$.

It will also be useful to decompose the quantity $g^{\alpha\beta} \partial_\alpha \varphi^A \partial_\beta \varphi^B$ as follows:

$$g^{\alpha\beta} \partial_\alpha \varphi^A \partial_\beta \varphi^B = (h^{\alpha\beta} - n^\alpha n^\beta) \partial_\alpha \varphi^A \partial_\beta \varphi^B = D^i \varphi^A D_i \varphi^B - 4K_\varphi^A K_\varphi^B. \quad (8.52)$$

8.4.2.1 Einstein's equations

The 3+1 decomposition of Einstein's equations with matter is given e.g. in Eqs. (2.4.6), (2.4.9) and (2.5.6) of [12]; in those equations the matter terms are expressed in terms of the quantities $\rho = n^\mu n^\nu T_{\mu\nu}$, $j^i = -h^{i\mu} n^\nu T_{\mu\nu}$, and $S_{ij} = h_i^\alpha h_j^\beta T_{\alpha\beta}$. We simply replace in those equations $T_{\mu\nu} \rightarrow T_{\mu\nu} + T_{\mu\nu}^{(\varphi)}$, where the explicit expression of $T_{\mu\nu}^{(\varphi)}$ is given in Eq. (8.41), i.e., we replace $\rho \rightarrow \rho + \rho^{(\varphi)}$, $j^i \rightarrow j^i + j^{i(\varphi)}$, $S_{ij} \rightarrow S_{ij} + S_{ij}^{(\varphi)}$, where:

$$8\pi G_\star \rho^{(\varphi)} = \gamma_{AB} [D^i \varphi^A D_i \varphi^B + 4K_\varphi^A K_\varphi^B] + 2V, \quad (8.53)$$

$$8\pi G_\star j^{i(\varphi)} = -2\gamma_{AB} D^i \varphi^A (-2K_\varphi^B) = 4\gamma_{AB} D^i \varphi^A K_\varphi^B, \quad (8.54)$$

$$8\pi G_\star S_{ij}^{(\varphi)} = 2\gamma_{AB} \left[D_i \varphi^A D_j \varphi^B + 2h_{ij} K_\varphi^A K_\varphi^B - \frac{1}{2} h_{ij} D_i \varphi^A D^i \varphi^B \right] - 2h_{ij} V. \quad (8.55)$$

We also have:

$$4\pi G_\star \left[(S^{(\varphi)} - \rho^{(\varphi)})h_{ij} - 2S_{ij}^{(\varphi)} \right] = -2\gamma_{AB}D_i\varphi^A D_j\varphi^B - 2h_{ij}V. \quad (8.56)$$

Then Eqs. (2.4.6), (2.4.9) and (2.5.6) of [12] give:

$${}^{(3)}R + K^2 - K_{\mu\nu}K^{\mu\nu} = 16\pi G_\star \rho + 2\gamma_{AB} \left[D^i\varphi^A D_i\varphi^B + 4K_\varphi^A K_\varphi^B \right] + 4V, \quad (8.57)$$

$$D_j(K^{ij} - h^{ij}K) = 8\pi G_\star j^i + 4\gamma_{AB}D^i\varphi^A K_\varphi^B \quad (8.58)$$

and

$$\begin{aligned} \mathcal{L}_n K_{ij} &= -D_i D_j (\ln \alpha) + {}^{(3)}R_{ij} + K K_{ij} - 2K_{ik} K_j^k + 4\pi G_\star [h_{ij}(S - \rho) - 2S_{ij}] \\ &\quad - 2\gamma_{AB}D_i\varphi^A D_j\varphi^B - 2h_{ij}V, \end{aligned} \quad (8.59)$$

where ${}^{(3)}R_{ij}$ and ${}^{(3)}R$ are the Ricci tensor and the Ricci scalar of the metric h_{ij} , respectively.

8.4.2.2 Scalar field equation

To decompose the scalar equation (8.45), i.e.

$$\square\varphi^A + \gamma_{CD}^A g^{\mu\nu} \partial_\mu\varphi^C \partial_\nu\varphi^D - \gamma^{AB} \frac{\partial V}{\partial\varphi^B} + 4\pi G_\star \gamma^{AB} \frac{\partial \log A}{\partial\varphi^B} T = 0, \quad (8.60)$$

we start by considering the first term, $\square\varphi^A$ (the single-scalar case was discussed in [398, 399]).

We have:

$$\begin{aligned} \square\varphi^A &= \nabla_\sigma (g^{\sigma\rho} \nabla_\rho \varphi^A) \\ &= \nabla_\sigma [(-n^\sigma n^\rho + h^{\sigma\rho}) \nabla_\rho \varphi^A] = \nabla_\sigma [2n^\sigma K_\varphi^a + D^\sigma \varphi^A] \\ &= 2\mathcal{L}_n K_\varphi^A - 2K K_\varphi^A + D_i D^i \varphi^A + D_\rho (\ln \alpha) D^\rho \varphi^A. \end{aligned} \quad (8.61)$$

Then, since $T = S - \rho$, the scalar field equation takes the form

$$\begin{aligned} \mathcal{L}_n K_\varphi^A &= K K_\varphi^A - \frac{1}{2} D_i D^i \varphi^A - \frac{1}{2} D^i \varphi^A D_i (\ln \alpha) - \frac{1}{2} \gamma_{CD}^A (D^i \varphi^C D_i \varphi^D - 4 K_\varphi^C K_\varphi^D) + \frac{1}{2} \gamma^{AB} \frac{\partial V}{\partial \varphi^B} \\ &\quad - 2\pi G_\star \gamma^{AB} \frac{\partial \log A}{\partial \varphi^B} (S - \rho). \end{aligned} \quad (8.62)$$

8.4.3 3 + 1 equations for 2-sphere and 2-hyperboloid

Let us now specialize to scalar fields living in a two-dimensional target space with maximal symmetry and positive or negative curvature, i.e. a sphere or hyperboloid. For simplicity we also assume a vanishing potential ($V \equiv 0$). As discussed in Appendix H, the sphere and hyperboloid are both described in stereographic coordinates by the metric

$$\gamma_{AB} = F \begin{pmatrix} 1 & 0 \\ 0 & 1 \end{pmatrix}, \quad (8.63)$$

with

$$F(Z, W) \equiv \frac{\mathbf{r}^4}{[(Z^2 + W^2)/4 + \mathbf{r}^2]^2}. \quad (8.64)$$

Here $\varphi^A = (Z, W)$, and \mathbf{r}^2 is positive (negative) for the sphere (hyperboloid). The Christoffel symbols (see Appendix H) are

$$\gamma_{AB}^Z = \frac{1}{Z^2 + W^2 + \mathbf{r}^2} \begin{pmatrix} -2Z & -2W \\ -2W & 2Z \end{pmatrix}, \quad \gamma_{AB}^W = \frac{1}{Z^2 + W^2 + \mathbf{r}^2} \begin{pmatrix} 2W & -2Z \\ -2Z & -2W \end{pmatrix},$$

and Einstein's equations can be written as

$$\begin{aligned} {}^{(3)}R + K^2 - K_{\mu\nu}K^{\mu\nu} &= 2\gamma_{AB} [D^i\varphi^A D_i\varphi^B + 4K_\varphi^A K_\varphi^B] + 16\pi G_\star \rho \\ &= 2F [D^i Z D_i Z + D^i W D_i W + 4(K_Z^2 + K_W^2)] + 16\pi G_\star \rho, \end{aligned} \quad (8.65)$$

$$\begin{aligned} D_j(K^{ij} - h^{ij}K) &= 4\gamma_{AB} D^i\varphi^A K_\varphi^B + 8\pi G_\star j^i \\ &= 4F(D^i Z K_Z + D^i W K_W) + 8\pi G_\star j^i, \end{aligned} \quad (8.66)$$

$$\begin{aligned} \mathcal{L}_n K_{ij} &= -D_i D_j(\ln \alpha) + {}^{(3)}R_{ij} + K K_{ij} - 2K_{ik} K_j^k \\ &\quad - 2\gamma_{AB} D_i\varphi^A D_j\varphi^B + 4\pi G_\star [h_{ij}(S - \rho) - 2S_{ij}] \\ &= -D_i D_j(\ln \alpha) + {}^{(3)}R_{ij} + K K_{ij} - 2K_{ik} K_j^k \\ &\quad - 2F(D_i Z D_j Z + D_i W D_j W) + 4\pi G_\star [h_{ij}(S - \rho) - 2S_{ij}]. \end{aligned} \quad (8.67)$$

Finally, the scalar field equations are

$$\begin{aligned} \mathcal{L}_n K_Z &= K K_Z - \frac{1}{2} D_i D^i Z - \frac{1}{2} D^i Z D_i(\ln \alpha) - \frac{1}{2} \gamma_{CD}^Z (D^i\varphi^C D_i\varphi^D - 4K_\varphi^C K_\varphi^D) \\ &= K K_Z - \frac{1}{2} D_i D^i Z - \frac{1}{2} D^i Z D_i(\ln \alpha) + \frac{1}{Z^2 + W^2 + \mathbf{r}^2} \\ &\quad \times [(Z D_i Z D^i Z - Z D_i W D^i W + 2W D_i Z D^i W) \\ &\quad - 4(Z K_Z^2 - Z K_W^2 + 2W K_Z K_W)] - 2\pi G_\star F^{-1} \frac{\partial \log A}{\partial Z} (S - \rho), \end{aligned} \quad (8.68)$$

$$\begin{aligned} \mathcal{L}_n K_W &= K K_W - \frac{1}{2} D_i D^i W - \frac{1}{2} D^i W D_i(\ln \alpha) - \frac{1}{2} \gamma_{CD}^W (D^i\varphi^C D_i\varphi^D - 4K_\varphi^C K_\varphi^D) \\ &= K K_W - \frac{1}{2} D_i D^i W - \frac{1}{2} D^i W D_i(\ln \alpha) + \frac{1}{Z^2 + W^2 + \mathbf{r}^2} \\ &\quad \times [(-W D_i Z D^i Z + W D_i W D^i W + 2Z D_i Z D^i W) \\ &\quad - 4(-W K_Z^2 + W K_W^2 + 2Z K_Z K_W)] - 2\pi G_\star F^{-1} \frac{\partial \log A}{\partial W} (S - \rho), \end{aligned} \quad (8.69)$$

where we used the expressions of the Christoffel symbols given in Appendix H.

8.5 Discussion and conclusions

In this chapter we have barely scratched the surface of the potentially rich phenomenology of gravitational theories with multiple scalar fields. Several important issues should be addressed in follow-up work. First of all, it is important to compute experimental bounds on the parameters β_0 , $|\beta_1|$, \mathbf{r} , $|\alpha|$ and $\arg \alpha - \frac{1}{2} \arg \beta_1$ that follow from binary pulsar timing [51, 169]. The quadrupole-order scalar and tensor radiation in TMS theories was computed in [117], but it is unclear whether the formalism of [117] is applicable to the theories that we have studied due to the discontinuity at $|\alpha| = 0$. In any case, drawing exclusion diagrams in the multidimensional phase space of the theory would require extensive stellar-structure calculations, that will be presented in future work. Preliminary results suggest that the target-space curvature radius \mathbf{r} enters the gravitational-wave flux (at least formally) at high post-Newtonian order, and therefore it is quite likely that \mathbf{r} will be poorly constrained by binary pulsars. This opens the possibility of interesting new phenomenology in the sensitivity window of advanced Earth-based gravitational-wave detectors. Furthermore, it is unclear whether binary pulsar observations will constrain β_0 , $|\beta_1|$, or some combination thereof, and the parameter $\arg \alpha - \frac{1}{2} \arg \beta_1$ (which according to our preliminary results plays a crucial role in “biscalarization”) is presently unconstrained.

In this chapter we have mainly presented various formal developments, but also some new physical results, which in our opinion are representative of the behavior of a wide class of TMS theories:

1. In theories with $\alpha = 0$, GR solutions co-exist with scalarized solutions but (besides the case of $O(2)$ -symmetric theories with $\beta_1 = 0$) we could not find any “biscalarized” solution for any value of β_0 . In other words, in this case either the real or the imaginary part of the complex scalar field scalarizes but not both, and the $O(2)$ symmetry of the $\beta_1 = 0$ case is broken.
2. The $\alpha \neq 0$ case is dramatically different. In this case – even when $|\alpha|$ is small enough

to be compatible with Solar System constraints – biscalarized solutions exist, and their existence depends quite critically on the value of $\arg \alpha - \frac{1}{2} \arg \beta_1$. These solutions seem to exist quite generically in the complex- α plane, but their properties strongly depend on the values of β_0 and $|\beta_1|$.

These results were obtained through extensive numerical searches. However, given the large dimensionality of the parameter space, we cannot exclude the existence of other solutions which were not found in our initial searches. An approximate analytical model which supports our results and a more detailed analysis of biscalarization will be presented elsewhere [222].

Some obvious extensions of the present results concern the study of rotating NSs in TMS theory (generalizing [119, 425, 153, 353]) and of the universal relations valid for NSs in general relativity [514, 515], which may or may not hold in this theory. Another possible extension is to relax the assumption of a vanishing potential in the action, i.e. to consider the multi-scalar generalization of massive Brans-Dicke theory [14, 52], and investigate the effect of the scalar field masses on the structure of scalarized NSs. The use of more realistic equations of state is pivotal in confronting TMS theory predictions on the evolution of binary pulsars with observations. Furthermore, we hope that the 3 + 1 split worked out in Section 8.4 will encourage other research groups to perform numerical simulations in TMS theories. This may lead to studies of phenomenological interest, such as investigations of dynamical multi-scalarization in neutron star binaries and evolutions of binary black-hole systems in the presence of non-trivial scalar field backgrounds.

CHAPTER 9

SLOWLY-ROTATING BLACK HOLE SOLUTIONS IN HORNDESKI GRAVITY

9.1 Introduction

GR has passed all experimental tests in the Solar System and in binary pulsars with flying colors [499]. Current observations mostly probe the weak-field/slow-motion regime of the theory (with the exception of binary pulsars, where the orbital motion is nonrelativistic but the individual binary members are compact objects), and some of the most interesting strong-field predictions of GR are still elusive and difficult to verify. Observational and theoretical issues with Einstein’s theory – including the dark matter and dark energy problems, the origin of curvature singularities and the quest for an ultraviolet completion of GR – have motivated strong efforts to develop modified theories of gravity which differ from GR in the infrared and ultraviolet regimes, while being consistent with the stringent observational bounds at intermediate energies [51]. The search for unambiguous signatures of modifications of GR in the strong-gravity regime is a major goal of several research fields, including cosmology [107], “standard” electromagnetic astronomy [376], and Earth- and space-based gravitational-wave astronomy [526, 174].

In this chapter we consider a class of modifications of GR known as Horndeski gravity [225]. This is the most general ST theory with a single scalar yielding second-order field equations for the metric and the scalar field (see e.g. [117, 221] for tensor-multiscalar theories, and [347, 97] for multiscalar versions of Horndeski gravity). All the terms present in the action of Horndeski gravity have been shown to be originating from Galileons, i.e. ST models having Galilean symmetry in flat space-time [332]. “Generalized Galileon” theories in curved space-time in any number of dimensions were studied in [131], and shown to be

equivalent to Horndeski gravity in four dimensions in [254]. Furthermore, Horndeski gravity can be shown to emerge from a Kaluza-Klein compactification of higher-dimensional Lovelock gravity (see e.g. [94] for an introduction to this topic, and for a discussion of the relation between exact solutions in Lovelock and Horndeski gravity).

The equations of motion of Horndeski gravity can be derived from the action

$$S = \sum_{i=2}^5 \int d^4x \sqrt{-g} \mathcal{L}_i , \quad (9.1)$$

where

$$\mathcal{L}_2 = G_2 , \quad (9.2)$$

$$\mathcal{L}_3 = -G_3 \square \phi , \quad (9.3)$$

$$\mathcal{L}_4 = G_4 R + G_{4X} [(\square \phi)^2 - \phi_{\mu\nu}^2] , \quad (9.4)$$

$$\mathcal{L}_5 = G_5 G_{\mu\nu} \phi^{\mu\nu} - \frac{G_{5X}}{6} [(\square \phi)^3 + 2\phi_{\mu\nu}^3 - 3\phi_{\mu\nu}^2 \square \phi] . \quad (9.5)$$

Here $g_{\mu\nu}$ is the metric tensor, $g \equiv \det(g_{\mu\nu})$, and R and $G_{\mu\nu}$ are the Ricci scalar and the Einstein tensor associated with $g_{\mu\nu}$, respectively. We have introduced the functions $G_i = G_i(\phi, X)$, which depend only on the scalar field ϕ and its kinetic energy $X = -\partial_\mu \phi \partial^\mu \phi / 2$, and we use units such that the reduced Planck mass $m_{\text{Pl}}^2 = (8\pi G)^{-1} = 1$. For brevity we have also defined the shorthand notation $\phi_{\mu\dots\nu} \equiv \nabla_\mu \dots \nabla_\nu \phi$, $\phi_{\mu\nu}^2 \equiv \phi_{\mu\nu} \phi^{\mu\nu}$, $\phi_{\mu\nu}^3 \equiv \phi_{\mu\nu} \phi^{\nu\alpha} \phi^\mu{}_\alpha$ and $\square \phi \equiv g^{\mu\nu} \phi_{\mu\nu}$. Horndeski theories are an interesting phenomenological playground for strong-field gravity because they include as special cases all dark energy and modified gravity models with a single scalar degree of freedom:

- (1) the GR limit corresponds to $G_4(\phi, X) = 1/2$, with $G_2 = G_3 = G_5 = 0$;
- (2) when the only nonzero term is $G_4(\phi, X) = F(\phi)$ we recover a ST theory with nonminimal coupling of the form $F(\phi)R$, and therefore Brans-Dicke theory and $f(R)$ gravity are special cases of Horndeski gravity;

(3) Einstein-dilaton-Gauss-Bonnet (EdGB) gravity, i.e. a theory with action

$$S = \int d^4x \sqrt{-g} \left(\frac{1}{2} R + X + \xi(\phi) R_{\text{GB}}^2 \right) , \quad (9.6)$$

where $R_{\text{GB}}^2 = R^2 - 4R_{\mu\nu}R^{\mu\nu} + R_{\alpha\beta\gamma\delta}R^{\alpha\beta\gamma\delta}$ is the Gauss-Bonnet invariant, corresponds to setting

$$G_2 = X + 8\xi^{(4)} X^2(3 - \ln X) , \quad (9.7)$$

$$G_3 = 4\xi^{(3)} X(7 - 3 \ln X) , \quad (9.8)$$

$$G_4 = \frac{1}{2} + 4\xi^{(2)} X(2 - \ln X) , \quad (9.9)$$

$$G_5 = -4\xi^{(1)} \ln X , \quad (9.10)$$

where $R_{\alpha\beta\gamma\delta}$ and $R_{\mu\nu}$ are the Riemann and Ricci tensors, and we have defined $\xi^{(n)} \equiv \partial^n \xi / \partial \phi^n$ [254];

(4) a theory with nonminimal derivative coupling of the form

$$S = \int d^4x \sqrt{-g} [\zeta R + 2\eta X + \beta G^{\mu\nu} \phi_\mu \phi_\nu - 2\Lambda_0] \quad (9.11)$$

(see e.g. [466, 403, 177, 178, 190] for cosmological studies of this type of action) corresponds to the following choice¹ of the coupling functions [252]:

$$G_2 = -2\Lambda_0 + 2\eta X , \quad (9.12)$$

$$G_4 = \zeta + \beta X , \quad (9.13)$$

$$G_3 = G_5 = 0 , \quad (9.14)$$

where Λ_0 , η , ζ and β are constants;

¹A coupling of the form $G^{\mu\nu} \phi_\mu \phi_\nu$ can also be obtained by setting $G_5 = -\phi$ and integrating by parts.

- (5) the Lagrangian \mathcal{L}_2 corresponds to the k-essence field [23, 22, 13] (and therefore part of the literature uses a different notation, where G_2 is denoted by K);
- (6) the covariant Galileon of Ref. [132] is recovered by setting $G_2 = -c_2 X$, $G_3 = -c_3 X/M^3$, $G_4 = M_{\text{Pl}}^2/2 - c_4 X^2/M^6$ and $G_5 = 3c_5 X^2/M^9$, where the c_i ($i = 2, \dots, 5$) are constants and M is a constant with dimensions of mass.

In this chapter we are interested in BH solutions in Horndeski gravity. As one of the most striking strong-field predictions of GR, BHs are ideal astrophysical laboratories to test gravity in the strong-field regime. Various authors explored nonrotating BH solutions in special classes of Horndeski gravity. Rinaldi [389] studied BH solutions in theories with a nonminimal derivative coupling to the Einstein tensor of the form $G^{\mu\nu}\phi_\mu\phi_\nu$. Minamitsuji [321] and Anabalon *et al.* [15] found more general solutions by adding a cosmological constant. Kobayashi and Tanahashi [252] studied BH solutions in a subclass of Horndeski theories that is both shift symmetric (i.e., symmetric under $\phi \rightarrow \phi + c$, with c a constant) and reflection symmetric (i.e., symmetric under $\phi \rightarrow -\phi$). Under these assumptions, the only nonzero terms in the action are \mathcal{L}_2 and \mathcal{L}_4 . Theories with nonminimal derivative coupling are both shift and reflection symmetric, and therefore they are a subclass of the theories considered in Ref. [252].

The nonrotating BH solutions found in the works listed above either reduce to the Schwarzschild solution or are not asymptotically flat. This is a consequence of the no hair theorem by Hui and Nicolis [229], which states that vacuum, static, spherically symmetric, asymptotically flat BHs have no-hair in Horndeski theories *with shift symmetry*. As pointed out by Sotiriou and Zhou [446, 447] the theorem actually has a loophole: asymptotically flat solutions can exist for theories of the EdGB type with $\xi(\phi) = \phi$ (these theories are still shift symmetric, because the Gauss-Bonnet combination is a topological invariant). The solutions found in Refs. [446, 447] are effectively special cases of the nonrotating EdGB BH solutions studied by Kanti *et al.* [243], that were subsequently generalized to slow rotation in

Refs. [356, 28, 305] and to rapid rotation in Refs. [249, 247]. Other possibilities to violate the no-hair theorems include adding a time dependence to the scalar (but not to the metric), as in the solution proposed by Babichev and Charmousis [29], or considering biscalar extensions of Horndeski gravity [97]. Reference [30] extended the solutions in [29] to the charged case, allowing for a coupling of the derivative of the scalar field to the energy-momentum tensor of the Maxwell field. Reference [261] argued that a phase transition to charged hairy BHs can be realized through a nonminimal derivative coupling to the Einstein tensor; in this case, however, the equations of motion were solved perturbatively.

The key question we address in this chapter is the following: does rotation produce interesting violations of the no-hair theorem at leading order in a slow-rotation expansion? In experimental terms, could we possibly observe violations of the no-hair theorem via frame-dragging experiments? The conclusion of our analysis is that frame-dragging corrections are *exactly the same as in GR* for all of the Horndeski BH solutions that we analyzed, with the (already known) exception of BH solutions in EdGB gravity [243, 356, 446, 447, 28, 305]. We do not expect this result to hold at second order in rotation, and this will be the topic of a follow-up study.

9.1.1 Organization of this chapter

The plan of the chapter is as follows. In Sec. 9.2 we present the equations of motion for slowly rotating BH space-times in Horndeski gravity, and we carry out some basic sanity checks (in particular, we check that GR and EdGB gravity are recovered in the appropriate limits). The field equations themselves are rather lengthy, and they are listed in Appendix K for the reader's convenience. In Sec. 9.3 we study slowly rotating BHs in theories with a nonminimal derivative coupling with the Einstein tensor, finding that frame-dragging corrections are exactly the same as in GR. In Sec. 9.4 we provide arguments (based on the work of Refs. [229, 446, 447]) to support this no-hair result. Finally, in Sec. 9.5 we present some conclusions and point out directions for future work.

9.2 The equations of motion

The equations of motion that follow from the action (9.1) can be written schematically as $\mathcal{E}_{\alpha\beta} = 0$ (from variations of the metric) and $\mathcal{E}_\phi = 0$ (from variations of the scalar field), where

$$\begin{aligned}
\mathcal{E}_{\alpha\beta} = & -\frac{g_{\alpha\beta}}{2}G_2 + G_{2X}X_{\alpha\beta} - \left[G_{3X}X_{\alpha\beta}\square\phi + \frac{1}{2}g_{\alpha\beta}G_{3\mu}\phi^\mu - G_{3(\alpha}\phi_{\beta)} \right] + G_{\alpha\beta}G_4 + G_{4X}X_{\alpha\beta}R \\
& + G_{4\mu}{}^\mu g_{\alpha\beta} - G_{4\alpha\beta} + \left[G_{4XX}X_{\alpha\beta} - \frac{1}{2}G_{4X}g_{\alpha\beta} \right] (\square\phi^2 - \phi_{\mu\nu}^2) + 2\square\phi G_{4X}\phi_{\alpha\beta} \\
& - 2\nabla_{(\alpha}[G_{4X}\phi_{\beta)}\square\phi] + \nabla_\mu[G_{4X}\phi^\mu\square\phi]g_{\alpha\beta} + 2\nabla_\mu[G_{4X}\phi_{(\alpha}\phi_{\beta)}^\mu] - \nabla_\mu[G_{4X}\phi^\mu\phi_{\alpha\beta}] \\
& - 2G_{4X}\phi_{\beta\nu}\phi^\nu{}_\alpha + G_{\mu\nu}\phi^{\mu\nu}(G_{5X}X_{\alpha\beta} - \frac{1}{2}G_5g_{\alpha\beta}) + 2G_5\phi^\mu{}_{(\beta}G_{\alpha)\mu} - \nabla^\mu[G_{5\phi_{(\alpha}G_{\beta)\mu}}] \\
& + \frac{1}{2}\nabla^\mu[G_{5\phi_\mu}G_{\alpha\beta}] + \frac{1}{2}\{RG_5\phi_{\alpha\beta} - R_{\alpha\beta}G_5\phi_\mu{}^\mu + \square(G_5\phi_{\alpha\beta}) + \nabla_\alpha\nabla_\beta(G_5\phi_\mu{}^\mu) \\
& - 2\nabla_\mu\nabla_{(\alpha}[G_{5\phi_{\beta)}^\mu] + g_{\alpha\beta}[\nabla_\mu\nabla_\nu(G_5\phi^{\mu\nu}) - \square(G_5\phi_\nu{}^\nu)]\} - \frac{1}{6}(G_{5XX}X_{\alpha\beta} \\
& - \frac{1}{2}g_{\alpha\beta}G_{5X})[(\square\phi)^3 + 2\phi_{\mu\nu}^3 - 3\phi_{\mu\nu}^2\square\phi] - \frac{1}{2}\{G_{5X}(\square\phi)^2\phi_{\alpha\beta} - 2\nabla_{(\alpha}[G_{5X}(\square\phi)^2\phi_{\beta)}] \\
& + \frac{1}{2}g_{\alpha\beta}\nabla^\mu[G_{5X}(\square\phi)^2\phi_\mu]\} - \{G_{5X}\phi_{\mu\alpha}\phi_{\beta\sigma}\phi^{\sigma\mu} - \nabla^\sigma[G_{5X}\phi_{(\alpha}\phi_{\mu\sigma}\phi_{\beta)}^\mu] \\
& + \frac{1}{2}\nabla^\sigma[G_{5X}\phi_\sigma\phi_{\mu\alpha}\phi_{\beta)}^\mu]\} + \frac{1}{2}\{G_{5X}(\phi_{\mu\nu}^2\phi_{\alpha\beta} + 2\square\phi\phi_{\alpha\mu}\phi_{\beta)}^\mu) - \nabla_{(\beta}[G_{5X}\phi_\alpha)\phi_{\mu\sigma}\phi^{\mu\sigma}] \\
& + \frac{1}{2}g_{\alpha\beta}\nabla^\sigma[G_{5X}\phi_\sigma\phi_{\mu\nu}\phi^{\mu\nu}] - 2\nabla^\mu[G_{5X}\square\phi\phi_{(\alpha}\phi_{\beta)\mu}] + \nabla^\mu[G_{5X}\square\phi\phi_\mu\phi_{\alpha\beta}]\}, \tag{9.15}
\end{aligned}$$

$$\begin{aligned}
\mathcal{E}_\phi = & G_{2\phi} + \nabla_\alpha(G_{2X}\phi^\alpha) - G_{3\alpha}{}^\alpha - \nabla_\alpha(G_{3X}\phi^\alpha\square\phi) - \square\phi G_{3\phi} + G_{4\phi}R + (\square\phi^2 - \phi_{\mu\nu}^2)G_{4X}\phi \\
& + \nabla^\alpha[G_{4XX}\phi_\alpha(\square\phi^2 - \phi_{\mu\nu}^2)] + \nabla^\alpha(G_{4X}\phi_\alpha R) + 2\square(G_{4X}\square\phi) - 2\nabla^\alpha\nabla^\beta(G_{4X}\phi_{\alpha\beta}) \\
& + G_{5\phi}G_{\alpha\beta}\phi^{\alpha\beta} + G_5^{\alpha\beta}G_{\alpha\beta} - \frac{1}{6}G_{5X\phi}[(\square\phi)^3 + 2\phi_{\mu\nu}^3 - 3\phi_{\mu\nu}^2\square\phi] + \nabla^\alpha[G_{5X}\phi_\alpha\phi_{\mu\nu}G^{\mu\nu}] \\
& - \frac{1}{6}\nabla^\alpha\{G_{5XX}\phi_\alpha[(\square\phi)^3 + 2\phi_{\mu\nu}^3 - 3\phi_{\mu\nu}^2\square\phi]\} - \frac{1}{2}\square[G_{5X}(\square\phi)^2] - \nabla^\alpha\nabla^\beta[G_{5X}\phi^\mu{}_\alpha\phi_{\mu\beta}] \\
& + \frac{1}{2}\square(G_{5X}\phi_{\mu\nu}^2) + \nabla^\alpha\nabla^\beta(G_{5X}\phi_{\alpha\beta}\square\phi). \tag{9.16}
\end{aligned}$$

Here we have defined $G_{i\alpha} \equiv \nabla_\alpha G_i$, $X_{\alpha\beta} \equiv \delta X/\delta g_{\alpha\beta}$, and $f_{1(\alpha}f_{2\beta)} \equiv (f_{1\alpha}f_{2\beta} + f_{1\beta}f_{2\alpha})/2$. These equations apparently contain higher derivatives, but they can be shown to be of second order using appropriate identities (cf. e.g. Appendix B of [254]).

To investigate the properties of slowly rotating BH solutions in Horndeski gravity we follow the approach developed by Hartle [203, 204], in which rotational corrections to the static, spherically symmetric background are introduced within a perturbative framework. At linear order in the BH angular velocity Ω , the metric can be written in the form

$$ds^2 = -A(r)dt^2 + \frac{dr^2}{B(r)} + r^2(d\theta^2 + \sin^2\theta d\varphi^2) - 2\omega(r)r^2 \sin^2\theta dt d\varphi, \quad (9.17)$$

where the frame-dragging function $\omega(r)$ is of order Ω .

Kobayashi et al. [250, 251] carried out a fully relativistic analysis of linear perturbations around static, nonrotating, spherically symmetric backgrounds. As a preliminary step for this perturbative analysis, they derived the equations of motion for general static, spherically symmetric vacuum space-times. Here we generalize these results to the slowly rotating case, deriving the equations of motion for the metric component $\omega(r)$. We also generalize the analysis of Refs. [250, 251] by allowing the scalar field to depend on the radial *and* time coordinates, since a nontrivial time dependence of ϕ allows for the existence of hairy BHs [29]. Following Refs. [29, 252], we assume the scalar field to have the functional form:

$$\phi = \phi(t, r) = qt + \psi(r). \quad (9.18)$$

Then the kinetic energy X is independent of t :

$$X = X(r) = \frac{1}{2} \left(\frac{q^2}{A(r)} - B(r)\psi'^2 \right), \quad (9.19)$$

where the prime means differentiation with respect to the radial coordinate r . Then in (9.15), $X_{\alpha\beta} = -\psi'^2 \delta^r_\alpha \delta^r_\beta / 2 - q^2 / 2 \delta^t_\alpha \delta^t_\beta$. The tt and rr components of Eq. (9.15) yield two

equations

$$\mathcal{E}_{tt} = 0, \tag{9.20}$$

$$\mathcal{E}_{rr} = 0, \tag{9.21}$$

and the scalar field equation of motion (9.16) in the background metric (9.17) is given by

$$\mathcal{E}_\phi = 0, \tag{9.22}$$

where the explicit form of the left-hand sides of (9.20)–(9.22) is quite lengthy, and it can be found in Appendix K. For a static scalar field ($q = 0$), Eqs. (9.20)–(9.22) reproduce the results obtained in [250, 251]; for reflection-symmetric theories, they reduce to the results of [252].

For slowly rotating solutions at linear order in the BH angular velocity, the only nonvanishing component of the equations of motion yields a second-order ordinary differential equation for the variable $\omega(r)$:

$$\mathcal{E}_{t\varphi} = 0. \tag{9.23}$$

Again, the explicit form of the left-hand side can be found in Appendix K.

Taken together, Eqs. (9.20)–(9.23) provide a full description of vacuum space-times at linear order in rotation. We now consider two special cases as sanity checks of the equations of motion.

9.2.1 General relativity

As stated in the introduction, the Einstein-Hilbert Lagrangian of GR corresponds to setting $G_4 = 1/2$ and all the other functions equal to zero. In this case the equation of

motion for the function $\omega(r)$ simply reads

$$\omega'' + \frac{\omega'}{2} \left(\frac{B'}{B} + \frac{8}{r} - \frac{A'}{A} \right) = 0, \quad (9.24)$$

in agreement with the frame-dragging equation found by Hartle [203]. If the nonrotating background is the Schwarzschild solution this further simplifies to

$$\omega'' + \frac{4}{r}\omega' = 0. \quad (9.25)$$

9.2.2 Einstein-dilaton-Gauss-Bonnet gravity

EdGB gravity [243] corresponds to the choice of Eqs. (9.7)-(9.10). If the coupling is linear in the field – i.e. $\xi(\phi) = \alpha\phi$ as in [446, 447], so that the theory is shift symmetric – and $q = 0$, we get

$$(8\alpha B\phi' - r)\omega'' + \left[12\alpha\phi'B' + 8\alpha B\phi'' + \frac{24\alpha}{r}B\phi' - 4\alpha B\phi'\frac{A'}{A} + \frac{r}{2} \left(\frac{A'}{A} - \frac{B'}{B} \right) - 4 \right] \omega' = 0. \quad (9.26)$$

If instead we use an exponential coupling of the form $\xi = e^\phi$ and we set $q = 0$, the frame-dragging equation becomes

$$\begin{aligned} \omega'' \left(\frac{2}{B}r^2 - 2re^\phi\phi' \right) + \frac{\omega'r}{B} \left(8 - r\frac{A'}{A} + \frac{B'}{B}r \right) \\ - \omega'e^\phi \left[2\phi''r + 6\phi' + r\phi' \left(3\frac{B'}{B} + 2\phi' - \frac{A'}{A} \right) \right] = 0, \end{aligned} \quad (9.27)$$

in agreement with the result of Ref. [356].

9.3 Nonminimal derivative coupling to the Einstein tensor

In this section we apply the formalism derived above to rotating solutions in a class of Horndeski theories characterized by a nonminimal derivative coupling with the Einstein tensor of the form (9.11). The theory defined by this action is invariant under both shift

symmetry ($\phi \rightarrow \phi + c$) and reflection symmetry ($\phi \rightarrow -\phi$). Shift symmetry allows us to write the equation of motion for the scalar field ϕ as a current conservation equation [29, 446, 447]:

$$\nabla_\mu J^\mu = 0. \quad (9.28)$$

In particular, for the action (9.11), the conservation equation (9.28) reduces to

$$(\eta g^{\mu\nu} - \beta G^{\mu\nu}) \nabla_\mu \partial_\nu \phi = 0. \quad (9.29)$$

Moreover, following [252] we shall parametrize our solutions in terms of three auxiliary functions:

$$\Lambda = -\frac{\eta}{\beta}, \quad (9.30)$$

$$\mathcal{F}(X) = -\frac{-2X\beta\eta + \zeta\eta + \beta\Lambda_0}{2X\beta^2}, \quad (9.31)$$

$$\mathcal{G}(X) = 2(\zeta - \beta X). \quad (9.32)$$

Using this parametrization, BH configurations within this theory can be easily obtained with the following procedure. The tt component of the equations of motion, Eq. (9.20), leads to the equation

$$-\frac{2A(r)^2}{q^2 r \mathcal{G}} \frac{d}{dr} [X \mathcal{G} (1 - r^2 \mathcal{F}(X))] = 0, \quad (9.33)$$

which can be integrated with the solution

$$X \mathcal{G}^2(X) [1 - r^2 \mathcal{F}(X)] = C, \quad (9.34)$$

where C is a constant. Equation (9.34) determines $X(r)$ algebraically. Then the metric function $A(r)$ can be found by solving Eq. (9.21), which yields

$$(rA)' = \frac{q^2}{2X} \frac{1 - r^2\Lambda}{1 - r^2\mathcal{F}(X)}. \quad (9.35)$$

Finally, the metric function $B(r)$ can be found from Eq. (9.28):

$$B(r) = \frac{2X}{q^2} [1 - r^2\mathcal{F}(X)] A(r). \quad (9.36)$$

With the choice (9.30), the frame-dragging equation for $\omega(r)$ has a particularly simple form:

$$\mathcal{G}\omega'' + \omega' \left[\mathcal{G}_X X + \frac{1}{2} \left(\frac{8}{r} - \frac{A'}{A} + \frac{B'}{B} \right) \mathcal{G} \right] = 0. \quad (9.37)$$

As an extension of Ref. [252], we now consider nonrotating BH solutions of Eqs. (9.34)-(9.36) in different subcases and investigate the slow-rotation corrections predicted by Eq. (9.37) for each of these solutions.

Case 1: $\mathcal{F} = 0$. One possibility to satisfy Eq. (9.34) is to impose $\mathcal{F}(X_f) = 0$, where following the notation of [252] we define X_f to be the value of X for which $\mathcal{F}(X_f) = 0$, and $C = X_f \mathcal{G}^2(X_f)$. In this case, the metric components and the scalar field read

$$A(r) = -\frac{\mu}{r} + \frac{q^2}{2X_f} \left(1 + \frac{\eta}{3\beta} r^2 \right), \quad (9.38)$$

$$B(r) = \frac{2X_f}{q^2} A(r), \quad (9.39)$$

$$\psi'(r)^2 = \frac{q^2 - 2X_f A(r)}{A(r)B(r)}, \quad (9.40)$$

where μ is an integration constant.

With a rescaling of the time variable $q^2 = 2X_f$, Eqs. (9.38)-(9.40) represent a BH solution with an effective cosmological constant $\Lambda = -\eta/\beta$ and a nontrivial profile for the

scalar field. Replacing this solution into Eq. (9.37) we find that $\omega(r)$ satisfies the same equation (9.25) as in GR. The standard solution of this equation is

$$\omega = c_1 + \frac{c_2}{r^3}, \quad (9.41)$$

where c_1 and c_2 are integration constants which can be fixed by imposing appropriate boundary conditions.

Case 2: $\mathcal{G} = 0$. Another class of solutions of Eq. (9.34) corresponds to choosing $\mathcal{G}(X_{\mathcal{G}}) = 0$. In this case, from Eq. (9.37) we see that the coefficients of both ω'' and ω' vanish, and there are no corrections at linear order.

Case 3: $q = 0$. Finally, we consider the case in which the scalar field is time independent ($q = 0$). Integration of the equations of motion for $A(r)$ and $B(r)$ leads to [321]

$$A(r) = \frac{1}{12\beta\zeta^2\eta^2r} \left\{ r(\zeta\eta - \beta\Lambda_0) [\zeta\eta(9\beta + \eta r^2) + \beta\Lambda_0(3\beta - \eta r^2)] - 24\beta\zeta^2\eta^2\mu \right\} + \frac{\sqrt{\beta}(\beta\Lambda_0 + \zeta\eta)^2 \arctan\left(\frac{\sqrt{\eta}r}{\sqrt{\beta}}\right)}{4\zeta^2\eta^{5/2}r}, \quad (9.42)$$

$$B(r) = \frac{4\zeta^2(\beta + \eta r^2)^2}{(2\beta\zeta - \beta\Lambda_0 r^2 + \zeta\eta r^2)^2} A(r), \quad (9.43)$$

where again μ is an integration constant, while for the scalar field we obtain:

$$\psi'(r)^2 = -\frac{(\beta\Lambda_0 + \zeta\eta)[r^3(\zeta\eta - \beta\Lambda_0) + 2\beta\zeta r]^2}{4\beta\zeta^2(\beta + \eta r^2)^3 A(r)}. \quad (9.44)$$

Replacing the former expressions into Eq. (9.37), we find that the frame-dragging function $\omega(r)$ satisfies once again the same equation (9.25) as in GR.

9.4 Why the baldness?

The no-hair theorems for static, spherically symmetric BHs proved in Refs. [229, 446, 447] rely crucially on shift symmetry, which allows us to write the equation of motion for ϕ as the conservation equation (9.28). In this section we discuss how these theorems can be generalized to the case where we consider first-order rotational corrections and time-dependent scalar fields of the form (9.18). In this case, we can show that the nontrivial components of J^μ are given by

$$\begin{aligned}
J^r = & B\psi' \left[-G_{2X} + \frac{B\psi'}{2} \left(\frac{A'}{A} + \frac{4}{r} \right) G_{3X} + \frac{2B}{r} \left(\frac{A'}{A} + \frac{B-1}{Br} \right) G_{4X} \right. \\
& \left. - \frac{2B^2\psi'^2}{r} \left(\frac{A'}{A} + \frac{1}{r} \right) G_{4XX} - \frac{B\psi' A'}{2r^2} (3B-1) G_{5X} + \frac{A' B^3\psi'^3}{A 2r^2} G_{5XX} \right] \\
& + \frac{q^2}{A} B\psi' \left[\frac{2B A'}{r A} G_{4XX} - \frac{B^2\psi' A'}{2r^2 A} G_{5XX} \right] \\
& + \frac{q^2}{A} \left[-\frac{B A'}{2 A} G_{3X} + \frac{B A'}{2r^2 A} (B-1) G_{5X} \right], \tag{9.45}
\end{aligned}$$

$$\begin{aligned}
\frac{A}{q} J^t = & G_{2X} - \left[B\psi'' + \frac{B}{2} \left(\frac{B'}{B} + \frac{A'}{A} + \frac{4}{r} \right) \psi' \right] G_{3X} - \frac{2}{r} \left(B' + \frac{B-1}{r} \right) G_{4X} + \frac{2B^2\psi'}{r} [2\psi'' \\
& + \left(\frac{B'}{B} + \frac{A'}{A} + \frac{1}{r} \right) \psi'] G_{4XX} + \frac{B}{r^2} \left[(B-1)\psi'' + \frac{1}{2} \left(\frac{A'}{A} B - \frac{B'}{B} - \frac{A'}{A} + 3B' \right) \psi' \right] G_{5X} \\
& - \frac{B^3\psi'^2}{2r^2} \left[2\psi'' + \left(\frac{A'}{A} + \frac{B'}{B} \right) \psi' \right] G_{5XX} \\
= & -\frac{J^r}{B\psi'} - \frac{2A}{r} \left[\left(G_{4X} - \frac{B\psi'}{2r} G_{5X} \right) \left(\frac{B}{A} \right)' \right. \\
& \left. + \left(2G'_{4X} + \frac{B\psi'}{2r} G'_{5X} - \frac{G'_5}{2r\psi'} \right) \frac{B}{A} - \frac{1}{2A\psi'} \left(rG'_3 + \frac{G'_5}{r} \right) \right]. \tag{9.46}
\end{aligned}$$

For shift-symmetric theories, $G_i = G_i(X)$. These expressions can be used to extend the no-hair theorems of Refs. [229, 446, 447] to the cases considered in this chapter.

For clarity and completeness, let us begin with a short summary of the original proof given in [229] (with the amendments of Refs. [446, 447]).

9.4.1 The no-hair theorem for nonrotating black holes with a time-independent scalar field

The no-hair theorem of Ref. [229] applies to static, spherically symmetric, asymptotically flat solutions in shift-symmetric theories. It consists of the following line of reasoning:

1. Assuming that the scalar field $\psi(r)$ has the *same symmetries as the metric* (the time-dependent scalar field of [29] obviously violates this first assumption), the only nonvanishing component of J^μ for a spherically symmetric background is J^r , i.e. $J^\mu = (J^r, 0, 0, 0)$.
2. Given a spherically symmetric space-time, defined by the line element (9.17) with $\omega(r) = 0$, we require $J^2 = J^\mu J_\mu$ to remain finite at the horizon r_h . Since

$$J^2 = \frac{(J^r)^2}{B} \tag{9.47}$$

5 and $B \rightarrow 0$ for $r \rightarrow r_h$, this regularity condition implies that $J^r = 0$ at the horizon.

3. For a spherically symmetric space-time, the conservation equation (9.28) reduces to

$$\frac{1}{\sqrt{-g}} \partial_\mu (\sqrt{-g} J^\mu) = \partial_r J^r + \frac{2}{r} J^r = 0, \tag{9.48}$$

which can be easily integrated. The solution is $J^r r^2 = K$, where K is an integration constant. At the horizon the areal radius r cannot be zero. This implies that $K = 0$, and therefore that

$$J^r = 0 \quad \forall r. \tag{9.49}$$

4. The current J^r can be schematically written as

$$J^r = B \psi' F(g, g', g'', \psi'), \tag{9.50}$$

where F is a generic function of the metric, its first and second derivatives, and ψ' .

At spatial infinity, asymptotic flatness implies that $B \rightarrow 1$ and $\psi' \rightarrow 0$, while F tends to a nonzero constant. This last condition is dictated by the requirement that the scalar field's kinetic energy should have the standard form: in the weak-field limit, the action contains a term that is quadratic in the field derivatives and $J_\mu \rightarrow \partial_\mu \phi$, up to an overall constant of normalization. If we now move “inward” towards the horizon, by continuity F and B will still be nonzero, and therefore $J^r \neq 0$, which contradicts Eq. (9.49). This contradiction can be avoided if $\psi' = 0$ for any choice of r , which fixes $\psi = \text{constant}$ or (without loss of generality, since the theory is shift symmetric) $\psi = 0$.

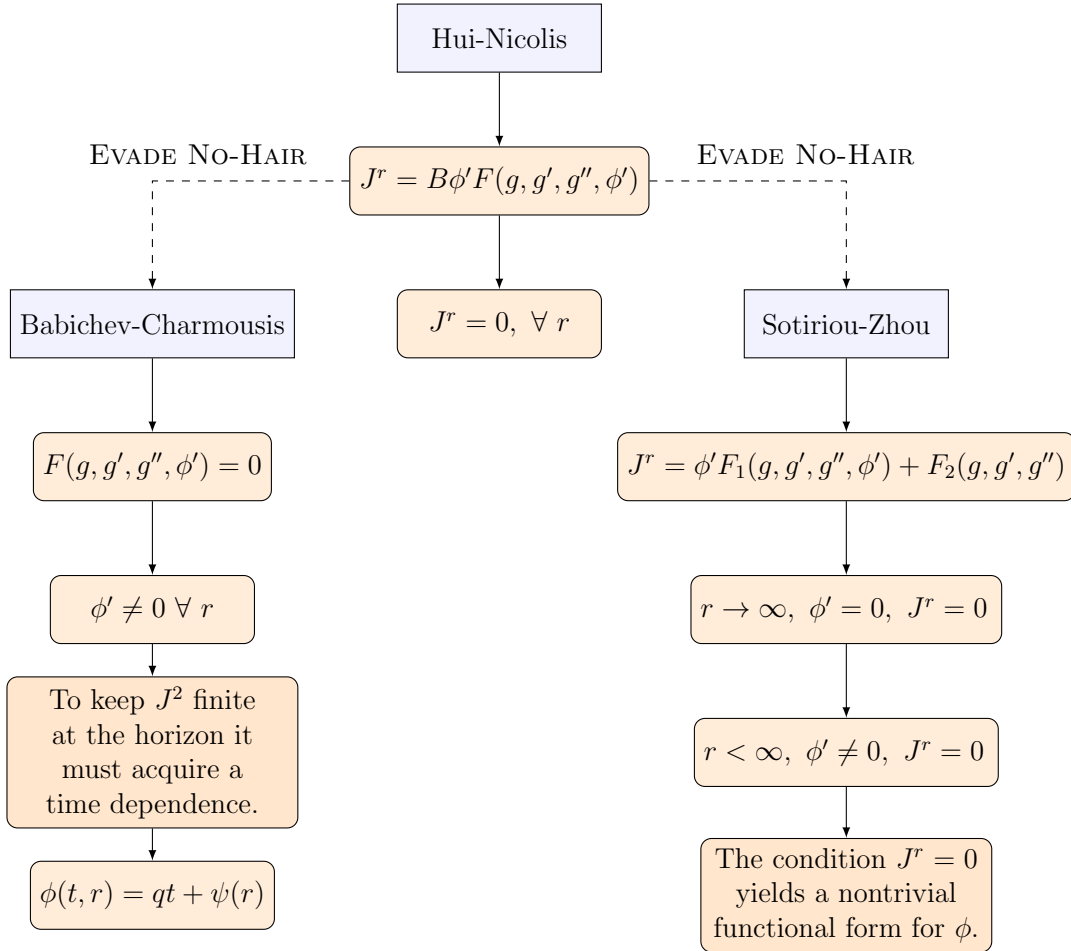


Figure 9.1: *Hair (and its absence) in Horndeski gravity.* A schematic representation of the Hui-Nicolis no-hair theorem for shift-symmetric Horndeski gravity, and two possible ways of violating it (adapted from Ref. [418]).

Sotiriou and Zhou [446, 447] pointed out a loophole in the last step of this proof. For Horndeski gravity theories with shift symmetry, the conserved current can be written as

$$\begin{aligned}
J^r = & -BG_{2X}\psi' + \frac{B^2\psi'^2}{2} \left(\frac{A'}{A} + \frac{4}{r} \right) G_{3X} + \frac{2B^2\psi'}{r} \left(\frac{A'}{A} - \frac{1}{Br} + \frac{1}{r} \right) G_{4X} \\
& - \frac{2B^3\psi'^3}{r} \left(\frac{A'}{A} + \frac{1}{r} \right) G_{4XX} - \frac{B^3\psi'^2}{2r^2} \frac{A'}{A} \left(\frac{3B-1}{B} \right) G_{5X} + \frac{A'}{A} \frac{B^4\psi'^4}{2r^2} G_{5XX}. \quad (9.51)
\end{aligned}$$

Depending on the particular form of the coupling functions G_i we have essentially two options:²

- (a) J^r depends linearly on ψ' . This is the case considered in Ref. [229], for which $F \rightarrow -G_{2X}$ as $r \rightarrow \infty$.
- (b) J^r contains terms which are independent of ψ' , but no negative powers of ψ' .

This second case represents a loophole for the no-hair theorem of Ref. [229]. Indeed, in this case the asymptotic behavior of F is not trivially determined.

This is illustrated most clearly by looking at two specific examples: EdGB gravity and theories with nonminimal derivative coupling to the Einstein tensor.

In the first case the conserved current reduces to

$$J_{\text{EdGB}}^r = -B\psi' - 4\alpha \frac{A'B(B-1)}{Ar^2}, \quad (9.52)$$

where we specialized to a linear coupling function $\xi(\phi) = \alpha\phi$ in Eq. (9.6), so that the theory becomes shift symmetric (recall that the Gauss-Bonnet combination is a topological invariant). The current (9.52) contains a term independent of ψ' as in case (b) above, corresponding to the loophole pointed out in Refs. [446, 447]. The current vanishes at infinity, but for smaller radii the choice of F is nontrivial and leads to scalar hair growth.

²A third case where J^r contains negative powers of ψ' can be excluded because it generally corresponds to theories that would not admit flat space with a trivial scalar configuration as a solution, leading to violations of local Lorentz symmetry [447].

For the nonminimal derivative coupling theory we have instead

$$J_{\text{Gg}}^r = B\psi' \left[-2\eta + \frac{2B}{r} \left(\frac{A'}{A} - \frac{1}{Br} + \frac{1}{r} \right) \beta \right]. \quad (9.53)$$

This expression for the current falls into case (a) above. The current depends linearly on ψ' , $F \rightarrow -2\eta$ for $r \rightarrow \infty$, and F stays finite even at finite radii by continuity, as required by the arguments of [229], so we are forced to set $\psi' = 0$ and ψ is a constant, which can be set to zero. Asymptotic flatness was of course a key ingredient in these arguments. Hairy solutions in theories with nonminimal derivative coupling are *not* asymptotically flat (see e.g. [389, 321, 15]).

Our discussion on the argument behind the proof of the no-hair theorem and its loopholes is summarized in Fig. 9.1.

9.4.2 Extension to slow-rotation and time-dependent scalar fields

What is crucial for the present work is that the arguments above apply also to rotating BH solutions at linear order in rotation. This is because, as argued in Ref. [446], the scalar field ϕ (like all scalar quantities) is affected by rotation only at second order, and therefore the expression (9.45) for the current J^r remains unchanged at linear order. Similarly, J^θ is still equal to zero at linear order. The component J^φ acquires a nonzero value proportional to the BH angular momentum; however J^φ is independent of φ , and therefore it does not contribute to the current conservation equation (9.28).

At first sight, the fact that no-hair theorems still hold true at linear order in rotation even for time-dependent scalar fields may be surprising. However this no-hair property can be proved through a simple extension of the arguments valid for static, nonrotating solutions. Let us extend the original argument to theories with time-dependent scalar fields of the form (9.18):

1. When ϕ has the form (9.18) the current has a nonzero time component, i.e. $J^\mu =$

$(J^r, 0, 0, J^t)$, and its norm becomes

$$J^2 = \frac{(J^r)^2}{B} - (J^t)^2 A. \quad (9.54)$$

2. By imposing regularity at the horizon, where $A \rightarrow 0$, $B \rightarrow 0$, we conclude that $J^r \rightarrow 0$ as $r \rightarrow r_h$. This is true as long as J^t does not diverge in the limit $r \rightarrow r_h$, i.e., as long as the quantity in square brackets in the last line of Eq. (9.46) is finite. For reflection-symmetric theories ($G_3 = G_5 = 0$), this latter requirement simplifies to the condition that $(B/A)'$ should be finite [252].

3. In principle, the current conservation equation (9.48) acquires an extra term because $J^t \neq 0$:

$$\partial_r J^r + \frac{2}{r} J^r + \partial_t J^t = 0. \quad (9.55)$$

However Eq. (9.46) shows that in the present case J^t is independent of time, so this term vanishes: $\partial_t J^t = 0$. Following the reasoning below Eq. (9.48), we conclude that $J^r = 0$ for all r even for scalar fields with a linear time dependence. Note that for a time-dependent scalar field, in general, the tr component of the gravitational equations $\mathcal{E}_{tr} = 0$ may be nontrivial, indicating the existence of an energy flux in the radial direction. However Ref. [30] showed that, for the linear-in-time ansatz (9.18), \mathcal{E}_{tr} is proportional to J^r under the assumptions of diffeomorphism invariance and shift symmetry. Therefore the condition $J^r = 0$ always ensures that $\mathcal{E}_{tr} = 0$: the linear time dependence (9.18) does not give rise to an energy flux in the radial direction.

4. The current (9.45) has the form (9.50), where $F(g, g', g'', \psi')$ is an unspecified function. This allows us to borrow in its entirety the reasoning of Ref. [447]. We can exclude cases where J^r contains negative powers of ψ' . When all terms in J^r contain positive powers of ψ' , $\psi' = 0$ for all r and the no-hair theorem of [229] applies. The only exception is the case where J^r contains one or more terms with no dependence on ψ' , but no

terms with negative powers of ψ' ; and then, following Sec. IIB of [447], shift symmetry and Lovelock's theorem imply that the action must contain a term proportional to the Gauss-Bonnet invariant.

This generalized no-hair theorem can be used to justify the absence of corrections to GR at linear order that we found in Sec. 9.3. For a theory with nonminimal derivative coupling to the Einstein tensor, the nonzero components of the current can be obtained by specializing Eqs. (9.45)-(9.46), with the result

$$J_{\text{Gg}}^r = B\psi' \left[-2\eta + \frac{2B}{r} \left(\frac{A'}{A} - \frac{1}{Br} + \frac{1}{r} \right) \beta \right], \quad (9.56)$$

$$\frac{A}{q} J_{\text{Gg}}^t = 2\eta + \frac{2B}{r} \left(\frac{1-B}{Br} - \frac{B'}{B} \right) \beta. \quad (9.57)$$

The J^r component is identical to the static case of Eq. (9.53), it does not contain any ψ' -independent terms, and the no-hair theorem of [229] implies that asymptotically flat solutions must be the same as GR.

In conclusion, the only no-hair violations at linear order in rotation when the scalar field depends linearly on time and when we require asymptotic flatness can occur in one of two cases:

- (i) if the scalar field has a linear coupling to the Gauss-Bonnet invariant, or
- (ii) if, as proposed in Ref. [29], the field equations of the theory guarantee that the current vanishes identically ($J^r = 0$) because $F(g, g', g'', \psi') = 0$ as a consequence of the field equations. Note that this is only possible for special forms of the functions G_i , and that the scalar field must then be time dependent (i.e., it must violate some of the symmetries of the metric) in order to be regular at the horizon.

9.5 Conclusions

In this work we studied leading-order rotational corrections to a broad class of BH solutions in Horndeski gravity. With the known exception of EdGB gravity [243, 356, 446,

447, 28, 305], we have found that the frame-dragging function $\omega(r)$, which describes the leading-order rotational corrections, is exactly the same as in GR for all of the Horndeski BH solutions known in the literature. This result applies even to asymptotically flat solutions that violate the no-hair theorems by requiring the scalar field to be time dependent (so that the scalar field does not respect the same symmetries as the metric), as proposed in Ref. [29].

The formalism developed in this chapter can be extended in various directions. First of all, the no-hair theorem proved in Sec. 9.4 at first order in rotation is not expected to hold at second order, where the continuity equation will be modified. Calculations of BH solutions at second order in rotation, along the lines of [28, 305], are already underway [304].

Even for nonrotating Horndeski BHs, studies of stability and perturbative dynamics (as encoded in their quasinormal mode spectrum: see e.g. [50] for a review) are still in their infancy. One of us [319] studied massless scalar field perturbations of static BH solutions in theories with field derivative coupling to the Einstein tensor. More in general, gravitational perturbations of static, nonrotating space-times can be explored using the formalism developed in Refs. [250, 251]. The present work lays the foundations to study quasinormal modes and look for super-radiant instabilities using the slow-rotation perturbative techniques reviewed, e.g., in Ref. [351].

Another important extension concerns compact stars in Horndeski gravity. Slowly rotating compact stars in EdGB gravity were studied in [355]. Cisterna et al. [104] investigated compact objects in theories with a nonminimal derivative coupling of the scalar field with the Einstein tensor. Our formalism can be extended relatively easily to study compact stars in broader classes of Horndeski gravity, and to understand whether genuine strong-field deviations from GR (similar to the “spontaneous scalarization” phenomena proposed by Damour and Esposito-Farèse [118]) can occur in some sectors of the Horndeski gravity action, see e.g. [100] for recent work in this direction. We explore some aspects of this problem in Chapter 10.

CHAPTER 10

NEUTRON STARS IN HORNDESKI GRAVITY

10.1 Introduction

The most recent cosmological observations are consistent with standard cosmological models built on general relativity (GR), but they imply the presence of a mysterious late-time acceleration phase. The late-time acceleration can be interpreted as due to the existence of new particle sectors beyond the Standard Model, or explained by assuming that GR itself is modified on cosmological scales. Modified gravity models differ widely in their physical motivations, but many of them can be reformulated in terms of ST theories of gravitation; i.e., they are mathematically equivalent to a gravitational theory whose degrees of freedom are the metric $g_{\mu\nu}$ and one or more scalar fields ϕ . Many of the simplest dark energy or modified gravity models – including the standard Λ CDM model – are plagued by the cosmological constant problem (i.e., the problem of fine-tuning the potentially huge quantum vacuum energy against the small value of the observed cosmological constant). However some ST theories allow for a “dynamical self-tuning mechanism” in which the effects of the cosmological constant may be compensated within the scalar field sector, so that they do not appear in the metric, by relaxing the assumptions of Weinberg’s no-go theorem [495]. Here we will focus on one such model, called “Fab Four” gravity in the literature, which is a special case of Horndeski’s theory.

10.1.1 Horndeski’s theory

Realistic models of dark energy or modified gravity must at the very least pass the stringent experimental constraints on deviations from GR [498, 51] and be theoretically viable. In particular, they must be free of the so-called “Ostrogradski ghost” [505]. Several

studies led to the conclusion that the most general models with a single additional scalar degree of freedom compatible with these requirements correspond to the ST theory formulated by Horndeski about 40 years ago, whose equations of motion contain at most second-order derivatives [225]. It was shown [254] that Horndeski's theory is equivalent to the generalization of a scalar field theory with Galilean shift symmetry in flat spacetime to curved spacetime [131], whose action reads

$$S = \sum_{i=2}^5 \int d^4x \sqrt{-g} \mathcal{L}_i, \quad (10.1)$$

where

$$\mathcal{L}_2 = G_2, \quad (10.2a)$$

$$\mathcal{L}_3 = -G_3 \square \phi, \quad (10.2b)$$

$$\mathcal{L}_4 = G_4 R + G_{4X} [(\square \phi)^2 - \phi_{\mu\nu}^2], \quad (10.2c)$$

$$\mathcal{L}_5 = G_5 G_{\mu\nu} \phi^{\mu\nu} - \frac{G_{5X}}{6} [(\square \phi)^3 + 2\phi_{\mu\nu}^3 - 3\phi_{\mu\nu}^2 \square \phi]. \quad (10.2d)$$

Here $g_{\mu\nu}$ is the metric tensor, and $g \equiv \det(g_{\mu\nu})$ its determinant. The Ricci scalar and Einstein tensor associated with $g_{\mu\nu}$ are denoted by R and $G_{\mu\nu}$, respectively. The functions $G_i = G_i(\phi, X)$ depend only on the scalar field ϕ and its kinetic energy $X = -\partial_\mu \phi \partial^\mu \phi / 2$. We also introduced the shorthand notations $\phi_{\mu\dots\nu} \equiv \nabla_\mu \dots \nabla_\nu \phi$, $\phi_{\mu\nu}^2 \equiv \phi_{\mu\nu} \phi^{\mu\nu}$, $\phi_{\mu\nu}^3 \equiv \phi_{\mu\nu} \phi^{\nu\alpha} \phi^\mu{}_\alpha$ and $\square \phi \equiv g^{\mu\nu} \phi_{\mu\nu}$.

Special cases of Horndeski's theory correspond to well-studied models of dark energy and modified gravity, including quintessence [384, 76], k-essence [23], the Dvali-Gabadadze-Porrati (DGP) model [157, 332], and $f(R)$ gravity [444, 476, 107, 333]. However it is desirable to restrict the large number of functional degrees of freedom of the action (10.1) by additional theoretical or phenomenological requirements. For example, it is desirable to restrict the Horndeski action to models that allow for dynamical self-tuning of the quantum vacuum

energy. This requirement leads to the Fab Four theory.

10.1.2 Fab Four theory

Starting from the Horndeski action (10.1), Charmousis et al. [95, 96] considered homogeneous isotropic cosmological models satisfying the following requirements:

1. The theory admits the Minkowski vacuum for any value of the vacuum energy.
2. The Minkowski vacuum persists across any phase transition where the vacuum energy changes instantaneously by a finite amount.
3. The theory admits nontrivial cosmological evolution in the presence of matter.

These requirements lead to the Fab Four action

$$S = \int d^4x \sqrt{-g} \left(\mathcal{L}_G[g_{\mu\nu}, \phi] + \mathcal{L}_M[g_{\mu\nu}, \Psi] \right), \quad (10.3)$$

where $\mathcal{L}_M[g_{\mu\nu}, \Psi]$ is the Lagrangian for matter fields, collectively represented by Ψ , and

$$\mathcal{L}_G[g_{\mu\nu}, \phi] = \mathcal{L}_{\text{george}} + \mathcal{L}_{\text{ringo}} + \mathcal{L}_{\text{john}} + \mathcal{L}_{\text{paul}}, \quad (10.4)$$

where

$$\mathcal{L}_{\text{george}} = V_{\text{george}}(\phi) R, \quad (10.5a)$$

$$\mathcal{L}_{\text{ringo}} = V_{\text{ringo}}(\phi) R_{\text{GB}}, \quad (10.5b)$$

$$\mathcal{L}_{\text{john}} = V_{\text{john}}(\phi) G^{\mu\nu} \nabla_\mu \phi \nabla_\nu \phi, \quad (10.5c)$$

$$\mathcal{L}_{\text{paul}} = V_{\text{paul}}(\phi) P^{\mu\nu\alpha\beta} \nabla_\mu \phi \nabla_\alpha \phi \nabla_\nu \nabla_\beta \phi. \quad (10.5d)$$

Here

$$R_{\text{GB}} \equiv R^{\alpha\beta\mu\nu} R_{\alpha\beta\mu\nu} - 4R^{\mu\nu} R_{\mu\nu} + R^2 \quad (10.6)$$

is the Gauss-Bonnet (GB) invariant, and the four potentials $V_{\text{george}}(\phi)$, $V_{\text{ringo}}(\phi)$, $V_{\text{john}}(\phi)$, and $V_{\text{paul}}(\phi)$ are functions of the scalar field. The quantity

$$P^{\mu\nu}{}_{\alpha\beta} \equiv -\frac{1}{4}\delta_{\sigma\lambda\alpha\beta}^{\mu\nu\gamma\delta}R^{\sigma\lambda}{}_{\gamma\delta}, \quad (10.7)$$

where

$$\delta_{\nu\beta\sigma\delta}^{\mu\alpha\rho\gamma} = \begin{vmatrix} \delta_{\alpha}^{\mu} & \delta_{\beta}^{\mu} & \delta_{\gamma}^{\mu} & \delta_{\delta}^{\mu} \\ \delta_{\alpha}^{\nu} & \delta_{\beta}^{\nu} & \delta_{\gamma}^{\nu} & \delta_{\delta}^{\nu} \\ \delta_{\alpha}^{\rho} & \delta_{\beta}^{\rho} & \delta_{\gamma}^{\rho} & \delta_{\delta}^{\rho} \\ \delta_{\alpha}^{\sigma} & \delta_{\beta}^{\sigma} & \delta_{\gamma}^{\sigma} & \delta_{\delta}^{\sigma} \end{vmatrix}, \quad (10.8)$$

is the double-dual of the Riemann tensor, which shares the symmetries of the Riemann tensor and satisfies $\nabla_{\mu}P^{\mu\alpha\nu\beta} = 0$. We assume that $g_{\mu\nu}$ is the Jordan frame metric, so that the matter fields Ψ do not couple directly to the scalar field ϕ .

“George” reduces to GR and “Ringo” – the Einstein-dilaton-Gauss-Bonnet (EdGB) term – becomes trivial in four dimensions when the respective potentials are constant. Compact objects in these theories (George and Ringo) have been studied in detail in the existing literature. The “John” and “Paul” terms are more crucial for self-tuning and will be the main focus of this chapter.

The correspondence between the Horndeski Lagrangians (10.2) and the Fab Four Lagrangians (10.5) was presented in [96], and we report it here for completeness:

$$G_2 = 2V_{\text{john}}''(\phi)X^2 - V_{\text{paul}}^{(3)}(\phi)X^3 + 6V_{\text{george}}''(\phi)X + 8V_{\text{ringo}}^{(3)}(\phi)X^2(3 - \ln(|X|)), \quad (10.9a)$$

$$G_3 = 3V_{\text{john}}'(\phi)X - \frac{5}{2}V_{\text{paul}}''(\phi)X^2 + 3V_{\text{george}}'(\phi) + 4V_{\text{ringo}}^{(3)}(\phi)X(7 - 3\ln(|X|)), \quad (10.9b)$$

$$G_4 = V_{\text{john}}(\phi)X - V_{\text{paul}}'(\phi)X^2 + V_{\text{george}}(\phi) + 4V_{\text{ringo}}''(\phi)X(2 - \ln(|X|)), \quad (10.9c)$$

$$G_5 = -3V_{\text{paul}}(\phi)X - 4V_{\text{ringo}}'(\phi)\ln(|X|). \quad (10.9d)$$

10.1.3 Cosmology and black holes in Fab Four theory

Cosmological evolution in Fab Four gravity in the presence of ordinary matter and radiation has been exhaustively investigated by Copeland et al. [112]. They demonstrated that for a specific choice of the Fab Four potentials in Eq. (10.5), even if the source is dominated by the vacuum energy and there is no explicit matter fluid, the cosmological evolution toward the self-tuned Minkowski attractor can mimic the matter-dominated evolution corresponding to dark matter. Moreover, Refs. [190, 21] demonstrated the existence of a self-tuned de Sitter (dS) attractor for a certain nonlinear combination of the canonical kinetic term to the Fab Four. References [302, 301] presented a systematic derivation of the most general subclass of Horndeski's theory that can allow for a spatially flat self-tuned dS vacuum. This new subclass of Horndeski's theory is expected to have a deep connection to the Fab Four theory, but it was derived in an independent way and their relation remains unclear. A specific form of John and Paul also appears in a proxy theory to nonlinear massive gravity [128], but a close inspection of cosmological dynamics revealed that there is no de Sitter attractor in this model [211].

A challenge to the Fab Four model is that self-tuning has been verified only for homogeneous, isotropic cosmological backgrounds. The presence of stars and black holes (BHs) in the Universe implies that self-tuning should still occur in the presence of local inhomogeneities of the spacetime, such as point masses or extended self-gravitating bodies. Whether self-tuning occurs in inhomogeneous spacetimes is a nontrivial question.

A first step towards answering this question is the investigation of BH solutions in Fab Four theory. Most studies of BH solutions in Horndeski's theory and Fab Four gravity have focused on the shift-symmetric subclass of the theories. An influential work by Hui and Nicolis [229] proved a BH no-hair theorem in Horndeski gravity. The theorem makes the following assumptions: (i) the spacetime is static and spherically symmetric; (ii) the scalar field shares the same symmetries as the spacetime, i.e. $\phi = \phi(r)$, where r is the radial coordinate; (iii) the theory is shift-symmetric (i.e. it is invariant under the transformation

$\phi \rightarrow \phi + c$, where c is a constant); and (iv) the spacetime is asymptotically flat.

Searches for hairy BH solutions followed two main routes: they either looked for loopholes in the Hui-Nicolis theorem, or relaxed the assumptions behind the theorem. All BH solutions found so far in Horndeski’s theory have secondary hair, i.e. the scalar charge is not independent of other charges, such as the mass (see e.g. [213] for a review of BH solutions with scalar hair).

Sotiriou and Zhou found a loophole in the Hui-Nicolis no-hair theorem [446, 447]. In our language, they considered the combination George+Ringo with $V_{\text{george}} = \text{constant}$ and $V_{\text{ringo}} \propto \phi$ in Eq. (10.5b). Other authors relaxed assumption (iv), finding asymptotically anti-de Sitter (AdS) BH solutions for actions of the John type (nonminimal coupling to the Einstein tensor) with $V_{\text{john}} = \text{constant}$ [389, 15, 321] (see [319, 103] for a stability analysis of BH solutions in theories of the John subclass). BH solutions that may be more relevant for astrophysics were found by Babichev and Charmousis [29] for theories of the George+John type, with V_{george} and V_{john} both constant, relaxing assumption (ii). Babichev and Charmousis introduced a linear time dependence in the scalar field that therefore does not possess the same symmetries as the metric. However the effective energy-momentum tensor remains static because of the shift symmetry. A particularly important asymptotically flat BH solution emerging from this analysis is a “stealth” solution in the George+John class: a Schwarzschild BH metric supports a nontrivial, regular scalar field configuration which does not backreact on the spacetime. By adding the canonical kinetic term for the scalar field and the cosmological constant Λ , Babichev and Charmousis also obtained a Schwarzschild-(A)dS solution. Interestingly, the effective cosmological constant one can read off from the Schwarzschild-(A)dS metric does *not* depend on Λ , and the Λ dependence appears only in the scalar field. Therefore this solution may be interpreted as an extension of the self-tuned dS vacuum to an inhomogeneous spacetime.

In Ref. [306], all of the above static, spherically symmetric BH solutions were generalized to slow rotation at leading order in the Hartle-Thorne approximation [203, 204]. For all

of these solutions, first-order corrections due to rotation were shown to be identical to GR. The Hui-Nicolis no-hair theorem was extended to slowly rotating BHs for which the scalar field is allowed to have a linear time dependence. Moreover, all the spherically symmetric solutions obtained for the John class can be naturally extended to the shift- and reflection-symmetric subclass of Horndeski’s theory, namely theories with $G_2 = G_2(X)$, $G_4 = G_4(X)$, and $G_3 = G_5 = 0$ [252].

In summary, nontrivial BH solutions in Fab Four gravity were found for the Ringo and John subclasses. In particular, the Schwarzschild-dS solution found in the case of nonminimal coupling with the Einstein tensor (John) can be seen as a self-tuned BH solution. On the other hand, to our knowledge, no analytic or numerical BH solutions have been reported for the Paul subclass. Because of the similarity between John and Paul, one may naively expect that Paul should also allow for self-tuned, inhomogeneous vacuum solutions. This question was partially addressed by Appleby [20], who claimed that self-tuned BH solutions would not exist in the Paul case. This is because in a Schwarzschild-dS spacetime the Weyl components of $P^{\mu\nu}{}_{\alpha\beta}$ and R_{GB} terms in the scalar field equation of motion contain an explicit dependence on the radial coordinate, and leave no redundancy in the scalar field equation of motion. This is in contrast to the case of “John,” where the scalar field equation of motion contains no Weyl component that could make it redundant for a Schwarzschild-dS metric. This also hints at the absence of similar BH solutions in the non-reflection-symmetric subclass of the shift-symmetric Horndeski theory with nonzero $G_3(X)$ and $G_5(X)$, although there are no detailed studies of this issue.

10.1.4 Plan of the chapter

The next natural step to test whether the Fab Four model is compatible with local inhomogeneities is to consider self-gravitating matter configurations, and in particular static or rotating NSs (NSs). The main goal of this chapter is precisely to investigate the existence and properties of slowly rotating NS solutions in Fab Four gravity.

The structure and stability of rotating NSs in GR (George) is, of course, textbook material [412, 171, 457]. In the past few years there has been significant progress in our understanding of slowly [355] and rapidly rotating [247, 248] NSs in Einstein-dilaton-Gauss-Bonnet gravity (Ringo), and there are also studies of stellar stability under odd-parity (axial) perturbations in this theory [61]. Recent investigations turned to theories with nonminimal coupling to the Einstein tensor (John) [104, 418, 105]. Here we complete and extend the analysis of NSs in the John subclass, and we look for solutions in theories containing the Paul term. We were unable to obtain NS solutions in theories involving the Paul term. Apparently, Paul does not want to be a star.

This chapter is organized as follows. In Sec. 10.2 we derive the stellar structure equations at first order in a slow-rotation expansion in generic shift-symmetric Horndeski theories. In Sec. 10.3 we specialize our analysis to each of the Fab Four subcases. In Sec. 10.5 we summarize our findings and point out possible directions for future research. We close with Section 10.4 discussing the relation between the moment of inertia and the stellar compactness in theories of the Ringo and John subclasses. Throughout the chapter, unless specified otherwise, we will use geometrical units ($G = c = 1$).

10.2 Slowly rotating stars in Fab Four theory

In this section we will consider the shift-symmetric subclass of Horndeski's theory that is invariant under the transformation

$$\phi \rightarrow \phi + c, \tag{10.10}$$

where c is a constant. From Eqs. (10.9), this assumption implies that V_{john} , V_{paul} , and V_{george} must be constant, while the Ringo (EdGB) term V_{ringo} can be a linear function of ϕ . For EdGB, a constant shift in ϕ only adds a trivial topological invariant to the action, and therefore it does not affect the field equations. Equations (10.4) and (10.5) represent the

basic building blocks of our theory, which will be described by the general action

$$S = S_G + S_M, \quad (10.11)$$

where S_M is the ordinary action for fluid matter and S_G is a combination of the Lagrangians (10.5c)-(10.5b).

To investigate slowly rotating solutions we follow the approach described by Hartle and Thorne [203, 204], in which spin corrections are considered as small perturbations on an otherwise static, spherically symmetric background. In particular, at first order in the star's angular velocity Ω the metric can be written as

$$ds^2 = -A(r)dt^2 + \frac{dr^2}{B(r)} + r^2 d\theta^2 + r^2 \sin^2 \theta d\varphi^2 - 2[\Omega - \tilde{\omega}(r)] \sin^2 \theta dt d\varphi, \quad (10.12)$$

where $\tilde{\omega}(r)$ is the angular velocity of the fluid as measured by a freely falling observer.

Varying the action (10.11) with respect to the metric and the scalar field we obtain the equations of motion for $g_{\alpha\beta}$ and ϕ , respectively:

$$\mathcal{E}_{\alpha\beta} = T_{\alpha\beta}, \quad \mathcal{E}_\phi = 0, \quad (10.13)$$

where

$$T_{\alpha\beta} = (\epsilon + p)u_\alpha u_\beta + pg_{\alpha\beta} \quad (10.14)$$

is the energy-momentum tensor of a perfect fluid. Here ϵ and p are the energy density and pressure of a fluid element with four-velocity $u^\mu = u^0(1, 0, 0, \Omega)$. The time component u^0 follows directly from the normalization condition $u^\mu u_\mu = -1$, which leads for the metric (10.12) to $u^0 = 1/\sqrt{A}$. The explicit form of $\mathcal{E}_{\alpha\beta}$ and \mathcal{E}_ϕ can be found in the Appendix of [306] (see [103] for a particular study in the case of John).

Moreover, in the Jordan frame, the energy-momentum tensor is conserved:

$$\nabla_{\mu} T^{\mu\nu} = 0. \quad (10.15)$$

To close the system of equations we need to specify the equation of state (EOS) for the NS, i.e., a relation between the pressure and energy density:

$$p = p(\epsilon). \quad (10.16)$$

Taken together, Eqs. (10.13), (10.15), and (10.16) provide the full description of a slowly rotating star.

In this chapter we will consider three realistic EOSs, namely, APR [10], SLy4 [155] and GNH3 [186] in decreasing order of stiffness. To facilitate comparisons with [104, 105] we will also consider a polytropic EOS of the form $p = K\rho^{\Gamma}$, with $K = 123M_{\odot}^2$ and $\Gamma = 2$. Here ρ is the mass density, related to the energy density by

$$\epsilon = \left(\frac{p}{K}\right)^{1/\Gamma} + \frac{p}{\Gamma - 1}. \quad (10.17)$$

In Table 10.1 we show the radius R and compactness $\mathcal{C} \equiv M/R$ of nonrotating models, as well as the moment of inertia I , for NSs with the “canonical” mass $M = 1.4 M_{\odot}$ constructed using different EOS models in GR. At fixed mass, the realistic EOSs APR, SLy4, and GNH3 (in this order) yield configurations with decreasing compactness, and therefore larger moment of inertia.

10.3 Fab Four neutron stars

In this section we discuss NSs in the four subclasses of Fab Four gravity, starting from the simplest Lagrangians.

EOS	R (km)	\mathcal{C}	I (10^{45} g cm ²)
APR	11.33	0.182	1.31
SLy4	11.72	0.176	1.37
GNH3	14.18	0.146	1.81
Polytrope	16.48	0.125	2.28

Table 10.1: The radius R , compactness \mathcal{C} , and moment of inertia I for a canonical NS with mass $M = 1.4 M_{\odot}$, in GR, using three different nuclear-physics based EOS models and a $\Gamma = 2$ polytrope.

10.3.1 George (General relativity)

The George Lagrangian for shift-symmetric theories corresponds to GR, so we refer the reader to standard treatments of rotating stars [412, 171, 457].

10.3.2 Ringo (Einstein-dilaton-Gauss-Bonnet gravity)

Nonrotating hairy BH solutions in EdGB gravity with a dilatonic coupling of the schematic form $V_{\text{ringo}} \sim \zeta e^{\gamma\phi}$ were found by Kanti et al. [243]. These solutions were then extended to slowly and rapidly rotating BHs [355, 249]. As stated in the introduction, Sotiriou and Zhou [446, 447] pointed out that hairy BH solutions exist in shift-symmetric EdGB theories, in violation of the Hui-Nicolis no-hair theorem (see [306] for an extension of these results to linear order in a slow-rotation approximation). Shift-symmetric EdGB theories can be seen as a small-field Taylor series expansion of the dilatonic coupling

$$V_{\text{ringo}} \simeq \zeta + \zeta\gamma\phi, \quad (10.18)$$

where the constant term ζ can be neglected since it gives rise to a topological invariant at the level of the action.

NSs in EdGB gravity with a dilatonic coupling were studied in [355, 247, 248] (see also [61] for axial perturbations). As it turns out, the bulk properties of NSs depend only on the combination $\zeta\gamma$; cf. the discussion around Eq. (29) of [355]. This is because the value of the scalar field is typically very small within the star, and therefore the Taylor

expansion (10.18) is an excellent approximation. For this reason, the analysis of NSs in Ref. [355] applies also to the shift-symmetric case of interest here, and we refer the reader to the treatment in that paper for calculations of stellar structure and observational bounds on the product $\zeta\gamma$.

10.3.3 John (Nonminimal coupling with the Einstein tensor)

A more interesting case is slowly rotating compact stars in theories with a nonminimal derivative coupling with the Einstein tensor, corresponding to the John Lagrangian (10.5c) [104, 418, 105]. These theories are described by the action

$$\begin{aligned} S_G &= \int d^4x \sqrt{-g} (\mathcal{L}_{\text{george}} + \mathcal{L}_{\text{john}} + \mathcal{L}_K) \\ &= \int d^4x \sqrt{-g} \left[\kappa R - \frac{1}{2} (\beta g^{\mu\nu} - \eta G^{\mu\nu}) \partial_\mu \phi \partial_\nu \phi \right], \end{aligned} \quad (10.19)$$

where $\mathcal{L}_K = \beta X = -(\beta \partial_\mu \phi \partial^\mu \phi)/2$ is a kinetic term for the scalar field, β and η are constants, and $\kappa = (16\pi)^{-1}$. Equation (10.19) can be obtained from the Horndeski Lagrangian by choosing

$$G_2 = \beta X, \quad G_4 = \kappa + \frac{\eta}{2} X, \quad G_3 = G_5 = 0. \quad (10.20)$$

We also consider a real scalar field of the form [29]

$$\phi(r, t) = qt + \psi(r), \quad (10.21)$$

where q is a constant scalar charge. With this choice, the field's kinetic energy is a function of r only:

$$X = \frac{1}{2} \left[\frac{q^2}{A(r)} - B(r) \psi'(r)^2 \right]. \quad (10.22)$$

In vacuum, the theory described by the action (10.19) leads to asymptotically AdS black hole solutions with a nontrivial scalar field configuration [389, 321, 15, 252, 29]. However, it has recently been shown that it is possible to construct “stealth” NS models for

which the exterior solution is given by the Schwarzschild spacetime [104].

For $\beta = 0$, the scalar field outside the star (where $T_{\mu\nu} = 0$) does not backreact on the metric, leading to “stealth solutions”. However inside the star (where $T_{\mu\nu} \neq 0$) the scalar field has a nontrivial effect, and the stellar structure is different from GR.

Hereafter we will focus on these stealth solutions, fixing $\beta = 0$. We recall that the action (10.19) is invariant under shift symmetry ($\phi \rightarrow \phi + c$). This allows us to write the equation of motion for the scalar field in terms of a conserved current J^μ :

$$\nabla_\mu J^\mu = 0, \quad (10.23)$$

with nonzero components given by

$$J^t = -\frac{q\eta}{r^2\kappa A}(rB' + B - 1), \quad (10.24)$$

$$J^r = \frac{\eta B}{r^2\kappa A}[A(B - 1) + rBA']\phi'. \quad (10.25)$$

We also remark that Eq. (10.23), using the line element (10.12), admits the solution

$$J^r = \sqrt{\frac{B}{A}} \frac{C_1}{r^2}, \quad (10.26)$$

with C_1 constant. In the following we will set $C_1 = 0$, as it has been shown that this choice is consistent with a vanishing radial energy flux, i.e., $\mathcal{E}_{tr} = 0$ [30].

Combining Eqs. (10.15), (10.25), and the (tt) and (rr) components of Eqs. (10.13), we obtain a set of differential equations for the spherically symmetric background. Moreover, at linear order in the angular velocity, the $(t\varphi)$ equation $\mathcal{E}_{t\varphi} - T_{t\varphi} = 0$ yields a differential equation for $\tilde{\omega}$. In summary, a slowly rotating NS at first order in the slow-rotation

approximation is described by the following set of equations:

$$A' = \frac{A}{r} \frac{1 - B}{B}, \quad (10.27)$$

$$B' = \frac{3q^2\eta B(B-1) - A[r^2\epsilon - 4\kappa + B(4\kappa + r^2(\epsilon + 6p))]}{r[A(4\kappa + r^2p) - 3q^2\eta B]}, \quad (10.28)$$

$$p' = -\frac{\epsilon + p}{2} \frac{A'}{A}, \quad (10.29)$$

$$\tilde{\omega}'' = \frac{4q^2\eta B^2 - A[4B(4\kappa + r^2p) - r^2(\epsilon + p)]}{rB[A(4\kappa + r^2p) - q^2\eta B]} \tilde{\omega}' - \frac{4A(\epsilon + p)}{B[q^2\eta B - A(4\kappa + r^2p)]} \tilde{\omega}, \quad (10.30)$$

$$(\phi')^2 = \frac{r^2 Ap - q^2\eta(B-1)}{\eta AB}. \quad (10.31)$$

Note that q and η always appear combined in the factor $q^2\eta$.

Expanding all variables in a power series around $r = 0$, we obtain the initial values for $(A, B, \tilde{\omega}, p, \phi)$ as

$$A = A_c - \frac{r^2 A_c^2 (3p_c + \epsilon_c)}{3(3q^2\eta - 4\kappa A_c)} + \mathcal{O}(r^3), \quad (10.32a)$$

$$B = 1 + \frac{2r^2 A_c (3p_c + \epsilon_c)}{3(3q^2\eta - 4\kappa A_c)} + \mathcal{O}(r^3), \quad (10.32b)$$

$$p = p_c + \frac{r^2 A_c (p_c + \epsilon_c)(3p_c + \epsilon_c)}{6(3q^2\eta - 4\kappa A_c)} + \mathcal{O}(r^3), \quad (10.32c)$$

$$\tilde{\omega} = \tilde{\omega}_c - \frac{2}{5} \frac{A_c(\epsilon_c + p_c)r^2}{q^2\eta - 4\kappa A_c} \tilde{\omega}_c + \mathcal{O}(r^3), \quad (10.32d)$$

$$(\phi')^2 = \frac{p_c}{\eta} r^2 - \frac{2q^2(3p_c + \epsilon_c)}{3(3q^2\eta - 4\kappa A_c)} r^2 + \mathcal{O}(r^3). \quad (10.32e)$$

where the subscript “ c ” means that the various variables are evaluated at the center of the star. Following [104] we set $A_c = 1$ and chose $\tilde{\omega}_c = 1$. Given a choice of EOS, the central pressure p_c uniquely determines a NS model.

From these expansions we can obtain constraints that must be satisfied by $q^2\eta$ to obtain physically acceptable solutions. If we demand that $p''(r) < 0$ [136], we obtain

$$q^2\eta < \frac{4\kappa}{3}, \quad (10.33)$$

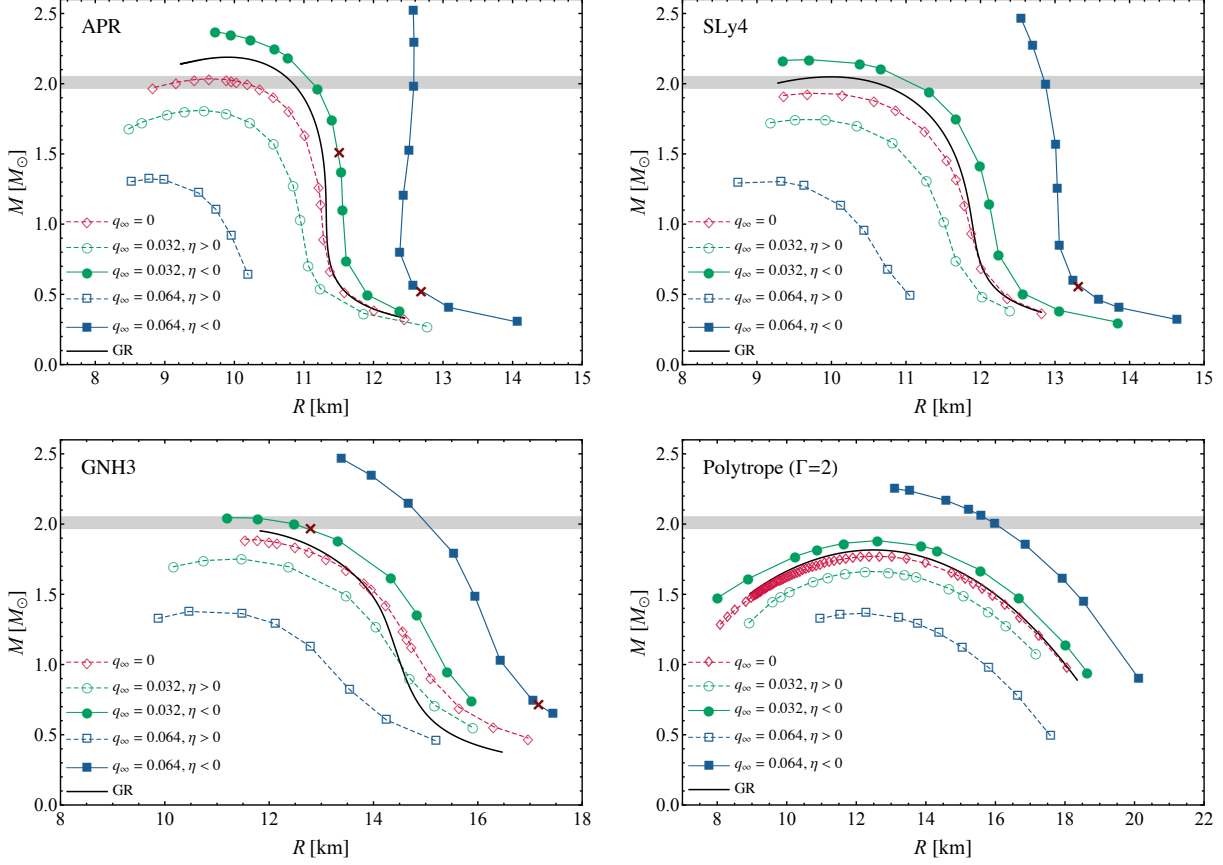


Figure 10.1: Mass-radius curves for different EOS models, selected values of q_∞ , and $\eta = \pm 1$. The various panels correspond to EOS APR (top left), SLy4 (top right), GNH3 (bottom left) and a polytropic (bottom right). Configurations with radii smaller than that identified by the orange cross do not satisfy the condition (10.34). The horizontal colored band corresponds to $M = 2.01 \pm 0.04 M_\odot$, the most massive NS mass known to date [138]. Note that the various panels have different x -axis ranges.

which is automatically satisfied when $\eta < 0$, but sets an upper bound on $q^2\eta$ when $\eta > 0$.

On the other hand, the requirement that the derivative of the scalar field should be real, i.e.,

$(\phi')^2 > 0$, implies

$$\frac{p_c}{\eta} - \frac{2q^2(3p_c + \epsilon_c)}{3(3q^2\eta - 4\kappa)} > 0. \quad (10.34)$$

For $\eta > 0$ this condition is always satisfied by virtue of Eq. (10.33). However, when $\eta < 0$ we obtain a lower bound on $q^2|\eta|$, namely,

$$q^2|\eta| > \frac{3}{4\pi} \frac{p_c}{2\epsilon_c - 3p_c}. \quad (10.35)$$

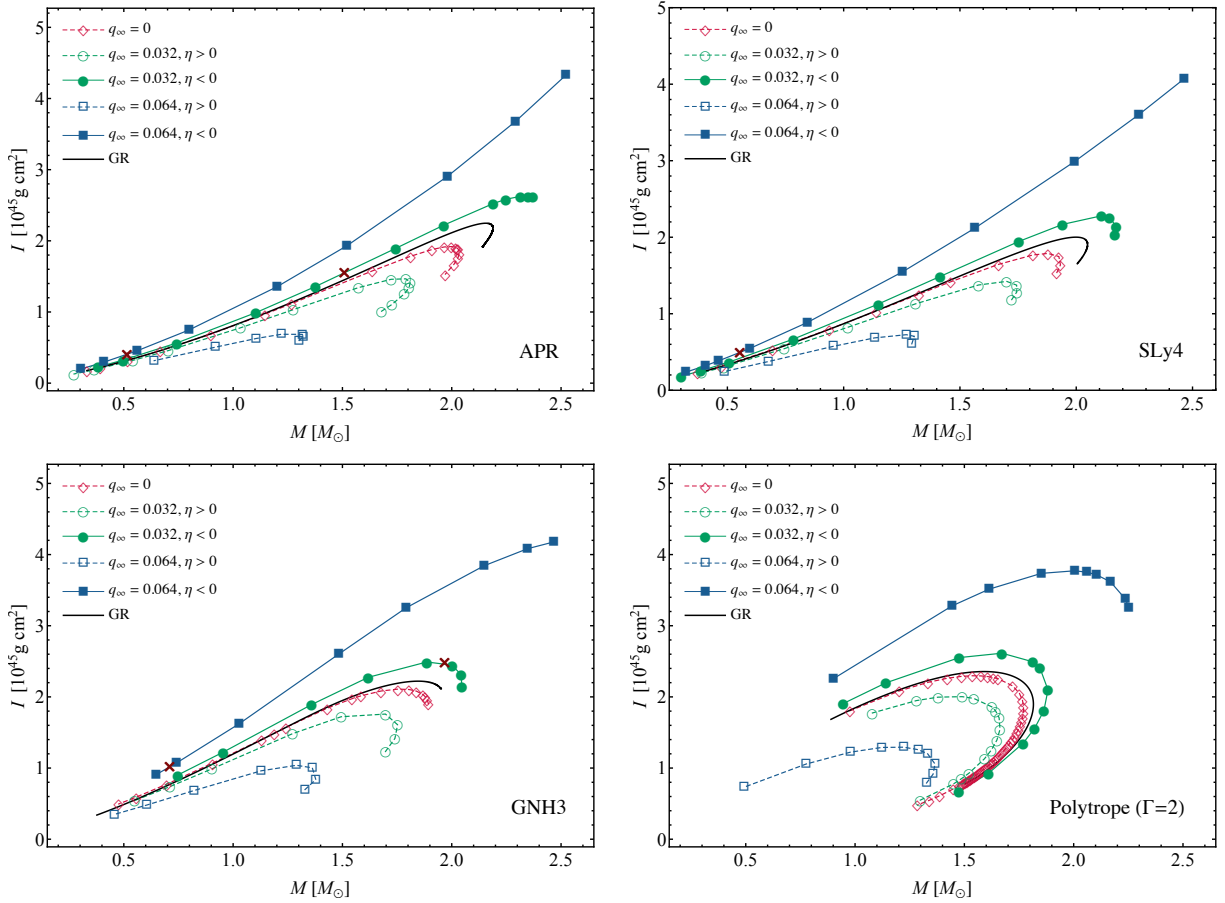


Figure 10.2: *Moment of inertia I as a function of the mass M .* The various panels correspond to EOS APR (top-left), SLy4 (top-right), GNH3 (bottom left) and a polytropic (bottom right). Configurations with masses larger than that identified by the orange cross do not satisfy the condition (10.34).

To construct NS models we integrate the system of equations (10.27)-(10.29), supplemented by the boundary conditions (10.32a)-(10.32c), from $r = 0$ up to the star's radius $r = R$, which corresponds to the point where the pressure vanishes, i.e., $p(R) = 0$. Then we match the interior solution to the exterior Schwarzschild metric. The NS mass is obtained by solving the system

$$A(R) = A_\infty \left(1 - \frac{2M}{R}\right), \quad A'(R) = A_\infty \frac{2M}{R^2}, \quad (10.36)$$

where A_∞ is an integration constant. Then we rescale the time variable ($t \rightarrow t\sqrt{A_\infty}$) so that

it represents the coordinate time measured by an observer at infinity. Because of the linear dependence of the scalar field on t , we correspondingly rescale q as

$$q_\infty = \frac{q}{\sqrt{A_\infty}}. \quad (10.37)$$

The stellar structure equations depend only on the combination $q^2\eta$, so we can set $\eta = \pm 1$ without loss of generality. The scalar field is computed from Eq. (10.31) for families of solutions with fixed values of q_∞ . To facilitate comparisons with [104], here we choose these values to be 0, 0.032, and 0.064. To obtain the solutions we apply a shooting method, adjusting the value q in each integration until we obtain the desired value of q_∞ .

We also integrate Eq. (10.30) for a given $\tilde{\omega}_c$ and we compute the star's angular velocity Ω and its angular momentum J , requiring that at the surface

$$\tilde{\omega}(R) = \Omega - \frac{2J}{R^3}, \quad \tilde{\omega}'(R) = \frac{6J}{R^4}. \quad (10.38)$$

The moment of inertia is computed through $I = J/\Omega$. We note that rescaling $\tilde{\omega}(r)$ by a constant factor does not affect Eq. (10.30). Therefore, once the solution $\tilde{\omega}_{\text{old}}$ has been found for given initial conditions, yielding a value Ω_{old} , a new solution $\tilde{\omega}_{\text{new}}$ can immediately be found via $\tilde{\omega}_{\text{new}} = \tilde{\omega}_{\text{old}}\Omega_{\text{new}}/\Omega_{\text{old}}$. The moment of inertia I is independent of the star's angular velocity.

In Fig. 10.1 we show the mass-radius diagram for all the EOS models used in this chapter. The polytropic case (bottom-right panel) matches the results in [104], except for what we believe to be a mislabeling of some curves in their Fig. 2.

As pointed out in [104], the limit $q_\infty \rightarrow 0$ does not correspond to GR, and indeed the corresponding mass-radius curves are different from those of GR (solid black lines). For any EOS and fixed q_∞ , positive (negative) values of η correspond to more (less) compact configurations. At fixed η , larger values of the scalar charge q_∞ corresponds to stellar models with larger radii. As a reference, the horizontal colored band correspond to the most massive

η	q_∞	I_{APR} (10^{45}g cm^2)	I_{GNH3} (10^{45}g cm^2)	I_{SLy4} (10^{45}g cm^2)
-	GR	1.31	1.81	1.37
-	0	1.28	1.80	1.35
-1	0.032	1.39	1.96	1.47
-1	0.064	1.70	2.42	1.81
1	0.032	1.17	1.64	1.22
1	0.064	-	-	-

Table 10.2: Moment of inertia for a NS with $M = 1.4M_\odot$ for selected values of q_∞ and for nuclear-physics-motivated EOS models. For $q_\infty = 0.064$ and $\eta = 1$, none of the EOS models considered here supports NSs with $M = 1.4 M_\odot$.

known NS, PSR J0348+0432, with $M = 2.01 \pm 0.04 M_\odot$ [138]. When $\eta > 0$, for all values of q_∞ and EOS models considered in this chapter such massive NSs are not supported.

In Fig. 10.2 we show the moment of inertia as a function of mass for the same stellar models and theory parameters as in Fig. 10.1. In addition, in Table 10.2 we list the values of I for a canonical NS with mass $M = 1.4M_\odot$. It is interesting that some theories with $\eta > 0$ cannot support stars with this value of the mass. As expected, deviations with respect to GR grow as the scalar charge increases, yielding larger (smaller) moments of inertia for $\eta < 0$ ($\eta > 0$). The relative deviation from GR can be of order 30% for $q_\infty = 0.064$ and $\eta = -1$.

In GR, the dimensionless moment of inertia $\bar{I} \equiv I/M^3$ was recently shown to be related to the NS compactness \mathcal{C} by a universal relation which is almost insensitive to the adopted EOS [71] (see [385, 272, 36, 276] for earlier studies):

$$\bar{I}_{\text{fit}} = a_1 \mathcal{C}^{-1} + a_2 \mathcal{C}^{-2} + a_3 \mathcal{C}^{-3} + a_4 \mathcal{C}^{-4}, \quad (10.39)$$

where the fitting coefficients a_i , $i = (1, \dots, 4)$, are listed in Table II of [71]. This I - \mathcal{C} relation reproduces numerical results with an accuracy better than 3%. The observed universality is reminiscent of the I -Love- Q relations between the moment of inertia, tidal deformability (as encoded in the so-called Love number) and rotational quadrupole moment Q [514, 520]. The

extension of these near-universal relations $I\text{-}\mathcal{C}$ relations to theories of the Ringo and John subclasses is discussed in the Appendix.

It is natural to ask whether these stealth NS models are stable. Vacuum, static, spherically symmetric solutions where the scalar field has a linear time dependence were shown to be free from ghost and gradient instabilities under odd-parity gravitational perturbations as long as the following conditions are met [341]:

$$\mathcal{F} > 0, \quad \mathcal{G} > 0, \quad \mathcal{H} > 0, \quad (10.40)$$

where

$$\mathcal{F} = 2 \left(G_4 - \frac{q^2}{A} G_{4X} \right) = 2 \left(\kappa + \frac{q_\infty^2 \eta}{4} - \frac{q_\infty^2 \eta A_\infty}{2A} \right), \quad (10.41)$$

$$\mathcal{G} = 2 \left(G_4 - 2XG_{4X} + \frac{q^2}{A} G_{4X} \right) = 2 \left(\kappa - \frac{q_\infty^2 \eta}{4} + \frac{q_\infty^2 \eta A_\infty}{2A} \right), \quad (10.42)$$

$$\mathcal{H} = 2 (G_4 - 2XG_{4X}) = 2 \left(\kappa - \frac{q_\infty^2 \eta}{4} \right). \quad (10.43)$$

Here we have used $X = q^2/(2A_\infty)$ as well as Eq. (10.37), which applies to the stealth BH solutions of [29]. For stealth BH solutions, $A \rightarrow 0$ in the vicinity of the event horizon; therefore the third term on the right-hand side of Eqs. (10.41) and (10.42) is the dominant one. As a consequence $\mathcal{F}\mathcal{G} < 0$, suggesting that these solutions are generically unstable [341].

A similar argument can be applied to our stealth NS solutions. In the exterior vacuum spacetime of the star, the metric function A , which satisfies $A < A_\infty$, remains positive and finite. When η is *positive*, \mathcal{G} is always positive as well, and the conditions $\mathcal{F} > 0$ and $\mathcal{H} > 0$ everywhere outside the star translate into

$$q_\infty^2 \eta < 4\kappa \frac{A(R)}{2A_\infty - A(R)} = 4\kappa \left(\frac{1 - 2\mathcal{C}}{1 + 2\mathcal{C}} \right), \quad (10.44)$$

$$q_\infty^2 \eta < 4\kappa, \quad (10.45)$$

respectively, where we have used Eq. (10.36).

We have numerically confirmed that all NS models presented in Fig. 10.1 satisfy the conditions (10.44) and (10.45) for the largest value of $q_\infty = 0.064$ considered in this chapter. For a typical NS the compactness is $\mathcal{C} \approx 0.2$, and the right-hand side of Eq. (10.44) is approximately 0.035, which is much larger than our choice $q_0^2 \eta = 0.064^2 \approx 0.004$. The condition (10.44) will be violated only for an unrealistically compact NS with $\mathcal{C} \approx 0.45$. This suggests that hypothetical ultracompact objects – such as Lemaitre stars [63, 183, 520] and gravastars [354, 81, 352] – may be unstable in the presence of a stealth scalar field.

Similarly, for *negative* values of η , \mathcal{F} and \mathcal{H} are always positive, and the condition $\mathcal{G} > 0$ is satisfied everywhere outside the star if

$$q_\infty^2 |\eta| < 4\kappa \frac{A(R)}{2A_\infty - A(R)} = 4\kappa \left(\frac{1 - 2\mathcal{C}}{1 + 2\mathcal{C}} \right). \quad (10.46)$$

We have also checked that for $q_\infty = 0.064$ and $\eta = -1$, all NS models presented in Fig. 10.1 satisfy (10.46). In the Newtonian limit $\mathcal{C} \ll 1$, the stealth NS spacetime is stable for $q_\infty^2 \eta < 4\kappa$ when $\eta > 0$, and for $q_\infty^2 |\eta| < 4\kappa$ when $\eta < 0$. For NSs with larger values of $q_\infty^2 |\eta|$ the exterior spacetime becomes unstable everywhere, including the Newtonian regime.

It is interesting to consider the nonrelativistic limit of theories of the John class. Introducing the usual mass function $m(r)$ such that $B(r) = 1 - 2m(r)/r$, we see that the pressure equation retains its standard form

$$\frac{dp}{dr} = -\frac{m\rho}{r^2}, \quad (10.47)$$

where ρ is the mass density. However the mass equation is reduced to

$$\frac{dm}{dr} = \frac{4\pi r^2 \rho}{1 - 12\pi q^2 \eta}. \quad (10.48)$$

This behavior looks reminiscent of “beyond Horndeski” theories [188, 187], where a partial

breakdown of the Vainshtein mechanism occurs, modifying the Newtonian limit [253]. In fact, several authors have advocated the use of this “feature” to constrain beyond Horndeski theories using Newtonian stars or white dwarfs [395, 394, 262, 235, 392]. While those theories modify the pressure equation (10.47), leaving the mass equation unaltered, theories of the John subclass seem to alter the Newtonian limit in the opposite way.

However, combining Eqs. (10.47)-(10.48) and restoring the gravitational constant G we obtain

$$\frac{1}{r^2} \frac{d}{dr} \left(\frac{r^2}{\rho} \frac{dp}{dr} \right) = -4\pi G_{\text{eff}} \rho, \quad (10.49)$$

which is equivalent to the ordinary hydrostatic equilibrium equation in Newtonian gravity with an *effective* gravitational constant

$$G_{\text{eff}} \equiv \frac{G}{1 - 12\pi q^2 \eta}. \quad (10.50)$$

Therefore the nonrelativistic limit of the “John” theories considered in this section is equivalent to Newtonian gravity with an effective gravitational constant G_{eff} . Incidentally, a similar result was found by Cisterna et al. [105] in the context of cosmology [cf. their Eq. (38)].

10.3.4 Paul (Double-dual of the Riemann tensor)

Let us now turn to NS solutions in theories containing the Paul Lagrangian (10.5d).

We start with the simplest model, given by the combination

$$\begin{aligned} \mathcal{L} &= \mathcal{L}_{\text{george}} + \mathcal{L}_{\text{paul}} \\ &= R - \frac{1}{3} \alpha P^{\mu\nu\alpha\beta} \nabla_\mu \phi \nabla_\alpha \phi \nabla_\nu \nabla_\beta \phi, \end{aligned} \quad (10.51)$$

which from Eqs. (10.9) corresponds to the following choice of the functions G_i :

$$G_2 = G_3 = 0, \quad G_4 = 1, \quad G_5 = \alpha X, \quad (10.52)$$

where α is a coupling parameter. As in Sec. 10.3.3, we consider a scalar field with linear time dependence of the form (10.21). This choice is crucial for $\phi(r)$ to have a nontrivial profile. Indeed, the nonvanishing components of the scalar current for the action (10.51) are

$$J^r = \frac{\alpha}{2r^2} \frac{B}{A} [q^2(B-1) + A(1-3B)B\phi'^2] \frac{A'}{A}, \quad (10.53)$$

$$J^t = \frac{q\alpha}{2r^2} \frac{B}{A} \left\{ \phi' \left[\frac{A'}{A}(B-1) + \frac{B'}{B}(3B-1) \right] + 2(B-1)\phi'' \right\}. \quad (10.54)$$

From the first equation we conclude that in the limit $q \rightarrow 0$ the condition $J^r = 0$ implies $\phi' = 0$; i.e., the scalar field must be constant. However for $q \neq 0$ we obtain

$$(\phi')^2 = q^2 \frac{1-B}{A(1-3B)B}. \quad (10.55)$$

Replacing this relation into the (tt) and (rr) components of Eqs. (10.13), we derive two first-order equations for the metric variables A and B :

$$B' = \frac{1-B-8\pi r^2 \epsilon}{r - \frac{q^3 \alpha \sqrt{1-B} [AB(1-3B)]^{3/2}}{A^3(1-3B)^3}}, \quad (10.56)$$

$$A' = \frac{A^3}{B} \frac{1-B+8\pi r^2 p}{A^2 r - \frac{q^3 \alpha B \sqrt{1-B} \sqrt{AB(1-3B)}}{(1-3B)^2}}. \quad (10.57)$$

Equations (10.55)-(10.57), together with a choice of EOS and the energy-momentum conservation equation (10.15), which gives

$$p' = -\frac{\epsilon + p}{2} \frac{A'}{A}, \quad (10.58)$$

form a closed system of differential equations, which can be integrated by imposing suitable initial conditions at the center of the star. These conditions can be found through a Taylor

expansion in r ,

$$A(r) = A_c + \frac{r^2}{q^6 \alpha^2} A_2(p_c, A_c) + \mathcal{O}(r^3), \quad (10.59a)$$

$$B(r) = 1 + \frac{r^2}{q^6 \alpha^2} B_2(p_c, A_c) + \mathcal{O}(r^3), \quad (10.59b)$$

$$p(r) = p_c + \frac{r^2}{q^6 \alpha^2} p_2(p_c, A_c) + \mathcal{O}(r^3), \quad (10.59c)$$

$$\phi'(r) = \pm \sqrt{\frac{B_2(p_c, A_c)}{2A_c}} \frac{r}{q^2 \alpha} + \mathcal{O}(r^3), \quad (10.59d)$$

where A_2 , B_2 , and p_2 are functions of the constant parameters A_c and p_c . Unlike Eqs. (10.56) and (10.57), which reduce to GR for $\alpha \rightarrow 0$ (or $q \rightarrow 0$), the initial conditions for the metric functions, $(\phi')^2$, and the pressure are ill defined.

Note that such a pathological behavior is not expected in the naive $\alpha \rightarrow 0$ limit of (10.56) and (10.57), because this is a “nonperturbative” effect such that the leading behavior $\sqrt{1 - B} \propto 1/\alpha$ obtained from (10.59b) cancels the α terms in (10.56) and (10.57), making the deviation from GR evident.

To better understand this issue, let us reconsider the $\eta \rightarrow 0$ limit of the John action. In that case, as we see from Eqs. (10.32a)-(10.32e), the only divergent quantity as $\eta \rightarrow 0$ is the derivative of the scalar field ϕ' , while all other metric and matter quantities have a finite limit. Since we work in the Jordan frame there is no direct coupling between the scalar field and matter. Furthermore the scalar field does not backreact on the spacetime in the stealth exterior, and therefore a singular behavior of the scalar field does not affect the geodesics of particles outside the star. In contrast, for the Paul case all physical quantities diverge in the limit $\alpha \rightarrow 0$, indicating a pathological behavior in the NS interior. Furthermore, at variance with the John case, we could not find a stealth exterior solution for Paul. Our results suggest that exterior stealth solutions for Paul do not exist under the ansatz (10.21) for the scalar field.

We observed a similar behavior for other Fab Four theories involving the Paul term.

We considered the following combinations:

$$\mathcal{L}_{\text{george}} + \mathcal{L}_{\text{paul}} + \mathcal{L}_{\text{K}} , \quad \phi(r) , \quad (10.60)$$

$$\mathcal{L}_{\text{george}} + \mathcal{L}_{\text{paul}} + \mathcal{L}_{\text{john}} + \mathcal{L}_{\text{K}} , \quad \phi(t, r) , \quad (10.61)$$

$$\mathcal{L}_{\text{george}} + \mathcal{L}_{\text{paul}} + \mathcal{L}_{\text{ringo}} + \mathcal{L}_{\text{K}} , \quad \phi(t, r) , \quad (10.62)$$

$$\mathcal{L}_{\text{george}} + \mathcal{L}_{\text{paul}} + \mathcal{L}_{\text{john}} + \mathcal{L}_{\text{ringo}} + \mathcal{L}_{\text{K}} , \quad \phi(t, r) . \quad (10.63)$$

In all of these cases the physical variables suffer from the same divergence when the coupling parameter α of the Paul term vanishes.

Appleby [20] found that the self-tuning mechanism is not applicable for spherically symmetric black hole spacetimes in theories of the Paul class. Our results strengthen his conclusions, suggesting that the Paul term does not allow for physically well-behaved compact object solutions.

10.4 An application: EOS-independent $I - \mathcal{C}$ relations in Horndeski gravity

As a short application of our results, let us discuss the existence EOS-independent relations connecting the moment of inertia and the compactness for NSs in theories of the John and Ringo subclasses. Our approach is very similar to what was done in Section 7.7 in the context of ST theories with disformal coupling. See also our discussion of EOS-independent relations in Chapter 2.

10.4.1 John (Nonminimal coupling with the Einstein tensor)

The behavior of I as function of q_∞ can be accurately described by a simple quadratic fit of the form

$$I = p_0 + p_1 q_\infty + p_2 q_\infty^2 , \quad (10.64)$$

where (p_0, p_1, p_2) are constants. In the top panel of Fig. 10.3 we compare this relation with numerical data for $\eta = -1$ (note that for this figure we have computed models with

additional values of q_∞ that were not displayed in Figs. 10.1 and 10.2 to avoid cluttering). The bottom panel of Fig. 10.3 shows that the relative errors between the numerical data and the fit are typically of order 0.1% or smaller.

To understand whether these relations hold also for theories of the John subclass, we have compared our numerical data against Eq. (10.39), computing the relative error $\Delta\bar{I}/\bar{I} = |1 - \bar{I}_{\text{fit}}/\bar{I}|$. The results are shown in the bottom panel of Fig. 10.4. Errors are always larger than in GR, and they can be as high as 40% for low-compactness configurations. A similar trend is observed for the I -Love- Q relations in GR in [419]. Deviations from the GR relation are due to the strong dependence of the star’s bulk properties on the scalar charge q_∞ , which spoils the (approximate) EOS universality of the relation proposed in [71]. Therefore we conclude that a theory-independent fit would perform poorly.

It is still possible to introduce approximately EOS-independent relations for I - \mathcal{C} at fixed values of the theory parameters q_∞ and η using the functional form given in Eq. (10.39). The relative errors between the numerical data and these fits are shown in Fig. 10.5, and the corresponding fitting coefficients are listed in Table 10.3. For almost all configurations the new relations perform better than Eq. (10.39), with relative errors that can be an order of magnitude smaller.

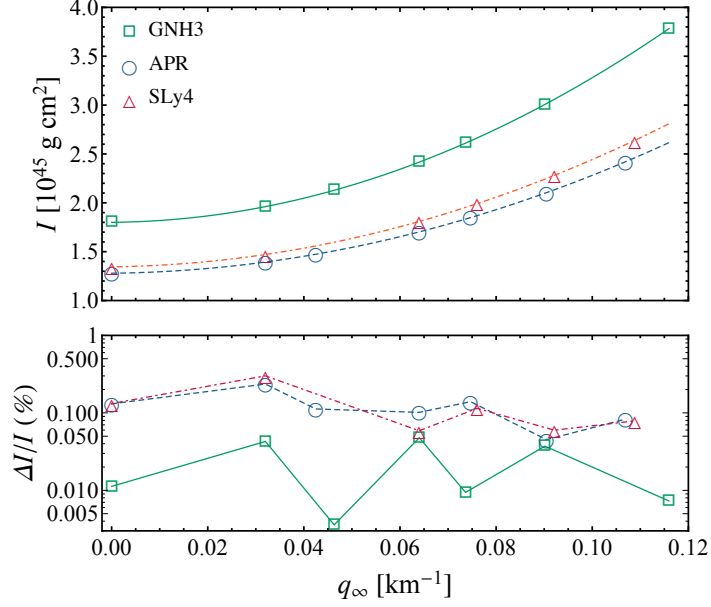


Figure 10.3: *The $I - q_\infty$ relations.* Top panel: The moment of inertia I versus charge q_∞ for a canonical NS with $M = 1.4 M_\odot$ and $\eta = -1$, and the realistic EOSs APR, GNH3, and SLy4. Bottom panel: Relative percentage errors between the numerical data and the relation (10.64).

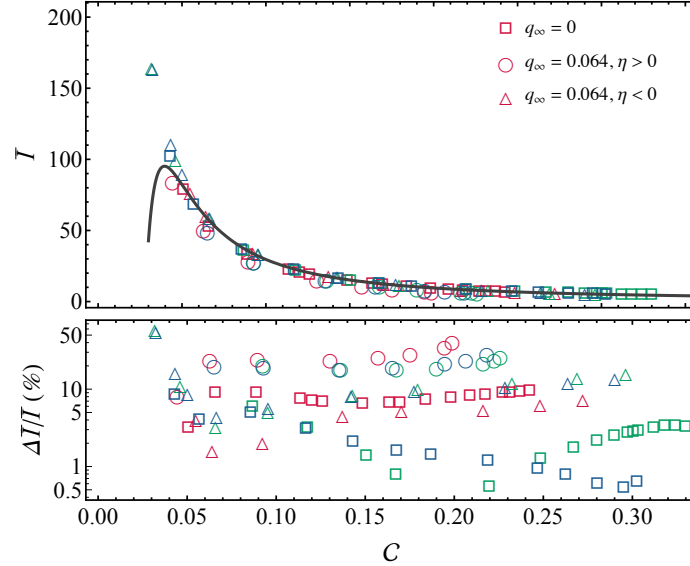


Figure 10.4: *The $\bar{I} - C$ relations.* Top panel: $\bar{I} - C$ relation for different values of the scalar charge q_∞ and the realistic EOS APR (blue), GNH3 (red), SLy4 (green). The solid curve represents the fit given by Eq. (10.39), obtained in [71]. Bottom panel: Relative errors between the numerical data and the analytic relation. For illustrative purposes, we show the cases $q_\infty = 0$ and $q_\infty = 0.064$. For the latter, deviations from GR are more dramatic.

q_∞	η	a_1	a_2	a_3	a_4
0	—	0.684	0.265	-0.0062	6.87×10^{-5}
0.032	1	0.666	0.240	-0.00364	-2.01×10^{-6}
0.032	-1	0.776	0.273	-0.00809	1.64×10^{-4}
0.064	1	0.0654	0.348	-0.0125	1.81×10^{-4}
0.064	-1	0.872	0.276	-0.00574	4.53×10^{-5}

Table 10.3: Numerical coefficients of the new universal I - \mathcal{C} relations, for fixed values of q_∞ and η .

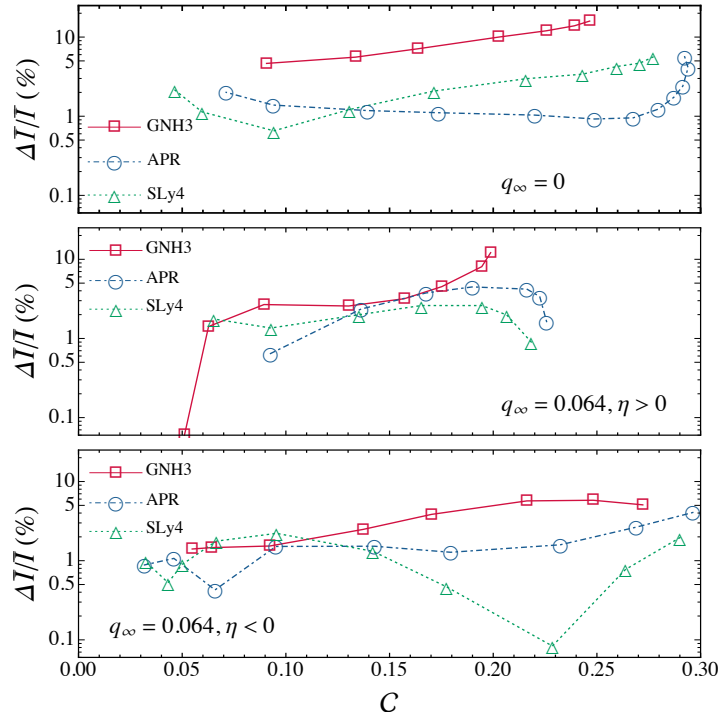


Figure 10.5: Relative errors between the improved fits and the numerical data. Top panel: $q_\infty = 0$. Middle panel: $q_\infty = 0.064$ and $\eta = 1$. Lower panel: $q_\infty = 0.064$ and $\eta = -1$.

10.4.2 Ringo (Einstein-dilaton-Gauss-Bonnet gravity)

We have also investigated the I - \mathcal{C} relations for theories of the Ringo subclass (EdGB gravity) using the numerical data from [355]. We found that the fit proposed in [71] works remarkably well for EdGB, with relative percentage errors $\lesssim 10\%$ for a wide range of compactness. This result is complementary to the I - Q relations in EdGB obtained in [247]. We recall, however, that our calculations are limited to slow rotation. The question of whether

or not rapidly rotating NSs in EdGB satisfy the same I - \mathcal{C} relations of [71] could be addressed following the analysis of [247, 248].

10.5 Conclusions

We have presented an exhaustive study of slowly rotating NS solutions in the shift-symmetric class of Fab Four gravity, namely, the subclass of Horndeski’s gravity that may allow for dynamical self-tuning of the quantum vacuum energy, and for this reason has been the subject of intense scrutiny in a cosmological context. Our main goal was to investigate whether Fab Four gravity is compatible with the existence of relativistic stars, such as NSs.

Among the nonminimal couplings in Fab Four gravity listed in Eqs. (10.5c)-(10.5b), we especially focused on the John (nonminimal derivative coupling to the Einstein tensor) and Paul (nonminimal derivative coupling to the double dual of the Riemann tensor) subclasses. This is both because George (GR) and Ringo (EdGB gravity) have been extensively studied in the past and because John and Paul are the crucial terms allowing for self-tuning of the quantum vacuum energy in cosmological scenarios.

In the case of John, if we make the assumption that the scalar field has a linear time dependence of the form (10.21), there is a stealth solution such that the scalar field does not backreact on the metric in the exterior, while it introduces nontrivial modifications of the interior stellar structure with respect to GR in the stellar interior. Our results on spherically symmetric NSs agree with previous work [104] and extend it to slowly rotating solutions. As pointed out in [104], in the limit of vanishing scalar charge ($q_\infty \rightarrow 0$) the mass-radius curves differ from GR. Irrespective of the chosen EOS, positive (negative) values of the coupling constant η in (10.19) yield more (less) compact stellar configurations. For positive values of η this fact can be used to put mild (EOS-dependent) constraints on the maximum value of q_∞ ; cf. Ref. [105].

We have also shown that the approximately EOS-independent relations between the moment of inertia I and compactness \mathcal{C} within GR break down in this theory. Therefore,

in principle, future measurements of I could potentially constrain the value of q_∞ [263]. We also obtained improved I - \mathcal{C} relations that depend of the value of q_∞ and are accurate within $\sim 5\%$.

Based on stability studies in the context of BH solutions [341], we have argued that the NS models studied here are generically stable under odd-parity gravitational perturbations. A systematic study of stellar perturbations within theories of the John subclass is desirable, and it could follow in the footsteps of similar studies for ST theory [438, 439, 420, 432] and EdGB gravity [61].

Surprisingly, we also found that in all subclasses of the Fab Four and its minimal extensions that involve Paul, not only the scalar field, but also all metric functions and the pressure diverge at the center of the star in the small-coupling limit. Therefore “healthy” BH and stellar solutions do not seem to exist in the shift-symmetric Paul subclass. It will be interesting to determine whether this conclusion still holds in the absence of shift symmetry.

As a straightforward generalization of the present study, one could search for NS solutions in Fab Four theories where the potentials (10.5c)-(10.5b) have nontrivial functional forms, as well as in more general (non-shift-symmetric) versions of Horndeski’s theory. The general formalism developed in [306] can be straightforwardly applied to these cases.

Barausse and Yagi [33] have recently shown that the so-called sensitivities of compact objects [158] vanish in shift-symmetric Horndeski gravity, which includes the Fab Four class. Consequently the dynamics of binaries involving NSs is, to leading post-Newtonian order, the same as in GR. It would be interesting to determine whether these conclusions hold at higher post-Newtonian orders, and whether gravitational waves can be used at all to constrain these theories.

BIBLIOGRAPHY

BIBLIOGRAPHY

- [1] LIGO SCIENTIFIC collaboration, AASI, J. ET AL., *Advanced LIGO*, *Class. Quant. Grav.* **32** (2015) 074001, [[1411.4547](#)].
- [2] VIRGO, LIGO SCIENTIFIC collaboration, ABBOTT, B. P. ET AL., *GW151226: Observation of Gravitational Waves from a 22-Solar-Mass Binary Black Hole Coalescence*, *Phys. Rev. Lett.* **116** (2016) 241103, [[1606.04855](#)].
- [3] VIRGO, LIGO SCIENTIFIC collaboration, ABBOTT, B. P. ET AL., *Observation of Gravitational Waves from a Binary Black Hole Merger*, *Phys. Rev. Lett.* **116** (2016) 061102, [[1602.03837](#)].
- [4] VIRGO, LIGO SCIENTIFIC collaboration, ABBOTT, B. P. ET AL., *Tests of general relativity with GW150914*, *Phys. Rev. Lett.* **116** (2016) 221101, [[1602.03841](#)].
- [5] ABRAMOWICZ, M. A. AND KLUZNIAK, W., *A Precise determination of angular momentum in the black hole candidate GRO J1655-40*, *Astron. Astrophys.* **374** (2001) L19, [[astro-ph/0105077](#)].
- [6] VIRGO collaboration, ACERNESE, F. ET AL., *Advanced Virgo: a second-generation interferometric gravitational wave detector*, *Class. Quant. Grav.* **32** (2015) 024001, [[1408.3978](#)].
- [7] ADAM, C., NAYA, C., SANCHEZ-GUILLEN, J., VAZQUEZ, R. AND WERESZCZYNSKI, A., *BPS Skyrmions as neutron stars*, *Phys. Lett.* **B742** (2015) 136, [[1407.3799](#)].
- [8] ADAM, C., NAYA, C., SANCHEZ-GUILLEN, J., VAZQUEZ, R. AND WERESZCZYNSKI, A., *Neutron stars in the Bogomol'nyi-Prasad-Sommerfield Skyrme model: Mean-field limit versus full field theory*, *Phys. Rev.* **C92** (2015) 025802, [[1503.03095](#)].
- [9] AGATHOS, M., MEIDAM, J., DEL POZZO, W., LI, T. G. F., TOMPITAK, M., VEITCH, J. ET AL., *Constraining the neutron star equation of state with gravitational wave signals from coalescing binary neutron stars*, *Phys. Rev.* **D92** (2015) 023012, [[1503.05405](#)].
- [10] AKMAL, A., PANDHARIPANDE, V. R. AND RAVENHALL, D. G., *The Equation of state of nucleon matter and neutron star structure*, *Phys. Rev.* **C58** (1998) 1804, [[nucl-th/9804027](#)].

- [11] ALBRECHT, A., BURGESS, C., RAVNDAL, F. AND SKORDIS, C., *Natural quintessence and large extra dimensions*, *Phys.Rev.* **D65** (2002) 123507, [[astro-ph/0107573](#)].
- [12] ALCUBIERRE, M., *Introduction to 3+1 Numerical Relativity*. Oxford University Press, 2008.
- [13] ALISHAHIHA, M., SILVERSTEIN, E. AND TONG, D., *DBI in the sky*, *Phys. Rev.* **D70** (2004) 123505, [[hep-th/0404084](#)].
- [14] ALSING, J., BERTI, E., WILL, C. M. AND ZAGLAUER, H., *Gravitational radiation from compact binary systems in the massive Brans-Dicke theory of gravity*, *Phys.Rev.* **D85** (2012) 064041, [[1112.4903](#)].
- [15] ANABALON, A., CISTERNA, A. AND OLIVA, J., *Asymptotically locally AdS and flat black holes in Horndeski theory*, *Phys. Rev.* **D89** (2014) 084050, [[1312.3597](#)].
- [16] ANDERSSON, N., FERRARI, V., JONES, D., KOKKOTAS, K., KRISHNAN, B. ET AL., *Gravitational waves from neutron stars: Promises and challenges*, *Gen.Rel.Grav.* **43** (2011) 409, [[0912.0384](#)].
- [17] ANDERSSON, N., BAKER, J., BELCZYNSKI, K., BERNUZZI, S., BERTI, E. ET AL., *The Transient Gravitational-Wave Sky*, *Class.Quant.Grav.* **30** (2013) 193002, [[1305.0816](#)].
- [18] ANTONIADIS, J., VAN KERKWIJK, M., KOESTER, D., FREIRE, P., WEX, N. ET AL., *The relativistic pulsar-white dwarf binary PSR J1738+0333 I. Mass determination and evolutionary history*, *Mon.Not.Roy.Astron.Soc.* **423** (2012) 3316, [[1204.3948](#)].
- [19] ANTONIADIS, J., FREIRE, P. C., WEX, N., TAURIS, T. M., LYNCH, R. S. ET AL., *A Massive Pulsar in a Compact Relativistic Binary*, *Science* **340** (2013) 6131, [[1304.6875](#)].
- [20] APPLEBY, S., *Self Tuning Scalar Fields in Spherically Symmetric Spacetimes*, *JCAP* **1505** (2015) 009, [[1503.06768](#)].
- [21] APPLEBY, S. A., DE FELICE, A. AND LINDER, E. V., *Fab 5: Noncanonical Kinetic Gravity, Self Tuning, and Cosmic Acceleration*, *JCAP* **1210** (2012) 060, [[1208.4163](#)].
- [22] ARMENDARIZ-PICON, C., DAMOUR, T. AND MUKHANOV, V. F., *k-inflation*, *Phys. Lett.* **B458** (1999) 209, [[hep-th/9904075](#)].
- [23] ARMENDARIZ-PICON, C., MUKHANOV, V. F. AND STEINHARDT, P. J., *Essentials of k-essence*, *Phys. Rev.* **D63** (2001) 103510, [[astro-ph/0006373](#)].
- [24] ARPONEN, J., *Internal structure of neutron stars*, *Nucl.Phys.* **A191** (1972) 257.

- [25] ARZOUMANIAN, Z. ET AL., *The neutron star interior composition explorer (NICER): mission definition*, in *Society of Photo-Optical Instrumentation Engineers (SPIE) Conference Series*, vol. 9144 of *Society of Photo-Optical Instrumentation Engineers (SPIE) Conference Series*, p. 20, 2014.
- [26] ASADA, H. AND SHIBATA, M., *Formulation for nonaxisymmetric uniformly rotating equilibrium configurations in the second postNewtonian approximation of general relativity*, *Phys.Rev.* **D54** (1996) 4944, [[gr-qc/9609024](#)].
- [27] AVILEZ-LOPEZ, A., PADILLA, A., SAFFIN, P. M. AND SKORDIS, C., *The Parametrized Post-Newtonian-Vainshteinian Formalism*, *JCAP* **1506** (2015) 044, [[1501.01985](#)].
- [28] AYZENBERG, D. AND YUNES, N., *Slowly-Rotating Black Holes in Einstein-Dilaton-Gauss-Bonnet Gravity: Quadratic Order in Spin Solutions*, *Phys.Rev.* **D90** (2014) 044066, [[1405.2133](#)].
- [29] BABICHEV, E. AND CHARMOUSIS, C., *Dressing a black hole with a time-dependent Galileon*, *JHEP* **1408** (2014) 106, [[1312.3204](#)].
- [30] BABICHEV, E., CHARMOUSIS, C. AND HASSAINE, M., *Charged Galileon black holes*, *JCAP* **1505** (2015) 031, [[1503.02545](#)].
- [31] BAMBI, C., *Testing black hole candidates with electromagnetic radiation*, [1509.03884](#).
- [32] BARAUSSE, E., PALENZUELA, C., PONCE, M. AND LEHNER, L., *Neutron-star mergers in scalar-tensor theories of gravity*, *Phys.Rev.* **D87** (2013) 081506, [[1212.5053](#)].
- [33] BARAUSSE, E. AND YAGI, K., *Gravitation-Wave Emission in Shift-Symmetric Horndeski Theories*, *Phys. Rev. Lett.* **115** (2015) 211105, [[1509.04539](#)].
- [34] BAYIN, S. S., *Anisotropic Fluid Spheres in General Relativity*, *Phys.Rev.* **D26** (1982) 1262.
- [35] BEJGER, M., BULIK, T. AND HAENSEL, P., *Moments of inertia of the binary pulsars J0737-3039A,B and the dense matter EOS*, *Mon. Not. Roy. Astron. Soc.* **364** (2005) 635, [[astro-ph/0508105](#)].
- [36] BEJGER, M. AND HAENSEL, P., *Moments of inertia for neutron and strange stars: Limits derived for the Crab pulsar*, *Astron. Astrophys.* **396** (2002) 917, [[astro-ph/0209151](#)].
- [37] BEKENSTEIN, J. D., *The Relation between physical and gravitational geometry*, *Phys. Rev.* **D48** (1993) 3641, [[gr-qc/9211017](#)].
- [38] BEKENSTEIN, J. D., *Relativistic gravitation theory for the MOND paradigm*, *Phys.Rev.* **D70** (2004) 083509, [[astro-ph/0403694](#)].

- [39] BEKENSTEIN, J. D. AND SANDERS, R. H., *Gravitational lenses and unconventional gravity theories*, *Astrophys. J.* **429** (1994) 480, [[astro-ph/9311062](#)].
- [40] BEKENSTEIN, J., *Novel ‘no scalar hair’ theorem for black holes*, *Phys.Rev.* **D51** (1995) 6608.
- [41] BELCZYNSKI, K., REPETTO, S., HOLZ, D. E., O’SHAUGHNESSY, R., BULIK, T., BERTI, E. ET AL., *Compact Binary Merger Rates: Comparison with LIGO/Virgo Upper Limits*, *Astrophys. J.* **819** (2016) 108, [[1510.04615](#)].
- [42] BENHAR, O., FERRARI, V., GUALTIERI, L. AND MARASSI, S., *Perturbative approach to the structure of rapidly rotating neutron stars*, *Phys. Rev.* **D72** (2005) 044028, [[gr-qc/0504068](#)].
- [43] BEREZHIANI, L., CHKAREULI, G. AND GABADADZE, G., *Restricted Galileons*, *Phys. Rev.* **D88** (2013) 124020, [[1302.0549](#)].
- [44] BERGMANN, P. G., *Comments on the scalar tensor theory*, *Int.J.Theor.Phys.* **1** (1968) 25.
- [45] BERNUZZI, S., DIETRICH, T. AND NAGAR, A., *Modeling the complete gravitational wave spectrum of neutron star mergers*, *Phys. Rev. Lett.* **115** (2015) 091101, [[1504.01764](#)].
- [46] BERNUZZI, S., NAGAR, A., BALMELLI, S., DIETRICH, T. AND UJEVIC, M., *Quasiuniversal properties of neutron star mergers*, *Phys. Rev. Lett.* **112** (2014) 201101, [[1402.6244](#)].
- [47] BERNUZZI, S., NAGAR, A., DIETRICH, T. AND DAMOUR, T., *Modeling the Dynamics of Tidally Interacting Binary Neutron Stars up to the Merger*, *Phys. Rev. Lett.* **114** (2015) 161103, [[1412.4553](#)].
- [48] BERNUZZI, S., NAGAR, A., THIERFELDER, M. AND BRUGMANN, B., *Tidal effects in binary neutron star coalescence*, *Phys. Rev.* **D86** (2012) 044030, [[1205.3403](#)].
- [49] BERTI, E., CARDOSO, V., GUALTIERI, L., HORBATSCH, M. AND SPERHAKE, U., *Numerical simulations of single and binary black holes in scalar-tensor theories: circumventing the no-hair theorem*, *Phys.Rev.* **D87** (2013) 124020, [[1304.2836](#)].
- [50] BERTI, E., CARDOSO, V. AND STARINETS, A. O., *Quasinormal modes of black holes and black branes*, *Class. Quantum Grav.* **26** (2009) 163001, [[0905.2975](#)].
- [51] BERTI, E. ET AL., *Testing General Relativity with Present and Future Astrophysical Observations*, *Class. Quant. Grav.* **32** (2015) 243001, [[1501.07274](#)].
- [52] BERTI, E., GUALTIERI, L., HORBATSCH, M. AND ALSING, J., *Light scalar field constraints from gravitational-wave observations of compact binaries*, *Phys.Rev.* **D85** (2012) 122005, [[1204.4340](#)].

- [53] BERTI, E., IYER, S. AND WILL, C. M., *A Post-Newtonian diagnosis of quasiequilibrium configurations of neutron star-neutron star and neutron star-black hole binaries*, *Phys. Rev. D* **77** (2008) 024019, [0709.2589].
- [54] BERTI, E. AND STERGIIOULAS, N., *Approximate matching of analytic and numerical solutions for rapidly rotating neutron stars*, *Mon. Not. Roy. Astron. Soc.* **350** (2004) 1416, [gr-qc/0310061].
- [55] BERTI, E., WHITE, F., MANIOPOULOU, A. AND BRUNI, M., *Rotating neutron stars: an invariant comparison of approximate and numerical spacetime models*, *Mon. Not. R. Astron. Soc.* **358** (2005) 923, [gr-qc/0405146].
- [56] BERTOTTI, B., IESS, L. AND TORTORA, P., *A test of general relativity using radio links with the Cassini spacecraft*, *Nature* **425** (2003) 374.
- [57] BETTONI, D. AND LIBERATI, S., *Disformal invariance of second order scalar-tensor theories: Framing the Horndeski action*, *Phys. Rev.* **D88** (2013) 084020, [1306.6724].
- [58] BETTONI, D., PETTORINO, V., LIBERATI, S. AND BACCIGALUPI, C., *Non-minimally coupled dark matter: effective pressure and structure formation*, *JCAP* **1207** (2012) 027, [1203.5735].
- [59] BETTONI, D. AND ZUMALACARREGUI, M., *Kinetic mixing in scalar-tensor theories of gravity*, *Phys. Rev.* **D91** (2015) 104009, [1502.02666].
- [60] BINNINGTON, T. AND POISSON, E., *Relativistic theory of tidal Love numbers*, *Phys. Rev.* **D80** (2009) 084018, [0906.1366].
- [61] BLÁZQUEZ-SALCEDO, J. L., GONZÁLEZ-ROMERO, L. M., KUNZ, J., MOJICA, S. AND NAVARRO-LÉRIDA, F., *Axial quasi-normal modes of Einstein-Gauss-Bonnet-dilaton neutron stars*, *Phys. Rev.* **D93** (2016) 024052, [1511.03960].
- [62] BONAZZOLA, S. AND GOURGOULHON, E., *Gravitational waves from pulsars: Emission by the magnetic field induced distortion*, *Astron. Astrophys.* **312** (1996) 675, [astro-ph/9602107].
- [63] BOWERS, R. L. AND LIANG, E. P. T., *Anisotropic Spheres in General Relativity*, *ApJ* **188** (1974) 657.
- [64] BRANS, C. AND DICKE, R., *Mach's principle and a relativistic theory of gravitation*, *Phys.Rev.* **124** (1961) 925.
- [65] BRAX, P. AND BURRAGE, C., *Constraining Disformally Coupled Scalar Fields*, *Phys. Rev.* **D90** (2014) 104009, [1407.1861].
- [66] BRAX, P. AND BURRAGE, C., *Explaining the Proton Radius Puzzle with Disformal Scalars*, *Phys. Rev.* **D91** (2015) 043515, [1407.2376].

- [67] BRAX, P., BURRAGE, C., DAVIS, A.-C. AND GUBITOSI, G., *Cosmological Tests of the Disformal Coupling to Radiation*, *JCAP* **1311** (2013) 001, [[1306.4168](#)].
- [68] BRAX, P., BURRAGE, C., DAVIS, A.-C. AND GUBITOSI, G., *Cosmological Tests of Coupled Galileons*, *JCAP* **1503** (2015) 028, [[1411.7621](#)].
- [69] BRAX, P., BURRAGE, C. AND ENGLERT, C., *Disformal dark energy at colliders*, *Phys. Rev.* **D92** (2015) 044036, [[1506.04057](#)].
- [70] BRAX, P., VAN DE BRUCK, C., DAVIS, A.-C., KHOURY, J. AND WELTMAN, A., *Detecting dark energy in orbit - The Cosmological chameleon*, *Phys. Rev.* **D70** (2004) 123518, [[astro-ph/0408415](#)].
- [71] BREU, C. AND REZZOLLA, L., *Maximum mass, moment of inertia and compactness of relativistic stars*, *Mon. Not. Roy. Astron. Soc.* **459** (2016) 646, [[1601.06083](#)].
- [72] BRITO, R., TERRANA, A., JOHNSON, M. AND CARDOSO, V., *Nonlinear dynamical stability of infrared modifications of gravity*, *Phys.Rev.* **D90** (2014) 124035, [[1409.0886](#)].
- [73] BRODERICK, A. E., JOHANNSEN, T., LOEB, A. AND PSALTIS, D., *Testing the No-Hair Theorem with Event Horizon Telescope Observations of Sagittarius A**, *Astrophys. J.* **784** (2014) 7, [[1311.5564](#)].
- [74] BROWN, D. A., HARRY, I., LUNDGREN, A. AND NITZ, A. H., *Detecting binary neutron star systems with spin in advanced gravitational-wave detectors*, *Phys. Rev.* **D86** (2012) 084017, [[1207.6406](#)].
- [75] BURGAY, M., D'AMICO, N., POSSENTI, A., MANCHESTER, R., LYNE, A. ET AL., *An Increased estimate of the merger rate of double neutron stars from observations of a highly relativistic system*, *Nature* **426** (2003) 531, [[astro-ph/0312071](#)].
- [76] CALDWELL, R. R., DAVE, R. AND STEINHARDT, P. J., *Cosmological imprint of an energy component with general equation of state*, *Phys. Rev. Lett.* **80** (1998) 1582, [[astro-ph/9708069](#)].
- [77] CAMELIO, G., GUALTIERI, L., PONS, J. A. AND FERRARI, V., *Spin evolution of a proto-neutron star*, *Phys. Rev.* **D94** (2016) 024008, [[1601.02945](#)].
- [78] CANUTO, V. AND CHITRE, S., *Crystallization of dense neutron matter*, *Phys.Rev.* **D9** (1974) 1587.
- [79] CARDOSO, V., CARUCCI, I. P., PANI, P. AND SOTIRIOU, T. P., *Black holes with surrounding matter in scalar-tensor theories*, *Phys.Rev.Lett.* **111** (2013) 111101, [[1308.6587](#)].
- [80] CARDOSO, V., CARUCCI, I. P., PANI, P. AND SOTIRIOU, T. P., *Matter around Kerr black holes in scalar-tensor theories: scalarization and superradiant instability*, *Phys.Rev.* **D88** (2013) 044056, [[1305.6936](#)].

- [81] CARDOSO, V., CRISPINO, L. C., MACEDO, C. F., OKAWA, H. AND PANI, P., *Light rings as observational evidence for event horizons: long-lived modes, ergoregions and nonlinear instabilities of ultracompact objects*, *Phys. Rev.* **D90** (2014) 044069, [[1406.5510](#)].
- [82] CARDOSO, V., PANI, P. AND RICO, J., *On generic parametrizations of spinning black-hole geometries*, *Phys.Rev.* **D89** (2014) 064007, [[1401.0528](#)].
- [83] CARTER, B. AND LANGLOIS, D., *Relativistic models for superconducting superfluid mixtures*, *Nucl.Phys.* **B531** (1998) 478, [[gr-qc/9806024](#)].
- [84] CATTOEN, C., FABER, T. AND VISSER, M., *Gravastars must have anisotropic pressures*, *Class.Quant.Grav.* **22** (2005) 4189, [[gr-qc/0505137](#)].
- [85] CHAGOYA, J., KOYAMA, K., NIZ, G. AND TASINATO, G., *Galileons and strong gravity*, *JCAP* **1410** (2014) 055, [[1407.7744](#)].
- [86] CHAKRABARTI, S., DELSATE, T., GÜRLEBECK, N. AND STEINHOFF, J., *I-Q relation for rapidly rotating neutron stars*, *Phys. Rev. Lett.* **112** (2014) 201102, [[1311.6509](#)].
- [87] CHAKRABARTY, D., *The Spin Distribution of Millisecond X-ray Pulsars*, *AIP Conf. Proc.* **1068** (2008) 67, [[0809.4031](#)].
- [88] CHAMEL, N. AND HAENSEL, P., *Physics of Neutron Star Crusts*, *Living Rev.Rel.* **11** (2008) 10, [[0812.3955](#)].
- [89] CHANDRASEKHAR, S., *The Post-Newtonian Equations of Hydrodynamics in General Relativity.*, *ApJ* **142** (Nov., 1965) 1488.
- [90] CHANDRASEKHAR, S., *An Introduction to the Study of Stellar Structure*. Dover Books on Astronomy Series. Dover Publications, 2012.
- [91] CHANDRASEKHAR, S. AND FERRARI, V., *On the non-radial oscillations of a star. III - A reconsideration of the axial modes*, *Royal Society of London Proceedings Series A* **434** (Aug., 1991) 449.
- [92] CHANDRASEKHAR, S. AND NUTKU, Y., *The Second Post-Newtonian Equations of Hydrodynamics in General Relativity*, *ApJ* **158** (1969) 55.
- [93] CHANDRASEKHAR, S., *The Mathematical Theory of Black Holes*. Clarendon Press, Oxford, U.K., 1983.
- [94] CHARMOUSIS, C., *From Lovelock to Horndeski's Generalized Scalar Tensor Theory*, *Lect. Notes Phys.* **892** (2015) 25, [[1405.1612](#)].
- [95] CHARMOUSIS, C., COPELAND, E. J., PADILLA, A. AND SAFFIN, P. M., *General second order scalar-tensor theory, self tuning, and the Fab Four*, *Phys. Rev. Lett.* **108** (2012) 051101, [[1106.2000](#)].

- [96] CHARMOUSIS, C., COPELAND, E. J., PADILLA, A. AND SAFFIN, P. M., *Self-tuning and the derivation of a class of scalar-tensor theories*, *Phys. Rev.* **D85** (2012) 104040, [[1112.4866](#)].
- [97] CHARMOUSIS, C., KOLYVARIS, T., PAPANTONOPOULOS, E. AND TSOUKALAS, M., *Black Holes in Bi-scalar Extensions of Horndeski Theories*, *JHEP* **07** (2014) 085, [[1404.1024](#)].
- [98] CHATZIOANNOU, K., CORNISH, N., KLEIN, A. AND YUNES, N., *Spin-Precession: Breaking the Black Hole–Neutron Star Degeneracy*, *Astrophys. J.* **798** (2015) L17, [[1402.3581](#)].
- [99] CHATZIOANNOU, K., YAGI, K., KLEIN, A., CORNISH, N. AND YUNES, N., *Probing the Internal Composition of Neutron Stars with Gravitational Waves*, *Phys. Rev.* **D92** (2015) 104008, [[1508.02062](#)].
- [100] CHEN, P., SUYAMA, T. AND YOKOYAMA, J., *Spontaneous scalarization: asymmetron as dark matter*, *Phys. Rev.* **D92** (2015) 124016, [[1508.01384](#)].
- [101] CHIBA, T., HARADA, T. AND NAKAO, K.-I., *Gravitational physics in scalar tensor theories: Tests of strong field gravity*, *Prog.Theor.Phys.Suppl.* **128** (1997) 335.
- [102] CHRUSCIEL, P. T., COSTA, J. L. AND HEUSLER, M., *Stationary Black Holes: Uniqueness and Beyond*, *Living Rev.Rel.* **15** (2012) 7, [[1205.6112](#)].
- [103] CISTERNA, A., CRUZ, M., DELSATE, T. AND SAAVEDRA, J., *Nonminimal derivative coupling scalar-tensor theories: odd-parity perturbations and black hole stability*, *Phys. Rev.* **D92** (2015) 104018, [[1508.06413](#)].
- [104] CISTERNA, A., DELSATE, T. AND RINALDI, M., *Neutron stars in general second order scalar-tensor theory: The case of nonminimal derivative coupling*, *Phys. Rev.* **D92** (2015) 044050, [[1504.05189](#)].
- [105] CISTERNA, A., DELSATE, T., DUCOBU, L. AND RINALDI, M., *Slowly rotating neutron stars in the nonminimal derivative coupling sector of Horndeski gravity*, *Phys. Rev.* **D93** (2016) 084046, [[1602.06939](#)].
- [106] CIUFOLINI, I. AND RUFFINI, R., *Equilibrium configurations of neutron stars and the parametrized post-Newtonian metric theories of gravitation*, *ApJ* **275** (1983) 867.
- [107] CLIFTON, T., FERREIRA, P. G., PADILLA, A. AND SKORDIS, C., *Modified Gravity and Cosmology*, *Phys. Rept.* **513** (2012) 1, [[1106.2476](#)].
- [108] COLAIUDA, A., FERRARI, V., GUALTIERI, L. AND PONS, J. A., *Relativistic models of magnetars: structure and deformations*, *Mon. Not. Roy. Astron. Soc.* **385** (2008) 2080, [[0712.2162](#)].
- [109] COLAIUDA, A. AND KOKKOTAS, K. D., *Magnetars oscillations in the presence of a crust*, *Mon.Not.Roy.Astron.Soc.* **414** (2011) 3014, [[1012.3103](#)].

- [110] COLLINS, N. A. AND HUGHES, S. A., *Towards a formalism for mapping the space-times of massive compact objects: Bumpy black holes and their orbits*, *Phys.Rev.* **D69** (2004) 124022, [[gr-qc/0402063](#)].
- [111] COOK, G. B., SHAPIRO, S. L. AND TEUKOLSKY, S. A., *Rapidly rotating neutron stars in general relativity: Realistic equations of state*, *Astrophys. J.* **424** (1994) 823.
- [112] COPELAND, E. J., PADILLA, A. AND SAFFIN, P. M., *The cosmology of the Fab-Four*, *JCAP* **1212** (2012) 026, [[1208.3373](#)].
- [113] CREMINELLI, P., GLEYZES, J., NORENA, J. AND VERNIZZI, F., *Resilience of the standard predictions for primordial tensor modes*, *Phys. Rev. Lett.* **113** (2014) 231301, [[1407.8439](#)].
- [114] DAMOUR, T. AND POLYAKOV, A. M., *String theory and gravity*, *Gen.Rel.Grav.* **26** (1994) 1171, [[gr-qc/9411069](#)].
- [115] DAMOUR, T. AND POLYAKOV, A. M., *The String dilaton and a least coupling principle*, *Nucl.Phys.* **B423** (1994) 532, [[hep-th/9401069](#)].
- [116] DAMOUR, T. AND SCHAEFER, G., *Higher Order Relativistic Periastron Advances and Binary Pulsars*, *Nuovo Cim.* **B101** (1988) 127.
- [117] DAMOUR, T. AND ESPOSITO-FARÈSE, G., *Tensor-multi-scalar theories of gravitation*, *Class.Quant.Grav.* **9** (1992) 2093.
- [118] DAMOUR, T. AND ESPOSITO-FARÈSE, G., *Nonperturbative strong field effects in tensor-scalar theories of gravitation*, *Phys.Rev.Lett.* **70** (1993) 2220.
- [119] DAMOUR, T. AND ESPOSITO-FARÈSE, G., *Tensor-scalar gravity and binary pulsar experiments*, *Phys.Rev.* **D54** (1996) 1474, [[gr-qc/9602056](#)].
- [120] DAMOUR, T. AND ESPOSITO-FARÈSE, G., *Testing gravity to second post-Newtonian order: A Field theory approach*, *Phys.Rev.* **D53** (1996) 5541, [[gr-qc/9506063](#)].
- [121] DAMOUR, T. AND ESPOSITO-FARÈSE, G., *Gravitational wave versus binary-pulsar tests of strong field gravity*, *Phys.Rev.* **D58** (1998) 042001, [[gr-qc/9803031](#)].
- [122] DAMOUR, T. AND NAGAR, A., *Relativistic tidal properties of neutron stars*, *Phys. Rev.* **D80** (2009) 084035, [[0906.0096](#)].
- [123] DAMOUR, T., NAGAR, A. AND VILLAIN, L., *Measurability of the tidal polarizability of neutron stars in late-inspiral gravitational-wave signals*, *Phys. Rev.* **D85** (2012) 123007, [[1203.4352](#)].
- [124] DE FELICE, A. AND TSUJIKAWA, S., *f(R) theories*, *Living Rev.Rel.* **13** (2010) 3, [[1002.4928](#)].

- [125] DE FELICE, A. AND TSUJIKAWA, S., *Conditions for the cosmological viability of the most general scalar-tensor theories and their applications to extended Galileon dark energy models*, *JCAP* **1202** (2012) 007, [[1110.3878](#)].
- [126] DE RHAM, C. AND GABADADZE, G., *Generalization of the Fierz-Pauli Action*, *Phys.Rev.* **D82** (2010) 044020, [[1007.0443](#)].
- [127] DE RHAM, C., GABADADZE, G. AND TOLLEY, A. J., *Resummation of Massive Gravity*, *Phys.Rev.Lett.* **106** (2011) 231101, [[1011.1232](#)].
- [128] DE RHAM, C. AND HEISENBERG, L., *Cosmology of the Galileon from Massive Gravity*, *Phys. Rev.* **D84** (2011) 043503, [[1106.3312](#)].
- [129] DEDEO, S. AND PSALTIS, D., *Towards New Tests of Strong-field Gravity with Measurements of Surface Atomic Line Redshifts from Neutron Stars*, *Phys. Rev. Lett.* **90** (2003) 141101, [[astro-ph/0302095](#)].
- [130] DEDEO, S. AND PSALTIS, D., *Testing strong-field gravity with quasiperiodic oscillations*, [astro-ph/0405067](#).
- [131] DEFFAYET, C., DESER, S. AND ESPOSITO-FARÈSE, G., *Generalized Galileons: All scalar models whose curved background extensions maintain second-order field equations and stress-tensors*, *Phys. Rev.* **D80** (2009) 064015, [[0906.1967](#)].
- [132] DEFFAYET, C., ESPOSITO-FARÈSE, G. AND VIKMAN, A., *Covariant Galileon*, *Phys.Rev.* **D79** (2009) 084003, [[0901.1314](#)].
- [133] DEFFAYET, C., GAO, X., STEER, D. AND ZAHARIADE, G., *From k-essence to generalised Galileons*, *Phys.Rev.* **D84** (2011) 064039, [[1103.3260](#)].
- [134] DEIBEL, A. T., STEINER, A. W. AND BROWN, E. F., *Magnetar giant flare oscillations and the nuclear symmetry energy*, *Phys.Rev.* **C00** (1969) 005800, [[1303.3270](#)].
- [135] DEL POZZO, W., LI, T. G. F., AGATHOS, M., VAN DEN BROECK, C. AND VITALE, S., *Demonstrating the feasibility of probing the neutron star equation of state with second-generation gravitational wave detectors*, *Phys. Rev. Lett.* **111** (2013) 071101, [[1307.8338](#)].
- [136] DELGATY, M. S. R. AND LAKE, K., *Physical acceptability of isolated, static, spherically symmetric, perfect fluid solutions of Einstein's equations*, *Comput. Phys. Commun.* **115** (1998) 395, [[gr-qc/9809013](#)].
- [137] DELSATE, T. AND STEINHOFF, J., *New insights on the matter-gravity coupling paradigm*, *Phys.Rev.Lett.* **109** (2012) 021101, [[1201.4989](#)].
- [138] DEMOREST, P., PENNUCCI, T., RANSOM, S., ROBERTS, M. AND HESSELS, J., *Shapiro Delay Measurement of A Two Solar Mass Neutron Star*, *Nature* **467** (2010) 1081, [[1010.5788](#)].

- [139] DEV, K. AND GLEISER, M., *Anisotropic stars: Exact solutions*, *Gen. Rel. Grav.* **34** (2002) 1793, [[astro-ph/0012265](#)].
- [140] DEV, K. AND GLEISER, M., *Anisotropic stars. 2. Stability*, *Gen. Rel. Grav.* **35** (2003) 1435, [[gr-qc/0303077](#)].
- [141] DEV, K. AND GLEISER, M., *Anisotropic stars: Exact solutions and stability*, *Int. J. Mod. Phys.* **D13** (2004) 1389, [[astro-ph/0401546](#)].
- [142] DHURANDHAR, S., TAGOSHI, H., OKADA, Y., KANDA, N. AND TAKAHASHI, H., *The cross-correlation search for a hot spot of gravitational waves*, *Phys. Rev.* **D84** (2011) 083007, [[1105.5842](#)].
- [143] DIETRICH, T., MOLDENHAUER, N., JOHNSON-MCDANIEL, N. K., BERNUZZI, S., MARKAKIS, C. M., BRÜGMANN, B. ET AL., *Binary Neutron Stars with Generic Spin, Eccentricity, Mass ratio, and Compactness - Quasi-equilibrium Sequences and First Evolutions*, *Phys. Rev.* **D92** (2015) 124007, [[1507.07100](#)].
- [144] DOMENECH, G., NARUKO, A. AND SASAKI, M., *Cosmological disformal invariance*, *JCAP* **1510** (2015) 067, [[1505.00174](#)].
- [145] DOMINIK, M., BERTI, E., O'SHAUGHNESSY, R., MANDEL, I., BELCZYNSKI, K., FRYER, C. ET AL., *Double Compact Objects III: Gravitational Wave Detection Rates*, *Astrophys. J.* **806** (2015) 263, [[1405.7016](#)].
- [146] DONEVA, D. D. AND KOKKOTAS, K. D., *Asteroseismology of rapidly rotating neutron stars - an alternative approach*, *Phys. Rev.* **D92** (2015) 124004, [[1507.06606](#)].
- [147] DONEVA, D. D. AND YAZADJIEV, S. S., *Gravitational wave spectrum of anisotropic neutron stars in Cowling approximation*, *Phys. Rev.* **D85** (2012) 124023, [[1203.3963](#)].
- [148] DONEVA, D. D. AND YAZADJIEV, S. S., *Rapidly rotating neutron stars with a massive scalar fieldstructure and universal relations*, *JCAP* **1611** (2016) 019, [[1607.03299](#)].
- [149] DONEVA, D. D., YAZADJIEV, S. S. AND KOKKOTAS, K. D., *The I-Q relations for rapidly rotating neutron stars in $f(R)$ gravity*, *Phys. Rev.* **D92** (2015) 064015, [[1507.00378](#)].
- [150] DONEVA, D. D., YAZADJIEV, S. S., KOKKOTAS, K. D. AND STEFANOV, I. Z., *Quasi-normal modes, bifurcations and non-uniqueness of charged scalar-tensor black holes*, *Phys. Rev.* **D82** (2010) 064030, [[1007.1767](#)].
- [151] DONEVA, D. D., YAZADJIEV, S. S., STAYKOV, K. V. AND KOKKOTAS, K. D., *Universal I-Q relations for rapidly rotating neutron and strange stars in scalar-tensor theories*, *Phys. Rev.* **D90** (2014) 104021, [[1408.1641](#)].

- [152] DONEVA, D. D., YAZADJIEV, S. S., STERGIIOULAS, N. AND KOKKOTAS, K. D., *Breakdown of I-Love-Q universality in rapidly rotating relativistic stars*, *Astrophys. J.* **781** (2013) L6, [[1310.7436](#)].
- [153] DONEVA, D. D., YAZADJIEV, S. S., STERGIIOULAS, N. AND KOKKOTAS, K. D., *Rapidly rotating neutron stars in scalar-tensor theories of gravity*, *Phys.Rev.* **D88** (2013) 084060, [[1309.0605](#)].
- [154] DONEVA, D. D., YAZADJIEV, S. S., STERGIIOULAS, N., KOKKOTAS, K. D. AND ATHANASIADIS, T. M., *Orbital and epicyclic frequencies around rapidly rotating compact stars in scalar-tensor theories of gravity*, *Phys.Rev.* **D90** (2014) 044004, [[1405.6976](#)].
- [155] DOUCHIN, F. AND HAENSEL, P., *A unified equation of state of dense matter and neutron star structure*, *Astron.Astrophys.* **380** (2001) 151, [[astro-ph/0111092](#)].
- [156] DUFF, M., *Kaluza-Klein theory in perspective*, [hep-th/9410046](#).
- [157] DVALI, G. R., GABADADZE, G. AND PORRATI, M., *4D gravity on a brane in 5D Minkowski space*, *Phys. Lett.* **B485** (2000) 208, [[hep-th/0005016](#)].
- [158] EARDLEY, D. M., *Observable effects of a scalar gravitational field in a binary pulsar*, *Astrophys. J.* **196** (1975) L59.
- [159] FARR, W. M., SRAVAN, N., CANTRELL, A., KREIDBERG, L., BAILYN, C. D., MANDEL, I. ET AL., *The Mass Distribution of Stellar-Mass Black Holes*, *Astrophys. J.* **741** (2011) 103, [[1011.1459](#)].
- [160] FAVATA, M., *Systematic parameter errors in inspiraling neutron star binaries*, *Phys. Rev. Lett.* **112** (2014) 101101, [[1310.8288](#)].
- [161] FEROCI, M. AND CONSORTIUM, T. L., *The Large Observatory for X-ray Timing (LOFT)*, *Exper.Astron.* **34** (2012) 415, [[1107.0436](#)].
- [162] FEROCI, M., HERDER, J., BOZZO, E., BARRET, D., BRANDT, S. ET AL., *LOFT: the Large Observatory For X-ray Timing*, *Proc.SPIE* **8443** (2012) 84432D, [[1209.1497](#)].
- [163] FIERZ, M., *On the physical interpretation of P. Jordan's extended theory of gravitation*, *Helv. Phys. Acta* **29** (1956) 128.
- [164] FINN, L. S., *Relativistic stellar pulsations in the Cowling approximation*, *MNRAS* **232** (1988) 259.
- [165] FISH, V. ET AL., *High-Angular-Resolution and High-Sensitivity Science Enabled by Beamformed ALMA*, [1309.3519](#).
- [166] FISH, V. L. ET AL., *1.3 mm Wavelength VLBI of Sagittarius A*: Detection of Time-Variable Emission on Event Horizon Scales*, *Astrophys. J.* **727** (2011) L36, [[1011.2472](#)].

- [167] FLANAGAN, E. E. AND HINDERER, T., *Constraining neutron star tidal Love numbers with gravitational wave detectors*, *Phys. Rev.* **D77** (2008) 021502, [[0709.1915](#)].
- [168] FOLOMEEV, V. AND DZHUNUSHALIEV, V., *Magnetic fields in anisotropic relativistic stars*, *Phys. Rev.* **D91** (2015) 044040, [[1501.06275](#)].
- [169] FREIRE, P. C., WEX, N., ESPOSITO-FARÈSE, G., VERBIEST, J. P., BAILES, M. ET AL., *The relativistic pulsar-white dwarf binary PSR J1738+0333 II. The most stringent test of scalar-tensor gravity*, *Mon. Not. Roy. Astron. Soc.* **423** (2012) 3328, [[1205.1450](#)].
- [170] FRIEDMAN, B. AND PANDHARIPANDE, V., *Hot and cold, nuclear and neutron matter*, *Nucl.Phys.* **A361** (1981) 502.
- [171] FRIEDMAN, J. L. AND STERGIIOULAS, N., *Rotating Relativistic Stars*. Cambridge University Press, Cambridge, 2013.
- [172] FUJII, Y. AND MAEDA, K.-I., *The Scalar-Tensor Theory of Gravitation*. Cambridge University Press, 2003.
- [173] GABLER, M., DURAN, P. C., STERGIIOULAS, N., FONT, J. A. AND MULLER, E., *Magneto-elastic oscillations of neutron stars with dipolar magnetic fields*, *Mon.Not.Roy.Astron.Soc.* **421** (2012) 2054, [[1109.6233](#)].
- [174] GAIR, J. R., VALLISNERI, M., LARSON, S. L. AND BAKER, J. G., *Testing General Relativity with Low-Frequency, Space-Based Gravitational-Wave Detectors*, *Living Rev.Rel.* **16** (2013) 7, [[1212.5575](#)].
- [175] GANDOLFI, S., CARLSON, J. AND REDDY, S., *The maximum mass and radius of neutron stars and the nuclear symmetry energy*, *Phys. Rev.* **C85** (2012) 032801, [[1101.1921](#)].
- [176] GENDREAU, K. C., ARZOUMANIAN, Z. AND OKAJIMA, T., *The Neutron star Interior Composition ExploreR (NICER): an Explorer mission of opportunity for soft x-ray timing spectroscopy*, in *Society of Photo-Optical Instrumentation Engineers (SPIE) Conference Series*, vol. 8443, 2012.
- [177] GERMANI, C. AND KEHAGIAS, A., *New Model of Inflation with Non-minimal Derivative Coupling of Standard Model Higgs Boson to Gravity*, *Phys. Rev. Lett.* **105** (2010) 011302, [[1003.2635](#)].
- [178] GERMANI, C. AND KEHAGIAS, A., *UV-Protected Inflation*, *Phys. Rev. Lett.* **106** (2011) 161302, [[1012.0853](#)].
- [179] GEROCH, R. P., *Multipole moments. I. Flat space*, *J. Math. Phys.* **11** (1970) 1955.
- [180] GEROCH, R. P., *Multipole moments. II. Curved space*, *J. Math. Phys.* **11** (1970) 2580.

- [181] GEROSA, D., SPERHAKE, U. AND OTT, C. D., *Numerical simulations of stellar collapse in scalar-tensor theories of gravity*, *Class. Quant. Grav.* **33** (2016) 135002, [1602.06952].
- [182] GLAMPEDAKIS, K. AND BABAK, S., *Mapping spacetimes with LISA: Inspiral of a test-body in a ‘quasi-Kerr’ field*, *Class.Quant.Grav.* **23** (2006) 4167, [gr-qc/0510057].
- [183] GLAMPEDAKIS, K., KAPADIA, S. J. AND KENNEFICK, D., *Superradiance-tidal friction correspondence*, *Phys. Rev.* **D89** (2014) 024007, [1312.1912].
- [184] GLAMPEDAKIS, K., PAPPAS, G., SILVA, H. O. AND BERTI, E., *Post-Tolman-Oppenheimer-Volkoff formalism for relativistic stars*, *Phys. Rev.* **D92** (2015) 024056, [1504.02455].
- [185] GLAMPEDAKIS, K., PAPPAS, G., SILVA, H. O. AND BERTI, E., *Astrophysical applications of the post-Tolman-Oppenheimer-Volkoff formalism*, *Phys. Rev.* **D94** (2016) 044030, [1606.05106].
- [186] GLENDENNING, N. K., *Neutron Stars Are Giant Hypernuclei?*, *Astrophys. J.* **293** (1985) 470.
- [187] GLEYZES, J., LANGLOIS, D., PIAZZA, F. AND VERNIZZI, F., *Exploring gravitational theories beyond Horndeski*, *JCAP* **1502** (2015) 018, [1408.1952].
- [188] GLEYZES, J., LANGLOIS, D., PIAZZA, F. AND VERNIZZI, F., *Healthy theories beyond Horndeski*, *Phys. Rev. Lett.* **114** (2015) 211101, [1404.6495].
- [189] GORIELY, S., CHAMEL, N. AND PEARSON, J. M., *Further explorations of Skyrme-Hartree-Fock-Bogoliubov mass formulas. XII: Stiffness and stability of neutron-star matter*, *Phys. Rev.* **C82** (2010) 035804, [1009.3840].
- [190] GUBITOSI, G. AND LINDER, E. V., *Purely Kinetic Coupled Gravity*, *Phys. Lett.* **B703** (2011) 113, [1106.2815].
- [191] GUPTA, A., GOPAKUMAR, A., IYER, B. R. AND IYER, S., *Padè approximants for truncated post-Newtonian neutron star models*, *Phys.Rev.* **D62** (2000) 044038, [gr-qc/0002094].
- [192] HAENSEL, P. AND PICHON, B., *Experimental nuclear masses and the ground state of cold dense matter*, *Astron.Astrophys.* **283** (1994) 313, [nucl-th/9310003].
- [193] HAENSEL, P., POTEKHIN, A. Y. AND YAKOVLEV, D. G., *Neutron stars 1: Equation of state and structure*. Springer, 2007.
- [194] HAGALA, R., LLINARES, C. AND MOTA, D. F., *Cosmological simulations with disformally coupled symmetron fields*, *Astron. Astrophys.* **585** (2016) A37, [1504.07142].

- [195] HAKIMOV, A., ABDUJABBAROV, A. AND AHMEDOV, B., *Magnetic fields of spherical compact stars in modified theories of gravity: $f(R)$ type gravity and Hořava-Lifshitz gravity*, *Phys.Rev.* **D88** (2013) 024008.
- [196] HANSEN, C. J. AND CIOFFI, D. F., *Torsional oscillations in neutron star crusts*, *ApJ* **238** (1980) 740.
- [197] HANSEN, R. O., *Multipole moments of stationary space-times*, *J. Math. Phys.* **15** (1974) 46.
- [198] HARADA, T., *Stability analysis of spherically symmetric star in scalar - tensor theories of gravity*, *Prog.Theor.Phys.* **98** (1997) 359, [gr-qc/9706014].
- [199] HARADA, T., *Neutron stars in scalar tensor theories of gravity and catastrophe theory*, *Phys.Rev.* **D57** (1998) 4802, [gr-qc/9801049].
- [200] HARADA, T., CHIBA, T., NAKAO, K.-I. AND NAKAMURA, T., *Scalar gravitational wave from Oppenheimer-Snyder collapse in scalar - tensor theories of gravity*, *Phys.Rev.* **D55** (1997) 2024, [gr-qc/9611031].
- [201] HARRISON, B. K., THORNE, K. S., WAKANO, M. AND WHEELER, J. A., *Gravitation Theory and Gravitational Collapse*. 1965.
- [202] HARTLE, J. B. AND THORNE, K. S., *Slowly Rotating Relativistic Stars. II. Models for Neutron Stars and Supermassive Stars*, *ApJ* **153** (1968) 807.
- [203] HARTLE, J. B., *Slowly rotating relativistic stars. I. Equations of structure*, *Astrophys.J.* **150** (1967) 1005.
- [204] HARTLE, J. B. AND THORNE, K. S., *Slowly Rotating Relativistic Stars. II. Models for Neutron Stars and Supermassive Stars*, *Astrophys.J.* **153** (1968) 807.
- [205] HAWKING, S. W., *Black holes in the Brans-Dicke theory of gravitation*, *Commun. Math. Phys.* **25** (1972) 167.
- [206] HE, X.-T., FATTOYEV, F. J., LI, B.-A. AND NEWTON, W. G., *Impact of the equation-of-state-gravity degeneracy on constraining the nuclear symmetry energy from astrophysical observables*, *Phys. Rev.* **C91** (2015) 015810, [1408.0857].
- [207] HEALY, J., BODE, T., HAAS, R., PAZOS, E., LAGUNA, P. ET AL., *Late Inspiral and Merger of Binary Black Holes in Scalar-Tensor Theories of Gravity*, *Class.Quant.Grav.* **29** (2012) 232002, [1112.3928].
- [208] HEBELER, K., LATTIMER, J., PETHICK, C. AND SCHWENK, A., *Equation of state and neutron star properties constrained by nuclear physics and observation*, *Astrophys. J.* **773** (2013) 11, [1303.4662].
- [209] HEINTZMANN, H. AND HILLEBRANDT, W., *Neutron stars with an anisotropic equation of state - Mass, redshift and stability*, *A&A* **38** (1975) 51.

- [210] HEISELBERG, H. AND HJORTH-JENSEN, M., *Phases of dense matter in neutron stars*, *Phys.Rept.* **328** (2000) 237, [[nucl-th/9902033](#)].
- [211] HEISENBERG, L., KIMURA, R. AND YAMAMOTO, K., *Cosmology of the proxy theory to massive gravity*, *Phys. Rev.* **D89** (2014) 103008, [[1403.2049](#)].
- [212] HERDEIRO, C. A. R. AND RADU, E., *Kerr black holes with scalar hair*, *Phys.Rev.Lett.* **112** (2014) 221101, [[1403.2757](#)].
- [213] HERDEIRO, C. A. R. AND RADU, E., *Asymptotically flat black holes with scalar hair: a review*, *Int. J. Mod. Phys.* **D24** (2015) 1542014, [[1504.08209](#)].
- [214] HERRERA, L. AND SANTOS, N. O., *Local anisotropy in self-gravitating systems*, *Phys. Rep.* **286** (1997) 53.
- [215] HESSELS, J. W. T., RANSOM, S. M., STAIRS, I. H., FREIRE, P. C. C., KASPI, V. M. AND CAMILO, F., *A radio pulsar spinning at 716-hz*, *Science* **311** (2006) 1901, [[astro-ph/0601337](#)].
- [216] HEUSLER, M., *The Uniqueness theorem for rotating black hole solutions of self-gravitating harmonic mappings*, *Class.Quant.Grav.* **12** (1995) 2021, [[gr-qc/9503053](#)].
- [217] HEUSLER, MARKUS, *Black Hole Uniqueness Theorems*. Cambridge University Press, Cambridge, 1996.
- [218] HINDERER, T., *Tidal Love Numbers of Neutron Stars*, *ApJ* **677** (2008) 1216, [[0711.2420](#)].
- [219] HINDERER, T., *Erratum: “Tidal Love Numbers of Neutron Stars”*, *ApJ* **697** (2009) 964.
- [220] HINDERER, T., LACKEY, B. D., LANG, R. N. AND READ, J. S., *Tidal deformability of neutron stars with realistic equations of state and their gravitational wave signatures in binary inspiral*, *Phys. Rev.* **D81** (2010) 123016, [[0911.3535](#)].
- [221] HORBATSCH, M., SILVA, H. O., GEROSA, D., PANI, P., BERTI, E., GUALTIERI, L. ET AL., *Tensor-multi-scalar theories: relativistic stars and 3 + 1 decomposition*, *Class. Quant. Grav.* **32** (2015) 204001, [[1505.07462](#)].
- [222] HORBATSCH, M., SILVA, H. O., GEROSA, D., PANI, P., BERTI, E., GUALTIERI, L. ET AL., *in preparation*, .
- [223] HORBATSCH, M. AND BURGESS, C., *Semi-Analytic Stellar Structure in Scalar-Tensor Gravity*, *JCAP* **1108** (2011) 027, [[1006.4411](#)].
- [224] HORBATSCH, M. AND BURGESS, C., *Cosmic Black-Hole Hair Growth and Quasar OJ287*, *JCAP* **1205** (2012) 010, [[1111.4009](#)].

- [225] HORNDESKI, G. W., *Second-order scalar-tensor field equations in a four-dimensional space*, *Int. J. Theor. Phys.* **10** (1974) 363.
- [226] HOROWITZ, C. J., *Gravitational Waves From Low Mass Neutron Stars*, *Phys. Rev.* **D81** (2010) 103001, [[0912.1491](#)].
- [227] HOROWITZ, C. AND HUGHTO, J., *Molecular Dynamics Simulation of Shear Moduli for Coulomb Crystals*, [0812.2650](#).
- [228] HORVAT, D., ILIJIC, S. AND MARUNOVIC, A., *Radial pulsations and stability of anisotropic stars with quasi-local equation of state*, *Class.Quant.Grav.* **28** (2011) 025009, [[1010.0878](#)].
- [229] HUI, L. AND NICOLIS, A., *No-Hair Theorem for the Galileon*, *Phys. Rev. Lett.* **110** (2013) 241104, [[1202.1296](#)].
- [230] HUPPENKOTHEN, D., WATTS, A. L. AND LEVIN, Y., *Intermittency and Lifetime of the 625 Hz Quasi-Periodic Oscillation in the 2004 Hyperflare from the Magnetar SGR 1806-20 as evidence for magnetic coupling between the crust and the core*, *Astrophys. J.* **793** (2014) 129, [[1408.0734](#)].
- [231] IIDA, K. AND OYAMATSU, K., *Symmetry energy, unstable nuclei, and neutron star crusts*, *Eur.Phys.J.* **A50** (2014) 42, [[1309.1592](#)].
- [232] IORIO, L., *Constraining on the Preferred-Frame α_1 , α_2 parameters from Solar System planetary precessions*, *Int. J. Mod. Phys.* **D23** (2014) 1450006, [[1210.3026](#)].
- [233] IP, H. Y., SAKSTEIN, J. AND SCHMIDT, F., *Solar System Constraints on Disformal Gravity Theories*, *JCAP* **1510** (2015) 051, [[1507.00568](#)].
- [234] ISRAEL, G., BELLONI, T., STELLA, L., REPHAELI, Y., GRUBER, D. ET AL., *Discovery of rapid x-ray oscillations in the tail of the SGR 1806-20 hyperflare*, *Astrophys.J.* **628** (2005) L53, [[astro-ph/0505255](#)].
- [235] JAIN, R. K., KOUVARIS, C. AND NIELSEN, N. G., *White Dwarf Critical Tests for Modified Gravity*, *Phys. Rev. Lett.* **116** (2016) 151103, [[1512.05946](#)].
- [236] JOHANNSEN, T., *Sgr A* and General Relativity*, *Class. Quant. Grav.* **33** (2016) 113001, [[1512.03818](#)].
- [237] JOHNSON-MCDANIEL, N. K., *Gravitational wave constraints on the shape of neutron stars*, *Phys. Rev.* **D88** (2013) 044016, [[1303.3259](#)].
- [238] JOHNSON-MCDANIEL, N. K. AND OWEN, B. J., *Maximum elastic deformations of relativistic stars*, *Phys. Rev.* **D88** (2013) 044004, [[1208.5227](#)].
- [239] JORDAN, P., *The present state of Dirac's cosmological hypothesis*, *Z. Phys.* **157** (1959) 112.

- [240] KAINULAINEN, K. AND SUNHEDE, D., *Dark energy from large extra dimensions*, *Phys.Rev.* **D73** (2006) 083510, [[astro-ph/0412609](#)].
- [241] KALOPER, N., *Disformal inflation*, *Phys. Lett.* **B583** (2004) 1, [[hep-ph/0312002](#)].
- [242] KAMIAB, F., BRODERICK, A. E. AND AFSHORDI, N., *The mass and radii of strongly magnetized neutron stars*, [1503.03898](#).
- [243] KANTI, P., MAVROMATOS, N. E., RIZOS, J., TAMVAKIS, K. AND WINSTANLEY, E., *Dilatonic black holes in higher curvature string gravity*, *Phys. Rev.* **D54** (1996) 5049, [[hep-th/9511071](#)].
- [244] KERR, R. P., *Gravitational field of a spinning mass as an example of algebraically special metrics*, *Phys. Rev. Lett.* **11** (1963) 237.
- [245] KHAN, E. AND MARGUERON, J., *Determination of the density dependence of the nuclear incompressibility*, *Phys. Rev.* **C88** (2013) 034319.
- [246] KIPPENHAHN, R. AND WEIGERT, A., *Stellar structure and evolution*. Astronomy and Astrophysics library. Springer, 1990.
- [247] KLEIHAUS, B., KUNZ, J. AND MOJICA, S., *Quadrupole Moments of Rapidly Rotating Compact Objects in Dilatonic Einstein-Gauss-Bonnet Theory*, *Phys. Rev.* **D90** (2014) 061501, [[1407.6884](#)].
- [248] KLEIHAUS, B., KUNZ, J., MOJICA, S. AND ZAGERMANN, M., *Rapidly Rotating Neutron Stars in Dilatonic Einstein-Gauss-Bonnet Theory*, *Phys. Rev.* **D93** (2016) 064077, [[1601.05583](#)].
- [249] KLEIHAUS, B., KUNZ, J. AND RADU, E., *Rotating Black Holes in Dilatonic Einstein-Gauss-Bonnet Theory*, *Phys. Rev. Lett.* **106** (2011) 151104, [[1101.2868](#)].
- [250] KOBAYASHI, T., MOTOHASHI, H. AND SUYAMA, T., *Black hole perturbation in the most general scalar-tensor theory with second-order field equations I: the odd-parity sector*, *Phys. Rev.* **D85** (2012) 084025, [[1202.4893](#)].
- [251] KOBAYASHI, T., MOTOHASHI, H. AND SUYAMA, T., *Black hole perturbation in the most general scalar-tensor theory with second-order field equations. II. The even-parity sector*, *Phys. Rev.* **D89** (2014) 084042, [[1402.6740](#)].
- [252] KOBAYASHI, T. AND TANAHASHI, N., *Exact black hole solutions in shift symmetric scalar-tensor theories*, *PTEP* **2014** (2014) 073E02, [[1403.4364](#)].
- [253] KOBAYASHI, T., WATANABE, Y. AND YAMAUCHI, D., *Breaking of Vainshtein screening in scalar-tensor theories beyond Horndeski*, *Phys. Rev.* **D91** (2015) 064013, [[1411.4130](#)].
- [254] KOBAYASHI, T., YAMAGUCHI, M. AND YOKOYAMA, J., *Generalized G-inflation: Inflation with the most general second-order field equations*, *Prog. Theor. Phys.* **126** (2011) 511, [[1105.5723](#)].

- [255] KOPYAKOV, D. AND PETHICK, C., *Dynamics of the inner crust of neutron stars: hydrodynamics, elasticity and collective modes*, *Phys.Rev.* **C87** (2013) 055803, [1303.1315].
- [256] KOIVISTO, T. AND NYRHINEN, H. J., *Stability of disformally coupled accretion disks*, **1503.02063**.
- [257] KOIVISTO, T., WILLS, D. AND ZAVALA, I., *Dark D-brane Cosmology*, *JCAP* **1406** (2014) 036, [1312.2597].
- [258] KOIVISTO, T. S., *Disformal quintessence*, **0811.1957**.
- [259] KOIVISTO, T. S., MOTA, D. F. AND ZUMALACARREGUI, M., *Screening Modifications of Gravity through Disformally Coupled Fields*, *Phys. Rev. Lett.* **109** (2012) 241102, [1205.3167].
- [260] KOKKOTAS, K. AND RUOFF, J., *Radial oscillations of relativistic stars*, *Astron.Astrophys.* **366** (2001) 565, [gr-qc/0011093].
- [261] KOLYVARIS, T., KOUTSOUMBAS, G., PAPANTONOPOULOS, E. AND SIOPSIS, G., *Scalar Hair from a Derivative Coupling of a Scalar Field to the Einstein Tensor*, *Class. Quant. Grav.* **29** (2012) 205011, [1111.0263].
- [262] KOYAMA, K. AND SAKSTEIN, J., *Astrophysical Probes of the Vainshtein Mechanism: Stars and Galaxies*, *Phys. Rev.* **D91** (2015) 124066, [1502.06872].
- [263] KRAMER, M. AND WEX, N., *The double pulsar system: A unique laboratory for gravity*, *Class. Quant. Grav.* **26** (2009) 073001.
- [264] KREIDBERG, L., BAILYN, C. D., FARR, W. M. AND KALOGERA, V., *Mass Measurements of Black Holes in X-Ray Transients: Is There a Mass Gap?*, *Astrophys. J.* **757** (2012) 36, [1205.1805].
- [265] KUULKERS, E., DEN HARTOG, P. R., IN 'T ZAND, J. J. M., VERBUNT, F. W. M., HARRIS, W. E. AND COCCHI, M., *Photospheric radius expansion x-ray bursts as standard candles*, *Astron. Astrophys.* **399** (2003) 663, [astro-ph/0212028].
- [266] LACKEY, B. D., KYUTOKU, K., SHIBATA, M., BRADY, P. R. AND FRIEDMAN, J. L., *Extracting equation of state parameters from black hole-neutron star mergers: aligned-spin black holes and a preliminary waveform model*, *Phys. Rev.* **D89** (2014) 043009, [1303.6298].
- [267] LAMM, H., *Can Galileons solve the muon problem?*, *Phys. Rev.* **D92** (2015) 055007, [1505.00057].
- [268] LANDRY, P. AND POISSON, E., *Dynamical response to a stationary tidal field*, *Phys. Rev.* **D92** (2015) 124041, [1510.09170].

- [269] LANDRY, P. AND POISSON, E., *Tidal deformation of a slowly rotating material body. External metric*, *Phys. Rev.* **D91** (2015) 104018, [[1503.07366](#)].
- [270] LANDULFO, A. G. S., LIMA, W. C. C., MATSAS, G. E. A. AND VANZELLA, D. A. T., *Particle creation due to tachyonic instability in relativistic stars*, *Phys. Rev.* **D86** (2012) 104025, [[1204.3654](#)].
- [271] LANDULFO, A. G. S., LIMA, W. C. C., MATSAS, G. E. A. AND VANZELLA, D. A. T., *From quantum to classical instability in relativistic stars*, *Phys.Rev.* **D91** (2015) 024011, [[1410.2274](#)].
- [272] LATTIMER, J. M. AND PRAKASH, M., *Neutron star structure and the equation of state*, *Astrophys. J.* **550** (2001) 426, [[astro-ph/0002232](#)].
- [273] LATTIMER, J. M., *The nuclear equation of state and neutron star masses*, *Ann. Rev. Nucl. Part. Sci.* **62** (2012) 485, [[1305.3510](#)].
- [274] LATTIMER, J. M. AND PRAKASH, M., *The Equation of State of Hot, Dense Matter and Neutron Stars*, *Phys. Rept.* **621** (2016) 127, [[1512.07820](#)].
- [275] LATTIMER, J. M. AND PRAKASH, M., *Neutron Star Observations: Prognosis for Equation of State Constraints*, *Phys. Rept.* **442** (2007) 109, [[astro-ph/0612440](#)].
- [276] LATTIMER, J. M. AND SCHUTZ, B. F., *Constraining the equation of state with moment of inertia measurements*, *Astrophys. J.* **629** (2005) 979, [[astro-ph/0411470](#)].
- [277] LATTIMER, J. M. AND STEINER, A. W., *Constraints on the symmetry energy using the mass-radius relation of neutron stars*, *Eur. Phys. J.* **A50** (2014) 40, [[1403.1186](#)].
- [278] LATTIMER, J. AND PRAKASH, M., *The physics of neutron stars*, *Science* **304** (2004) 536, [[astro-ph/0405262](#)].
- [279] LETELIER, P. S., *Anisotropic fluids with two-perfect-fluid components*, *Phys. Rev. D* **22** (1980) 807.
- [280] LEWIN, W. H. G., VAN PARADIJS, J. AND TAAM, R. E., *X-Ray Bursts*, *Space Sci. Rev.* **62** (Sept., 1993) 223.
- [281] LI, B.-A. AND HAN, X., *Constraining the neutron-proton effective mass splitting using empirical constraints on the density dependence of nuclear symmetry energy around normal density*, *Phys. Lett.* **B727** (2013) 276, [[1304.3368](#)].
- [282] LI, B.-A., RAMOS, A., VERDE, G. AND VIDANA, I., *Topical issue on nuclear symmetry energy*, *Eur. Phys. J.* **A50** (2014) 9.
- [283] LIMA, W. C., MATSAS, G. E. AND VANZELLA, D. A., *Awaking the vacuum in relativistic stars*, *Phys.Rev.Lett.* **105** (2010) 151102, [[1009.1771](#)].
- [284] LINDBLOM, L., *Determining the nuclear equation of state from neutron-star masses and radii*, *ApJ* **398** (1992) 569.

- [285] LINDBLOM, L., *The Relativistic Inverse Stellar Structure Problem*, *AIP Conf. Proc.* **1577** (2014) 153, [[1402.0035](#)].
- [286] LINDBLOM, L. AND INDIK, N. M., *A Spectral Approach to the Relativistic Inverse Stellar Structure Problem*, *Phys.Rev.* **D86** (2012) 084003, [[1207.3744](#)].
- [287] LINDBLOM, L. AND INDIK, N. M., *Spectral Approach to the Relativistic Inverse Stellar Structure Problem II*, *Phys.Rev.* **D89** (2014) 064003, [[1310.0803](#)].
- [288] LITTENBERG, T. B., FARR, B., COUGHLIN, S., KALOGERA, V. AND HOLZ, D. E., *Neutron stars versus black holes: probing the mass gap with LIGO/Virgo*, *Astrophys. J.* **807** (2015) L24, [[1503.03179](#)].
- [289] LO, K.-W. AND LIN, L.-M., *The spin parameter of uniformly rotating compact stars*, *Astrophys. J.* **728** (2011) 12, [[1011.3563](#)].
- [290] LORENZ, C. P., RAVENHALL, D. G. AND PETHICK, C. J., *Neutron star crusts*, *Phys. Rev. Lett.* **70** (1993) 379.
- [291] LORIMER, D. R., *Binary and millisecond pulsars at the new millennium*, *Living Rev. Rel.* **4** (2001) 5, [[astro-ph/0104388](#)].
- [292] LORIMER, D. R., *Binary and Millisecond Pulsars*, *Living Rev. Rel.* **11** (2008) 8, [[0811.0762](#)].
- [293] LYNE, A., BURGAY, M., KRAMER, M., POSSENTI, A., MANCHESTER, R. ET AL., *A Double - pulsar system - A Rare laboratory for relativistic gravity and plasma physics*, *Science* **303** (2004) 1153, [[astro-ph/0401086](#)].
- [294] MACEDO, C. F., PANI, P., CARDOSO, V. AND CRISPINO, L. C. B., *Astrophysical signatures of boson stars: quasinormal modes and inspiral resonances*, *Phys.Rev.* **D88** (2013) 064046, [[1307.4812](#)].
- [295] MAGUEIJO, J., *New varying speed of light theories*, *Rept. Prog. Phys.* **66** (2003) 2025, [[astro-ph/0305457](#)].
- [296] MAJCZYNA, A., MADEJ, J., JOSS, P. C. AND ROZANSKA, A., *Model atmospheres and x-ray spectra of iron-rich bursting neutron stars. 2. Iron rich Comptonized spectra*, *Astron. Astrophys.* **430** (2005) 643, [[astro-ph/0412644](#)].
- [297] MAJUMDER, B., YAGI, K. AND YUNES, N., *Improved Universality in the Neutron Star Three-Hair Relations*, *Phys. Rev.* **D92** (2015) 024020, [[1504.02506](#)].
- [298] MANDEL, I., HASTER, C.-J., DOMINIK, M. AND BELCZYNSKI, K., *Distinguishing types of compact-object binaries using the gravitational-wave signatures of their mergers*, *Mon. Not. Roy. Astron. Soc.* **450** (2015) L85, [[1503.03172](#)].
- [299] MANDEL, I. AND O'SHAUGHNESSY, R., *Compact Binary Coalescences in the Band of Ground-based Gravitational-Wave Detectors*, *Class. Quant. Grav.* **27** (2010) 114007, [[0912.1074](#)].

- [300] MANOLIDIS, D., *Neutron Star Models in Alternative Theories of Gravity*. PhD thesis, Washington University in St. Louis, 2014.
- [301] MARTÍN-MORUNO, P., NUNES, N. J. AND LOBO, F. S. N., *Attracted to de Sitter: cosmology of the linear Horndeski models*, *JCAP* **1505** (2015) 033, [[1502.05878](#)].
- [302] MARTIN-MORUNO, P., NUNES, N. J. AND LOBO, F. S. N., *Horndeski theories self-tuning to a de Sitter vacuum*, *Phys. Rev.* **D91** (2015) 084029, [[1502.03236](#)].
- [303] MARTINEZ, J. G., STOVALL, K., FREIRE, P. C. C., DENEVA, J. S., JENET, F. A., MCLAUGHLIN, M. A. ET AL., *Pulsar J0453+1559: A Double Neutron Star System with a Large Mass Asymmetry*, *Astrophys. J.* **812** (2015) 143, [[1509.08805](#)].
- [304] MASELLI, A. ET AL., *in preparation*, .
- [305] MASELLI, A., PANI, P., GUALTIERI, L. AND FERRARI, V., *Rotating black holes in Einstein-Dilaton-Gauss-Bonnet gravity with finite coupling*, *Phys. Rev.* **D92** (2015) 083014, [[1507.00680](#)].
- [306] MASELLI, A., SILVA, H. O., MINAMITSUJI, M. AND BERTI, E., *Slowly rotating black hole solutions in Horndeski gravity*, *Phys. Rev.* **D92** (2015) 104049, [[1508.03044](#)].
- [307] MASELLI, A., SILVA, H. O., MINAMITSUJI, M. AND BERTI, E., *Neutron stars in Horndeski gravity*, *Phys. Rev.* **D93** (2016) 124056, [[1603.04876](#)].
- [308] MCDERMOTT, P. N., VAN HORN, H. M. AND SCHOLL, J. F., *Nonradial g-mode oscillations of warm neutron stars*, *ApJ* **268** (1983) 837.
- [309] MCMANUS, R., LOMBRISER, L. AND PEARRUBIA, J., *Finding Horndeski theories with Einstein gravity limits*, *JCAP* **1611** (2016) 006, [[1606.03282](#)].
- [310] MEHRA, J., *One month in the history of the discovery of general relativity theory*, *Foundations of Physics Letters* **11** (1998) 41.
- [311] MENDES, R. F. P., *Possibility of setting a new constraint to scalar-tensor theories*, *Phys. Rev.* **D91** (2015) 064024, [[1412.6789](#)].
- [312] MENDES, R. F. P., MATSAS, G. E. A. AND VANZELLA, D. A. T., *Instability of nonminimally coupled scalar fields in the spacetime of slowly rotating compact objects*, *Phys. Rev.* **D90** (2014) 044053, [[1407.6405](#)].
- [313] MENDES, R. F. P. AND ORTIZ, N., *Highly compact neutron stars in scalar-tensor theories of gravity: Spontaneous scalarization versus gravitational collapse*, *Phys. Rev.* **D93** (2016) 124035, [[1604.04175](#)].
- [314] MENDES, R. F., MATSAS, G. E. AND VANZELLA, D. A., *Quantum versus classical instability of scalar fields in curved backgrounds*, *Phys.Rev.* **D89** (2014) 047503, [[1310.2185](#)].

- [315] MESSIOS, N., PAPADOPOULOS, D. B. AND STERGIIOULAS, N., *Torsional oscillations of magnetized relativistic stars*, *Mon.Not.Roy.Astron.Soc.* **328** (2001) 1161, [[astro-ph/0105175](#)].
- [316] MILLER, M. C., *Astrophysical Constraints on Dense Matter in Neutron Stars*, [1312.0029](#).
- [317] MILLER, M. C. AND LAMB, F. K., *Determining Neutron Star Properties by Fitting Oblate-star Waveform Models to X-ray Burst Oscillations*, *Astrophys. J.* **808** (2015) 31, [[1407.2579](#)].
- [318] MILLER, M. C. AND MILLER, J. M., *The Masses and Spins of Neutron Stars and Stellar-Mass Black Holes*, *Phys.Rept.* **548** (2014) 1, [[1408.4145](#)].
- [319] MINAMITSUJI, M., *Black hole quasinormal modes in a scalar-tensor theory with field derivative coupling to the Einstein tensor*, *Gen. Rel. Grav.* **46** (2014) 1785, [[1407.4901](#)].
- [320] MINAMITSUJI, M., *Disformal transformation of cosmological perturbations*, *Phys. Lett.* **B737** (2014) 139, [[1409.1566](#)].
- [321] MINAMITSUJI, M., *Solutions in the scalar-tensor theory with nonminimal derivative coupling*, *Phys. Rev.* **D89** (2014) 064017, [[1312.3759](#)].
- [322] MIRSHEKARI, S. AND WILL, C. M., *Compact binary systems in scalar-tensor gravity: Equations of motion to 2.5 post-Newtonian order*, *Phys.Rev.* **D87** (2013) 084070, [[1301.4680](#)].
- [323] MISNER, C. W., THORNE, K. S. AND WHEELER, J. A., *Gravitation*. San Francisco: W.H. Freeman and Co., 1973.
- [324] MIYATSU, T., YAMAMURO, S. AND NAKAZATO, K., *A new equation of state for neutron star matter with nuclei in the crust and hyperons in the core*, *Astrophys. J.* **777** (2013) 4, [[1308.6121](#)].
- [325] MORA, T. AND WILL, C. M., *A PostNewtonian diagnostic of quasiequilibrium binary configurations of compact objects*, *Phys. Rev.* **D69** (2004) 104021, [[gr-qc/0312082](#)].
- [326] MOROIANU, A., *Lectures on Kähler Geometry*. Cambridge University Press, 2007.
- [327] MOTOHASHI, H. AND WHITE, J., *Disformal invariance of curvature perturbation*, *JCAP* **1602** (2016) 065, [[1504.00846](#)].
- [328] MUELLER, H. AND SEROT, B. D., *Relativistic mean field theory and the high density nuclear equation of state*, *Nucl.Phys.* **A606** (1996) 508, [[nucl-th/9603037](#)].
- [329] NELMES, S. AND PIETTE, B., *Phase Transition and Anisotropic Deformations of Neutron Star Matter*, *Phys.Rev.* **D85** (2012) 123004, [[1204.0910](#)].

- [330] NEVEU, J., RUHLMANN-KLEIDER, V., ASTIER, P., BESANCON, M., CONLEY, A., GUY, J. ET AL., *First experimental constraints on the disformally coupled Galileon model*, *Astron. Astrophys.* **569** (2014) A90, [[1403.0854](#)].
- [331] NEWTON, W. G., HOOKER, J., GEARHEART, M., MURPHY, K., WEN, D.-H., FATTOYEV, F. J. ET AL., *Constraints on the symmetry energy from observational probes of the neutron star crust*, *European Physical Journal A* **50** (Feb., 2014) 41, [[1506.02207](#)].
- [332] NICOLIS, A., RATTAZZI, R. AND TRINCHERINI, E., *The Galileon as a local modification of gravity*, *Phys. Rev.* **D79** (2009) 064036, [[0811.2197](#)].
- [333] NOJIRI, S. AND ODINTSOV, S. D., *Unified cosmic history in modified gravity: from $F(R)$ theory to Lorentz non-invariant models*, *Phys. Rept.* **505** (2011) 59, [[1011.0544](#)].
- [334] NOLLER, J., *Derivative Chameleons*, *JCAP* **1207** (2012) 013, [[1203.6639](#)].
- [335] NORDTVEDT, K. J. AND WILL, C. M., *Conservation Laws and Preferred Frames in Relativistic Gravity. II. Experimental Evidence to Rule Out Preferred-Frame Theories of Gravity*, *Astrophys.J.* **177** (1972) 775.
- [336] NOVAK, J., *Neutron star transition to strong scalar field state in tensor scalar gravity*, *Phys.Rev.* **D58** (1998) 064019, [[gr-qc/9806022](#)].
- [337] NOVAK, J., *Spherical neutron star collapse in tensor - scalar theory of gravity*, *Phys.Rev.* **D57** (1998) 4789, [[gr-qc/9707041](#)].
- [338] NOVAK, J. AND IBANEZ, J. M., *Gravitational waves from the collapse and bounce of a stellar core in tensor scalar gravity*, *Astrophys.J.* **533** (2000) 392, [[astro-ph/9911298](#)].
- [339] NUTKU, Y., *The Post-Newtonian Equations of Hydrodynamics in the Brans-Dicke Theory*, *ApJ* **155** (Mar., 1969) 999.
- [340] OGATA, S. AND ICHIMARU, S., *First-principles calculations of shear moduli for Monte Carlo-simulated Coulomb solids*, *Phys. Rev. A* **42** (Oct., 1990) 4867.
- [341] OGAWA, H., KOBAYASHI, T. AND SUYAMA, T., *Instability of hairy black holes in shift-symmetric Horndeski theories*, *Phys. Rev.* **D93** (2016) 064078, [[1510.07400](#)].
- [342] ONO, K., EDA, K. AND ITOH, Y., *New estimation method for mass of an isolated neutron star using gravitational waves*, *Phys. Rev.* **D91** (2015) 084032, [[1503.01231](#)].
- [343] OPPENHEIMER, J. R. AND VOLKOFF, G. M., *On massive neutron cores*, *Phys. Rev.* **55** (Feb, 1939) 374.
- [344] OYAMATSU, K. AND IIDA, K., *Saturation of nuclear matter and radii of unstable nuclei*, *Prog. Theor. Phys.* **109** (2003) 631, [[nucl-th/0204033](#)].

- [345] ÖZEL, F., BAYM, G. AND GÜVER, T., *Astrophysical Measurement of the Equation of State of Neutron Star Matter*, *Phys.Rev.* **D82** (2010) 101301, [[1002.3153](#)].
- [346] ÖZEL, F., PSALTIS, D., NARAYAN, R. AND MCCLINTOCK, J. E., *The Black Hole Mass Distribution in the Galaxy*, *Astrophys. J.* **725** (2010) 1918, [[1006.2834](#)].
- [347] PADILLA, A. AND SIVANESAN, V., *Covariant multi-galileons and their generalisation*, *JHEP* **04** (2013) 032, [[1210.4026](#)].
- [348] PALENZUELA, C., BARAUSSE, E., PONCE, M. AND LEHNER, L., *Dynamical scalarization of neutron stars in scalar-tensor gravity theories*, *Phys.Rev.* **D89** (2014) 044024, [[1310.4481](#)].
- [349] PALENZUELA, C. AND LIEBLING, S. L., *Constraining scalar-tensor theories of gravity from the most massive neutron stars*, *Phys. Rev.* **D93** (2016) 044009, [[1510.03471](#)].
- [350] PANDHARIPANDE, V. R., *Hyperonic matter*, *Nuclear Physics A* **178** (Dec., 1971) 123.
- [351] PANI, P., *Advanced Methods in Black-Hole Perturbation Theory*, *Int.J.Mod.Phys.* **A28** (2013) 1340018, [[1305.6759](#)].
- [352] PANI, P., *I-Love-Q relations for gravastars and the approach to the black-hole limit*, *Phys. Rev.* **D92** (2015) 124030, [[1506.06050](#)].
- [353] PANI, P. AND BERTI, E., *Slowly rotating neutron stars in scalar-tensor theories*, *Phys.Rev.* **D90** (2014) 024025, [[1405.4547](#)].
- [354] PANI, P., BERTI, E., CARDOSO, V., CHEN, Y. AND NORTE, R., *Gravitational wave signatures of the absence of an event horizon. I. Nonradial oscillations of a thin-shell gravastar*, *Phys. Rev.* **D80** (2009) 124047, [[0909.0287](#)].
- [355] PANI, P., BERTI, E., CARDOSO, V. AND READ, J., *Compact stars in alternative theories of gravity. Einstein-Dilaton-Gauss-Bonnet gravity*, *Phys. Rev.* **D84** (2011) 104035, [[1109.0928](#)].
- [356] PANI, P. AND CARDOSO, V., *Are black holes in alternative theories serious astrophysical candidates? The Case for Einstein-Dilaton-Gauss-Bonnet black holes*, *Phys.Rev.* **D79** (2009) 084031, [[0902.1569](#)].
- [357] PANI, P., CARDOSO, V., BERTI, E., READ, J. AND SALGADO, M., *The vacuum revealed: the final state of vacuum instabilities in compact stars*, *Phys.Rev.* **D83** (2011) 081501, [[1012.1343](#)].
- [358] PANI, P., DELSATE, T. AND CARDOSO, V., *Eddington-inspired Born-Infeld gravity. Phenomenology of non-linear gravity-matter coupling*, *Phys.Rev.* **D85** (2012) 084020, [[1201.2814](#)].

- [359] PANI, P., GUALTIERI, L. AND FERRARI, V., *Tidal Love numbers of a slowly spinning neutron star*, *Phys. Rev. D* **92** (2015) 124003, [[1509.02171](#)].
- [360] PANI, P., GUALTIERI, L., MASELLI, A. AND FERRARI, V., *Tidal deformations of a spinning compact object*, *Phys. Rev. D* **92** (2015) 024010, [[1503.07365](#)].
- [361] PAPPAS, G., *What can quasi-periodic oscillations tell us about the structure of the corresponding compact objects?*, *MNRAS* **422** (May, 2012) 2581, [[1201.6071](#)].
- [362] PAPPAS, G. AND SOTIRIOU, T. P., *Geodesic properties in terms of multipole moments in scalar-tensor theories of gravity*, *MNRAS* **453** (Nov., 2015) 2862, [[1505.02882](#)].
- [363] PAPPAS, G. AND SOTIRIOU, T. P., *Multipole moments in scalar-tensor theory of gravity*, *Phys. Rev. D* **91** (Feb., 2015) 044011, [[1412.3494](#)].
- [364] PAPPAS, G. AND APOSTOLATOS, T. A., *Effectively universal behavior of rotating neutron stars in general relativity makes them even simpler than their Newtonian counterparts*, *Phys. Rev. Lett.* **112** (2014) 121101, [[1311.5508](#)].
- [365] PAPPAS, G. AND SOTIRIOU, T. P., *Geodesic properties in terms of multipole moments in scalar-tensor theories of gravity*, *Mon. Not. Roy. Astron. Soc.* **453** (2015) 2862, [[1505.02882](#)].
- [366] PAPPAS, G. AND SOTIRIOU, T. P., *Multipole moments in scalar-tensor theory of gravity*, *Phys. Rev. D* **91** (2015) 044011, [[1412.3494](#)].
- [367] PEARSON, J. M., CHAMEL, N., GORIELY, S. AND DUCOIN, C., *Inner crust of neutron stars with mass-fitted Skyrme functionals*, *Phys. Rev. C* **85** (2012) 065803, [[1206.0205](#)].
- [368] PEARSON, J. M., GORIELY, S. AND CHAMEL, N., *Properties of the outer crust of neutron stars from Hartree-Fock-Bogoliubov mass models*, *Phys. Rev. C* **83** (2011) 065810.
- [369] POISSON, E. AND WILL, C., *Gravity: Newtonian, Post-Newtonian, Relativistic*. Cambridge University Press, 2014.
- [370] POLCHINSKI, J., *String theory*. Cambridge University Press, 1998.
- [371] PONCE, M., PALENZUELA, C., BARAUSSE, E. AND LEHNER, L., *Electromagnetic outflows in a class of scalar-tensor theories: Binary neutron star coalescence*, *Phys. Rev. D* **91** (2015) 084038, [[1410.0638](#)].
- [372] POPOV, S. B., BLASCHKE, D., GRIGORIAN, H. AND PROKHOROV, M. E., *Neutron star masses: dwarfs, giants and neighbors*, *Astrophys. Space Sci.* **308** (2007) 381, [[astro-ph/0606308](#)].

- [373] POSTNIKOV, S., PRAKASH, M. AND LATTIMER, J. M., *Tidal Love Numbers of Neutron and Self-Bound Quark Stars*, *Phys. Rev.* **D82** (2010) 024016, [[1004.5098](#)].
- [374] POTEKHIN, A. Y., DE LUCA, A. AND PONS, J. A., *Neutron stars - thermal emitters*, *Space Sci. Rev.* **191** (2015) 171, [[1409.7666](#)].
- [375] POTEKHIN, A. Y., FANTINA, A. F., CHAMEL, N., PEARSON, J. M. AND GORIELY, S., *Analytical representations of unified equations of state for neutron-star matter*, *Astron. Astrophys.* **560** (2013) A48, [[1310.0049](#)].
- [376] PSALTIS, D., *Probes and Tests of Strong-Field Gravity with Observations in the Electromagnetic Spectrum*, *Living Rev. Rel.* **11** (2008) 9, [[0806.1531](#)].
- [377] PSALTIS, D., *Testing General Metric Theories of Gravity with Bursting Neutron Stars*, *Phys. Rev.* **D77** (2008) 064006, [[0704.2426](#)].
- [378] PSALTIS, D. AND JOHANNSEN, T., *Sgr A*: The Optimal Testbed of Strong-Field Gravity*, *J. Phys. Conf. Ser.* **283** (2011) 012030, [[1012.1602](#)].
- [379] PSALTIS, D., ÖZEL, F. AND CHAKRABARTY, D., *Prospects for Measuring Neutron-Star Masses and Radii with X-Ray Pulse Profile Modeling*, *Astrophys. J.* **787** (2014) 136, [[1311.1571](#)].
- [380] PSALTIS, D., WEX, N. AND KRAMER, M., *A Quantitative Test of the No-Hair Theorem with Sgr A* using stars, pulsars, and the Event Horizon Telescope*, *Astrophys. J.* **818** (2016) 121, [[1510.00394](#)].
- [381] RAMAZANOĞLU, F. M. AND PRETORIUS, F., *Spontaneous Scalarization with Massive Fields*, *Phys. Rev.* **D93** (2016) 064005, [[1601.07475](#)].
- [382] RANDALL, L. AND SUNDRUM, R., *A large mass hierarchy from a small extra dimension*, *Phys. Rev. Lett.* **83** (1999) 3370, [[hep-ph/9905221](#)].
- [383] RANDALL, L. AND SUNDRUM, R., *An alternative to compactification*, *Phys. Rev. Lett.* **83** (1999) 4690, [[hep-th/9906064](#)].
- [384] RATRA, B. AND PEEBLES, P. J. E., *Cosmological Consequences of a Rolling Homogeneous Scalar Field*, *Phys. Rev.* **D37** (1988) 3406.
- [385] RAVENHALL, D. G. AND PETHICK, C. J., *Neutron star moments of inertia*, *ApJ* **424** (Apr., 1994) 846.
- [386] RAY, P. S., CHAKRABARTY, D., WILSON-HODGE, C. A., PHILIPS, B. F., REMILLARD, R. A. ET AL., *AXTAR: Mission Design Concept*, *Proc.SPIE Int.Soc.Opt.Eng.* **7732** (2010) 48, [[1007.0988](#)].
- [387] READ, J. S., BAIOTTI, L., CREIGHTON, J. D. E., FRIEDMAN, J. L., GIACOMAZZO, B., KYUTOKU, K. ET AL., *Matter effects on binary neutron star waveforms*, *Phys. Rev.* **D88** (2013) 044042, [[1306.4065](#)].

- [388] READ, J. S., MARKAKIS, C., SHIBATA, M., URYU, K., CREIGHTON, J. D. E. AND FRIEDMAN, J. L., *Measuring the neutron star equation of state with gravitational wave observations*, *Phys. Rev.* **D79** (2009) 124033, [0901.3258].
- [389] RINALDI, M., *Black holes with non-minimal derivative coupling*, *Phys. Rev.* **D86** (2012) 084048, [1208.0103].
- [390] RUDERMAN, M., *Pulsars: structure and dynamics*, *Ann.Rev.Astron.Astrophys.* **10** (1972) 427.
- [391] RYAN, F. D., *Gravitational waves from the inspiral of a compact object into a massive, axisymmetric body with arbitrary multipole moments*, *Phys. Rev. D* **52** (1995) 5707.
- [392] SAITO, R., YAMAUCHI, D., MIZUNO, S., GLEYZES, J. AND LANGLOIS, D., *Modified gravity inside astrophysical bodies*, *JCAP* **1506** (2015) 008, [1503.01448].
- [393] SAKSTEIN, J., *Disformal Theories of Gravity: From the Solar System to Cosmology*, *JCAP* **1412** (2014) 012, [1409.1734].
- [394] SAKSTEIN, J., *Hydrogen Burning in Low Mass Stars Constrains Scalar-Tensor Theories of Gravity*, *Phys. Rev. Lett.* **115** (2015) 201101, [1510.05964].
- [395] SAKSTEIN, J., *Testing Gravity Using Dwarf Stars*, *Phys. Rev.* **D92** (2015) 124045, [1511.01685].
- [396] SAKSTEIN, J., *Towards Viable Cosmological Models of Disformal Theories of Gravity*, *Phys. Rev.* **D91** (2015) 024036, [1409.7296].
- [397] SAKSTEIN, J. AND VERNER, S., *Disformal Gravity Theories: A Jordan Frame Analysis*, *Phys. Rev.* **D92** (2015) 123005, [1509.05679].
- [398] SALGADO, M., *The Cauchy problem of scalar tensor theories of gravity*, *Class.Quant.Grav.* **23** (2006) 4719, [gr-qc/0509001].
- [399] SALGADO, M., RIO, D. M.-D., ALCUBIERRE, M. AND NUNEZ, D., *Hyperbolicity of scalar-tensor theories of gravity*, *Phys. Rev.* **D77** (2008) 104010, [0801.2372].
- [400] SAMPSON, L., YUNES, N., CORNISH, N., PONCE, M., BARAUSSE, E. ET AL., *Projected Constraints on Scalarization with Gravitational Waves from Neutron Star Binaries*, **1407.7038**.
- [401] SAMUELSSON, L., *Stellar Models in General Relativity*. PhD thesis, Stockholm University, 2003.
- [402] SAMUELSSON, L. AND ANDERSSON, N., *Neutron Star Asteroseismology. Axial Crust Oscillations in the Cowling Approximation*, *Mon.Not.Roy.Astron.Soc.* **374** (2007) 256, [astro-ph/0609265].

- [403] SARIDAKIS, E. N. AND SUSHKOV, S. V., *Quintessence and phantom cosmology with non-minimal derivative coupling*, *Phys. Rev.* **D81** (2010) 083510, [1002.3478].
- [404] SATHYAPRAKASH, B. ET AL., *Scientific Objectives of Einstein Telescope*, *Class. Quant. Grav.* **29** (2012) 124013, [1206.0331].
- [405] SAWYER, R., *Condensed π -phase in neutron star matter*, *Phys.Rev.Lett.* **29** (1972) 382.
- [406] SCHUMAKER, B. L. AND THORNE, K. S., *Torsional oscillations of neutron stars*, *MNRAS* **203** (1983) 457.
- [407] SCHUNCK, F. AND MIELKE, E., *General relativistic boson stars*, *Class.Quant.Grav.* **20** (2003) R301, [0801.0307].
- [408] SCHWAB, J., HUGHES, S. A. AND RAPPAPORT, S., *The Self-Gravity of Pressure in Neutron Stars*, **0806.0798**.
- [409] SENNETT, N. AND BUONANNO, A., *Modeling dynamical scalarization with a resummed post-Newtonian expansion*, *Phys. Rev.* **D93** (2016) 124004, [1603.03300].
- [410] SEROT, B. D., *A relativistic nuclear field theory with π and ρ mesons*, *Physics Letters B* **86** (Sept., 1979) 146.
- [411] SHAM, Y. H., LIN, L. M. AND LEUNG, P., *Testing universal relations of neutron stars with a nonlinear matter-gravity coupling theory*, *Astrophys.J.* **781** (2014) 66, [1312.1011].
- [412] SHAPIRO, S. L. AND TEUKOLSKY, S. A., *Black Holes, White Dwarfs, and Neutron Stars: the Physics of Compact Objects*. John Wiley, 1983.
- [413] SHAPIRO, S. T. AND LIGHTMAN, A. P., *Rapidly rotating, post-Newtonian neutron stars*, *ApJ* **207** (1976) 263.
- [414] SHEN, H., TOKI, H., OYAMATSU, K. AND SUMIYOSHI, K., *Relativistic equation of state of nuclear matter for supernova and neutron star*, *Nucl. Phys.* **A637** (1998) 435, [nucl-th/9805035].
- [415] SHIBATA, M., TANIGUCHI, K., OKAWA, H. AND BUONANNO, A., *Coalescence of binary neutron stars in a scalar-tensor theory of gravity*, *Phys.Rev.* **D89** (2014) 084005, [1310.0627].
- [416] SHINKAI, H.-A., *Truncated post-Newtonian neutron star model*, *Phys.Rev.* **D60** (1999) 067504, [gr-qc/9807008].
- [417] SILVA, H. O., MACEDO, C. F. B., BERTI, E. AND CRISPINO, L. C. B., *Slowly rotating anisotropic neutron stars in general relativity and scalar-tensor theory*, *Class. Quant. Grav.* **32** (2015) 145008, [1411.6286].

- [418] SILVA, H. O., MASELLI, A., MINAMITSUJI, M. AND BERTI, E., *Compact objects in Horndeski gravity*, *Int. J. Mod. Phys. D* **25** (2016) 1641006, [1602.05997].
- [419] SILVA, H. O., SOTANI, H. AND BERTI, E., *Low-mass neutron stars: universal relations, the nuclear symmetry energy and gravitational radiation*, 1601.03407.
- [420] SILVA, H. O., SOTANI, H., BERTI, E. AND HORBATSCH, M., *Torsional oscillations of neutron stars in scalar-tensor theory of gravity*, *Phys. Rev. D* **90** (2014) 124044, [1410.2511].
- [421] KAGRA collaboration, SOMIYA, K., *Detector configuration of KAGRA: The Japanese cryogenic gravitational-wave detector*, *Class. Quant. Grav.* **29** (2012) 124007, [1111.7185].
- [422] SOTANI, H., KOKKOTAS, K. AND STERGIOULAS, N., *Torsional Oscillations of Relativistic Stars with Dipole Magnetic Fields*, *Mon.Not.Roy.Astron.Soc.* **375** (2007) 261, [astro-ph/0608626].
- [423] SOTANI, H., *Probing Tensor-Vector-Scalar Theory with Gravitational Wave Asteroseismology*, *Phys.Rev. D* **80** (2009) 064035, [0909.2411].
- [424] SOTANI, H., *Stellar Oscillations in Tensor-Vector-Scalar Theory*, *Phys.Rev. D* **79** (2009) 064033, [0903.2424].
- [425] SOTANI, H., *Slowly Rotating Relativistic Stars in Tensor-Vector-Scalar Theory*, *Phys.Rev. D* **81** (2010) 084006, [1003.2575].
- [426] SOTANI, H., *Toroidal oscillations of slowly rotating relativistic star in tensor-vector-scalar theory*, *Phys.Rev. D* **82** (2010) 124061, [1012.2143].
- [427] SOTANI, H., *Constraints on Pasta Structure of Neutron Stars from Oscillations in Giant Flares*, *Mon. Not. Roy. Astron. Soc.* **417** (2011) L70, [1106.2621].
- [428] SOTANI, H., *Torsional oscillations in tensor-vector-scalar theory*, *Phys.Rev. D* **83** (2011) 124030, [1106.3913].
- [429] SOTANI, H., *Slowly Rotating Relativistic Stars in Scalar-Tensor Gravity*, *Phys.Rev. D* **86** (2012) 124036, [1211.6986].
- [430] SOTANI, H., *Electron screening effects on crustal torsional oscillations*, *Phys.Lett. B* **730** (2014) 166, [1401.6977].
- [431] SOTANI, H., *Observational discrimination of Eddington-inspired Born-Infeld gravity from general relativity*, *Phys.Rev. D* **89** (2014) 104005, [1404.5369].
- [432] SOTANI, H., *Scalar gravitational waves from relativistic stars in scalar-tensor gravity*, *Phys. Rev. D* **89** (2014) 064031, [1402.5699].
- [433] SOTANI, H., *Stellar oscillations in Eddington-inspired Born-Infeld gravity*, *Phys.Rev. D* **89** (2014) 124037, [1406.3097].

- [434] SOTANI, H., *Magnetized relativistic stellar models in Eddington-inspired Born-Infeld gravity*, *Phys. Rev.* **D91** (2015) 084020, [[1503.07942](#)].
- [435] SOTANI, H., IIDA, K. AND OYAMATSU, K., *Constraining the density dependence of the nuclear symmetry energy from an X-ray bursting neutron star*, *Phys. Rev.* **C91** (2015) 015805, [[1501.01698](#)].
- [436] SOTANI, H., IIDA, K. AND OYAMATSU, K., *Possible identifications of newly observed magnetar quasi-periodic oscillations as crustal shear modes*, *New Astron.* **43** (2016) 80, [[1508.01728](#)].
- [437] SOTANI, H., IIDA, K., OYAMATSU, K. AND OHNISHI, A., *Mass and radius formulas for low-mass neutron stars*, *PTEP* **2014** (2014) 051E01, [[1401.0161](#)].
- [438] SOTANI, H. AND KOKKOTAS, K. D., *Probing strong-field scalar-tensor gravity with gravitational wave asteroseismology*, *Phys. Rev.* **D70** (2004) 084026, [[gr-qc/0409066](#)].
- [439] SOTANI, H. AND KOKKOTAS, K. D., *Stellar oscillations in scalar-tensor theory of gravity*, *Phys. Rev.* **D71** (2005) 124038, [[gr-qc/0506060](#)].
- [440] SOTANI, H., NAKAZATO, K., IIDA, K. AND OYAMATSU, K., *Effect of superfluidity on neutron star crustal oscillations*, *Mon.Not.Roy.Astron.Soc.* **428** (2013) L21, [[1210.0955](#)].
- [441] SOTANI, H., NAKAZATO, K., IIDA, K. AND OYAMATSU, K., *Possible Constraints on the Density Dependence of the Nuclear Symmetry Energy from Quasiperiodic Oscillations in Soft Gamma Repeaters*, *Mon. Not. Roy. Astron. Soc.* **434** (2013) 2060, [[1303.4500](#)].
- [442] SOTIRIOU, T. P., *Gravity and Scalar Fields*, [1404.2955](#).
- [443] SOTIRIOU, T. P., *Black Holes and Scalar Fields*, *Class. Quant. Grav.* **32** (2015) 214002, [[1505.00248](#)].
- [444] SOTIRIOU, T. P. AND FARAONI, V., *f(R) Theories Of Gravity*, *Rev. Mod. Phys.* **82** (2010) 451, [[0805.1726](#)].
- [445] SOTIRIOU, T. P. AND FARAONI, V., *Black holes in scalar-tensor gravity*, *Phys.Rev.Lett.* **108** (2012) 081103, [[1109.6324](#)].
- [446] SOTIRIOU, T. P. AND ZHOU, S.-Y., *Black hole hair in generalized scalar-tensor gravity*, *Phys. Rev. Lett.* **112** (2014) 251102, [[1312.3622](#)].
- [447] SOTIRIOU, T. P. AND ZHOU, S.-Y., *Black hole hair in generalized scalar-tensor gravity: An explicit example*, *Phys. Rev.* **D90** (2014) 124063, [[1408.1698](#)].
- [448] STAYKOV, K. V., DONEVA, D. D. AND YAZADJIEV, S. S., *Moment-of-inertiacompactness universal relations in scalar-tensor theories and \mathcal{R}^2 gravity*, *Phys. Rev.* **D93** (2016) 084010, [[1602.00504](#)].

- [449] STAYKOV, K. V., DONEVA, D. D., YAZADJIEV, S. S. AND KOKKOTAS, K. D., *Slowly rotating neutron and strange stars in R^2 gravity*, *Journal of Cosmology and Astroparticle Physics* **2014** (2014) 006, [[1407.2180](#)].
- [450] STEFANOV, I. Z., YAZADJIEV, S. S. AND TODOROV, M. D., *Phases of 4D scalar-tensor black holes coupled to Born-Infeld nonlinear electrodynamics*, *Mod. Phys. Lett.* **A23** (2008) 2915, [[0708.4141](#)].
- [451] STEINER, A. W., GANDOLFI, S., FATTOYEV, F. J. AND NEWTON, W. G., *Using Neutron Star Observations to Determine Crust Thicknesses, Moments of Inertia, and Tidal Deformabilities*, *Phys. Rev.* **C91** (2015) 015804, [[1403.7546](#)].
- [452] STEINER, A. W., LATTIMER, J. M. AND BROWN, E. F., *The Equation of State from Observed Masses and Radii of Neutron Stars*, *Astrophys. J.* **722** (2010) 33, [[1005.0811](#)].
- [453] STEINER, A. W., LATTIMER, J. M. AND BROWN, E. F., *The Neutron Star Mass-Radius Relation and the Equation of State of Dense Matter*, *Astrophys. J.* **765** (2013) L5, [[1205.6871](#)].
- [454] STEINER, A. W., PRAKASH, M., LATTIMER, J. M. AND ELLIS, P. J., *Isospin asymmetry in nuclei and neutron stars*, *Phys. Rept.* **411** (2005) 325, [[nucl-th/0410066](#)].
- [455] STELLA, L. AND VIETRI, M., *Lense-Thirring Precession and Quasi-periodic Oscillations in Low-Mass X-Ray Binaries*, *ApJ* **492** (Jan., 1998) L59, [[astro-ph/9709085](#)].
- [456] STELLA, L. AND VIETRI, M., *khz quasiperiodic oscillations in low-mass x-ray binaries as probes of general relativity in the strong-field regime*, *Phys. Rev. Lett.* **82** (1999) 17.
- [457] STERGIOULAS, N., *Rotating stars in relativity*, *Living Rev. Relativ.* **6** (2003) 3, [[gr-qc/0302034](#)].
- [458] STEVENSON, S., OHME, F. AND FAIRHURST, S., *Distinguishing compact binary population synthesis models using gravitational-wave observations of coalescing binary black holes*, *Astrophys. J.* **810** (2015) 58, [[1504.07802](#)].
- [459] STROBEL, K., SCHAAB, C. AND WEIGEL, M. K., *Properties of nonrotating and rapidly rotating protoneutron stars*, *Astron. Astrophys.* **350** (1999) 497, [[astro-ph/9908132](#)].
- [460] STROHMAYER, T., VAN HORN, H. M., OGATA, S., IYETOMI, H. AND ICHIMARU, S., *The shear modulus of the neutron star crust and nonradial oscillations of neutron stars*, *ApJ* **375** (1991) 679.

- [461] STROHMAYER, T. E. AND WATTS, A. L., *Discovery of fast x-ray oscillations during the 1998 giant flare from SGR 1900+14*, *Astrophys.J.* **632** (2005) L111, [[astro-ph/0508206](#)].
- [462] STROHMAYER, T. E. AND WATTS, A. L., *The 2004 Hyperflare from SGR 1806-20: Further Evidence for Global Torsional Vibrations*, *Astrophys.J.* **653** (2006) 593, [[astro-ph/0608463](#)].
- [463] SULEIMANOV, V., POUTANEN, J. AND WERNER, K., *X-ray bursting neutron star atmosphere models: spectra and color corrections*, *Astron. Astrophys.* **527** (2011) A139, [[1009.6147](#)].
- [464] SULEIMANOV, V., POUTANEN, J., REVNIVTSEV, M. AND WERNER, K., *Neutron star stiff equation of state derived from cooling phases of the X-ray burster 4U 1724-307*, *Astrophys. J.* **742** (2011) 122, [[1004.4871](#)].
- [465] SUMIYOSHI, K., IBÁÑEZ, J. M. AND ROMERO, J. V., *Thermal history and structure of rotating protoneutron stars with relativistic equation of state*, *A&AS* **134** (Jan., 1999) 39.
- [466] SUSHKOV, S. V., *Exact cosmological solutions with nonminimal derivative coupling*, *Phys. Rev.* **D80** (2009) 103505, [[0910.0980](#)].
- [467] TAKAHASHI, T. ET AL., *The ASTRO-H X-ray Observatory*, *Proc. SPIE Int. Soc. Opt. Eng.* **8443** (2012) 1Z, [[1210.4378](#)].
- [468] TALUKDER, D., THRANE, E., BOSE, S. AND REGIMBAU, T., *Measuring neutron-star ellipticity with measurements of the stochastic gravitational-wave background*, *Phys. Rev.* **D89** (2014) 123008, [[1404.4025](#)].
- [469] TANIGUCHI, K., ASADA, H. AND SHIBATA, M., *Irrotational and incompressible ellipsoids in the first post-Newtonian approximation of general relativity*, *Prog.Theor.Phys.* **100** (1998) 703, [[gr-qc/9809039](#)].
- [470] TANIGUCHI, K., SHIBATA, M. AND BUONANNO, A., *Quasiequilibrium sequences of binary neutron stars undergoing dynamical scalarization*, *Phys. Rev.* **D91** (2015) 024033, [[1410.0738](#)].
- [471] TAURIS, T. M., LANGER, N. AND PODSIADLOWSKI, P., *Ultra-stripped supernovae: progenitors and fate*, *Mon. Not. Roy. Astron. Soc.* **451** (2015) 2123, [[1505.00270](#)].
- [472] TOOPER, R. F., *General Relativistic Polytropic Fluid Spheres.*, *ApJ* **140** (1964) 434.
- [473] TOOPER, R. F., *Adiabatic Fluid Spheres in General Relativity.*, *ApJ* **142** (1965) 1541.
- [474] TSANG, M. B. ET AL., *Constraints on the symmetry energy and neutron skins from experiments and theory*, *Phys. Rev.* **C86** (2012) 015803, [[1204.0466](#)].

- [475] TSANG, M. B., ZHANG, Y., DANIELEWICZ, P., FAMIANO, M., LI, Z., LYNCH, W. G. ET AL., *Constraints on the density dependence of the symmetry energy*, *Phys. Rev. Lett.* **102** (2009) 122701, [[0811.3107](#)].
- [476] TSUJIKAWA, S., *Modified gravity models of dark energy*, *Lect. Notes Phys.* **800** (2010) 99, [[1101.0191](#)].
- [477] TSUJIKAWA, S., *Disformal invariance of cosmological perturbations in a generalized class of Horndeski theories*, *JCAP* **1504** (2015) 043, [[1412.6210](#)].
- [478] TUROLLA, R., ZANE, S. AND WATTS, A., *Magnetars: the physics behind observations. A review*, *Rept. Prog. Phys.* **78** (2015) 116901, [[1507.02924](#)].
- [479] URBANEC, M., MILLER, J. C. AND STUHLIK, Z., *Quadrupole moments of rotating neutron stars and strange stars*, *Mon. Not. Roy. Astron. Soc.* **433** (2013) 1903, [[1301.5925](#)].
- [480] VAINSHTEIN, A., *To the problem of nonvanishing gravitation mass*, *Phys.Lett.* **B39** (1972) 393.
- [481] VAN DE BRUCK, C. AND MORRICE, J., *Disformal couplings and the dark sector of the universe*, *JCAP* **1504** (2015) 036, [[1501.03073](#)].
- [482] VAN DE BRUCK, C., KOIVISTO, T. AND LONGDEN, C., *Disformally coupled inflation*, *JCAP* **1603** (2016) 006, [[1510.01650](#)].
- [483] VAN DE BRUCK, C., MIFSUD, J. AND NUNES, N. J., *The variation of the fine-structure constant from disformal couplings*, *JCAP* **1512** (2015) 018, [[1510.00200](#)].
- [484] VAN DE BRUCK, C., MORRICE, J. AND VU, S., *Constraints on Nonconformal Couplings from the Properties of the Cosmic Microwave Background Radiation*, *Phys. Rev. Lett.* **111** (2013) 161302, [[1303.1773](#)].
- [485] VAVOULIDIS, M., STAVRIDIS, A., KOKKOTAS, K. AND BEYER, H. R., *Torsional Oscillations of Slowly Rotating Relativistic Stars*, *Mon.Not.Roy.Astron.Soc.* **377** (2007) 1553, [[gr-qc/0703039](#)].
- [486] VELTEN, H., OLIVEIRA, A. M. AND WOJNAR, A., *A free parametrized TOV: Modified Gravity from Newtonian to Relativistic Stars*, *PoS MPC2015* (2016) 025, [[1601.03000](#)].
- [487] VINES, J., FLANAGAN, E. E. AND HINDERER, T., *Post-1-Newtonian tidal effects in the gravitational waveform from binary inspirals*, *Phys. Rev.* **D83** (2011) 084051, [[1101.1673](#)].
- [488] VOLKOV, M. S., *Hairy black holes in the XX-th and XXI-st centuries*, [1601.08230](#).

- [489] WADE, L., CREIGHTON, J. D. E., OCHSNER, E., LACKEY, B. D., FARR, B. F., LITTENBERG, T. B. ET AL., *Systematic and statistical errors in a bayesian approach to the estimation of the neutron-star equation of state using advanced gravitational wave detectors*, *Phys. Rev.* **D89** (2014) 103012, [[1402.5156](#)].
- [490] WAGONER, R. V. AND MALONE, R. C., *Post-Newtonian Neutron Stars*, *ApJ* **189** (1974) L75.
- [491] WAGONER, R. V., *Scalar tensor theory and gravitational waves*, *Phys.Rev.* **D1** (1970) 3209.
- [492] WATANABE, Y., NARUKO, A. AND SASAKI, M., *Multi-disformal invariance of non-linear primordial perturbations*, *Europhys. Lett.* **111** (2015) 39002, [[1504.00672](#)].
- [493] WATTS, A., XU, R., ESPINOZA, C., ANDERSSON, N., ANTONIADIS, J. ET AL., *Probing the neutron star interior and the Equation of State of cold dense matter with the SKA*, [1501.00042](#).
- [494] WATTS, A. L., *Neutron starquakes and the dynamic crust*, [1111.0514](#).
- [495] WEINBERG, S., *The Cosmological Constant Problem*, *Rev. Mod. Phys.* **61** (1989) 1.
- [496] WEX, N., *Testing Relativistic Gravity with Radio Pulsars*, [1402.5594](#).
- [497] WILL, C. M. AND ZAGLAUER, H. W., *Gravitational Radiation, Close Binary Systems, and the Brans-dicke Theory of Gravity*, *Astrophys. J.* **346** (1989) 366.
- [498] WILL, C. M., *The Confrontation between general relativity and experiment*, *Living Rev. Rel.* **9** (2006) 3, [[gr-qc/0510072](#)].
- [499] WILL, C. M., *The Confrontation between General Relativity and Experiment*, *Living Rev. Rel.* **17** (2014) 4, [[1403.7377](#)].
- [500] WILL, C. M., *The Confrontation between General Relativity and Experiment*, *Living Rev.Rel.* **17** (2014) 4, [[1403.7377](#)].
- [501] WILL, C. M. AND NORDTVEDT, J., KENNETH, *Conservation Laws and Preferred Frames in Relativistic Gravity. I. Preferred-Frame Theories and an Extended PPN Formalism*, *Astrophys.J.* **177** (1972) 757.
- [502] WILL, C., *Theory and Experiment in Gravitational Physics*. Cambridge University Press, 1993.
- [503] WILL, C., *Was Einstein Right?: Putting General Relativity to the Test*. Basic Books, 1993.
- [504] WILLIAMS, J. G., TURYSHEV, S. G. AND BOGGS, D. H., *Lunar laser ranging tests of the equivalence principle with the earth and moon*, *Int.J.Mod.Phys.* **D18** (2009) 1129, [[gr-qc/0507083](#)].

- [505] WOODARD, R. P., *Ostrogradsky's theorem on Hamiltonian instability*, *Scholarpedia* **10** (2015) 32243, [[1506.02210](#)].
- [506] XIE, Y., NI, W.-T., DONG, P. AND HUANG, T.-Y., *Second post-Newtonian approximation of scalar-tensor theory of gravity*, *Adv.Space Res.* **43** (2009) 171, [[0704.2991](#)].
- [507] YAGI, K. private communication, 2016.
- [508] YAGI, K., BLAS, D., BARAUSSE, E. AND YUNES, N., *Constraints on Einstein-Æther theory and Hořava gravity from binary pulsar observations*, *Phys.Rev.* **D89** (2014) 084067, [[1311.7144](#)].
- [509] YAGI, K., BLAS, D., YUNES, N. AND BARAUSSE, E., *Strong Binary Pulsar Constraints on Lorentz Violation in Gravity*, *Phys.Rev.Lett.* **112** (2014) 161101, [[1307.6219](#)].
- [510] YAGI, K., KYUTOKU, K., PAPPAS, G., YUNES, N. AND APOSTOLATOS, T. A., *Effective No-Hair Relations for Neutron Stars and Quark Stars: Relativistic Results*, *Phys. Rev.* **D89** (2014) 124013, [[1403.6243](#)].
- [511] YAGI, K., STEIN, L. C., PAPPAS, G., YUNES, N. AND APOSTOLATOS, T. A., *Why I-Love-Q: Explaining why universality emerges in compact objects*, *Phys. Rev.* **D90** (2014) 063010, [[1406.7587](#)].
- [512] YAGI, K., STEIN, L. C. AND YUNES, N., *Challenging the Presence of Scalar Charge and Dipolar Radiation in Binary Pulsars*, *Phys. Rev.* **D93** (2016) 024010, [[1510.02152](#)].
- [513] YAGI, K., STEIN, L. C., YUNES, N. AND TANAKA, T., *Post-Newtonian, Quasi-Circular Binary Inspirals in Quadratic Modified Gravity*, *Phys.Rev.* **D85** (2012) 064022, [[1110.5950](#)].
- [514] YAGI, K. AND YUNES, N., *I-Love-Q*, *Science* **341** (2013) 365, [[1302.4499](#)].
- [515] YAGI, K. AND YUNES, N., *I-Love-Q Relations in Neutron Stars and their Applications to Astrophysics, Gravitational Waves and Fundamental Physics*, *Phys. Rev.* **D88** (2013) 023009, [[1303.1528](#)].
- [516] YAGI, K. AND YUNES, N., *Love can be Tough to Measure*, *Phys. Rev. D* **89** (2014) 021303, [[1310.8358](#)].
- [517] YAGI, K. AND YUNES, N., *I-Love-Q anisotropically: Universal relations for compact stars with scalar pressure anisotropy*, *Phys. Rev.* **D91** (2015) 123008, [[1503.02726](#)].
- [518] YAGI, K. AND YUNES, N., *Relating follicly-challenged compact stars to bald black holes: A link between two no-hair properties*, *Phys. Rev.* **D91** (2015) 103003, [[1502.04131](#)].

- [519] YAGI, K. AND YUNES, N., *Binary Love Relations*, *Class. Quant. Grav.* **33** (2016) 13LT01, [[1512.02639](#)].
- [520] YAGI, K. AND YUNES, N., *I-Love-Q Relations: From Compact Stars to Black Holes*, *Class. Quant. Grav.* **33** (2016) 095005, [[1601.02171](#)].
- [521] YASUDA, J. ET AL., *Extraction of anti-analog giant dipole resonance and neutron skin thickness for ^{208}Pb* , *PTEP* **2013** (2013) 063D02.
- [522] YAZADJIEV, S., *Relativistic models of magnetars: Nonperturbative analytical approach*, *Phys. Rev.* **D85** (2012) 044030, [[1111.3536](#)].
- [523] YAZADJIEV, S. S., DONEVA, D. D. AND POPCHEV, D., *Slowly rotating neutron stars in scalar-tensor theories with a massive scalar field*, *Phys. Rev.* **D93** (2016) 084038, [[1602.04766](#)].
- [524] YUNES, N., PANI, P. AND CARDOSO, V., *Gravitational Waves from Quasicircular Extreme Mass-Ratio Inspirals as Probes of Scalar-Tensor Theories*, *Phys. Rev.* **D85** (2012) 102003, [[1112.3351](#)].
- [525] YUNES, N. AND PRETORIUS, F., *Fundamental Theoretical Bias in Gravitational Wave Astrophysics and the Parameterized Post-Einsteinian Framework*, *Phys. Rev.* **D80** (2009) 122003, [[0909.3328](#)].
- [526] YUNES, N. AND SIEMENS, X., *Gravitational-Wave Tests of General Relativity with Ground-Based Detectors and Pulsar Timing-Arrays*, *Living Rev. Rel.* **16** (2013) 9, [[1304.3473](#)].
- [527] YUNES, N., YAGI, K. AND PRETORIUS, F., *Theoretical Physics Implications of the Binary Black-Hole Mergers GW150914 and GW151226*, *Phys. Rev.* **D94** (2016) 084002, [[1603.08955](#)].
- [528] ZAGLAUER, H., *Neutron stars and gravitational scalars*, *Astrophys. J.* **393** (1992) 685.
- [529] EXTP collaboration, ZHANG, S. N. ET AL., *eXTP – enhanced X-ray Timing and Polarimetry Mission*, *Proc. SPIE Int. Soc. Opt. Eng.* **9905** (2016) 99051Q, [[1607.08823](#)].
- [530] ZHANG, X., ZHAO, W., HUANG, H. AND CAI, Y., *Post-Newtonian parameters and cosmological constant of screened modified gravity*, *Phys. Rev.* **D93** (2016) 124003, [[1603.09450](#)].
- [531] ZUMALACARREGUI, M., KOIVISTO, T. S., MOTA, D. F. AND RUIZ-LAPUENTE, P., *Disformal Scalar Fields and the Dark Sector of the Universe*, *JCAP* **1005** (2010) 038, [[1004.2684](#)].
- [532] ZUMALACÁRREGUI, M. AND GARCÍA-BELLIDO, J., *Transforming gravity: from derivative couplings to matter to second-order scalar-tensor theories beyond the Horndeski Lagrangian*, *Phys. Rev.* **D89** (2014) 064046, [[1308.4685](#)].

- [533] ZUMALACARREGUI, M., KOIVISTO, T. S. AND MOTA, D. F., *DBI Galileons in the Einstein Frame: Local Gravity and Cosmology*, *Phys. Rev.* **D87** (2013) 083010, [[1210.8016](#)].

APPENDICES

APPENDIX A

DIMENSIONAL ANALYSIS OF POST-NEWTONIAN TERMS

In this appendix we develop an algorithm for constructing PN terms using dimensional analysis techniques. Barring PN terms involving the three potentials U , E , Ω , the available parameters for generating PN terms are $\{p, \rho, m, r, \Pi\}$. From these quantities plus the gravitational constant G and the speed of light c we can build the dimensionless combination¹:

$$\Lambda = p^\alpha \rho^\beta m^\gamma r^\delta \Pi^\theta G^\kappa c^\lambda, \quad (\text{A.1})$$

for a suitable choice of integers $\alpha, \beta, \gamma, \delta, \kappa, \lambda$ (these are not to be confused with the PPN parameters of Section 3.2). Since Π is already dimensionless, there is no a priori dimensional restriction on θ (apart from one coming from the PN order of Λ) and therefore that factor can be omitted in the dimensional analysis. Using the scalings

$$p \sim G \frac{m\rho}{r}, \quad m \sim \rho r^3, \quad (\text{A.2})$$

we obtain the following form for Λ in terms of mass, length and time dimensions:

$$\Lambda \sim [M]^{\alpha+\beta+\gamma-\kappa} [L]^{-\alpha+\delta-3\beta+\lambda+3\kappa} [T]^{-2\alpha-\lambda-2\kappa}. \quad (\text{A.3})$$

Since Λ is required to be dimensionless, we have the three algebraic relations:

$$\lambda = -2(\alpha + \kappa), \quad \kappa = \alpha + \beta + \gamma, \quad (\text{A.4})$$

and

$$-\alpha + \delta - 3\beta + \lambda + 3\kappa = 0. \quad (\text{A.5})$$

The first two relations simply express λ and κ in terms of the other parameters. Using them in (A.5) we obtain

$$\gamma + \delta = 2(\alpha + \beta), \quad (\text{A.6})$$

¹Note that this combination is oblivious to the presence of dimensional coupling constants that might appear in modified theories of gravity.

which represents the true dimensional degree of freedom. It is straightforward (if tedious) to verify that all PN terms appearing in the PPN equations of Section 3.2 are consistent with (A.6).

All $\alpha < 0$ terms are divergent at the surface and need not be considered. As we shall shortly see, all terms with $\alpha \geq 4$ are divergent at $r = 0$ in both structure equations, and therefore should be discarded. The $\alpha = 3$ terms are singular in the dp/dr equation and can be discarded by the same argument; $\alpha = 3$ terms are regular in the dm/dr equation, but they are always dominated in magnitude by the $\alpha < 3$ terms, and therefore will not be presented in detail here. Therefore our strategy hereafter is to focus on the particular cases $\alpha = 0$ (no pressure dependence) and $\alpha = 1, 2$ (linear and quadratic scaling with the pressure).

A.1 Terms with $\alpha = 0$

Starting with the $\alpha = 0$ case we have

$$\gamma + \delta = 2\beta. \tag{A.7}$$

The resulting form of Λ in geometric units is

$$\Lambda \sim (r^2\rho)^\beta \left(\frac{m}{r}\right)^\gamma. \tag{A.8}$$

Formally, this combination is of order $(m/r)^{\beta+\gamma}$. Therefore, we can generate N -PN terms if $\beta + \gamma = N$. These are of the form

$$\Lambda_N(\beta) \sim (r^2\rho)^\beta \left(\frac{m}{r}\right)^{N-\beta}, \tag{A.9}$$

with $\beta = 0, \pm 1, \pm 2, \dots$. For instance, the first few 1PN and 2PN terms of this series are (we start from $\beta = -1$ for reasons explained below):

$$\Lambda_1(-1) \sim \frac{m^2}{r^4 \rho}, \quad \Lambda_1(0) \sim \frac{m}{r}, \quad \Lambda_1(1) \sim r^2 \rho, \quad (\text{A.10})$$

$$\Lambda_2(-1) \sim \frac{m^3}{r^5 \rho}, \quad \Lambda_2(0) \sim \frac{m^2}{r^2}, \quad \Lambda_2(1) \sim r \rho m. \quad (\text{A.11})$$

A.2 Terms with $\alpha = 1$

The $\alpha = 1$ group of terms can be obtained with the same procedure. We have

$$\gamma + \delta = 2(1 + \beta), \quad (\text{A.12})$$

and this leads to terms of the form

$$\Lambda \sim r^2 p (r^2 \rho)^\beta \left(\frac{m}{r}\right)^\gamma. \quad (\text{A.13})$$

Since $r^2 p$ is a 2PN term, the resulting N -PN combination should take the form:

$$\Lambda_N(\beta) \sim r^2 p (r^2 \rho)^\beta \left(\frac{m}{r}\right)^{N-2-\beta}. \quad (\text{A.14})$$

The first few 1PN and 2PN terms generated from this expression are:

$$\Lambda_1(-1) \sim \frac{p}{\rho}, \quad \Lambda_1(0) \sim \frac{r^3 p}{m}, \quad \Lambda_1(1) \sim \frac{r^6 \rho p}{m^2}, \quad (\text{A.15})$$

$$\Lambda_2(-1) \sim \frac{pm}{\rho r}, \quad \Lambda_2(0) \sim r^2 p, \quad \Lambda_2(1) \sim \frac{r^5 \rho p}{m}. \quad (\text{A.16})$$

A.3 Terms with $\alpha = 2$

Finally, we consider the $\alpha = 2$ terms. The corresponding Λ_N combination is,

$$\Lambda_N(\beta) = (r^2 p)^2 (r^2 \rho)^\beta \left(\frac{m}{r}\right)^{N-4-\beta}, \quad (\text{A.17})$$

and from this we have:

$$\Lambda_1(-1) \sim \frac{r^4 p^2}{m^2 \rho}, \quad \Lambda_1(0) \sim \frac{r^7 p^2}{m^3}, \quad (\text{A.18})$$

$$\Lambda_2(-1) \sim \frac{r^3 p^2}{\rho m}, \quad \Lambda_2(0) \sim \frac{r^6 p^2}{m^2}. \quad (\text{A.19})$$

A.4 Generic N -PN order terms and constraints.

It is now not too difficult to see that a N -PN order term with an arbitrary p^α scaling and with Π re-introduced is given by the universal formula,

$$\Lambda_N(\alpha, \beta, \theta) \sim \Pi^\theta (r^2 p)^\alpha (r^2 \rho)^\beta \left(\frac{m}{r}\right)^{N-2\alpha-\beta-\theta}. \quad (\text{A.20})$$

As discussed in Section 3.3.2, different threads of reasoning lead to the constraint $\beta \geq -1$. The first one has to do with avoiding a divergence at the stellar surface (this already has allowed us to filter out all $\alpha < 0$ terms). An inspection of the two stellar structure equations reveals that terms with $\alpha = \theta = 0$ should scale as

$$\rho \Lambda_N(0, \beta, 0) \sim \rho^{1+\beta}, \quad (\text{A.21})$$

in the vicinity of the surface, and therefore we ought to take $\beta \geq -1$ in order to avoid a surface singularity. This argument still allows for $\beta < -1$ values in the Λ_N terms with $\alpha, \theta > 0$, since these terms have a smoother profile as a result of the vanishing of p and Π at

the surface.

The second thread is no more than a heuristic argument and has to do with the expectation that for a broad family of gravity theories the solution for the metric (and its derivatives) should scale as $\sim (\epsilon + \tau p)^n = \rho^n (1 + \Pi + \tau p/\rho)^n$ with the fluid parameters (where τ and n are $\mathcal{O}(1)$ numbers). From this it follows that negative powers of ρ will come in the form of dimensionless PN terms $\sim \rho^{n-1} (p/\rho)^k$, where $k = n, n-1, \dots$ (note that a factor ρ has been absorbed by the Newtonian prefactor in the structure equations). As a consequence, ρ^{-1} is the only possible negative power in a PN expansion. Obviously, this argument automatically takes care of the regularity of any $\Lambda_N(\alpha, \beta, \theta)$ term at the surface.

The exclusion of all $\alpha \geq 4$ terms comes about as a consequence of regularity at the stellar center. Near the origin (where p, ρ, Π take finite non-zero values) a $\Lambda_N(\alpha, \beta, \theta)$ term behaves as

$$\Lambda_N(r \rightarrow 0) \sim r^{2(N-\alpha-\theta)}. \quad (\text{A.22})$$

The corresponding terms in the stellar structure equations will behave as

$$\frac{dp}{dr} \sim \frac{\rho m}{r^2} \Lambda_N \sim r^{2(N-\alpha-\theta)+1}, \quad (\text{A.23})$$

$$\frac{dm}{dr} \sim r^2 \rho \Lambda_N \sim r^{2(N-\alpha-\theta+1)}. \quad (\text{A.24})$$

and therefore regularity at the center dictates the following limits for each equation:

$$\frac{dp}{dr} : \quad 0 \leq \alpha \leq N - \theta, \quad (\text{A.25})$$

$$\frac{dm}{dr} : \quad 0 \leq \alpha \leq N + 1 - \theta. \quad (\text{A.26})$$

We can also see that these conditions entail the following limits for θ :

$$\frac{dp}{dr} : \quad 0 \leq \theta \leq N, \quad \frac{dm}{dr} : \quad 0 \leq \theta \leq N + 1. \quad (\text{A.27})$$

For the particular case of 2PN order terms we then have:

$$\frac{dp}{dr} : \quad 0 \leq \theta \leq 2, \quad 0 \leq \alpha \leq 2 - \theta, \quad (\text{A.28})$$

$$\frac{dm}{dr} : \quad 0 \leq \theta \leq 3, \quad 0 \leq \alpha \leq 3 - \theta, \quad (\text{A.29})$$

which shows that all $\alpha \geq 4$ terms are to be excluded and that $\alpha = 3$ terms can only appear in the mass equation.

APPENDIX B

THE NEWTONIAN AND RELATIVISTIC LANE-EMDEN EQUATIONS

In this appendix we review the nonrelativistic and relativistic Lane-Emden equations. The former equation is classic textbook material (see e.g. [90]) and therefore is just sketched here. The somewhat less familiar relativistic extension was developed by Tooper [472, 473] and is discussed in some more details. Our definition for the polytropic EOS, i.e. $p = K\rho^{1+1/n}$, is the same as the one adopted in [473] but is different to the one used in Tooper’s earlier paper [472], i.e. $p = K\epsilon^{1+1/n}$. This subtle difference, combined with the choice between p_c/ρ_c or p_c/ϵ_c (the “c” index refers to the stellar center) for the scale of the system, leads to slightly different Lane-Emden equations.

B.1 The Newtonian Lane-Emden equation

In Newtonian gravity, one can express the hydrostatic equilibrium equation for spherical non-rotating stars in terms of dimensionless parameters for the pressure, the density and the radial coordinate. If the EOS is polytropic (i.e., according to our definition, $p = K\rho^{1+1/n}$) the equations governing the dimensionless quantities are scale-invariant, depending only on the polytropic index n . By writing the density and the pressure as

$$\theta^n \equiv \frac{\rho}{\rho_c}, \quad p = K\rho_c^{1+1/n}\theta^{n+1}, \quad (\text{B.1})$$

and introducing the dimensionless radial coordinate

$$r = \alpha\xi, \quad \alpha \equiv \left[\frac{(n+1)K}{4\pi G} \rho_c^{-1+1/n} \right]^{1/2}, \quad (\text{B.2})$$

the Newtonian stellar structure equations

$$\frac{dp}{dr} = -\frac{Gm_{\text{N}}}{r^2}\rho, \quad (\text{B.3})$$

$$\frac{dm_{\text{N}}}{dr} = 4\pi r^2\rho, \quad (\text{B.4})$$

lead to

$$\frac{1}{\xi^2} \frac{d}{d\xi} \left(\xi^2 \frac{d\theta}{d\xi} \right) = -\theta^n. \quad (\text{B.5})$$

This is the famous Lane-Emden equation, and its scale-invariant solutions describe all possible fluid configurations in terms of the single parameter n .

B.2 The relativistic Lane-Emden equations

Generalizing the Lane-Emden formalism to GR is a straightforward task, but this comes at the price of losing the scale-invariance property of the Newtonian treatment. In relativity we can define the polytropic EOS in the same way as before, where ρ is the baryonic rest mass density. The polytropic exponent is defined as

$$\Gamma = 1 + \frac{1}{n} = \frac{\rho dp}{p d\rho} = \frac{\epsilon + p dp}{p d\epsilon}. \quad (\text{B.6})$$

Then the energy density ϵ and the internal energy Π are given by

$$\epsilon = \rho + np, \quad (\text{B.7})$$

which implies

$$\Pi = n \frac{p}{\rho}. \quad (\text{B.8})$$

This observation was used in the argument leading to Eq. (3.52).

We can now introduce the relativistic version of the Lane-Emden equations. In analogy with the Newtonian case we define $\rho = \rho_c \theta^n$, $r = a\xi$, and $p = K \rho_c^{1+1/n} \theta^{n+1}$. The ratio between the central pressure and the central energy density

$$\lambda \equiv \frac{p_c}{\epsilon_c} = \frac{K \rho_c^{1+1/n}}{\rho_c + nK \rho_c^{1+1/n}}, \quad (\text{B.9})$$

is a convenient measure of the importance of relativistic effects in the system. Note that our

definition deviates from Tooper's [473], who prefers to use the ratio p_c/ρ_c .

The energy density is then 5

$$\epsilon = \rho_c \theta^n + nK\rho_c^{1+1/n}\theta^{n+1} = \epsilon_c [1 + n\lambda(\theta - 1)] \theta^n. \quad (\text{B.10})$$

We now want to derive a dimensionless form of the TOV equations (3.7). The definition of the mass function m_Γ implies

$$\frac{dm_\Gamma}{d\xi} = 4\pi\epsilon_c a^3 [1 + n\lambda(\theta - 1)] \theta^n \xi^2. \quad (\text{B.11})$$

In terms of the dimensionless mass

$$\bar{m} \equiv \frac{m_\Gamma}{a^3 \epsilon_c}, \quad (\text{B.12})$$

this becomes

$$\frac{d\bar{m}}{d\xi} = 4\pi [1 + n\lambda(\theta - 1)] \theta^n \xi^2. \quad (\text{B.13})$$

From the TOV equation for the pressure we similarly obtain, after some manipulations,

$$\frac{d\theta}{d\xi} = -\frac{\bar{m}}{\xi^2} (1 - n\lambda) \left[1 + (n+1) \frac{\lambda}{1 - n\lambda} \theta \right] \left(1 + \lambda \frac{4\pi\xi^3 \theta^{n+1}}{\bar{m}} \right) \left[1 - 2(n+1)\lambda \frac{\bar{m}}{\xi} \right]^{-1}. \quad (\text{B.14})$$

In the present case the characteristic length scale is

$$a = [(n+1)K\rho_c^{-1+1/n} (1 - n\lambda)^2]^{1/2}. \quad (\text{B.15})$$

At this point we would like to define dimensionless quantities that come from the relativistic Lane-Emden equations. The central baryonic rest-mass density is related to λ as [see Eq. (B.9)]:

$$\rho_c = K^{-n} \ell^n, \quad \ell \equiv \frac{\lambda}{1 - n\lambda}. \quad (\text{B.16})$$

The factor K^{-n} has units of mass density (or inverse square length in geometrical units),

therefore the dimensionless rest-mass density is

$$\bar{\rho} \equiv \rho K^n = \ell^n \theta^n. \quad (\text{B.17})$$

Similarly, the length scale a takes the form

$$a = K^{n/2} \sqrt{(n+1)\ell^{1-n}} (1 - n\lambda), \quad (\text{B.18})$$

where $K^{n/2}$ has dimensions of length. The dimensionless radius is defined as

$$\bar{r} \equiv r K^{-n/2} = \sqrt{(n+1)\ell^{1-n}} (1 - n\lambda) \xi. \quad (\text{B.19})$$

The remaining dimensionless parameters are

$$\bar{\epsilon} \equiv \epsilon K^n = \left(\frac{\ell^n}{1 - n\lambda} \right) [1 + n\lambda(\theta - 1)] \theta^n, \quad (\text{B.20})$$

$$\bar{\mu} \equiv m_{\text{T}} K^{-n/2} = \left[\sqrt{(n+1)\ell^{1-n}} (1 - n\lambda) \right]^3 \left(\frac{\ell^n}{1 - n\lambda} \right) \bar{m}, \quad (\text{B.21})$$

$$\bar{p} \equiv p K^n = \ell^{n+1} \theta^{n+1}, \quad (\text{B.22})$$

$$\Pi = n \frac{\bar{p}}{\bar{\rho}} = n \ell \theta. \quad (\text{B.23})$$

All of the above dimensionless profiles are functions of ξ , n and λ . At variance with the Newtonian treatment, the relativistic Lane-Emden formalism does not allow for a simple algebraic mass-radius relation $M(R)$. This is also related to the fact that the system is not scale-invariant, due to the presence of λ in the equations.

APPENDIX C

THE PPN POTENTIALS

The goal of this appendix is to study the behavior of the potentials U , E and Ω appearing in the PPN stellar structure equations (3.9), first derived by Ciufolini and Ruffini [106]. By means of a mass function redefinition (see Section 3.2) these potentials can be eliminated at 1PN order, but they could still appear at 2PN order and higher.

Given the 2PN precision of our calculations we can write these potentials as:

$$U(r) = - \int_0^r dr' \frac{m_N}{r'^2} + U(0), \quad (\text{C.1a})$$

$$E(r) = 4\pi \int_0^r dr' r'^2 \rho \Pi, \quad (\text{C.1b})$$

$$\Omega(r) = -4\pi \int_0^r dr' r' \rho m_N, \quad (\text{C.1c})$$

where all right-hand side quantities are computed in Newtonian theory. In Eqs. (C.1), $m_N(r)$ denotes the Newtonian mass function

$$m_N(r) = 4\pi \int_0^r dr' \rho r'^2 = 4\pi m_b \int_0^r dr' n_b r'^2, \quad (\text{C.2})$$

where n_b is the baryon number density. The integral quantities U , E and Ω represent the system's gravitational potential energy, internal energy, and gravitational potential energy respectively [369]. They appear as dimensionless PN terms in the form of reduced potentials: U , E/m_N , Ω/m_N [see Eqs. (3.9)].

The radial profiles of the three potentials inside the star can be determined by first integrating the Newtonian hydrostatic equilibrium equations, Eqs. (B.3) and (B.4), to find m_N and p as functions of r . Using realistic EOS data tables for $p(\rho)$ we can subsequently compute the internal density per unit mass $\Pi(p)$ and the mass density $\rho(p) = m_b n_b(p)$, and then numerically evaluate the potentials inside the star by integration.

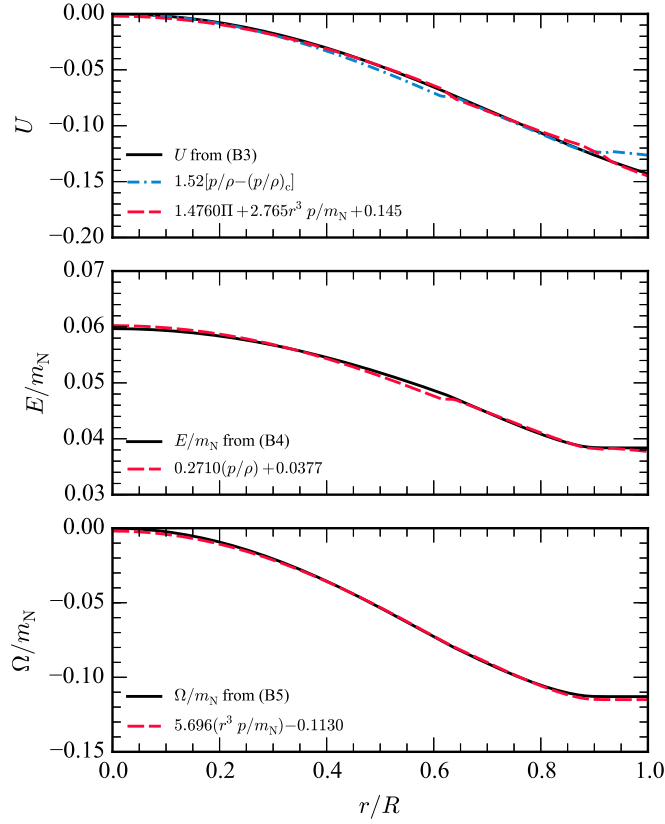


Figure C.1: *Integral PN potentials and 1PN terms.* The radial profiles of the integral potentials U , E/m_N and Ω/m_N are well fitted by linear functions of the non-integral potentials p/ρ and $r^3 p/m_N$. In all plots, the radial coordinate is normalized to the stellar radius R .

Some insight into the nature of these potentials can be obtained by rewriting Eqs. (C.1) in the form

$$U = \frac{m_N}{r} + 4\pi \int_r^R dr' r' \rho, \quad (\text{C.3a})$$

$$\frac{E}{m_N} = \Pi - \frac{1}{m_N} \int_0^r dr' m_N \frac{d\Pi}{dr'}, \quad (\text{C.3b})$$

$$\frac{\Omega}{m_N} = -\frac{m_N}{2r} - \frac{1}{2m_N} \int_0^r dr' \left(\frac{m_N}{r'} \right)^2 = 4\pi \frac{r^3 p}{m_N} - \frac{12\pi}{m_N} \int_0^r dr' r'^2 p. \quad (\text{C.3c})$$

Note that the integration constant for U has been fixed by requiring $U(R) = M/R$ at the stellar surface, while those for E and Ω have been set to zero in order to have regularity of

E/m_N and Ω/m_N at $r = 0$. The values of the potentials at the stellar center are:

$$U(0) = 4\pi \int_0^R dr r \rho, \quad \frac{\Omega}{m_N}(0) = 0, \quad \frac{E}{m_N}(0) = \Pi_c. \quad (\text{C.4})$$

From Eqs. (C.3) we can see that E/m_N and Ω/m_N are (partially) expressed in terms of the non-integral 1PN terms

$$\frac{m_N}{r}, \Pi, \frac{r^3 p}{m_N}. \quad (\text{C.5})$$

This suggests the possibility that the behavior of all three potentials could be captured by linear combinations of non-integral 1PN terms. If true, this would mean that any 2PN term involving U , E/m_N or Ω/m_N is effectively accounted for by the presence of the other terms in the post-TOV formulae. For instance, this idea can be demonstrated for U and for the special case of a polytropic system. Starting from (C.1a) and expressing m_N in terms of dp/dr , after an integration by parts and use of (B.6) we arrive at

$$U = (n + 1) \left(\frac{p}{\rho} - \frac{p_c}{\rho_c} \right) + U(0). \quad (\text{C.6})$$

We know that for a polytrope $\Pi = np/\rho$, which means that we can also write

$$U = \frac{(n + 1)}{n} (\Pi - \Pi_c) + U(0). \quad (\text{C.7})$$

For a polytropic model, therefore, U can be written exactly as a linear function of p/ρ or Π .

We have verified that U , E/m_N and Ω/m_N can be approximated by similar linear functions for the case of realistic EOSs. As an illustration, in Fig. C.1 we consider a stellar model built using the APR EOS with central mass density of 0.58×10^{15} g/cm³, Newtonian mass $m_N = 1.50M_\odot$ and radius $R = 14.8$ km. For this model we plot the radial profiles of U (top panel), E/m_N (middle panel) and Ω/m_N (bottom panel). The figure shows that the profiles of the three potentials can be accurately reproduced by linear combinations of the 1PN terms in Eq. (C.5), and that U is reasonably well fit by a linear function of p/ρ ,

as suggested by (C.6). This latter fit breaks down near the surface, but with a different combination of 1PN terms (namely, Π and $r^3 p/m_N$) one can produce a near-perfect fit.

In conclusion, the addition of the integral potentials U , E/m_N and Ω/m_N in the 2PN terms is unnecessary because their behavior can be captured by linear combinations of the non-integral PN terms which are already included in the post-TOV equations (3.1).

APPENDIX D

INTEGRAL REPRESENTATION OF THE MOMENT OF INERTIA OF A SLOWLY
ROTATING ANISOTROPIC STAR IN SCALAR-TENSOR THEORY

In this Appendix we present a derivation of the integral (5.29), used to compute the moment of inertia I of slowly rotating stars in scalar-tensor theory. We begin by noting that

$$\frac{d\Lambda}{dr} = \frac{r}{r-2\mu} \left(\frac{1}{r} \frac{d\mu}{dr} - \frac{\mu}{r^2} \right), \quad (\text{D.1})$$

where Eq. (5.15) implies that $\Lambda = -(1/2) \log(1 - 2\mu/r)$ and where $d\mu/dr$ is given by Eq. (5.20). Introducing the auxiliary variable $j \equiv e^{-\Phi-\Lambda}$ we find, using Eqs. (5.21) and (D.1), that

$$\frac{dj}{dr} = -j \left[4\pi A^4(\varphi) \frac{r^2}{r-2\mu} (\tilde{\epsilon} + \tilde{p}) + r\psi^2 \right]. \quad (\text{D.2})$$

Multiplying the frame dragging equation (5.24) by j and rearranging, we obtain

$$\frac{1}{r^4} \frac{d}{dr} \left(r^4 j \frac{d\bar{\omega}}{dr} \right) = 16\pi A^4(\varphi) \frac{j r^2}{r-2\mu} (\tilde{\epsilon} + \tilde{p}) \left(1 - \frac{\tilde{\sigma}}{\tilde{\epsilon} + \tilde{p}} \right) \frac{\bar{\omega}}{r}. \quad (\text{D.3})$$

If we multiply by r^4 , integrate from $r = 0$ to infinity and use the fact that

$$j = 1 + \mathcal{O}(r^{-1}), \quad \text{and} \quad \frac{d\bar{\omega}}{dr} = \frac{6 I \Omega}{r^4} + \mathcal{O}(r^{-5}). \quad (\text{D.4})$$

as $r \rightarrow \infty$, we finally get Eq. (5.29).

APPENDIX E

A SIMPLE APPROXIMATE FORMULA FOR THE CRUST THICKNESS-TO-RADIUS RATIO OF NEUTRON STARS IN SCALAR TENSOR THEORY

In this Appendix we present the derivation of Eq. (6.23). Making use of Eq. (5.21), we rewrite Eq. (5.23) as

$$\frac{d\tilde{p}}{dr} = -(\tilde{\epsilon} + \tilde{p}) \left[4\pi A^4(\varphi) \frac{r^2 \tilde{p}}{r - 2m} + \frac{1}{2} r \psi^2 + \frac{m}{r(r - 2m)} + \alpha(\varphi) \psi \right]. \quad (\text{E.1})$$

Let us assume that the following approximations hold true in the NS crust: (i) $m_s \approx M$, and therefore $e^{-2\Lambda} = 1 - 2M/r_s$; (ii) the pressure \tilde{p} is negligible in comparison to $\tilde{\epsilon}$ [402]; (iii) $\varphi \approx \varphi_s$ and $\psi \approx \psi_s$; (iv) $A(\varphi) \approx 1$. We also assume that the EOS has the polytropic form $\tilde{\epsilon} = k\tilde{p}^{1/\Gamma}$, where k and Γ are constants. Then Eq. (E.1) becomes

$$\frac{d\tilde{p}}{dr} \approx -\tilde{p} e^{2\Lambda} \frac{M}{r} - \tilde{\epsilon} \left[\frac{1}{2} r \psi_s^2 + \alpha(\varphi_s) \psi_s \right], \quad (\text{E.2})$$

where $\alpha(\varphi_s) = \beta\varphi_s$. Integrating this equation from $r = r_b$ to $r = r_s$ and imposing $\tilde{p}(r_s) = 0$ we obtain

$$0 = \sigma + M e^{2\Lambda} \left(\frac{1}{r_s} - \frac{1}{r_b} \right) - \psi_s^2 (r_s^2 - r_b^2) - \alpha(\varphi_s) \psi_s (r_s - r_b), \quad (\text{E.3})$$

where we have defined $\sigma \equiv \xi \tilde{p}_b / \tilde{\epsilon}_b$ and $\xi \equiv \Gamma / (\Gamma - 1)$ (recall that the subscript b denotes quantities evaluated at the crust basis).

We now make the additional assumption that $\psi_s^2 (r_s^2 - r_b^2)$ is negligible compared to $\alpha(\varphi_s) \psi_s (r_s - r_b)$. We have verified this assumption by explicitly evaluating these two terms for different stellar models: typically $\alpha(\varphi_s) \psi_s (r_s - r_b)$ is larger than $\psi_s^2 (r_s^2 - r_b^2)$ by at least a factor 10. Rewriting Eq. (E.3) in terms of \mathcal{R} we obtain the quadratic equation

$$0 = \frac{\beta\xi}{\sigma} \mathcal{R}^2 - \left[1 + \frac{1}{\sigma} (\mathcal{C} e^{2\Lambda} + \beta\zeta) \right] \mathcal{R} + 1, \quad (\text{E.4})$$

where we introduced $\zeta = \zeta(\mathcal{C}) \equiv \varphi_s \psi_s r_s$, which must be obtained by interpolation, given a family of stellar models, as a function of \mathcal{C} . Choosing the solution of Eq. (E.4) that reduces to the GR result (6.22) when $\beta \rightarrow 0$ and defining $\mathcal{F} \equiv 1 + (\mathcal{C} e^{2\Lambda} + \beta\zeta) / \sigma$, we finally obtain Eq. (6.23).

APPENDIX F

EQUIVALENCE OF THE PERTURBATION EQUATIONS IN EINSTEIN AND
JORDAN FRAMES

Here we show that the perturbation equation (6.38) could also be obtained by starting with the energy-momentum conservation law in the Einstein frame,

$$\nabla_{*\mu} T_*^{\mu\nu} - \alpha(\varphi) T_* \nabla_*^\nu \varphi = 0.$$

For odd (axial) perturbations in the Cowling approximation, the perturbed Einstein-frame energy-momentum tensor $\delta T_{*\mu\nu}$ satisfies

$$\partial_\mu \delta T_{*\nu}^\mu + \Gamma_{*\sigma\mu}^\mu \delta T_{*\mu}^\sigma - \Gamma_{*\nu\mu}^\sigma \delta T_{*\sigma}^\mu - \alpha(\varphi) \delta T_* \nabla_*^\nu \varphi = 0. \quad (\text{F.1})$$

Using the relation $T_{*\nu}^\mu = A^4(\varphi) \tilde{T}_\nu^\mu$ – which implies $\delta T_{*\nu}^\mu = A^4(\varphi) \delta \tilde{T}_\nu^\mu$ – and the trace relation $T_* = A^4(\varphi) \tilde{T}$, we obtain upon substitution into Eq. (F.1) that

$$4A^3(\varphi) \frac{A(\varphi)}{d\varphi} \partial_\mu \delta \tilde{T}_\nu^\mu + A^4(\varphi) \left[\partial_\mu \delta \tilde{T}_\nu^\mu + \Gamma_{*\sigma\mu}^\mu \delta \tilde{T}_\nu^\sigma - \Gamma_{*\nu\mu}^\sigma \delta \tilde{T}_\sigma^\mu - \alpha(\varphi) \partial_\nu \varphi \delta \tilde{T} \right] = 0. \quad (\text{F.2})$$

Dividing by $A^4(\varphi)$ we recover Eq. (6.38).

APPENDIX G

DISFORMAL INVARIANCE

In this appendix, we study how the physical quantities associated with properties of a slowly-rotating star transform under disformal transformations [cf. Eq. (7.2)] introduced in Chapter 7:

$$\tilde{g}_{\mu\nu} = A^2(\varphi) [g_{\mu\nu} + \Lambda B^2(\varphi) \varphi_\mu \varphi_\nu]$$

We start by writing the line elements for slowly-rotating spacetimes in the Einstein and Jordan frames as

$$ds^2 = -e^{\nu(r)} c^2 dt^2 + e^{\lambda(r)} dr^2 + r^2 (d\theta^2 + \sin^2 \theta d\phi^2) + 2(\omega - \Omega) r^2 \sin^2 \theta dt d\phi, \quad (\text{G.1})$$

and

$$d\tilde{s}^2 = -e^{\bar{\nu}(\bar{r})} c^2 dt^2 + e^{\bar{\lambda}(\bar{r})} d\bar{r}^2 + \bar{r}^2 (d\theta^2 + \sin^2 \theta d\phi^2) + 2(\bar{\omega} - \bar{\Omega}) \bar{r}^2 \sin^2 \theta dt d\phi. \quad (\text{G.2})$$

We can relate Eqs. (G.1) and (G.2) using the disformal relation (7.2) as

$$e^{\bar{\nu}} = A^2(\varphi) e^\nu, \quad (\text{G.3})$$

$$e^{\frac{\bar{\lambda}}{2}} d\bar{r} = A(\varphi) \sqrt{\chi} e^{\frac{\lambda}{2}} dr, \quad (\text{G.4})$$

$$\bar{r} = r A(\varphi), \quad (\text{G.5})$$

$$\bar{\omega} - \bar{\Omega} = \omega - \Omega, \quad (\text{G.6})$$

where we recall that due the symmetries of the problem $\varphi = \varphi(r)$. From Eqs. (G.4) and (G.5) we get

$$e^{\bar{\lambda}} = \frac{\chi}{(1 + r\alpha\varphi')^2} e^\lambda. \quad (\text{G.7})$$

Introducing μ and $\bar{\mu}$ in the Einstein and Jordan frames by

$$e^{-\lambda} = 1 - \frac{2\mu}{r}, \quad e^{-\bar{\lambda}} = 1 - \frac{2\bar{\mu}}{\bar{r}}, \quad (\text{G.8})$$

and using Eqs. (G.5) and (G.7) we find

$$\bar{\mu} = -\frac{rA(\varphi)}{2} \left[\left(1 - \frac{2\mu}{r}\right) \frac{(1 + r\alpha(\varphi)\varphi')^2}{\chi} - 1 \right]. \quad (\text{G.9})$$

As it is reasonable to set $\varphi_0 = 0$ and $\varphi'_0 = 0$ at asymptotic infinity, in the class of models considered in the text [Eq. (7.74)], $A(\varphi_0) = 1$, $\alpha(\varphi_0) = 0$ and $\chi(\varphi_0, \varphi'_0) = 1$, we find that the ADM mass obtained from the leading-order values of μ and $\bar{\mu}$ at asymptotic infinity is disformally invariant

$$\bar{M} = M. \quad (\text{G.10})$$

The energy-momentum tensors of the matter fields in the Einstein and Jordan frames are defined by

$$\begin{aligned} T_{(m)\mu\nu} &= \rho c^2 u_\mu u_\nu + p_r k_\mu k_\nu + p_t (g_{\mu\nu} + u_\mu u_\nu - k_\mu k_\nu), \\ \bar{T}_{(m)\mu\nu} &= \bar{\rho} c^2 \bar{u}_\mu \bar{u}_\nu + \bar{p}_r \bar{k}_\mu \bar{k}_\nu + \bar{p}_t (\bar{g}_{\mu\nu} + \bar{u}_\mu \bar{u}_\nu - \bar{k}_\mu \bar{k}_\nu), \end{aligned} \quad (\text{G.11})$$

where u^μ (\bar{u}^μ) and k^μ (\bar{k}^μ) are the four-velocity and unit radial vectors in the Einstein (Jordan) frame, respectively [417]. Within the first order of Hartle-Thorne's slow-rotation approximation [204], in the Einstein frame

$$u^\mu = \left(\frac{1}{\sqrt{-g_{tt}}}, 0, 0, \frac{\Omega}{\sqrt{-g_{tt}}} \right), \quad k^\mu = \left(0, \frac{1}{\sqrt{g_{rr}}}, 0, 0 \right),$$

and in the Jordan frame \bar{u}^μ and \bar{k}^μ are defined in the same way as Eq. (G.12) with an overbar. The nonvanishing components of the energy-momentum tensors in both frames are

then given by

$$T_{(m)t}{}^t = -\rho c^2, \quad T_{(m)r}{}^r = p_r, \quad T_{(m)\theta}{}^\theta = T_{(m)\phi}{}^\phi = p_t, \quad (\text{G.12a})$$

$$\bar{T}_{(m)t}{}^t = -\bar{\rho} c^2, \quad \bar{T}_{(m)\bar{r}}{}^{\bar{r}} = \bar{p}_{\bar{r}}, \quad \bar{T}_{(m)\theta}{}^\theta = \bar{T}_{(m)\phi}{}^\phi = \bar{p}_t, \quad (\text{G.12b})$$

and

$$T_{(m)\phi}{}^t = \left(\rho + \frac{p_t}{c^2} \right) e^{-\nu} \omega r^2 \sin^2 \theta, \quad (\text{G.13a})$$

$$\bar{T}_{(m)\phi}{}^t = \left(\bar{\rho} + \frac{\bar{p}_t}{c^2} \right) e^{-\bar{\nu}} \bar{\omega} \bar{r}^2 \sin^2 \theta. \quad (\text{G.13b})$$

In the Jordan frame, we then make a coordinate transformation from $\bar{x}^\mu = (t, \bar{r}, \theta, \phi)$ to $x^\mu = (t, r, \theta, \phi)$, such that

$$\tilde{T}_{(m)\mu}{}^\nu := \frac{\partial \bar{x}^\rho}{\partial x^\mu} \frac{\partial x^\nu}{\partial \bar{x}^\sigma} \bar{T}_{(m)\rho}{}^\sigma. \quad (\text{G.14})$$

Introducing the components of the energy-momentum tensor $\tilde{T}_{(m)\mu\nu}$ as (G.12a)-(G.12b) with a tilde, we find

$$\bar{\rho} = \tilde{\rho}, \quad \bar{p}_{\bar{r}} = \tilde{p}_r, \quad \bar{p}_t = \tilde{p}_t, \quad (\text{G.15})$$

and consequently

$$\bar{T}_{(m)\phi}{}^t = \tilde{T}_{(m)\phi}{}^t. \quad (\text{G.16})$$

The components of the energy-momentum tensor in the Einstein and Jordan frames are related by (7.23) and

$$T_{(m)\phi}{}^t = A^4(\varphi) \sqrt{\chi} \tilde{T}_{(m)\phi}{}^t. \quad (\text{G.17})$$

Now, substituting Eqs. (7.23), (G.3), (G.5), (G.13a), (G.13b), (G.15) and (G.16) into Eq.

(G.17) we find

$$\bar{\omega} = \omega, \quad (\text{G.18})$$

and, therefore, from (G.6)

$$\bar{\Omega} = \Omega. \quad (\text{G.19})$$

The angular momenta in the Einstein and Jordan frames are given by

$$J = \int dr d\theta d\phi r^2 \sin \theta e^{\frac{\nu+\lambda}{2}} T_{(m)\phi}{}^t, \quad (\text{G.20})$$

$$\bar{J} = \int d\bar{r} d\theta d\phi \bar{r}^2 \sin \theta e^{\frac{\bar{\nu}+\bar{\lambda}}{2}} \bar{T}_{(m)\phi}{}^t. \quad (\text{G.21})$$

Using again (G.3), (G.4), (G.5), (G.16) and (G.17), we find that the angular momentum is disformally invariant

$$\bar{J} = J. \quad (\text{G.22})$$

From Eqs. (G.19) and (G.22) we find that the moments of inertia in the Einstein and Jordan frames, $I = J/\Omega$ and $\bar{I} = \bar{J}/\bar{\Omega}$, are also disformally invariant

$$\bar{I} = I. \quad (\text{G.23})$$

Thus all quantities associated with rotation are disformally invariant. Our arguments in this appendix can be applied to a generic class of the Horndeski theory connected by the disformal transformation [57].

APPENDIX H

SPHERICAL AND HYPERBOLOIDAL TARGET SPACES

In TMS theory [117], the scalar field $\varphi^A(x^\mu)$ is an application from the space-time manifold \mathcal{M} to the target-space manifold \mathcal{T} . This target-space manifold is Riemannian, and its metric is denoted by $\gamma_{AB}(\varphi^C)$. The dimensionality of \mathcal{T} (i.e. the number of scalar fields) is N . Since one-dimensional manifolds are necessarily flat, the simplest non-trivial case is $N = 2$. Furthermore, the simplest two-dimensional manifolds are the maximally symmetric ones, i.e. spherical, hyperbolic and flat spaces. In these spaces, the curvature radius $\hat{r} > 0$ is constant; the Ricci scalar is $\mathcal{R} = 2/\hat{r}^2$ for spherical space, $\mathcal{R} = -2/\hat{r}^2$ for hyperbolic space, and $\mathcal{R} = 0$ for flat space. For convenience we define $\mathbf{r} = \hat{r}$, $i\hat{r}$ for spherical and hyperbolic spaces, respectively, so that the Ricci scalar has the form $\mathcal{R} = 2/\mathbf{r}^2$ in both cases.

Here we derive the expression for the target-space line element $\gamma_{AB}d\varphi^A d\varphi^B = 2\gamma d\varphi d\bar{\varphi}$ in terms of the complexified scalar field $\varphi = Z + iW$ for the spherical and hyperbolic cases; the result is Eq. (8.16) in the main text.

H.1 Spherical target space

The 2-sphere can be defined from its embedding in a three-dimensional Euclidean space of coordinates (x, y, z) through the equation

$$x^2 + y^2 + z^2 = \hat{r}^2. \quad (\text{H.1})$$

It can be parametrized in polar coordinates, defining $\varphi^{A'} = (\Theta, \Phi)$, where:

$$x = \hat{r} \sin \Theta \cos \Phi, \quad y = \hat{r} \sin \Theta \sin \Phi, \quad z = \hat{r} \cos \Theta. \quad (\text{H.2})$$

The target-space metric in these coordinates is

$$\gamma_{A'B'} = \begin{pmatrix} \hat{r}^2 & 0 \\ 0 & \hat{r}^2 \sin^2 \Theta \end{pmatrix}. \quad (\text{H.3})$$

This frame has undesirable features: in the flat-space limit $\hat{r} \rightarrow \infty$ the metric diverges, and the kinetic term in the action (8.40) [where for simplicity we set $V(\Theta, \Phi) = 0$]

$$S = \frac{1}{4\pi G_\star} \int d^4x \sqrt{-g} \left[\frac{R}{4} - \frac{1}{2} g^{\mu\nu} \hat{r}^2 (\partial_\mu \Theta \partial_\nu \Theta + \sin^2 \Theta \partial_\mu \Phi \partial_\nu \Phi) \right] \quad (\text{H.4})$$

diverges as well. Moreover, the polar frame is not the most suitable for numerical implementation, because it has coordinate singularities at the boundary of the open intervals $0 < \Theta < \pi$, $0 < \Phi < 2\pi$ where the coordinate system is defined. To fix this problem we perform a stereographic projection from the north pole of the sphere (which is the only point of the manifold not covered by this chart) to the plane $\varphi^A = (Z, W)$ tangent to the south pole:

$$Z = \frac{2\hat{r}}{\hat{r} - z} x = 2\hat{r} \frac{\sin \Theta}{1 - \cos \Theta} \cos \Phi, \quad (\text{H.5})$$

$$W = \frac{2\hat{r}}{\hat{r} - z} y = 2\hat{r} \frac{\sin \Theta}{1 - \cos \Theta} \sin \Phi. \quad (\text{H.6})$$

With this projection the equator is mapped to the circle $Z^2 + W^2 = 4\hat{r}^2$; the upper and lower hemispheres are mapped to the exterior and interior of this circle, respectively, and the north pole is mapped to infinity. Using $\sin \Theta / (1 - \cos \Theta) = \cot(\Theta/2)$, the complex field $\varphi = Z + iW$ is written in a more compact form as

$$\varphi = 2\hat{r} \cot(\Theta/2) e^{i\Phi}. \quad (\text{H.7})$$

In the coordinate frame $\varphi^A = (Z, W)$ the target-space metric is

$$\gamma_{AB} = \frac{(1 - \cos \Theta)^2}{4} \delta_{AB} = \frac{\hat{r}^4}{[(Z^2 + W^2)/4 + \hat{r}^2]^2} \delta_{AB}; \quad (\text{H.8})$$

note that $(Z^2 + W^2)/4 + \hat{r}^2 = 2\hat{r}^2 / (1 - \cos \Theta)$. In terms of the complex field φ , $\delta_{AB} d\varphi^A d\varphi^B = d\varphi d\bar{\varphi}$, therefore $\gamma_{AB} d\varphi^A d\varphi^B = 2\gamma d\varphi d\bar{\varphi}$ (note that we denote $\gamma = \gamma_{a\bar{b}}$, because a, b can only

take the value 1), and

$$\gamma = \frac{1}{2} \left(1 + \frac{\varphi\bar{\varphi}}{4\hat{r}^2} \right)^{-2}. \quad (\text{H.9})$$

H.2 Hyperbolic target space

The two-dimensional hyperbolic space of two sheets can also be defined from its embedding into $\mathbb{R}^{1,2}$ with coordinates (x, y, z) through the equation

$$-x^2 - y^2 + z^2 = \hat{r}^2. \quad (\text{H.10})$$

It can be parametrized in terms of $\varphi^{A'} = (\Theta, \Phi)$ as

$$x = \hat{r} \sinh \Theta \cos \Phi, \quad y = \hat{r} \sinh \Theta \sin \Phi, \quad z = \pm \hat{r} \cosh \Theta. \quad (\text{H.11})$$

The target-space metric in these coordinates is

$$\gamma_{A'B'} = \begin{pmatrix} \hat{r}^2 & 0 \\ 0 & \hat{r}^2 \sinh^2 \Theta \end{pmatrix}. \quad (\text{H.12})$$

As in the case of spherical space (see above) the metric diverges when $\hat{r} \rightarrow \infty$, and the kinetic term in the action diverges as well. Therefore we perform a stereographic projection from the point at the top of the lower branch to the plane $\varphi^A = (Z, W)$ tangent to the bottom of the upper branch. With this projection, the upper branch is mapped to the interior of the circle $Z^2 + W^2 = 4\hat{r}^2$, and the lower branch is mapped to the exterior of this circle. The stereographic mapping reads

$$Z = \frac{2\hat{r}}{z + \hat{r}} x = 2\hat{r} \frac{\sinh \Theta}{\cosh \Theta + 1} \cos \Phi, \quad (\text{H.13})$$

$$W = \frac{2\hat{r}}{z + \hat{r}} y = 2\hat{r} \frac{\sinh \Theta}{\cosh \Theta + 1} \sin \Phi. \quad (\text{H.14})$$

for the upper branch, and

$$Z = \frac{2\hat{r}}{-z - \hat{r}}x = 2\hat{r} \frac{\sinh \Theta}{\cosh \Theta - 1} \cos \Phi, \quad (\text{H.15})$$

$$W = \frac{2\hat{r}}{-z - \hat{r}}y = 2\hat{r} \frac{\sinh \Theta}{\cosh \Theta - 1} \sin \Phi \quad (\text{H.16})$$

for the lower branch. The complex field $\varphi = Z + iW$ is then $\varphi = 2\hat{r} \tanh(\Theta/2)e^{i\Phi}$ for the upper branch, and $\varphi = 2\hat{r} \coth(\Theta/2)e^{i\Phi}$ for the lower branch.

In the coordinate frame $\varphi^A = (Z, W)$ the target-space metric is

$$\gamma_{AB} = \frac{(1 \pm \cosh \Theta)^2}{4} \delta_{AB} = \frac{\hat{r}^4}{[-(Z^2 + W^2)/4 + \hat{r}^2]^2} \delta_{AB} \quad (\text{H.17})$$

where the upper (lower) sign refers to the upper (lower) branch; note that $-(Z^2 + W^2)/4 + \hat{r}^2 = 2\hat{r}^2/(1 \pm \cos \Theta)$. In terms of the complex field φ , then, the target-space metric is $2\gamma d\varphi d\bar{\varphi}$ with

$$\gamma = \frac{1}{2} \left(1 - \frac{\varphi\bar{\varphi}}{4\hat{r}^2}\right)^{-2}. \quad (\text{H.18})$$

H.3 Field equations for two-dimensional spherical and hyperbolic spaces

In summary, the expressions (H.9), (H.18) for the target-space metric in the (two-dimensional) spherical and hyperbolic cases can be written in the form of Eq. (8.16), i.e.

$$\gamma = \frac{1}{2} \left(1 + \frac{\varphi\bar{\varphi}}{4\mathbf{r}^2}\right)^{-2}, \quad (\text{H.19})$$

where $\mathbf{r} = \hat{r}$ for a spherical space, and $\mathbf{r} = i\hat{r}$ for a hyperbolic space. In the coordinate frame $\varphi^A = (Z, W)$ the target-space metric is

$$\gamma_{AB} = \frac{\mathbf{r}^4}{[(Z^2 + W^2)/4 + \mathbf{r}^2]^2} \delta_{AB} \quad (\text{H.20})$$

for both the spherical and hyperbolic space. Therefore, Eqs. (H.19), (H.20) describe a spherical space if $\mathbf{r}^2 > 0$, an hyperbolic space if $\mathbf{r}^2 < 0$. The limit $\mathbf{r} \rightarrow \infty$ yields flat space. If

$\mathbf{r} \rightarrow \infty$ and the scalar field is restricted to real values, one recovers the single-scalar case.

The Christoffel symbols are:

$$\gamma^Z_{ZZ} = -\frac{2Z}{\mathbf{r}^2 + Z^2 + W^2}, \gamma^W_{ZZ} = \frac{2W}{\mathbf{r}^2 + Z^2 + W^2}, \gamma^Z_{ZW} = -\frac{2W}{\mathbf{r}^2 + Z^2 + W^2}, \quad (\text{H.21})$$

$$\gamma^W_{WW} = -\frac{2W}{\mathbf{r}^2 + Z^2 + W^2}, \gamma^Z_{WW} = \frac{2Z}{\mathbf{r}^2 + Z^2 + W^2}, \gamma^W_{ZW} = -\frac{2Z}{\mathbf{r}^2 + Z^2 + W^2}. \quad (\text{H.22})$$

In terms of the complex field φ , writing explicitly the indices a, b in $\gamma_{a\bar{b}}$ (which can only take the value 1) we get

$$\gamma^{\bar{c}}_{a\bar{b}} = \frac{1}{2} \partial_\varphi \log \gamma = -\frac{\bar{\varphi}}{4\mathbf{r}^2 + \bar{\varphi}\varphi}, \quad \gamma^c_{a\bar{b}} = \frac{1}{2} \partial_{\bar{\varphi}} \log \gamma = -\frac{\varphi}{4\mathbf{r}^2 + \bar{\varphi}\varphi}. \quad (\text{H.23})$$

The Ricci tensor and Ricci scalar of the target space are $\mathcal{R}_{AB} = \mathbf{r}^{-2} \delta_{AB}$ and $\mathcal{R} = 2\mathbf{r}^{-2}$, respectively.

Replacing the expression of the metric (H.18) and of the Christoffel symbols (H.23) in Eqs. (8.14) and (8.15) with $V(\varphi) = 0$ we find the field equations for a maximally symmetric two-dimensional target space, i.e. Eqs. (8.17) and (8.18).

APPENDIX I

SOLAR SYSTEM CONSTRAINTS ON TENSOR-MULTI-SCALAR THEORY

The weak-field limit of TMS theories has been worked out in [117]. Specializing these results to the theory constructed in the body of the text, and rewriting them in complex notation, one finds that the gravitational constant measured in a Cavendish experiment is given by

$$G = G_{\star} A_{\infty}^2 (1 + \bar{\kappa}_{\infty} \kappa_{\infty}), \quad (\text{I.1})$$

where the subscript ∞ denotes evaluation at $\varphi_{\infty} = 0$ and we defined the complex function $\kappa(\varphi, \bar{\varphi})$ as in Eq. (8.19). Using Eq. (8.20), one finds that $\kappa_{\infty} = 2\alpha^*$.

It is straightforward to show that the post-Newtonian parameter γ_{PPN} reads [117]

$$\gamma_{\text{PPN}} - 1 = -\frac{2\bar{\kappa}_{\infty}\kappa_{\infty}}{1 + \bar{\kappa}_{\infty}\kappa_{\infty}} = -\frac{8|\alpha^*|^2}{1 + 4|\alpha^*|^2}, \quad (\text{I.2})$$

and therefore the Cassini bound $|\gamma_{\text{PPN}} - 1| < 2.3 \cdot 10^{-5}$ [56] implies the constraint

$$|\alpha^*|^2 < 3 \cdot 10^{-6} \quad (\text{I.3})$$

on the coupling constants α^* and $\bar{\alpha}^*$ appearing in Eq. (8.20). Crucially, the one above is a bound on $|\alpha^*|$, whereas $\arg \alpha^*$ is completely unconstrained in the weak-field limit.

On the other hand, the post-Newtonian parameter β_{PPN} reads [117]

$$\beta_{\text{PPN}} - 1 = \frac{\bar{\kappa}_{\infty}\kappa_{\infty}\beta_{\infty}}{2(1 + \bar{\kappa}_{\infty}\kappa_{\infty})^2}, \quad (\text{I.4})$$

where the real-valued function $\beta(\varphi, \bar{\varphi})$ is defined by

$$\beta(\varphi, \bar{\varphi}) \equiv \frac{1}{2} \left(1 + \frac{\bar{\varphi}\varphi}{4\mathbf{r}^2} \right) \left(\kappa \frac{\partial}{\partial \bar{\varphi}} + \bar{\kappa} \frac{\partial}{\partial \varphi} \right) \log(\bar{\kappa}\kappa). \quad (\text{I.5})$$

Using the definitions above and Eq. (8.20) we obtain

$$\begin{aligned}\beta_{\text{PPN}} - 1 &= \frac{\alpha^* \alpha^* \bar{\beta}_1^* + 2\alpha^* \bar{\alpha}^* \beta_0 + \bar{\alpha}^* \bar{\alpha}^* \beta_1^*}{(1 + 4\alpha^* \bar{\alpha}^*)^2} \\ &= \frac{2|\alpha^*|^2}{(1 + 4|\alpha^*|^2)^2} \left(\beta_0 + |\beta_1^*| \cos(2 \arg \alpha^* - \arg \beta_1^*) \right).\end{aligned}\quad (\text{I.6})$$

Finally, the bound $|\beta_{\text{PPN}} - 1| < 1.1 \cdot 10^{-4}$ coming from the combination of Cassini and Lunar Laser Ranging measurements [504] implies a constraint on some combination of the parameters β_0 , $|\beta_1^*|$, and $\arg \alpha^* - \frac{1}{2} \arg \beta_1^*$. However, note that if $|\alpha^*| \rightarrow 0$ the observational constraint $|\beta_{\text{PPN}} - 1| < 1.1 \cdot 10^{-4}$ is satisfied for any value of β_0 , $|\beta_1^*|$ and $\arg \alpha^* - \frac{1}{2} \arg \beta_1^*$, and therefore these parameters are unconstrained by weak-field observations in this limit.

APPENDIX J

LINEARIZED FIELD EQUATIONS AND SCALARIZATION IN
TENSOR-MULTI-SCALAR THEORY

Here we consider the ST theory defined by Eqs. (8.21) and (8.23) with $\alpha = 0$, which admits GR solutions with $\psi \equiv 0$. We will perturb these GR solutions, and linearize the field equations in the perturbations. This is valid when the amplitudes of the scalar fields are small and consequently the metric back-reaction on the scalar field can be neglected. This approximation is well motivated at the onset of scalarization.

The field equations acquire a particularly simple form when linearized to first order in $Z \equiv \text{Re}[\psi]$ and $W \equiv \text{Im}[\psi]$. In this case, the tensor field equations (8.21) reduce to

$$R_{\mu\nu} = 8\pi G_\star \left(T_{\mu\nu} - \frac{1}{2} T g_{\mu\nu} \right), \quad (\text{J.1})$$

and therefore the background geometry to $\mathcal{O}(Z, W)$ is described by a GR solution. The scalar-field equation (8.22) becomes

$$\square Z = -4\pi G_\star (\beta_0 + \beta_1) T Z, \quad (\text{J.2})$$

$$\square W = -4\pi G_\star (\beta_0 - \beta_1) T W, \quad (\text{J.3})$$

where, in this perturbative expansion, the box operator is evaluated on the GR background solution and the trace of the perfect fluid energy-momentum tensor T attains its GR value, i.e. $T = -(8\pi G_\star)^{-1} R = 3P - \rho$. Note that the equations for Z and W decouple in this limit, reducing to the same equation as in the single-scalar case, $\square\varphi = -4\pi G_\star \beta T \varphi$, but with effective coupling parameters $\beta = \beta_0 + \beta_1$ and $\beta = \beta_0 - \beta_1$, respectively.

In the case of a single scalar, the term on the right-hand side of the scalar equation can be interpreted as an effective mass term (cf. e.g. [51])

$$m_{\text{eff}}^2 = -4\pi G_\star \beta T. \quad (\text{J.4})$$

Because in typical configurations $T \sim -\rho < 0$, the effective mass squared is negative when $\beta < 0$. This signals a possible tachyonic instability which is associated with an exponentially

growing mode and causes the growth of scalar hair in a process known as *spontaneous scalarization* [118], as discussed in the main text. In the case of static compact stars, it turns out that this instability occurs for $\beta \lesssim -4.35$, the threshold value depending only mildly on the equation of state [198, 336, 417].

The same reasoning can be applied to Eqs. (J.2) and (J.3). Because the latter are completely equivalent to two copies of a single-scalar equation, scalarization is expected whenever

$$\beta_0 + \beta_1 \lesssim -4.35 \quad \text{or} \quad \beta_0 - \beta_1 \lesssim -4.35. \quad (\text{J.5})$$

Note that these conditions were derived assuming that each scalar field acquires a non-vanishing expectation value independently and by perturbing a static GR solution. In particular, they do not imply that *both* fields scalarize when both conditions (J.5) are satisfied. In fact, biscalarization can be investigated in this perturbative framework by studying the linear perturbations of (say) the scalar field W on the background of a previously scalarized solution where Z has a non-trivial profile.

APPENDIX K

THE FIELD EQUATIONS OF HORNDESKI GRAVITY

In this appendix we list the left-hand side of the field equations, cf. Eqs. (9.15) and (9.16). For clarity, we split all of the left-hand sides of the field equations as a sum of two contributions, so that the case of time-independent scalar fields can more easily be recovered by setting $q = 0$:

$$\mathcal{E}_{\alpha\beta} = \mathcal{E}_{\alpha\beta}^{(0)} + \frac{q^2}{A} \mathcal{E}_{\alpha\beta}^{(t)} , \quad (\text{K.1})$$

$$\mathcal{E}_{\phi} = \mathcal{E}_{\phi}^{(0)} + \frac{q^2}{A} \mathcal{E}_{\phi}^{(t)} . \quad (\text{K.2})$$

Let us remark that the equations of motion still depend on the specific form of the G_i 's, which are functions of the kinetic energy (9.19), and therefore may contain q -dependent terms; therefore we must evaluate all of the functions G_i at $q = 0$ to recover the time-independent limit. The explicit forms of the various terms are

$$\begin{aligned} \mathcal{E}_{tt}^{(0)} = & G_2 + B\psi'^2 G_{3\phi} - \frac{B\psi'^2}{2} (B'\psi' + 2B\psi'') G_{3X} - \frac{2}{r} \left(\frac{B-1}{r} + B' \right) G_4 \\ & - \frac{2B^2\psi'}{r} \left(\frac{\psi'}{r} + 2\frac{B'}{B}\psi' + 2\psi'' \right) G_{4X} - B \left(\frac{4}{r}\psi' + \frac{B'}{B}\psi' + 2\psi'' \right) G_{4\phi} \\ & + \frac{2B^2\psi'^3}{r} (B'\psi' + 2B\psi'') G_{4XX} - B^2\psi'^2 \left(\frac{4}{r}\psi' - \frac{B'}{B}\psi' - 2\psi'' \right) G_{4X\phi} \\ & - 2B\psi'^2 G_{4\phi\phi} + \frac{B\psi'^2}{2r^2} (5B'B\psi' + 6B^2\psi'' - B'\psi' - 2B\psi'') G_{5X} \\ & + \frac{B^3\psi'^3}{r} \left(\frac{\psi'}{r} - \frac{B'}{B}\psi' - 2\psi'' \right) G_{5X\phi} - \frac{B^3\psi'^4}{2r^2} (B'\psi' + 2B\psi'') G_{5XX} \\ & + \frac{B\psi'}{r} \left(3B'\psi' + 4B\psi'' + \frac{\psi'}{r} + B\frac{\psi'}{r} \right) G_{5\phi} + \frac{2B^2\psi'^3}{r} G_{5\phi\phi} , \end{aligned} \quad (\text{K.3})$$

$$\begin{aligned}
\mathcal{E}_{tt}^{(t)} &= -G_{2X} + G_{3\phi} + \frac{B}{2} \left(4\frac{\psi'}{r} + \frac{B'}{B}\psi' + 2\psi'' \right) G_{3X} + \frac{2}{r} \left(\frac{B-1}{r} + B' \right) G_{4X} \\
&\quad - \left(\frac{4B}{r}\psi' + B'\psi' + 2B\psi'' \right) G_{4X\phi} - \frac{2B\psi'}{r} \left(B'\psi' + 2B\psi'' + \frac{B}{r}\psi' \right) G_{4XX} \\
&\quad - \frac{1}{2r^2} (3B'B\psi' - B'\psi' - 2B\psi'' + 2B^2\psi'') G_{5X} - \frac{1}{r} \left(\frac{B-1}{r} + B' \right) G_{5\phi} \\
&\quad + \frac{B\psi'}{r} \left(B'\psi' + 2B\psi'' + \frac{B}{r}\psi' \right) G_{5X\phi} + \frac{B^2\psi'^2}{2r^2} (B'\psi' + 2B\psi'') G_{5XX} , \tag{K.4}
\end{aligned}$$

$$\begin{aligned}
\mathcal{E}_{rr}^{(0)} &= G_2 + B\psi'^2 G_{2X} - B\psi'^2 G_{3\phi} - \frac{B^2\psi'^3}{2} \left(\frac{4}{r} + \frac{A'}{A} \right) G_{3X} - \frac{2}{r} \left(B\frac{A'}{A} + \frac{B-1}{r} \right) G_4 \\
&\quad - B\psi' \left(\frac{4}{r} + \frac{A'}{A} \right) G_{4\phi} - \frac{2B\psi'^2}{r} \left(2B\frac{A'}{A} + \frac{2B-1}{r} \right) G_{4X} + B^2\psi'^3 \left(\frac{4}{r} + \frac{A'}{A} \right) G_{4X\phi} \\
&\quad + \frac{2B^3\psi'^4}{r} \left(\frac{A'}{A} + \frac{1}{r} \right) G_{4XX} + \frac{B\psi'^2}{r} \left(3B\frac{A'}{A} + \frac{3B-1}{r} \right) G_{5\phi} + \frac{B^2\psi'^3}{2r^2} \frac{A'}{A} (5B-1) G_{5X} \\
&\quad - \frac{B^3\psi'^4}{r} \left(\frac{A'}{A} + \frac{1}{r} \right) G_{5X\phi} - \frac{B^4\psi'^5}{2r^2} \frac{A'}{A} G_{5XX} , \tag{K.5}
\end{aligned}$$

$$\begin{aligned}
\mathcal{E}_{rr}^{(t)} &= -G_{3\phi} + \frac{B\psi'}{2} \frac{A'}{A} G_{3X} + \frac{2B}{r} \frac{A'}{A} G_{4X} + 2G_{4\phi\phi} - \frac{2B^2\psi'^2}{r} \frac{A'}{A} G_{4XX} + B\psi' \left(\frac{4}{r} - \frac{A'}{A} \right) G_{4X\phi} \\
&\quad - \frac{2B\psi'}{r} G_{5\phi\phi} - \frac{B\psi'}{2r^2} \frac{A'}{A} (3B-1) G_{5X} + \frac{B^2\psi'^2}{r} \left(\frac{A'}{A} - \frac{1}{r} \right) G_{5X\phi} + \frac{B^3\psi'^3}{2r^2} G_{5XX} \\
&\quad + \frac{1}{r} \left(\frac{B-1}{r} - B\frac{A'}{A} \right) G_{5\phi} , \tag{K.6}
\end{aligned}$$

$$\begin{aligned}
\mathcal{E}_{t\varphi}^{(0)} = & \omega G_2 + B\psi'^2 \omega G_{3\phi} - \frac{B\psi'^2}{2} \omega (B'\psi' + 2B\psi'') G_{3X} \\
& + \frac{B}{2} \left[- \left(\frac{2B'}{rB} + 2\frac{A''}{A} + \frac{B'A'}{BA} - \frac{A'^2}{A^2} + \frac{2A'}{rA} \right) \omega + \left(\frac{B'}{B} + \frac{8}{r} - \frac{A'}{A} \right) \omega' + 2\omega'' \right] G_4 \\
& - \left[\left(\frac{A'}{A} B\psi' + B'\psi' + 2B\psi'' + \frac{2}{r} B\psi' \right) \omega - \omega' B\psi' \right] G_{4\phi} \\
& + \frac{B^2\psi'}{2} \left[- \left(\frac{2A'}{rA} \psi' + \frac{4B'}{rB} \psi' + 2\frac{A''}{A} \psi' - \frac{A'^2}{A^2} \psi' + 2\frac{B'A'}{BA} \psi' + 2\frac{A'}{A} \psi'' + \frac{4}{r} \psi'' \right) \omega \right. \\
& \left. + 2\psi' \omega'' + \left(\frac{8\psi'}{r} + \frac{2B'}{B} \psi' + 2\psi'' - \frac{A'}{A} \psi' \right) \omega' \right] G_{4X} \\
& + B^2\psi'^2 \left[\left(\frac{B'}{B} \psi' - \frac{A'}{A} \psi' + 2\psi'' - \frac{2}{r} \psi' \right) \omega + \psi' \omega'' \right] G_{4X\phi} - 2B\psi'^2 \omega G_{4\phi\phi} \\
& + \frac{B^2\psi'^3}{2} \left[\left(\frac{2}{r} \psi' B' + \psi' B' \frac{A'}{A} + \frac{4}{r} B\psi' \psi'' + 2B \frac{A'}{A} \psi'' \right) \omega - (\psi' B' + 2B\psi'') \omega' \right] G_{4XX} \\
& + \frac{B^3\psi'^2}{4r} \left[- \left(5\frac{B'}{B} \psi' - \frac{A'}{A} \psi' + 6\psi'' + \frac{6}{r} \psi' \right) \omega' + \left(5\frac{B'A'}{BA} \psi' - \frac{A'^2}{A^2} \psi' + 6\frac{A'}{A} \psi'' + 2\frac{A''}{A} \psi' \right) \omega \right. \\
& \left. - 2\psi' \omega'' \right] G_{5X} + \frac{B^2\psi'^3}{4} \left[\left(\psi' B' + 2B\psi'' - \frac{2B}{r} \psi' \right) \omega' - \left(\psi' B' \frac{A'}{A} + 2B \frac{A'}{A} \psi'' \right. \right. \\
& \left. \left. - \frac{2}{r} B\psi' \frac{A'}{A} + \frac{2}{r} \psi' B' + \frac{4}{r} B\psi'' \right) \omega \right] G_{5X\phi} \\
& + \frac{B^3\psi'^4}{4r} \left[(\psi' B' + 2B\psi'') \omega' - \frac{A'}{A} (\psi' B' + 2B\psi'') \omega \right] G_{5XX} \\
& + \frac{B\psi'}{4} \left[\left(\frac{A'}{A} B\psi' - \frac{8}{r} B\psi' - 4B\psi'' - 3B'\psi' \right) \omega' \right. \\
& \left. + \left(3B' \frac{A'}{A} \psi' - \frac{BA'^2}{A^2} \psi' + \frac{2A'}{rA} B\psi' + 2B \frac{A''}{A} \psi' + \frac{6}{r} B'\psi' + \frac{8}{r} B\psi'' + 4\frac{A'}{A} B\psi'' \right) \omega \right. \\
& \left. - 2B\psi' \omega'' \right] G_{5\phi} + \frac{B^2\psi'^3}{2} \left[\left(\frac{2}{r} + \frac{A'}{A} \right) \omega - \omega' \right] G_{5\phi\phi} , \tag{K.7}
\end{aligned}$$

$$\begin{aligned}
\mathcal{E}_{t\varphi}^{(t)} = & -\frac{B\psi' A'}{2A}\omega G_{3X} - \omega G_{3\phi} \\
& + \left[\left(\frac{2B A'}{r A} + 2B \frac{A''}{A} - 2B \frac{A'^2}{A^2} + B' \frac{A'}{A} \right) \frac{\omega}{2} - \left(B' + \frac{8B}{r} - 2B \frac{A'}{A} \right) \frac{\omega'}{2} - B\omega'' \right] G_{4X} \\
& + \left[\left(3 \frac{A'}{A} B\psi' + \frac{2B}{r} \psi' + B' \psi' + 2B\psi'' \right) \omega - \omega' B\psi' \right] G_{4X\phi} \\
& + \frac{B}{2} \left[B\psi' \left(\frac{B'}{B} \psi' + 2\psi'' - \psi' \frac{A'}{A} \right) \omega' \right. \\
& \left. - \frac{A'}{A} B\psi' \left(\frac{B'}{B} \psi' - \frac{A'}{A} \psi' + 2\psi'' - \frac{2}{r} \psi' \right) \omega \right] G_{4XX} + 2\omega G_{4\phi\phi} \\
& + \left[\frac{B^2}{4r} \left(\frac{6\psi'}{r} - 3 \frac{A'}{A} \psi' + 3 \frac{B'}{B} \psi' + 2\psi'' \right) \omega' \right. \\
& \left. - \frac{B^2}{4r} \left(3 \frac{B'}{B} \frac{A'}{A} \psi' + 2 \frac{A'}{A} \psi'' + 2 \frac{A''}{A} \psi' - 3 \frac{A'^2}{A^2} \psi' \right) \omega + \frac{B^2 \psi'}{2r} \omega'' \right] G_{5X} \\
& + \left[\frac{B^2 \psi'}{4} \left(\frac{A'}{A} \psi' - \frac{B'}{B} \psi' - 2\psi'' + \frac{2}{r} \psi' \right) \omega' \right. \\
& \left. - \frac{B^2 \psi'}{4} \left(\frac{A'^2}{A^2} \psi' - \frac{B'}{B} \frac{A'}{A} \psi' - 2 \frac{A'}{A} \psi'' + \frac{6}{r} \frac{A'}{A} \psi' + \frac{2}{r} \frac{B'}{B} \psi' + \frac{4}{r} \psi'' \right) \omega \right] G_{5X\phi} \\
& + \frac{B^3 \psi'^2 A'}{4r A} \left[\left(\psi' - \frac{AB'}{A'B} \psi' - \frac{2A}{A'} \psi'' \right) \omega' + \left(\frac{B'\psi'}{B} - \frac{A'\psi'}{A} + 2\psi'' \right) \omega \right] G_{5XX} \\
& + \frac{B}{4} \left[\left(-\frac{2A'}{r A} + 3 \frac{A'^2}{A^2} - 2 \frac{A''}{A} + \frac{2B'}{r B} - \frac{B' A'}{B A} \right) \omega + \left(\frac{8}{r} + \frac{B'}{B} - 3 \frac{A'}{A} \right) \omega' + 2\omega'' \right] G_{5\phi} \\
& + \frac{B}{2} \left[- \left(2 \frac{A'}{A} \psi' + \frac{B'}{B} \psi' + 2\psi'' + \frac{2}{r} \psi' \right) \omega + \psi' \omega' \right] G_{5\phi\phi} \\
& + \frac{q^2 B A'}{A 4 A} \left(\frac{A'}{A} \omega - \omega' \right) \left(G_{5X\phi} - 2G_{4XX} + \frac{B\psi'}{r} G_{5XX} \right), \tag{K.8}
\end{aligned}$$

$$\begin{aligned}
\mathcal{E}_\phi^{(0)} = & G_{2\phi} + B\psi' \left(\frac{A'}{2A} + \frac{B'}{2B} + \frac{2}{r} + \frac{\psi''}{\psi'} \right) G_{2X} + B\psi'^2 G_{2X\phi} - B\psi'^3 \left(\frac{B'}{2} + \frac{B\psi''}{\psi'} \right) G_{2XX} \\
& - B\psi' \left(\frac{B'}{B} + \frac{A'}{A} + \frac{4}{r} + \frac{2\psi''}{\psi'} \right) G_{3\phi} - B^2\psi'^2 \left(\frac{3A'B'}{4AB} + \frac{3B'}{Br} + \frac{A'\psi''}{A\psi'} + \frac{4\psi''}{\psi'r} + \frac{A''}{2A} - \frac{A'^2}{4A^2} \right. \\
& + \left. \frac{2A'}{Ar} + \frac{2}{r^2} \right) G_{3X} + B^2\psi'^3 \left(\frac{\psi''}{\psi'} - \frac{A'}{2A} + \frac{B'}{2B} - \frac{2}{r} \right) G_{3X\phi} + B^3\psi'^4 \left(\frac{B'}{Br} + \frac{A'B'}{4AB} + \frac{2\psi''}{r\psi'} \right. \\
& + \left. \frac{A'\psi''}{2A\psi'} \right) G_{3XX} - B\psi'^2 G_{3\phi\phi} + B \left(\frac{A'^2}{2A^2} - \frac{A''}{A} - \frac{A'B'}{2AB} - \frac{2A'}{Ar} - \frac{2B'}{Br} - \frac{2}{r^2} + \frac{2}{Br^2} \right) G_{4\phi} \\
& + B^2\psi' \left(\frac{A'^2}{A^2r} - \frac{2A''}{Ar} - \frac{3A'B'}{ABr} - \frac{3A'}{Ar^2} - \frac{3B'}{Br^2} + \frac{A'}{ABr^2} - \frac{2A'\psi''}{A\psi'r} - \frac{2\psi''}{\psi'r^2} + \frac{B'}{B^2r^2} + \frac{2\psi''}{B\psi'r^2} \right) G_{4X} \\
& + B^3\psi'^3 \left(\frac{2A''}{Ar} - \frac{A'^2}{A^2r} + \frac{6A'B'}{ABr} + \frac{3A'}{Ar^2} + \frac{6B'}{Br^2} + \frac{8A'\psi''}{A\psi'r} + \frac{8\psi''}{\psi'r^2} - \frac{B'}{B^2r^2} - \frac{2\psi''}{B\psi'r^2} \right) G_{4XX} \\
& + B^2\psi'^2 \left(\frac{A''}{A} - \frac{A'^2}{2A^2} + \frac{2A'B'}{AB} + \frac{4A'}{Ar} + \frac{8B'}{Br} + \frac{4}{r^2} + \frac{2}{Br^2} + \frac{3A'\psi''}{A\psi'} + \frac{12\psi''}{\psi'r} \right) G_{4X\phi} \\
& + B^2\psi'^3 \left(\frac{A'}{A} + \frac{4}{r} \right) G_{4X\phi\phi} + B^3\psi'^4 \left(\frac{2A'}{Ar} - \frac{2B'}{Br} - \frac{A'B'}{2AB} - \frac{A'\psi''}{A\psi'} - \frac{4\psi''}{\psi'r} + \frac{2}{r^2} \right) G_{4XX\phi} \\
& - B^3\psi'^5 \left(\frac{A'B'}{Ar} + \frac{B'}{r^2} + \frac{2A'B\psi''}{A\psi'r} + \frac{2B\psi''}{\psi'r^2} \right) G_{4XXX} + B^2\psi' \left(\frac{2A''}{Ar} - \frac{A'^2}{A^2r} + \frac{3A'}{Ar^2} + \right. \\
& + \left. \frac{3A'B'}{ABr} + \frac{3B'}{Br^2} - \frac{A'}{ABr^2} + \frac{2A'\psi''}{A\psi'r} + \frac{2\psi''}{\psi'r^2} - \frac{B'}{B^2r^2} - \frac{2\psi''}{\psi'Br^2} \right) G_{5\phi} \\
& + B^3\psi'^2 \left(\frac{3A''}{2Ar^2} - \frac{3A'^2}{4A^2r^2} + \frac{15A'B'}{4ABr^2} + \frac{A'^2}{4A^2Br^2} - \frac{A''}{2ABr^2} - \frac{3A'B'}{4AB^2r^2} + \frac{3A'\psi''}{A\psi'r^2} - \frac{A'\psi''}{AB\psi'r^2} \right) G_{5X} \\
& + B^4\psi'^4 \left(\frac{A'^2}{4A^2r^2} - \frac{A''}{2Ar^2} - \frac{5A'B'}{2ABr^2} - \frac{7A'\psi''}{2\psi'Ar^2} + \frac{A'B'}{4AB^2r^2} + \frac{A'\psi''}{2AB\psi'r^2} \right) G_{5XX} \\
& + B^3\psi'^3 \left(\frac{A'^2}{2A^2r} - \frac{A''}{Ar} - \frac{7A'B'}{2ABr} - \frac{A'}{2Ar^2} - \frac{7B'}{2Br^2} - \frac{A'}{2ABr^2} - \frac{5A'\psi''}{A\psi'r} - \frac{5\psi''}{\psi'r^2} \right. \\
& + \left. \frac{B'}{2B^2r^2} + \frac{\psi''}{\psi'Br^2} \right) G_{5X\phi} + B^2\psi'^2 \left(\frac{A'}{Ar} - \frac{1}{Br^2} + \frac{1}{r^2} \right) G_{5\phi\phi} - B^3\psi'^4 \left(\frac{A'}{Ar} + \frac{1}{r^2} \right) G_{5X\phi\phi} \\
& + B^4\psi'^5 \left(\frac{A'B'}{2ABr} - \frac{A'}{2Ar^2} + \frac{B'}{2Br^2} + \frac{A'\psi''}{A\psi'r} + \frac{\psi''}{\psi'r^2} \right) G_{5XX\phi} \\
& + B^4\psi'^6 \left(\frac{A'B'}{4Ar^2} + \frac{A'B\psi''}{2Ar^2\psi'} \right) G_{5XXX} , \tag{K.9}
\end{aligned}$$

$$\begin{aligned}
\mathcal{E}_\phi^{(t)} = & -G_{2X\phi} - \frac{A'B\psi'}{2A}G_{2XX} + \left(\frac{BA'}{Ar} - \frac{3BA'^2}{4A^2} + \frac{A'B'}{4A} + \frac{BA''}{2A} \right) G_{3X} \\
& + G_{3\phi\phi} + B\psi' \left(\frac{B'}{2B} + \frac{2}{r} + \frac{3A'}{2A} + \frac{\psi''}{\psi'} \right) G_{3X\phi} \\
& + B^2\psi'^2 \left(\frac{A'}{Ar} + \frac{A'^2}{4A^2} - \frac{A'\psi''}{2A\psi'} - \frac{A'B'}{4AB} \right) G_{3XX} \\
& + B^2\psi' \left(\frac{4A'^2}{A^2r} - \frac{2A''}{Ar} - \frac{3A'B'}{ABr} - \frac{A'}{Ar} - \frac{2A'\psi''}{A\psi'r} - \frac{A'}{ABr^2} \right) G_{4XX} \\
& + \left(\frac{2A'^2B}{A^2} - \frac{BA''}{A} - \frac{A'B'}{2A} - \frac{2A'B}{Ar} + \frac{2B'}{r} + \frac{2(B-1)}{r^2} \right) G_{4X\phi} \\
& - B\psi' \left(\frac{2A'}{A} + \frac{B'}{B} + \frac{2\psi''}{\psi'} + \frac{4}{r} \right) G_{4X\phi\phi} \\
& - B^2\psi'^2 \left(\frac{6A'}{Ar} + \frac{2B'}{Br} - \frac{A'B'}{2AB} - \frac{A'\psi''}{A\psi'} + \frac{A'^2}{2A^2} + \frac{2}{r^2} + \frac{4\psi''}{\psi'r} \right) G_{4XX\phi} \\
& + B^2\psi'^3 \left(\frac{A'B'}{Ar} + \frac{2A'B\psi''}{A\psi'r} - \frac{A'^2B}{A^2r} - \frac{A'B}{Ar^2} \right) G_{4XXX} \\
& + B^2 \left(\frac{3A'^2}{4A^2r^2} - \frac{A''}{2Ar^2} - \frac{3A'B'}{4ABr^2} - \frac{3A'^2}{4A^2Br^2} + \frac{A''}{2ABr^2} + \frac{A'B'}{4AB^2r^2} \right) G_{5X} \\
& + B^2\psi'^2 \left(\frac{A''B}{2Ar^2} - \frac{3A'^2B}{2A^2r^2} + \frac{3A'B'}{2Ar^2} + \frac{3A'B\psi''}{2A\psi'r^2} - \frac{A'B'}{4ABr^2} - \frac{A'\psi''}{2A\psi'r^2} + \frac{A'^2}{4A^2r^2} \right) G_{5XX} \\
& + B^2\psi' \left(\frac{A''}{Ar} - \frac{5A'^2}{2A^2r} + \frac{3A'B'}{2ABr} - \frac{A'}{2Ar^2} - \frac{3B'}{2Br^2} + \frac{3A'}{2ABr^2} + \frac{A'\psi''}{A\psi'r} - \frac{\psi''}{\psi'r^2} \right. \\
& \left. + \frac{B'}{2B^2r^2} + \frac{\psi''}{\psi'Br^2} \right) G_{5X\phi} - \left(\frac{B-1}{r^2} + \frac{B'}{r} \right) G_{5\phi\phi} + B^2\psi'^2 \left(\frac{2A'}{Ar} + \frac{B'}{Br} + \frac{2\psi''}{\psi'r} + \frac{1}{r^2} \right) G_{X\phi\phi} \\
& + B^3\psi'^3 \left(\frac{3A'}{2Ar^2} - \frac{A'B'}{2ABr} - \frac{A'\psi''}{A\psi'r} + \frac{B'}{2Br^2} + \frac{\psi''}{\psi'r^2} + \frac{A'^2}{2A^2r} \right) G_{5XX\phi} \\
& - B^4\psi'^4 \left(\frac{A'B'}{4ABr^2} + \frac{A'\psi''}{2A\psi'r^2} - \frac{A'^2}{4A^2r^2} \right) G_{5XXX} . \tag{K.10}
\end{aligned}$$

VITA

Hector Okada da Silva

University of Mississippi

Department of Physics and Astronomy

108 Lewis Hall, Room 204

University, MS 38677-1848 USA

Education

- 2005–2008, BSc. in Physics, Departamento de Física, Universidade Federal do Pará, Brazil
- 2009–2011, MSc. in Physics, Departamento de Física, Universidade Federal do Pará, Brazil

Awards, Honors & Scholarships

- 2006–2008, National Council for Scientific and Technological Development (CNPq) Scholarship
- 2008–2009, Foundation for Research Support of the State of Pará (FAPESPA) Scholarship
- 2009–2011, National Council for Scientific and Technological Development (CNPq) Scholarship
- 2012–2017, University of Mississippi, Department of Physics and Astronomy, Zdravko Stipcevic Honors Fellowship

- 2015, Summer Research Assistantship, Graduate School, University of Mississippi
- 2015, The Blue Apple Award, 8th Gulf Coast Gravity Meeting, University of Florida, American Physical Society Topical Group in Gravitation
- 2016, Elected member of the Sigma Pi Sigma, the Physics Honor Society
- 2016, Graduate Achievement Award, University of Mississippi
- 2016, Dissertation Fellowship – Spring 2017, University of Mississippi

Publications

- *Quantum radiation force on the moving mirror of a cavity, with Dirichlet and Neumann boundary conditions for a vacuum, finite temperature, and a coherent state*
D. T. Alves, E. R. Granhen, H. O. Silva and M. G. Lima,
Phys. Rev. D **81** 025016 (2010).
- *Exact behavior of the energy density inside an one-dimensional oscillating cavity with a thermal state*
D. T. Alves, E. R. Granhen, H. O. Silva and M. G. Lima,
Phys. Lett. A **374** 3899-3907 (2010)
- *Simple model for the dynamical Casimir effect for a static mirror with time-dependent properties*
H. O. Silva and C. Farina,
Phys. Rev. D **84** 045003 (2011)
- *New signatures of the dynamical Casimir effect in a superconducting circuit*
A. L. C. Rego, H. O. Silva, D. T. Alves and C. Farina,
Phys. Rev. D **90** 025003 (2014)

- *Torsional oscillations of neutron stars in scalar-tensor theory of gravity*
H. O. Silva, H. Sotani, E. Berti and M. Horbatsch,
Phys. Rev. D **90** 124044 (2014)
- *Slowly rotating anisotropic neutron stars in general relativity and scalar-tensor theory*
H. O. Silva, C. F. B. Macedo, E. Berti and L. C. B. Crispino,
Class. Quantum Grav. **32** 145008 (2015)
- *Post-Tolman-Oppenheimer-Volkoff formalism for relativistic stars,*
K. Glampedakis, G. Pappas, H. O. Silva and E. Berti,
Phys. Rev. D **92** 024056 (2015)
- *Tensor-multi-scalar theories: relativistic stars and 3+1 decomposition,*
M. Horbatsch, H. O. Silva, D. Gerosa, P. Pani, E. Berti, L. Gualtieri and U. Sperhake,
Class. Quantum Grav. **32** 204001 (2015)
- *Slowly rotating black hole solutions in Horndeski gravity,*
A. Maselli, H. O. Silva, M. Minamitsuji and E. Berti,
Phys. Rev. D **92** 104049 (2015)
- *Low-mass neutron stars: universal relations, the nuclear symmetry energy and gravitational radiation,*
H. O. Silva, H. Sotani and E. Berti,
Mon. Not. Roy. Astron. Soc **459** 4378 (2016)
- *Neutron stars in Horndeski gravity,*
A. Maselli, H. O. Silva, M. Minamitsuji and E. Berti,
Phys. Rev. D **93** 124056 (2016)
- *Relativistic stars in scalar-tensor theories with disformal coupling,*
M. Minamitsuji and H. O. Silva,
Phys. Rev. D **93** 124041 (2016)

- *Astrophysical application of the Post-Tolman-Oppenheimer-Volkoff formalism*,
K. Glampedakis, G. Pappas, H. O. Silva and E. Berti,
Phys. Rev. D **94** 044030 (2016)